Lecture Notes in Electrical Engineering 251

Tong-Cun Zhang
Pingkai Ouyang
Samuel Kaplan
Bill Skarnes *Editors*

Proceedings of the 2012 International Conference on Applied Biotechnology (ICAB 2012)

Volume 3

Springer

Lecture Notes in Electrical Engineering

Volume 251

For further volumes:
http://www.springer.com/series/7818

Tong-Cun Zhang · Pingkai Ouyang
Samuel Kaplan · Bill Skarnes
Editors

Proceedings of the 2012 International Conference on Applied Biotechnology (ICAB 2012)

Volume 3

Springer

Editors
Tong-Cun Zhang
College of Bioengineering
Tianjin University of Science
and Technology
Tianjin
People's Republic of China

Pingkai Ouyang
Nanjing University of Technology
Nanjing
People's Republic of China

Samuel Kaplan
Department of Microbiology, Houston
Medical School
University of Texas
Texas, TX
USA

Bill Skarnes
Wellcome Trust Sanger Institute
Cambridge
UK

ISSN 1876-1100 ISSN 1876-1119 (electronic)
ISBN 978-3-642-37924-6 ISBN 978-3-642-37925-3 (eBook)
DOI 10.1007/978-3-642-37925-3
Springer Heidelberg New York Dordrecht London

Library of Congress Control Number: 2013945796

Printed on acid-free paper

Springer is part of Springer Science+Business Media (www.springer.com)

Preface

2012 International Conference on Applied Biotechnology (ICAB2012) was organized by Tianjin University of Science and Technology, Tianjin Institute of Industrial Biotechnology, Chinese Academy of Sciences was held from October 18–19, 2012 in Tianjin, China.

The conference served as a forum for exchange and dissemination of ideas and the latest findings among all parties involved in any aspects of applied biotechnology. The following distinguished professors gave keynote speeches: Hassan Ashktorab (Howard University, USA), William Carl Skarnes (The Wellcome Trust Sanger Institute, UK), Hiroyuki Takenaka (Kyushu Kyoritsu University, Japan) and Xueli Zhang (Tianjin Institute of Industrial Biotechnology, Chinese Academy of Sciences, China). The conference was complemented by talks given by other 51 professors and investigates.

More than 200 authors from 44 different universities, institutes and companies submitted conference papers. A lot of fields have been covered, ranging from fermentation engineering, cell engineering, genetic engineering, enzyme engineering and protein engineering.

Special thanks are given to the Academic Committee, Organizing Committee and Secretary Staff of the conference for the commitment to the conference organization. We would like also to thank all the authors who contributed with their papers to the success of the conference.

This book gathers a selection of the papers presented at the conference; it contains contributions from both academic and industrial researchers providing a unique perspective on the research and development of applied biotechnology from all over the world. The scientific value of the papers also helps the researchers in this field to get more valuable results.

Tianjin, China

Tong-Cun Zhang
Pingkai Ouyang
Samuel Kaplan
Bill Skarnes

Committees

Sponsor

Chinese Society of Biotechnology

Organizers

Tianjin University of Science and Technology
Key Lab of Industrial Fermentation Microbiology, Ministry of Education
Tianjin Institute of Industrial Biotechnology, Chinese Academy of Sciences

Co-Organizers

Tianjin Society for Microbiology
Tianjin International Joint Academy of Biotechnology and Medicine
College of Biotechnology and Pharmaceutical Engineering, Nanjing University of Technology
College of Life Science, Nankai University
School of Biotechnology, Jiangnan University
College of Life Science and Technology, Beijing University of Chemical Technology
School of Bioscience and Bioengineering, South China University of Technology
College of Biotechnology, Chongqing University
State Key Laboratory of Bioreactor Engineering, East China University of Science and Technology
School of Biological Engineering, Dalian Polytechnic University
School of Food and Bioengineering, Shandong Polytechnic University

Academic Committee

Chairman

Pingkai Ouyang, Academician, Nanjing University of Technology, China

Executive Chairman

Zixin Deng, Academician, Shanghai Jiao Tong University, China
Baoguo Sun, Academician, Beijing Technology and Business University, China
Tianwei Tan, Academician, Beijing University of Chemical Technology, China
Prof. George Fu Gao, Institute of Microbiology of Chinese Academy of Sciences, China
Prof. Xiaohong Cao, Tianjin University of Science and Technology, China
Prof. Jian Chen, Jiangnan University, China
Prof. Yanhe Ma, Tianjin Institute of Industrial Biotechnology, Chinese Academy of Sciences, China

Members

Prof. Baishan Fang, Xiamen University, China
Prof. Cheng Yang, Tianjin International Joint Academy of Biotechnology and Medicine, China
Prof. Cunjiang Song, Nankai University (Tianjin Society for Microbiology), China
Prof. Danqun Huo, Chongqing University, China
Prof. Fang Liu, Nankai University, China
Prof. Fuping Lu, Tianjin University of Science and Technology, China
Prof. Guocheng Du, Jiangnan University, China
Prof. He Huang, Nanjing University of Technology, China
Prof. Hongzhang Chen, Institute of Process Engineering, Chinese Academy of Sciences, China
Prof. Jianhe Xu, East China University of Science and Technology, China
Prof. Jianjiang Zhong, Shanghai Jiao Tong University, China
Prof. Jianjun Liu, Shandong Academy of Food and Fermentation Industries, China
Prof. Jibin Sun, Tianjin Institute of Industrial Biotechnology, Chinese Academy of Sciences, China
Prof. Lirong Yang, Zhejiang University, China
Prof. Longjiang Yu, Huazhong University of Science and Technology, China
Prof. Min Wang, Tianjin University of Science and Technology, China
Prof. Muyi Cai, China National Research Institute of Food and Fermentation Industries, China

Prof. Ning Chen, Tianjin University of Science and Technology, China
Prof. Qipeng Yuan, Beijing University of Chemical Technology, China
Prof. Ruiming Wang, Shandong Polytechnic University, China
Prof. Shiru Jia, Tianjin University of Science and Technology, China
Prof. Shuyi Qiu, Guizhou University, China
Prof. Shuangjiang Liu, Institute of Microbiology of Chinese Academy of Sciences, China
Prof. Youshu Xia, Sichuan Academy of Food and Fermentation Industries, China
Prof. Siliang Zhang, East China University of Science and Technology, China
Prof. Tong-Cun Zhang, Tianjin University of Science and Technology, China
Prof. Xianzhen Li, Dalian University of Technology, China
Prof. Xiaolei Wu, Beijing University, China
Prof. Xinhui Xing, Tsinghua University, China
Prof. Xueming Zhao, Tianjin University, China
Prof. Yin Li, Institute of Microbiology of Chinese Academy of Sciences, China
Prof. Yinbo Qu, Shandong University, China
Prof. Ying Lin, South China University of Technology, China

Organizing Committee

Chairman

Prof. George Fu Gao, Vice Dean, Beijing Institute of Life Sciences, Chinese Academy of Sciences, China

Executive Chairman

Prof. Shuheng Ma, Vice Dean, Tianjin Institute of Industrial Biotechnology, Chinese Academy of Sciences, China
Prof. Dongguang Xiao, Dean, Tianjin University of Science and Technology, China

Members

Yinhua Wan, Deputy Secretary General, Chinese Society of Biotechnology, China
Lei Ma, Director, President's Office, Tianjin University of Science and Technology, China
Feng Wen, Secretary of the Party Committee, College of Bioengineering, Tianjin University of Science and Technology, China
Dingcheng Liu, Vice Dean, Division of Science and Technology, Tianjin

University of Science and Technology, China
Cunjiang Song, Secretary General, Tianjin Society of Microbiology, China
Cheng Yang, Vice Dean, Tianjin International Joint Academy of Biotechnology and Medicine, China

Secretariat

Secretary General

Prof. Shuheng Ma, Vice Dean, Tianjin Institute of Industrial Biotechnology, Chinese Academy of Sciences, China

Deputy Secretary General

Prof. He Huang, Dean, Division of Science and Technology, Nanjing University of Technology, China
Prof. Cunjiang Song, Secretary General, Tianjin Society of Microbiology, China
Prof. Tong-Cun Zhang, Director, Key Laboratory of Industrial Fermentation Microbiology (Tianjin University of Science and Technology), Ministry of Education, China

Members

Yue Wang, Juke Wang, Hongling Wang, Jiaming Wang, Yanbing Shen, Yihan Liu, Jian Zhang, Chaozheng Zhang, Kui Lu, Hao Zhou, Xuegang Luo, Cheng Zhong, Qingyang Xu, Bin Jia, Xuewu Guo, Zhilei Tan.

Contents

Part V Biotechnology Applications

137 Molecular Cloning and Expression of the β-Galactosidase Gene from *Bifidobacterium longum* LL04 in *Escherichia coli* 1279
Fanzhu Li, Xian Zhang and Seongil Lim

138 Identification of Symbiotic or Epiphyte Microbe F17 from *Pinctada Fucata* and Analysis of Its Main Metabolites by GC–MS 1291
Yanyan Wu, Yan Zhang, Laihao Li, Xianqing Yang, Wei Shi and Zhengyi Shao

139 Construction of Genomic Expression Library Vaccines Against Avian *Pasteurella Multocida* and Detection of the Immune Efficacy 1301
Qiang Gong, Cuili Qin and Ming Cheng

140 Expression of Recombinant Human Bone Morphogenetic Protein 2 in Insect Cells, Purification and Activity Analysis . . . 1309
Wen Chu, Shenheng Luo, Lihong Xu, Minhui Long and Aipo Diao

141 Biotechnology of Azobenzene-Modified DNA and RNA 1317
Xingguo Liang and Jing Li

142 Evaluation of a Whole Genome Amplification Method Based on Improved Ligation-Mediated PCR 1333
Xiaoming Pan, Weikai Chen, Xiushuang Jia, Ping Dong and Xingguo Liang

143 Isolation and Identification of a Bacterial Strain with Pullulanase Activity and the Cloning of the Pullulanase Gene 1345
Guixiu Dong, Tao Xia, Yongqian Qiu, Xiaoliang Si, Yiyu Liu, Pingping Yang, Xiangzhao Mao and Lizhong Guo

144 Study on ^{60}Coγ-Ray Irradiation Mutation of *Bacillus subtils* natto 1353
Yufeng Xie and Yingliang Ge

145 Effects of Different Processing Methods on Oyster DNA 1361
Ping Dong, Ran An, Xiushuang Jia, Dong Han and Xingguo Liang

146 Design and Synthesis of Resveratrol Analogs 1373
Yuanmou Chen, Fei Hu, Yinghao Gao, Na Ji, Weizhu Liu and Erbing Hua

147 Elongation of Trinucleotide Repeats by DNA Polymerase 1383
Yang Wang, Ping Dong and Xingguo Liang

148 Hydroxylation of Dehydroepiandrosterone by *Penicillium decumbens* ph-13 1393
Song Zhang, Peihui Liu, Lin Zhao and Xinli Liu

149 Preparation and Characterization of Cross-Linked Enzyme Aggregates of Amyloglucosidase 1399
Jiandong Cui and Yanan Zhang

150 An Extraction Method Suitable for Two-Dimensional Electrophoresis of Low-Abundant Proteins from Ginseng Roots 1407
Rui Jiang, Liwei Sun, Rui Ma, Xiujuan Lei and Daqing Zhao

151 Purification of Alkaline Pectinase in Engineering *Bacillus subtilis* 1419
Ming Li, Xin Sun, Liying Zhou, Hongxin Wang, Dongxia Li, Shuya Wang and Fuping Lu

152 In situ Preparation and Characteristics of a New Water-Soluble Heme Iron Via Hemin-Arginate Coacervation 1431
Wenhang Wang, Ting Liu, Ying Zhang, Rujie Chen and Anjun Liu

153 Enzymatic Extraction and Characteristics of Collagen Fibers from Cattle Skin 1441
Wenhang Wang, Ke Zhao, Wei Ren, Ting Liu and Ying Zhang

154 Detection of DNA Target with Highly Enhanced Specificity by Self-Circularization Rolling Circle Amplification 1449
Xingyu Wang, Xiaoliang Wang, Ping Dong, Masatomo Suzuki, Hiroyuki Asanuma and Xingguo Liang

155 Effect of Proteinase a Propeptide Deletion on Its Enzyme Activity in *Saccharomyces cerevisiae* 1459
Deguang Wu, Yefu Chen, Jun Lu, Yanan Qi, Cuiying Zhang and Dongguang Xiao

156 Corncob Residue Pretreatment for 2,3-Butanediol Production by Simultaneous Saccharification and Fermentation 1469
Xiaopei Peng, Cuiying Zhang, Yujie Tian, Xuewu Guo, Yanwen Liu and Dongguang Xiao

157 The Comparison on the Genotype of *idh-1* Between *Paralichthys olivaceus* and *Scophthalmus maximus* 1481
Zhiyi Qiao, Shi Dong, Jinhui Sun, Yue Pei and Qi Wang

158 Production of Natural Chitosan from Xylose by *Actinomucor elegans* Culture 1489
Xi Wang, Hua Zhao, Xin Feng and Jing Yang

159 Inhibition of α-Amylase Activities by Extracts of Chinese Yam 1499
Sai Qu, Liming Zhang, Xiaobian Zhang and Zhengjun Li

160 *VvpGLT,* a Grapevine Gene Encoding for a Plastidic Localized Glucose Transporter 1507
Lei Zeng, Yanjie Yi, Huaijian Tang and Jinshui Wang

161 Preparation and Characterization of New GA Carboxylic Acid Derivatives 1517
Caiju Zhou, Yong-En Guo, Laitao Zhang, Baoguo Wang, Longjiang Chen and Tong-Cun Zhang

162 Separation and Purification of Hyaluronic Acid from Fermentation Broth 1523
Yunshuang Wang, Jian Zhang and Hao Liu

163 In Vitro Cytotoxicity of the Bile Acids and Bile Acid Derivatives 1531
Xiangzheng Hu, Hongjian Zhou, Guangzhen Song, Anjun Liu and Lixia Wang

164 Studying on Extraction of Betulin from the White Birch and Synthesis of Betulinic Acid 1541
Tong-Cun Zhang, Weiwei Xu, Nan Wang, Xuegang Luo, Jing Wang and Xiangzheng Hu

165 Research on the Optimum Conditions and the Effect of Antioxidant Peptide from Scallop Protein 1551
Yuan Liu, Jian Wang, Zhisheng Zhang and Jie Wang

166 Tracing the Origin of Pigment in Broilers by Stable Nitrogen and Carbon Isotopes Analysis 1561
Huiwen Wang, Fengmei Sun and Shuming Yang

167 Vascular Endothelial Growth Factor Induces Bone Marrow-Derived Mesenchymal Stem Cells Differentiation into Endothelial Cells 1567
Nan Wang, Rui Zhang, Shuijing Wang, Jianjie du, Yanyang Tang and Tong-Cun Zhang

168 Fasting Effects on the Content of Liver and Muscle Glycogen in Sparrow 1575
Xingjun Xu, Shuli Shao, Huaiyong Li, Ziqiang Wang, Guangjun Zhang, Chenyang Jin, Yabo Sun and Shijie Zhao

169 Antibacterial Activity of Polyprenols and Other Lipids from *Ginkgo biloba* L. Leaves 1581
Ran Tao, Chengzhang Wang and Zhenwu Kong

170 Effect of *Lactococcus lactis subsp.* on Production of Pigment and Citrinin by Monascus 1591
Shichao Wang, Shuxin Zhao, Hongxia Mu, Fengyun Sun and Peng Chen

171 Prediction of NH_4^+ Concentration During the Temperature Triggered Glutamate Fermentation Using At-Line Near-Infrared Spectroscopy 1601
Jingbo Liang, Dalong Zhang, Xuan Guo, Qingyang Xu, Xixian Xie, Chenglin Zhang and Ning Chen

172 Studies on Protein Extraction from *Caragana korshinskii* Kom. Using Acetone Precipitation Method 1609
Cheng Zhong, Zhao Zhou, Rui Wang, Peipei Han and Shiru Jia

173 Signaling Pathways in Cardiac Hypertrophy 1617
Man Li, Nan Wang, Wenjing Liu, Xin Zhi and Tong-Cun Zhang

174 Progress in Heparin-Functionalized Biomaterials 1627
Yingfeng Wu, Juan Li, Feipeng Zhu and Hao Wang

175 Identification of an Antifungal Bacillus Strain and Studies on Its Antifungal Active Ingredients 1637
Yingde Shen, Ruibin Liu, Yuehua Chen and Jun Cai

176 Enrichment of Flavonoids and Removal of Organic Acid by Treatment of Weak-Base Anion Resins 1645
Yuping Zhao, Shuyang Sun, Zuli Sun, Wenguang Jiang, Jianrong Yang, Pu Song, Xiangping Zheng and Tiantian Tian

177 Study on the Decolourization Methods of Crude Alkaline Protease 1657
Hongbin Wang, Zhijia Lv, Jing Wang and Fuping Lu

178 Research Progress of the Polysaccharide O-Acetylated Pustulan-Type Glucans from *Umbilicariaceae lichens* 1665
Junjie Sun, Xinli Wei and Jiangchun Wei

179 Effects of UV-B Radiation and NaCl Stress on the Protein Expression in *Nostoc flagelliforme* 1671
Lei Yang, Haifeng Yu and Hongxian Lv

180 Study on Antibacterial Activity of *Radix isatidis* Extracts and Preliminary Investigation of Their Antibacterial Mechanism 1681
Lin Tian and Zhan Wang

181 Optimization Research of Sufu by Enzymatic Accelerated Maturation 1689
Jianming Wang, Feng Hu, Ping Li, Changsheng Qiao, Yuan Geng and Hengxing Yang

182 Optimization of the Electroporation Conditions for DNA Transformation of *Staphylococcus carnosus* 1699
Qiang Gao, Mengxiao Wang, Changyan Yu, Lin Huang, Xiu Zheng and Yan Zhu

183 Neutralization of the Residual Alkaline Solution of Chitosan with CO_2 Gas 1709
Ainan Guo, Shiru Jia, Yujie Dai, Peipei Han, Guojuan Xu, Xintong Zheng and Yanyan Li

184 Study on Method for Cooking Wheat Straw Pulp at Atmosphere by Microwave Radiation Mixed-Alkali Method 1717
Yu Deng and Zhimin Zhang

185 Biologic Chromatography for Purifying Filamentous Fungi Contaminated with Bacteria 1727
Jianping Zhang and Feifei Sun

186 Cross-Linked Enzyme Aggregates of *β*-Galactosidase from Different Source by Dialdehyde Starch as Cross-Linker 1733
Kang Wang, Yang Gao, Zhang Wang and Guangying Meng

187 Research Development on Vanadium-Dependent Haloperoxidases in Marine Algae 1741
Tao Wang, Yong-chao Lu, Dong-mei Cao, Shu-bao Gao and Yu-shan Zhang

188 The Cells of *Gluconacetobacter xylinus* Response to Exposure 1749
Xintong Zheng, Cheng Zhong, Miao Liu, Ainan Guo, Yanyan Li and Shiru Jia

189 Purification and Characterization of Cholinesterase from Duck Plasma 1759
Chang Liu and Fusheng Chen

190 Study on the Sensitivity of Two-Line Hybrid Rice's Self-Fruitful Rates on Temperature Changes: A Numerical Study 1771
Zhiwei Wang, Qingdai Liu and Zetian Hua

191 The Changes in Physicochemical Properties of Lacquer Wax by Physical Adsorption and UV Light 1777
Yuan-Feng He, Cheng-Zhang Wang, Yan-he Dong, Jian-Zhong Ye, Hao Zhou and Hong-Xia Cheng

192 The Effect of Ethanol on Steroid Δ^1-Dehydrogenase from *Arthrobacter simplex* 1789
Jianmei Luo, Yongxin Cheng, Lina Liu, Jianfeng Wang, Yu Zheng, Yanbing Shen and Min Wang

193 Rapid Assessment of Cell Viability of *Lactobacillus casei* after Freeze-Drying by Measurement Cell Membrane Using Flow Cytometry and Fluorescence Probes 1799
Lin Wang, Xiaohui Liu and Jinghua Yu

194 Molecular Cloning, Characterization and Expression Analysis of a Gene Encoding Hydroxyphenylpyruvate Reductase Involved in Rosmarinic Acid Biosynthesis Pathway from *Perilla frutescens* 1807
Xiaoling Lu, Lei Hao, Fang Wang and Chen Huang

195 Design, Synthesis, and Biological Evaluation of Nedd4 E3 Ubiquitin Ligase Small Molecule Inhibitors 1821
Xiaoli Fu, Jie Chu, Yuyin Li, Shasha Wang, Jie Zhou, Yujie Dai and Aipo Diao

196 Improvement of Electrotransformation Efficiency by Lysozyme Treatment in *Cronobacter sakazakii* 1829
Xinjun Du, Fei Wang, Yue Ge, Lu Meng and Shuo Wang

197 Multiplex Plasmid Engineering (MPE) for Fine Tuning the Expression Level of Red Fluorescent Protein 1837
Qun Gu, Yifan Li, Zhenquan Lin, Tao Chen, Xueming Zhao and Zhiwen Wang

198 Study on the Influencing Conditions in the Electro-Transformation Efficiency of *Bacillus licheniformis* ATCC14580 1845
Yihan Liu, Yanjing Xu, Shuai Fan, Jiaxin Bo, Jianling Wang and Fuping Lu

199 Determination of Folic Acid in Serum by SPE and High Performance Liquid Chromatography with Photochemical Spectrofluorimetry 1855
Caiju Zhou, Haijie Hu and Tong-Cun Zhang

200 Design and Synthesis of 2-Arylbenzothiazole Analogues as Novel SIRT1 Activators 1863
Shaolong Jia, Fei Hu, Yinghao Gao, Qiuyue Wang, Yingying Wang and Erbing Hua

201 UV-B Irradiation Regulates Apoptosis in Yeast 1869
Kun Chen, Nailong Liang, Jing Yang and Hua Zhao

Part V
Biotechnology Applications

Chapter 137
Molecular Cloning and Expression of the β-Galactosidase Gene from *Bifidobacterium longum* LL04 in *Escherichia coli*

Fanzhu Li, Xian Zhang and Seongil Lim

Abstract A *Bifidobacterium* strain with β-galactosidase (β-gal) activity was isolated from infant feces on transgalactooligosaccharide (tGOS) propionate plates and de Man, Rogosa, and Sharpe (MRS) plates containing 5-bromo-4-chloro-3-indolyl-β-D-galacto-pyranoside (X-gal). The strain was identified as a *Bifidobacterium longum* and was named *B. longum* LL04. The gene encoding the β-galactosidase enzyme *β-gal* from *B. longum* LL04 was revealed by nucleotide sequence analysis as a 3.2-kb DNA fragment. *B. longum β-gal* (3,069 bp) is a 1,023-amino acid-long polypeptide with a predicted molecular mass of 114.5 kDa. The amino acid sequence of β-gal was homologous to those found in the LacZ families. The acid-base, nucleophilic, and substrate-recognition sites conserved in the LacZ family were found in β-gal. The coding region of the β-gal gene was then cloned downstream of a T7 promoter for overexpression in *Escherichia coli*.

Keywords *Bifidobacterium longum* LL44 · β-galactosidase gene · Cloning · *Escherichia coli* · Expression

137.1 Introduction

Bifidobacterium species comprise immobile, gram-positive, anaerobic bacteria that were first isolated by Tissier from the feces of breast-fed infants in 1989 [1]. They were once considered to belong to other genera such as *Bacillus* or *Lactobacillus*

F. Li · X. Zhang
Department of Food Science and Technology, Agricultural College of Yanbian University, Yanji 133002, People's Republic of China

F. Li · S. Lim (✉)
Fermentation and Functionality Research Group, Korea Food Research Institute, Seongnam 463-746, R. Korea
e-mail: silim@kfri.re.kr

T.-C. Zhang et al. (eds.), *Proceedings of the 2012 International Conference on Applied Biotechnology (ICAB 2012)*, Lecture Notes in Electrical Engineering 251,
DOI: 10.1007/978-3-642-37925-3_137,

because of their morphological and physiological similarities. However, the enzymatic characteristics and molecular genetics of this species are distinct enough to exclude them from other genera [2, 3]. Currently, a total of 32 species are included in this genus [4]. The application of bifidobacteria to food products started in Japan in the 1980s, and has become popular worldwide in recent years. Bifidobacteria constitute one of the major classes of organisms in the intestines of healthy humans, and are helpful in maintaining normal intestinal flora [5]. The reduction or disappearance of bifidobacteria in the intestine often coincides with poor health status. To maintain high counts of bifidobacteria and protect the intestinal tract from the proliferation of harmful bacteria, live bifidobacteria, or certain selective compounds defined as "prebiotics" [6] have been used as dietary supplements. For instance, prebiotics such as galactooligosaccharides (GaOS), when administered orally, increased the bifidobacterial counts in the human fecal flora [7]. *Bifidobacterium longum* is one of the species frequently used in *Bifidobacterium*-containing probiotic products. There is increasing interest in exploiting the enzymatic characteristics of *B. longum*. β-galactosidase, one of the hydrolytic enzymes expressed by *Bifidobacterium*, is also produced by eukaryotes and several other bacteria, where it is involved in the digestion of transgalactooligosaccharides (tGOS) [8]. Several studies have been published concerning the isolation and characterization of plasmids from bifidobacteria [9, 10] and construction of vectors using *Bifidobacterium* plasmids [11, 12].

The β-galactosidase (β-galactoside galactosylation; EC 3.2.1.23) not only was used in the food industry more and more extensively, but also played an important role in the other fields, such as genetic engineering, enzyme engineering and protein engineering. Recently it was also used in the medicine field extensively [13]. However, its transgalactosylation activity, which yields GaOS, has been less studied than the hydrolytic reaction. GaOS synthesized via β-galactosidases promotes the growth of bifidobacteria [14] and intestinal bacteria, which play important roles in maintaining human health [15, 16]. This has prompted interest in studying other β-galactosidases. In this report, the molecular cloning and expression of the β-galactosidase gene from *B. longum* LL04 in *Escherichia coli* are discussed.

137.2 Materials and Methods

137.2.1 Bacterial Strains, Plasmid, and Growth Conditions

Two strains of *E. coli*, DH5α and ER2566, were used as host strains (NEB Inc., MA, USA). A *Bifidobacterium* strain with β-galactosidase (β-gal) activity was isolated from infant feces on transgalactooligosaccharide (tGOS) propionate agar and de Man, Rogosa, and Sharpe (MRS) (Difco, Detroit, MI, USA) agar containing 5-bromo-4-chloro- 3-indolyl-β-D-galactopyranoside (X-gal; Sigma, St.

Louis, MO, USA) [4]. The strain was identified as *B. longum* and was named *B. longum* LL04. Genomic cloning was performed using the pBR322 plasmid (Life Technologies, Carlsbad, CA, USA). *E. coli* cells were propagated at 37 °C in Luria–Bertani (LB) broth (Difco, Detroit, MI, USA) with vigorous shaking or on LB medium solidified with 1.5 % agar. When appropriate, ampicillin (200 g/mL), and kanamycin (40 g/mL) were added.

137.2.2 Chemicals and Enzymes

All restriction enzymes, T7 DNA ligase, X-gal, and agarose were purchased from Boehringer Mannheim or Life Technologies, while o-nitrophenyl-β-D-galactopyranose (ONPG) and 4-o-methyl-umbelliferyl-β-D-galactoside (4MeUmG) were purchased from Sigma.

137.2.3 Enzyme and Protein Assays

β-Gal activity was measured by incubating enzymes with 10 mM ONPG in 50 mM sodium phosphate buffer (pH 7.5) at 37 °C for 10 min, and the reaction was stopped by adding 1.0 M sodium carbonate. The released o-nitrophenol was quantified by measuring the A420 nm of the reaction solution. One unit of activity was defined as the amount of enzyme liberating 1 mol of o-nitrophenol per minute [17]. Specific activity was defined as units per milligram of protein. The protein concentration was determined by the Bradford method [18] using bovine serum albumin as a standard.

137.2.4 Gel Electrophoresis and ß-gal Activity Staining

Proteins were analyzed by polyacrylamide gel electrophoresis (PAGE) by using 10 % (w/v) polyacrylamide gels and stained with Coomassie blue. For β-gal activity determination [19], the crude cell lysates were loaded and electrophoresed on a nondenaturing PAGE system. β-Gal activity was then detected by incubating the gel in a 4-o-methylumbelliferyl-β-D-galactoside (4MeUmG; Sigma, St. Louis, MO, USA) solution (0.2 mg/mL in phosphate buffer, pH 7.0) for 30 min. Fluorescent bands were visualized under UV light on a transilluminator.

137.2.5 DNA Isolation, Manipulation, and Transformation

Bifidobacterium genomic DNA was isolated with Lim's method [17]. DNA was precipitated by isopropanol, washed with 70 % ethanol, and dissolved in TE buffer (10 mM Tris-1 mM EDTA [pH 8]). Small-scale *E. coli* plasmid preparations were prepared with the QIAprep Spin Miniprep kit (Qiagen, Valencia, CA, USA). All DNA manipulations in this study were performed according to standard procedures. T4 DNA ligase and other DNA-modifying enzymes were purchased from New England Biolabs, Inc., Life Technologies, or Amersham Pharmacia Biotech, Inc., and were used according to the manufacturers' specifications. Electroporation was performed with a Gene-Pulser II electroporation apparatus (Bio-Rad) according to the manufacturer's specifications.

137.2.6 16S rRNA Sequence Analysis for Identification of Bifidobacterium with β-gal Activity

The PCR was performed with lm26 (Forward, 5′-GATTCTGGCTCA GGATGAACG-3′) and lm3 (Reverse, 5′-CGGGTGCTICCCCACTTTCATG-3′) as probes for *Bifidobacterium*-specific 16S rRNA [4] and chromosomal DNA from *Bifidobacterium* LL04 with β-galactosidase activity as a template. The PCR product was then ligated to pDrive (pD16S). Primers targeting the pDrive T7 and SP6 promoters were then used to sequence the cloned PCR product.

137.2.7 Construction and Screening of the B. longum β-gal Genomic Library

The isolated chromosomal DNA from *B. longum* LL04 was partially digested with the restriction enzyme *Eco*RI and analyzed by DNA electrophoresis. DNA fragments ranging from 2.0 to 12.0 kb were isolated using a QIA quick gel extraction kit (Qiagen, Valencia, CA, USA), and then ligated to the pBR322 vector that had been digested with *Eco*RI and dephosphorylated. The ligation mixture was transformed into *E. coli* DH5α-competent cells to create a plasmid library. For the detection of β-gal activity of the transformed *E. coli*, X-gal plates were prepared using LB medium supplemented with X-gal at 40 μg/mL.

137.2.8 Subcloning and Sequencing

Restriction maps of pBRgal are shown in Fig. 137.1. The two subclones, namely, pBRgal38 and pBRgal27, were constructed by deleting the fragment from the right end to the *Bam*HI site of pBRgal and by deleting the fragment from the left end to the *Bam*HI site of pBRgal, respectively. A 2.7-kb fragment of pBRgal27 was subcloned into pDrive for nucleotide sequence determination; the latter was performed by the dideoxy chain termination method [20] using the Sequenase cycle sequencing kit (US Biochemical, Cleveland, OH, USA). T7 and SP6 primers were used as sequencing primers.

137.2.9 Polymerase Chain Reaction

Polymerase Chain Reaction (PCR) were performed with Lim's method [17]. PCR products were analyzed by electrophoresis in 0.8 % agarose gels containing ethidium bromide (1 μg/mL) and purified with the QIAquick PCR purification kit (Qiagen, Valencia, CA, USA).

137.2.10 DNA Sequencing and Sequence Analysis

The nucleotide sequences were determined by fluorescent-labeled dye terminator reactions with an Applied Biosystems 373 stretch automated sequencer. DNA sequence assembly and analysis were performed with DNASIS for Windows (Hitachi Software Engineering America Ltd. MiraiBio Group).

137.2.11 Overexpression Vector Construction

The gene encoding β-gal from *B. longum* LL04 was cloned into pET36(+) (Novagen, Madison, WI, USA) by PCR using pBRgal (pBR322 with a 6.5-kb

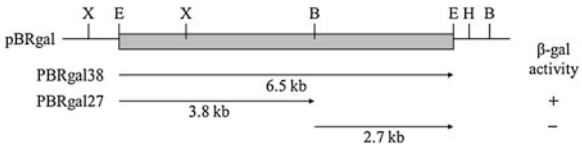

Fig. 137.1 Restriction enzyme maps of pBRgal and their derivatives. X, E, B, and H designate restriction enzymes sites for *Xmn*I, *Eco*RI, *Bam*HI, and *Hin*dIII

*Eco*RI–*Eco*RI insert from *B. longum* LL04 chromosomal DNA) as the template. To create the overexpression plasmid pBGal36b, the *β*-gal gene was amplified with the primers *β*-gal-F and *β*-gal-R (5′-AGC ATA TGA CAG ACG TCA CAC ATG TCG-3′ and 5′-ATA AGC TTC AGA TCA GCT CGA GGT C-3′, respectively). An *Nde*I site was designed in primer *β*-gal-F and a *Hin*dIII site was created in primer *β*-gal-R to include the start codon sequence and the stop codon (TGA) sequence, respectively. Cloning into the *Nde*I-*Hind*III sites of pET36b(+) resulted in the translational fusion of the *β*-gal gene (3 kb of PCR product) to the T7 promoter and *E. coli* ribosome-binding site of the plasmid. Plasmid pBGal36b was created in *E. coli* DH5α and transformed into *E. coli* ER2566 (*F- l- fhuA2 [lon] ompT lacZ::T7 genel gal sulA11D (mcrC-mrr)114::IS10R (mcr-73::mini Tn10-Tet^s)2 R(zgb-210::Tn10-Tet^s) endA1 [dcm]*, New England BioLabs Inc., Ontario, Canada) for the overexpression studies.

137.3 Results and Discussion

137.3.1 Identification of Bifidobacterium with β-galactosidase Activity

Bifidobacteria were isolated from infant feces on tGOS propionate agar. The colony of an isolate, designated LL04, turned dark blue in color on MRS agar containing X-gal, indicating the presence of *β*-gal activity. The 16S rRNA sequence of isolated *Bifidobacterium* sp. LL04. When the sequence of the PCR fragment was compared with other genes in the data library, the sequence showed 99 % homology with 16S rRNA genes of *B. longum* strains (Accession No. AE014295, AY850359, AY735403, AY675246, and AY151399). *Bifidobacterium* LL04 was, therefore, designated *B. longum* LL04.

137.3.2 Cloning and Sequence Analysis of the β-gal Gene from B. longum LL04

To identify the gene(s) encoding *β*-gal activity in *B. longum* LL04, an *Eco*RI-digested genomic library was created in pBR322 and screened in *E. coli* DH5α cells. One positive clone was identified by the formation of a blue colony on the selective medium (LBX-gal) supplemented with 200 μg/mL ampicillin and was designated as pBRgal. Preliminary restriction enzyme analysis revealed that pBRgal contained a 6.5-kb-long insert. With the *Bam*HI site of the insert in pBRgal, two subclones, pBRgal38 (*Eco*RI-*Bam*HI fragment, 5.5-kb-long insert) and pBRgal27 (*Bam*HI-*Eco*RI fragment, 2.7-kb-long insert), were constructed with pBR322 as the vector (Fig. 137.1). For confirmation of *β*-gal activity, the two

plasmids were retransformed into *E. coli* DH5α. However, all the transformants showed no colored colonies on the X-gal and ampicillin agar plates. A comparison of the partial nucleotide (966-bp-long) sequence of the 2.7-kb-long insert to the database by BLAST analysis revealed highest similarities to the LacZ of *B. longum* NCC2705 [963/966(99 %) identity (GenBank Accession No. AE014295)]. Significant similarities were also found to the β-gal genes of several *Bifidobacterium* strains [959/966 (99 %) and 949/966 (98 %) identity] (GenBank Accession Nos. AJ242596 and AF192265). In case of the partial nucleotide sequence, the nucleotide sequence of β-gal in pBRgal was analyzed (Fig. 137.2). The coding region of β-gal (3,072-bp-long) started with ATG at nucleotide 168 and ended with TGA at nucleotide 3,240. The putative ribosome-binding sequence (RBS) AGAAAG (Fig. 137.2) was found nine bases upstream of the β-gal translation start site (ATG). The β-gal gene was almost identical to the complete genome of *B. longum* NCC2705 [(AE014295, 99 % identity (3057/3072)], and β-galactosidase I gene, complete cds of *B. infantis* strain HL96 [(AE014295, 99 % identity (3057/3072)]. The β-gal gene of *B. longum* LL04 encodes a protein containing 1,023 amino acids. The deduced protein had a theoretical molecular mass of 1,14,542 Da and a pI of 4.86. The alignments of the deduced amino acid sequences of β-gal with other homologous β-galactosidases are summarized in Table 137.1. β-Gal featured some sequence homology with β-galactosidases from various microorganisms, including LacZ. Comparison of the amino acid sequence of the β-gal gene from LL04 with that from AE014295 from the database by BLAST analysis showed six different amino acids (0.6 %). Comparison of the β-gal from LL04 and β-gal I from *B. infantis* strain HL96 revealed a homology of 97 %. A difference of only 29 amino acids was found.

The high similarity between β-galactosidase from *B. longum* and *B. infantis* is not surprising. Immunological and DNA–DNA hybridization approaches have demonstrated that *B. longum* and *B. infantis* have a close phylogenetic relationship [21]. Significant similarities were also found to the β-galactosidase of several *Lactobacillus* strains (40–44 % identity) (GenBank Accession Nos. M55068, AY616518, and X82287), as well as to β-gal enzymes of *Streptococcus* strains (44–45 %) (GenBank Accession Nos. CP000024, AF389474, and AY460089), *Bacillus* strain (44 %) (GenBank Accession Nos. CAA04267 and BA000004), *Thermotoga* strain (33 %) (GenBank Accession No. NC000853), *Arthrobacter* strain (31 %) (GenBank Accession No. AJ457162), and *Lactococcus* strain (30 %) (GenBank Accession No U60828) (Table 137.1).

Three regions of the *E. coli* LacZ, two flanking a glutamate residue at the amino acid positions 461 and 537, respectively, and one flanking a glycine residue at the position 794, were reported to be the acid-base, nucleophilic, and substrate-recognition sites [22–24]. These three regions are well conserved in almost all β-galactosidases of the LacZ family. Similarly, these three conserved regions were revealed in the β-gal from *B. longum* LL04, with two glutamates located at the residues 469 and 536 and a glycine located at the residue 793 (Fig. 137.3).

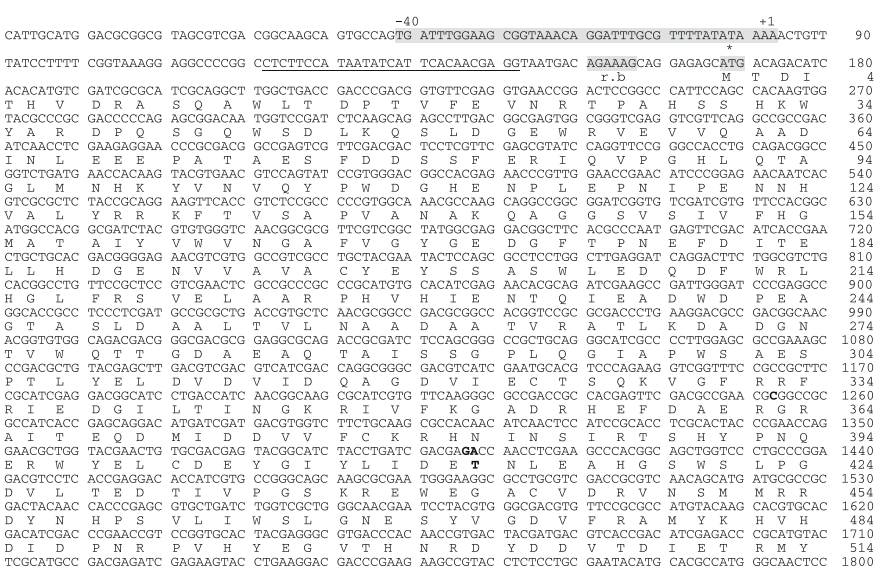

Fig. 137.2 Nucleotide sequence of *β*-gal gene in pBRgal. The coding region of *β*-gal starts from base 168, ends at base 3240. The deduced amino acid sequence is shown by capital letters below the nucleotide sequence. The predicted ribosome-binding sites(r.b) for *β*-gal and permease are underlined. Possible +1 to −40 sequences for *β*-gal and permease gene is highlighted

137.3.3 Overexpression of the B. longum β-gal Gene in E. coli

To further investigate the *β*-galactosidase gene product, we made use of the T7 RNA polymerase expression system for the overexpression of the *B. longum β*-gal gene in *E. coli*. The coding region of *β*-gal was cloned into pET36b, under the

Table 137.1 A comparison between *B. longum* β-gal and other β-galactosidases

Enzyme source	No. of aa[a]	Similarity (%)	Identity (%)	Reference
Bifidobacterium longum LL04	1023	100	100	This study
Bifidobacterium longum NCC2705	1023	99	99	33
Bifidobacterium infantis	1022	97	96	34
Streptococcus thermophilus	1026	62	44	35
Lactobacillus bulgaricus	1007	62	44	36
Escherichia coli LacZ	1060	45	30	37
Bacillus megaterium	1034	55	40	38
Bacillus halodurans	1014	56	40	39
Thermotoga maritima	1087	50	33	40
Lactococcus lactis	1045	46	30	41
Arthrobacter spp.	1056	45	31	42

[a] aa amino acid

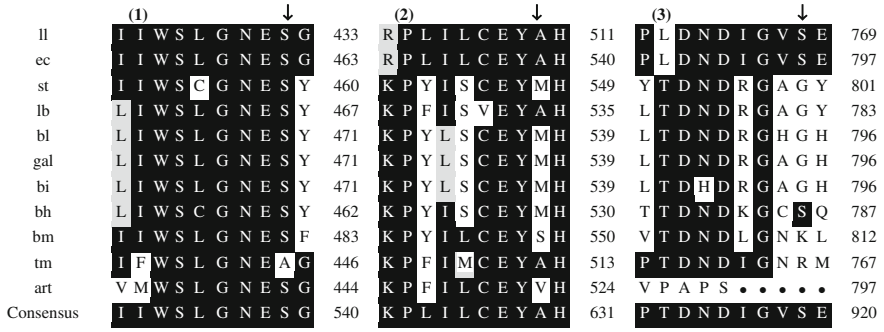

Fig. 137.3 Multiple alignment of the possible acid-base, nucleophilic, and substrate-recognition sites of β-gal and of 11 listed β-galactosidases. Abbreviations; ll, *Lactococcus lactis*; ec, *E. coli* LacZ; st, *Streptococcus thermophilus*; lb, *Lactobacillus bulgaricus*; bl, *Bifidobacterium longum* NCC2705; gal, *Bifidobacterium longum* LL04 β-Gal; bi, *Bifidobacterium infantis*; bh, *Bacillus halodurans*; bm, *Bacillus megaterium*; tm, *Thermotoga maritima*; art, *Arthrobacter* spp. Conserved amino acids are highlighted. *Down arrow*, amino acids proposed to be the key residues in the active sites. Multiple alignment was done using the PrettyBox program of the genetics computer group

control of a T7 promoter. Gene expression in *E. coli* was induced by IPTG and analyzed by assaying ONPG hydrolysis activity and by SDS-PAGE and nondenaturing PAGE. After the addition of IPTG, a dramatic increase in β-gal enzyme activity was seen at 3 h (Fig. 137.4). The effect of IPTG on the growth curve of ER2566 (pBgal36b) was observed by measuring the density at 595 nm every hour during the induction period, using the growth curve of ER2566 (pBgal36b) without IPTG induction as reference. The growth of ER2566 (pBgal36b) was found to be inhibited by IPTG (Fig. 137.5). A protein with an apparent molecular mass of approximately 115 kDa was overproduced from pBgal36b (Fig. 137.5), in close

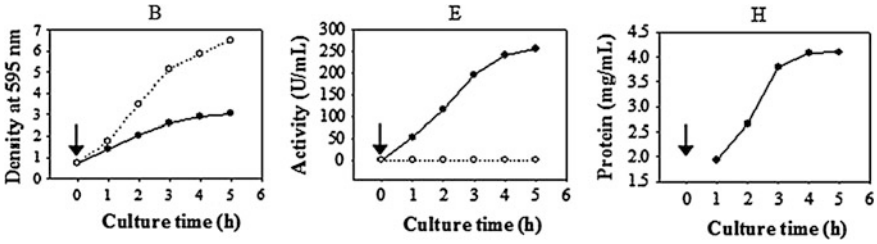

Fig. 137.4 Effect of IPTG on cell growth **a**, β-galactosidase activity (U/mL) **b**, and protein concentration (mg/mL) **c** of ER2566 (pBgal36b). The *down arrow* indicates the culture time for adding IPTG. Black circles, +IPTG; open circles, −IPTG

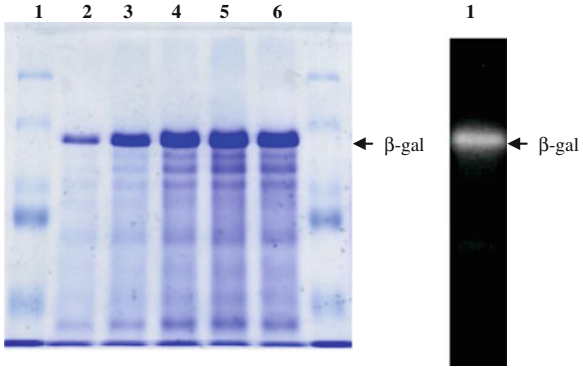

Fig. 137.5 SDS-PAGE and β-gal activity staining using nondenaturing PAGE analysis of the *B. longum* β-gal gene overexpressed in *E. coli* ER2566 containing pBgal36b induced by 1 mM IPTG. **a** SDS-PAGE. Lane 1, marker protein (molecular masses are indicated); lanes 2, 3, 4, 5, and 6, induction for 1, 2, 3, 4, and 5 h, respectively. *Arrow* indicates overexpressed β-gal. **b** Activity staining on a nondenaturing polyacrylamide gel. Lane 1, soluble fraction of IPTG-induced *E. coli* ER2566 containing pBgal36b obtained after sonication

agreement with the predicted molecular weight of the *B. longum* LL04 β-gal gene. Active staining of the nondenaturing PAGE with 4MeUmG confirmed the presence of β-gal.

137.4 Conclusion

A β-galactosidase gene (LLGal) from *Bifidobacterium longum* LL04 was cloned and expressed at high levels in *Escherichia coli*. The β-galactosidase belongs to the LacZ family and shares high degree of sequence similarity with other lactobacillus β-galactosidases. The purified LLGal displayed optimum activity at acidic pH and remained stable over a broad pH range [17]. Results of this project will provide a solid base for farther study and application in the future.

References

1. Bezkorovainy A, Miller-Catchpole R (1989) Classification of bifidobacteria. Biochemistry and physiology of bifidobacteria, pp 2–28
2. De Vries W, Stouthamer AH (1967) Pathway of glucose fermentation in relation to the taxonomy of *bifidobacteria*. J Bacteriol 93:574–576
3. Sebald M, Gasser F, Werner H (1965) DNA base composition and classification. application to group of *bifidobacteria* and related genera. Ann Inst Pasteur 109:251–269
4. Kaufmann P, Pfefferkorn A, Teber M et al (1997) Identification and quantification of *bifidobacterium* species isolated from food with genus-specific 16S rRNA targeted probes by colony hybridization and PCR. Appl Environ Microbiol 63:1268–1273
5. Mitsuoka T (1990) *Bifidobacteria* and their role in human health. J Ind Microbiol 6:263–268
6. Gibson GR, Roberfroid MB (1995) Dietary modulation of the human colonic *microbiota*: Introducing the concept of prebiotics. J Nutr 125:1401–1412
7. Anne MB (2012) Galactooligosaccharides, Next generation prebiotics. Dietary fiber and health 25:359–368
8. Gibson GR, Rabiu B, Rycroft CE et al (2004) Trans-Galactooligosaccharides as prebiotics. Handbook of functional dairy products, pp 91–108
9. Yongseo P, Kihwan K, Juhui P et al (2008) Isolation and molecular characterization of a cryptic plasmide from *Bifidovacterium longum*. Biotechnol Lett 30:145–151
10. Juhoon L, Deniel JO (2006) Sequence analysis of two cryptic plasmids from *Bifidobacterium longum* DJO10A and construction of a shuttle cloning vector. Appl Environ Microbiol 72:527–535
11. Klijn A, Moine D, Delley M et al (2006) Construction of a reporter vector for the analysis of *Bifidobacterium longum* promoters. Appl Environ Microbiol 72:7401–7405
12. Simone G, Matti K, Diego M et al (2007) Molecular characterization of *Bifidobacterium longum* Biovar *longum* NAL8 plasmids and construction of a novel replicon screening system. Appl Microbiol Biotechnol 74:1053–1061
13. Li Z, Qingzhang L, Lei T (2009) Research advancement of β-galactosidase. J Northeast Agric Univ 40:128–131
14. Jorgensen F, Hansen OC, Srougaard P (2001) High-deiciency of oligosaccharides with a truncated β-galactosidase from *Bifidobacterium bifidum*. Appl Microbiol Biotechnol 57:647–652
15. Robert AR, Glenn RG, Harsharnjit SG et al (2005) Modulation of the microbial ecology of the human colon by probiotics, Prebiotics and synbiotics to enhance human health: An overview of enabling science and potential applications. FEMS Microbiol Ecol 52:145–152
16. Tanaka R, Takayama H, Morotomi M et al (1985) Effects of administration of TOS and *Bifidobacterium breve* 4006 on the human fecal flora. Bifidobact Microflora 2:17–24
17. Seongil L, Geunbae K, Sunghun Y et al (2006) Characteristics of a *Bifidobacterium longum* LL04 β-Galactosidase(recombinant) produced in *Escherichia coli*. Food Sci Biotechnol 15:908–913
18. Bradford MM (1970) A rapid and sensitive method for the quantitation of microgram quantities of protein utilizing the principle of protein-dye binding. Anal Biochem 72:248–254
19. Laemmli UK (1970) Cleavage of structural proteins during the assembly of the head of bacteriophage T4. Nature (London) 227:680–685
20. Sanger F, Nicklen S, Coulson AR (1977) DNA sequencing with chain-determinating inhibitors. Proc Natl Acad Sci USA 74:5463–5467
21. Shinji S, Maki K, Mitsuo S et al (2002) Unification of *Bifidobacterium infantis* and *Bifidobacterium suis* as *Bifidobacterium longum*. Int J Syst Evol Microbiol 52:1945–1951
22. Douglas HJ, Tom H, Andrea V et al (2001) A structural view of the action *of Escherichia coli*(lacZ) β-Galactosidase. Biochemistry 40:14781–14794

23. Gebler JC, Aebersold R, Withers SG (1992) Glu-537, Not Glu-461, is the nucleophile in the active site of (lacZ) β-galactosidase from *Escherichia coli*. J Biol Chem 267:11126–11130
24. Martinez-Bilbao M, Holdsworth RE, Edwards LA et al (1991) A highly reactive beta-galactosidase (*Escherichia coli*) resulting from a substitution of an aspartic acid for Gly-794. J Biol Chem 266:4979–4986

Chapter 138
Identification of Symbiotic or Epiphyte Microbe F17 from *Pinctada Fucata* and Analysis of Its Main Metabolites by GC–MS

Yanyan Wu, Yan Zhang, Laihao Li, Xianqing Yang, Wei Shi and Zhengyi Shao

Abstract The strain F17 which had broad antibacterial spectrum and strong antibacterial activity was isolated from *Pinctada fucata* sample collected from Sanya, China. This strain was finally identified as *Bacillus flexus* based on morphological, biochemical characteristics, and 16S rRNA sequence. Antifungal spectrum was confirmed by oxford piate assay system and showed that F17 had significant inhibitory effect against *Escherichia coli, Bacillus subtilis, Staphylococcus aureus, Listeria monocytogenes, Pseudomoas aerunginosa, Salmonella typhimurium, Vibrio parahaemolyticus, Shigella dysenteriae*, etc. The volatilis components of the extracellular metabolites of F17 were analyzed by GC–MS. The results showed that the main chemical compositions were 2-Methyl butyric acid, Dioctyl phthalate, 2,3-Butanediol, 4-Chloro-2-nitrobenzyl alcohol, and Glycyl-L-proline in the fermentation fluid extracted by ethyl acetate. In those, 2-Methyl butyric acid and 2,3-Butanediol can be used in food flavor; 4-Chloro-2-nitrobenzyl alcohol has certain development potential for antiseptic. Glycyl-L-proline is an

Y. Wu (✉) · Y. Zhang · L. Li · X. Yang
South China Sea Fisheries Research Institute, Chinese Academy of Fishery Sciences, Guangzhou 510300, People's Republic of China
e-mail: wuyygd@163.com

Y. Wu · Y. Zhang · L. Li · X. Yang
National R&D Center For Aquatic Product Processing, Guangzhou 510300, People's Republic of China

Y. Wu · Y. Zhang · L. Li · X. Yang
Key Lab of Aquatic Product Processing, Ministry of Agriculture, Guangzhou 510300, People's Republic of China

Y. Zhang · Z. Shao
College of Food Science and Technology, Shanghai Ocean University, Shanghai 201306, People's Republic of China

W. Shi
Guangdong Huankai Microbial Science and Technology Co., Ltd, Guangzhou 510663, People's Republic of China

T.-C. Zhang et al. (eds.), *Proceedings of the 2012 International Conference on Applied Biotechnology (ICAB 2012)*, Lecture Notes in Electrical Engineering 251,
DOI: 10.1007/978-3-642-37925-3_138,

important raw material in pharmaceutical and nutrient food industry. The experiments showed the metabolites of F17 had great potential as food additives.

Keywords *Bacillus flexus* · Identification · GC–MS · Extracellular metabolites

138.1 Introduction

Symbiotic or epiphyte microorganisms mean the microorganisms which attach to surfaces or live in the body of hosts, with relationship of mutual benefit or benefit by oneself existing among them [1]. *Pinctada. fucata* is one of the important economic seashell in south of China [2–4]. Many researches indicated that marine symbiotic or epiphyte microorganisms can produce active compounds similar or identical to the hosts. In 1994, Oclarit reported [5] that a strain obtained from the sponge homogenate, can produce an antimicrobial peptide. Incidentally, this antimicrobial peptide was ever found in sponge extract. Further investigations found similar evidences in other marine invertebrate [6, 7]. In this paper, we present the strain F17 to the identification. Main metabolites analyzed by GC–MS were also presented. All above researches aimed to provide scientific basis for application in food, medical, and forage industries.

138.2 Materials and Methods

138.2.1 Strains and Culture Media

The strain F17 was isolated from the mucous substance of *P. fucata* collected from Lingshui sea waters in Sanya, China.*E. coli*, *B. subtilis*, *S. aureus*, L. monocytogenes, *P. aerunginosa*, *S. typhimurium*, *V. parahaemolyticus*, *S. dysenteriae* were used as indicator bacteria for inhibitory effect. The strain F17 and all indicator bacteria were stored at −20 °C in the water containing 20 % of glycerol [8–10]. We should subculture twice before using in the manipulations. Nutrient agar and Zobell 2216E agar were used for culturing indicator bacteria and strain F17, respectively.

138.2.2 Preparation of Culture Supernatant

The strain F17 was incubated aerobically in 150 mL erlenmeyer flask containing 50 mL of seed medium (Zobell 2216E broth) on rotary shaker (250 rpm) at 28 °C for 24 h. Then, this seed culture (15 % v/v) was transferred to 1 L production

medium consisting of 2 % glucose, 0.1 % yeast extract, 0.5 % tryptone, 0.05 % K_2HPO_4, and 0.05 % $MgSO_4 \cdot 7H_2O$ with pH 7.2 ~ 7.4, and incubated on an orbital shaker at 150 rpm (72 h, 28 °C). Cells were harvested by centrifugation at 12,000×*g* for 20 min. The obtained culture supernatant was filtered through 0.22 μm membranes and stored at −4 °C.

138.2.3 Antimicrobial Activity

Eight different indicator bacteria were used to measure antimicrobial activity of the culture supernatant by agar diffusion assay [11]. First, various indicator bacteria were diluted their cell densities to approximately 10^8 CFU/mL [12]; Second, 1 mL of corresponding indicator bacteria were added into 100 mL of nutrient agar at 50 °C, respectively; Third, Petri dishes with 20 mL of nutrient agar consisting corresponding indicator bacteria were prepared. Once solidified, four wells (+7.8 mm) were made and filled with 100 μL culture supernatant in the wells, then diffuse 2 h at 4 °C. Finally, the inoculated plates were incubated for 24 h at 37 °C. The diameter of inhibition zone was measured with vernier caliper.

138.2.4 Taxonomic Studies of the Strain F17

138.2.4.1 Taxonomic Studies of the Strain F17

The strain F17 was morphologically and biochemical characterized by the method described in Simbert's paper [12].

138.2.4.2 Molecule Biology Identification

The extraction of genomic DNA was performed according to the method as described by Cui [13]. The 16S rRNA gene was amplified with primers Eubac27 (5′-3′: AGAGTTTGATCMTGGCTCAG) and Eubac1492R (5′-3′:GGTTACCTTGTTACGACTT) [14, 15]. Each 60 μL PCR reaction mixture contained 0.2 μL of MightyAmp DNA Polymerase (1.25 U/μL), 30 μL of 2×MightyAmp Buffer Ver.2 (4) mM Mg+, 800 μM dNTP, 1.5 μL of each primer (100 ng/μL), and 2 μL template DNA (10.0 ng/μL). The reaction was then heated to 96 °C for 32 min, followed by 40 cycles of denaturation at 96 °C for 10 s, annealing at 55 °C for 15 s, and extension at 68 °C for 90 s. A final extension stage of the PCR was carried out at 75 °C for 4 min. The amplified DNA fragment was separated on 1 % agarose gel, and observed the purpose fragments under the ultraviolet lamp. If the amplified DNA fragment amplified was successfull, then sequences it by the BigDye terminator kit ABI310 Genetic Analyzer. Phylogenetic

analysis was performed using the software package MEGA version 4.0, after multiple alignments of data by CLUSTAL_X. The phylogenetic tree was reconstructed using the neighbor-joining method [16].

138.2.5 GC–MS Analysis of the Metabolites

The supernatant was extracted with ethyl acetate [17, 18]. 40 mL of ethyl acetate was added into 100 mL of culture supernatant sample (extraction for 30 min) for three times. The extract liquor will be concentrated to 5 mL on a revolving evaporator at 40 °C. Use the same way to blank liquids fermentation for extraction, named it as blank for the solution control. 2 μL of the derivative samples were injected into GC–MS, respectively. A D25 fused silica capillary column (30 m × 0.25 mm × 0.25 μm) was used for the separation with high pure helium carrier gas at flow rate of 1.0 mL min^{-1}. The GC oven was initially set at 40 °C for 10 min, increased to 250 °C at a rate of 10 °C min^{-1}, and then kept at 250 °C. Splitless mode injection was used. MS detection was conducted with EI mode with electron energy of 70 eV and full scan mode with m/z of 20–500 u.

138.3 Results and Analysis

138.3.1 Spectrum of Antimicrobial Activity

The result shows that culture supernatant had different effects against various common pathogens in food. Among which, the antibacterial function to *E. coli* was the best and antibacterial circle diameter up to 25.35 ± 0.31 mm. And the *S. typhimurium* was the weakest, but the antibacterial circle diameter still reach to 9.78 ± 0.21 mm. Therefore, culture supernatant had broad antibacterial spectrum, strong antibacterial activity (Table 138.1).

Table 138.1 Antimicrobial spectrum of strain F17 (n = 3, x ± SD)

Indicator microorganisms	Antibacterial circle diameter (mm)
Staphyloccocus aureus	19.87 ± 0.18
Escherichia coli	25.35 ± 0.31
Bacillus subtilis	22.94 ± 0.24
Listeria monocytogenes	12.02 ± 0.14
Pseudomoas aerunginosa	12.34 ± 0.25
Vibrio parahaemolyticus	21.12 ± 0.09
Salmonella typhimurium	9.78 ± 0.21
Shigella dysenteriae	19.10 ± 0.20

Table 138.2 Results of biochemical identification

Tests	Results	Tests	Results
Oxidase	+	Acid production	
Catalase	+	Ribose	+
Citrate assimilation	−	Glucose	+
Nitrate reduction	+	Sucrose	+
Phenylalanine deaminase	−	Maltose	+
V–P	+	Trehalose	+
Indole	+	Galactose	+
H_2S production	−	Fructose	
Growth temperature		Mannitol	+
5 °C	−	Hydrolytic	
30 °C	+	Starch	+
50 °C	−	Gelatin	+
Growth in NaCl		Decrarboxylation of Amino acids	
2 %	+	Lysine	+
5 %	+	Arginine	+
7 %	+	Tyrosine	−

138.3.2 Identification Results of the Strain F17

138.3.2.1 Results of Morphological and Biochemical Identification

Morphological of the strain F17 showed the colony was milky white, not clear, brightness and regular edges, and under the light microscope, a gram-positive bacterium with gemmas, short rod single cell in shape. Biochemical characterizations of the strain were listed in Table 138.2.

138.3.2.2 Sequence Analysis of 16 s rRNA Gene

Primary sequence data of the strain F17 was aligned and phylogenetically classified by CLUSTAL_X program. The phylogenetic tree was constructed by neighbor-joining method with 1,000 replications in bootstrap analysis (Fig. 138.1). The result showed that its sequenced RNA fragment was 1405-bp long, and the 16S rRNA sequence analysis indicated that it belonged to the branch of *B. flexus* IFO 15715^T, with a similarity of 99.929 %. According to the morphological, biochemical characteristics, and sequence analysis of 16S rRNA, the strain F17 was finally identified as *B. flexus*.

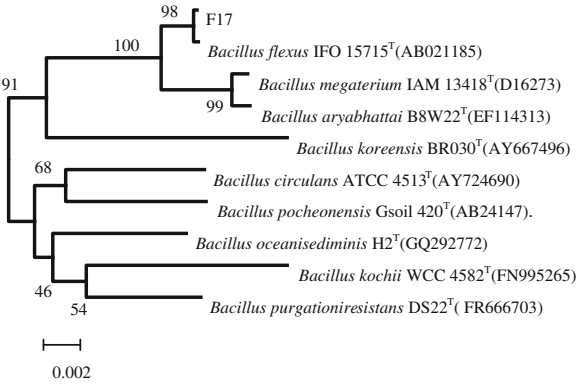

Fig. 138.1 Phylogenetic tree derived from 16S rRNA gene sequence of strain F17

138.3.3 Analysis of Components on Extracellular Metabolites

The ethyl acetate extract was identified by GC–MS, respectively. Figure 138.2 shows that total ion chromatograms on contrast liquid Fig. 138.2a and strain fermented liquid Fig. 138.2b. After searching NIST standard database, and with the help of Agilent GC–MS software, showed 173 components in strain fermented liquid and 169 components in contrast liquid in total.

From Fig. 138.2 and Table 138.3, We found the relative content of some components in contrast liquid were decreased significantly, such as Bis-acrylamide; 1,2-Benzened carboxylic acid bi(2-methylpropyl)ester; 2,4-Bis (1,1-dimethylethyl)-phenol, L-Ascorbic acid 2,6-dihexadecanoate. This demonstrated that

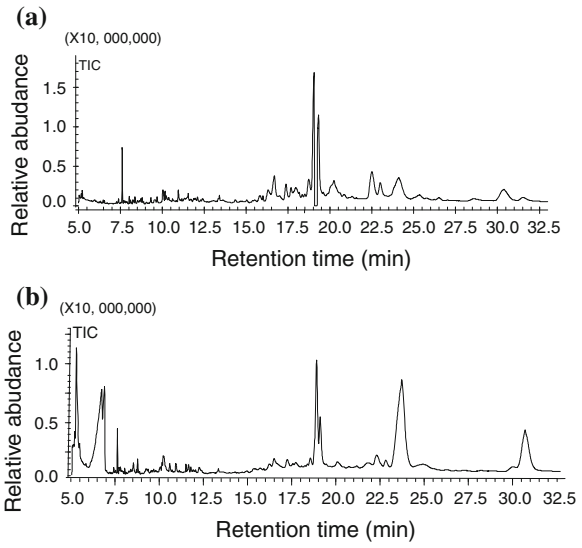

Fig. 138.2 **a** GC–MS total ion chromatograms on contrast liquid **b** GC–MS total ion chromatograms on strain fermented liquid

Table 138.3 Comparison of main constituents and contents between strain F17 and contrast

No.	Retention time/min		Compound	Molecular formula	Relative content/ %		Comparability/ %	
	Strain	Contrast			Strain	Contrast	Strain	Contrast
1.	6.724	6.726	2-Methylbutyric acid	$C_5H_{10}O_2$	13.09	0.09	92	92
2.	6.881	6.884	3-Methylbutanoic acid	$C_5H_{10}O_2$	7.49	0.03	92	92
3.	7.597	7.601	2,2,4,6,6-Pentamethyl-Heptane	$C_{12}H_{26}$	1.06	3.96	96	96
4.	13.439	13.441	Glycyl-L-proline	$C_7H_{12}N_2O_3$	4.02	0.91	92	92
5.	16.608	16.611	1,2-Benzenedicarboxylic acid bis(2-methylpropyl) ester	$C_{16}H_{22}O_4$	1.26	5.63	91	92
6.	18.695	18.698	Bis-acrylamide	$C_7H_{10}N_2O_2$	1.08	7.17	87	88
7.	19.312	19.315	2,4-Bis(1,1-dimethylethyl)-phenol	$C_{15}H_{24}O$	5.13	23.94	89	90
8.	20.355	20.358	[1,2-a]-pyrazine-1,4-dione,hexahydro-3-(2-methylpropyl)-Pyrrolo	$C_{11}H_{18}N_2O_2$	1.02	5.42	90	90
9.	22.508	22.510	L-Ascorbic acid 2,6-dihexadecanoate	$C_{38}H_{68}O_8$	6.54	13.62	90	91
10.	24.011	24.014	Dioctyl phthalate	$C_{24}H_{38}O_4$	31.52	12.1	95	96
11.	5.042	–	Lactic acid	$C_3H_6O_3$	2.45	–	92	–
12.	5.274	–	2,3-Butanediol	$C_4H_{10}O_2$	10.33	–	93	–
13.	10.241	–	Benzeneacetic acid	$C_8H_8O_2$	0.95	–	68	–
14.	30.983	–	4-Chloro-2-nitrobenzyl alcohol	$C_7H_6ClNO_3$	10.97	–	95	–

Note Means that corresponding compound had been not detected

strain F17 was using them during the metabolism. Through comparison, the relative content of four components increased enormously after fermentation which was 2-Methyl butyric acid, 3-Methylbutanoic acid, Glycyl-L-proline, and Dioctyl phthalate, respectively. There were four new components in fermented liquid as the No.11–14 in the Table 138.3, most similar to lactic acid, 2,3-Butanediol, Benzeneacetic acid, and 4-Chloro-2-nitrobenzyl alcohol with the similarity rate 92, 93, 68, 95 %, respectively. It is worthwhile to note that the similarity rate of No.13 component is only 68 %, and most similar to Benzeneacetic acid. So we need further studies to identify this unidentified compound. The main chemical compositions of fermentation fluid extracted by ethyl acetate were 2-Methyl butyric acid, Dioctyl phthalate, 2,3-Butanediol and 4-Chloro-2-nitrobenzyl alcohol, and the relative content were all more than 10 %. According to The National Standard of the People's Republic of China—Food additives using standard GB2760-2011, 2-Methyl butyric acid can be used as allowable essence in food industry. On lower concentrations condition, it has sweet fruit on the smell. Dioctyl phthalate is an important and popular type plasticizer that can be used as food packaging material in food industry. 2,3-Butanediol can be added to liquor in china, which could evidently increase pit flavor in liquor and improve liquor smell flavor, and strengthen liquor harmony. 4-Chloro-2-nitrobenzyl alcohol has antibacterial activity in vitro and dilute form as a disinfectant and antiseptic. Besides, Glycyl-L-proline in fermented liquid had higher relative content comparing with contrast liquid. For the present, Glycyl-L-proline has been widely used in medicine and food industry. In medicine industry, it was the important raw material in aminophenol transfusion and synthesize, it was also an important intermediate during synthesizing an antihypertensive drug. In food industry, it can occur Maillard reaction with sugar, so as to produce flavoring substance, Glycyl-L-proline can be used to synthetic edible essence.

138.4 Conclusion

According to morphological, biochemical characteristics, and sequence analysis of 16S rRNA, the strain F17 was finally identified as *B. flexus*.

Our research first showed that the strain F17 may produce new sources of antimicrobial substances. The main chemical compositions of fermentation fluid can be used as antiseptic and edible essence in food industry (Table 138.3). The fermentation fluid with wide antimicrobial spectrum may be caused by producing 4-Chloro-2-nitrobenzyl alcohol and kinds of organic acid during the process of fermentation. Hitomi also reported [19] *B. flexus*, *B. cereus*, *B. coagulans*, *B. thuringiensis* can ferment organic acid in 1996. The strain F17 may also be a probiotic strain. However, the downside of this research only analyze the volatile of the components, the physiological active substance may be not volatile, so the extracellular metabolites of the stain F17 is worth studying further. In a word, we must conduct toxicology text which should be carried out to estimate biological

security before any kind of active substances of the strain F17 and before application in food, medical, and forage industries.

Acknowledgments This work was financially supported by National Science and Technology Planning Project (2012BAD28B05), Hainan Key Science and Technology Project (ZDXM20100005), Guangdong province Science and Technology Project (2011B031200009).

References

1. George SW, David AR, Sham VN (2011) Antimicrobial activity of surface attached marine bacteria in biofilms. Microbiol Res 166:437–448
2. Tang JW, Zhang FZ, Chen B (2009) Achievement and development trend of genetics and breeding of mariculture varieties in China. J South China Fish Sci 4:77–82
3. Yu DH, Li YN, Wu KC (2005) Analysis on sequence variation of ITS 2 rDNA in *Pinctada fucata* from China, Japan and Australia. J South China Fish Sci 2:1–6
4. Tang J, Liu WG, Lin JS (2011) Evaluation on mid-term growth of 9 families of pearl oyster *pinctada facata*. J South China Fish Sci 5:30–34
5. Oclarit JM, Okada H, Ohta S et al. (1994) Anti-bacillus substance in the marine sponge, Hyatella species, produced by an associated Vibrio species bacterium. Microbios 78:7–16
6. Gill MS, Fenical W (1992) Embryos of *Homarus americanus* are protected by epibiotic bacteria. Biol Bull 182:105–108
7. Fenical W (1993) Chemical studies on marine bacteria: developing a new resource. Chem Rev 5:1673–1683
8. Lee HJ, Joo CS, Park SH et al (1999) Purification and characterization of a bacteriocin produced by *Lactococcus lactis* subsp. lactis H-559 isolated from kimchi. J Biosci Bioeng 88: 153-159
9. Huang X, Lu Z, Bie XM et al (2007) Optimization of inactivation of endospores of *Bacillus cereus* by antimicrobial lipopeptides from *Bacillus subtilis* fmbj strains using a response surface method. Appl Microbiol Biotechnol 74:454–461
10. Olinda CS, Paula VML, Juliana FM et al (2010) Isolation, characterization and phylogeny of sponge-associated bacteria with antimicrobial activities from Brazil. Res Microbiol 161: 604–612
11. Bauer AW, Kirby W, Sherris J (1966) Antibiotic susceptibility testing by a standardized single disc diffusion method. Am Soc Microbiol 45:493–496
12. Simbert RM, Krieg NR (1997) Phenotypic characterization. In: Gerhardt P, Murray RGE, Wood WA, Krieg NR (eds) Methods for general and molecular bacteriology, vol 2. American Society for Microbiology, Washington, pp 607–653
13. Cui XL, Mao P, Zeng M (2001) *Streptimonospora salinagen*. nov., a new member of the family *Nocardiopsaceae*. Int J Syst Evol Microbiol 51:357–363
14. Nakano MM, Marahiel MA, Zuber P (1988) Identification of a genetic locus required for biosynthesis of the lipopeptide antibiotic surfactin in *Bacillus subtilis*. J Bacteriol 170:5662–5668
15. James HJ, Mary JF (1998) Antimicrobial susceptibility testing general principles and contemporary practices. Clin Infect Dis 26:973–980
16. George SW, David AR, Shannon LC (2010) Diversity and antimicrobial activities of surface-attached marine bacteria from Sydney Harbour, Australia. Microbiol Res 165:300–311
17. Alapati K, Peddikotla P, Manchala N (2010) Isolation, characterization and biological evaluation of bioactive metabolites from *Nocardia levis* MK-VL113. Microbiol Res 165:199–210

18. Chun WB, Yanni T, Ben W (2011) Separation and identification of norcantharidin metabolites in vivo by GC-MS method. J Chromatogr 879:1741–1747
19. Hitomi O, Masahito Y (1996) L-Lactic acid production by *Bacillus* sp. in anaerobic and aerobic culture. J Ferment Bioeng 3:272–274

Chapter 139
Construction of Genomic Expression Library Vaccines Against Avian *Pasteurella Multocida* and Detection of the Immune Efficacy

Qiang Gong, Cuili Qin and Ming Cheng

Abstract The random DNA fragments (500–3000 bp), which obtained from genomic of avian *Pasteuella multocida* CVCC474 with restriction enzyme *Sau*3AI were cloned into the *Bam*HIsite of the eukaryotic expression vector pcDNA3.1(+) to construct the genomic expression library. The library was subdivided into five clone pools and the recombinant plasmids were extracted from each group. The Balb/c mice named groups 1–5 were vaccinated with these recombinant plasmids respectively, and the mice injected with pcDNA3.1(+) and PBS were negative control. After immunization the serum antibodies were tested by ELISA. Immunized mice were challenged with virulent of avian *Pasteurella multocida,* the relative protection rate was counted. The results showed the levels of antibodies and the relative protection rate in group one was significantly higher than 1–4 groups ($P < 0.05$) and control groups ($P < 0.01$). The results indicated genomic expression library vaccines provide a promising approach for the prevention of avian pasteurellosis.

Keywords Avian *Pasteurella multocida* · Expression library · Immunization · Vaccine

139.1 Introduction

Avian *Pasteuella multocida* is the etiological agent of avian pasteurellosis (fowl cholera), which is a widely distributed disease of poultry, particularly chickens, turkeys, ducks, and geese in many countries [1]. The high morbidity and mortality associated with fowl cholera result in significant economic losses to the poultry

Q. Gong (✉) · C. Qin · M. Cheng
He Nan university of Science and technology, Luoyang 471023, China
e-mail: qianggong79@yahoo.com.cn

T.-C. Zhang et al. (eds.), *Proceedings of the 2012 International Conference on Applied Biotechnology (ICAB 2012)*, Lecture Notes in Electrical Engineering 251,
DOI: 10.1007/978-3-642-37925-3_139,

industry. The major control measures against this disease are drug treatment, particularly antibiotics. However, the disease is easy to relapse after drug withdrawal, the pathogen susceptible to drug resistance after long-term medication, and also may produce significant toxic effects to avian. Laying rate may significantly decrease in layers and drug residue in broilers. Therefore, it is necessary to immunoprophylaxis with available vaccines to fundamentally control the prevalence of fowl cholera.

Currently, the vaccines for prevention of fowl cholera include attenuated vaccine and inactivated vaccine. However, the protective effect achieved through commercial live vaccine is not ideal. The attenuated vaccine has some shortcomings, for instance, short-term immunoprotection and poor protective effect. Residual virulence may lead to degression of laying rate, and the disease may be outbreak after incorrect use [2]. The immunological effect of inactivated vaccine is not as good as live vaccine, therefore, the inactivated vaccine is rarely applied.

The lack of an effective vaccine for preventing this disease has stimulated the search for new candidate immunogens for novel vaccine. Expression library immunization (ELI) is an alternative approach that has the potential to identify the vaccine antigens. ELI was first reported by Barry et al. [3]. Piedrafita et al. demonstrated that DNA vaccination with genomic libraries of mycoplasma pulmonis can induced protection against challenge exposure of parental strain in mice [4]. The research of Hernández showed experimental animals immunized with the genomic expression library of mycobacterium tuberculosis had a significant reduction of viable bacteria in lungs and less pulmonary tissue damage [5].

In this study, we constructed the genomic expression library of Avian *Pasteuella multocida*. The recombinant plasmids were extracted and mice were vaccinated with these plasmids. The levels of antibodies and efficacy of protection were tested. The aim of this study was to lay a foundation for screening of immunogens and for the development of vaccines against *Pasteurella multocida* infection.

139.2 Materials and Methods

139.2.1 Mice, Bacteria Strains, Plasmids, and Cells

Female Balb/c mice (6 weeks old) were purchased from Experimental Animal Center of Henan Province. Avain *Pasteurella multocida*-CVCC474 strain was purchased from Chinese Institute of Veterinary Drug Control (IVDC). Competent cell TG1, the eukaryotic expression vector pcDNA3.1(+) was conserve in the laboratory of He Nan University of Science and Technology in China.

139.2.2 Construction of the Library

Genomic DNA was extract from avain *Pasteurella multocida*-CVCC474 strain as previously described [6] and digested with the restriction enzyme *Sau*3AIto median sizes of 500–3000 bp. These fragments were purified using the gel extraction kit. The eukaryotic expression vector pcDNA3.1(+) was digested with *Bam*HIand treated with alkaline phosphatase. Then it was ligated with Sau3AI-digested gene fragments and transformed into competent *E.coli* TGl by electroporation [7]. The *E.coli* cells were plated into Luria-Bertani (LB) agar plates supplied with and incubated overnight at 37 °C resulting in the genomic expression library about 10^6 clones.

139.2.3 Identification of Library and Extraction of Recombinant Plasmids

Eight clones were randomly selected from the library and inoculated in 5 ml LB with ampicillin (50 μg/ml) and cultivated overnight at 37 °C. The recombinant plasmids were extracted and identified with restriction enzyme *Eco*RI and *Hin*dIII. Then the library was randomly assigned to five clone pools. The plasmids of each pool were prepared on a large scale using the alkaline lysis method, and the plasmid preparations were adjusted to 1 μg/μl using phosphate-buffered saline (PBS, 0.01 M, pH 7.2) for further experiments.

139.2.4 DNA Immunization of Mice

Six-weeks-old female Balb/c mice ($n = 75$) were randomly assigned to seven groups, named groups 1–5, pcDNA3.1(+) group and PBS group. The mice of groups 1–5 and pcDNA3.1(+) group were immunized intramuscularly with 100 μg of plasmids from clone pools 1–5 and empty vector pcDNA3.1, respectively. Mice in the PBS group were injected with 100 μl PBS (0.01 M, pH 7.2). The animals in each of the above groups were immunized three times at 2-week intervals.

139.2.5 Elisa

Blood samples were drawn from mice with tail cutting every week after immunization, and then the serum specimens were isolated. The serum antibody titers were determined using indirect enzyme-linked immunosorbent assay (ELISA). ELISA was performed as following: Flat bottomed 96-well plates were coated

with 100 μl ultrasound lysates (20 μg/ml) of avain *Pasteurella multocida*-CVCC474. The plates were washed with 0.01 M phosphate buffer saline with 0.05 % tween-20 (PBST, pH7.2) and blocked with 3 % Sodium caseinate for 2 h at 37 °C. Then the plates were incubated for 1.5 h at 37 °C with 100 μl of the serum samples (diluted 1/100 with PBST). The plates were washed three times with PBST and goat antimouse IgG- Horseradish peroxidase was added and incubated at 37 °C for 1.5 h. Plates were washed three times with PBST, then 50 μl Ortho-phenylene diamine was added and incubated for 20 min. Enzyme activity was stopped by adding an equal volume of 2 M H2SO4, and the absorption was measured at 492 nm. Antibody titers were determined for up to 6 weeks before challenge. All the serum samples of each weekly extraction were studied in the same ELISA plate, with two replicates.

139.2.6 Challenge Study

Fifteen days after the final vaccination, the mice were challenged with 3×10^2 (5LD50) virulent strain CVCC474 subcutaneously. The mice were observed for 15 days, the survival number and the relative protection rate was counted.

139.2.7 Analysis of Data

Results corresponding to ELISA and challenge experiment were analyzed employing the origin75 software. Analysis of variance was used to determine the significance of differences in means between the experimental groups. Difference with $P < 0.05$ was considered significant.

139.3 Results

139.3.1 Identification of Library

Clones were selected randomly from the library and recombinant plasmids were extracted. They were digested with two kinds of restriction endonucleases EcoRI and HindIII. The Enzyme-digested products were analyzed by agarose gel electrophoresis. As shown in Fig. 139.1, the DNA fragments between 500–3000 bp were obtained, indicating the genomic expression library of avian *Pasteuella multocida* CVCC474 were constructed successfully.

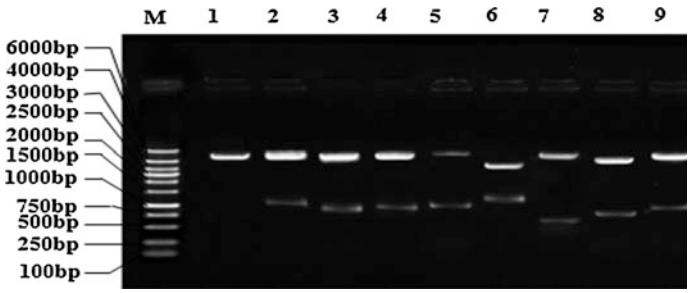

Fig. 139.1 Electrophoresis of recombinant plasmids digested with EcoRI and HindIII. *M* Wide Range DNA Marker (100–6000); *1* pcDNA3.1(+) empty plasmid; *2–9* recombinant plasmids digested by EcoRI and HindIII

139.3.2 Serum Antibody Levels

Conserved plates containing library clones were combined and assigned to five clone pools. The plasmids of each pools were extracted on a large scale and injected mice. The serum specimens from vaccinated mice were isolated 1–6 weeks after the first immunization and were assayed for the presence of specific antibodies using indirect enzyme-linked immunosorbent assay (ELISA). As shown in Fig. 139.2, after immunization, antibody level of serum of all the experimental groups (groups 1–5) presented the rising trend. The serum antibody levels in the group 1 was significantly higher than those in groups 2–5 ($P < 0.05$) and in the two negative control groups (pcDNA3.1(+) group and PBS group, $P < 0.01$). There are no difference in the antibody levels among other experimental groups ($P > 0.05$), though the group 2 was slightly higher than the others. In addition, the serum antibody levels in groups 1–5 were significantly higher than those in pcDNA3.1(+) groups ($P < 0.01$).

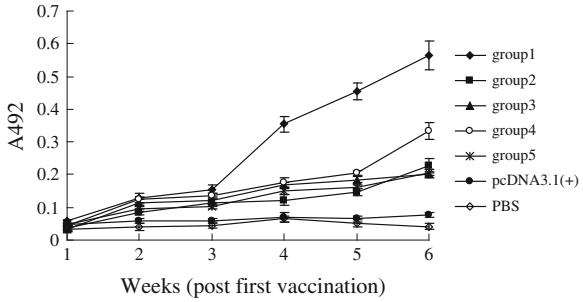

Fig. 139.2 The dynamic changes of serum antibody level in serum from immunized mice. Following the first immunization, serum antibody levels were measured by indirected ELISA weekly until 6 weeks. Group 1 (◆); group 2 (■); group 3 (▲); group 4 (○▼); group 5 (*);pcDNA3.1(+) vector (●); PBS (◇)

Table 139.1 The protective efficacy against lethal challenge with avian *Pasteurella multocida* ($^{a}P < 0.05$, $^{b}P < 0.01$.)

Groups	Survival number/Total	Mortality (%)	The relative protection rate (%)
Group 1	10/15	33.33	64.29[b]
Group 2	5/15	66.67[a]	28.57[a]
Group 3	3/15	80.00[b]	14.29
Group 4	7/15	46.67[a]	50.00[a]
Group 5	5/15	66.67[a]	28.57[a]
pcDNA3.1(+)	2/15	86.67[b]	0
PBS	1/15	93.33[b]	0

The relative protection rate (%) = (1-Mortality of experimental groups/Mortality of control group) × 100 %

139.3.3 Protection Against Challenge with Avian Pasteuella Multocida CVCC474

Groups of mice were challenged with live virulent avian *Pasteurella multocida* CVCC474 strain 15 days after the third immunization. Survival number and relative protection rate were counted till 15 days (Table 139.1). The mortality of mice receiving PBS were 93.33 % after challenge, and the pcDNA3.1(+) group were 86.67 %. The relative protection rate of group 1, group4, and group 5 was higher than other groups ($P < 0.05$). Particularly, the immunoprotection efficiency of group 1 was optimal, the relative rate of protection was 64.29 %.

139.4 Discussion

Currently, candidates for avian *Pasteurella multocida* DNA vaccine antigens include Outer membrane proteins (Omps), capsule, and Type 4 fimbriae [8–10]. However, there are large differences between the immune efficacies of DNA vaccines constructed using these genes. Their protective efficacy hardly exceeds that of attenuated live vaccine. Thus, screening and research of novel protective antigen genes is required to develop effective vaccines for controlling avian pasteurellosis. Immunization with genomic expression libraries has emerged as a novel technology for the discovery of vaccine candidate genes against some pathogens. Some studies have showed the identification of individual protective genes by the sequential fraction of cDNA or genomic expression libraries [11–13]. Identify vaccine candidates against avian *Pasteurella multocida* by means of this technology is promising, since other study has demonstrated that fusion and combined DNA vaccines against avian pasteurellosis could induce a higher immune response than monovalent DNA vaccines [14].

At present study, we constructed the genomic expression library of avian *Pasteurella multocida* and evaluated the immune efficacy. Humoral

immunoresponse is an important factor in resistance to avian *Pasteurella multocida* infection. In this study, we detected the levels of antibodies induced by the recombinant plasmids extracted from clone pools 1–5 of the library in mice (group1–5), and found that the level of antibody response of group 1, which was vaccinated with clone pool 1 plasmids, was higher than the other groups.

The challenge experiment is one of the important indexes to evaluate the protective efficacy of vaccines. In this study, mice immunized with various recombinant plasmids were challenged with virulent avian *Pasteurella multocida*. Among these DNA vaccines, the plasmids from clone pool 1 showed promise.

A future direction for our studies could therefore include investigating co-delivery of interleukins such as IL-2 and IL-10, that have been shown to modulate immune responses to DNA vaccines, with our novel antigens delivered as DNA vaccines to mice in attempts to elicit long-lived antibody and cell-mediated immune responses in our vaccinated animals [15, 16]. There are a lot of screening which antigenic ingredient in the better immune protection clone had played a role in immune effects need to be done. The task now is to identify specific antigens from our novel library that can be formulated in a subunit and DNA vaccine to induce a protective immune response against fowl cholera. In conclusion, we demonstrated that expression library immunization enabled screening of the avian *Pasteurella multocida* genome for potential vaccine candidates, and provided a valuable reference for the design of future DNA vaccines against fowl cholera.

Acknowledgments This work was supported by a grant from the Natural scientific research Project of Henan province, China (No. 2011B180019).

References

1. Davies RL, MacCorquodale R, Caffrey B (2003) Diversity of avian *Pasteurella Multocida* strains based on capsular PCR typing and variation of the OmpA and OmpH outer membrane Pproteins. Vet Microbiol 19:169–182
2. Mariana S, Hirst R (2000) The immunogenicity and pathogenicity of *Pasteurella Multocida* isolated from poultry in Indonesia. Vet Microbiol 72:27–36
3. Barry MA, Laiand WC, Johnston SA (2002) Protection against mycoplasma infection using expression library immunization. Nature 377:632–635
4. Piedrafita D, Xu D, Hunter D et al (1999) Protective immune responses induced by vaccination with an expression genomic library of leishmania major. J Immunol 163:1467–1472
5. Hernández YL, Corona DY, Rodríguez SS et al (2006) Immunization of mice with a mycobacterium tuberculosis genomic expression library results in lower bacterial load in lungs after challenge with BCG. Tubercul 86:247–254
6. Moore RJ, Lenghaus C, Sheedy SA et al (2001) Improved vectors for expression library immunization-application to mycoplasma hyopneumoniae infection in pigs. Vaccine 20:115–120
7. Tollefsen S, Vordermeier M, Olsen I et al (2003) DNA injection in combination with Eelectroporation: a novel method for vaccination of farmed ruminants. Scand J Immunol 57:29–38

8. Entomack B, Sawada T, Kataoka Y et al (2003) A 39 kDa protein mediates adhesion of avian *Pasteurella Multocida* to chicken embryo fibroblast cells. Vet Microbiol 97:29–243
9. Hatfaludi T, Al-Hasani K, Boyce JD (2010) Outer membrane proteins of *Pasteurella Multocida*. Vet Microbiol 144:1–17
10. Prado ME, Dabo SM, Confer AW (2005) Immunogenicity of iron-regulated outer membrane proteins of *Pasteurella Multocida* A:3 in cattle: molecular characterization of the immunodominant Heme Acquisition System Receptor (HasR) protein. Vet Microbiol 105:269–280
11. Melby P, Ogden G, Flores H et al (2000) Identification of vaccine candidates for experimental visceral leishmaniasis by immunization with sequential fractions of a cDNA expression library. Infect Immun 8:5595–5602
12. Lvey FD, Magge DM, Woitaske MD et al (2003) Identification of a protective antigen of coccidioides immitis by expression library immunization. Vaccine 21:4359–4367
13. Halea S, Kaltenboeckb B, DeGravesb FJ et al (2005) Screening the whole genome of a pathogen in vivo for individual protective antigens. Vaccine 23:3016–3025
14. Gong Q, Niu MF, Qin CL et al (2011) Out membrane protein (Omp) DNA vaccines for protective immunity against virulent avian *pasteurella multocida* in chickens. ICBBT bioinformatics Biomedical technician 3rd conference: 375–378
15. Williman A, Lockhart E, Slobbe L et al (2006) The use of Th1 cytokines, IL-12 and IL-23, to modulate the immune response raised to a DNA vaccine delivered by gene gun. Vaccine 24:4471–4474
16. Huang L, Babiuk A, Hurk SD (2006) The Cell-Mediated Immune Response Induced by Plasmid Encoding Bovine Herpesvirus 1 Glycoprotein B is Enhanced by Plasmid Encoding IL-12 when Delivered Intramuscularly or by Gene Gun, but not after Intradermal Injection. Vaccine 24:5349–5359

Chapter 140
Expression of Recombinant Human Bone Morphogenetic Protein 2 in Insect Cells, Purification and Activity Analysis

Wen Chu, Shenheng Luo, Lihong Xu, Minhui Long and Aipo Diao

Abstract The aim was to produce recombinant human bone morphogenetic protein 2 (BMP2) using baculovirus-insect cell protein expression system. The recombinant protein was purified by high affinity Ni-charged resin, then the bio-activity of recombinant protein was detected by alkaline phosphatase assay, and the result showed that the recombinant BMP2 stimulated alkaline phosphatase activity in MC3T3-E1 cells, which lay the foundation for further study and application of recombinant BMP2.

Keywords Human bone morphogenetic protein 2 · Baculovirus-insect cells protein expression system · High5 · Alkaline phosphatase

140.1 Introduction

Bone morphogenetic proteins (BMPs) belong to the members of the transforming growth factor TGF-β super genes family [1], people have already separated BMP from many animals' bone matrix like cows, pigs, sheeps, mice, rabbits and people [2], there are 21 members in BMP family [3], they have the ability to induce mesenchymal cells and osteoprogenitor cells to differentiate into chondrocytes and bone cells, which can induce new bone formation except BMP1 [4–6]. Along with the wide application of genetic engineering and deeper research of the bone induction and BMP biological characteristics, BMPs had been proved to be the most important differentiation factors [7] for normal embryonic period bone [8] and adult bone repair [9–11]. This group of proteins have important value no

W. Chu · S. Luo · L. Xu · M. Long · A. Diao (✉)
College of Biotechnology, Tianjin University of Science and Technology, Tianjin 300457, People's Republic of China
e-mail: diaoaipo@tust.edu.cn

T.-C. Zhang et al. (eds.), *Proceedings of the 2012 International Conference on Applied Biotechnology (ICAB 2012)*, Lecture Notes in Electrical Engineering 251,
DOI: 10.1007/978-3-642-37925-3_140,

matter for the basic biological research, or for the clinical application. So they had been the hotspot in the field of bone since they found [12].

In this experiment, the Sf9 insect cells were cotransfected with plasmids of pBAC-2CP-BMP2 and baculovirus flashBAC DNA to produce recombinant baculovirus, containing the BMP2 mature peptide encoded gene. High5 insect cells were infected with recombinant baculovirus to express BMP2 recombinant protein mature peptides efficiently, the expressed BMP2 protein was purified by high affinity Ni-charged resin, the bioactivity of recombinant protein was detected by alkaline phosphatase assay and the result showed that the recombinant BMP2 could stimulate alkaline phosphatase activity in MC3T3-E1 cells.

140.2 Materials and Methods

140.2.1 Materials

Restriction enzyme BamHI, EcoRI and T4 DNA ligase, pfu and Taq DNA polymerase were bought from Fermentas company; DNA purification and Miniprep plasmid extraction kit were bought from Tiangen company; Insect cell expression vector pBAC-2CP was from Novagen; Insect cells culture medium, DMEM medium and bovine serum were bought from GIBCO company; Escherichia Coli TOP10 competent cells, Sf9 insect cells, High5 insects cells, MC3T3-E1 mice fibroblast cells were preserved in the laboratory.

140.2.2 Methods

140.2.2.1 Insect Cell Culture

Insect cells were grown at 28 °C without CO_2 in a monolayer are split 1:5–1:8 every 3–4 days when confluence was between 85 and 95 %. To initiate shake culture from monolayer cultures, cells were dislodged from flask by pipetting medium over cells, and diluted with pre-warmed 28 °C medium to final concentration of 0.75×10^6 cells/ml [13]. Sf9 or High5 insect cells were grown and maintained in suspension culture in a temperature controlled orbital shaker operating at 150 rpm.

140.2.2.2 Production of Recombinant Baculovirus

To produce recombinant baculovirus, insect cells were co-transfected with transfer plasmid DNA and flashBAC DNA in 35 mm culture dish, cells were grown at

28 °C without CO_2 for 6 days. Homologous recombination between these two molecules yielded a baculovirus genome with the promoter and target sequence from the transfer plasmid located between the ORF1629 and the lef2 loci. The recombination also restored the function of the essential viral ORF1629, enabling the recombinant baculovirus to replicate and produce a population of recombinant viruses, which were released into the medium [14]. Six days after, the recombinant baculovirus in the supernatant was collected.

140.2.2.3 Amplification of Recombinant Virus

1 ml recombinant viruses were added to 10 cm sf9 insect cells culture dish, cells were grown at 28 °C without CO_2. Six days later, the supernatant was collected. Prepared 100 ml suspension culture of sf9 cells at an appropriate cell density, cells should be infected at a low multiplicity of infection, appropriate recombinant virus seed stock harvested from 10 cm sf9 insect cells culture dish was added to suspension culture cells. Incubated with shaking until cells were well infected (usually 6 days). When cells appeared to be well infected with viruses, cell culture medium was collected by centrifugation at 3,000 rpm for 4 min at 4 °C. Stored supernatant (recombinant virus stock) in dark at 4 °C and took out a small amount for PCR test.

140.2.2.4 BMP2 Protein Expression

Prepared 500 ml suspension culture of High5 cells at an appropriate cell density, appropriate recombinant virus seed stock harvested from 100 ml sf9 insect cells culture dish was added to suspension culture High5 cells, cells were grown at 28 °C for 3 days, cells and culture medium were collected at different time points after infection (24, 48 and 72 h) and protein expression were evaluated by SDS-PAGE analysis.

140.2.2.5 Protein Purification

The recombinant protein was purified using high affinity Ni-charged resin (GenScript). Cell pellet was resuspended in 50 mM sodium phosphate buffer containing 8 M urea, after centrifugation the supernatant wase incubated with Ni-charged resin for 1 h at 4 °C. The Ni-charged resin was washed with buffer containing gradient concentration of urea (6 M, 4 M, 2 M, 1 M, 0 M) and 20 mmol imidazole. Purified protein was eluted with 0.5 M imidazole and dialysed in PBS. The purified protein was analysed by SDS-PAGE.

140.2.2.6 Activity Assays of BMP2 Protein

The bioactivity of recombinant BMP2 protein was detected by alkaline phosphatase assay. MC3T3-E1 cells were cultured in 96-well with the density of the cells at 10^5 cells/ml, 100 μl each well, cells were grown at 37 °C for 1 day. Different concentration protein samples and standard samples were added, parallel and controls were set, then cells were grown at 37 °C for further 5 days. Five days later, the medium was removed, 100 μl 1 % Triton X-100 solution was added and placed at 4 °C for 1 h, then repeated freeze-thaw three times. 50 μl alkaline phosphatase reaction liquid substrates (1 mmol/L PNPP, 0.1 mol/L MgCl2) were added, placed at 37 °C for 1 h then 1.25 mol/L NaOH was added to terminate the reaction. Enzyme standard instrument was used to determine the spectrophotometry at 405 nm wavelength.

140.3 Results and Discussion

140.3.1 Production and Amplification of Recombinant Baculovirus

The DNA fragment encoded human BMP2 mature peptide was amplified by PCR, and inserted into insect cell expression vector pBAC-2CP to produce recombinant plasmid pBAC-2CP-BMP2, and indentified by DNA sequencing. Sf9 cells were co-transfected with plasmid pBAC-2CP-BMP2 and flashBAC DNA in 35 mm culture dish to produce recombinant baculovirus containing the BMP2 mature peptide encoded gene. To indentify the recombinant baculovirus, the virus DNA was extracted by proteinase K and indentified by PCR. Figure 140.1 showed that the BMP2 mature peptide encoded DNA fragment was successfully inserted into the virus genome to produce recombinant baculovirus.

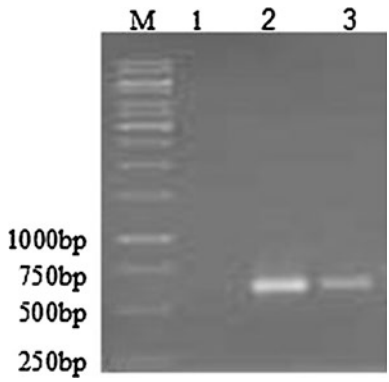

Fig. 140.1 Identification of recombinant virus by PCR. *M* DNA marker, *1* negative control (without template), *2* positive control (pBAC-2CP-BMP2 plasmid), *3* pBAC-2CP-BMP2 virus DNA

140.3.2 BMP2 Protein Expression

Appropriate recombinant virus seed stock harvested from 100 ml sf9 insect cells culture dish was added to 500 ml suspension culture High5 cells, when the cell density reach 2×10^6 cells/ml, placed at room temperature for 1 h, then 200 ml fresh medium was added, cells were grown at 28 °C for 3 days. Samples were taken everyday and the protein expression was evaluate by SDS-PAGE analysis. The result showed that recombinant BMP2 started to express 2 days after infection, with the highest expression level at the third day (Fig. 140.2).

140.3.3 Protein Purification

High5 cells were harvested 3 days after infection and resuspended in 50 mM sodium phosphate buffer containing 8 M urea. The recombinant protein was

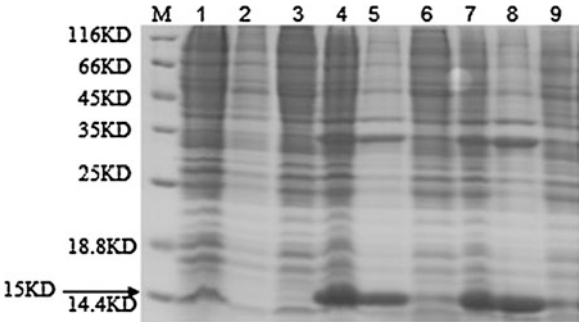

Fig. 140.2 Expression assays of BMP2 protein. *M* protein marker (14/18/25/35/45/66/116 kDA), *1* Bmp2 (1 day)-total, *2* Bmp2 (1 day)-pellet, *3* Bmp2 (1 day)-supernatant, *4* Bmp2 (2 days)-total, *5* Bmp2 (2 days)-pellet, *6* Bmp2 (2 days)-supernatant, *7* Bmp2 (3 days)-total, *8* Bmp2 (3 days)-pellet, *9* Bmp2 (3 days)-supernatant

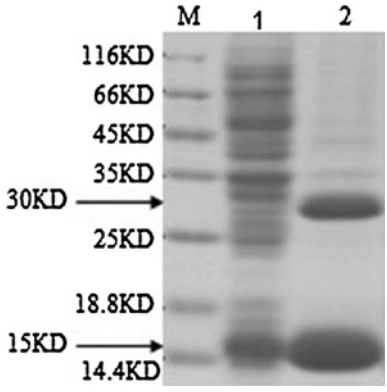

Fig. 140.3 Purification assays of BMP2 protein. *M* protein marker, *1* BMP2 total, *2* BMP2 purified

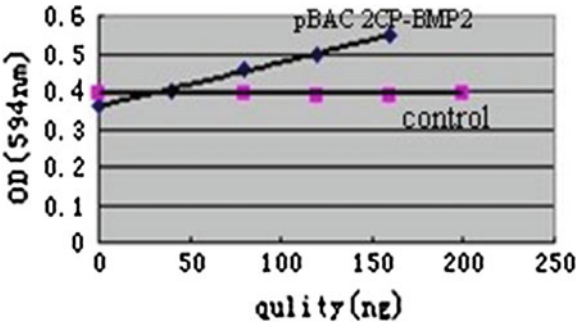

Fig. 140.4 Activity assays of BMP2 protein

refolded and purified using high affinity Ni-charged resin. The purified protein contains ~15 kDa BMP2 protein monomer and ~30 kDa BMP2 protein dimer (Fig. 140.3).

140.3.4 Activity Assays of BMP2 Protein

The differentiation of osteoblasts and the activity of intracellular alkaline phosphatase can be stimulated by BMP2 [15]. The bioactivity of recombinant BMP2 protein was detected by alkaline phosphatase assay using MC3T3-E1 cells. The activity of intracellular alkaline phosphatase increased obviously with the increasing concentration of recombinant BMP2 protein, but not for the control using recombinant protein His-interferon α (Fig. 140.4).

140.4 Conclusion

Bone morphogenetic proteins (BMPs) are a group of growth factors, originally discovered by their ability to induce the formation of bone and cartilage. The natural BMP2 protein was separated and purified in 1988, which plays a key role in osteoblast differentiation [16]. Recombinant human BMP2 protein has been produced using genetic-engineering technology, however, because recombinant BMP2 had lower activity to induce ossify, it still not widely used in clinic [17].

In this experiment, baculovirus-insect cells protein expression system was used to express recombinant human BMP2 protein. Baculovirus expression system is an eukaryotic protein expression system widely used in recent years [18–20], it has some advantages including: high protein expression level; expressed protein has proper modification (glycosylation) and easy to operate. We successfully produced recombinant human BMP2 using baculovirus-insect cell protein expression system, and the recombinant BMP2-stimulated alkaline phosphatase activity in MC3T3-E1 cells, which lay the foundation for further study and application of recombinant BMP2.

References

1. Croteau S, Rauch F, Silvestri A et al (1999) Bone morphogenetic proteins in orthopedics: from basic science to clinical practice. Orthopedics 22(7):686
2. Bessho K, Tagawa T, Murat AM et al (1992) Comparison of bone matrix derived bone morphogenetic proteins from various animals. J Oral Maxil Surg 50:496–501
3. Lindholm TS (1999) Thirty years of bone morphogenetic protein research. In: Lindholm TS (ed) Bone morphogenetic proteins experimental and clinical aspects today, Tampere, Finland, pp 1–2
4. Hots G, Herr G (1994) Bone substitute with osteoinductive biomaterials—current and future clinical applications. Int J Oral Maxillofac Surg 23:413–420
5. Wang EA, Rosen VD, Alessandro JS et al (1990) Recombinant human bone morphogenetic protein induces bone formation. Proc Natl Acad Sci USA 87:2220–2224
6. Riley EH, Lane JM, Urist MR et al (1996) Bone morphogenetic protein-2: biology and applications. Clin Orthop Rel Res 324:39–46
7. Wozney JM, Rosen V, Wang EA et al (1998) Novel regulators of bone formation: molecular clone and activities. Science 242:1528–1534
8. Nakashima M, Reddi AH (2003) The application of bone morphogenetic proteins to dental tissue engineering. Nat Biotechnol 21(9):1025–1032
9. Wang EA, Rosen V, Cordes P et al (1990) Purification and characterization of other distinct bone-inducing factors. Proc Natl Acad Sci USA 85:9484
10. Lioborman JR, Le LQ, Wu L et al (1998) Regional gene therapy with BMP-2 producing murine stromal cell line induces heterotopic and orthotopic bone formation in rodents. J Orthop Res 16:330–339
11. Yamaguchi A, Katagiri T, Ikeda T et al (1991) Recombinant human bone morphogenetic protein-2 stimulates osteoblastic maturation and inhibits myogenic differentiation in vitro. J Cell Biol 113(3):681–687
12. Hogan BLM (1996) Bone morphogenetic proteins: multifunctional regulators of vertebrate development. Gene Dev 10:1580–1594
13. Novagen user protocol TB459 Rev. E 1208:4–5
14. Novagen user protocol TB459 Rev. E 1208:6
15. Alborzi A, Mac K, Glackin CA et al (1996) Endochondral and intramembranous fetal bone development: osteoblastic cell proliferation, and expression of alkaline phosphatase, m-twist, and histone H4. J Craniofac Genet Dev Biol 16(2):94–106
16. Wu Y (1996) Bone induction and BMP research situation and expectation. Chin J Orthop Trauma 34(10):579
17. Hughs FJ, Collyer J, Stanfield M et al (1995) The effects of bone morphogenetic protein-2, -4 and -6 on differentiation of rat osteoblast cells in vitro. Endocrinology 136(6):2671
18. Maeda S (1989) Expression of foreign genes in insects using baculovirus vector. Annu Rev Entomol 34:351–372
19. Hongsheng Lv (1998) Insects virus molecular biology. China's Agricultural Science and Technology Publishing, Beijing
20. Ailor E, Betenbaugh MJ (1999) Modifying secretion and posttranslational processing in insect cells. Curr Opin Biotechnol 10:142–145

Chapter 141
Biotechnology of Azobenzene-Modified DNA and RNA

Xingguo Liang and Jing Li

Abstract Chemically modified nucleic acids have been widely investigated as antisense and RNAi candidates for therapeutic applications, agents, and probes for nucleic acid analysis, as well as tools for understanding the biological process. On the other hand, artificial regulation of gene expression using light as the external trigger has aroused much interest. In this study, we describe the molecular design of chemical modification of nucleic acid by introducing azobenzene, which can reversibly photoisomerize between *trans* and *cis* forms. By using the DNA modified by multiple azobenzenes, the duplex formation and dissociation were efficiently photoregulated. Several enzymatic reactions such as transcription, RNA cleavage, and gene expression were also efficiently photo-controlled. Furthermore, the azobenzene-modified DNA was utilized as a novel nanomaterial to create an artificial double helix for constructing functional nanostructures and nanodevices.

Keywords Azobenzene · Modified nucleic acid · Nanotechnology · Photoregulation

141.1 Introduction

Chemical modification of nucleoside, nucleotide, and oligonucleotide has been extensively studied both as therapeutic agents and as tools for biological analysis. The modified nucleic acids have been used in a large variety of fields, such as diagnostics, detection, therapeutics, sequencing, as well as basic molecular biology

X. Liang (✉) · J. Li
College of Food Science and Engineering, Ocean University of China, Qingdao 266003, People's Republic of China
e-mail: liangxg@ouc.edu.cn

T.-C. Zhang et al. (eds.), *Proceedings of the 2012 International Conference on Applied Biotechnology (ICAB 2012)*, Lecture Notes in Electrical Engineering 251,
DOI: 10.1007/978-3-642-37925-3_141,

[1, 2]. On the other hand, novel technologies using photochemistry have become powerful and contribute greatly to the modern industry [3]. Light is also an ideal external trigger to switch a biological reaction either in vitro or in vivo [4]. Accordingly, modification of biological molecules with photoresponsive groups is extremely attractive because control of their functions can be easily realized by simple light irradiation [5]. Other merits using photons as external stimulus are (1) light irradiation is easily controlled spatially at a pinpoint position; (2) both amount and time of irradiation can be tuned by will; (3) light irradiation is a noninvasive approach that causes almost no secondary perturbation of cellular processes; (4) wavelength can also be selected when various modified photoresponsive groups are used. Obviously, modification of nucleic acids with photoresponsive molecules is a direct way to reach the aim of photocontrolling gene expression.

Basically, there are two ways to modify nucleic acids and render them the photoresponsive capacity [6, 7]. One method is attaching a "caged" group to a nucleic acid molecule [8]. Another method is attaching to the nucleic acid a photoswitch that can isomerize between two chemical structures by light irradiation of various wavelengths. The ideal modification is that the function of modified nucleic acid is highly active when the attached molecule takes one structure (e.g., trans-azobenzene); on the other hand the function is turned off when the attached molecule is photoisomerized to another structure (e.g., cis-azobenzene) [9]. The approach of caging has a merit of complete function recovery once the cage group is removed. Its main demerits include (1) the removed cage group may contaminate the system; (2) photoregulation cannot be reversible; (3) in some cases, the high light strength is required for efficient removal of cage group and efficient regulation becomes difficult. As comparison, the photoswitch approach can easily achieve reversible regulation, although it is a challenge for modified nucleic acid to retain its function.

Azobenzene is an ideal molecule for photoswitch due to its clean photochemistry and drastic structure change with trans-cis isomerization [9, 10]. From the late 1990s, nucleic acid chemists have started to modify DNA using azobenzene as a photoswitch [11]. In 1998, Asanuma et al. introduced azobenzene as an analog of nucleobase to oligonucleotides through an acyclic linker [12]. The photoregulation of DNA duplex formation and dissociation was first realized. Later, structures of both linker and azobenzene were optimized for clear-cut photoregulation. In the present review, I will summarize the molecular design of azobenzene-modified nucleic acids and their applications to photoregulation of DNA/RNA biofunctions. The construction of photoresponsive DNA nanostructures and light-driven DNA nanomachines will also be described.

141.2 Modification of Nucleic Acid with Azobenzene Derivatives for Photoregulation of its Hybridization

141.2.1 Distinguishing Features of Introducing Azobenzene Via an Acyclic Linker

As we know, a tiny change in the structure of biomolecules usually causes complete loss of their functions. Normally, modification is carried out at 5-position of thymine, 2′-position of ribose, or the phosphodiester linkage to minimize the structural perturbations by modification [1]. However, the difficult chemical procedures are usually required to perform this kind of modification. Another approach is to synthesize a phosphoramidite monomer involving the functional group so that it can be easily introduced to any sequence on a DNA synthesizer. Obviously, it is a challenge to retain the binding of a protein at the modified site because even the backbone is greatly changed. In order to develop an artificial photoresponsive oligonucleotide which can be easily synthesized and utilized for photoregulation of DNA function, we designed a phosphoramidite monomer in which azobenzene is attached to a dinol linker [12, 13].

Figure 141.1 shows the structure of azobenzene-modified DNA we synthesized. As a type of 1, 3-propanediol linker (abbreviated as a C3 scaffold), 2, 2-bis(hydroxymethyl) propionic acid (C3–COOH) was first used as the acyclic linker for attaching azobenzene [13]. Obviously, both the backbone and side chain (formed by nucleobases A, G, C, and T in native DNA) changed greatly after modification. As the size of azobenzene is much bigger than a nucleobase, when the azobenzene-modified oligonucleotide forms a duplex with a non-modified one, the azobenzene moiety is like a wedge to insert between two adjacent base pairs (Fig. 141.2) [141.14]. The modified oligonucleotide is longer than its complementary strand by one nucleotide. Interestingly, the asymmetry of the structure does not affect much the stability of the duplex because the destabilization effect caused by the steric torsion is compensated by the strong stacking of azobenzene with base pairs. When a short C2 linker (C2-COOH) is used (Fig. 141.1), more stable duplex can be obtained, although the improvement is not so notable [15]. These results also demonstrate that DNA duplex has big structural flexibility, and even drastic structure change is allowed for its modification.

As DNA duplex is usually right-handed helix, chirality is important for stabilizing the duplex. When threoninol (C3–NH2) was used as the linker, for example, the D-configuration fits well with B-form DNA duplex, and shows more stabilization effect [16]. Structural analysis by 2D NMR revealed that R-configuration of C3–COOH (similar configuration as D-threoninol) fits well with B-form right-hand duplex (Fig. 141.2) [14]. For S-configuration of C3-COOH and L-threoninol, the hydrophobic azobenzene also intercalates well between two adjacent base pairs. The less stability as compared with R- or D-configuration is caused by the more steric stress due to the torsion of the linker.

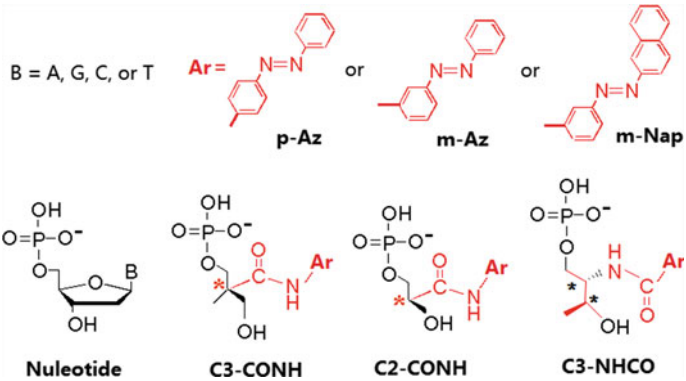

Fig. 141.1 Structures of a nucleotide and the artificial units in photoresponsive oligonucleotides

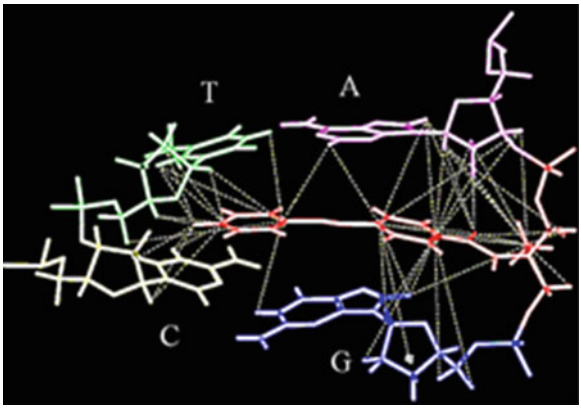

Fig. 141.2 NMR structure of a DNA duplex involving azobenzene moiety

141.2.2 Photoregulation of DNA Duplex and Triplex Formation by Using Azobenzene-Modified DNA

As we know, almost all functions of nucleic acids are related to the dissociation of the double helix. Our assumption is direct and simple: once the duplex formation and dissociation can be photocontrolled, many functions of nucleic acids can be regulated by light irradiation. Accordingly, we first checked whether photoisomerization can dissociate the duplex.

As shown in Fig. 141.3, photoisomerization of azobenzene to *cis* form did cause partial dissociation of DNA duplex, although only 10–20 % duplex could open after UV light irradiation (300–400 nm) at a fixed temperature. The efficiency of photoregulation was evaluated by the difference in T_m between *trans* and *cis* form (ΔT_m). For an 8 bp duplex, the photoisomerization of azobenzene showed a ΔT_m of only 8.9 °C [13]. The less efficiency, very short sequence, and limited

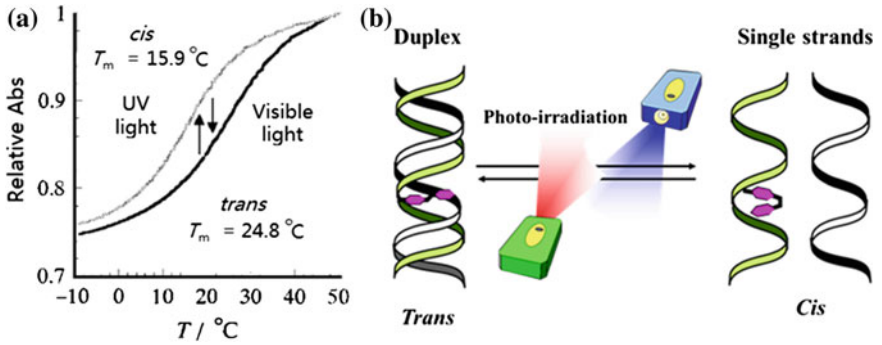

Fig. 141.3 Photoregulation of DNA duplex formation by using azobenzene-modified DNA. **a** T_m curves of a duplex with an azobenzene either in *trans* or *cis* form; **b** Schematic illustration of the regulation with light of various wavelengths

temperature range for regulation did not dampen scientists' enthusiasm for making use of photons to regulate gene expression in a controllable manner. The concept and creative novelty are very attractive. Another interesting point is that the regulation is completely reversible, and no deterioration of azobenzene was found during light irradiation.

The mechanism of photoregulation is easily understood: hydrophobic planar *trans*-azobenzene intercalates between base pairs and stabilizes the duplex by stacking interaction; non-planar *cis*-azobenzene destabilizes the duplex by steric hindrance. More strong interaction of *trans*-azobenzene with adjacent base pairs causes more difference in stability between *trans*- and *cis*-azobenzene [15].

The modified DNA can also be used as the third strand (TFO, triplex formation oligonucleotide) to photoregulate the DNA triplex formation and dissociation [17, 18]. One azobenzene in the middle position of a 13 nt TFO can cause a ΔT_m of 36.2 °C. However, the strong interaction between base pairs and azobenzene decreases greatly its efficiency of *cis*-to-*trans* photoisomerization. Only about 40 % of azobenzene can be isomerized to *cis* form at 20 °C.

141.2.3 Optimization of the Acyclic Linker and Azobenzene Derivatives

Although potential photoregulation ability had been shown by introducing azobenzene to DNA, several requirements should be satisfied. (1) The stability of *cis* form should be improved because the thermal *cis*-to-*trans* isomerization causes problems during photoregulation. (2) The photoregulation efficiency was too low. (3) The efficiency of *trans*-to-*cis* photoisomerization decreased when *trans*-azobenzene intercalates into a duplex. (4) The activity of an enzyme or a cell is affected when UV light is used. (5) When a prochiral linker like C3–COOH is

used, multiple introduction of azobenzene becomes difficult. (6) The asymmetry structure reduces the photoregulation efficiency. (7) Big structure change in the duplex blocks the interaction of DNA with other biomolecules. (8) As the backbone changes a lot, the modified oligonucleotides cannot be used as the template for DNA or RNA synthesis. (9) The azobenzene moiety cannot be introduced using an enzymatic way because polymerase cannot use the corresponding triphosphate of azobenzene monomer as the substrate. Accordingly, molecular design should be modulated for various requirements and applications.

At first, we used *meta*-aminoazobenzene (m-Az in Fig. 141.1) to replace *para*-aminoazobenzene (p-Az), and the half-life of *cis* form increased from 1.0 to 64 h at 37 °C [19]. This result proved again that the conjugation of substitute group on azobenzene with N = N double bond causes low thermal stability of *cis*-azobenzene. However, the photoregulation efficiency decreased to some extent as compared with the *para* one. We tried *meta*-naphthalene (m-Nap in Fig. 141.1), which has bigger size for more structure change between *trans* and *cis* isomers, the thermal stability of *cis* form decreased [20].

For C3–COOH, two diastereomers are obtained when one azobenzene moiety is introduced. When n azobenzenes are attached, the number of structures is 2^n, and it is difficult to purify them. Although a chiral C2-linker was used to solve this problem, and photoregulation efficiency increased a little, the problem of thermal stability of *cis* form remained unsolved [15]. More than 30 % of *cis* form isomerized to *trans*-form even during T_m measurement.

Based on the above efforts, we noticed that chiral threoninol is the best option to solve problems of both thermal stability and multiple introductions. Reynolds first use L-threoninol to attach a functional group [21]. Our experiments showed that half-life of *cis*-C3NHCO using D-threoninol as the linker was 3.3 h at 60 °C [22]. The change in T_m (ΔT_m) of a 12 bp duplex caused by photoisomerization of one azobenzene was 5.7 °C. It was proved that D-threoninol could satisfy the basic requirement of photoregulation and it was used as the standard linker from then on [16].

For improving the regulation efficiency of a long DNA duplex, introduction of multiple azobenzenes is required. When 9 azobenzenes were introduced via D-threoninol into a 20 bp duplex, the ΔT_m increased to 62 °C, although the duplex was highly asymmetric [23]. Even in this case, if the temperature of irradiation is fixed, only about 50 % of DNA duplex can be photoregulated. Further improvement in photoregulation efficiency was also required.

To improve the photoregulation ability, several methyl substituted azobenzene derivatives were used as photoswitches (Fig. 141.4). Interestingly, in the case that two methyl groups are present at the two ortho positions of the distal benzene ring (2′6′-Azo), ΔT_m increased from 5.7 to 14.6 °C when one azobenzene derivative was introduced into a 12 bp duplex [22]. For the derivative with two methyl groups at other positions or only one methyl group, no obvious effect was found. More interestingly, the thermal stability of *cis*-2′6′-Azo ($t_{1/2}$ = 25 h at 60 °C) is about 8 times higher than that of non-substituted azobenzene. However, the *trans*-to-*cis* isomerization becomes difficult, and only 65–70 % of 2′6′-Azo can be isomerized to *cis* form at most.

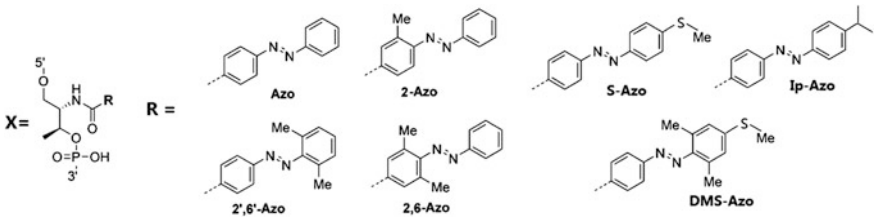

Fig. 141.4 Improvement of photoregulation efficiency by using various azobenzene derivatives

When a large substitute group is present in the *para* position of the distal benzene ring, *cis*-azobenzene forms much more stable duplex than *trans* form [24]. For the 12 bp duplex, T_m of *cis* form is higher than *trans* one by 6.7 °C. This reverse photoswitch effect can be explained as follows: the hydrophobic alkyl group in *cis* form interacts with hydrophobic part in the major group; in *trans* form, the big substitute group causes large steric hindrance toward the deoxyribose of the complementary strand.

For all azobenzene derivatives we tried up to now, *cis*-azobenzene could only be obtained by UV light irradiation with a wavelength shorter than 380 nm. In order to reduce the possible harm to biological molecules as well as improve the diversity of photoregulation styles, the light with wavelength longer than 400 nm should be used. When dimethylthiomethylazobenzene (DMS-Azo, Fig. 141.4) was used, 400 nm light could photoisomerize it to *cis* form, and ΔT_m of the 12 bp duplex was as large as 12 °C. In addition, $t_{1/2}$ of *cis*- DMS-Azo attached to an oligonucleotide is 6.4 h at 60 °C, which is longer than the non-substituted azobenzene [25].

141.2.4 Photoregulation of RNA Duplex Formation

For antisense strategy, DNA/RNA or RNA/RNA duplex is more important than DNA/DNA duplex. DNA/RNA duplex can be photoregulated efficiently when azobenzene is tethered on the DNA strand. Azobenzene derivatives can also be introduced into short RNA for photoregulation of RNA/RNA or RNA/DNA duplex formation. In some cases, even a larger ΔT_m can be obtained as compared with DNA/DNA duplex [26]. However, T_m of azobenzene-modified DNA/RNA, RNA/RNA, or RNA/DNA duplex is similar or lower than that of native duplex, probably because the intercalators usually cannot stabilize A-form duplex.

An acceleration effect of RNAi was observed by using modified RNA as compared with the non-modified one [27]. The Off-Target effect was greatly reduced by the modification. The possibility of RNA-induced silencing (DISC) complex formation with the non-target strand was greatly decreased due to the steric hindrance.

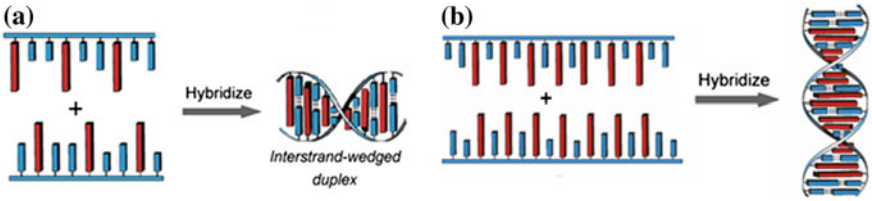

Fig. 141.5 Models of interstrand-wedged motif (**a**) and Azo–Azo pairing motif (**b**). The long bars indicate the azobenzene groups, and the short ones are nucleobases. Only *trans* forms are shown, and duplexes are completely dissociated in *cis* form

141.2.5 Efficient Photoregulation by Introducing Multiple Azobenzenes in a Symmetric Style

When targeting a native DNA or RNA strand, azobenzens have to be introduced into only one strand. However, when azobenzene-modified oligonucleotides are used as nanomaterials, azobenzenes can be present in both strands. As shown in Fig. 141.5, an artificial duplex can be built with the ratio of azobenzene and base pair being 1:1 [28]. The symmetry is greatly improved, although the azobenzene also inserts like a wedge and the structure is asymmetric locally. Interestingly, this artificial duplex is much more stable than the native duplex with the same sequence. More interestingly, complete ON–OFF photoregulation becomes possible.

NMR analysis also proved that hydrogen bonds in a base pair formed tightly between two azobenzene molecules [29]. Very strong negative-positive cotton effect indicates that a regular right-hand duplex was formed. More interestingly, the recognition ability between two complementary strands is even higher than the native duplex, and the mismatch between two azobenzenes causes a greater decrease of T_m.

Furthermore, two azobenzenes and one base pair (2:1 ratio) is also possible (Fig. 141.5) [30]. In this artificial duplex, two azobenzene molecules form an Azo–Azo pair, and the structure is highly symmetric. Clear-cut photoregulation was also obtained.

141.3 Photoregulation of Bioreactions Using Azobenzene-Modified Nucleic Acids

141.3.1 Photocontrol of Enzymatic Reaction by Using the Photoregulation of DNA Duplex Formation

We have the problem that *cis* form cannot be obtained at 37 °C with a high efficiency, usually less than 50 % of azobenzene can be isomerized to *cis* form

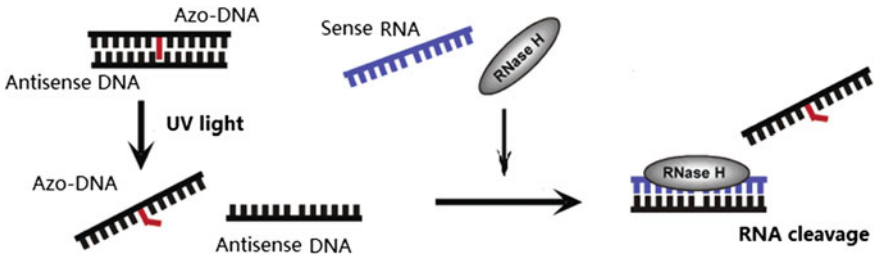

Fig. 141.6 Photoregulation of RNA cleavage by RNase H. Partial dissociation of the native antisense DNA caused by photoisomerization of azobenzene to *cis* form is enough to hybridize with sense RNA for its cleavage by RNase H

when *trans*-azobenzene intercalates between base pairs. In some cases, the content of *cis* form is even less than 30 %. Therefore, for a clear-cut photoregulation, the efficiency of OFF is more important. It is good that content of *trans*-azobenzene can be more than 98 % under visible light, especially when the azobenzene interacts strongly with base pairs at a relatively lower temperature. So our molecular design is: complete OFF at *trans* form, and ON at *cis* form. However, in cases such as antisense strategy, RNA/DNA formation activates (Turn ON) the block of gene expression. We made an interesting molecular design as shown in Fig. 141.6 [31]. The complementary antisense DNA strand can dissociate from the photoresponsive DNA duplex after UV light irradiation (*cis* form). The native strand can bind the target RNA (sense RNA) so that RNase H can cut the RNA. Even by this design, the complete OFF is also difficult because a small amount of Dn can bind and cause cleavage of RNA in a rapid turnover style.

A strand modified by azobenzene at 5′-end was also used to block primer extension by a DNA polymerase [32]. The modified strand hybridized to the DNA template as a modulator. After visible light irradiation, the primer extension stopped at the position of azobenzene; after UV light irradiation, the DNA polymerase kept on primer extension to the end of the template [32].

141.3.2 Photoregulation of Transcription

During transcription, the DNA duplex has to partly dissociate to expose the template for RNA synthesis. We tried to introduce azobenzenes to realize photoregulation of RNA transcription. Here, the concept is different from the simple photoregulation of DNA duplex formation, no complete and permanent dissociation occurs during transcription, and the structure change itself should be the main factor for efficient photoregulation. The T7 promoter was used as a model system. When only one azobenzene was introduced either in the template or non-template strand, no clear-cut photoregulation was obtained, and only two folds of increase was observed for *cis* form as compared with *trans* one. Interestingly, when two

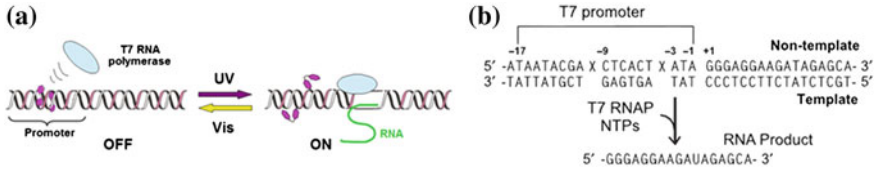

Fig. 141.7 Photoregulation of RNA transcription by azobenzene-modified T7 promoter. **a** A schematic illustration. **b** Sequence of T7 promoter and positions of azobenzenes are shown

azobenzenes were attached at −9 and −3 positions (Fig. 141.7), a synergistic effect appeared and the difference increased by 6–10 folds [33]. In *trans* form, the azobenzenes intercalate between base pairs so that the structure changes greatly. Thus T7 RNA polymerase cannot bind to start the transcription. In *cis* form, however, the azobenzenes prefer to flip out from the duplex so that the structure is similar to the non-modified one, and the activity of transcription recovers.

The detail mechanism of photoregulation was also clarified by introducing two kinds of azobenzenes (Azo and DMazo, in Fig. 141.4) with different thermal isomerization rate of *cis* form. By this well-considered molecular design, the isomers of cis–trans (the azobenzene group at −9 position is in *cis* form and the other one at −3 position in *trans* form) and trans–cis form were obtained [34]. The results showed that the *trans* to *cis* isomerization at −9 position mainly causes increase in the affinity (smaller K_m) of T7 RNA polymerase, and the *trans* to *cis* isomerization at −3 position mainly causes an increase in reaction rate (bigger k_{cat}). Cis-cis is the most active form.

The expression of protein can also be photoregulated by photoswitching the transcription. Here the light of 370 nm was used. However, the UV light irradiation at 340 nm harms the non-cell protein synthesis system we used (named PURE System) and the amount of protein decreases greatly. To improve the regulation efficiency, a thiomethyl azobenzene (S-Azo, Fig. 141.4) was used and *trans* to *cis* photoisomerization was carried out by 400 nm light. However, the difference between *trans* and *cis* form became lower, i.e., the photoregulation efficiency decreased. The main reason is that *para*-substitution decreases the duplex even in *trans* form. The improvement by using DMS-Azo is expected.

141.4 Photoresponsive Nanostructures or Nanodevices

Obviously, there are several limits by using directly azobenzene-modified nucleic acid to photoswitch bioreactions. For example, regulating a gene expression of eukaryotic gene will be difficult because there are so many factors related to the formation of transcription complex. Another difficulty is that a lot of positions in the DNA have to be tested to find a proper one. A new strategy is required.

We noticed that DNA can be used as the nanomaterial to either construct nanostructures such as DNA oligami, nano soccer ball, or even well-designed nanomachine with open-close, rotation, and transportation functions. In these cases, azobenzenes can be introduced to any positions and no direct enzyme binding is required. By ingenious designs, photoswitching of bioreactions can also be obtained by attaching the nanostructures to some functional nucleic acids. The photoresponsiveness of this kind of nanostructures may extend the application of DNA nanotechnology.

141.4.1 Photoresponsive Nanostructure

In many cases, the construction of 2D and 3D nanostructures was based on the hybridization of 4–6 nt sticky ends of basic parts. The molecular design for building a photoresponsive nanostructure can be very simple. Photoresponsiveness can be obtained by adding several azobenzenes to the sticky ends. In *trans* form, the nanostructure formed stably; in *cis* form on the other hand, the nanostructure is broken. The efficiency can be very high because dozens of sticky ends are present in one nanoparticle and even hundreds of azobenzenes can be introduced. The cascade effect can also be expected: after initiation of the destroying process, more and more azobenzenes can be photoisomerized to *cis* form so that the nanostructure is broken completely.

As shown in Fig. 141.8, a photoresponsive soccer ball is made of three kinds of oligonucleotides [35]. As the introduction of *trans* azobenzenes stabilizes the duplex formed between sticky ends, the formation of DNA nanostructure is even more stable than the native one. After 30 s of UV light irradiation, the nanoball was broken. This broken procedure was also recorded by real-time AFM.

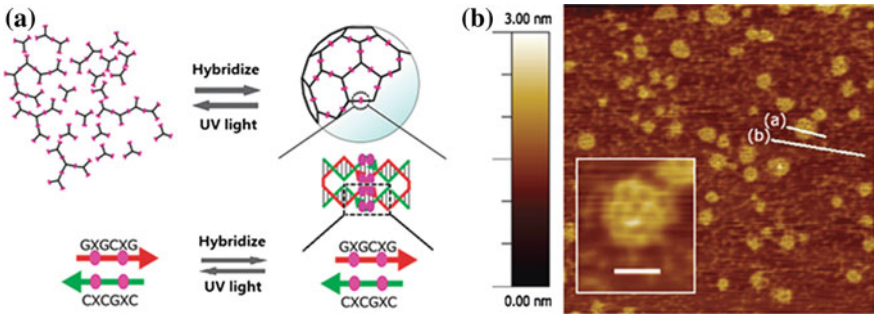

Fig. 141.8 A photoresponsive DNA nanosoccer ball involving azobenzene-modified sticky ends. **a** The molecular design of the sticky ends. **b** AFM image of the nanoball under visible light

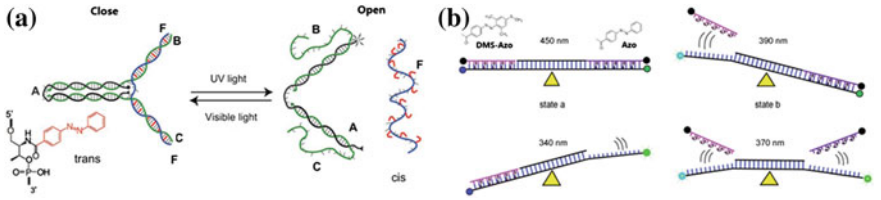

Fig. 141.9 Photoresponsive DNA nanomachines constructed by various azobenzene-modified oligos. **a** Photon-driven DNA tweezers; **b** A DNA seesaw driven by light of various wavelengths

141.4.2 Photon-Driven DNA Nanomachines

Many DNA nanomachines have been reported. The operation is based on the strand displacement or strand migration in which the formation and dissociation of duplex occurred. DNA oligos are usually the fuel for driving these devices. One problem caused by this approach is that the addition of DNA fuel is required for each cycle of the operation. A waste of duplex DNA is produced inevitably. The azobenzene-modified DNA can reversibly photoregulate the formation and dissociation. Accordingly, the azobenzene-modified oligos can be used as the fuel and simple repeats of UV and visible light irradiation are enough. Figure 141.9a shows one model of photoresponsive nanomachine [36]. The operations were easily repeated by irradiating UV light and visible light, and no waste was produced. It was also evolved to a single-molecule photoresponsive DNA nanomachine that cleaves RNA with a DNAzyme as the functional nucleic acid [37].

Another merit of using azobenzene-modified oligos to construct nanomachine is that more complex operations are possible by the combination of various azobenzene derivatives. We have photoswitches of reverse direction (Ip-Azo, Fig. 141.1) and capable of photoisomerization at various wavelengths. Figure 141.9b shows a light-driven DNA seesaw involving both Azo and DMS-Azo [25].

141.5 Conclusion

Various DNA functions have been photoregulated using azobenzene-modified DNA or RNA. It is interesting that the acyclic linker can be used to introduce functional molecules to confer new functions on nucleic acid. Surprisingly, DNA functions such as being the template for transcription were maintained even when two azobenzenes are present, although the high-dimensional structures are changed greatly. Azobenzene-modified DNA could even be used as the template for ligating two native DNA oligos at exactly the azobenzene site with a high yield [38].

The features of photoregulation can be simply diversified by using various azobenzene derivatives. Users can select different photoswitches for various

applications, such as photoswitches of reverse style, thermal-stable *cis* form, and capable of isomerizing to *cis* form under visible light. Especially for DNA nanotechnology, a great variety of nanostructures and nanodevices can be designed. Several groups are using our azobenzene-modified nucleic acids for various applications [39, 40]. Although further improvement (e.g., higher photo-isomerization efficiency at low temperature) is expected, we believe that the biotechnology and biology of azobenzene-modified DNA and RNA are promising to be well developed in the near future.

Acknowledgments Recruitment programs of "Wanren Plan," "Fund for Distinguished Young Scholars" of Shandong province, and "National Youth Qianren Plan," and "Program for Changjiang Scholars and Innovative Research Team in University (PCSIRT)" are acknowledged.

References

1. Venkatesan N, Seo YJ, Bang EK et al (2006) Chemical modification of nucleic acids toward functional nucleic acid systems. Bull Korean Chem Soc 27:613–630
2. Kuwahara M, Sugimoto N (2010) Molecular evolution of functional nucleic acids with chemical modifications. Molecules 15:5423–5444
3. Lee S, Kang HS, Park JK (2012) Directional photofluidization lithography: micro/nanostructural evolution by photofluidic motions of azobenzene materials. Adv Mater 24:2069–2103
4. Deiters A (2009) Light activation as a method of regulating and studying gene expression. Curr Opin Chem Boil 13:678–686
5. Gorostiza P, Isacoff EY (2008) Optical switches for remote and noninvasive control of cell signaling. Science 322:395–399
6. Young DD, Deiters A (2007) Photochemical control of biological processes. Org Biomol Chem 5:999–1005
7. Tang X, Dmochowski IJ (2007) Regulating gene expression with light-activated oligonucleotides. Mol BioSyst 3:100–110
8. Mayer G, Heckel A (2006) Biologically active molecules with a "light switch". Angew Chem Int Ed Engl 45:4900–4921
9. Beharry AA, Woolley GA (2011) Azobenzene photoswitches for biomolecules. Chem Soc Rev 40:4422–4437
10. Diau EW-G (2004) A new trans-to-cis photoisomerization mechanism of azobenzene on the S1 (n, π^*) surface. J Phys Chem A 108:950–956
11. Yamana K, Yoshikawa A, Nakano H (1996) Synthesis of a new photoisomerizable linker for connecting two oligonucleotide segments. Tetrahedron Lett 37:637–640
12. Asanuma H, Ito T, Komiyama M (1998) Photo-responsive oligonucleotides carrying azobenzene in the side-chains. Tetrahedron Lett 39:9015–9018
13. Asanuma H, Ito T, Yoshida T et al (1999) Photoregulation of the formation and dissociation of a DNA-duplex by using the cis-trans isomerization of azobenzene. Angew Chem Int 38:2547–2549
14. Liang XG, Asanuma H, Kashida H et al (2003) NMR study on the photo-responsive DNA tethering an azobenzene. J Am Chem Soc 125:16408–16415
15. Liang XG (2001) Studies on the photoregulation of DNA duplex and triplex formation. Doctoral dissertation of the university of Tokyo, Japan

16. Asanuma H, Takarada T, Yoshida T et al (2001) Enantioselective incorporation of azobenzene into oligodeoxyribonucleotide for effective photoregulation of duplex formation. Angew Chem Int Ed 40:2671–2673
17. Asanuma H, Liang XG, Yoshida T et al (2000) Photocontrol of triple-helix formation by using azobenzene-bearing oligo(thymidine). Angew Chem Int Ed 39:1316–1319
18. Liang XG, Asanuma H, Komiyama M (2002) Photoregulation of DNA triplex formation by azobenzene. J Am Chem Soc 124:1877–1883
19. Asanuma H, Liang XG, Komiyama M (2000) Meta-aminoazobenzene as a thermo-insensitive photo-regulator of DNA duplex formation. Tetrahedron Lett 41:1055–1058
20. Liang XG, Asanuma H, Komiyama M (2001) Phenylazonaphthalene as a superb photo-regulator for DNA-triplex formation. Tetrahedron Lett 42:6723–6725
21. Reynolds MA, Beck TA, Hogrefe RI et al (1992) A nonnucleotide-based linking method for the preparation of psoralen-derivatized methylphosphonate oligonucleotides. Bioconjuate Chem 3:366–374
22. Nishioka H, Liang XG, Kashida H et al (2007) 2,6-dimethylazobenzene as an efficient and thermo-stable photo-regulator for the photoregulation of DNA hybridization. Chem Commun 14:4354–4356
23. Asanuma H, Liang XG, Nishioka H et al (2007) Synthesis of azobenzene-tethered DNA for reversible photo-regulation of DNA functions: hybridization and transcription. Nat Protocol 2:203–212
24. Liang XG, Takenaka N, Nishioka H et al (2008) Molecular design for reversing the photoswitching mode of turning on and off DNA hybridization. Chem Asian J 3:553–560
25. Nishioka H, Liang XG, Kato T et al (2012) Photon-fueled DNA nanodevice carrying two different photoswitches. Angew Chem Int Ed 51:1165–1168
26. Ito H, Liang XG, Nishioka H et al (2010) Construction of photoresponsive RNA for photoswitching RNA hybridization. Org Biomol Chem 8:5519–5524
27. Ito H, Urushihara M, Liang XG et al (2012) Improvement of RNAi activity and strand-selectivity of RISC formation by modified siRNA involving intercalators near 5'-termini. Chem bio chem 13:311–315
28. Liang XG, Mochizuki T, Asanuma H (2009) A supra-photoswitch involving sandwiched DNA base pairs and azobenzenes for light-driven nanostructures and nanodevices. Small 5:1761–1768
29. Liang XG, Nishioka H, Mochizuki T et al (2010) An interstrand-wedged duplex composed of alternating DNA base pairs and covalently attached intercalators. J Mater Chem 20:575–581
30. Liang XG, Mochizuki T, Fujii T et al (2011) Design of a functional nanomaterial with recognition ability for constructing light-driven nanodevices. Lect Notes Comput Sc 6518:112–122
31. Matsunaga D, Asanuma H, Komiyama M (2004) Photoregulation of RNA digestion by RNase H with azobenzene-tethered DNA. J Am Chem Soc 126:11452–11453
32. Yamazawa A, Liang XG, Asanuma H et al (2000) Photoregulation of DNA polymerase reaction by oligonucleotides bearing an azobenzene. Angew Chem Int Ed 39:2356–2358
33. Liu M, Asanuma H, Komiyama M (2006) Abenzene-tethered T7 promoter for efficient photoregulation of transcription. J Am Chem Soc 128:1009–1015
34. Liang XG, Wakuda R, Fujioka K et al (2010) Photoregulation of DNA transcription by using photoresponsive T7 promoters and clarification of its mechanism. FEBS J 277:1551–1561
35. Tanaka F, Mochizuki T, Liang XG et al (2010) Robust and photo-controllable DNA capsules using azobenzenes. Nano Lett 10:3560–3565
36. Liang XG, Nishioka H, Takenaka N et al (2008) A DNA nanomachine powered by light irradiation. ChemBioChem 9:702–705
37. Zhou MG, Liang XG, Mochizuki T et al (2010) A light-driven DNA nanomachine for efficiently photoswitching RNA digestion. Angew Chem Int Ed 49:2167–2170
38. Liang XG, Fujioka K, Asanuma H (2011) Nick sealing by T4 DNA ligase on a modified DNA template tethering a functional molecule on D-threoninol. Chem Eur J 17:10388–10396

39. Yuan Q, Zhang Y, Chen Y et al (2011) Using silver nanowire antennas to enhance the conversion efficiency of photoresponsive DNA nanomotors. PNAS 108:9331–9336
40. Yan Y, Chen JI, Ginger DS (2012) Photoswitchable oligonucleotide-modified gold nanoparticles: controlling hybridization stringency with photon dose. Nano Lett 12:2530–2536

Chapter 142
Evaluation of a Whole Genome Amplification Method Based on Improved Ligation-Mediated PCR

Xiaoming Pan, Weikai Chen, Xiushuang Jia, Ping Dong and Xingguo Liang

Abstract DNA sequencing, genotyping, detection, and SNPs analysis usually require large amount of DNA. In the case that only tiny amount of DNA can be collected from samples, the whole genome amplification (WGA) technique is a good choice for its high efficiency. As a WGA method, ligation-mediated PCR (LM-PCR) has the shortcoming that strict conditions are required to avoid biased DNA amplification. Here, we used TspR I endonuclease to digest the target DNA into fragments with 9-nt-long (NNCASTGNN) sticky ends in which 4–5 different bases from other fragments are present. After ligation of these fragments to a universal adaptor, all the fragments will have ends with the same sequence for PCR, and the outstanding WGA was obtained by using only a uniform primer. The efficiency and sensitivity of this technique were evaluated and its application for DNA detection was also discussed.

Keywords Ligation-mediated PCR · High sensitivity · Whole genome amplification · TspR I endonuclease

142.1 Introduction

In many genetic studies such as DNA sequencing, genotyping, and detection of SNPs large quantities of DNA are required. However, in many cases only a small amount of target DNA can be collected because the quantity or quality of samples were not good enough, e.g., formalin-fixed paraffin-embedded tissues [1, 2]. Thus, the whole genome amplification (WGA) technique was employed to overcome this limitation. As a powerful tool, WGA plays an important role in various

X. Pan · W. Chen · X. Jia · P. Dong · X. Liang (✉)
College of Food Science and Engineering, Ocean University of China, Qingdao 266003, People's Republic of China
e-mail: liangxg@ouc.edu.cn

T.-C. Zhang et al. (eds.), *Proceedings of the 2012 International Conference on Applied Biotechnology (ICAB 2012)*, Lecture Notes in Electrical Engineering 251,
DOI: 10.1007/978-3-642-37925-3_142,

high-throughput genetic areas because it can provide sufficient DNA for large-scale genetic studies. Among the WGA methods, multiple displacement amplification (MDA) and ligation-mediated polymerase chain reaction (LM-PCR) were frequently used.

The MDA method, which relies on the strong strand displacement activity of the φ29 DNA polymerase, is an isothermal amplification approach based on rolling cycle amplification [3, 4]. In MDA, a primer with random sequence (e.g., a pool of all the hexamer primers) is usually used. LM-PCR is based on the PCR technique and inherited its high efficiency. LM-PCR was originally introduced in the field of footprinting for studying interactions of proteins with DNA in vivo [5–8]. By some modifications it can also be applied to perform methylation analysis and study of human diseases [9, 10].

For WGA, balanced amplification of all sequences is the basic performance. The application of traditional LM-PCR is limited, because it usually shows some deviation during amplification. The key procedure of LM-PCR is to prepare the fragments with a universal sequence at both ends. After digestion by a restriction enzyme, a universal adaptor with the same sticky end is ligated to all the fragments. One of the reasons of deviation during amplification is that ligation between digested fragments cannot be avoided because restriction enzyme digestion usually produce a 4–6-nt sticky end with palindromic sequence (e.g., AATT for EcoRI). Obviously, the unexpected ligation can also occur between the sticky ends of the adaptor. In this study, for improving the uniformity of LM-PCR, an improved approach using TspR I endonuclease as the restriction enzyme is developed. TspR I can digest DNA into fragments with 9-nt-long sticky ends, which can be used to decrease the self-ligation between fragments. A single-stranded adaptor is used and the self-ligation of adaptor molecules is avoided.

142.2 Materials and Methods

142.2.1 Materials

The 2686-bp-long pUC18 plasmid was extracted from bacteria culture solution. The extraction and purification procedures were referred to Molecular Cloning: A Laboratory Manual (the 3rd edition). Briefly, 500 mL of culture medium was centrifuged under 4 °C for 15 min to collect the cell pellets, resuspended the pellets with 200 mL of STE buffer (10 mM Tris–HCl, 0.1 mM NaCl, 1.0 mM EDTA, pH 8.0) and centrifuged again, then added 18 mL of lysis buffer I (50 mM glucose, 25 mM Tris–HCl, 10 mM EDTA, pH 8.0) and 20 mg lysozyme, added 40 mL of lysis buffer II (0.2 M NaOH, 1 % SDS) and stored at room temperature for 5–10 min. Then 20 mL of lysis buffer III (5.0 M potassium acetate 60.0 mL, acetic acid 11.5 mL, H_2O 28.5 mL) was added and kept on ice for 10 min. After that, samples were centrifuged for 30 min, liquid supernatant was collected, 0.6

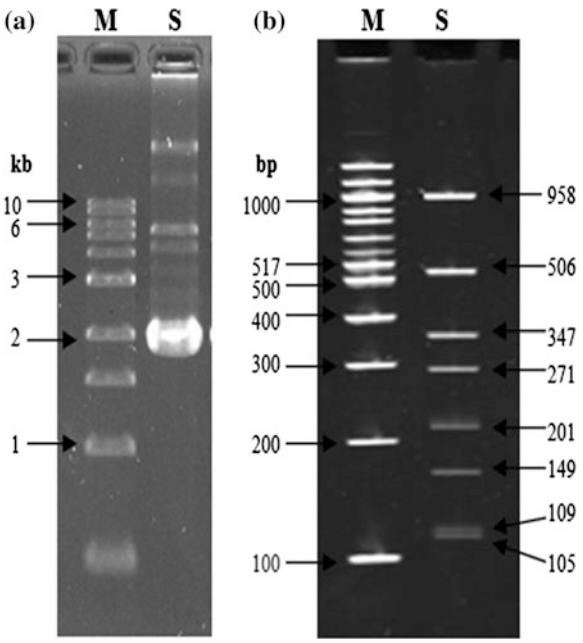

Fig. 142.1 Purification **a** and digestion **b** results of pUC18 plasmid

times volume of isopropanol was added to precipitate the DNA for 10 min at room temperature. After another centrifuge, precipitate was washed with 70 % ethanol, and resolved with 3 mL of TE buffer (10 mM Tris–HCl, 1 mM EDTA, pH 8.0). After extraction step, polyethylene glycol (PEG) precipitation method was used to purify the plasmid [11]. The concentration of pUC18 was determined by Nanodrop 2000 (Thermo Scientific). An amount of 2 μL of purification product was electrophoresed on 1.2 % (w/v) agarose with TBE buffer and stained in 0.5 μg/mL ethidium bromide for 20 min. Then 1 μg pUC18 plasmid was digested by TspR I ednonuclease (New England Biolabs, Inc.). The reaction mixture contains 50 mM KAc, 20 mM Tris-Ac, 10 mM $Mg(Ac)_2$, 1 mM DTT, 100 μg/mL BSA, the total mixture was incubated at 65 °C for 2 h and 2 μL of digestion product was electrophoresed on 8 % (w/v) polyacrylamide gel electrophoresis. The purification and digestion results were shown in Fig. 142.1.

The adapter and primer were synthesized by IDT (Integrated DNA Technologies, Inc.). Adapter: CTCACTCTCACCAACGTCGACAGCTTNNCASTGNN, Primer: CTCACTCTCACCAACGTCGACAGCTT [12].

142.2.2 Impact of Different DNA Ligase

The ligation reaction was the key procedure in the whole experiment and the ligation results mainly depended on the efficiency of DNA ligase. Here two

different ligase, T4 DNA ligase and Taq ligase were used to evaluate their effect to the Improved LM-PCR.

The ligation reaction was performed under the manufacture's protocol. The reaction mixture contains 5 pg pUC18 plasmid fragments, 0.2 pmol adapter, and 5.0 U DNA liagse. The total volume was 20 μL and the reaction with T4 DNA ligase (Fermentas) was incubated at 16 °C overnight while the reaction with Taq ligase (New England Biolabs, Inc.) was incubated at 45 °C, respectively. Use ddH_2O instead of DNA ligase for negative control. After ligation, PCRs that used ligation product as template were performed under uniform conditions: 1.0 μL of ligation product added to 19 μL of PCR mixture [10 mM Tris–HCl, 50 mM KCl, 1.5 mM $MgCl_2$, pH 8.3, 1 U DreamTaq DNA polymerase (Fermentas), 0.25 mM dNTPs, 0.75 μM primer], the mixture was incubated at 72 °C for 5 min for the 3′-end filling reaction. PCRs were performed as follows: initial denaturation at 94 °C for 3 min and 30 cycles of denaturation at 94 °C for 30 s, annealing at 60 °C for 30 s, and primer extension at 72 °C for 1 min [13, 14]. The samples were incubated at 72 °C for another 5 min and 2 μL of PCR product was electrophoresed on polyacrylamide gel electrophoresis.

142.2.3 Impact of Ligation Time and Temperature

The high efficiency of T4 DNA ligase depends on the ligation temperature and time. Two sets of experiments were done respectively to evaluate the effect of ligation time and temperature. The ligation and PCR reactions were referred to 2.2. The ligation time used were 4, 8, 12, 16 h and the ligation temperature were 16, 25, and 37 °C, respectively.

142.2.4 Impact of Primer Annealing Temperature

The primer annealing temperature used above was calculated by primer premier 6.0 (PREMIER Biosoft international, Palo Alto, CA) and maybe not the optimal temperature in actual experiment. Gradient annealing PCR were performed. The annealing temperatures were set up as 57, 60, and 63 °C, respectively. All other parameters were the same as mentioned in 2.3.

142.2.5 Improved LM-PCR Performed on E. coli Genome

Various concentrations of *E. coli* genome digestion product was used as template and the reaction conditions were the same as the conditions mentioned above.

142.3 Results

142.3.1 Principle of Improved LM-PCR

Similar to traditional LM-PCR, the Improved LM-PCR can be mainly divided into 3 steps: (1) preparation of DNA fragments by TspR I: double-strand DNA was digested by TspR I endonuclease into numerous fragments with different length and the same sticky end of NNCASTGNN. (2) ligation of adapter to both ends of the fragments: fragments were ligated with adapter which comprised of a primer sequence and a linker sequence. The linker sequence NNCASTGNN ligated to the 3′ sticky end produced by TspR I and the primer sequence served as template for primer extension thus created a substrate for PCR with uniform primer bonding site at each end. (3) amplification of the newly formed fragments by PCR: after PCR with universal primer, all of the fragments with the same end sequence could be amplified (Fig. 142.2).

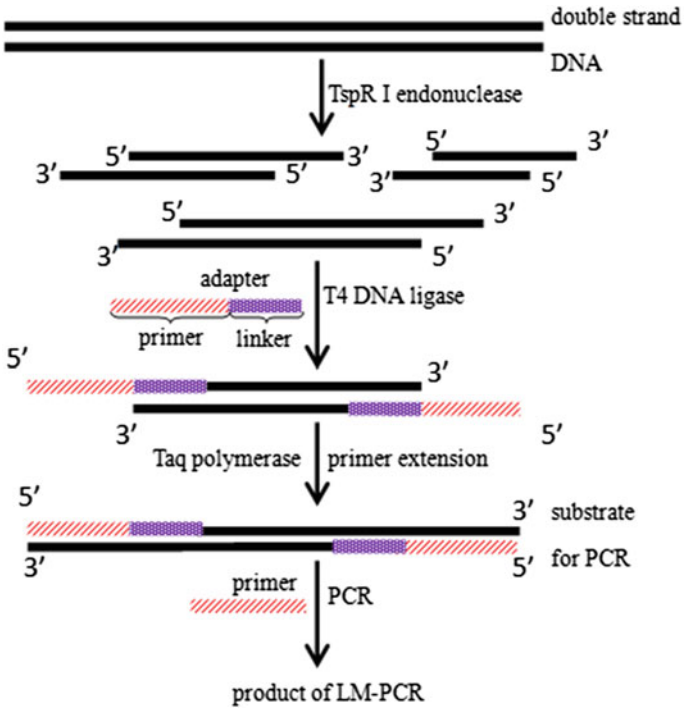

Fig. 142.2 Flowchart of improved LM-PCR

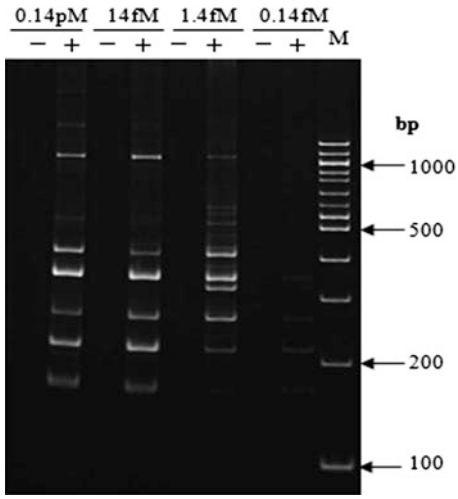

Fig. 142.3 Results of improved LM-PCR. "−" means negative control without DNA ligase. Ligation condition: 0.2 pmol adapter, 16 °C, 12 h

142.3.2 Results of Improved LM-PCR

The effect of Improved LM-PCR performed on pUC18 plasmid was shown in Fig. 142.3. The sensitivity was also evaluated by using 10-fold serial diluted template. The results showed that the Improved LM-PCR amplified the whole sequence of pUC18 plasmid successfully and the sensitivity was very high. When the concentration of template was 1.4 fM (∼50 fg), all of the eight fragments could be amplified; when the concentration lowered to 0.14 fM (∼5 fg), amplification of five of them could still be detected.

142.3.3 Results of Different DNA Ligase

T4 DNA ligase and Taq ligase were two mainly used ligases in genetic studies. The effect of the two ligases was shown in Fig. 142.4. When using T4 DNA ligase, all of the eight target bands could be seen, but less were obtained by Taq ligase. The results showed that the efficiency of T4 ligase was higher than Taq ligase.

142.3.4 Results of Different Ligation Temperature and Time

The high efficiency of T4 DNA ligase depends on the optimal reaction temperature and reaction time. At a higher temperature of 37 °C the band was indistinct and smaller fragments were not obtained. At lower temperature of 25 and 16 °C the number of target bands obtained was seven and eight, which means that 16 °C was better (Fig. 142.5a). The result of reaction time experiment showed that 12 h was the optimal reaction time (Fig. 142.5b).

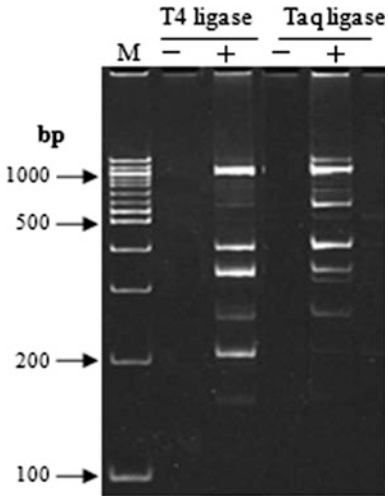

Fig. 142.4 Results of different DNA ligase. Ligation with T4 ligase was at 16 and 45 °C for Taq ligase

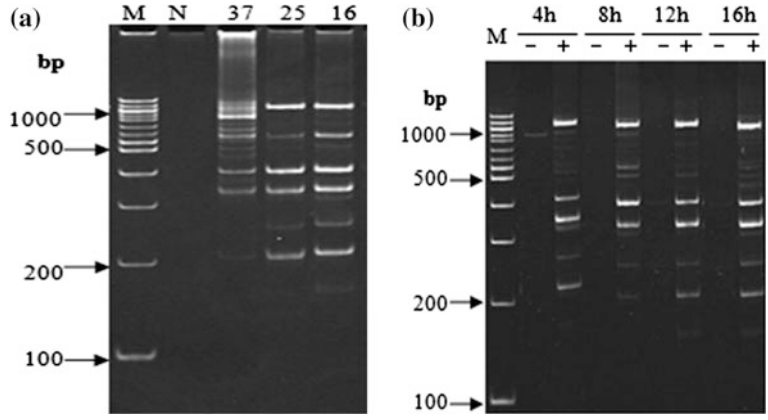

Fig. 142.5 Different ligation temperature and reaction time with T4 DNA ligase. **a** Ligation at various temperatures. **b** Ligation with various times

142.3.5 Results of Different Annealing Temperature

The annealing temperature used previously was calculated by software theoretically and need to be verified in actual experiment. The results indicated that with annealing temperature of 57, 60, and 63 °C the amplification efficiency was almost the same and 60 °C was slightly better (Fig. 142.6). Compared to other factors, the annealing temperature had less impact on this experiment.

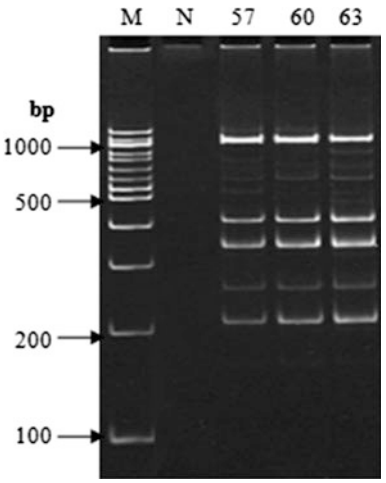

Fig. 142.6 Impact of annealing temperature. N: negative control without DNA ligase. Gradient annealing temperature was set on S1000 thermal cycler (BIO-RAD) with 57, 60 and 63 °C

142.3.6 Effect of Improved LM-PCR Performed on E. coli Genome

The continuous bands in Fig. 142.7 indicated that large amount of *E. coli* genome fragments were amplified. Plenty of bands could be seen even the concentration of genome was 8 aM. Most of the fragments ranged from 100 to 1000 bp and larger fragments that more than 1000 bp could also be amplified (Fig. 142.7). The results showed that Improved LM-PCR could amplify the whole genome with high sensitivity.

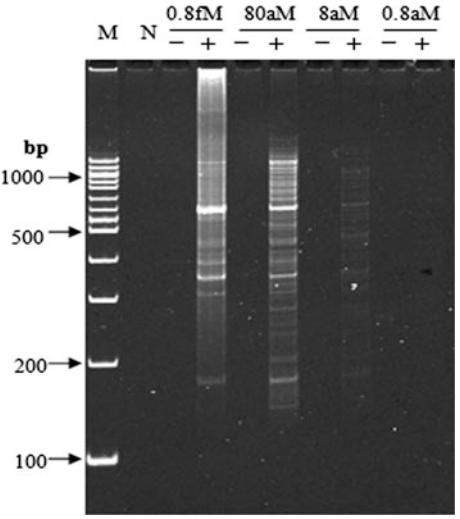

Fig. 142.7 Results of amplify the whole genome of *E. coli* with improved LM-PCR. N: negative control that no templates were added

142.4 Discussion

Theoretically, pUC18 plasmid could be cut into ten fragments by TspR I endonuclease but only eight of them could be examined on polyacrylamide gel electrophoresis either because the amount of the other two fragments (27 and 13 bp) run too fast in the gel or they were too little to be stained by ethidium bromide, e.g., the 13 bp fragment only owe 4 bp double strand and the 9 bp long was single strand. Thus our aim was to amplify the eight fragments obtained by digestion. The final LM-PCR products were 61 bp longer than the original fragments due to the ligation of adapter on both ends.

Compared to others work that used double-strand adapter, the adapter we used was single strand. As described before single strand is easier to operate [15]. The 9-nt-long sticky end produced by TspR I promised the ligation efficiency. Traditional LM-PCR that employed only one endonuclease tends to cause the self-ligation between fragments because all the fragments had the same end. But TspR I endonuclease could resolve this problem due to its sticky end was NNCASTGNN. This sticky end makes all of the fragments have at most 5 bases different to each other which will reduce the probability of self-ligation. Before ligation reaction, digestion product was serial diluted to even 10^7 times. Thus the effect of TspR I endonuclease that still existed in the sample could be ignored, and the loss of DNA during the removal of endonuclease procedure could also be avoided. The amplification efficiency may be affected by varieties of factors and among them the DNA polymerase was one of the key factors, some reports suggested that combination of *pfu* exo$^-$ and Taq polymerase at primer extension step and amplification step could improve the efficiency [16].

The sensitivity of WGA was especially important when there was not sufficient sample, thus, the LM-PCR technique based on high sensitivity PCR could play an important role in such conditions. Compared to other PCR-based WGA technique, degenerate oligonucleotide primer PCR (DOP-PCR) and primer extension pre-amplification PCR (PEP-PCR) also have high sensitivity that even one single cell could be used to perform WGA, but the main challenges were fidelity and balanced amplification [17–21]. LM-PCR was performed under strict conditions to avoid the biased amplification and our results showed that 50 fg plasmid in 20 μL of ligation reaction solution can still obtain all the eight target bands, and five of them could be obtained when only 5 fg plasmid was used, which indicated the high sensitivity and balanced amplification of Improved LM-PCR. Compared to the genome of *E. coli*, the pUC18 plasmid was small and simple. The result of LM-PCR performed on *E. coli* genome indicated that LM-PCR could amplify the whole genome well but more work is needed to evaluate the cover rate of LM-PCR used on larger genome DNA.

142.5 Conclusion

As a WGA method, the efficiency of Improved LM-PCR was evaluated in our study. The results showed that Improved LM-PCR may overcome the problem existed in the traditional LM-PCR. The effect of different reaction conditions was also evaluated. Under the optimal conditions, 1.4 fM plasmid in the ligation reaction could be amplified completely which showed that Improved LM-PCR has high sensitivity, and the results of LM-PCR performed on *E. coli* genome showed that Improved LM-PCR could also be used to perform WGA on larger genome with very low template concentration. All of the data obtained above indicated that improved LM-PCR could be a very useful tool in a variety of genetic analyses.

Acknowledgments Recruitment programs of "Wanren Plan", "Fund for Distinguished Young Scholars" of Shandong province, and "National Youth Qianren Plan", "Program for Changjiang Scholars and Innovative Research Team in University (PCSIRT)" are acknowledged.

References

1. Liu D, Liu C, DeVries S et al (2004) LM-PCR permits highly representative whole genome amplification of DNA isolated from small number of cells and paraffin-embedded tumor tissue sections. Diagn Mol Pathol 13:105–115
2. Tanabe C, Aoyagi K, Sakiyama T et al (2003) Evaluation of a whole-genome amplification method based on adaptor-ligation PCR of randomly sheared genomic DNA. Genes Chromosomes Cancer 38:168–176
3. Lovmar L, Syvanen AC (2006) Multiple displacement amplification to create a long-lasting source of DNA for genetic studies. Hum Mutat 27:603–614
4. Detter JC, Jett JM, Lucas SM et al (2002) Isothermal strand displacement amplification applications for high-throughput genomics. Genomics 80:691–698
5. Dai SM, Chen HH, Chang C et al (2000) Ligation-mediated PCR for quantitative in vivo footprinting. Nat Biotechnol 18:1108–1111
6. Garrity PA, Wold BJ (1992) Effects of different DNA polymerases in ligation-mediated PCR-enhanced genomic sequencing and in vivo footprinting. Proc Natl Acad Sci USA 89:1021–1025
7. Törmänen VT, Swiderski PM, Kaplan BE et al (1992) Extension product capture improves genomic sequencing and DNase I footprinting by ligation-mediated PCR. Nucleic Acids Res 20:5487–5488
8. Pfeifer GP, Tornaletti S (1997) Footprinting with UV irradiation and LMPCR. Methods 11:189–196
9. Pfeifer GP, Steigerwald SD, Mueller PR et al (1989) Genomic sequencing and methylation analysis by ligation mediated PCR. Science 246:810–813
10. Hughes S, Arneson N, Done S et al (2005) The use of whole genome amplification in the study of human disease. Prog Biophys Mol Biol 88:173–189
11. Sambrook J, Russell DW (2001) Molecular Cloning: A laboratory Manual (3rd ed), 32–36. Cold Spring Harbor Laboratory Press, Cold Spring Harbor
12. Masny A, Plucienniczak A (2003) Ligation mediated PCR performed at low denaturation temperatures—PCR melting profiles. Nucleic Acids Res 31:e114

13. Guilfoyle RA, Leeck CL, Kroening KD et al (1997) Ligation-mediated PCR amplification of specific fragments from a class-II restriction endonuclease total digest. Nucleic Acids Res 25:1854–1858
14. O'Malley RC, Alonso JM, Kim CJ et al (2007) An adapter ligation-mediated PCR method for high-throughput mapping of T-DNA inserts in the Arabidopsis genome. Nat Protoc 2:2910–2917
15. Prod'hom G, Guilhot C, Gutierrez MC et al (1997) Rapid discrimination of Mycobacterium tuberculosis Complex Strains by Ligation-Mediated PCR Fingerprint Analysis. J Clin Microbiol 35:3331–3334
16. Angers M, Cloutier JF, Castonguay A et al (2001) Optimal conditions to use *Pfu* exo$^-$ DNA polymerase for highly efficient ligation-mediated polymerase chain reaction protocols. Nucleic Acids Res 29:e83
17. Telenius H, Carter NP, Bebb CE et al (1992) Degenerate oligonucleotide primed PCR: general amplification of target DNA by a single degenerate primer. Genomics 13:718–725
18. Cheung VG, Nelson SF (1996) Whole genome amplification using a degenerate oligonucleotide primer allows hundreds of genotypes to be performed on less than one nanogram of genomic DNA. Proc Natl Acad Sci USA 93:14676–14679
19. Barbaux S, Poirier O, Cambien F (2001) Use of degenerate oligonucleotide primed PCR (DOP-PCR) for the genotyping of low-concentration DNA samples. J Mol Med 79:329–332
20. Dietmaier W, Hartmann A, Wallinger S et al (1999) Multiple mutation analyses in single tumor cells with improved whole genome amplification. Am J Pathol 154:83–95
21. Zhang L, Cui X, Schmitt K et al (1992) Whole genome amplification from a single cell: implications for genetic analysis. Proc Natl Acad Sci USA 89:5847–5851

Chapter 143
Isolation and Identification of a Bacterial Strain with Pullulanase Activity and the Cloning of the Pullulanase Gene

Guixiu Dong, Tao Xia, Yongqian Qiu, Xiaoliang Si, Yiyu Liu, Pingping Yang, Xiangzhao Mao and Lizhong Guo

Abstract A novel bacterial strain OPF-0031 with pullulanase activity was isolated from mud sample of the sea. With the analysis of the 16S rDNA sequence and the characterization of biochemical reactions, the strain was identified to be *Bacillus cereus*. A 2641 bp DNA fragment including a pullulanase gene from the genome of OPF-0031, was present. The nucleotide sequence of the gene encoding pullulanase was cloned and analyzed in *Escherichia coli*.

Keywords Gene cloning · Isolation · 16SrDNA · Pullulan hydrolase activity · Phylogenetic dendrogram

143.1 Introduction

Pullulanases are widely distributed among animals, plants, fungi, and bacteria, which hydrolyze the α-1,6-glucosidic linkages in pullulan, amylopectin, starch and related oligosaccharides [1].

Since a variety of microbial pullulanases have been obtained, they have been classified into four groups based on substrate specificities and reaction products [2,

G. Dong · T. Xia · Y. Qiu · X. Si · Y. Liu · X. Mao (✉)
College of Food Science and Engineering, Ocean University of China, Qingdao 266003, People's Republic of China
e-mail: xzhmao@ouc.edu.cn

G. Dong · P. Yang
School of Food and Bioengineering, Shandong Institute of Light Industry, Jinan 250353, People's Republic of China

L. Guo (✉)
Shandong Province Key Lab of Applied Mycology, Qingdao Agricultural University, Qingdao 266109, People's Republic of China
e-mail: lzgou@qau.edu.cn

T.-C. Zhang et al. (eds.), *Proceedings of the 2012 International Conference on Applied Biotechnology (ICAB 2012)*, Lecture Notes in Electrical Engineering 251,
DOI: 10.1007/978-3-642-37925-3_143,

3]: (i) neopullulanase (EC 3.2.1.135): pullulan hydrolase type I attacks α-1,4 glycosidic linkages in pullulan, forming panose; (ii) isopullulanase (EC 3.2.1.57): pullulan hydrolase type II can hydrolyze α-1,4 glycosidic linkages in pullulan, forming isopanose; (iii) In branched oligosaccharides or pullulan, pullulanase type I (EC 3.2.1.41) specifically attacks α-1,6 glycosidic linkages, linear oligomers or maltotriose were formed, respectively; and (iv) amylopullulanase: pullulanase type II attacks both α-1,6 glycosidic linkages in pullulan and branched substrates and the α-1,4 glycosidic linkages in polysaccharides.

Based on its characteristic, pullulanase has attracted significant attention as a useful tool in starch industry. So far, high value of pullulanase has been applied in the preparing resistant starch, cyclodextrin, maltotriose syrup, beer brewing, and maltotriose syrup.

To date, a large number of different microorganisms with pullulanases activity have been characterized [4–7]. Some of the isolates have been identified to be moderately aerobic thermophilic bacteria *Bacillus acidopullulyticus* [8], Bacillus flavocaldarius KP 1228 [9], *Thermus aquaticus* YT-1 [10], *Thermus caldophilus* GK-24 [11], extreme anaerobic bacterium *Thermotoga maritima* [12], and *Anaerobranca gottschalkii* [13]. Due to high temperatures of 95–105 Centigrade running in the liquefaction process of starch, the absence of thermostable pullulanase has been essential [14]. Most of strains have no potential interest in the industries, for their low expression level or thermolability. Some strategies which include optimization of the culture conditions [15] and the construction of mutant strain et al. were carried out to enhance the enzyme yield from the wild strains by many investigators. To change the culture condition of pullulanase production, some genes of hyperthermophilic strains have been cloned and expressed by the inducer appearance in the host *Escherichia coli* [16] and *B. Subtilis* [17]. Mutant strain, which is catabolite repression resistant, was also screened for enzyme synthesis [18]. However, low biomass yield and complicated culture conditions of recombinant and wild strains lead to higher production costs. Up to now, the only strains used for enzyme industrial production, were *Bacillus acidopullulyticus* and *Bacillus deramificans* from Novo and Genencor respectively. In this study, the work which focuses on the isolation and identification of the microorganism with pullulanase activity was described. Based on the physiological and biochemical characteristics and the analysis of 16S rDNA gene sequence, the strain OPF-0031 was classified to be genus *Bacillus cereus*. Furthermore, the gene encoding pullulanase has been obtained and analyzed, which would be used in the expression of the recombinant enzyme.

143.2 Materials and Methods

143.2.1 Culture Conditions

The enrichment medium contained, per liter: 15 g glutinous rice starch, 10 g peptone, 2 g yeast powder, 0.5 g $MgSO_4 \bullet 7H_2O$, 1 g NaCl, 1 g K_2HPO_4, pH 7.0.

Screening agar plates contained, per liter: 10 g glutinous rice starch, 5 g peptone, 0.1 g Na_2HPO_4, 0.15 g KH_2PO_4, 0.5 g $MgSO_4 \bullet 7H_20$, 1 g NaCl, 18 g agar, pH 7.0.

Fermentation cultures contained, per liter: 15 g soluble starch, 10 g peptone, 5 g yeast powder, 0.5 g $MgSO_4 \bullet 7H_2O$, 1 g NaCl, 1 g K_2HPO_4, pH 7.0.

143.2.2 Pullulan-Utilizing Strain Isolation

5 g soil samples were collected from the sea in China and diluted with 50 mL of sterile physiological water.

1 mL of diluted mud soil were inoculated in 50 mL of sterile enrichment medium in a 250 mL flask and were grown with shaking at 200 rpm in an incubator at 32 °C. After 24 h of incubation, a 1 mL enrichment medium was diluted to 10–7 dilution of the original soil sample with sterile physiological water. The serial dilutions spreaded on solid medium were incubated at 32 °C for 48 h. To ensure the selected isolations containing pullulanase degrading strains, they were inoculated in fermentation cultures and incubated under the same conditions mentioned above.

143.2.3 Enzyme Assays

One unit of enzyme activity was defined as the amount of enzyme that releases 1 mmol of reducing sugars per minute and expressed as U/mL.

Cell-free fermentation cultures were obtained by centrifugation (8000×g for 10 min at 4 °C) and incubated with pullulan for determining pullulanase activity by measuring the amount of reducing sugars. To 500 μL of 1 % (wt/vol) pullulan dissolved in 300 μL of 0.2 M phosphate buffer (pH 7.0), 200 μL of culture filtrate was added and the samples were incubated at 32 °C for 30 min. The reaction was terminated and the amount of reducing sugars released was assayed by the DNS. Blanks were prepared to correct for the reducing sugars of fermentation cultures [19].

143.2.4 Identification of Strain OPF-0031

Chromosomal DNA of strain OPF-0031 was obtained with TIANamp Bactria DNA kit (Tiangen Biotech (Beijing) Co., Ltd) and used as template for amplification. Two primers 27F (5′-AGAGTTTGATCCTGGCTCAG-3′) and 1492R (5′-GGTTACCTTGTTAC-GACTT-3′) designed from the conserved zones of 16S rDNA operon in *E. coli*, were used for PCR amplification of the 16S rDNA gene. The genomic DNA of OPF-0031 was used as template with PCR profile carried out at the following temperature: denaturation at 94 °C for 4 min, 30 cycles of denaturation at 94 °C for 30 s, primer annealing at 60 °C for 30 s and extension at 72 °C for 90 s, and the final extension at 72 °C for 90 s. Amplicons were purified using TIANgel Midi Purification (Tiangen Biotech (Beijing) Co., Ltd). After purification, PCR products were sequenced by Sangon Biotech (Shanghai) Co., Ltd. The nucleotide sequences of 16S rRNA gene have been assayed by BLAST search algorithm and public databases of GeneBank.

143.2.5 Molecular Cloning of a Gene Encoding Pullulanase

Two primers BC-1 (5′-GGAATTCCATATGGT-GCAAATTACAAAA-3′) and BC-2 (5′-CGGGATCC-TTATTTAATCGGTTTCTCT-3′) designed from the conserved zones of pullanase gene, were used for PCR amplification and sequencing of the gene encoding pullulanase. The sample with genomic DNA of OPF-0031 as the template was heat-denatured for 7 min at 94 °C and the thermal profile consisted of 32 cycles of denaturation at 94 °C for 45 s, annealing at 52 °C for 45 s, and extension at 72 °C for 3.30 min, and the final extension at 72 °C for 8 min. The PCR product linked with PMD19-T vector for sequencing was cloned into *E. coli* [20]. The recombinant stains were spread on LB agar plates for 16 h at 37 °C of positive clones allowed the identification of recombinant plasmid carrying the pullulanase gene (pulOPF-0031) from OPF-0031. The nucleotide sequences of recombinant plasmid have been assayed by Sangon Biotech (Shanghai) Co., Ltd. After gel electrophoresis, the PCR products was isolated with a TIANgel Midi Purification (Tiangen Biotech (Beijing) Co., Ltd). Recombinant plasmids were purified with a TIANprep Mini Plasmid kit (Tiangen Biotech (Beijing) Co., Ltd).

143.3 Results and Discussion

143.3.1 Isolation and Physiological Characteristics of the Bacterium

A novel Gram+, nonmotile bacteria named OPF-0031 were isolated from mud samples of the sea in China and showed pullulan hydrolysis activity in flask fermentation. The detailed physiological characteristics of OPF-0031 were investigated and compared with *Bacillus cereus* as shown in Table 143.1. Catalase reaction was positive, as well as liquefaction of gelatin, starch hydrolysis, pullulan reduction, voges-proskauer test, urease, methyl red test, and hydrolysis of casein. However, oxidase reaction was negative; so were tests for hydrolysis of chitin. The isolate OPF-0031 could utilize glucose, fructose, and maltose. But arabinose, mannose, sucrose, lactose, galactose, and D-sorbitol were not observed to be resolved. Pellicle was not observed in process of the fermentation, too.

Table 143.1 Comparison of conventional chemical characteristics for strain OPF-0031 and *Bacillus Cereus*

Characteristics	OPF-0031	*Bacillus cereus*
Catalase	+	+
Hydrolysis of gelatin	+	+
Hydrolysis of starch	+	+
Voges-Proskauer test	+	+
Methyl red test	+	+
Urease	+	−
Hydrolysis of casein	+	+
Hydrolysis of chitin	−	+
Glucose	+	+
Fructose	+	+
Maltose	+	+
Arabinose	−	+
Mannose	−	−
Sucrose	−	+
Lactose	−	−
Galactose	−	−
D-sorbitol	−	−
Pellicle	−	−

+ Positive, − negative

143.3.2 Identification of Strain Opf-0031

By means of analyzing nucleotide sequences of known bacteria in NCBI, the isolate OPF-0031 were inferred to be the genus Bacillus and showed a closest match (99 %) with *Bacillus cereus* strain Cr-50 (accession no. JF895490.1). The sequence was deposited in the GenBank database with accession no. JQ824137. Based on the physiological characteristics and its 16SrDNA gene sequence, the strain OPF-0031 was identified as a number of *Bacillus cereus*, and thus named as *Bacillus cereus* OPF-0031.

143.3.3 Molecular Cloning of a Gene Encoding Pullulanase Activity

The 2641 bp PCR fragment was obtained through the method described above. Several recombinants AmpR clones were tested for pullulanase activity. A total of three clones, which carried an insert of 2641 bp pullulanase gene (pulOPF-0031) fragment from *Bacillus cereus* OPF-0031 strain, were detected by colony PCR. The cultivation of three positive clones in LB medium allowed the extraction of the recombinant plasmid. The entire nucleotide sequence of the gene is shown in NCBI.

The sequence of pulOPF-0031 has a very high similarity (99 %) with the pullulanase gene of *Bacillus cereus* F837/76 (accession no. CP003187.1) listed in gene bank. The sequence was deposited in the GenBank database with accession No. JQ707952.

In this study, a bacterial strain, which has been isolated and identified, offers new industrial opportunities in the saccharification of starch. The pullulanase reducing unhydrolysed residues may be more compatible with the amylases in the process of amylopectin hydrolysis at high temperatures. In further research, medium compositions of *Bacillus cereus* OPF-0031 would be optimized and optimal recombinants would also be constructed to improve the yield of pullulanase.

Acknowledgments This work was supported by the Fundamental Research Funds for the Central Universities (201262021) and Grants from National Undergraduate Innovative Experiment Plan.

References

1. Norman BE (1982) A novel debranching enzyme for application in the glucose syrup industry. Starch/Stärke 34:340–346
2. Bertoldo C, Duffner F, Jorgensen PL et al (1999) Pullulanase type I from *Fervidobacterium pennavorans* Ven5: cloning, sequencing and expression of the gene and biochemical characterization of the recombinant enzyme. Appl Environ Microb 65:2084–2091

3. Fiona D, Costanzo B, Jens TA et al (2000) A New thermoactive pullulanase from *Desulfurococcus mucosus*: cloning, sequencing, purification, and characterization of the recombinant enzyme after expression in *Bacillus subtilis*. J Bacteriol 22:6331–6338
4. Amitava R, Messaoud EB, Bejar S (2003) Isolation and purification of an acidic pullulanase type II from newly isolated *Bacillus* sp. US149. Enzyme Microb Tech 33:720–724
5. Melasniemi H (1987) Characterization of alpha-amylase and pullulanase activities of *Clostridium thermohydrosulfuricum*. Biochem J 246:193–197
6. Kim JH, Sunako M, Ono H et al (2003) Characterization of gene encoding amylopullulanase from plant-originated lactic acid bacterium, *Lactobacillus plantarum* L137. J Biosci Bioeng 106:449–459
7. Fujita N, Toyosawa Y, Utsumi1 Y et al (2009) Characterization of pullulanase (PUL)-deficient mutants of rice (*Oryza sativa L.*) and the function of PUL on starch biosynthesis in the developing rice endosperm. J Exp Bot 60:1009–1023
8. SChülein M, Pedersen BH (1984) Characterization of a new class of thermophilic pullulanases from Bacillus acidopullulyticus. Ann N Y Acad Sci 434:271–274
9. Suzuki Y, Htagaki K, Oda H (1986) A hyperthermostable pullulanase produced by an extreme thermophile, *Bacillus flavocaldarius* KP 1228, and evidence for the proline theory of increasing thermostability. Appl Microbiol Biotechnol 34:707–714
10. Plant AR, Morgan HW, Daniel RM (1986) A highly stable pullulanase from *Thermus aquaticus* YT-1. Enzyme Microbiol Technol 8:668–672
11. Bertoldo C, Armbrecht M, Becker F et al (2004) Cloning, sequencing, and characterization of a heat- and alkali-stable type I pullulanase from *Anaerobranca gottschalkii*. Appl Environ Microbiol 70:3407–3416
12. Kim CH, Nashiru O, Ko JH (1996) Purification and biochemical characterisation of pullulanase type I from *Thermus caldophilus* GK-24. FEMS Microbiol Lett 138:147–152
13. Bibel M, Brettl C, Gosslar U et al (1998) Isolation and analysis of genes for amylolytic enzymes of the hyperthermophilic bacterium *Thermotoga maritima*. FEMS Microbiol Lett 158:9–15
14. Koch R, Canganella F, Hippe H et al (1997) Purification and properties of a thermostable pullulanase from a newly isolated thermophilic anaerobic bacterium, Fervidobacterium pennavorans Ven5. Appl Environ Microbiol 63:1088–1094
15. Rama Mohan Reddy P, Reddy G, Seenayya G (1999) Production of thermostable pullulanase by *Clostridium thermosulfurogenes* SV2 in solid-state fermentation: optimization of nutrients levels using response surface methodology. Bioproc Biosyst Eng 21:497–503
16. Albertson GD, McHale RH, Gibbs MD (1997) Cloning and sequence of a type I pullulanase from an extremely thermophilic anaerobic bacterium, *Caldicellulosiruptor saccharolyticus*. Biochim Biophys Acta 1354:35–39
17. Duffner F, Bertoldo C, Andersen JT et al (2000) A new thermoactive pullulanase from *Desulfurococcus mucosus*: cloning, sequencing, purification, and characterization of the recombinant enzyme after expression in *Bacillus subtilis*. J Bacteriol 182:6331–6338
18. Hyun HH, Zeikus JG (1985) Regulation and genetic enhancement of glucoamylase and pullulanase production in *Clostridium thermohydrosulfuricum*. J Bacteriol 164:1146–1152
19. Miller GL, Chem A (1959) Use of dinitrosalicylic acid reagent for determination of reducing sugars. Anal Chem 31:426–428
20. Doman-Pytka M, Bardowski J (2004) Pullulan degrading enzymes of bacterial origin. Crit Rev Microbiol 30:107–121

Chapter 144
Study on ^{60}Coγ-Ray Irradiation Mutation of *Bacillus subtils* natto

Yufeng Xie and Yingliang Ge

Abstract Soybean meal (SBM) was widely used as raw material in plant protein industry. *Bacillus subtilis* natto was the beneficial bacteria of generating a variety of protease, which could degrade plant protein of SBM, so as to improve the hydrolysis degree (DH) of plant protein. *Bacillus subtilis natto* was commonly treated by ultraviolet ray(UV), Lithium chloride(LiCl), nitrosoguanidine (NTG), diethyl sulphate (DES) at home and abroad, but it had not been reported that bacillus natto was treated by ^{60}Coγ gamma rays (^{60}Coγ). Different dosages of ^{60}Coγ irradiation and 0.85 % Lithium chloride were used as mutagen in treating *Bacillus subtils* natto HRBX0. Result showed that when 400 Gy dosage was used, which led to a 95 % spore death rate with the positive mutation rate 14.5 %, good mutagenic effect occured. DH of defatted SBM in solid-state fermentation of the mutant HRBX6 increased from original 19.5 % to 30.6 %, increased by 56.9 %. It showed a good genetic stability and stably DH of defatted SBM with the experiments of the mutant after continuous cultivation for five generations and obviously exceeded the original strain. It showed that ^{60}Coγ was an effective factor of mutagenic breeding of *Bacillus subtilis* natto.

Keywords ^{60}Coγ · Mutation · DH · *Bacillus subtils* natto

Y. Xie (✉) · Y. Ge
Department of Food Engineering, Haerbin University, Haerbin 150080, China

Y. Xie
College of Biotechnology, Tianjin University of Science and Technology, Tianjin 300457, China

T.-C. Zhang et al. (eds.), *Proceedings of the 2012 International Conference on Applied Biotechnology (ICAB 2012)*, Lecture Notes in Electrical Engineering 251,
DOI: 10.1007/978-3-642-37925-3_144,

144.1 Introduction

Bacillus species have been major workhorse industrial microorganisms with roles in applied microbiology, which date back more than a thousand years, since the production of natto by solid-state fermentation of SBM using *Bacillus subtilis* natto is first practiced in Japan. The production of protein for raw materials has exceeded 100 million tons with the development of China in the past 20 years, but at the same time it has become a prominent problem on shortage of resources especially the protein for raw materials [1]. SBM is the major source of protein in animal diets used in China and several other countries, and is widely used as the plant protein industrial raw material [2].

Not high DH is obtained by using the current strains. Much is now known about the biochemistry, physiology, and genetics of *B. subtilis* natto, which facilitates further development and greater exploitation of these organisms in industrial processes. So we need mutants of *B. subtilis* natto. It is reported that *B. subtilis* natto is almost handled by a various of physical or chemical mutagens in domestic and foreign by using UV, LiCl, NTG, DES, and so on [3]. It has not been reported that *B. subtilis* natto is handled by ^{60}Coγ. When SBM is subjected to fermentation with the mutant strain HRBX6, most of the total amino acids increased significantly and only few of them suffer a decrease depending on the type of the fermentation.

Bacillus subtilis natto HRBX0(HRBX0) was used as the original strain. It was processed by different doses of ^{60}Coγ, and then screened the mutant strain. So the HRBX6 with the high DH was obtained. The results showed that the nutritional quality of SBM and its utilization rate of the protein industry was improved.

144.2 Materials and Methods

144.2.1 Original Strain

HRBX0: It was preserved by microbiology laboratory in Harbin institute.

144.2.2 Materials

144.2.2.1 SBM

Defatted SBM containing 48 % protein was purchased from market.

144.2.2.2 Chemicals

PITC (phenylisothiocyanate 99 %) and DL-norleucine were obtained from Sigma. Medium were from "Beijing Land Bridge Technology Co., Ltd". All the other analytical chemicals were from Merck.

144.2.2.3 Medium

Liquid broth medium(%): yeast extract 0.3, peptone 1.0, sodium chloride 0.5, pH 7.4–7.6, and sterilization for 20 min at 121 °C.

Solid broth medium(%): yeast extract 0.3, peptone 1.0, sodium chloride 0.5, agar 2.0, pH 7.0 ~ 7.2, and sterilization for 20 min at 121 °C.

Fermentation medium(%): SBM: bran(35) = 9:1, water 65, pH 5.4 ~ 6.6, and sterilization for 20 min at 121 °C.

144.2.3 Strain Breeding

144.2.3.1 Mutagenic Treatment

0.85 % LiCl and saline were added in the fresh slant HRBX0, and made the bacterial suspension of the concentration 10^8 cfu/ml with filtered by cotton after shocking [4]; HRBX0 was irradiated with the dosage of 100 Gy, 200 Gy, 300 Gy, 400 Gy, 500 Gy, and 600 Gy; The number of the bacterial suspension before and after radiation was counted by using the plate dilution method, the number of the unirradiated colony C and irradiated colony D was counted, and the death rate R and the positive mutation rate P was calculated

$$P = S/D \tag{1}$$

P positive mutation rate
S degree of hydrolysis after the irradiated to improve the number of colonies
D after the irradiated the sum total of colonies.

144.2.3.2 Screening Mutations

Plate after diluting the bacterial suspension of mutagenic treatment with appropriate method was spreaded, 30 °C for 2 days, the number of colonies was observed and counted. The single colony with big shape, smooth surface, surrounding sticky to screening was selected. The single colony of screening was

rescreened in the fermentation medium under the condition 37 °C, 60 h [5]. DH of SBM in the fermentation broth was determined and calculated, and the strains were saved which can make the DH of SBM higher.

144.2.3.3 Verify the Genetic Stability of Mutations

The rescreening strains were transferred continuously to culture to the fifth generation and ferment separately, DH of SBM was determined and calculated, the DH with their each original strain was compared, genetic stability was observed [6].

144.2.4 Culture Method

HRBX0 was grown in stock and maintained on Solid broth medium for 9 h at 37 °C. The cells were washed twice in sterile saline solution and inoculated to give a final inoculation of 10^7 cfu/ml. HRBX0 was grown in Liquid broth medium broth for 14 h at 37 °C, and then washed twice in sterile saline solution and inoculated to give a final inoculation of 10^7 cfu/ml.

144.2.5 Fermentation

Seven small-scale solid fermentations were performed in fermentation medium, including natural fermentation (carried out with the only microorganisms HRBX0), and six different induced fermentations with each of the microorganisms mentioned above in Sect. 144.2.3. Suspensions of fermentation medium were prepared and were allowed to ferment either spontaneously (no microorganisms added). The fermentation processes were carried out in a fermentor for 60 h at 37 °C. Samples were collected at times 0 and 60 h for pH and microbiological analyses. Fermented samples were freeze-dried for further analysis.

144.2.6 Analytical Methods

144.2.6.1 Determinations of Biomass

Method of absorbance values at 660 nm, method of dry weight.

144.2.6.2 Counts of Bacterial Suspension

The fermentation process was monitored by withdrawing samples at times 0 and 48 h using plate counts to determine changes in viable cells. It was measured by microscope count method and plate count method.

144.2.6.3 Analysis of Amino Acids by HPLC

Determination of amino acids was carried out by acid hydrolysis, derivatization, and HPLC quantification. In brief, 200 μl (0.2 mmol/ml) of DL-norleucine were added to 50 mg of sample as internal standard. Protein hydrolysis was carried out with 6 M HCl for 21 h at 110° C in a vacuum closed vial. Hydrolysates were dried under vacuum and rinsed twice with water. PITC (phenylisothiocyanate 99 %) was used for amino acid derivatization.

144.2.6.4 DH

Alpha-amino nitrogen (AN) was assayed in duplicate by the formol titration procedure. Total nitrogen (TN) was measured also in duplicate by the microK-jeldahl method. The percent degree of hydrolysis (DH) was calculated as in (1):

$$\% \text{ DH} = \text{An}_\text{h} - \text{AN}_\text{c}/\text{TN} \times \text{P}_\text{f} \times 100 \quad (2)$$

where An_h and AN_cwere the percent amino nitrogen of the hydrolysate and intact SBM, respectively. No significant difference was found between total nitrogen of the intact SBM and that of the hydrolysates.

Therefore, TN in Eq. (1) referred to the mean percent total nitrogen of the intact SBM solution and all hydrolysate samples, and P_f was a correction factor for side chain nitrogen which could not be converted to amino nitrogen by hydrolysis of peptide bonds. The P_f factor (0.777) was calculated from the amino acid profile of SBM.

144.3 Results and Discussion

144.3.1 Selection of the Dose of ^{60}Coγ

HRBX0 was irradiated with the dosage of 100 Gy, 200 Gy, 300 Gy, 400 Gy, 500 Gy, 600 Gy, and the death rate and the positive mutation rate were calculated, the results were shown in Figs. 144.1 and 144.2.

As shown in Fig. 144.1, different doses of rays all had the lethal effect to HRBX0, and death rate increased with the increasing of the radiation dose; when the radiation dose was 100 Gy, the death rate of the cells reached 68.25 %, and when 500 Gy, the death rate almost 100 %.

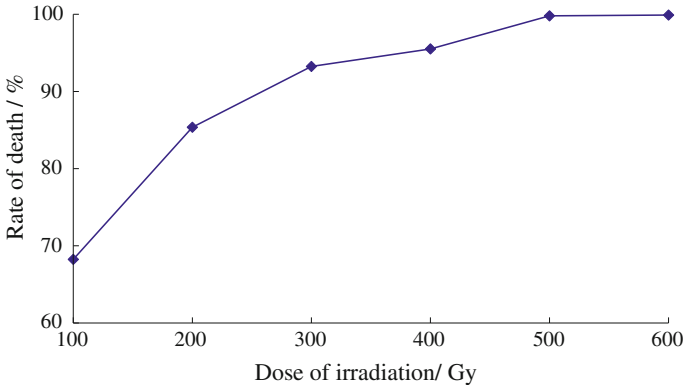

Fig. 144.1 Relationship between irradiation dose and rate of death

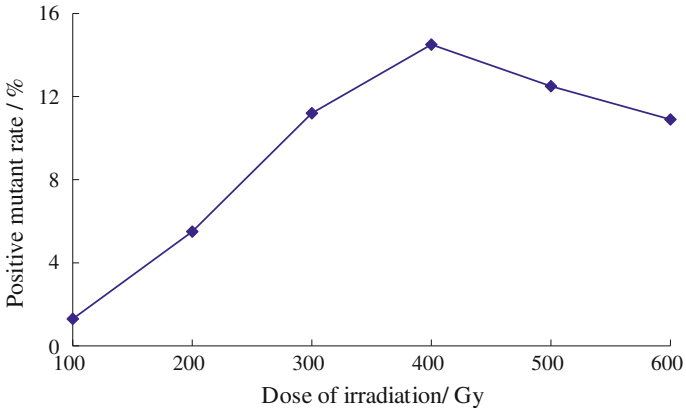

Fig. 144.2 Relationship between irradiation dose and positive mutation rate

As shown in Fig. 144.2, varying degrees of positive mutation rate of the strains appeared with different radiation doses, it showed that the mutagenesis by using ^{60}Coγ is effective; mutants had higher positive mutation rate when the radiation dose was 400 Gy or 500 Gy, especially when 400 Gy, positive mutation rate reached 14.5 %. In order to improve test efficiency, the mutants were selected which were irradiated with the radiation dose 400 Gy to fermentations test for screening the mutants of higher DH.

144.3.2 Result of ^{60}Coγ Irradiation

HRBX0 was irradiated with the dosage of 400 Gy, and the death rate and the positive mutation rate were calculated, the DH of SBM were obtained by fermentations test, the results were shown in Table 144.1.

Table 144.1 Result of $^{60}Co\gamma$ irradiation on HRBX0 strains

Irradiation dose/ Gy	Death rate/ %	Positive mutant rate/ %	DH (average value)/ %	Increase rate/ %
400	95.51	14.5	30.6	56.9

Table 144.2 Effect of generation on stability of degree of hydrolysis of mutation strains

Bacillus subtilis *natto*	Generation					
	1	2	3	4	5	Average value
HRBX0(DH)/%	19.3	19.0	19.7	19.3	19.5	19.36
HRBX6(DH)/%	31.1	30.5	30.2	30.8	30.7	30.62

Positive mutation rate of HRBX0 was 14.5 % with the optimized conditions of $^{60}Co\gamma$, the DH of SBM in solid-state fermentation of the mutant HRBX6 increased from original 19.5 to 30.6 %, increased by 56.9 %. The capacity of hydrolyzing soybean meal improved significantly higher than the original strain.

144.3.3 Result of Solid-State Fermentation and Stability Test with the Positive Mutant HRBX6

The positive mutant HRBX6 was obtained by screening, DH of defatted SBM with the fermentation experiments of the mutant after continuous cultivation for five generations were compared, the results were given in Table 144.2.

The positive mutation strain HRBX6 showed a good stably DH of defatted SBM with the experiments after continuous cultivation for five generations, the average of the DH increased from original 19.36 to 30.62 %, increased by 58.1 %. The capacity of the degree of hydrolysis was close from the fifth generation to first generation of mutant strain HRBX6, and it showed a good genetic stability of HRBX6.

144.4 Conclusion

Different doses of rays all have the lethal effect to HRBX0, and death rate increases with the increasing of the radiation dose; when the radiation dose is 100 Gy, the death rate of the cells reach 68.25 %, and when the radiation dose is 500 Gy, the death rate of the cells reach almost 100 %, and mutants have higher positive mutation rate when the radiation dose is 400 and 500 Gy, especially when 400 Gy, positive mutation rate reach 14.5 %.

HRBX0 was used as the original strain. It was processed by different doses of ^{60}Coγ, and then screened the mutant strain. The mutation strain HRBX6 with the high DH was obtained by different doses of ^{60}Coγ and screened the mutant strain, it showed a good genetic stability and the DH increased from original 19.36 to 30.62 %, increased by 58.1 %. ^{60}Coγ is an effective factor of mutagenic breeding of *Bacillus subtilis* natto.

Acknowledgments The authors wish to thank the projects supported by the Research of Science and Technology of Education Bureau of Heilongjiang Province, China(Grant No12523032).

References

1. Shih IL, Yu YT (2005) Simultaneous and selective production of levan and poly(γ-glutamic acid) by Bacillus subtilis. Biotechnol Lett 27:103–106
2. Ma XN, Hui M, Niu TG (2005) The isolation of a flocculant-producing bacillus and identification of microbial flocculant. Microbiol 32:26–31
3. Barbosa AM et al (2010) Extracellular β-glucosidase production by the yeast Debaryomyces pseudopolymorphus UCLM-NS7A: optimization using response surface methodology. New Biotech 27:374–381
4. Shi QQ, Wu SG (2003) Industrial microbial breeding science. Science Press, Beijing
5. SANG L, XU H, LI H et al (2004) Screening of Bacillus subtilis PGAN-12 and production of γ-polyglutamic acid by fermantation. " Chin J process Eng" (in Chinese) 4:462466
6. Huang J,Mei LH,Hu S et al (2005) Screening of Bacillus subtilis natto from traditional Japanese food natto and separation of nattokinase. "J Chem Eng Chin Univ" (in Chinese) 19:518522

Chapter 145
Effects of Different Processing Methods on Oyster DNA

Ping Dong, Ran An, Xiushuang Jia, Dong Han and Xingguo Liang

Abstract Chemical state of nucleic acids in oyster affects its flavor and gene analysis. In this study, the effect of food processing on oyster DNA was studied. After processing fresh oysters by microwave, freeze−thaw , grinding, salting, high temperature, DNA, and free bases were extracted. DNA was analyzed by gel electrophoresis, and free bases were determined by LC-MS. The results showed that oyster DNA was affected differently by the five processing methods. Microwave brought out the denatured DNA, high-temperature caused the rupture of genomic DNA, both freeze–thaw and grinding affected the molecular weight of oyster DNA slightly, while salting can increase the stability of DNA in oyster. Bases showed different sensitivity to the applied processing methods. Base pair G-C escaped from DNA strands together. High-temperature caused depurination. The results will be helpful for the development of typical flavor food, analysis of DNA from processing food, and studies on nucleic acids metabolism diseases.

Keywords Oyster · DNA · Free base · Processing

145.1 Introduction

Oyster is a group of bivalve molluscs living in temperate and tropic sea. As a very important economy shell fish, oyster is the main components of mollusc production [1]. As we known, oyster is so delicious that it is greatly popular all over the world. A lot of oyster products were developed to meet the needs of the consumers, including raw oyster, stream oyster, fried oyster, canned oyster, salty

P. Dong · R. An · X. Jia · D. Han · X. Liang (✉)
College of Food Science and Engineering, Ocean University of China,
Qingdao 266003, People's Republic of China
e-mail: Liangxg@ouc.edu.cn

T.-C. Zhang et al. (eds.), *Proceedings of the 2012 International Conference on Applied Biotechnology (ICAB 2012)*, Lecture Notes in Electrical Engineering 251,
DOI: 10.1007/978-3-642-37925-3_145,

oyster, smoked oyster, dried oyster, etc. And it is also the major material to make oyster sauce which is a popular flavoring sauce in China.

As reported, oyster is a kind of sea food with higher nucleic acids content. Only mentioning purines, the total content is up to 176 mg/100 g [2]. Intake of nucleic acids still has some controversies. (1) Germany researchers investigated foreign DNA in mammalian systems from 1990s. Their results demonstrated that some foreign DNA fragments supplied by daily food survived from gastrointestinal (GI) tract and retrieved in many organs, including blood, peripheral leukocytes, spleen, and liver [3]. Surprisingly, the uptaken foreign DNA can also penetrate the placental circulatory system and reach the offspring of pregnant animals [4]. The survival foreign DNA may have some biological significance on host mammalians. It is inconsistent to the traditional nucleic acids metabolism theory considering that the foreign DNA is broken into nucleotides, nucleosides, and bases before assimilated by small intestine [5]. The metabolite excretes with urine. (2) Metabolic abnormalities of nucleic acids, especially purine, are supposed to be one pivotal cause of gout and hyperuricacidemia [6, 7]. (3) Supplementary nucleic acids in animal feed are getting more and more attentions. It is reported that dietary supplements will enhance immunity and disease resistance of fish and pigs [8, 9]. Nucleic acids also play important roles in infant milk because of the significant differences in the nonprotein nitrogen nucleotide pool between bovine and human milk [10, 11]. (4) Moreover, nucleotides or other nucleic acids degradation products, like IMP and GMP, may significantly contribute to food flavor. They can greatly enhance the food flavor by combination with monosodium glutamate [12, 13].

As described above, nucleic acids in oyster may have effects on its quality and its biofunctions. We need to figure out the state of nucleic acids in a food, which is also important for the gene analysis. Obviously, food processing may cause great structure changes of nucleic acids. However, effects of food processing on nucleic acids have not been reported. Here, we adopted DNA in oyster (Qingdao, China) as our study material to investigate the changes of DNA sizes and removal of bases during microwave, freeze–thaw, grinding, salting, and high-temperature processing.

145.2 Materials and Methods

145.2.1 Materials

Oyster was collected in the local farm in Qingdao, Shandong province, China. They were kept in iced sea water during the transportation. After arrived in the lab, they were processed immediately.

Ethidium bromide, proteinase K, and marine animals genomic DNA extraction kit were purchased from Tiangen Biotech (Beijing) Co., Ltd. Acrylamide, N, N'-methylenebisacrylamide, ammonium persulfate (AP) and N, N, N', N'-tetramethylethylenediamine

(TEMED) were supplied by Sangon Biotech (Shanhai) Co., Ltd. Ladder of Lambda DNA-HindIII digest, 1 kb ladder and 100 bp ladder were bought from New England Biolabs Inc. (Ipswich, MA, US). Regular agarose G-10 was manufactured by Biowest SAS (France). Guanine (G), adenine (A), cytosine (C), and thymine (T) were purchased from Sigma-Aldrich Co. LLC. HPLC-grade ethanol was supplied by J.T. Baker Chemical Company (USA). Highly purified water (resistivity $\geq$ 18 M, E-pure water system, Sartorius, German) was used. All other chemicals were analytical reagent grade or HPLC-grade supplied by local companies.

145.2.2 Processing Methods

Oyster was processed with five methods.

(1) Microwave. Oyster was cooked with high, medium, and low power styles. The employed microwave instrument is a normal household microwave oven with 2,450 MHz frequency and 20 L volume. We choose three power steps, high level (HL), medium level (ML), and low level (LL). Output power of HL step is 100 % of microwave energy, ML step is 77 % and LL step is 55 %. One whole fresh oyster meat around 2–3 g was collected into a 10 cm petri dish and covered with a piece of cling film. The cooked time is 0.5–2 min.
(2) High temperature. One whole fresh oyster meat around 2–3 g was collected into a 100 mL beaker and sealed with a piece of parafilm. Oyster samples were treated at 121 °C or 100 °C in sterilization pot for 10 min or 20 min.
(3) Grinding. One whole oyster meat was grinded continuously in a mortar for 10 min under room temperature.
(4) Freeze–thaw. Fresh oyster meat was frozen under −20 °C overnight. Then put it in the room temperature to thaw completely. Repeat these freeze–thaw procedures for 10 times.
(5) Salting. Fresh oyster meat was mixed with NaCl (3.0 g/g oyster meat) and placed under room temperature for 24 h. Then salted oyster meat was washed with distilled water three times, ready for DNA and free bases extraction.

145.2.3 Extraction of DNA

DNA of fresh and processed oyster meat was extracted using optimized "Marine Animals Genomic DNA Extraction Kit (Tiangen Biotech, Beijing)" procedures. One whole oyster meat was cut into small pieces and mixed together. Around 30 mg meat was weighted and put into a 1.5 ml centrifuge tube. 200 μL of GA buffer and 20 μL of proteinase K solution (20 mg/mL) were added into the tube, mixing well by vortex. Left the tube at 56 °C for about 1 h to dissolve the animal tissue completely. Then add 200 μL of GB buffer, put the tube at 70 °C for 10 min. After that, 200 μL of 100 % ethanol and CB3 column were added,

centrifuge at 12,000 rpm for 30s, and remove the upper solution. Then wash CB3 column with 500 μL of GD buffer, 700 μL of PW solution, and 500 μL of PW solution. Leave CB3 column at room temperature for several minutes to dry the wash solution. Then add 50–200 μL elution solution into the middle of CB3 column, 5 min latter centrifuge it at 12,000 rpm for 2 min. The upper solution was collected for electrophoresis analysis.

145.2.4 Extraction of Free Bases

Free bases were extracted by distilled water. Two grams of fresh or processed oyster meat were homogenated and dipped in 3.0 mL distilled water. Mixtures of meat and water were sonicated for 20 min. Then mixtures were centrifuged with 10,000 rpm for 5 min. The supernatant was collected. Repeat the extraction procedures three times. Combined the supernatants and added water to 10 mL. The extracted solutions were filtrate with 0.45 μm film, ready for HPLC analysis.

145.2.5 Analysis of Genomic DNA in Oyster Meat by Electrophoresis

Extracted DNA solutions (8.0 μL) were electrophoresed on 1 % agarose gel as described previously [14].

145.2.6 Analysis of Free Bases by LC-MS

Extracted free bases solutions and standard bases solution were analyzed with an Agilent G6410B series (Palo Alto, CA), an Agilent G1314A variable wavelength detector (VWD) and an YMC C18 column (4.5×150 mm, particle size 3 μm). The flow rate was 0.5 mL/min, the column temperature was 25 °C, the detection wavelength was 260 nm, and the injection volume was 10 μL. The mobile phases were composed of 0.05 mol/L ammonium formate (dissolved in water) and methanol. Gradient elution was applied in our analysis, 2 % methanol was increased to 12 % in 20 min, and then methanol went back to 2 % in 5 min.

Electrospray ionization (ESI) was performed in the positive mode with an ionspray voltage of 4,000 V. The heated nebulizer temperature was set at 350 °C and flow rate was set at 9 L/min.

Standard bases solutions including guanine (G), adenine (A), cytosine (C), and thymine (T) were diluted in 0.6 % HCl with concentrations from 5.0 to 50 μg/mL. The peaks were recognized by MS spectrum, while the peak areas were calculated

with the absorbance under 260 nm. Calibration curves were obtained by peak areas of bases against the concentrations of standard solutions. Every concentration level was analyzed in three replications. Concentrations of the free bases in fresh or processed oyster were calculated using the calibration curves.

145.3 Results and Discussion

145.3.1 Analysis of DNA from Fresh Oyster

Genomic DNA in fresh oyster meat was shown in Fig. 145.1. A wide smeared band ranged from 200 bp to 20 kb and a bright band around 20 kb was observed (Lane 3 in Fig. 145.1).

145.3.2 Effects of Microwave Processing

After processing by three different microwave power levels, genomic DNA in oyster meat was analyzed by agarose gel electrophoresis. Result was shown in Fig. 145.2. Compared to DNA in fresh oyster meat, DNA in microwave processed oyster meat was gathered in gel wells, especially ML and HL microwave processed oyster (lane 5 and lane 6). It demonstrated that state of DNA in oyster meat was changed greatly by microwave. DNA in gel wells was thought to be denatured DNA or DNA and protein complex probably formed by instantaneous heat of microwave.

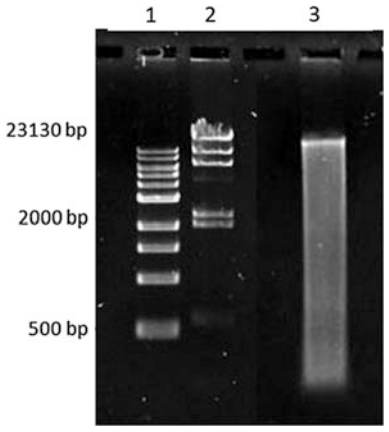

Fig. 145.1 Gel electrophoresis of DNA in fresh oyster meat. Lane 1, 1.0 kb ladder; lane 2, ladder of Lambda DNA-HindIII digest; lane 3, fresh oyster meat

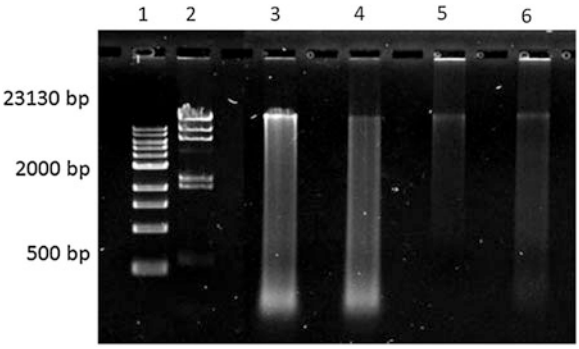

Fig. 145.2 Gel electrophoresis of DNA in oyster processed by different microwave power level. Lane 1, 1.0 kb ladder; lane 2, ladder of lambda DNA-HindIII digest; lane 3, fresh oyster; lane 4, low level 2.0 min; lane 5, medium level 2.0 min; lane 6, high level 2.0 min

145.3.3 Effects of High-Temperature Processing on DNA

Fresh oyster was processed by 100 °C or 121 °C, the processing time is 10 or 20 min. DNA in high-temperature processed oyster analyzed by agarose gel electrophoresis was shown in Fig. 145.3. We can figure out that oyster DNA was broken into small pieces. When the processing temperature was 100 °C, DNA in processed oyster meat was shown to be smaller than 4.0 kb. Even more, after processed by 121 °C, DNA was broken into small segments less than 2.0 kb. The influence of temperature on DNA of oyster was obvious, but the influence of processing time seemed not that significant.

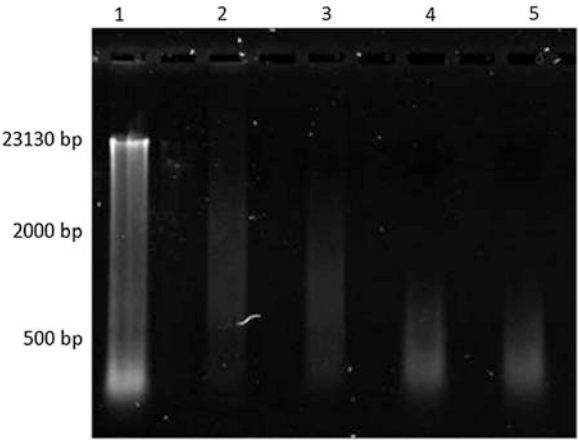

Fig. 145.3 Gel electrophoresis of DNA in oyster meat processed by high temperature. Lane 1, Fresh oyster; Lane 2, 100 °C, 10 min; Lane 3, 100 °C, 20 min; Lane 4, 121 °C, 10 min; Lane 5, 121 °C, 20 min

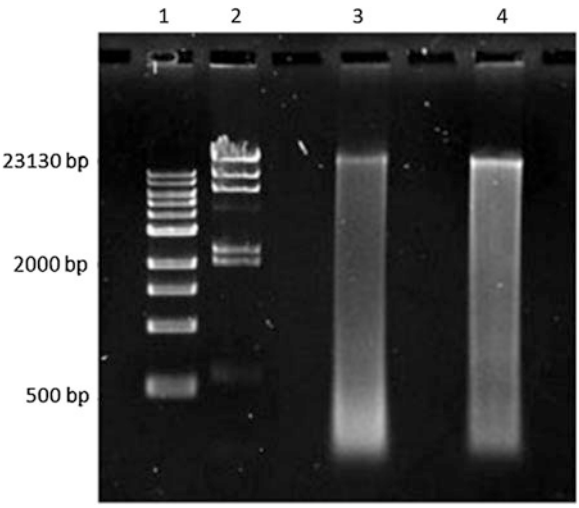

Fig. 145.4 Gel electrophoresis of DNA in oyster freeze–thaw under −20 °C for 10 times. Lane 1, 1 kb ladder; Lane 2, lambda DNA-HindIII digest; Lane 3, freeze–thaw oyster; Lane 4, fresh oyster

145.3.4 Effects of Freeze–Thaw Processing on Oyster DNA

After 10 times freeze–thaw, DNA in oyster meat was analyzed by agarose gel electrophoresis (Fig. 145.4). Results showed that the freeze–thaw process had little influence on oyster genomic DNA.

145.3.5 Effects of Grinding

Figure 145.5 showed the gel electrophoresis of DNA in oyster after grinding for 10 min. Band of 20 kb decreased and segments lower than 500 bp increased. It revealed that some genomic DNA was broken down into small segments during grinding.

145.3.6 Effects of Salting

As shown in Fig. 145.6, increase of lower Mw DNA was not found in salting oyster. However, content of higher Mw DNA increased. This illuminated that salting process may enhance the stability of genomic DNA in oyster. In the fresh oyster meat, nuclease-like Dnase may destroy DNA during DNA extraction, while salt can decrease the activity of nuclease to some extent.

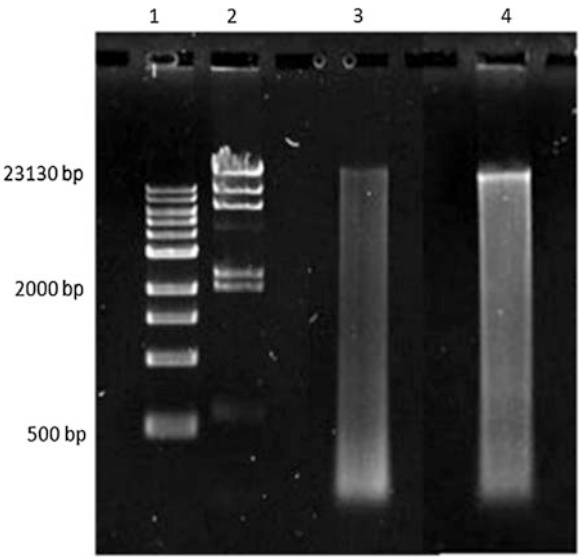

Fig. 145.5 Gel electrophoresis of DNA in oyster meat after grinding for 10 min. Lane 1, 1.0 kb ladder; Lane 2, Lambda DNA-HindIII digest; Lane 3, Grinding oyster; Lane 4, Fresh oyster

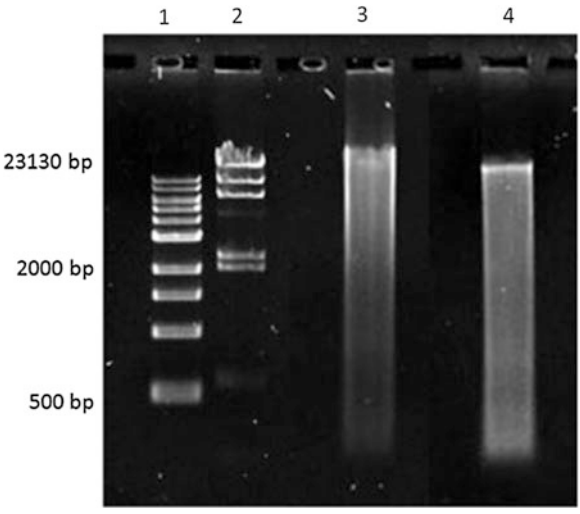

Fig. 145.6 Gel electrophoresis of DNA in salting oyster meat. in fresh oyster1, 1.0 kb ladder; Lane 2, lambda DNA-HindIII digest; Lane 3, salting oyster; Lane 4, fresh oyster

145.3.7 Effects of Processing Methods on Free Bases

Free bases in fresh oyster meat or processed oyster meat were extracted and determined by LC-MS. The peaks were recognized by MS spectrum (data not shown). Concentration of each base was calculated by peak area with absorbance under 260 nm. Results of free bases were listed in Table 145.1. The LC-MS chromatography of free bases in fresh oyster meat was shown in Fig. 145.7b.

Table 145.1 Free bases concentrations in oyster meat after different processing methods

No.	Processing methods	Cytosine	Guanine	Thymine	Adenine	Total μg/g
1	Fresh	*	*	33.74	*	33.74
2	HL microwave 2.0 min	*	*	14.72	9.81	24.53
3	High-temperature (121 °C, 20 min)	10.08	56.83	*	109.21	176.12
4	Freeze–thaw	163.08	173.62	277.88	*	614.58
5	Grinding	*	*	35.25	*	35.25
6	Salting	32.57	53.53	31.72	*	117.82
7	Total	205.73	283.98	393.31	119.02	

* Not detected

Compared to standard bases (Fig. 145.7a), concentrations of free thymine (T) were calculated as 33.74 μg/g. Free cytosine (C), guanine (G), and adenine (A) were not detected.

Line 2 showed the concentrations of free C, G, T, A, and total free bases in oyster meat which was processed by HL microwave for 2 min. Concentrations of free bases did not change much after the microwave processing. Only A and T were detected, concentrations of thymine and adenine were 14.72 μg/g and 9.81 μg/g, respectively. Similarly, grinding processing also did not affect the free bases in oyster meat (Lane 5, Table 145.1). After grinding processing composition and concentration of free bases was both similar to fresh oyster.

Changes of free bases after high-temperature process were shown in Lane 3 Table 145.1. Free bases increased greatly, especially A and G. After processed by 121 °C for 20 min, free adenine in oyster meat increased to 109.21 μg/g and free guanine increased to 56.83 μg/g. However, free thymine was not detected after the high-temperature processing. It may be that because of some reactions under high temperature, free thymine might change into other compounds and be used up after processing. It indicated that high temperature caused the loss of purines from DNA strands.

Among all the five processing methods, freeze–thaw processing affected the loss of bases from DNA strands (Lane 4, Table 145.1) the most significantly. Total concentration of free bases in freeze–thaw processed oyster was 614.58 μg/g, it is almost 20 times compared to total free bases in fresh oyster. After freeze–thaw processed, free cytosine, guanine, and thymine were all higher than 160 μg/g. Concentration of free thymine was up to 277.88 μg/g, from almost nine times of free thymine in fresh oyster. The LC-MS chromatography was shown in Fig. 145.7c.

As discussed in Sect. 145.3.6, salting process was supposed to protect the DNA in oyster meat. However, free cytosine and guanine increased during salting (Lane 6, Table 145.1). They escaped from DNA strands up to 32.57 μg/g and 53.53 μg/g, respectively. It supposed that salting process caused G-C base pair breaking off from DNA strands.

Compared these five processes to fresh oyster, three processing methods including high temperature, freeze–thaw, and salting induced the rupture of bases

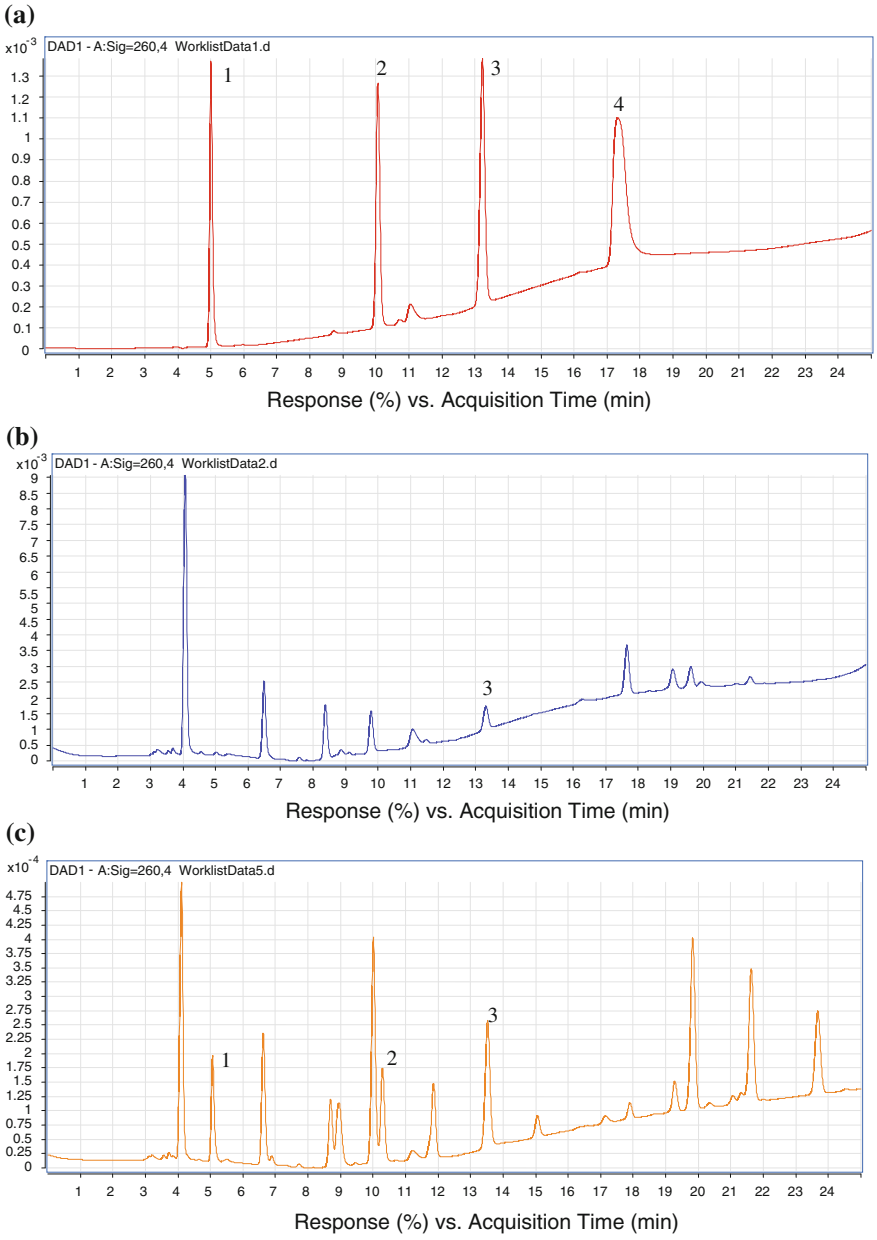

Fig. 145.7 Chromatographs of free bases in fresh oyster meat, peaks were recognized by MS spectrum. **a** standard bases, peak 1 is cytosine, peak 2 is guanine, peak 3 is thymine and peak 4 is adenine; **b** free bases in fresh oyster meat; **c** free bases in freeze–thaw processed oyster meat

from DNA strands. Especially, they all caused the increase of free cytosine and guanine. The result implied the base pairs composed of G-C escaped from DNA strands together during food processing. As we know three hydrogen bonds were needed to compose the base pair G-C, however, A-T base pair were composed of two hydrogen bonds. Therefore, G and C were connected more tightly. When the high-temperature strike to DNA strands, G-C will escape together from the strands. Hydrogen bonds in A-T base pair were less stable, the rupture will happen inside A-T base pair, then A and T will not escape from DNA strands simultaneously. Moreover, purines including guanine and adenine were affected significantly by high temperature. This result indicated that the super-hot condition will cause the depurination. The mechanism should be investigated in the future.

145.4 Conclusion

Genomic DNA of oyster processed by different methods was investigated in our study. Processing methods included microwave, high temperature, freeze–thaw, grinding, and salting. Microwave will bring out DNA and protein gathered together. The instantaneous heat caused by microwave should be the main reason. High temperature will cause the rupture of DNA. Under high temperature oyster DNA was denatured. The denatured DNA is unstable, then break of hydrogen bonds and phosphodiester bonds will come up. Slight rupture of DNA during of freeze–thaw was attributed to ice crystal. Shape of ice crystal during freeze–thaw can break the oyster meat cells, DNase comes out together with genomic DNA, and slow hydrolysis of DNA will happen. And considerable loss of free bases from DNA strands may attribute to both the breakage of DNA strands by ice crystal and the release of DNase. Similar as freeze–thaw, process of grinding will also break oyster cells. Moreover, grinding will generate heat, increase of temperature may be another reason of the DNA rupture. However, to some extent salting can increase the stability of DNA in oyster meat. It will attribute to the existence of NaCl. On the one hand, high concentration of NaCl can destroy the Dnase in oyster cells; the inactivation of enzyme protected DNA from degradation. On the other hand, increase of ion in the system will promote the separation of DNA and protein; neutralize the negative charge of DNA strands. The increased stability of DNA will prevent the DNA rupture by processing.

Changes of free bases concentrations in oyster meat will reflect the loss of bases from DNA strands. Our study indicated that G-C and A-T base pairs have different sensitivities to processing. G-C escaped from DNA strands together and showed a universal sensitivity to the applied processing methods in this paper. This result may attribute to the different strength of hydrogen bonds inside base pairs. Moreover, purines, but not pyrimidine, were sensitive to high-temperature processing. As we know, purine is supposed to be related to the cause of gout and some other metabolism diseases [6, 7], the difference performances of pyrimidine and purine during high-temperature processing were thought-provoking.

Different processing methods do have influences on oyster DNA. The influences can affect the flavor, nutrition, DNA separation, and determination of processed oyster. Changes of DNA or other nucleic acids during processing should be paid more attention. However, to reveal the mechanism of these phenomena, we need to devote more work in the future.

Acknowledgments This work was supported by program for "Changjiang Scholars and Innovative Research Team in University", recruitment programs of "Wanren Plan", "Fund for Distinguished Young Scholars" of Shandong province, "National Youth Qianren Plan", and doctoral fund of ministry of education of China (RFDP, No. 20100132120018).

References

1. Food and Agriculture Organization of the United Nations (2010) World review of fisheries and aquaculture
2. Kiyoko K (2007) 食品に含まれるプリン体について：血清尿酸値に影響を与える食品と食品中のプリン体含量. Gout Nucleic Acid Metab 31:119–131 (in Japanese)
3. Doerfler W, Hohlweg U, Müller K et al (2001) Foreign DNA integration: perturbations of the genome—oncogenesis. Ann N Y Acad Sci 945:276–288
4. Schubbert R, Hohlweg U, Renz D et al (1998) On the fate of orally ingested foreign DNA in mice: chromosomal association and placental transmission to the fetus. Mol Gen Genet 259:569–576
5. Ho CY, Miller KV, Savaiano DA et al (1979) Absorption and metabolism of orally administered purines in fed and fasted rats. J Nutr 109:1377–1382
6. Pande I (2006) An update on gout. Indian J Rheumatol 1:60–65
7. Dalbeth N, Haskard DO (2005) Mechanisms of inflammation in gout. Rheumatology 44:1090–1096
8. Li P, Gatlin DM III (2006) Nucleotidenutrition in fish: current knowledge and future applications. Aquaculture 251:141–152
9. Martinez PD, Manzanillab EG, Moralesc J et al (2007) Dietary nucleotide supplementation reduces occurrence of diarrhoea in early weaned pigs. Livest Sci 208:276–279
10. Thorell L, Sjöberg LB, Hernell O (1996) Nucleotides in human milk: sources and metabolism by the newborn infant. Pediatr Res 40:845–852
11. Gill BD, Indyk HE (2007) Development and application of a liquid chromatographic method for analysis of nucleotides and nucleosides in milk and infant formulas. Int Dairy J 17:596–605
12. Sommer I, Schwartz H, Solar S et al (2010) Effect of gamma-irradiation on flavor 50-nucleotides, tyrosine, and phenylalanine in mushrooms (*Agaricus bisporus*). Food Chem 123:171–174
13. Hiltz DF, Bishop LJ (1975) Postmortem glycolytic and nucleotide degradative changes in muscle of the atlantic queen crab (*Chionoecetes opilio*) upon iced storage of unfrozen and of thawed meat, and upon cooking. Comp Biochem Physiol B 52:453–458
14. Reuter T, Aulrich K (2003) Investigations on genetically modified maize (Bt-maize) in pig nutrition: fate of feed-ingested foreign DNA in pig bodies. Eur Food Res Technol 216:185–192

Chapter 146
Design and Synthesis of Resveratrol Analogs

Yuanmou Chen, Fei Hu, Yinghao Gao, Na Ji, Weizhu Liu and Erbing Hua

Abstract Resveratrol (3,5,4′-trihydroxy-trans-stilbene), a naturally occurring hydroxystilbene, is considered as an essential anti-oxidative and possessing chemopreventive properties, and is found in various medical plants. It has been proven that resveratrol is a Sirt1 activator and kinds of biological activities. In this paper, we designed and synthesized a series of resveratrol derivatives through a five-step synthetic procedure. Total 11 resveratrol derivatives were prepared from two kinds of hydroxybenzoic acid by methylation and reduction followed by bromination and reaction with triethyl phosphate to get methoxylated diethyl benzylphosphonates, then condensation with a series of aromatic aldehydes by Wittig-Horner reaction to offer the desired compounds in overall yield of about 17.2–48.5 %. These synthesized compounds were characterized on the basis of 1H NMR.

Keywords Resveratrol analogs · Synthesis · Sirt1 activator · Wittig-Horner reaction

146.1 Introduction

Resveratrol (3,5,4′-trihydroxystilbene) was identified as one ingredient of red wine, which could cause the so-called "French paradox" [1]. This compound, which is a naturally occurring phytoalexin produced by a wide range of plants in response to environmental stress or pathogenic attack, was first isolated from the roots of the white hellebore lily Veratrum grandiflorum by O. Loes in 1940 [2]. Since the discovery of its cardioprotective activity in 1992, resveratrol research has steadily accelerated.

Y. Chen · F. Hu · Y. Gao · N. Ji · W. Liu · E. Hua (✉)
Key Laboratory of Industrial Microbiology of Ministry of Education,
College of Biotechnology, Tianjin University of Science & Technology,
Tianjin 300457, People's Republic of China
e-mail: huarb@tust.edu.cn

T.-C. Zhang et al. (eds.), *Proceedings of the 2012 International Conference on Applied Biotechnology (ICAB 2012)*, Lecture Notes in Electrical Engineering 251,
DOI: 10.1007/978-3-642-37925-3_146,

In past years, there have been a large of reports about resveratrol that exerts a variety of biological activities. Among the most significant activities of resveratrol are its cancer chemo-preventive properties [3, 4], antioxidant [5], antibacterial, and anti-inflammatory activities [6–8]. Some of these have been reported to inhibit LDL oxidation in human [9], in addition to its blocking of platelet aggregation [10] and vasorelaxing activities [11]. In yeast assays, resveratrol was also found to significantly mimic calorie restriction by stimulating Sirt2 which is the most homologic homolog of Sirt1 of mammalian and extended lifespan by 70 % [12].

In recent years, a large number of papers have been published on resveratrol, which report a wide range of novel discoveries, such as new extraction methods, new applications [13–15], and resveratrol analogs [16–18]. This intrigued us to prepare its analogs and their derivatives. In order to increase its stability and water-solubility, we designed and synthesized some methoxylated analogs of resveratrol. The methoxylation of hydroxyl groups results in an increase in lipophilicity and a loss of hydrogen bond donor property. These changes will influence bioavailability, susceptibility to metabolism, and possibly the pharmacological profile of the resulting analog.

146.2 Experimental

146.2.1 Materials and Measurements

^{1}H NMR spectra was obtained at Bruker AM-400 NMR spectrometer using $CDCl_3$ as the solvent except where otherwise specified, the chemical shifts are reported in δ values (ppm) relative to Me_4Si line as internal standard and J values are reported in Hertz. Unless otherwise stated, reagents and solvents were of reagent grade and used as obtained from commercial sources without further purification. Dichloromethane was distilled from CaH_2, THF from sodium prior to use and DMF were dried over anhydrous sodium sulfate. Reaction temperatures were controlled by oil bath with temperature modulator and dewars. Thin layer chromatography (TLC) was performed using E. Merck silica gel 60 GF_{254} precoated plates (0.25 mm). Silica gel (particle size 200–400 mesh) was used for flash chromatography.

146.2.2 General Procedures

The route to prepare the resveratrol analogs was presented in Scheme 146.1.

146.2.2.1 General Procedure 1 (Gp 1) for the Preparation of Aromatic Esters from Hydroxybenzoic Acid

In a round-bottomed flask, to a well-stirred suspension of a mixture of hydroxybenzoic acid (1 eq.), freshly powered anhydrous K_2CO_3 (5 eq.), and

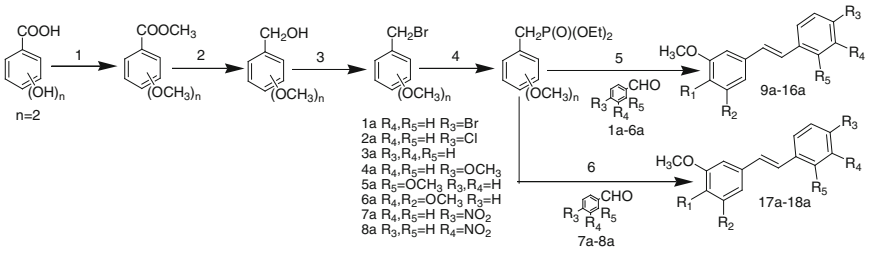

Scheme 146.1 Synthetic pathway for stilbenes 9a–18a. Reagents and conditions: *1* $(CH_3O)_2CO$, Bu_4NBr, DMF, K_2CO_3, reflx; *2* $LiAlH_4$, THF, 0 °C; *3* PBr_3, CH_2Cl_2, rt; *4* $P(O)(OEt)_3$, reflux; *5* NaH, ArCHO, THF, 0 °C; *6* CH_3ONa, ArCHO, DMF, 100 °C

tetrabutylammonium bromide (0.5 eq.) in DMF (10 ml) was added dimethyl carbonate (50 ml, 30 eq.) at room temperature. After the mixture was stirred at 140 °C for 38 h, the dimethyl carbonate was removed under reduced pressure and water (80 ml) was added to the residue. The resulted mixture was extracted with ethyl acetate and the organic layer was washed with water and brine, dried over anhydrous sodium sulfate. The solvent was concentrated in vacuo to yield the pure product as a white solid in moderate yield aromatic esters.

146.2.2.2 General Procedure 2 (Gp 2) for the Preparation of Aromatic Alcohol from Aromatic Esters

$LiAlH_4$ (0.5 eq.) was added slowly to a solution of aromatic esters (1 eq.) in THF (50 mL) at 0 °C for 1 h. The reaction mixture was stirred for 10 h at room temperature. Ice water (10 mL) was added slowly to the reaction mixture and stirred for 10 min, followed by concentrated 2 M HCl to neutralize the base. The reaction mixture was extracted with ethyl acetate, and the ethyl acetate layer was washed with water and brine, dried over anhydrous sodium sulfate. The solvent was removed in vacuo to yield the pure product in good yield aromatic alcohol.

146.2.2.3 General Procedure 3 (Gp 3) for the Preparation of Benzyl Bromine from Aromatic Alcohol

A solution of tribromophosphine (3 eq.) in CH_2Cl_2 (15 mL) was added dropwise to a solution of aromatic alcohol (1 eq.) in CH_2Cl_2 (30 mL) at 0 °C. The reaction mixture was stirred for 2 h and then warmed up to room temperature. After 4 h, the solution was poured into 50 mL ice water and stirred for 10 min. Then the organic layer was washed with water and aq $NaHCO_3$ (3 × 20 mL), dried over anhydrous sodium sulfate, and evaporated to yield the pure product as a solid benzyl bromine.

146.2.2.4 General Procedure 4 (Gp 4) for the Preparation of Methoxylated Diethyl Benzylphosphonates from Benzyl Bromine (Arbuzov Rearrangement)

A mixture of bromide (1 eq.) and triethyl phosphite (2 mL 5 eq.) was stirred at 135 °C for 3 h [19]. Triethyl phosphate (2 mL 5 eq.) was added again and stirred another 4 h. After the reaction was completely finished, the mixture was cooled to room temperature and purified by distillation at 4×10^{-3} bar and 120 °C to yield yellow oils methoxylated diethyl benzylphosphonates. The crude product was used directly for the next step without further purification.

146.2.2.5 General Procedure 5 (Gp 5) for Synthesis of Compounds 9a–16a (Wittig-Hornor Condensation)

Methoxylated diethyl benzylphosphonates (1 eq.) in the round-bottomed flask was added dropwise to a suspension of NaH (4 eq.) in THF (20 mL) at 0 °C and stirred for 1 h [20]. Then the mixture was treated with aromatic carboxaldehyde (1a–6a) (1 eq.) at 0 °C for 2 h. The reaction mixture was warmed up to room temperature and further stirred for 15 h. The solution was poured into 150 mL ice water, neutralized with 2 M HCl, and extracted with ethyl acetate. The ethyl acetate layer was washed with water and brine, dried over anhydrous sodium sulfate, and concentrated. The crude product purified by crystallization or flash column chromatography to afford (E)-stilbenes.

146.2.2.6 General Procedure 6 (Gp 6) for the Nitro Groups and Stilbenes (Compounds 17a–18a)

To a stirred suspension of CH_3ONa (3 eq.), DMF (25 mL) was added dropwise to the corresponding methoxylated diethyl benzylphosphonate (1 eq.) at 0 °C in a round-bottomed flask and the mixture was stirred for 1 h. Then the corresponding benzaldehyde (7a–8a) (1 eq.) were added. The mixture was stirred at room temperature for 1 h, then heated to 100 °C under argon for 10 h. The solution was poured into 150 mL ice water, the precipitate as filtered off and recrystallized from diluted or pure ethanol to afford the nitro groups and stilbenes.

146.2.3 Syntheses

146.2.3.1 3,5-Dimethoxyl-4′-bromo-trans-stilbene (9a)

This compound was prepared in 59.2 % yield by following GP 4 and 5. White solid: 1H NMR (400 MHz CDCl3): δ/ppm 7.47 (d, $J = 8.4$ Hz, 2H), 7.36

(d, $J = 8.4$ Hz, 2H), 7.01(s, 2H), 6.65 (d, $J = 2.4$ Hz, 2H), 6.41 (t, $J = 2.2$ Hz, 1H), 3.83 (s, 6H).

146.2.3.2 3,5-Dimethoxyl-4′-chloro-trans-stilbene (10a)

This compound was prepared in 65.8 % yield by following GP 4 and 5. White solid: ^{1}H NMR (400 MHz $CDCl_3$): δ/ppm 7.42 (d, $J = 8.4$ Hz, 2H), 7.32 (d, $J = 8.4$ Hz, 2H), 7.01 (d, $J = 1.6$ Hz, 2H), 6.65 (d, $J = 2.4$ Hz, 2H), 6.41 (t, $J = 2.4$ Hz, 1H), 3.83 (s, 6H).

146.2.3.3 3,5-Dimethoxyl-trans-stilbene (11a)

This compound was prepared in 45.6 % yield by following GP 4 and 5. White solid: ^{1}H NMR (400 MHz $CDCl_3$): δ/ppm 7.55 (d, $J = 7.6$ Hz, 2H), 7.40 (t, $J = 7.6$ Hz, 2H), 7.31 (t, $J = 7.2$ Hz, 1H), 7.14 (d, $J = 16.4$ Hz, 1H), 7.08 (d, $J = 16.4$ Hz, 1H), 6.73 (d, $J = 2$ Hz, 2H), 6.45 (t, $J = 2.4$ Hz, 1H), 3.87 (s, 6H).

146.2.3.4 3,5,4′-Trimethoxyl-trans-stilbene (12a)

This compound was prepared in 37.1 % yield by following GP 4 and 5. White solid: ^{1}H NMR (400 MHz $CDCl_3$): δ/ppm 7.44 (d, $J = 8.4$ Hz, 2H), 7.04 (d, $J = 16$ Hz, 1H), 6.91 (t, $J = 6.4$ Hz, 3H), 6.65 (s, 2H), 6.37 (s, 1H), 3.83 (s, 9H).

146.2.3.5 3,5,2′-Trimethoxyl-trans-stilbene (13a)

This compound was prepared in 46.2 % yield by following GP 4 and 5. White solid: ^{1}H NMR (400 MHz $CDCl_3$): δ/ppm 7.57 (d, $J = 7.6$ Hz, 2H), 7.45 (d, $J = 16.4$ Hz, 1H), 7.22–7.26 (m, 1H), 7.04 (d, $J = 16.4$ Hz, 1H), 6.96 (t, $J = 7.2$ Hz, 1H), 6.90 (d, $J = 8.4$ Hz, 1H), 6.69 (d, $J = 2$ Hz, 2H), 6.38 (t, $J = 2.4$ Hz, 1H), 3.88 (s, 3H), 3.83 (s, 6H).

146.2.3.6 3,5,2′,3′-Tetramethoxyl-trans-stilbene (14a)

This compound was prepared in 48.8 % yield by following GP 4 and 5. White solid: ^{1}H NMR (400 MHz $CDCl_3$): δ/ppm 7.42 (d, $J = 16.4$ Hz, 1H), 7.23 (d, $J = 9.2$ Hz, 1H), 7.06 (t, $J = 9.2$ Hz, 1H), 7.05 (d, $J = 16.4$ Hz, 1H), 6.84 (d, $J = 9.6$ Hz, 1H), 6.70 (d, $J = 2$ Hz, 2H), 6.4 (t, $J = 2.4$ Hz, 1H), 3.88 (s, 3H), 3.85 (s, 3H), 3.84 (s, 6H).

146.2.3.7 3,4,2′-Trimethoxyl-trans-stilbene (15a)

This compound was prepared in 44.9 % yield by following GP 4 and 5. White solid: ^{1}H NMR (400 MHz $CDCl_3$): δ/ppm 7.58 (d, $J = 9.2$ Hz, 1H), 7.33 (d, $J = 16.4$ Hz, 1H), 7.21 (t, $J = 4.8$ Hz, 1H), 7.10 (d, $J = 1.6$ Hz, 1H), 7.06 (d, $J = 16.4$ Hz, 1H), 7.05 (d, $J = 8.4$ Hz, 1H), 6.96 (t, $J = 7.6$ Hz, 1H), 6.90 (d, $J = 8$ Hz, 1H), 6.85 (d, $J = 8.4$ Hz, 1H), 3.95 (s, 3H), 3.90 (d, $J = 1.2$ Hz, 6H).

146.2.3.8 3,4,2′,3′-Tetramethoxyl-trans-stilbene (16a)

This compound was prepared in 37.6 % yield by following GP 4 and 5. White solid: ^{1}H NMR (400 MHz $CDCl_3$): δ/ppm 7.31 (d, $J = 16.4$ Hz, 1H), 7.22 (d, $J = 9.6$ Hz, 1H), 7.09 (d, $J = 16.4$ Hz, 1H), 7.09 (s, 1H), 7.08 (t, $J = 6.4$ Hz, 1H), 7.04 (d, $J = 8$ Hz, 1H), 6.87 (d, $J = 8.8$ Hz, 1H), 6.83 (d, $J = 9.6$ Hz, 1H), 3.95 (s, 3H), 3.91 (s, 3H), 3.89 (s, 3H), 3.86 (s, 3H).

146.2.3.9 3,5-Dimethoxyl-4′-nitro-trans-stilbene (17a)

This compound was prepared in 76.5 % yield by following GP 4 and 6. Yellow solid: ^{1}H NMR (400 MHz $CDCl_3$): δ/ppm 8.22 (d, $J = 8.4$ Hz, 2H), 7.63 (d, $J = 8.8$ Hz, 2H), 7.20 (d, $J = 16.4$ Hz, 1H), 7.11 (d, $J = 16.4$ Hz, 1H), 6.96 (t, $J = 7.2$ Hz, 1H), 6.70 (s, 2H), 6.46 (t, $J = 2$ Hz, 1H), 3.85 (s, 6H).

146.2.3.10 3,5-Dimethoxyl-3′-nitro-trans-stilbene (18a)

This compound was prepared in 78.3 % yield by following GP 4 and 6. Orange solid: ^{1}H NMR (400 MHz $CDCl_3$): δ/ppm 8.36 (s, 1H), 8.09 (d, $J = 9.6$ Hz, 1H), 7.79 (d, $J = 8$ Hz, 1H), 7.52 (t, $J = 8$ Hz, 1H), 7.16 (d, $J = 16.4$ Hz, 1H), 7.09 (d, $J = 16.4$ Hz, 1H), 6.69 (d, $J = 2.4$ Hz, 2H), 6.45 (t, $J = 2.4$ Hz, 1H), 3.84 (s, 6H).

146.2.3.11 3,5-Dimethoxy-4′-amino-trans-stilbene (19a)

Ferric chloride hexahydrate (0.1 g) and activated carbon (1 g) were added to a solution of compound 17a (1.42 g, 5 mmol) in ethanol (55 mL). Then the reaction mixture was heated to 80 °C and hydrazine hydrate (9 mL, 15 mmol) was added dropwise to the mixture. The mixture was stirred under reflux for 5 h. The mixture was filtered and the solvent was removed. Water was added to the residue and the aqueous layer was extracted by ethyl acetate and the organic layer was washed by brine, and dried over anhydrous sodium sulfate. The solvent was evaporated in

vacuo to provide a yellow solid that was recrystallized from ethyl acetate and hexane to yield a pure yellow solid (1.09 g, 85.6 %): ^{1}H NMR (400 MHz $CDCl_3$): δ/ppm 7.33 (d, $J = 8.4$ Hz, 2H), 7.00 (d, $J = 16.4$ Hz, 1H), 6.84 (d, $J = 16.4$ Hz, 1H), 6.67 (d, $J = 8.4$ Hz, 2H), 6.63 (d, $J = 2.4$ Hz, 2H), 6.36 (t, $J = 2.4$ Hz, 1H), 3.82 (s, 6H), 3.75 (br, 2H).

146.3 Results and Discussion

In this work, we used the Wittig-Horner reaction to synthesize resveratrol derivatives. It was found that Wittig-Horner reaction is much better in forming double bond of resveratrol due to its mild reaction conditions, simple manipulation, high purity, and yield than Perkin or Heck reaction.

In this work, methoxylated analogs of resveratrol were synthesized through 3,5-dihydroxybenzoic acid or 3,4-trihydroxybenzoic acid followed by aromatic esters formation in moderate yield, which was reduced with $LiAlH_4$ to alcohol, and subsequent treatment with tribromophosphine afforded benzyl bromine in about 85.0 %. With Wittig-Horner reaction methoxylated diethyl benzylphosphonates were obtained by refluxing benzyl bromine with $P(OEt)_3$, which was condensed with ArCHO in CH_3ONa/DMF or NaH/THF to give compounds 9a–18a, only the trans isomer was obtained. Compounds 9a–18a were prepared according to Scheme 146.1 and the structures of these compounds were listed in Table 146.1. The nitro group of the analog 17a was reduced to provide the amine derivatives 19a in satisfactory yields (Scheme 146.2).

It is reported that some methylated derivatives of resveratrol show better potential antifungal, anti-proliferative, anticancer, and other activities than resveratrol. For instance, compound 12a was reported to inhibit invasion of human

Table 146.1 Chemical structures of compounds 9a–18a

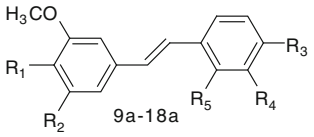

Compound	R_1	R_2	R_3	R_4	R_5
9a	H	OCH_3	Br	H	H
10a	H	OCH_3	Cl	H	H
11a	H	OCH_3	H	H	H
12a	H	OCH_3	OCH_3	H	H
13a	H	OCH_3	H	H	OCH_3
14a	H	OCH_3	H	OCH_3	OCH_3
15a	OCH_3	H	H	H	OCH_3
16a	OCH_3	H	H	OCH_3	OCH_3
17a	H	OCH_3	NO_2	H	H
18a	H	OCH_3	H	NO_2	H

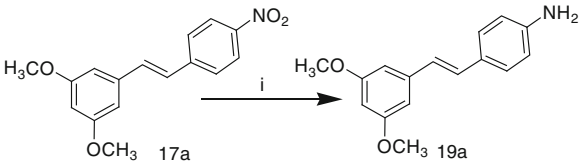

Scheme 146.2 Synthetic pathway for stilbenes 19a. Reagents and conditions: (i) $FeCl_3/C$, H_2NNH_2, EtOH, reflux

lung adenocarcinoma cells [21]. In addition, compound 19a also displayed potent QR2 inhibitory activity [22] and compound 11a possesses potent NQO1 induction activity [23] and other articles reported that they have inhibitory activity of prostaglandin E2 [24]. So the biological activities of these resveratrol derivatives lead us to synthesize novel derivatives and further study their other biological activities such as anti-diabetes.

146.4 Conclusion

In summary, we designed and synthesized some methoxylated analogs of resveratrol. The synthetic route is a five-step convenient procedure via Wittig-Horner reaction which is the key step to prepare resveratrol derivatives including compounds 9a–18a in overall yield 17.2–48.5 %. The compounds 17a–18a were prepared in 76.5–78.3 % yield by following GP 4 and 6, however, yield would be a range from 35.5 to 37.6 % by following GP 4 and 5. It was possible that compounds 7a–8a could cause Cannizzaro reaction when the reactions took GP 5, resulting in lower yield. The analogs 17a were reduced by hydrazine hydrate to get the compound 19a in yield 85.0 %.

Acknowledgments This work was supported by National Natural Science Foundation of China (No: 81072521) and Tianjin University of Science & Technology (No: 20100411).

References

1. Richard JL (1987) Coronary risk factors: The French paradox. Arch Mal Coeur Vaiss 80:17–21
2. Takaoka MJ (1940) Of the phenolic substances of white hellebore. J Faculty Sci 3:1–16
3. Kopp P (1998) Resveratrol, a phytoestrogen found in red wine. A possible explanation for the conundrum of the 'French paradox'? Eur J Endocrinol 138:619–620
4. Jang M, Pezzuto JM (1999) Cancer chemopreventive activity of resveratrol. Drugs Exp Clin Res 25:65–771
5. Stivala LA, Savio M, Carafoli F et al (2001) Specific structural determinants are responsible for the antioxidant activity and the cell cycle effects of resveratrol. J Biol Chem 276:22586–22594
6. Daroch F, Hoeneisen M, Gonzalez CL et al (2001) In vitro antibacterial activity of Chilean red wines against Helicobacter pylori. Microbios 104:79–85

7. Wang WB, Lai HC, Hsueh PR et al (2006) Inhibition of swarming and virulence factor expression in Proteus mirabilis by resveratrol. J Med Microbiol 55:1313–1321
8. Zaidi SF, Ahmed K, Yamamoto T et al (2009) Effect of resveratrol on Helicobacter pylori-induced interleukin-8 secretion, reactive oxygen species generation and morphological changes in human gastric epithelial cells. Biol Pharm Bull 32:1931–1935
9. Arichi H, Kimura Y, Okuda H et al (1982) Effects of stilbene components of the roots of Polygonum cuspidatum on lipid metabolism. Chem Pharm Bull (Tokyo) 30:1766–1770
10. Pace-Asciak CR, Hahn S, Diamandis EP et al (1996) The red wine phenolics trans-resveratrol and quercetin block human platelet aggregation and eicosanoid synthesis: implications for protection against coronary heart disease. Clin Chim Acta 235:207–219
11. Chen CK, Pace-Asciak CR (1996) Vasorelaxing activity of resveratrol and quercetin in isolated rat aorta. Gen Pharmacol 27:363–366
12. Howitz KT, Bitterman KJ, Cohen HY et al (2003) Small molecule activators of sirtuins extend Saccharomyces cerevisiae lifespan. Nature 425:191–196
13. Wang RH, Sengupta K, Li C et al (2008) Impaired DNA damage response, genome instability, and Tumorigenesis in SIRT1 mutant mice. Cancer Cell 14:312–323
14. Rocha-Gonzalez HI, Ambriz-Tututi M, Granados-Soto V (2008) Resveratrol: a natural compound with pharmacological potential in neurodegenerative diseases. CNS Neurosci Ther 14:234–247
15. Vieira de Almeida LM, Pineiro CC, Leite Marina MC et al (2008) Protective effects of resveratrol on hydrogen peroxide induced toxicity in primary cortical astrocyte cultures. Neurochem Res 33:8–15
16. Ali HA, Kondo K, Tsuda Y (1992) Synthesis and nematocidal activity of hydroxystilbenes. Chem Pharm Bull 40:1130–1136
17. Thakkar K, Geahlen RL, Gushman M (1993) Synthesis and protein-tyrosine kinase inhibitory activity of polyhydroxylated stilbene analogs of piceatannol. J Med Chem 36:2950–2955
18. Murias M, Handler N, Erker T et al (2004) Resveratrol analogues as selectivecyclooxygenase-2 inhibitors: synthesis and structure—activity relationship. Bioorg Med Chem 12:5571–5578
19. Bhattacharya Alok K, Thyagarajan G (1981) Michaelis-Arbuzov rearrangement. Chem Rev 81:415–430
20. Cristau HJ, Darviche F, Torreilles E (1998) Mechanistic investigations of the formation of TTF derivatives via the phosphonate way. Tetrahedron Lett 39:2103–2106
21. Yang YT, Weng CJ, Ho CT et al (2009) Resveratrol analog-3,5,4′-trimethoxy-trans-stilbene inhibits invasion of human lung adenocarcinoma cells by suppressing the MAPK pathway and decreasing matrix metalloproteinase-2 expression. Mol Nutr Food Res 53:407–416
22. Sun B, Hoshino J, Jermihov K et al (2010) Design, synthesis, and biological evaluation of resveratrol analogues as aromatase and quinone reductase 2 inhibitors for chemoprevention of cancer. Bioorg Med Chem 18:5352–5366
23. Park EJ, Min HY, Park HJ et al (2011) Nuclear factor E2-related factor 2-mediated induction of NAD(P)H:quinone oxidoreductase 1 by 3,5-dimethoxy-trans- stilbene. J Pharmacol Sci 116:89–96
24. Park EJ, Min HY, Ahn YH et al (2004) Synthesis and inhibitory effects of pinosylvin derivatives on prostaglandin E2 production in lipopolysaccharide-induced mouse macrophage cells. Bioorg Med Chem Letters 14:5895–5898

Chapter 147
Elongation of Trinucleotide Repeats by DNA Polymerase

Yang Wang, Ping Dong and Xingguo Liang

Abstract The wide present simple repetitive sequences in genomes are significant for studying molecular evolution, genetic diversity, and some hereditary diseases. Here, elongation of 64 (3^4) kinds of 18 nucleotides long sequences with trinucleotide tandem repeats by DNA polymerase was studied. The result showed that all of the repeats, apart from several strands made up with single nucleotide, could be elongated, although the efficiency depended on the sequences and reaction temperatures. More GC content required a higher temperature for efficient elongation. For double strands, elongation products had a narrow size distribution, and the length of synthesized DNA increased linearly with reaction time. Single-stranded sequences could also be elongated with even higher efficiency, and products longer than 10 kb were obtained in several hours. Our results are promising to be used for explanation of molecular evolution, as well as unusual amplification of repetitive sequences during gene amplification and detection.

Keywords Repetitive sequences · Isothermal amplification · Molecular evolution

147.1 Introduction

Tandem short repetitive sequences are strands of DNA made up with short units connected with each other, which are also known as satellite DNA [1, 2], such as $(AT)_n$ and $(CAG)_n$. They are widely distributed in eukaryotic and prokaryotic organisms and show polymorphism in length even in closely related individuals.

Y. Wang · P. Dong · X. Liang (✉)
College of Food Science and Engineering, Ocean University of China, Qingdao 266003, People's Republic of China
e-mail: liangxg@ouc.edu.cn

T.-C. Zhang et al. (eds.), *Proceedings of the 2012 International Conference on Applied Biotechnology (ICAB 2012)*, Lecture Notes in Electrical Engineering 251,
DOI: 10.1007/978-3-642-37925-3_147,

Tandem repeats are closely related to many aspects of biological and medical science like molecular evolution, genetic diversity, molecular markers, and genetic diseases [3]. It has been revealed that more than 10 serious diseases, such as Huntington's disease and Myotonic dystrophy, are caused by expansion of trinucleotide repetitive sequences [4]. As the result of easy mutation of these short repeats, they contribute greatly to biological evolution and diversity of species. Moreover, these repeats have already been widely used as gene specific markers [5]. On the other hand, although human genome project has just been completed 10 years ago, what we know about repetitive sequences is definitely not enough to understand their abundant presence as well as to solve relevant problems. Accordingly, in-depth study of these repetitive sequences, especially the mechanism of abnormal expansion is required.

There are many proposed mechanisms for repetitive sequence expansion, such as intra or intermolecular recombination, slipped strand mispairing, and illegitimate elongation model [6–8]. Ogata studied the amplification of repeats with palindromic sequences, considering that formation of hairpin structures plays an important role in the initiation stage for elongation, and further elongation is carried out in a slippage style [9, 10]. After noticing these mechanisms were inadequate to explain the high efficiency of expansion, especially at low concentrations, Liang et al. proposed a mechanism to show that the hairpin formation at the end of a DNA duplex contributed to the efficient and continuous elongation, although further experiments were required to clarify this model [11, 12]. At presents, we believe that expansion of repetitive sequence may be carried out according to various mechanisms, which depend on the sequences and the reaction conditions.

Up to now, some scattered researches have shown that many simple repetitive sequences such as $(TA)_n$, $(GAA)_n/(TTC)_n$, $(CCTG)_n$, and $(dG)_n/(dC)_n$ could be expanded by polymerase to 10 kb long [13, 14]. However, no reasonable explanation was provided. On the other hand, repetitive sequences were synthesized ab initio (i.e., in the absence of any initial nucleic acid) from dNTPs by thermophilic DNA polymerases [15]. More and more results supported that modern coding sequences of DNA might evolve from primordial simple sequence repeats. Thus, for both clarifying the mechanism of synthesis of repetitive sequences and understanding their biological significance, systematic study on elongation of simple repetitive sequences is essential. Here, abnormal expansion of all of the 18 nt trinucleotide repetitive sequences by DNA polymerase is studied comprehensively for understanding the expansion mechanism, providing some hints for molecular evolution, as well as explaining the nonspecific amplification in gene detection and diagnose.

147.2 Materials and Methods

147.2.1 Materials

Sixty four kinds of sequences of 18 bp trinucleotide repeats used in this study were purchased from Integrated DNA Technologies. $(AGC)_6$ and $(GCT)_6$ indicate the single-stranded oligonucleotides; and $(AGC)_6/(GCT)_6$ and $(ATA)_6/(TAT)_6$. indicate corresponding duplexes. The oligonucleotides were dissolved in H_2O to 100 μM as stock solutions. The oligos were then diluted to 1.0 μM as the stock for elongation (to a final concentration of 100 nM in reaction). Vent and Vent (exo^-) DNA polymerase, restriction enzyme ApeKI (recognition sequence: G↓CWGC, W = A or T), AluI (recognition sequence: AG↓CT), SmaI (recognition sequence: CCC↓GGG), plasmid PUC18, and RNase-free DNase I were purchased from New England Biolabs. Deoxyribonucleoside Triphosphates (dNTPs) was obtained from Tiangen, T4 DNA ligase was from Fermentas.

147.2.2 Elongation of Short Repetitive Sequences

In principal, standard reaction solution contains 50 nM or 100 nM short repeats, 0.5 mM each dNTPs and 20 U/mL Vent or Vent (exo^-) DNA polymerase. 1 × Thermolpol buffer contains 20 mM Tris-HCl, 10 mM $(NH4)_2SO_4$, 10 mM KCl, 2.0 mM $MgSO_4$, 0.1 % Triton X-100, pH 8.8 at 25 °C. For elongation of double strands, the repeats were pretreated by incubating in 1 × ThermolPol buffer at 90 °C for 3 min followed by slowly cooling to room temperature. The reaction mixture were added to the 96 well plates and performed on life express Thermal cycler (BIOER). Aliquots of the reaction solution were next loaded on a 0.8 % nondenaturing agarose or 8.0 % polyacrylamide gel and then stained with ethidium bromide.

147.2.3 Digestion of Elongated Products by Restriction Enzyme

Elongated products were purified by PCI (phenol: chloroform: isoamyl alcohol = 25:24:1), CIA (chloroform: isoamyl alcohol = 24:1) treatment and precipitated with ethanol. The products were then digested by restriction enzymes ApeKI and AluI for sequence analysis. The reaction was carried out at 75 °C by 100 U/mL ApeKI in 20 μL 1 × NEBuffer 3 (100 mM NaCl, 50 mM Tris–HCl, 10 mM $MgCl_2$, 1.0 mM Dithiothreitol, pH 7.9 at 25 °C) and at 37 °C by 250 U/mL AluI in 20 μL 1 × NEBuffer 4 (50 mM KAc, 20 mM Tris-Ac, 10 mM $Mg(Ac)_2$, 1.0 mM DTT, pH 7.9 at 25 °C).

147.2.4 Molecular Cloning of the Elongated Products

After purification by PCI and CIA treatment and precipitated with ethanol, elongated products were digested slightly with 0.4 U/mL of DNase I in the presence of $MnCl_2$ to generate fragments with blunt ends. The products were then purified again, cloned into the SmaI site of a PUC18 plasmid vector. The strands of the insert DNA were sequenced by the dideoxy chain termination method.

147.2.5 T_m Measurement

1.0 μM 18 nt or 18 bp short repeats were added to 1 × Thermopol Detergent Free buffer (10 mM KCl, 10 mM $(NH4)_2SO_4$, 20 mM Tris-HCl, 2.0 mM $MgSO_4$, pH 8.8 at 25 °C). Change of absorbance at 260 nm with temperature was recorded on UV-1800 equipped with temperature-controlling device (Shimadsu).

147.3 Results and Discussion

147.3.1 Elongation of Single-Stranded Sequences by DNA Polymerase

Elongation of all the single strands of repetitive sequences were first performed at 70 °C using 100 nM short repeats seeds in the presence of 0.5 mM dNTPs by polymerase. The elongation products were analyzed by 0.8 % agarose gel. For single strands, The sequences with higher GC content, such as $(TCG)_6$ were inclined to expand efficiently. Products up to 10 kb were observed in some cases within 1 h (Fig. 147.1). For most of other sequences, this kind of phenomenon was also observed. Similar results were also obtained when a denaturing agarose gel (30 mM NaOH) was used.

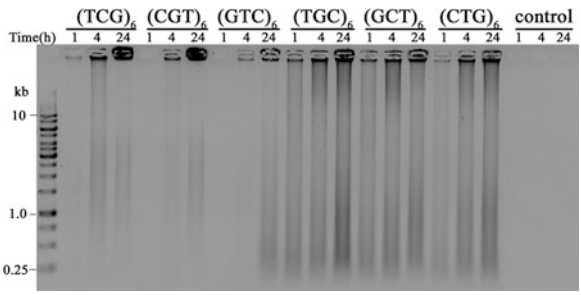

Fig. 147.1 Gel electrophoresis analysis of expansion products of several single strands repeats at 70 °C for 4 h

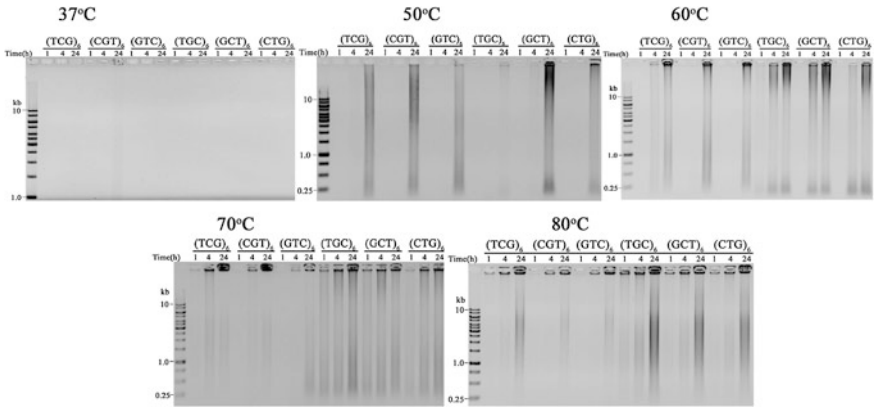

Fig. 147.2 Extensions of single-stranded short trinucleotide repeats at various temperatures

Next, we checked the effect of reaction temperature on the elongation of short repeats. As shown in Fig. 147.2, for $(TCG)_6$ very long DNA was obtained within 1 h at 70 and 80 °C; at 50 and 60 °C, the speed of elongation became slower, and products could only be observed after 4 or 24 h; at 37° C, basically no elongation was observed under the conditions we used. Other short repeats were also analyzed and similar results were obtained, showing that temperature had great effect on their expansion. Repeats with different GC content have different optimal reaction temperatures. For all the short repeats, the suitable temperatures were increased according to the increasing GC content.

147.3.2 Elongation of Double-Stranded Sequences by DNA Polymerase

To catalyze single strands elongation, we used Vent (exo^-) to substituted Vent, because there have been reports describing primer and template-free de novo synthesis of DNA by Vent DNA polymerase [10, 16, 17], especially in high temperature (70–80 °C) for several hours. However, we found that short duplex with repetitive sequence could produce nearly uniform long DNA with Vent polymerase better than with Vent (exo^-). So for double strands repeats, Vent DNA polymerase was used in our study, and the smear band at high temperature can be regarded as de novo synthesis or single strands elongation.

For double strands repeats, the products after elongation had a narrow size distribution (Fig. 147.3), especially for those with more AT content, such as $(AAG)_6$/$(AGG)_6$ and $(ATG)_6$/$(CTA)_6$. When the GC content is 2/3, although more smeared products were observed, the narrow bands around 500 bp could also be clearly seen. The repeats with 100 % AT contents did not give lots of products at 70 °C after 4 h of reaction; on the other hand, except for $(GGG)_6$/$(CCC)_6$, short

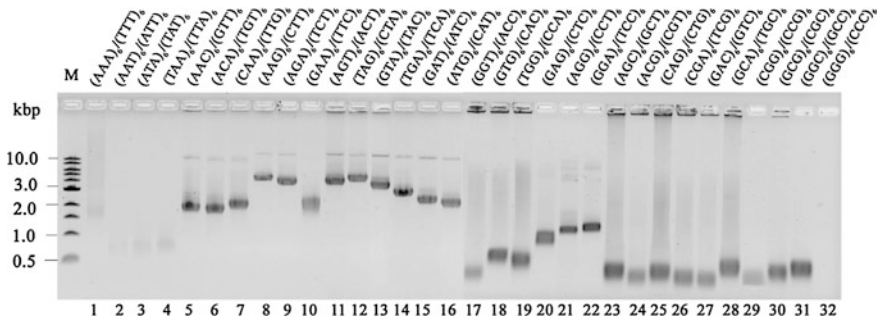

Fig. 147.3 Gel electrophoresis analysis of expansion products of 32 duplexes of trinucleotide repeats at 70 °C for 4 h. 1–16: Short repeats with 0 or 1/3 GC content; 17–32: short repeats with 2/3 or 100 % GC content. Reaction conditions: 50 nM short repeats, 10 U/mL Vent, 0.5 mM dNTPs, in 20 μL of 1 × Thermopol Buffer. The products were analyzed on a 0.8 % agarose gel

repeats with 100 % GC content can be elongated and narrow bands were observed (Fig. 147.2). Obviously, the average elongation speed of each repeats changed with the variation of the sequences. Repeats with 1/3 GC content grew fastest, with a speed of more than 8.0 bp/min. Repeats which have the same GC content but different sequence grew similarly.

In order to find out the effect of temperature to amplification double stands, only duplex $(AGC)_6/(GCT)_6$ and $(GAT)_6/(ATC)_6$ were studied specially. For $(AGC)_6/(GCT)_6$ at all temperatures, narrow bands were observed, although smear bands were also present in some cases. At 37 and 50 °C, the reactions were very slow and weak bands could only be observed after 20 h; at a temperature higher than 60 °C, the products were observed in just 1 h. For $(GAT)_6/(ATC)_6$, narrow bands could be observed from 37 to 70 °C, although the smear bands were obviously present at 50 and 60 °C. As compared with $(AGC)_6/(GCT)_6$, whose GC content is 2/3, elongation speed for $(GAT)_6/(ATC)_6$ (1/3 GC content) was up to 8.5 bp/min at 70 °C. Unexpectedly, elongation was carried out for both $(AGC)_6/(GCT)_6$ and $(GAT)_6/(ATC)_6$, although the efficiency is not so high. It should be noticed that the optimum reaction temperature of Vent DNA polymerase is 70–80 °C.

147.3.3 Sequence Analysis of Elongated Products by Restriction Enzyme Digestion and Sequencing of Elongated Products

To check whether the long products were surely elongated from short repeats, the elongated DNA expanded from $(AGC)_6$, $(GCT)_6$, and $(AGC)_6/(GCT)_6$ were digested by restriction enzyme ApekI with recognition site G↓CWGC and AluI with recognition site AGCT (Fig. 147.4). The expansion products of single and double strands were digested efficiently and almost no DNA was left with ApekI after 1 h,

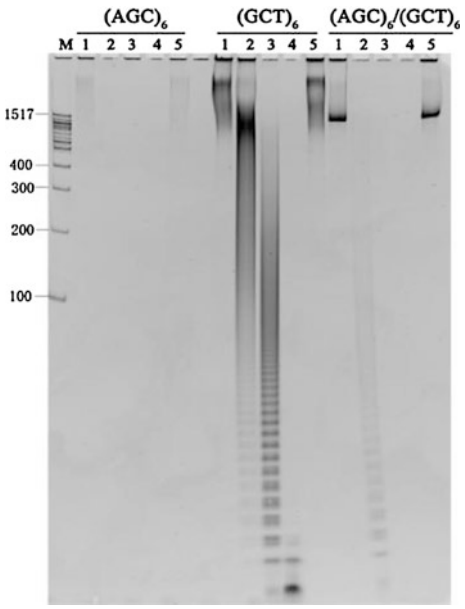

Fig. 147.4 Digestion of elongated products of short repeats by restriction enzyme. *Lane 1* Elongated products without. *Lane 2–4* ApeKI treatment for 10, 30, 60 min, respectively. *Lane 5* AluI treatment for 60 min. The standard reaction conditions were used and the DNA products were analyzed by nondenaturing polyacrylamide gel (6 %) electrophoresis

indicating that the products have a large amount of GCAGC and/or GCTGC sequence at short intervals. On the other hand, AluI could not digest these kinds of long DNA after 1 h showing that little AGCT sequence existed (Fig. 147.4).

The products sequencing of $(CAG)_6$ showed that the sequences of elongated products were basically tandem repeats of seeds (data not shown). There were up to 64 CTG in the long products without any interruption, indicating that slippage occured during elongation. It can be inferred from the result that the long DNA were made up of a large amount of trinucleotide repetitive sequences. Although several point mutations appeared. These may be the result of misincorporation by Vent (exo^-) DNA polymerase, which lacks proof-leading activity.

147.3.4 Proposed Mechanism of Elongation of Short Repetitive Sequences

From above results, we concluded that trinucleotide repetitive sequences had the potential to expand generally. Almost all of the trinucleotide repeats could be elongated, but the sequence had a great effect on it. It showed that no matter for single strands or for double strands, the repeats with more GC contents could easily proceed. For single strands, the expansion was so quick that the products of more than 10 kb could be got even in 1 h. We proposed a new model to explain this unusual elongation (Fig. 147.5a). The 18 nt short repeats can form transient hairpin at 3′ end, then DNA polymerase catch it to complete the template/primer

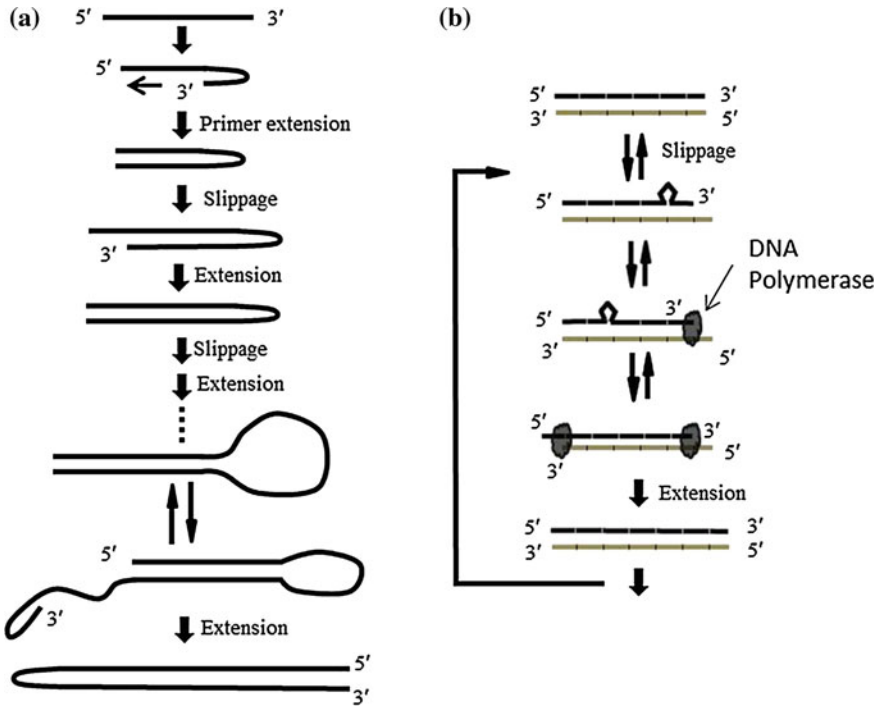

Fig. 147.5 Proposed mechanism for elongation of tandem repetitive sequence. **a** Mechanism proposed of the slippage and hairpin extension model for single strands repeats. **b** Possible mechanism for duplex repeats. The $(ATC)_6/(GAT)_6$ was set as an example to explain this slippage synthesis model

extension to form a bigger hairpin. Slippage happened in this duplex followed by filling the 5′ by DNA polymerase. After several slippage-extension cycles, the 3′ end slips to form a overhang, which was long enough to be in favor of a new hairpin. In this situation the self-priming extension happened again to prolong the repeats, then accessed to next expansion cycle.

According to this model, most of the results can be explained. The elongated products of $(AGC)_6$ and $(GCT)_6$ can be digested completely by ApeKI to give very clear bands, indicating that the elongated products consist of only repetitive sequence of short repeated seeds. At the beginning, for example, the hairpin of $(GAT)_6$ at the end is difficult to form at the reaction temperatures (60–70 °C). However, in the present of DNA polymerase, which can strongly bind to the template/primer to form the expansion complex, the transient hairpin formation can be caught by a DNA polymerase and carry out primer extension quickly. On the other hands, with the products becoming longer, the T_m can be up to 75.9 °C, in which the slippage can be easier to process and expansion become quick evidently. At lower temperatures, the duplex is difficult to slip; at higher temperatures, the transient hairpin formation is difficult to be caught by DNA polymerase so that the efficiency of primer extension becomes lower.

For duplex extension, the obvious bright single band showed that something different from single strands elongation had happened. Some other studies have discovered similar phenomenon and put forward several mechanisms [13, 17]. The slippage model is the orthodox view but few practical data and theoretical explanation could give supports. Moreover, this slippage required very high activation energy for inter-strands slippage when the reaction temperature is much lower than the T_m of repeats. We found that almost all of the double trinucleotide repetitive sequences increased linearly with time in some extent, and the extension speed is not related to the length of prolonged products, which is unacceptable to explain with the existing model. We proposed a model as shown in Fig. 147.5b. It was reported that several base pair opening (breathing) could happen transiently blew the T_m of duplex [18, 19]. Generally, base pairs are much easier to open at the end of the duplex [20]. Strand slippage inclines to happen for repetitive sequences. If the six base pair in the end of duplex opens to take a bulge form, the trinucleotide slippage will happen, then DNA polymerase binds to the 3′ end to prevent it from returning back to normal duplex. This kind of unstable trinucleotide bulge will slip to the other end to form a template-primer complex and filled by polymerase. The slippage-loop-filling cycle makes duplex extend gradually. The duplex expanded linearly as the even speed of loop forming, which could account for the result of our research. When product is elongated to more than 1.0 kb, the loop becomes easier to slip to left and right and need more time to wave to the end, which makes the expansion to slow down.

147.4 Conclusions

From above results, we concluded that all of the trinucleotide repetitive sequences, no matter single strand or duplex, can be used as the seeds for synthesizing long DNA by DNA polymerase under isothermal conditions, except several strands with uniform nucleotide. The temperature and sequence of repeats had great effect on it. The products were made up of a large number of trinucleotide repeats. New model on these two kinds of elongation was proposed. Single strands repeat expanded quickly to more than 10 kb. The high efficiency may be due to the continuous slippage and hairpin formation for self-priming and primer extension. For duplex repeats, as a result of slippage of duplex and spread of loop, the elongation product prolonged gradually with a narrow size distribution, and the length of synthesized DNA increases linearly with reaction time. These models may be helpful for clarifying the molecular evolution of nucleic acids and the nonspecification during DNA detection.

Acknowledgments Recruitment programs of “Wanren Plan”, “Fund for Distinguished Young Scholars” of Shandong province, and “National Youth Qianren Plan”, “Program for Changjiang Scholars and Innovative Research Team in University (PCSIRT)” are acknowledged.

References

1. Hastings PJ, Lupski JR, Rosenberg SM et al (2009) Mechanisms of change in gene copy number. Nat Rev Genet 10:551–564
2. Heidenfelder BL, Topal MD (2003) Effects of sequence on repeat expansion during DNA replication. Nucleic Acids Res 31:7159–7164
3. Treangen TJ, Salzberg SL (2012) Repetitive DNA and next generation sequencing: computational challenges and solutions. Nat Rev Genet 13:36–46
4. Mohmood S, Sherwani A, Khan F et al (2003) DNA trinucleotide repeat expansion in neuropsychiatric patients. Med Sci Monitor 9:237–245
5. Kumar RS, Parthiban KT, Rao MG (2009) Molecular characterization of jatropha genetic resources through inter-simple sequence repeat (ISSR) markers. Mol Biol Rep 36:1951–1956
6. Heale SM, Petes TD (1995) The stabilization of repetitive tracts of DNA by variant repeats requires a functional DNA mismatch repair system. Cell 83:539–545
7. Aquilina G, Hess P, Branch P et al (1994) A mismatch recognition defect in colon carcinoma confers DNA microsatellite instability and a mutator phenotype. P Natl Acad Sci USA 91:8905–8909
8. Elizabeth FS, Linda J (2000) Dinucleotide repeat expansion catalyzed by bacteriophage T4 DNA polymerase in vitro. J Biol Chem 275:31528–31535
9. Ogata N, Miura T (1998) Creation of genetic information by DNA polymerase of the thermus thermophilus. Nucleic Acids Res 26:4657–4661
10. Ogata N, Miura T (2000) Elongation of tandem repetitive DNA by the DNA polymerase of the hyperthermophilic archaeon thermococcus litoralis at a hairpin-coil transitional state: a model of amplification of a primordial simple DNA sequence. Biochemistry 39:13993–14001
11. Liang XG, Jensen K, Frank-Kamenetskii MD (2004) Very efficient template/primer-independent DNA synthesis by thermophilic DNA polymerase in the presence of a thermophilic restriction endonuclease. Biochemistry 43:13459–13466
12. Liang XG, Kato T, Hiroyuki A (2008) Mechanism of DNA elongation during de novo DNA synthesis. Nucleic Acids Res Supple 52:411–412
13. Kotlyar AB, Borovok N, Molotsky T et al (2005) In vitro synthesis of uniform poly (dG)-poly(dC) by klenow exo$^-$ fragment of polymerase I. Nucleic Acids Res 33:525–535
14. Tuntiwechapikul W, Salazar M (2002) Mechanism of in vitro expansion of long DNA repeats: effect of temperature, Repeat length, repeat sequence, and DNA polymerases. Biochemistry 41:854–860
15. Ogata N, Miura T (1998) Creation of genetic information by DNA polymerase of the archaeon thermococcus litoralis: influences of temperature and ionic strength. Nucleic Acids Res 26:4652–4656
16. Liang XG, Kato T, Hiroyuki A (2007) Unexpected efficient ab initio DNA synthesis at low temperature by using thermophilic DNA polymerase. Nucleic Acids Res supple 51:351–352
17. Jorg SH, Eric TK (2005) Efficient isothermal expansion of human telomeric and minisatellite repeats by thermococcus litoralis DNA polymerase. Nucleic Acids Res 33:4922–4927
18. Krueger A, Protozanova E, Frank-Kamenetskii MD (2006) Sequence-dependent base pair opening in DNA double helix. Biophys J 90:3091–3099
19. Frank-Kamenetskii M (1987) How the double helix breathes. Nature 328:17–18
20. Smolina IV, Demidov VV, Soldatenkov VA et al (2005) End invasion of peptide nucleic acids (PNAs) with mixed base composition into linear DNA duplexes. Nucleic Acids Res 33:e146

Chapter 148
Hydroxylation of Dehydroepiandrosterone by *Penicillium decumbens* ph-13

Song Zhang, Peihui Liu, Lin Zhao and Xinli Liu

Abstract Dehydroepiandrosterone was hydroxylated by biotranformation with typical *Penicillium decumbens* ph-13. The two products were obtained and identified by NMR and polarimeter. The results indicate that they are 1α-hydroxy-dehydroepiandrosterone and 7α-hydroxy-dehydroepiandrosterone, respectively. The hydroxylation of dehydroepiandrosterone by *Penicillium decumbens* ph-13 offers a gentle and promising way of producing the desired compounds that is not available by chemical synthesis.

Keywords Biotransformation · Dehydroepiandrosterone · Hydroxylation · Penicillium decumbens

148.1 Introduction

Dehydroepiandrosterone (DHEA, 3β-hydroxy pregna-5-ene-17-one), naturally occurring in human blood, is an ACTH-regulated C-19 steroid derived from cholesterol and classified with the adrenal androgens, androstenedione, and testosterone [1–5]. It has been shown to be effective in potential antiaging properties, longevity, improvement in lipid profiles, and protection against development of atherosclerosis, osteoporosis, and modulation of immunological mechanisms [6–9].

More recently, the attention has been focused on the hydroxylation of steroid in order to obtain more functionalized compounds due to high regio- and stereoselectivity of these reactions [10, 11]. As far as DHEA is concerned, the hydroxylated DHEA plays a very significant role in medicine field. For example,

S. Zhang · P. Liu · L. Zhao · X. Liu (✉)
Shandong Provincial Key Laboratory of Microbial Engineering,
School of Food and Bioengineering, Shandong Polytechnic University,
Jinan 250353, People's Republic of China
e-mail: vip.lxl@163.com

T.-C. Zhang et al. (eds.), *Proceedings of the 2012 International Conference on Applied Biotechnology (ICAB 2012)*, Lecture Notes in Electrical Engineering 251,
DOI: 10.1007/978-3-642-37925-3_148,

1α-hydroxy-dehydroepiandrosterone and 7α-hydroxy-dehydroepiandrosterone are important drug intermediates for the synthesis of active vitamin D3 and its analogues, which are wildly used in therapy of osteoporosis, hyperparathyroidism, psoriasis, cancer, and immune diseases [7, 8].

However, it is very difficult to introduce hydroxy group at C-1 and C-7 position of DHEA molecule by chemical synthesis. To the best of our knowledge, we have not found in literature any reports on the hydroxylation of DHEA by chemical method at C-1 position. For this reason, the present investigation highlights this valuable hydroxylation of DHEA for the first time by a typical *Penicillium decumbens* ph-13.

148.2 Materials and Methods

148.2.1 Microorganism

The screening of strains was performed from the oil and the objective strain was identified as *Penicillium decumbens* ph-13 by 18S rDNA sequence and morphological observation.

148.2.2 Cultivation Medium and Main Chemicals

The strain was maintained on agar slants composed of potato (200 g/L), glucose (20 g/L), agar (18 g/L). The seed medium consisted of 1 % soluble starch, 0.5 % glucose, 0.5 % peptone, 0.3 % N–Z-case, 0.2 % yeast extract, 0.1 % dipotassium hydrogen phosphate, 0.05 % magnesium sulfate, and 0.3 % calcium carbonate. The pH was adjusted to 7.0 with NaOH solution. The transformation medium components were sucrose 4.75 %, sodium nitrate 3.69 %, magnesium sulfate 0.31 %, ferrous sulfate 0.002 %, and manganese sulfate 0.001 %. DHEA was purchased from Wuhan Hezhong Chemical Company. 1α-hydroxy-dehydroepiandrosterone was donated by Professor YASUHIRO IGARASHI from TOYAMA Prefectural University.

148.2.3 Experimental Methods

The spore of *Penicillium decumbens* ph-13 were scraped from the slants and suspended in sterilized water [12]. The suspension was transferred to 300 mL Erlenmeyer flask containing 70 mL of the seed medium. The incubation was carried out at the temperature of 30 °C for 72 h, until the proper growth of the microorganisms was

achieved. The mycelia were washed three times with sterilized water, and then inoculated to transformation medium. After cultivated at the temperature of 30 °C for 72 h on a rotary shaker (180 r/min), the hydroxylation substrate (DHEA) was dissolved in acetone and added to the culture medium at the concentration of 0.6 g/L. In addition, culture controls containing only the fermentation medium and the microorganism (without substrate) were employed to help distinguish biotransformation products from naturally occurring products. The hydroxylation was completed after incubation for 72 h under the above conditions.

The microorganism and the fermentation medium were separated by vacuum filtration in a BÜchner funnel. The collected solids on the filter paper and the filtrate was extracted separately with dichloromethane for several times, all of the extracts were combined, concentrated by rotary evaporators, and washed with petroleum ether four times. The products was purified by silica gel column chromatography (4 × 50 cm, 200–300 mesh), using acetic ether/ethylether (20:1) as eluent. Fractions were collected in 50 mL aliquots. Thin layer chromatography (TLC) was performed using silica gel GF254 with a mobile phase of acetic ether/ethylether (20:1). It was visualized with 10 % sulfuric acid. 1α-hydroxy-dehydroepiandrosterone offered by Professor YASUHIRO IGARASHI was employed as reference. Two main crude products (I and II) were obtained. The crude product I was dissolved with small portions of methylene chloride, and preparative thin-layer chromatography (PTLC) was carried out, a mixed solvent of chloroform/methanol (13:1) was employed as the mobile phase. The target silica gel was scraped, pulverized, and eluted by silica gel column chromatography (2 × 15 cm), using chloroform/methanol (5:1) as eluent. The eluent was concentrated, crystallized, and washed by acetic ester. The white needle-shaped crystals were obtained. Similar method was employed to purify the crude product II, and the white powder was obtained.

The high performance liquid chromatography (HPLC) was performed on Elite instrument for quantitative analysis of the two products. Resolution was achieved using an analytical ODS-BP reverse phase column from Shimadzu (4.6 × 200 mm); the elution was methanol/H_2O solution (3:2); detection at 240 nm; flow for analytical resolution 0.8 mL/min. The ^{1}H and ^{13}C nuclear magnetic resonance (NMR) spectra were obtained using a Bruker Avance 600 spectrometer at 600 and 150 MHz, respectively, with tetramethylsilane as internal standard in $CDCl_3$, and chemical shifts are given as δ values. The optical activity was measured by polarimeter (WZZ-2B Automatic Polarimeter).

148.3 Results and Discussion

The hydroxylation of DHEA was performed by *Penicillium decumbens* ph-13 which was screened in our laboratory from soil around the chemical factories and pharmaceutical factories in Jinan, China. The microbiological hydroxylation mechanism of steroids has been illustrated in terms of a triangular relationship

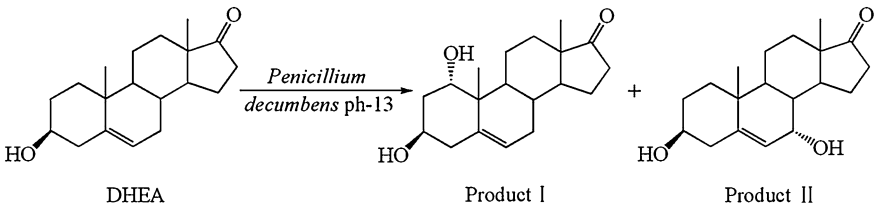

Fig. 148.1 Products of microorganism hydroxylation of DHEA

between two binding sites and the site of hydroxylation [13–16]. The biological activity and application of the hydroxylation products is up to their oxidoreduction. As seen in Fig. 148.1, in our experiments the two products are obtained, one is white needle-shaped crystals (product I), the other is white powder (product II). After optimized hydroxylation process conditions, the yields are about 18.83 and 21.55 %, respectively.

The chemical structures of the products were identified by NMR spectra data (^{1}H-NMR, ^{13}C-NMR, HMBC), and optical activity. The data of ^{1}H-NMR and ^{13}C-NMR for product I and II are given in Tables 148.1 and 148.2, respectively. The spectra of product I show that the compound contains 28 hydrogen atoms, 19 carbon atoms, 1 carbonyl group, 1 carbon double bonds, 1 olefins hydrogen atoms, 2 methyl groups, 2 carbon-hydrogen group-bearing oxygen atoms. Combining with HMBC spectra, we can confirm that the resonance of C-5 correlates with H-1 and H-bearing C-18. The hydroxyl group was introduced to C-1 position by comparing the spectra of the substrate of DHEA (Spectral Database for Organic Compounds SDBS. Therefore the product I is 1-hydroxy-dehydroepiandrosterone.

The molecular configuration brings out the optical activity. For steroids, the configuration of the introduced hydroxyl group can be deduced from the difference of the specific optical activity between the hydroxylated compound and the parent compound. The difference of specific rotation of product I and DHEA is 11.8° (c 0.12, MeOH). According to Van't Hoff rule [17] and the empirical, semi-empirical rule [18, 19] of optical activity, we can confirm that the Product I is 1α-hydroxy-dehydroepiandrosterone.

Similarly, the spectra of product II indicate the similar structure, but the resonance of C-5 and C-6 correlates with H-7, the resonance of C-5 correlates with H-bearing C-18. The conclusion was drawn that the substrate of DHEA was hydroxylated at C-7 position. Comparison of the spectra data of this compound with the reported data [20] led to the identification as known hydroxylated DHEA, 7α-hydroxy-dehydroepiandrosterone.

Table 148.1 1H NMR ($CDCl_3$, 600 MHz) data of the products

H (δ/ppm)	Product I	Product II
1-H	3.97 m	
3-H	3.56 m	3.57 m
6-H	5.32 m	5.64 m
7-H		3.98 m
18-H	1.08 s	0.89 s
19-H	0.90 s	1.02 s

Table 148.2 ^{13}C NMR ($CDCl_3$, 150 MHz) data of products

C (δ/ppm)	Product I	Product II
1	72.9	35.8
2	31.2	31.1
3	71.3	71.1
4	41.6	41.9
5	143.7	146.5
6	125.5	123.5
7	36.9	64.3
8	40.5	37.2
9	48.2	42.6
10	36.7	37.5
11	20.4	20.1
12	31.5	31.3
13	47.8	47.1
14	51.2	44.9
15	24.2	21.9
16	36.0	36.9
17	221.1	221.1
18	13.6	13.3
19	19.2	18.3

148.4 Conclusion

The two hydroxylated DHEA were obtained by biotransformation with *Penicillium decumbens* ph-13. One is 1α-hydroxy-dehydroepiandrosterone; the other is 7α-hydroxy-dehydroepiandrosterone. The yields are about 18.83 and 21.55 %, respectively. It can be concluded that the hydroxylation by *Penicillium decumbens* ph-13 offer a gentle and promising way of producing the desired hydroxylated compounds.

Acknowledgments The work was supported by natural science fund of Shandong Province (ZR2011CQ006) and Postdoctoral innovation project special fund of Shandong Province (No. 200903077).

References

1. Oberbeck R, Deckert H, Bangen J et al (2007) Dehydroepiandrosterone: a modulator of cellular immunity and heat shock protein 70 production during polymicrobial sepsis. Intensive Care Med 33:2207–2213
2. Kalimi M, Shafagoj Y, Loria R et al (1994) Anti-glucocorticoid effects of dehydroepiandrosterone (DHEA). Mol Cell Biochem 131:99–104
3. Duan RS, Link H, Xiao BG (2003) Dehydroepiandrosterone therapy ameliorates experimental autoimmune myasthenia gravis in lewis rats. J Clin Immunol 23:100–106
4. Parker LN (1989) Adrenal androgens in clinical medicine. Academic Press, San Diego
5. Baulieu E, Corpechot C, Dray F et al (1965) An adrenal secreted 'androgen': Dehydroisoandrosterone sulfate. Its metabolism, and a tentative generalization on the metabolism of other steroid conjugates in man. Rec Prog Horm Res 21:411–500
6. Kumar P, Taha A, Sharma D et al (2008) Effect of dehydroepiandrosterone (DHEA) on monoamine oxidase activity, lipid peroxidation and lipofuscin accumulation in aging rat brain regions. Biogerontology 9:235–246
7. Wolf OT, Kirschbaum C (1999) Brain Res Rev 30:264–288
8. Brown AJ (2001) Microbiological Hydroxylation of steroids part VII. The pattern of dihydroxylation of mono-oxo-5-androstanes and 5-estranes with the fungus *Rhizopus nigricans*. Am J Kidney Dis 38:3–19
9. Bemd GJ, Pols HA, Leeuwen JP (2000) Anti-tumor effects of 1, 25-dihydroxyvitamin D3 and vitamin D analogs. Curr Pharm Des 6:717–732
10. Bartmanska A, Dmochowska-Gładysz J, Huszcza E (2005) Steroids' transformations in *Penicillium notatum* culture. Steroids 70:193–198
11. Ahmad S, Johri BN (1993) Microbial transformation of sterols in organic media. Indian J Chem 32:67–69
12. Parshikov IA, Freeman JP, Lay JO et al (1999) Regioselective transformation of ciprofloxacin to *N*-acetylciprofloxacin by the fungus *Mucor ramannianus*. FEMS Microbiol Lett 177:131–135
13. Browne JW, Denny WA, Jones ERH et al (1973) Microbiological hydroxylation of steroids part VII. The pattern of dihydroxylation of mono-oxo-5α-androstanes and 5α-estranes with the fungus *Rhizopus nigricans*. J Chem Soc Perkin Trans I:1493–1499
14. Chambers VEM, Denny WA, Evans JM et al (1973) Microbiological hydroxylation of steroids part VIII. The pattern of monohydroxylation of diketones and keto-alcohols derived from 5α-androstane with cultures of the fungus, *Rhizopus nigricans*. J Chem Soc Perkin Trans I:1500–1511
15. Coon MJ, Ding X (1992) Cytoehrome P450: progress and predietions. FASEB J 6:669–673
16. Peterson JA, Graham SE et al (1998) Structure 6:1079–1085
17. Van't Hoff JH (1894) Die Lagerung der Atome im Raume. Kessinger Publlc, Vieweg, Braunschweig
18. Brewster JH (1961) Some applications of the conformational dissymmetry rule. Tetrahedron 13:106–122
19. Freudenberg K, Todd J, Seidler R et al (1933) Ann Chem 501:191–199
20. Li HP, Liu HM, Ge WZ et al (2005) Synthesis of 7α-hydroxy-dehydroepiandrosterone and 7β-hydroxy-dehydroepiandrosterone. Steroids 70:970–973

Chapter 149
Preparation and Characterization of Cross-Linked Enzyme Aggregates of Amyloglucosidase

Jiandong Cui and Yanan Zhang

Abstract Cross-linked enzyme aggregates of glucoamylase (GAs-CLEAs) were prepared. The effect and concentration of aggregating agent as well as those of cross-linking agent were studied. It was effective for GAs-CLEAs production to use ammonium sulfate (80 %-saturation), and subsequently cross-link for 2 h with 4.5 % (v/v) glutaraldehyde. Some changes in optimum pH and temperature values of the enzyme activity were recorded after immobilization. Moreover, the thermal stability of the resulting GAs-CLEAs was also investigated. Compared to the free enzyme, the GAs-CLEAs exhibited the expected increasing thermal stability. These CLEAs are suitable for all starch-based industries. To the best of our knowledge, this is the first report of immobilization of GAs as cross-linked enzyme aggregates.

Keywords Glucoamylase · Cross-linked enzyme aggregates · Preparation · Characterization · Biocatalysis

149.1 Introduction

Enzymes as biocatalysts are useful tools for a green and sustainable industry. However, large-scale industrial use of enzymes is hampered by high cost and instability. Therefore, the stabilization of enzymes has attracted more and more attention. Generally, immobilized enzymes are more stable than their counterparts

J. Cui (✉)
College of Bioscience and Bioengineering, Hebei University of Science and Technology, Shijiazhuang 050018, People's Republic of China
e-mail: cjd007cn@163.com

Y. Zhang
Library, Hebei University of Science and Technology, Shijiazhuang 050018, People's Republic of China

T.-C. Zhang et al. (eds.), *Proceedings of the 2012 International Conference on Applied Biotechnology (ICAB 2012)*, Lecture Notes in Electrical Engineering 251,
DOI: 10.1007/978-3-642-37925-3_149,

in solution; they have the potential of circumventing catalyst stabilization against thermal and chemical denaturation. Furthermore, immobilized enzymes can be recovered. However, the disadvantage of immobilization on a solid support is the low enzyme/support weight ratio and high production cost. Recently, carrier-free enzyme immobilization approach has attracted more attention due to clear advantages: highly concentrated enzyme activity in the catalyst, high stability and the low production cost due to the exclusion of an additional carrier [1, 2]. In particular, preparation of cross-linked enzyme aggregates (CLEAs) has emerged as a promising carrier-free immobilization strategy [3]. The simple process of preparing CLEAs consists of two steps: protein precipitation and cross-linking with bifunctional agent (such as glutaraldehyde). Moreover, it is worth mentioning that CLEAs can be obtained from crude enzyme [1]. Successful preparation of CLEAs from a broad range of enzymes, including nitrilase, lipases, and laccases, have been reported [4–6], however, until now, immobilization of glucoamylase (E.C. 3.2.1.3-GAs), as cross-linked enzyme aggregates, has not been described. GAs, is one of the most important enzyme for all starch-based industries (food, textile, brewing, paper, and alcohol industries) and also for the pharmaceutical and fine chemical industries because it is capable of achieving complete breakdown of the starch to glucose [7–9]. However, GAs from most sources is unstable at higher temperatures industrial saccharification. To eliminate the disadvantages present in the conventional process, the enzyme has been immobilized using different methods [10–12]. GAs was immobilized on various insoluble carriers with the retention of its catalytic properties which can be used repeatedly. A novel affinity covalent immobilization technique of glucoamylase enzyme onto ρ-benzoquinone-activated alginate beads was presented and compared with a traditional entrapment. The results showed that there was no shift in the optimum temperature and pH of immobilized enzymes. Km values of free and entrapped glucoamylase were found to be almost identical, while the covalently immobilized enzyme has lower affinity for substrate. Moreover, the Vm value of covalently immobilized enzyme was lower compared to the free counterpart's [13]. GAs was immobilized using a combined method of adsorption of the enzyme to gelatinized cornstarch and subsequent alginate fiber entrapment. The immobilization resulted in 22 % relative activity and has been active for 21 days without decrease in activity [14]. However, preparation of cross-linked enzyme aggregates of amyloglucosidase (GAs-CLEAs) has not been reported. In this work, the preparation of GAs-CLEAs was first introduced, including the analysis of the main immobilization parameters which affects the final volumetric activity of the biocatalyst. In addition, the stability and applicability of GAs-CLEAs for the production of glucose from starch have also been assessed.

149.2 Materials and Methods

149.2.1 Materials

Glutaraldehyde was obtained from Sigma-Aldrich Inc. (St. Louis, MO, U.S.A.). All other reagents were of analytical grade. Industrial glucoamylase (amyloglucosidase; exo-1,4-α-glucosidase; EC 3.2.1.3 from *Aspergillus niger*) was supplied from Novo Nordisk (Beijing, China).

149.2.2 Preparation of CLEAs

GAs-CLEA was prepared using the GAs alone. The different concentrations ammonium sulfate as precipitant was added dropwise to the GAs solution under gentle stirring at 20 °C for 1 h. The different concentrations of glutaraldehyde (1.5, 2.5, 3.5, 4.5, 5.5 %) were added in the mixture for the cross-linking of the aggregates. Samples were shaken continuously during this addition. Then, the mixture was kept at 4 °C for 1 h with constant shaking at 200 rpm and then centrifuged at 10000 ×g for 10min. Afterwards, The supernatant was decanted and the residue was washed with the relevant solvents until no more activity was determined in the supernatant. The resulted CLEA was washed three times with 25 mM Tris-HCl buffer pH 7.0. Finally, CLEA preparation was kept in the same buffer at 4 °C prior to use.

149.2.3 Activity assay

The activities of both free and GAs-CLEA were determined by measuring the glucose content in the medium according to a method described previously [15]. In the assay conditions, using soluble starch as the substrate, soluble starch, 10 ml of 2 % (w/v) in 25 mM acetate buffer solution (pH 5.5), was reacted with immobilized or free GAs at 60 °C for 20 min. The reaction mixture was agitated at 500 rev/min with a magnetic stirrer. After reaction, agitation was stopped, and then the reaction was terminated by adding 5 mL of NaOH solution (0.1 M). The amount of glucose formed was determined by using the DNS method [16]. The amount of glucose was obtained from the calibration curve and used in the calculation of enzyme activity. One unit of GAs activity is defined as the amount of enzyme that produces 1.0 mmol of glucose from dissolubility starch per minute in assay conditions. The activity recovery in CLEAs was calculated as given in Eq. (1):

$$\text{Activity recovery (\%)} = \frac{\text{Activity of CLEAs}}{\text{Activity of free enzyme}} \quad (1)$$

149.3 Results and discussion

149.3.1 Preparation of GAs-CLEAs

As mentioned above, CLEA preparation consists of two steps: aggregation by precipitation and cross-linking. Thus, the impact of the formation procedures on the activity of GAs-CLEAs was studied in two steps: (1) determining the best precipitant and its concentration and (2) determining the impact of cross-linker concentration and cross-link time. Figure 149.1 shows activity recovery using different concentration of ammonium sulfate. The best results (recovery of about 85 % of the initial GAs activity) were obtained using 80 % (w/v) of ammonium sulfate as precipitant. Figure 149.2 is the effect of pH on precipitation. Excellent activity recoveries were observed with the GAs at pH 4–6. A dramatic decrease in activity was observed at pH 8. The highest activity recoveries were obtained at pH 4.5. In addition, different concentrations of glutaraldehyde (1.5–5.5 %) were used to determine the optimum quantity required for stable cross-linking of GAs. At lower concentrations, very little insoluble aggregates could be obtained; whereas at higher concentrations, the amount of insoluble aggregates increased, but no significant activity was detected. The highest activity recovery could be obtained when 4.5 % glutaraldehyde solution and 2 h cross-linked time was adopted (Fig. 149.3).

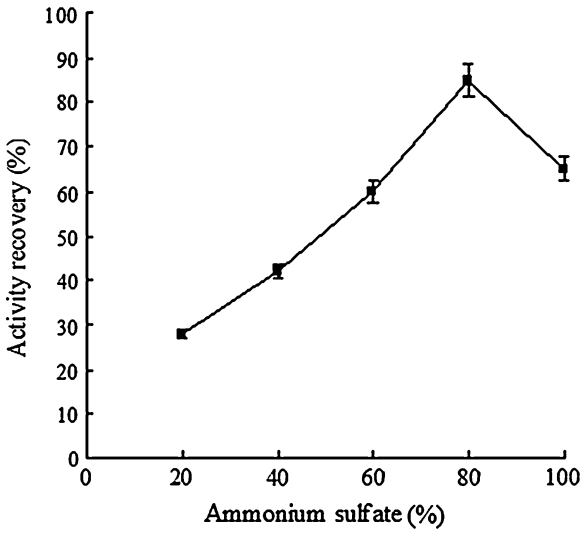

Fig. 149.1 Effect of precipitants on PAL activity recovery

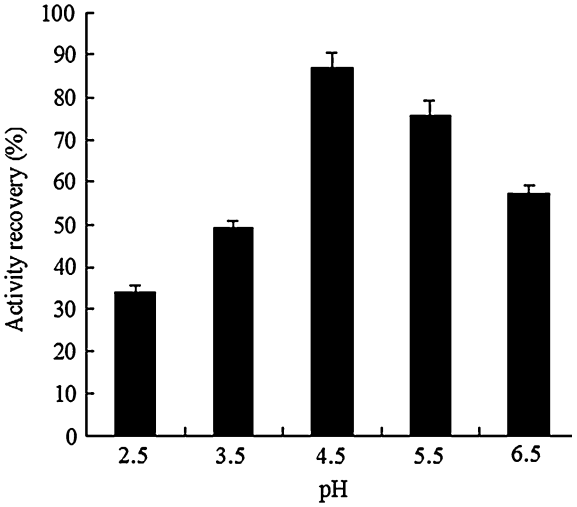

Fig. 149.2 Effects of pH on precipitation

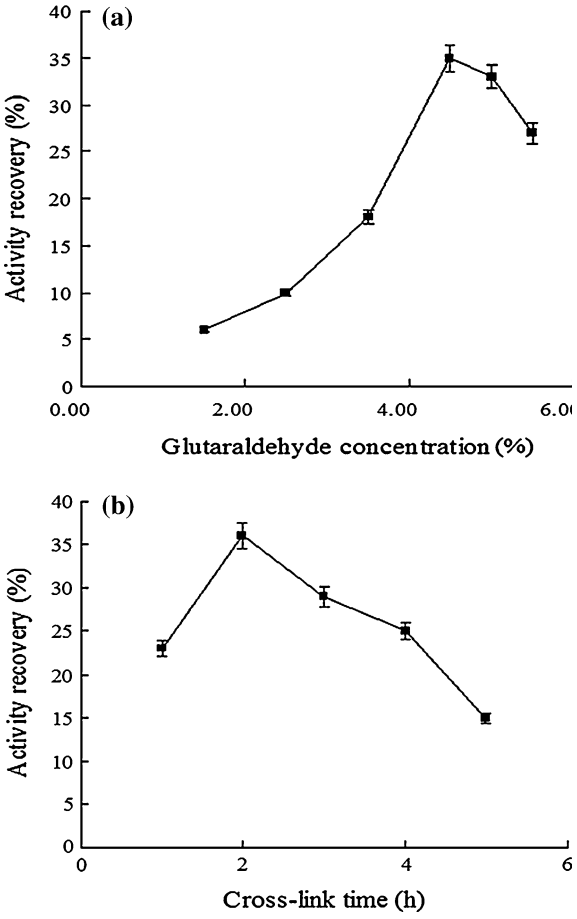

Fig. 149.3 Effect of glutaraldehyde concentration and cross-link time on CLEAs' activity recovery

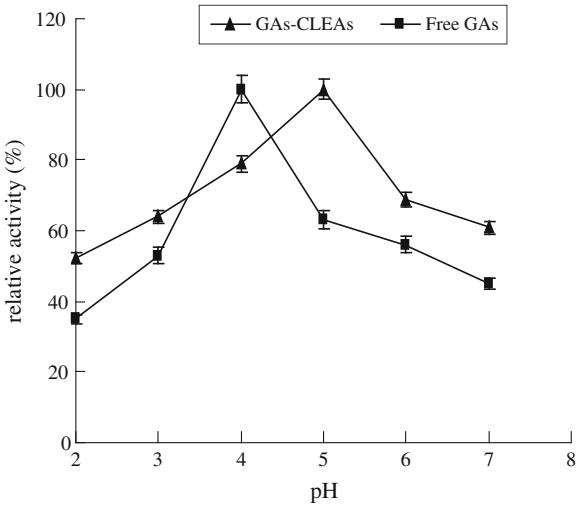

Fig. 149.4 The effect of pH on CLEAs

149.3.2 The Effect of pH and Temperature on the Activity of Soluble and CLEAs

Many studies have shown that the activity and stability of an immobilized enzyme can differ considerably from that of its soluble counterpart [17, 18]. Therefore, the properties of the CLEAs were compared with those of the native GAs. The pH and temperature effect on both free tyrosinase and CLEA activities were determined in the pH range of 2.0–7.0 and temperature range of 30–80 °C. The optimal pH values and temperature for activity of GAs-CLEAs were 5.0 and 70 °C, and these of the soluble enzyme were 4.0 and 60 °C (Figs. 149.4, 149.5). Thus, cross-linking

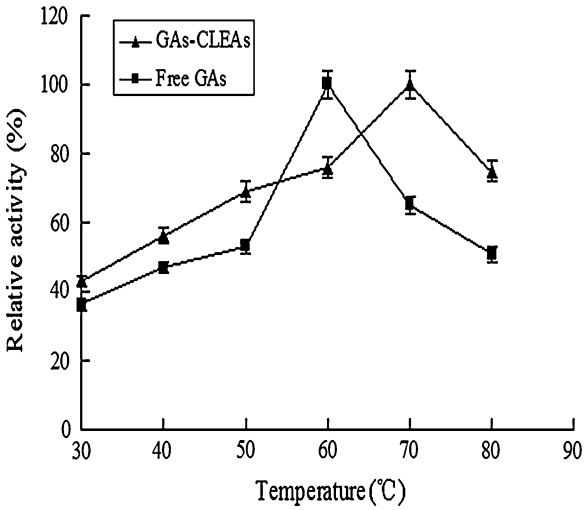

Fig. 149.5 The effect of temperature on CLEAs

the enzyme results in the temperature optimum increased by an impressive 10 °C. Furthermore, the immobilized enzyme was active in a broader pH range, indicating a higher operational stability. Aytar et al. (2008) reported that some changes of the optimum pH values of cross-linked tyrosinase aggregate were observed. Moreover, the optimum temperature of cross-linked tyrosinase aggregate was changed. They considered that this shift could be resulted from the change in acidic and basic amino acid side chain ionizations in the microenvironment around the active site, which was caused by the newly formed interactions between basic residues of the enzyme and glutaraldehyde during cross-linking. This shift in the optimum temperature can be explained by covalent bond formation between proteins caused by glutaraldehyde during CLEA preparation [1]. The same phenomenons were observed by Cerdobbel et al. [18].

149.3.3 Thermal Stability

Thermal stability experiments of both free enzyme and CLEAs were conducted by incubating enzyme samples in the absence of substrate at 50 °C at various time intervals. GAs-CLEAs maintained approximately 62 % activity when stored at 50 °C for 24 h, whereas its soluble counterpart only maintained 40 % of its activity at the same temperature. Thus, the GAs-CLEAs were observed to confer excellent thermal stability to the enzyme. This enhancement in stability can be due to inter- and intramolecular covalent cross-links that prevent the conformational changes [19].

149.4 Conclusions

GAs-CLEAs were first prepared in this study. It demonstrated that the concentrations of ammonium sulfate, glutaraldehyde, cross-linking period, and pH could significant affect CLEA activity. Moreover, after immobilization, thermal stability of glucoamylase was significantly increased. These CLEAs are suitable for all starch-based industries.

Acknowledgements The Project Partially Supported by the National Natural Science Foundation of China (NSFC, Project No. 21072041), Open Funding Project of the National Key Laboratory of Biochemical Engineering (No. KF2010-12), and the Foundation (NO. 2012IM004) of Ministry of Education Key Laboratory of Industrial Fermentation Microbiology (Tianjin University of Science & Technology), P. R. China, and Foundation of Hebei University of Science and technology for Distinguished Young Scientists.

References

1. Aytar BS, Bakir U (2008) Preparation of cross-linked tyrosinase aggregates. Process Biochem 43:125–131
2. Mateo C, Palomo JM, Langen LM et al (2004) A new, mild cross-linking methodology to prepare cross-linked enzyme aggregates. Biotechnol Bioeng 15:273–276
3. Sheldon RA (2007) Cross-linked enzyme aggregates (CLEAs): stable and recyclable biocatalysts. Biochem Soc T 35:1583–1587
4. Cabana H, Jones JP, Agathos SN (2007) Preparation and characterization of cross-linked laccase aggregates and their application to the elimination of endocrine disrupting chemicals. J Biotechnol 132:23–31
5. Gupta P, Dutt K, Misra S et al (2009) Characterization of cross-linked immobilized lipase from thermophilic mould *Thermomyces lanuginosa* using glutaraldehyde. Bioresource Technol 100:4074–4076
6. Kaul P, Stolz A, Banerjee UC (2007) Cross-linked amorphous nitrilase aggregates for enantioselective nitrile hydrolysis. Adv Synth Cat 349:2167–2176
7. Gupta RP, Gigras H, Mohapatra VK et al (2003) Microbial α-amylases: A biotechnological perspective. Process Biochem 38:1599–1616
8. Sanchez JM, Perillo MA (2000) α–Amylase kinetic parameters modulation by lecithin vesicles: Binding versus entrapment. Colloid Surfaces B 18:31–40
9. Saville BA, Khavkine M, Seetharam G et al (2004) Characterization and performance of immobilized amylase and cellulose. Appl Biochem Biotechnol 113:251–259
10. Bahar T, Celebi SS (1998) Characterization of glucoamylase immobilized on magnetic poly(styrene) particles. Enzyme Microb Tech 23:301–304
11. Yajima H, Hirose A, Ishii T et al (1989) Immobilization of glucoamylase onto alternative acrylonitrile-butadiene copolymer by amidination reaction. Biotechnol Bioeng 33:795–798
12. Oh JT, Kim JH (2000) Preparation and properties of immobilized amyloglucosidase on nonporous PS/PNaSS microspheres. Enzyme Microb Tech 27:356–356
13. Eldin MMS, Seuror EI, Nasr MA et al (2011) Affinity covalent immobilization ofglucoamylase onto ρ–benzoquinone-activated alginate beads: Π. Enzyme immobilization and characterization. Appl Biochem Biotechnol 164:45–57
14. Aziz T, Yıldız BU, Senay D (2002) A novel method for the immobilization of glucoamylase to produce glucose from maltodextrin. Enzyme Microb Tech 30:406–409
15. Nelson NJ (1944) A photometic adaptation of the somogyi method for the determination of glucose. J Biol Chem 153:375–380
16. Miller GN (1959) Use of dinitrosalicylic acid reagent for determination of reducing sugar. Anal Chem 81:426–428
17. Mateo C, Grazu V, Pessela BCC et al (2007) Advances in the design of new epoxy supports for enzyme immobilization-stabilization. Biochem Soc T 35:1593–1601
18. An Cerdobbel, Winter KDe, Desmet T et al (2010) Sucrose phosphorylase as cross-linked enzyme aggregate: Improved thermal stability for industrial applications. Biotechnol J 5:1192–1197
19. Migneault I, Dartiguenave C, Bertrand MJ et al (2004) Glutaraldehyde: behavior in aqueous solution, reaction with proteins, and application to enzyme cross-linking. Biotechniques 37:790–802

Chapter 150
An Extraction Method Suitable for Two-Dimensional Electrophoresis of Low-abundant Proteins from Ginseng Roots

Rui Jiang, Liwei Sun, Rui Ma, Xiujuan Lei and Daqing Zhao

Abstract Four lysis buffers, which contain different concentration ratio of urea and thiourea, and three extraction methods (sonication extraction, osmotic extraction, and freeze–thaw extraction) were used to optimize the extraction conditions of low-abundant proteins from ginseng roots based on protein extraction efficiency, the good quality of the 2-DE patterns, and the results of mass spectrometry (MS) identification. Our results have shown that when lysis buffer II (7 M urea, 2 M thiourea, 2 % CHAPS, 1 % PMSF, and 1 % protease inhibitor) combined with sonication was used, higher protein extraction efficiency, lower background, more protein spots (987 ± 31), and higher spot intensities of low-abundant proteins were obtained, which indicated that the optimized protocol was suitable for proteomic studies of ginseng root. Moreover, those results provided the foundation for further researches on the significant functional proteins of ginseng roots.

Keywords Two-dimensional electrophoresis · Ginseng root · Low-abundant proteins · Protein extraction

R. Jiang · R. Ma · D. Zhao (✉)
Changchun University of Chinese Medicine, Changchun 130117,
People's Republic of China
e-mail: zhaodaqing1963@163.com

R. Jiang · L. Sun (✉)
Beihua University, Jilin 132013, People's Republic of China
e-mail: sunliwei1970@yahoo.cn

X. Lei
The Chinese Academy of Agricultural Sciences Institute of Specialty, Jilin 132011,
People's Republic of China

T.-C. Zhang et al. (eds.), *Proceedings of the 2012 International Conference on Applied Biotechnology (ICAB 2012)*, Lecture Notes in Electrical Engineering 251,
DOI: 10.1007/978-3-642-37925-3_150,

150.1 Introduction

Panax ginseng C. A. Meyer is a well-known traditional Chinese medicine (TCM) and has been used in China, Korea, and other Asian countries for over 2,000 years. Although ginsenosides are considered to be the main active pharmacological compounds in ginseng roots [1], various pharmacological effects of ginseng proteins have been reported now, such as antioxidative activity [2], serum lipid and blood pressure reducing activity [3, 4], antifatigue activity [5], radioresistance effect [6], regulating immune function [7], antifungal effect [8]. However, less than 100 functional proteins of ginseng roots have been reported [9–13]. It would be quite necessary to systematically study the ginseng proteins that performed important bioactive functional effects.

With the development of functional genomics and proteomics technology, the plant proteomics technology has been improved rapidly. It has been used to rapidly identify hundreds of proteins, discover special functional proteins, elucidate the underlying mechanisms of plant growth metabolism, regulation, and stress resistance. Plant proteomics is also becoming an essential technology in the study of TCM functional proteins.

Two-dimensional electrophoresis (2-DE) is commonly used to separate total proteins in proteomics, in which sample preparation is the key step to determine the success or failure of 2-DE figures. Because of the tough cell walls of ginseng roots and the interference of compounds such as lignins, polyphenols, tannins, alkaloids, and pigments in the roots, it is already difficult to acquire a smart and reproducible 2-DE gel image [1]. It has reported that ginseng roots contained a large proportion of abundant storage proteins which hindered the isolation and characterization of low-abundant proteins and it remained a challenge to isolate both abundant and less abundant proteins using conventional extraction methods [14]. Therefore, to optimize the extraction protocol, especially for low-abundant proteins of important biological function, is crucial to the acquisition of a clear 2-DE gel image.

In this study, we optimized two parameters affecting 2-DE quality, including four lysis buffers and three extraction methods to obtain well-separated protein profiles and enrich low-abundant proteins. The improvement of this extraction protocol was quite important for identification of new significant functional proteins of ginseng roots, and would be also useful to clarify the pharmacologic mechanism of ginseng roots.

150.2 Materials and Methods

150.2.1 Chemicals

IPGphor (7 cm, 24 cm, and pH 3–10), IPG buffer (pH 3–10), protease inhibitor, and mineral oil were obtained from GE. Urea, β-mercaptoethanol, thiourea, CHAPS, PMSF, SB3-10, TECP, DTT, acrylamide, and other imported chemicals were obtained from Sigma. All other chemicals were of analytical grade.

150.2.2 Sample Preparation

Five-year-old fresh *panax ginseng* C. A. Meyer (ginseng) roots were purchased from Fusong, Jilin, China. The roots were cut into small piece and ground in a mortar with liquid nitrogen. 1.5 g of these samples were incubated in 1 ml cold 10 % TCA/acetone containing 0.07 % (v/v) β-mercaptoethanol at −20 °C for 2 h. After centrifugation at 14,000 rpm at 4 °C for 15 min, the pellets were washed with 2 ml cold acetone containing 0.07 % (v/v) β-mercaptoethanol at least three times in order to remove contaminants, dried, and stored at −20 °C until use [15].

150.2.3 Protein Extraction

Dried samples were resolved in four different lysis buffers, respectively [16–20]. The common components they contained were 2 % CHAPS, 1 % PMSF, and 1 % protease inhibitor; and the differences were lysis buffers I: 8 M urea; Lysis buffers II: 7 M urea, 2 M thiourea; Lysis buffers III: 6 M urea, 2 M thiourea; Lysis buffers IV: 5 M urea, 2 M thiourea. Further handling followed one of the following extraction methods: Method A: The samples were sonicated on ice and centrifuged at 14,000 rpm at 4 °C for 15 min. These supernatants were collected, centrifuged at 14,000 rpm at 4 °C for 15 min, again stored at −80 °C [17, 21]. Method B: Instead of sonicating the mixture, the samples were shaken on ice for 2 h. Insoluble substance was removed by centrifugation at 14,000 rpm at room temperature for 15 min and stored at −80 °C [17, 22]. Method C: The samples were cooled at −80 °C for 15 min and then incubated at room temperature for 20 min. This sequence was repeated three times. The samples were clarified by centrifugation at 14,000 rpm at room temperature for 15 min and stored at −80 °C [16, 17]. The protein contents were measured by using Bradford assay [23].

150.2.4 2-DE

2-DE was performed according to the IPG principles and methods of GE with some modifications. In the first dimension, 125 μl of each sample containing 250 μg total proteins in 5 M urea, 2 M thiourea, 2 % CHAPS, 2 % SB3-10, 20 mM DTT, 5 mM TCEP, 0.25 % carrier ampholytes (pH 4–7), and 0.5 % carrier ampholytes (pH 3–10) was used to rehydrate IPG strips (7 cm) in the rehydration cassette for 12 h at 30 V. The running conditions were 200 V, step, 1 h; 500 V, step, 1 h; 1,000 V, Grad, 1 h; 5,000 V, Grad, 4,000 Vhr, 5,000 V, step, 6,000 Vhr. Following IEF, the gel strip was equilibrated with equilibration buffer 1 of 1 % DTT and equilibration buffer 2 of 2.5 % iodoacetamide for 15 min each on a shaker. SDS-PAGE was carried out on a 12.5 % acrylamide gel with tris-glycine buffer system. After electrophoresis, the gels were visualized by staining with colloidal Coomassie blue G-250. The gel profiles of protein spots were scanned using Image Scanner (GE Healthcare), and then the images were analyzed by Image Master two-dimensional Platinum Software and Version 6.0 (GE Healthcare). A mean of three replicates was made for each gel to produce a master image.

150.2.5 2-DE by the Optimized Protocol and Protein Identification

In order to evaluate the separation effect of the optimized protocol, the total proteins of ginseng roots were extracted by that method and were separated by 24 cm pH 3–10 linear IPG strips in 1-DE and 12.5 % acrylamide gel (24 × 18 cm) in 2-DE (methods as above).

150.2.6 Protein Identification

Selected protein spots were exercised manually from gels and digested in-gel with trypsin. The peptides were analyzed by MALDI-TOF-TOF MS experiments. The peptide mass fingerprinting data were used to search for viridiplantae in MSDB databases using the Mascot program.

150.3 Results and Discussion

150.3.1 Comparison of the Protein Contents of Different Lysis Buffers and Extraction Methods

Protein content is one of the main targets to evaluate the protein extraction method for 2-DE. Four different lysis buffers, which contained different concentration ratio of urea and thiourea, were compared, and the protein contents were shown in Fig. 150.1. As shown in Fig. 150.1a, protein concentration of lysis buffer II was highest and increased with nearly 2 times compared with lysis buffer I yielded the lowest of protein concentration using the same extraction method. The similar results were also acquired by using method B (Fig. 150.1b) and method C (Fig. 150.1c). It was shown that urea in combination with thiourea could increase the solubility of proteins and effectively enhance the concentrations of extraction proteins.

Next, we examined three different extraction methods for their ability to enhance the protein concentrations of extract (Fig. 150.1d). There was no significant difference among the three extraction methods in the protein concentration ($P > 0.05$). However, compared with the other methods, sonication method (method A) had the characteristics of simpler to operate and fewer steps, which leaded to better yields.

Moreover, it was noteworthy that ultrasonic time and ultrasound power made strong impacts on the protein extraction efficiency [21]. Therefore, we optimized ultrasonic time and ultrasound power in order to extract most proteins from ginseng roots. In Fig. 150.1e, along with prolongation of the ultrasonic time, the protein concentrations of extract increased continuously, and reached a maximum after sonicate extraction for 40 min. There was higher protein concentration using sonication extraction method at 100 W compared with at 200 W.

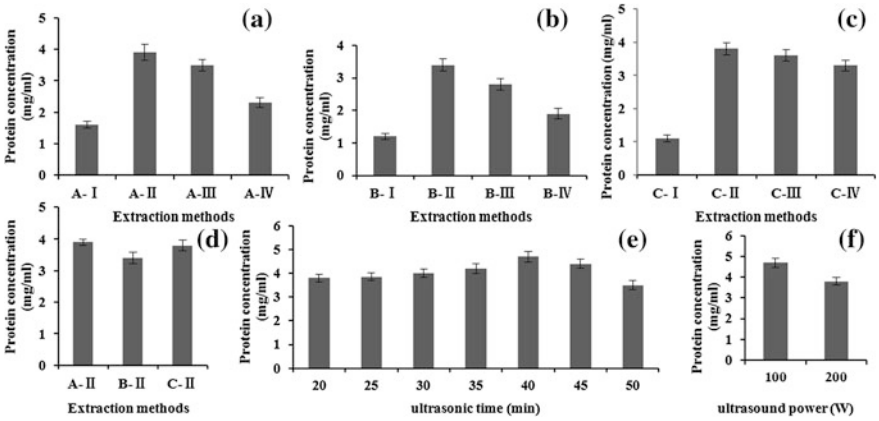

Fig. 150.1 Comparison of the protein concentration by different lysis buffers and extraction methods

So according to the protein concentrations of extract, lysis buffer II (7 M urea, 2 M thiourea, 2 % CHAPS, 1 % PMSF, and 1 % protease inhibitor), combined with sonication at 100 W, 40 min, was the most favorable for preparing samples for 2-DE.

150.3.2 Comparison of 2-DE Profiles of Different Lysis Buffers and Extraction Methods

Enrichment of low-abundant proteins of biological importance to bring them into detectable range is a key standard to evaluate the 2-DE gel profiles [17]. As we all know, there were the tough cell walls in ginseng roots which were less easily disrupted so as to influence the extraction efficiency of proteins, and a large number of the interference substances such as polyphenols, polysaccharides, nucleic acids, alkaloids, pigments in ginseng roots, which would seriously interfere with the proteins of the first-dimension IEF step of 2-DE [1]. A large proportion of abundant storage proteins in ginseng roots could hinder the isolation and characterization of low-abundant proteins and it was also a challenge to enrich less abundant proteins using conventional extraction methods [14]. Unfortunately, using the existing methods of lysis buffers I [16] and lysis buffers II [24] combining with Freeze–thaw extraction method, the profiles of 2-DE obtained were poor quality, high background, a few low-abundant proteins. The optimization of the extraction protocols was significant for identification of new low-abundant proteins that may play an important biological function.

We compared 2-DE patterns using four different lysis buffers and the same extraction method, and the results had shown in Fig. 150.2. The number of protein spots detected in gels (7 cm strips): lysis buffer I, 196 ± 14 spots, lysis buffer II, 389 ± 16 spots, lysis buffer III, 285 ± 12 spots and lysis buffer IV, 235 ± 16 spots. Lysis buffer II (7 M urea, 2 M thiourea) yielded the most number of detectable protein spots, and lysis buffer I yielded the lowest number, consistent with previous research. More proteins ranging in size from 25 to 75 kDa, 5.0 to 6.9 pI, in lysis buffer II, were obtained than in other three lysis buffers (data not shown) and it significantly improved the extraction efficiency of low-abundant in the acid area, as shown in the box of Fig. 150.2a–d, which contained a large quantity of low-abundant proteins of important biological function. This may be because of urea in lysis buffer II, which was commonly used as the denaturant in 2-DE, solubilized and unfolded most proteins to their fully random conformation [17]. Using thiourea combined with urea can further improved solubilization, particularly of membrane proteins [17], and the optimum concentration ratio of urea and thiourea was 7 M/2 M.

As shown in Fig. 150.3, the protein patterns of three extraction methods seemed similar with the proteins ranging in size from 10 to 150 kDa. The total number of

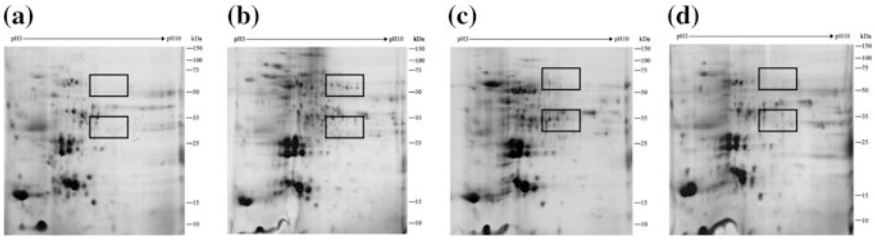

Fig. 150.2 Optimization of lysis buffers for the solubilization of ginseng roots proteins. **a** lysis buffer I, **b** lysis buffer II, **c** lysis buffer III, **d** lysis buffer IV

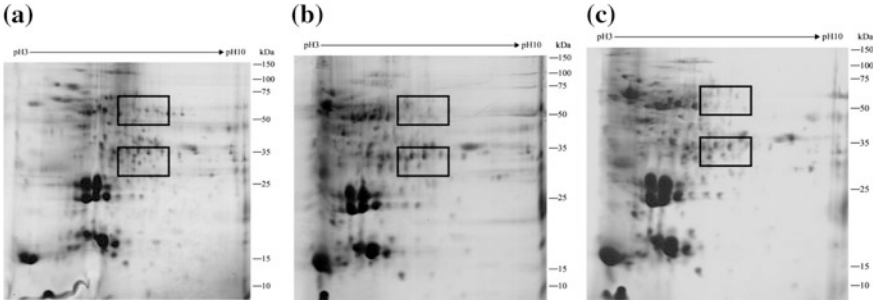

Fig. 150.3 2-DE analysis of ginseng roots proteins extracted by different extraction methods. **a** sonication extraction method, **b** osmotic extraction method, **c** freeze–thaw extraction method

protein spots on 2-DE gels of method A was 389 ± 16, which were increased more than 2.5 fold compared with the results reported [16, 24–26], and method B and method C were only 294 ± 13 and 345 ± 16 respectively. Relative to other extraction methods, the area in size from 25 to 75 kDa of method a, had less horizontal streaking and more protein spots (as shown in the box of Fig. 150.3a–c). Sonication, a vigorous lysis method, can increase the motion velocity and enhance the penetrating power of the molecules of the medium, and break up nucleic acids and glucosides of the sample in order to remarkable increase protein solubility and enrich low-abundant proteins [17]. Therefore, method A combining with lysis buffer II was better suited to obtain high quality proteins of ginseng roots for 2-DE.

150.3.3 2-DE by the Optimized Protocol

The total proteins of 2-DE (24 cm strips) were extracted according to the optimized protocol and 2-DE was performed according to the above methods (Fig. 150.4). The overall quality of the protein profiles were good, with less

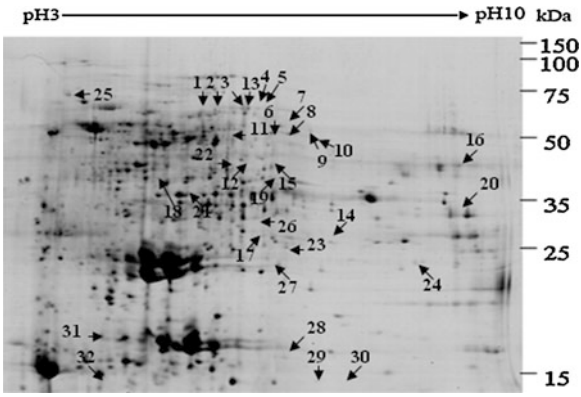

Fig. 150.4 Application of the optimized protocol for protein extraction from ginseng roots

vertical and horizontal streaking and smearing, and the number of protein spots was 987 ± 33, being far above the results reported [16, 24–26]. The optimized protocol can also be suitable for 2-DE of 24 cm strips.

150.3.4 Protein Identification

On the basis of mechanical fluctuant effect, cavitation effect and thermal effect, the ultrasonic extraction as an advanced extraction method, can increase the motion velocity and enhance the penetrating power of the molecules of the medium to improve the extraction efficiency of the proteins from the samples. However, it also had some damage effects to the sample cells and then destroyed the proteins extracted from the samples. Therefore, we identified the new found low-abundant protein spots in acid area using the optimized protocol by MALDI-TOF-TOF MS and locations map was as shown in Fig. 150.4. 20 protein spots of total 31 protein spots were successfully identified (Table 150.1). All these proteins were not the destruction products of the same protein by sonication. Those identified proteins were different functional proteins and involved in metabolism, stress, and other functional proteins, and all the functional proteins were not reported in ginseng roots except catalase and 40S ribosomal protein S21e. It was shown that the optimized protocol of urea/thiourea lysis buffer combined with sonication did not destroy the proteins and could resolve both abundant and less abundant proteins, a number of which were firstly reported in ginseng roots. So it was a suitable method for 2-DE separation and identification of ginseng roots.

Table 150.1 Summary of proteins identified by MALDI-TOF-TOF MS

ID	Protein id	Accession number	Protein mw	PI	Pep. count
01	Hypothetical protein SELMODRAFT_236040[*Selaginella moellendorffii*]	gil300141644	38213.8	9.02	13
02	Cofactor-independent phosphoglyceromutase[*Apium graveolens*]	gil6706331	60896.7	5.26	10
03	Malic enzyme, putative[*Ricinus communis*]	gil255550956	65041.7	6.43	12
06	Serine hydroxymethyltransferase 2[*Glycine max*]	gil222142531	54542.6	8.22	13
07	Predicted: hypothetical protein[*Vitis vinifera*]	gil225433510	51873.2	7.17	10
08	Catalase[*Populus trichocarpa*]	gil224081479	56908.5	7.09	12
09	Catalase[*Populus trichocarpa*]	gil224081479	56908.5	7.09	15
10	Catalase[*Populus trichocarpa*]	gil224081479	56908.5	7.09	14
12	GDH2[*Actinidia chinensis*]	gil149938958	44800.8	6.28	6
15	Monodehydroascorbate reductase[*Vitis vinifera*]	gil146432261	47249.7	5.93	7
17	Hypothetical protein[*Vitis vinifera*]	gil147862790	24295.9	7.03	11
18	Unnamed protein product[*Vitis vinifera*]	gil297736283	118733.5	5.38	25
19	Unnamed protein product[*Vitis vinifera*]	gil270253313	102134.3	6.84	20
21	Predicted protein[*Populus trichocarpa*]	gil224112088	40841.5	6.25	8
22	Predicted protein[*Populus trichocarpa*]	gil224099005	41135.6	6.25	8
26	Recname: full = malate dehydrogenase, mitochondrial; flags: precursor	gil126896	36178.2	8.88	7
27	Aldo/keto reductase, putative[*Ricinus communis*]	gil255552045	39151.3	5.69	9
28	Unknown[*Picea sitchensis*]	gil148905774	17181.2	6.32	10
30	40S ribosomal protein S21e, putative[*Ricinus Communis*]	gil255551737	9278.6	7.82	3
32	Unknown[*Picea sitchensis*]	gil116779029	18612.5	7.6	4

150.4 Conclusion

In summary, lysis buffer II (7 M urea, 2 M thiourea, 2 % CHAPS, 1 % PMSF, and 1 % protease inhibitor) combined with sonication was the optimized protocol in our study based on protein extraction efficiency, the good quality of the 2-DE patterns, and the result of MS identification. Using the method, higher protein extraction efficiency, lower background, more protein spots (987 ± 31), and higher spot intensities of low-abundant proteins were obtained, which indicated that the optimized protocol was suitable for proteomic studies of ginseng roots. Moreover, those results provided the foundation for further researches on the significant functional proteins of ginseng roots.

Acknowledgments This work was supported by two national key technology R&D programs (No. 2011BAI03B01 and No. 2012BAI29B05), a foundation of national natural science (No. 81041091), national science and technology major project (No. 2010ZX09401-305-02).

References

1. Nam MH, Kim SI, Ryol J et al (2005) Proteomic analysis of Korean ginseng (*Panax ginseng* C. A. Meyer). J Chromatogr B 815:147–155
2. Li HY, Zhao Y, Cao Y et al (2010) Purification and characterization of a superoxide dismutase from *Panax ginseng*. Biomed Chromatogr 24:1203–1207
3. Xu YF, Zhao Y, Yao BJ et al (2011) Effect of ginseng protein on decreasing blood lipid in rat models with hyperlipidemia. Tradit Chin Drug Res Clin Pharmacol 22:138–141
4. Song J, Li HT, Cheng HT et al (2011) Extraction of angiotensin I-converting enzyme inhibitory protein from ginseng. Chin Agric Sci Bull 27:133–136
5. Xu YF, Xing NN, Yang F et al (2011) Study on anti-fatigue effects of ginseng protein on mice. Sci Tech Food Ind 32:406–407
6. Li HY, Zhao Y, Sun XD et al (2010) Effect of ginseng protein against radiation injury in mice. Lishizhen Med Mater Medica Res 21:2143–2144
7. Li HY, Zhao Y, Sun XD et al (2010) Effect of ginseng protein on immune function in mice. Asia-Pacific Tradit Med 6:14–16
8. Nga TB, Wang HX (2001) Panaxagin, a new protein from Chinese ginseng possesses anti-fungal, anti-viral, translation-inhibiting and ribonuclease activities. Life Sci 68:739–749
9. Tansakul P, Shibuya M, Kushiro T et al (2006) Dammarenediol-II synthase, the first dedicated enzyme for ginsenoside biosynthesis, in *Panax ginseng*. FEBS Lett 580:5143–5149
10. Lee MH, Jeong JH, Seo JW et al (2004) Enhanced triterpene and phytosterol biosynthesis in *Panax ginseng* Overexpressing Squalene Synthase Gene. Plant Cell Physiol 45:976–984
11. Han JY, Kwon YS, Yang DC et al (2006) Expression and RNA Interference-Induced Silencing of the dammarenediol synthase gene in *Panax ginseng*. Plant Cell Physiol 47:1653–1662
12. Han JY, In JG, Kwon YS et al (2010) Regulation of ginsenoside and phytosterol biosynthesis by RNA interferences of squalene epoxidase gene in *Panax ginseng*. Phytochemistry 71:36–46
13. Purev M, Kim YJ, Kim MK et al (2010) Isolation of a novel catalase (Cat1) gene from *Panax ginseng* and analysis of the response of this gene to various stresses. Plant Physiol Biochem 48:451–460
14. Natarajana SS, Krishnanb HB, Lakshmana S et al (2009) An efficient extraction method to enhance analysis of low abundant proteins from soybean seed. Anal Biochem 394:259–268
15. Méchin V, Consoli L, Guilloux ML et al (2003) An efficient solubilization buffer for plant proteins focused in immobilized pH gradients. Proteomics 3:1299–1302
16. Kim SI, Kim JY, Kim EA et al (2003) Proteome analysis of hairy root from *Panax ginseng* C. A. Meyer using peptide fingerprinting, internal sequencing and expressed sequence tag data. Proteomics 3:2379–2392
17. Wu YP, Zhou JY, Zhang X et al (2009) Optimized sample preparation for two-dimensional gel electrophoresis of soluble proteins from chicken bursa of fabricius. Proteome Sci 7:1–12
18. Xie H, Pan S, Liu S et al (2007) A novel method of protein extraction from perennial bupleurum root for 2-DE. Electrophoresis 28:871–875
19. Nam MH, Heo EJ, Kim JY et al (2003) Proteome analysis of the responses of *Panax ginseng* C. A. Meyer leaves to high light: use of electrospray ionization quadrupole-time of flight mass spectrometry and expressed sequence tag data. Proteomics 3(12):2351–2367
20. Xi JH, Wang X, Li SY et al (2006) Polyethylene glycol fractionation improved detection of low-abundant proteins by two-dimensional electrophoresis analysis of plant proteome. Phytochemistry 67:2341–2348
21. Liu B, Ma HL, Li SJ et al (2011) Study on the structure of defatted wheat germ protein isolate under ultrasonic treatment. Guang Pu Xue Yu Guang Pu Fen Xi 31(8):2220–2225
22. Méchin V, Consoli L, Guilloux ML et al (2003) An efficient solubilization buffer for plant proteins focused in immobilized pH gradients. Proteomics 3:1299–1302

23. Bradford MM (1976) A rapid and sensitive method for the quantitation of microgram quantities of protein utilizing the principle of protein-dye binding. Anal Biochem 7:248–254
24. Lum JH, Fung KL, Cheung PY et al (2002) Proteome of oriental ginseng *Panax ginseng* C. A. Meyer and the potential to use it as an identification tool. Proteomics 2:1123–1130
25. Kim ST, Bae DW, Lee K et al (2008) Proteomic analysis of Korean ginseng (*Panax ginseng* C. A. Meyer) following exposure to salt stress. J Plant Biotechnol 35:185–193
26. Nagappan A, Karunanithi N, Sentrayaperumal S et al (2012) Comparative root protein profiles of Korean ginseng (*Panax ginseng*) and Indian ginseng (withania somnifera). Am J Chin Med 40:203–218

Chapter 151
Purification of Alkaline Pectinase in Engineering *Bacillus subtilis*

Ming Li, Xin Sun, Liying Zhou, Hongxin Wang, Dongxia Li, Shuya Wang and Fuping Lu

Abstract The alkaline pectinase in fermentation liquid of engineering Bacillus subtilis was isolated and purified by using centrifugation, ultrafiltration, ammonium sulfate precipitation, and ion exchange chromatography, and the optimum conditions of ion exchange chromatography were determined. The results showed that, the recovery rate of crude enzymes ultrafiltrated by an ultrafiltration membrane with molecular weight cut-off 10000 Dalton reached 73.3 %, and the specific activity was 259.7 U/mg; after fractional salting out, the recovery rate was up to 62.9 %, and the specific activity was 1084 U/mg. With the DEAE-Sephorose CL-4B anion exchange chromatography under gradient elution with 0–1.0 mol/L NaCl (buffer solution of Gly-NaOH at pH8.6), the specific activity increased to 1230 U/mg. Subsequently, Sephadex-G75 column chromatography was applied and the specific activity increased to 2352 U/mg. The purity was 12.5 times of the crude enzyme, with the recovery rate of 21.6 %. The molecular weight of finally obtained alkaline pectinase was 43 kDa and the SDS polyacrylamide gel electrophoresis displayed that it was electrophoretically pure.

Keywords Alkaline pectinase · Isolation and purification · Ultrafiltration · Chromatography

151.1 Introduction

Alkaline pectinase refers to the pectinase with higher activity under basic condition. Pectate lyase mainly acts in alkaline environment, occupying a large proportion in alkaline pectinase, thus alkaline pectinase generally refers to pectate lyase [1].

M. Li · X. Sun · L. Zhou · H. Wang · D. Li · S. Wang · F. Lu (✉)
Key Laboratory of Industrial Fermentation Microbiology, Ministry of Education, National Engineering Laboratory for Industrial Enzymes, The College of Biotechnology, Tianjin University of Science and Technology, Tianjin 300457, People's Republic of China
e-mail: liming09@tust.edu.cn

T.-C. Zhang et al. (eds.), *Proceedings of the 2012 International Conference on Applied Biotechnology (ICAB 2012)*, Lecture Notes in Electrical Engineering 251,
DOI: 10.1007/978-3-642-37925-3_151,

Alkaline pectinase is widely used in leather and silk industry, and shows wide application prospect in food, feed, and particularly in the extraction and washing for plant drugs in the field of medicine.

A strain of *Bacillus subtilis* TCCC11485 with high yield of alkaline pectinase was constructed in our laboratory. The enzyme produced by the engineering bacteria has high expression activity, short fermentation period, fast degumming for pectinase, and small influence on fiber quality, which has potential application in the textile industry.

The purification of alkaline pectinase is the prerequisite and foundation for the effective utilization of alkaline pectinase.

The purification methods for alkaline pectinase produced by bacteria, mold, and yeast reported at home and abroad were different. In the initial separation, salting out or organic solvents were usually used to precipitate it and the commonly used organic solvents are methanol, ethanol, isopropanol, and acetone. Schjter and Marcus precipitated pectin esterase and polygalacturonase from *Botrytis cinereaPers* with 20 % and 66 % acetone respectively, which were purified by 5 times and 6 times respectively [2]. Compared with ammonium sulfate fractionation, the biggest drawback of organic solvent precipitation was the partially inactivation of the enzyme.

DEAE-cellulose chromatography, DEAE-Sephadex, and CM-Sephadex have good application in the purification of pectinase [3–6]. In addition, affinity chromatography also has certain applications in the separation of enzymes. Rombouts and Pilnik crosslinked pectic acid or sodium pectinate (high molecular weight) with epichlorohydrin under alkaline conditions, and methyl esterified the products to separate pectin esterase from the orange. Two peaks of pectin esterase were obtained [7]. Tibensky et al. used crosslinked products without methyl esterification to isolate endo-polygalacturonase from *Aspergillus niger* with the pH 6 elution condition [8].

Sephadex gel filtration was one of the common means used in pectinase purification process. Tagawa and Kaji used Sephadex G-100 to separate polygalacturonase from *Cuoticium rolfsii* after affinity chromatography, having good results [9]. In the separation of pectinases from mutant of *Cladosporium herbarum*, Wu Meihua et al. compared several different Sephadax fixed materials and elution conditions, and found that QAE Sephadex A-25 gradient elution can achieve better results [10]. In fact, Sephadex gel filtration combined with other methods had been widely used in the purification of pectinase.

To sum up, the purification process of pectinase is flexible and diverse, so in the working practice, the methods could be combined according to the specific circumstances, but the primary separation with ammonium sulfate and organic solvent is necessary.

In the fermentation of *B. subtilis* engineering baterium, except alkaline pectinase, there were also other proteins produced by *B. subtilis* and some remaining medium components, which affected the purification of alkaline pectinase. Thus, this article focus on the purification method of alkaline pectinase from *B. subtilis*

TCCC11485, in order to lay the foundation for the further study of structure and properties, such as remixing with other enzymes or auxiliary agents for the application in the textile industry.

151.2 Materials and Methods

151.2.1 Materials

Bacillus subtilis TCCC11485 with the high yield of alkaline pectinase was constructed by Enzyme and Applied Microbiology Laboratory in Tianjin University of Science and Technology. Polygalacturonic acid was purchased from sigma. Molecular weight makers, acrylamide, bis acrylamide, ammonium persulfate, sodium dodecyl sulfate (SDS), coomassie brilliant blue, DEAE-Sephorose CL-4B, and Sephadex-G75 were purchased from Sangon Biotech (Shanghai) Co., Ltd. (China), and Bradford Protein Assay Kit was purchased from Beyotime Institute of Biotechnology (Shanghai) Co., Ltd. (China),and neutral protease was bought from Tianjin Noao Science and Technology Co., Ltd.(China), and other reagents were analytically pure and made in China.

151.2.2 Preparation of Alkaline Pectinase Crude Enzyme

Single colony of engineering *B. subtilis* TCCC11485 was selected and inoculated in LB seed culture medium with the culture at 37 °C and 200 r/min for 12 h, which was then inoculated in a 5 L fermentation tank with the inoculation amount of 4 % for fermentation of 24 h. The dissolved oxygen concentration was controlled to 15–20 % in the fermentation process, and the temperature was controlled at 41 °C in 0–4 h, and at 35 °C in 4–22 h, and the speed was 500 r/min in 0–5 h, and 600 r/min after 5 h. The initial pH of the fermentation medium was 7.0.

After fermentation, the fermentation liquid was centrifuged at 4 °C and 6,000 r/min for 20 min to collect the supernatant, which was alkaline pectinase crude enzyme, and then preserved at 4 °C.

151.2.3 Purification of Alkaline Pectinase

151.2.3.1 Ultrafiltration of Alkaline Pectinase Crude Enzyme

The crude enzyme was concentrated by an ultrafiltration membrane with molecular weight cut-off of 10,000 Dalton to 1/5 of the original volume, and the concentrate was collected.

151.2.3.2 Ammonium Sulfate Fractionation

First according to ammonium sulfate fractionation curve, the suitable saturation was selected for salting out.

500 mL of concentrated crude enzyme was put in ice bath, and 50 % saturation ammonium sulfate salting out was conducted overnight for precipitation of other proteins, then it was centrifuged in high-speed refrigerated centrifuge at 9000 r/min for 15 min to remove the precipitation, and 80 % saturation ammonium sulfate was added to the supernatant for overnight to precipitate target enzyme, subsequently, it was centrifuged in high-speed refrigerated centrifuge at 9000 r/min for 15 min to remove the supernatant, and the precipitation was the fractionation of crude enzyme.

Dialysis was conducted using a dialysis bag immersed into balance buffer with the volume more than 5 times that of the crude enzyme in 4 °C refrigerator. After a few hours, balance buffer was replaced and repeated until the precipitation cannot be seen after dropping 10 % BaCl2 solution.

151.2.3.3 DEAE-Sephorose CL-4B Anion Exchange Chromatography

(1) The choice of pH value of ion exchange eluate

1 mL anion exchanger was aspirated to 10 test tubes, and washed by buffer with different pH values for 10 times. After the ion exchange resin being equilibrated, 1 mL buffer was added, and 100 μL alkaline pectinase solution salted out with ammonium sulfate was added and mixed and then in the marinade for 10 min. The activity of the enzyme in the supernatant was detected to judge whether target protein existed.

(2) Purification of alkaline pectinase

The samples after desaltation were added into DEAE- Sephorose CL-4B anion exchange chromatography column being balanced with pH 8.6 Gly-NaOH buffer, and eluted with pH 8.6 Gly-NaOH buffer at 1 mL/min for 120 min, and then linearly gradient eluted with pH 8.6 Gly-NaOH buffer containing 0–1 mol/L NaCl, with the eluting rate of 1 mL/min. The elution solution was collected automatically with the speed of 1 min/pipe.

151.2.3.4 Sephadex-G75 Column Chromatography

Glass column packed with Sephadex G-75 dextran gel was balanced with pH 8.6 Gly-NaOH buffer, and sampled, and then eluted with pH 8.6 Gly-NaOH buffer, with the flow rate of 1 mL/min, and the effluent was on-line detected by UV

detector at the wavelength of 214 nm, to record ultraviolet absorption peak curve. The components were collected, used for the determination of enzyme activity and protein content.

151.2.4 Determination of Alkaline Pectinase Activity

(1) The definition of enzyme unit: the amount of the enzyme in 1 mL enzyme solution that catalyzes polygalacturonic acid to degenerate into 1 μmol unsaturated polygalacturonic acid per minute at 45 °C and pH 9.0.
(2) The measurement of enzyme activity [11]: 20 μL crude enzyme dilution and 2 mL glycine-NaOH (0.2 mol/L) buffer solution containing 0.2 % polygalacturonic acid (pH 9.0, containing 0.44 mmol/L CaCl2) were included in measurement system. The solution with no activity was taken as the blank control. Buffer solution containing substrate was added to start enzymatic reaction. The reaction was conducted at 45 °C for 15 min, and 3 mL 0.03 mol/L phosphoric acid was added to terminate reaction, and the absorbance values were measured at 235 nm. Enzyme blank parallel to the samples was used for zeroing.

Enzyme blank: 2 mL of above buffer system was insulated for 2 min, and then 3 mL 0.03 mol/L phosphoric acid was added, subsequently, 20 μL inactivate enzyme solution of the same dilution ratio with the sample was added and mixed. Other operations were same as those for the samples.

$$\text{Enzyme activity(U/ml)} = \frac{10^3 \times \text{t} \times 4,600 \times \text{volume of enzyme preparation}}{\text{OD}_{235} \times 10^6 \times \text{dilution factor} \times \text{volume of mixture}}$$

in which, 4,600 ($L.mol^{-1}$ cm^{-1}) was the molar absorptivity of unsaturated polygalacturonic acid at 235 nm.

t (min) Enzymatic reaction time (within the linear range of enzymatic reaction)
b (cm) The thickness of cuvette

to be simplified as: enzyme activity (U/ml) = 3.6232 × dilution multiple × OD235.

151.2.5 Determination of Protein Content and SDS–Polyacrylamide Gel Electrophoresis (SDS-PAGE)

Protein content was determined by Bradford [12] method, and SDS-PAGE was conducted according to the methods from the literature [13] to identify enzyme purity.

151.3 Results and Discussion

151.3.1 Fermentation Results in 5 L Fermentor

The fermentation curve is shown in Fig. 151.1.

As seen in Fig. 151.1: the whole fermentation process lasted for 26 h. In 0–4 h, due to self-decomposition of nutrients in fermentation medium, pH value declined; after 4 h, with the substantial growth and reproduction of bacteria, pH value of fermentation liquid rose gradually to make the bacteria grow in the optimal environment; at 18 h, nucleic acid reached peak, and bacteria reached stable; at 22 h, enzyme activity reached the maximum value, and alkaline pectinase activity in the final fermentation liquid reached 1536 U/mL. 2133 mL supernatant was obtained by centrifugation to remove bacteria from the fermentation liquid, with the total enzyme activity of 3276288 U.

151.3.2 Ultrafiltration

Fermentation liquid was centrifuged to remove bacteria, and crude enzyme was ultrafiltrated by an ultrafiltration membrane with molecular weight cut-off 10,000 Dalton, and about 500 mL concentrated liquid was collected. After ultrafiltration, pectinase activity was 4,802.6 U/mL, and the total enzyme activity was 240,1307 U. The activity loss was around 26.7 %.

The loss of enzyme activity was the result of some enzymes which were deactivated with the ultrafiltration time. It was probably due to a small part of enzyme molecules adsorbed in hollow fiber membrane.

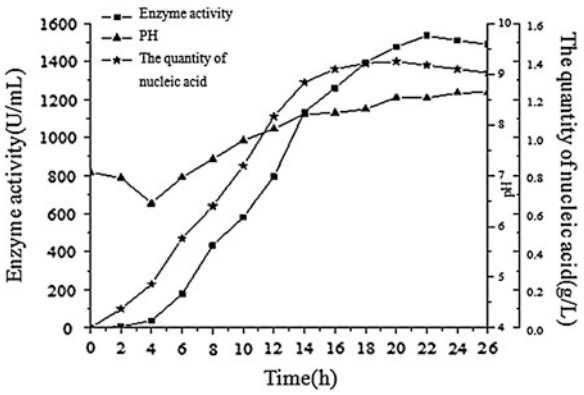

Fig. 151.1 Fermentation curve

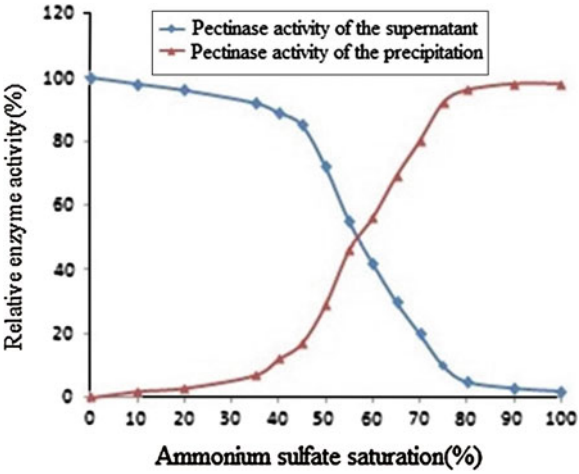

Fig. 151.2 Ammonium sulfate fractionation curve

151.3.3 Ammonium Sulfate Fractionation

The fractionation curve is shown in Fig. 151.2.

Figure 151.2 showed that, when ammonium sulfate was saturated to 50–80 %, enzyme activities of the precipitation increased and that of the supernatant decreased significantly with the saturation. When the saturation rate reached 80–100 %, enzyme activities of the supernatant and precipitation did not change significantly. Thereafter fractional salting out should be adopted. First 50 % saturated ammonium sulfate was added for salting out to remove impure proteins, and then 80 % saturated ammonium sulfate was added to the supernatant to precipitate the target protein.

The target protein after salting out was redissolved with 200 mL buffer. The enzyme activity determined was 10303.2 U/mL, and the total enzyme activity was 2060635 U, with the activity loss of about 37.1 %. The loss of enzyme activity may be due to the protein denaturation under higher salt concentration.

The crude enzyme salted out was desalted and dried in freeze drying conditions to obtain about 1.9 g enzyme powder. The final product was preserved at 4 °C.

151.3.4 Choice of pH Value for DEAE-Sephorose CL-4B Ion Exchange Eluate

The results were shown in Fig. 151.3. When the pH value was 9.0, there was only a very low enzyme activity value of alkaline pectinase determined in the supernatant, which indicated that pectinase was adsorbed to the column at this pH value.

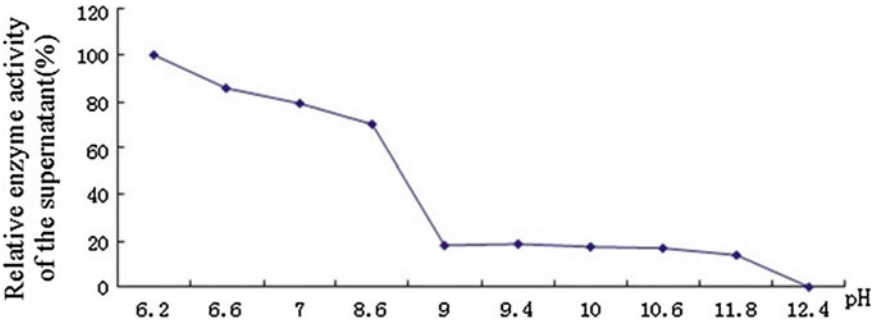

Fig. 151.3 Change of relative enzyme activity of the supernatant (%) with pH value for DEAE-Sephorose CL-4B eluate

When pH was 8.6, alkaline pectinase was not absorbed but impure proteins were adsorbed, thus the crude enzyme can be purified. By comprehensive consideration, the most suitable pH for alkaline pectinase was 8.5, thus pH 8.6 buffer should be chosen.

151.3.5 DEAE-Sephorose CL-4B Anion Exchange Chromatography

0.05 g enzyme powder was dissolved in 10 mL buffer and centrifuged to remove small amounts of insoluble materials. The supernatant was then purified with DEAE- Sephorose CL-4B ion exchange column.

The results were shown in Fig. 151.4. When the desalted alkaline pectinase was eluted first with pH 8.6 Gly-NaOH buffer, two kinds of protein components were washed off, and when the column was gradiently eluted with pH 8.6 Gly-NaOH buffer containing 0–1 mol/L NaCl, three proteins were washed off. The elution curve was detected at 214 nm. By the detection of enzyme activity, it was found the first elution peak was active component while other elution peaks were inactive, which illustrated that alkaline pectinase was not adsorbed on ion exchange chromatography column, and can be separated completely from impure proteins.

About 60 mL of the first elution peak was collected with enzyme activity of 565.3 U/mL, and then the protein purity was identified with the SDS-PAGE. The total activity was 1301277 U, and enzyme activity lost around 60.3 %. The activity loss may be resulted from the adsorption of a small amount of enzyme in ion exchange column and was not washed off.

The eluted liquid was dried in freeze drying conditions at −70 °C, and concentrated to be stored at 4 °C.

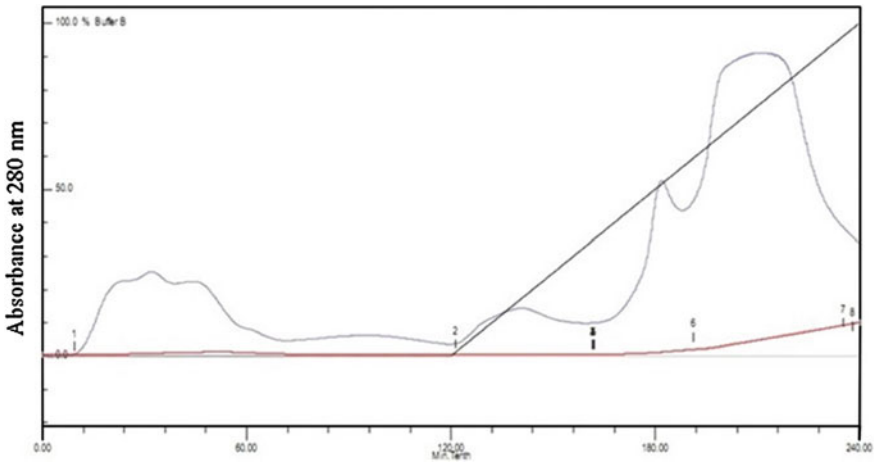

Fig. 151.4 Elution curve of DEAE-Sephorose CL-4B anion exchange chromatography

151.3.6 Sephadex-G75 Column Chromatography

After salting out, dialysis and anion exchange chromatography, crude enzyme solution was subjected to Sephadex-G75 column chromatography to further remove impure proteins. The sample volume was 2 mL. The elution curve was drawn with time as abscissa and absorption of the liquid in each tube as ordinate. As shown in Fig. 151.5, there were two protein peaks in the elution process. By the detection of enzyme activity, the first elution peak was determined as active component, whose shape was nearly symmetric and the baseline was close to zero, which indicated that it could be separated from another protein group.

About 37 mL corresponding to the first elution peak was collected with the enzyme activity of 303.6 U/mL, and total enzyme activity of 707,715 U. After the purification through the steps described previously, the total recovery rate was 21.6 %, and purification multiples reached 12.5 times.

151.3.7 Purity Identification

The molecular weight of the purified alkaline pectinases was detected by Coomassie brilliant blue staining and SDS polyacrylamide gel electrophoresis. Figure 151.6 showed it was 43 kDa, with the electrophoretical purity.

M: molecular weight makers; 1. fermentation liquid; 2. ultrafiltration; 3. concentrated ammonium sulfate salting out solution; 4. DEAE-Sephorose CL-4B ion exchange chromatography; 5, 6. Sephadex-G75 column chromatography.

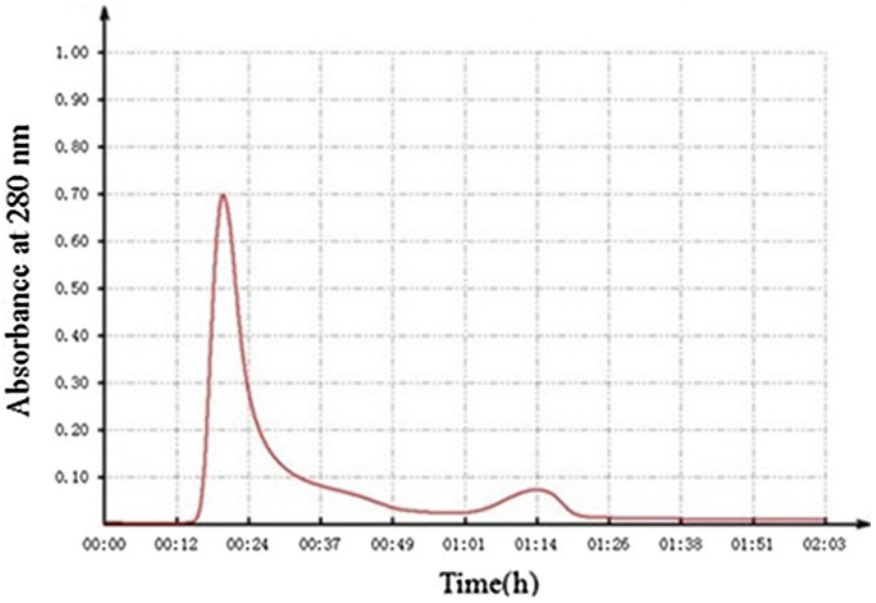

Fig. 151.5 Sephadex-G75column chromatography elution curve

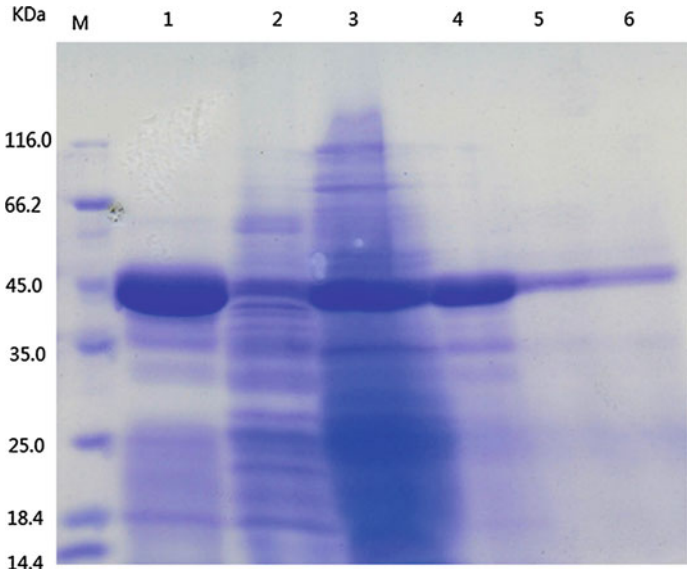

Fig. 151.6 Polyacrylamide gel electrophoretogram

Table 151.1 The purification results of alkaline pectinase

	Total activity (U)	Protein content (mg)	Specify activity (U/mg)	Purification multiple	Recovery rate (%)
Fermentation liquid	3276288	17400	188.2	1	100
Ultrafiltration	2401307	9246	259.7	1.4	73.3
Ammonium sulfate	2060635	1900	1084	5.8	62.9
DEAE-Sephorose CL-4B	1301277	1057	1230	6.5	39.7
Sephadex-G75	707715	301	2352	12.5	21.6

151.4 Conclusions

By the processes of centrifugation, ultrafiltration, ammonium sulfate precipitation, DEAE-Sephorose CL-4B anion exchange chromatography and Sephadex-G75 column chromatography for the fermentation liquid, the specific activity of electrophoretically pure alkaline pectinase finally obtained, which was 12.5 times higher than that of the original enzyme with the recovery rate up to 21.6 %. It can be seen that the purification route described above can improve the purity of the alkaline pectinase, with high recovery rate. It was an effective purification method (Table 151.1).

This experiment uses the previous purification methods of microbial pectinase for reference, and combines ammonium sulfate salting out, ion exchange chromatography, gel filtration, and other conventional separation methods, to establish a kind of separation method for alkaline pectinase with low cost and good purification effect, which will be helpful to further research on enzyme properties and advanced structure of alkaline pectinase, laying the foundation for remixing with other enzymes or auxiliary agents to be applied in degumming in the textile industry.

Acknowledgments This work was supported by Key Technology Research and Development Program of Tianjin, China (No. 11ZCKFSY00900), Tianjin Research Program of Application Foundation and Advanced Technology (No. 11JCYBJC 09600) and National Natural Science Foundation of China (No. 21176190).

References

1. Zhang JH, Li Y, Liu H et al (2005) Isolation, phylogenetic analysis of a bacterium with high yield of alkaline pectate lyase and optimization of its culture conditions. Chinese J App And 11(3):354–358
2. Schejterand A, Marcus L (1988) Isozymes of pectinesterase and polygalacturonase from *Botrytis cinerea Pers*. Methods Enzymol 161:366–373
3. Haruyoshi K (1998) Endopectate lyase from *Erwinia aroideae*. Methods Enzymol 161:381–385
4. Konno H (1988) Galacturan, 1,4-α-Galactuionidase from *Carrot Daucus carota* and *Liverwort Marchantia polymorpha*. Methods Enzymol 161:373–380
5. Pitt D (1988) Pectin lyase from *Phoma medicaginisrar pinodella*. Methods Enzymol 161:350–354
6. Forster H (1988) Pectinesterases from *Phytophthora infestans*. Methods Enzymol 161:355–361
7. Rombouts FM, Wissenburg AK, Pilnik W (1979) Chromtographic separation of orange pectinesterase isoenzymes on pectates with different degrees of crosslinking. J Chromatogr, 168:151-161
8. Lubomira RB, Vladimir TB (1972) Selective purification of *Aspergillus niger* endopolygalacturonase by affinity chromatography on cross-linked pectic acid. Acta Bioch Bioph Sin 268:187–193
9. Tagawa K, Kaji A (1988) Polygalacturonase from *Corticium rolfsii*. Methods Enzymol 161:361–365
10. Wu HM, Zhou J (1997) The purification and characterization of pectinases from *Cladosporium herbarum* and its mutants. Guizhou Science 15(3):163–170
11. Li S, Dong RA, He YM (2007) Study on the detection conditions of pectate lyase produced by Bacillus. Life Sci Instrum 5(9):18–21
12. Wang JZ, Fan M (2001) Protein technology handbook. Science Press, Beijing
13. Bradford MM (1976) A rapid and sensitive method for the quantitation of microgram quantities of protein utilizing the principle of protein-dyebinding. Anal Biochem 72:248–254

Chapter 152
In situ Preparation and Characteristics of a New Water-Soluble Heme Iron Via Hemin-Arginate Coacervation

Wenhang Wang, Ting Liu, Ying Zhang, Rujie Chen and Anjun Liu

Abstract A new water-soluble heme iron (WSHI) was prepared and characterized. Crystalline hemin and L-arginate in molar proportions of 1:3 were mixed in a acetone solution (acetone: water = 100:10, V: V), stirred at 25 °C, for 12 h, and then centrifuged, washed with acetone, freeze-dried, referred to as WSHI. No clear differences in UV spectrum, IR spectrum between hemin-arginate and hemin was founded, while a notable distinct of thermal sensitivity occurred by differential thermal analysis (DTA), which partly explained dissolution elevation of hemin-arginate. Hemin-arginate is stable and no coagulate occurred in Carbonate solution, phosphate solution, or tea water, respectively. So, Hemin-arginate can be used as a new heme iron supplement in food additives, functional foods, and pharmaceuticals.

Keywords Hemin · L-arginate · Coacervation · Dissolution · Stability

152.1 Introduction

Iron is the most abundant essential trace elements in the body, the main component of hemoglobin, myoglobin, and cytochrome enzymes, and involved in oxygen transshipment, carbon dioxide exchange, and tissue respiration process [1, 2]. In addition, iron participate in red blood cell formation and maturation, and associated with the catalytics of β-carotene into vitamin A, purine and collagen

W. Wang (✉) · T. Liu · R. Chen · A. Liu
Key Laboratory of Food Nutrition and Safety, Ministry of Education, Tianjin University of Science and Technology, Tianjin 300457, People's Republic of China
e-mail: wangwenhang@tust.edu.cn

Y. Zhang
Department of Ecology, Environment Management College of China, Qinhuangdao 066004, People's Republic of China

T.-C. Zhang et al. (eds.), *Proceedings of the 2012 International Conference on Applied Biotechnology (ICAB 2012)*, Lecture Notes in Electrical Engineering 251,
DOI: 10.1007/978-3-642-37925-3_152,

synthesis, antibody production, lipid transportation from the blood and drugs detoxification in liver [3].

Iron deficiency anemia is one of the world's highest incidence of nutritional deficiency diseases, which is storage iron in the body cannot meet the needs of normal erythropoiesis, due to insufficient iron intake, low absorption, increased demand, and losing too much [4, 5]. About 500 million people worldwide suffer from anemia, of which nearly half of the iron deficiency anemia. Iron deficiency anemia has become the most serious public health problem with the prevalence rate second only to tuberculosis. World Health Report (2002) of World Health Organization pointed that iron deficiency is one of ten top preventable health risk factors in world [6].

A lot of iron supplement have been on the market recently, but most is some nonheme iron supplement, such as ferrous chloride, ferrous sulfate, ferrous lactate, ferrous fumarate, and ferrous gluconate. Due to the impact of food phytic acid, oxalic acid, tannic acid, phosphate, carbonate, nonheme iron supplement has a low absorption rate for the body, which is generally 5–8 %. In addition, some side effects (prone to nausea, bloating or abdominal pain, digestive disorders, diarrhea, constipation, and other symptoms), and special metal taste of rust cause its difficulty of long-term consumption. Excessive intake of nonheme iron in body leads to iron overload in the body, resulting in iron accumulation poisoning [7–9].

Heme, also known as porphyrin iron, is a key assistance factor of many biologically active macromolecules, such as hemoglobin, myoglobin, cytochrome, and peroxidase. Heme is a natural class of porphyrin compounds, a combination with the organic molecules, widely present in the animal's blood, muscle, and some plant tissues [10]. The basic structure of the heme is composed of porphyrin and ferrous. Two N atoms of the porphyrin ring was covalently combined with the iron, the other two N atoms is contacted the iron with a Coordination bond, that is to say, the entire molecule of heme is in a resonance state. When heme combines with oxygen, the molecule of the heme iron is oxidized to trivalent heme namely as hemin; when the separation of heme with oxygen, the heme iron molecule is reduced to divalent, which is called heme [11]. Heme iron is a well-known, ideal antianemia drug, due to good promotion of bone marrow hematopoietic, treatment of animals hemolytic, and hemorrhagic anemia [12, 13].

Heme iron is usually extracted from pork or cow blood with acetone-HCl method. In fact, Probable formation of large insoluble heme polymers in digestion was another disadvantage for heme application although its good absorption, so some research efforts to improve the water-soluble porphyrin iron dispersion [14, 15].

This paper was focused on preparation WSHI via hemin-arginate coacervation, in order to improve the solubility of the heme iron. At the same time, UV, IR, and DTA of WSHI were characterized and its stability in different solutions (tea, phosphate, and carbonate) was studied.

152.2 Materials and Methods

152.2.1 Reagents and Materials

Fresh pork blood was obtained from Jingwu meat food Co., Ltd., added with 0.5 % sodium citrate for anticoagulation. Other reagents were of analytical grade.

152.2.2 Preparation of WSHI

Anticoagulated blood was centrifuged at 4,000 r/min, for 15 min. the upper was discarded and, the bottom red blood cells was Collected. Red blood cells were added with a final concentration of 0.2 % Na_2SO_3. After mixing, adding five times volume of acetone solution (acetone:6 mol/L HCl = 100:3, v:v), the reactive substances was disturbed for 2 h, and then filtrated. The filtered liquid was added with constantly dropping 1 mol/L NaOH solution until pH 4.6, and then precipitated by the sodium acetate solution with the final concentration of 1 %. The precipitation was separated with centrifugation, spurred by repeated washing with ethanol and distilled water, crystallization. The dried matter is hemin.

Crystalline hemin and L-arginate in molar proportions of 1:3 were mixed in an acetone solution (acetone: water = 100:10, V: V). the mixture was stirred vigorously to react, at 25 °C, for 12 h, and then was centrifuged at 10,000 g, for 5 min. The precipitates were collected, washed with acetone, and freeze-dried. The dried matter is WSHI [16].

152.2.3 Detection of Hemin Content

Hemin content of WSHI was detected with the Colorimetry method [17]. 20 mg hemin sample was completely dissolved at 100 mL 0.1 mol/L NaOH solution. 0.5, 1.0, 2.0, 4.0, 5.0 mL of the above solution was mixed with 100 mL 0.1 mol/L NaOH solution again, respectively. With Solvent blank as control, all absorbance values were measured at 392 nm, and the standard curve of hemin is drawn. 20 mg WSHI sample was detected by the same above procedure. According to standard curve of hemin, the hemin content of WSHI was calculated.

152.2.4 UV: Visible Absorption Spectroscopy

0.5 g WSIH and hemin were dissolved in 0.1 mol/L NaOH solution, fully stirred and centrifuged. The supernatant was scanned in 300–800 nm with 0.1 mol/L NaOH solution for blank sample.

152.2.5 IR Absorption Spectroscopy

1 mg WSIH and hemin was ground into about 2 μm particles, and mixed with 100 mg spectroscopically pure KBr powder, followed grinding again. The mixture was made into a thickness of 1 mm, diameter of 10 mm, transparent sheets under 10 MPa pressure. Absorption spectrums of the sheets were observed in 4,000–500 cm^{-1}.

152.2.6 Differential Scanning Calorimetry (DSC)

Differential scanning calorimetry analysis was carried out using a Polymer differential scanning calorimetry DSC141 (seraram corp., France). Temperature was raised from 50 to 200 °C, at a heating rate of 10 °C/min^{-1} [18].

152.2.7 Stability of WSIH

0.1 g of ferrous lactate, ferrous fumarate, ferrous gluconate, WSHI, ferrous chloride, and ferrous sulfate was weighed, divided in each test tube, and labeled. About 5 g green tea was boiled in 100 mL deionized water for 2 min and then cooled. The cold tea water was filtered for next detection. 10 ml tea water was added slowly and mixed completely. After 20 min standing, the change of the solution was observed. The stability of different iron supplement in the 0.2 mol/L sodium phosphate and 0.1 mol/L sodium carbonate was detected at the same procedure.

152.3 Results and Discussion

152.3.1 Hemin Content of WSHI

A new, water-soluble heme iron named WSHI was prepared via hemin-alrginate coacervation. WSHI was completely dissolved in distilled water.

The standard curve of hemin was showed in Fig. 152.1, with a linear relationship between absorbance and the hemin concentration in the range of 0 μg/mL–10 μg/mL. The regression equation was $Y = 0.0844\ X + 0.0112$, Y represented absorbance, X represented concentration. According to the formula in Fig. 152.1, the purity of WSHI prepared is 86.9 %.

152.3.2 UV, IR Spectrum

Absorption Spectroscopy of WSHI and hemin in the range of 300–800 nm were showed in Fig. 152.2. According to Fig. 152.2, the maximum absorption peak in visible spectrum of WSHI and hemin was found at the wave length of 392 nm. No other apparent differences were observed in absorption of WSHI and hemin.

The infrared absorption spectra of WSHI and hemin were shown in Fig. 152.3. The common characteristic absorption peak were determined at the wave number of 2919, 1717, 1272, 939, 841, and 719 cm^{-1}.

An absorption peak appeared at 2,919 cm^{-1} is attributed to carboxyl group stretching, while 1,272 cm^{-1} indicated C–N stretching, and 939 cm^{-1} and 841 cm^{-1} is attributed to C–H bending vibration of hydrocarbon compounds. In addition, 719 cm^{-1} indicated C–H bending vibration of benzene compounds.

From Fig. 152.3, A distinct absorption of at 3,422 cm^{-1} and 1626 cm^{-1} occurred in WSHI. 3,422 cm^{-1} is mainly caused by alcohols or phenols structure

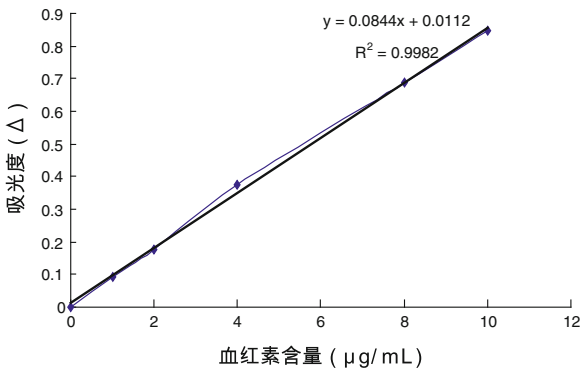

Fig. 152.1 Standard curve of hemin

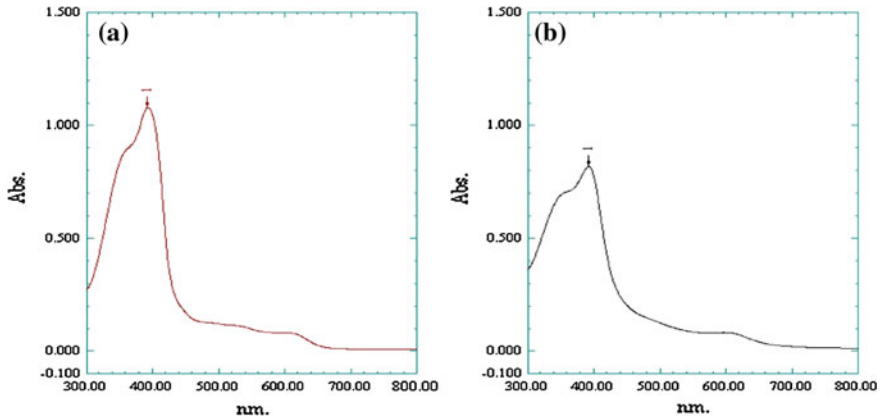

Fig. 152.2 UV spectrum of WSHI and hemin. **a** Hemin. **b** WSHI

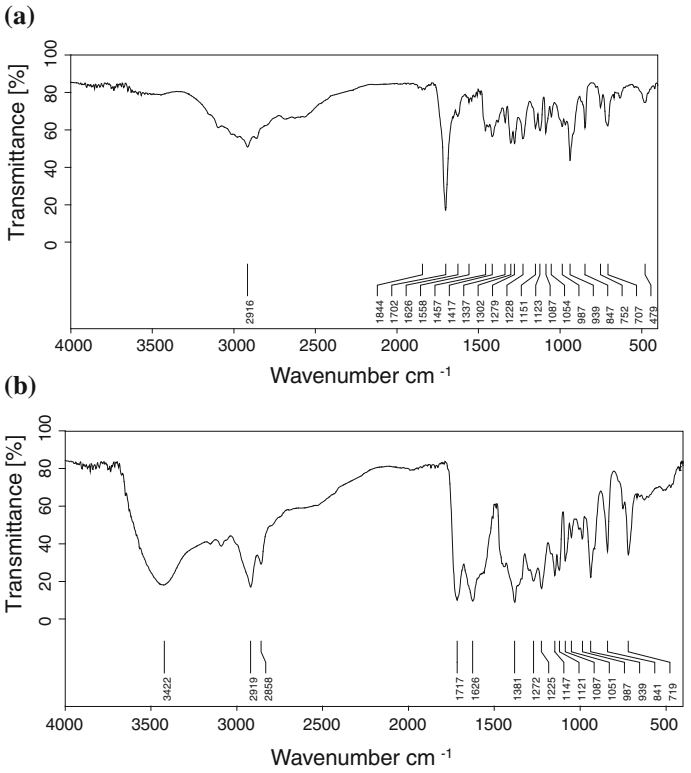

Fig. 152.3 IR spectrum of WSHI and hemin. **a** Hemin. **b** WSHI

in the OH stretching vibration, 1,626 cm^{-1}, amine compounds of NH bending vibration. It contributes to peptide of WSHI.

152.3.3 DSC Analysis

Figure 152.4 showed that hemin melted at 341.1 °C, but WSHI melted at 52.9 °C. It is obvious that both of them did not have fixed melting point.

From Fig. 152.4, hemin began to melt at 341.44 °C. There may be two melting range, 359.08 °C first endothermic peak, 380 °C second endothermic peak. WSHI began to melt at 52.92 °C, and along with the temperature gradually increasing, to generate other substances in the late degeneration due to thermal instability of it. It began to release heat at about 175 °C, and the maximum amount of heat release was obtained at 158 °C.

152.3.4 Stability of WSHI

Many green vegetables, such as seek, spinach, parsley all contain carbonate, and the ferrous lactate, ferrous chloride, ferrous sulfate iron in iron combine to form the insoluble precipitate, thus affecting the iron absorption. Patients with anemia in the iron at the same time, large-scale use of these substances would greatly reduce the absorption rate of iron precipitation can also cause stomach discomfort and indigestion [19, 20].

Stability of WSHI in different solutions was studied with other iron supplements for comparisons.

From Fig. 152.5a, except WSHI, other iron supplements rapidly produced a black precipitate after mixing with tea water. This is because tea contains large amounts of tannic acid, which being iron-binding agents reacted with many nonheme irons, such as Ferrous lactate, ferrous fumarate, ferrous gluconate, ferrous sulfate, ferrous chloride, to form insoluble tannin iron precipitation.

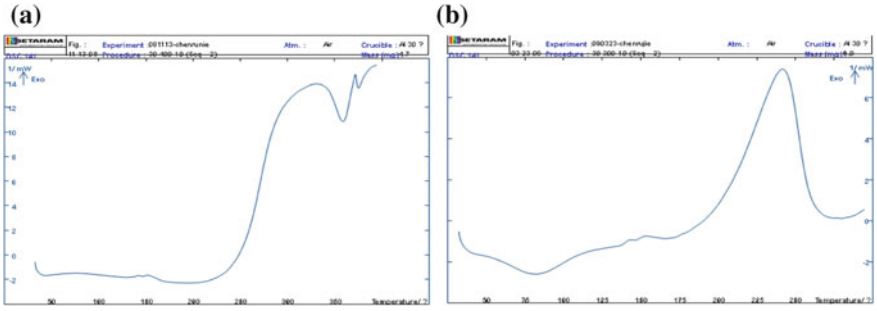

Fig. 152.4 DTA analysis of WSHI and hemin. **a** Hemin. **b** WSHI

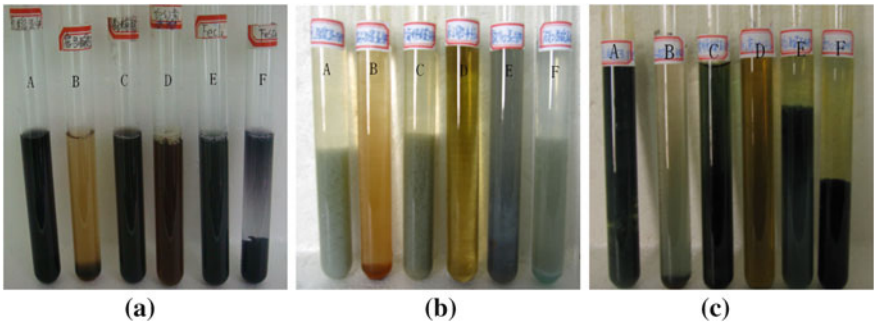

Fig. 152.5 stability of iron supplements in solutions. **a** Stability of irons in tea water. **b** Stability of irons in 0.2 % sodium phosphate solution. **c** Stability of irons in 0.1 % Sodium carbonate solution. A: Ferrous lactate; B: ferrous fumarate; C: ferrous gluconate; D: WSHI; E: ferrous sulfate; F: ferrous chloride

An insoluble precipitate formed in 0.2 % sodium Phosphate solutions, after all nonheme iron supplements added to while WSHI is an exception, as shown in Fig. 152.5b.

It can be seen from Fig. 152.5c, after mixed 0.1 % carbonate buffer solution with a variety of iron supplement, ferrous lactate, ferrous chloride, ferrous sulfate, a dark green flocculent precipitate occurred.

152.4 Conclusions

The UV spectrogram and Infrared absorption spectrum of WSHI was analogous to hemin, but differential thermal analysis was significantly different from hemin. WSHI was soluble and stable in distilled water and other solution, such as in Carbonate, phosphate, and tea water, which indicated its potential application as a new heme iron supplement in food additives, functional foods, and pharmaceuticals.

Acknowledgments The present work was supported by grants from the Special Fund for Agroscientific Research in the Public Interest (No. 201303082-3), National Natural Science Foundation of China (No. 31000755), and Key Project of Chinese Ministry of Education (No. 211008).

References

1. Wang J, Pantopoulos K (2011) Regulation of cellular iron metabolism. Biochem J 434:365–381
2. Dorota F, Piotr F (2011) An overall view of the process of the regulation of human iron metabolism. J Biotechnol Comput Biol Bionanotechnol 92(2):193–207
3. Clinton KS (1998) Lycopene: chemistry, biology and implication for human health and disease. Nutr Rev 56(2):35–51

4. Roughead ZK, Johnson LK, Hunt JR (1999) Dietary Copper Primarily affects antioxidant capacity and dietary iron mainly affects iron status in a surface response study of female rats fed varying concentrations of iron, zinc and copper. Am Soc Nutr Sci 99:1368–1376
5. Agostoni C, Decsi T, Fewtrell M et al (2008) Complementary feeding: A commentary by ESPGHAN committee on nutrition. J Pediatr Gastroenterol Nutr 46:99–110
6. Martĺnez-Navarretea N, Camachoa MM, Martĺnez-Lahuertab J et al (2002) Iron deficiency and ironfortified foods—a review. Food Res Int 35:225–231
7. McKie AT, Barrow D, Latunde-Dada GO et al (2001) An iron -regulated ferric reductase associated with the absorption of dietary iron. J Sci 291:1755–1759
8. Hinton PS, Giordano C, Brownlie T (2000) Iron supplementation improves endurance after training in iron-depleted, nonanemic women. J Appl Physiol 88(3):1103–1111
9. Hiroshe K (1993) Effect of lacterr in on iron solubility under neutral conditions. Biosci Biotech Biochem 57(8):1376–1377
10. Kappas A, Drummond GS (1986) Control of heme metalbolism with synthetic metalloporphyrins. J Chin 2(77):335
11. Frederic L, Anne B (1998) Solubility of heme in heme-iron enriched bovine hemoglobin hydrolysate. J Agric Food Chem 46:5017–5025
12. Qian ZM, Xiao DS, Liao QK (2002) Effect of different durations of exercise on transferring-bound iron uptake by rat erythroblast. J Nutr Biochem 13(1):47–54
13. Weiss G, Houston T, Kastner S (1997) Regulation of cellular iron metabolism by erythropoietin: activation of iron-regulatory protein and upregulation of transferrin receptor expression in erythroid cells. 89(2):680–687
14. Róbert H, György L, Ottó H (2007) Air-stable, heme-like water-soluble iron (II) porphyrin: in situ preparation and characterization. J Biol Inorg Chem 12:68–690
15. In Man-Jin, Chae Hee Jeong, Nam-Soon Oh (2002) Process development for heme-enriched peptide by enzymatic hydrolysis of hemoglobin. Bioresour Technol 84:63–68
16. Grels DI, Ritva LAP, Reino O et al (1995) Process for preparation of a new hemin complex P. US patent 5,008,388
17. Rita KU, David PH et al (1997) Direct observation of nitrosylated heme in myoglobin and hemoglobin by electrospray ionization mass spectrometry. J Am Chem Soc 119:10424–10429
18. Chaijan M, Benjakul S, Visessanguan W et al (2007) Characterisation of myoglobin from sardine (*Sardinella gibbosa*) dark muscle. Food Chem 100:156–164
19. Brie KF, Christopher DV, Gregory JA (2012) Intestinal iron absorption. J Trace Elem Med Biol 26:115–119
20. Meehye K, Dong-Tae L, Yeon-Sook L (1995) Iron absorption and intestinal solubility in rats are influenced by dietary proteins. Nutr Res 15:1705–1716

Chapter 153
Enzymatic Extraction and Characteristics of Collagen Fibers from Cattle Skin

Wenhang Wang, Ke Zhao, Wei Ren, Ting Liu and Ying Zhang

Abstract Collagen fibers from cattle skin were enzymatically extracted and analyzed. The results of texture analyzer determination and microscopic observation of collagen fibers showed that extract efficiency was affected by pH, enzyme concentration, and combined ratio. The optimal conditions were obtained as follows: adding 0.5 ml 6 ‰ complex enzyme solution (alkaline proteinase: neutral protease = 1:1, w/w) into 1 g leather, ultrasonic shocking for 20 min, incubating in the shaking box at 30 °C for 24 h, and soaking in the pH = 2 hydrochloric acid solution for 7 h. Extracted collagen fibers are potentially used in edible film production and casing making.

Keywords Cattle skin · Collagen fibers · Extraction · Characteristics

153.1 Introduction

When thought about the packaging innovations for the twenty-first century, the most interesting thing to review was the technologies that are enabling these changes. As packaging innovations were researched across the food industry, there

W. Wang (✉) · K. Zhao · T. Liu
Key Laboratory of Food Nutrition and Safety, Ministry of Education, Tianjin University of Science and Technology, Tianjin 300457, People's Republic of China
e-mail: wangwenhang@tust.edu.cn

W. Ren
China National Research Institute of Food and Fermentation Industries, Beijing 100027, People's Republic of China

Y. Zhang
Department of Ecology, Environmental Management College of China, Qinhuangdao 066004, People's Republic of China

T.-C. Zhang et al. (eds.), *Proceedings of the 2012 International Conference on Applied Biotechnology (ICAB 2012)*, Lecture Notes in Electrical Engineering 251,
DOI: 10.1007/978-3-642-37925-3_153,

are numerous examples of breakthrough innovations in meat, snack, and beverage industry [1], such as high-density polyethylene coffee containers and polyethylene plastic bags. However, these new materials were not so friendly to the environment in some way. Many polyethylene plastic bags were found to be flying all around in the street at one time. So interest in edible films was rooted in attempts to develop easily degradable packaging, nonaggressive to the environment, thus improving the quality of food products and providing new markets for the materials used in the manufacture of these films [2]. The new food packaging technologies are also developing as a response to consumer demands or industrial production trends toward mildly preserved, fresh, tasty, and convenient food products with prolonged shelf life and controlled quality [3].

Edible films are defined as a thin layer of material which can be consumed and provides a barrier to moisture, oxygen, and solute movement for the food. The material can manufacture a complete food coating or can be disposed as a continuous layer between food components [4]. Edible films can be formed as food coatings and free-standing films, and have the potential to be used with food as gas aroma barrier [5].

Edible films can be produced from materials with film forming ability. During manufacturing, film materials must be dispersed and dissolved in a solvent such as water, alcohol, or mixture of water and alcohol or a mixture of other solvents. Plasticizers, antimicrobial agents, colors, or flavors can be added in this process. Adjusting the pH and heating the solutions may be done for the specific polymer to facilitate dispersion. Film solution is then casted and dried at a desired temperature and relative humidity to obtain free-standing films. In food applications, film solutions could be applied to food by several methods such as dipping, spraying, brushing, and panning followed by drying. Components used for the preparation of edible films can be classified into three categories: hydrocolloids (such as proteins, polysaccharides, and alginate), lipids (such as fatty acids, acyl glycerol, and waxes), and composites [6].

In their native states, proteins generally exist as either fibrous proteins or globular proteins [7]. Fibrous proteins are fully extended and associated closely with each other in parallel structures, generally through hydrogen bonding, to form fibers [8]. At the same time, proteins can assured their biodegradability and environmental compatibility to form films [9], and films made from protein can supplement the nutritional value of the food [10].

Collagen is widely found in nature as the major constituent of skin, bones and connective tissue, which has a high value whether in the field of food or medicine, and cosmetics. So the extraction of collagen from cattle skin will have a high cost-effectiveness and practical value. Plasticizers, antimicrobial agents, colors, or flavors have been added to improve its characteristics, such as mechanical properties and water vapor permeability. Chambi and Grosso [11] produced edible films with gelatin and casein cross-linked with transglutaminase. Vanin et al. [12] studied the effects of plasticizers and their concentrations on the thermal and functional properties of gelatin-based films.

Found by the preceding work, collagen fibers were mainly extracted by chemical methods, such as acid, alkali, which caused serious environment pollution and potential toxicity. Few researches were reported by enzymatic methods, although enzymatic hydrolysis has already used in gelatin production, collagen hydrolyte extraction, which showed enzymatic extraction is an efficient, environment-friendly way for collagen treatment.

The objective of this work was to study the enzymatic extraction conditions for collagen fibers from cattle skin, and to characterize their mechanical properties, providing a basic for produce potentially used in edible film production and casing making.

153.2 Materials and Methods

153.2.1 Materials

Cattle skins were obtained from Longbao Collagen Co., Ltd, and the initial pH was 12. Enzymes were purchased from Tianjin Nuoao Technology Co., Ltd. For simplicity in this article, trypsin and high alkali alkaline proteinase were abbreviated as Try and Haap. Alkaline proteinase and neutral protease in food and industry grade were abbreviated as Apf, Api, Npf, and Npi, respectively.

153.2.2 Collagen Fibers Production

Initial cattle skins were washed to the neutral pH, dried in the air, and then cut into pieces, vibrated 20 min in the ultrasonic oscillator, and cultivated with different enzyme solutions at 30 °C for 24 h. After washed up the residual enzyme, skins were put in hydrochloric acid in order to swell the collagen fibers, and neutralize the acid finally. In control group, cattle skins were treated with distilled water [13, 14]. Each sample was examined in triplicate.

153.2.3 Mechanical Properties

Firmness and shear force were determined according to the NY/T 1180-2006 using a texture analyzer (TA-XT Plus, Stable Micro Systems, SMS, UK), and the software Texture Expert V 5.1.2.0. The trigger force was 40 g. The speed before and after used initially was 1.50 and 10.00 mm/s, respectively [15]. Mechanical measurements were done in triplicate.

153.2.4 Histological Study

Cattle skins were cut into small pieces, embedded in the sample care using the Tissue Freezing Medium, sectioned at 4–6 μm thickness using a Freezing splicer (Leica CM1950). After fixed by the stationary liquid [16], the sections were stained with hematoxylin and eosion for microscopic examination using confocal laser scanning microscopy [17, 18].

153.3 Results and Discussion

153.3.1 Mechanical Properties

The firmness and shear force of cattle skins were determined using a Texture Analyzer. The data can react rough understanding of the enzymatic degree. The firmness and shear force of cattle skins were studied using six enzymes at 2, 4, 6, and 8 ‰ (w/w) concentrations. Figure 153.1 showed the changes of firmness and shear force under six different enzymes. The initial cattle skin firmness and shear force were 500.424 N and 639.7 N/s, respectively. The firmness and shear force of control group were 258.58 N and 201 N/s, respectively.

In Fig. 153.1, it was obvious that the firmness of skins treated with different enzymes had similar trend with the shear force. Compared with the control group, cattle skins dealt with Npf and Npi were obviously tougher than other groups. However, the Apf, Api, and Haap groups were almost twice softer than first three groups. Try was similar with animal proteinase in the way to degrade collagen, and it also acted on 780–781 sector of the amino acid sequence which is close to the sectors animal proteinase acted [19]. The optimum pH of Npf and Npi is 6.0–7.5, while APf, Api, and Haap is 9–11. Figure 153.1 showed that it was better to choose Apf, Api, or Haap to degrade the collagen.

With enzyme concentration increasing, firmness and shear force decreased quickly under 6 ‰. When the concentration was higher, firmness and shear force increased immediately. In this case, the best concentration of enzyme was 6 ‰.

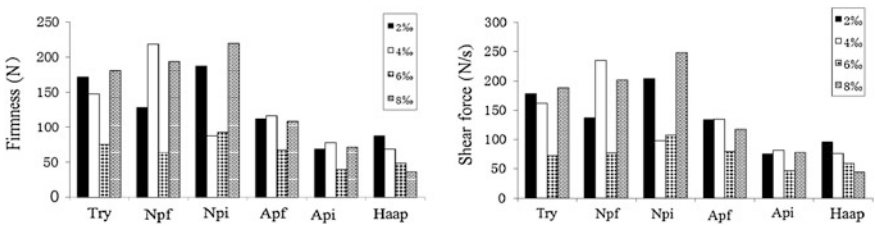

Fig. 153.1 Firmness and shear force of different enzymes at different concentrations

In Fig. 153.2, firmness and shear force of different enzymes with different ratios (1:1, 1:2, 2:1) were researched. The concentration of different complex enzyme was fixed to 6 ‰ according to Fig. 153.1. It was obvious that the effect was best when Npf/Apf was 1:1. Other groups were similar each other, but they were all too tough compared to the best group. So the best condition was to add 0.5 ml 6 ‰ complex enzyme solution (alkaline proteinase: neutral protease = 1:1, w/w) into 1 g leather.

After cattle skins were broken by enzymes, the isolated protein and many other components were cleaned up together. So the content of fibers was increased relatively. Then it was swelled by acid. Fibers became rougher, and space between fibers was not so tight. As is well-known, protein is hydrophilic, so its size becomes bigger when it absorbs water. However, fibers will be used to manufacture collagen casings by drying it, so the casings contain fibers most, and they have strong tensile strength. The better the fibers are swelled, the stronger casings are made. Figure 153.3 showed that when pH was 2, firmness and shear force of the fibers were both better than pH was 5.

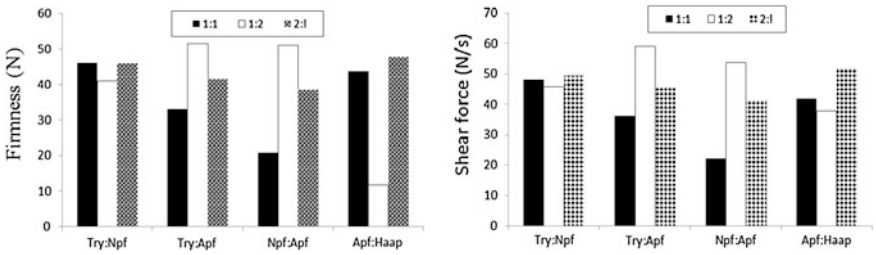

Fig. 153.2 Firmness and shear force of different enzymes with different ratios (1:1, 1:2, 2:1)

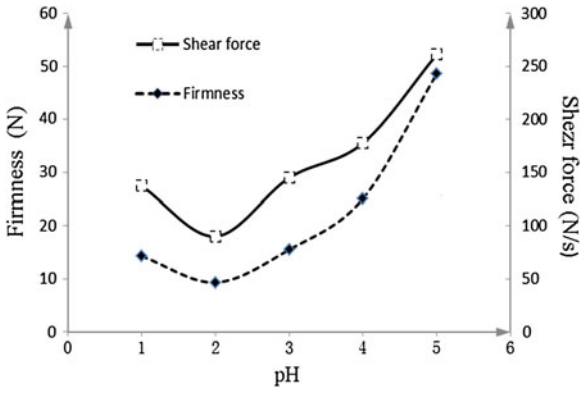

Fig. 153.3 Firmness and shear force of different pH values

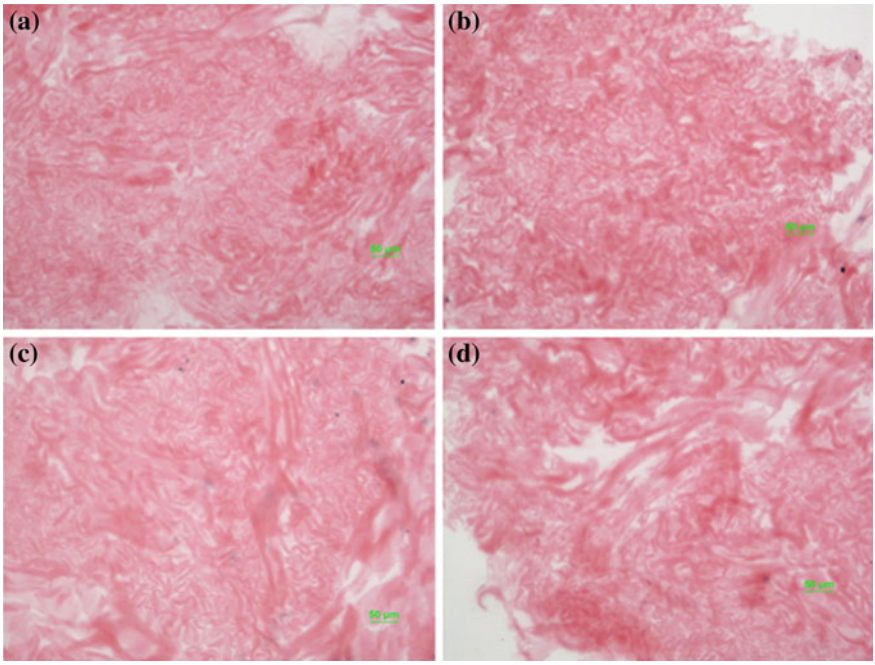

Fig. 153.4 Fibers micrographs in different conditions: **a** the control group, **b** Api (2 ‰), **c** Api (6 ‰), **d** complex enzyme (6 ‰). Magnification: 100X

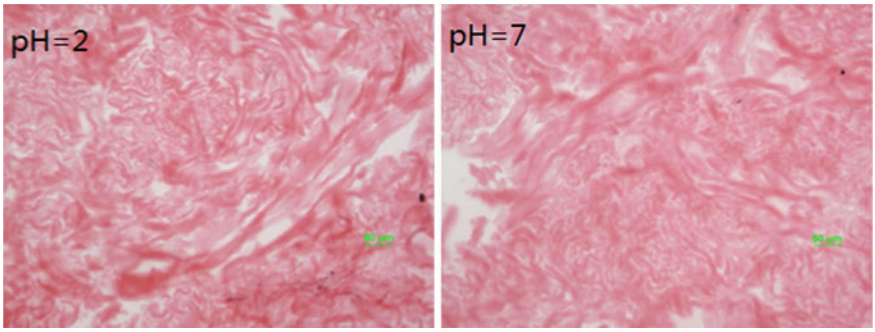

Fig. 153.5 Fibers micrographs in pH = 2 and pH = 7. Magnification: 100X

153.3.2 Microscope Imaging

Figure 153.4 showed four micrographs of the cattle skin in different enzyme conditions: the control group, Api (2 ‰), Api (6 ‰), and the complex enzyme (6 ‰). Enzyme can get rid of the dissociate protein. It was obvious in the micrographs that the majority of materials in cattle skin were collagen fibers.

Fibers rank tidily and regularly according to certain directions in the casings [20]. When cattle skins were dealt with alkali proteinase, extracted fibers were obviously thicker than the control ones, which add nothing to the cattle skins. Moreover, with the increasing concentration of enzyme, the fibers were thicker, and the gap between fibers was broader. In addition, it also showed that it was better when enzymes were mixed and the most suitable result was found when the complex enzymes (Alkaline proteinase/Neutral protease) ratio was 1:1.

After enzymatic extraction, collagen fibers were soaked in the hydrochloric acid. When the pH was too low, as well as the concentration of hydrochloric acid was too high, acid can break protein [21], and make it degeneration, so fibers were broken, casings can not be made. Figure 153.5 showed that when pH = 2, fibers were thicker than pH = 7. What is more, the gap between fibers became broader.

153.4 Conclusions

The collagen fibers from cattle skins were extracted by using the combined enzymolysis method. Effects of enzyme addition, solid-liquor ratio on the extraction, as well as pH efficiency of collagen fibers were investigated in this paper. The optimal processing conditions were obtained as follows: adding 0.6 % compound enzyme solution into 1 g leather, ultrasonic shocking for 20 min, then incubation at 30 °C in shaking box for 24 h, soaked in the pH = 2 hydrochloric acid solution. The results of texture analyzers determination and frozen section microscope observation of collagen fibers showed that in all conditions, the condition with alkaline proteinase/neutral protease = 1:1 was best.

Acknowledgements The present work was supported by grants from the Foundation of National 863 Plan (No.2013AA102204), National Natural Science Foundation of China (No. 31000755), and Key Project of Chinese Ministry of Education (No. 211008).

References

1. Eilert SJ (2005) New packaging technologies for the 21st century. Meat Sci 71:122–127
2. Chen H (1995) Functional properties and applications of edible films made of milk proteins. J Dairy Sci 78:2563–2583
3. Dainelli D, Gontard N, Spyropoulos D, Beuken EZ, Tobback P (2008) Active and intelligent food packaging: legal aspects and safety concerns. Trends Food Sci Tech 19:S103–S112
4. Guilbert S (1986) Technology and application of edible protective films. Food package preserv 1986:371–394
5. Kester JJ, Fennema OR (1986) Edible films and coatings: a review. Food Tech 40(12):47–59
6. Donhowe IG, Fennema OR (1993) The effects of plasticizers on crystallinity, permeability, and mechanical properties of methylcellulose films. J Food Process Preserv 17:247–257
7. Scope RK (1993) Separation by precipitation. In: Protein purification, principles and practice. Springer, New York, pp 71–101

8. Bourtoom T (2008) Review article edible films and coatings: characteristics and properties. Int Food Res J 15(3):237–248
9. Krochta JM, Johnston C (1997) Edible and biodegradable polymer films: challenges and opportunities. Food Tech 51:61–64
10. Gennadios A, Weller L (1990) Edible films and coatings from wheat and corn proteins. Food Tech 44:438–443
11. Chambi H, Grosso C (2006) Edible films produced with gelatin and casein cross-linked with transglutaminase. Food Res Int 39:446–458
12. Vanin FM, Sobral PJA, Menegalli FC et al (2005) Effects of plasticizers and their concentrations on the thermal and functional properties of gelatin-based films. Food Hydrocolloids 19:899–907
13. Ya H (2007) Edible collagen casing and application in meat industry. Meat Ind 10:17–19
14. Li P (2010) Collagen casing and film production. Sci Technol Gelatin 30(2):80–82
15. NY/T 1180-2006 (2006) Determination of meat tenderness and shear force method. Ministry of Agricultre of the PRC, Beijing
16. Yao HS, Yang J, Jin XL et al (1998) The fixed method improvement of frozen section. Shanhai Med 21(5):309–310
17. Adedeji AA, Liu L, Ngadi MO (2011) Microstructural evaluation of deep-fat fried chicken nugget batter coating using confocal laser scanning microscopy. J Food Eng 102:49–57
18. Achir N, Vitrac O, Trystram G (2010) Direct observation of the surface structure of French fries by UV-VIS confocal laser scanning microscopy. Food Res Int 43:307–314
19. Zhao SN (1998) Research of collagen extracted from fresh pig skin. Sci Tech Food Ind 5:16–17
20. Ye Y, Wang KY, Wang B (2003) Characteristics of collagen-chitosan-poval complex film. China Leather 32(23):1–4
21. Li X, Li YT, Wei SZ (2004) Study on production technology of acid-hydrolysis amino acid seasoning. China Brewing 3:11–15

Chapter 154
Detection of DNA Target with Highly Enhanced Specificity by Self-Circularization Rolling Circle Amplification

Xingyu Wang, Xiaoliang Wang, Ping Dong, Masatomo Suzuki, Hiroyuki Asanuma and Xingguo Liang

Abstract DNA detection is widely used for gene analysis. However, false-positive results are difficult to be avoided due to the non-specific amplification. Here, we described a novel RCA approach to improve the specificity. With the help of TspR I (endonuclease), DNA was cleaved into smaller duplex fragments, including the target DNA fragment, with 9 nt sticky ends. A duplex adaptor with two sticky ends which were complementary to that of the target fragment was designed. After hybridization of the adaptor with the target fragments, T4 DNA ligase was used to ligate them to form a circular ds DNA with a gap. Then RCA was carried out from the free 3′-end of the open strand by Phi29 DNA polymerase with two primers which were complementary to the target sequence. Different from the traditional padlock-RCA, SC-RCA showed excellent specificity by amplifying the specific DNA target other than the added probe.

Keywords RCA · DNA detection · DNA amplification · Gene analysis

Xingyu Wang and Xiaoliang Wang—these authors contributed equally to this article.

X. Wang · X. Wang · P. Dong · X. Liang (✉)
College of Food Science and Engineering, Ocean University of China,
Yushan Road, No.5, Shinan-qu, Qingdao 266003, People's Republic of China
e-mail: liangxg@ouc.edu.cn

M. Suzuki · H. Asanuma
Department of Molecular Design and Engineering, Graduate School of Engineering,
Nagoya University, Chikusa,
Nagoya 464-8603, Japan

T.-C. Zhang et al. (eds.), *Proceedings of the 2012 International Conference on Applied Biotechnology (ICAB 2012)*, Lecture Notes in Electrical Engineering 251,
DOI: 10.1007/978-3-642-37925-3_154,

154.1 Introduction

DNA amplification technology has greatly facilitated the development of molecular biology. Based on the amplification protocols, nucleic acid detection for harmful bacteria and virus won the edge in diagnosis, infectious disease prevention, environment monitor, and food industry [1]. As a traditional amplification approach, polymerase chain reaction (PCR) has been widely used for detecting DNA targets with high specificity and sensitivity. However, besides the elaborate routine for primer design, since PCR requires expensive equipment for fast thermal cycles and precise temperature control, its application in low-cost and rapid DNA detection has been limited [2]. Also, PCR can lead to sequence-dependent bias due to the mismatched primer-target hybridization and the intense thermal cycles [3].

As an isothermal detection method for overcoming the shortcomings of PCR, RCA (rolling circle amplification) has gained a great attention over the past decade [4]. The most distinguished feature of RCA is that it can be easily carried out on a chip for high-throughput detections [5]. However, the specificity of traditional padlock-RCA is not high enough and various methods have been tried to improve it [6]. The specificity of padlock-RCA is based on the specific hybridization of two ends of a pre-circular DNA (probe) with the target sequence, followed by circularization of the probe with the help of ligase. With the specifically formed circular probe, RCA can be carried out. Nonetheless, even in the case that several mismatches are present at the position not close to the ligation site, the probe can also be circularized and end up with false-positive results [7]. Moreover, the amplification reaction of padlock-RCA only generates tandem copies of the probe itself but not the DNA target [8].

Here we present a novel DNA detection method, termed "Self-Circularization Rolling Circle Amplification" (SC-RCA), which features the sensitivity comparable to that of padlock-RCA but with much higher specificity. Unlike padlock-RCA, in SC-RCA procedure, the DNA target but not the probe is circularized and amplified sequentially. Furthermore, its specificity is as well be enhanced by branched RCA using oligonucleotide primers complementary to the DNA target sequence. Therefore, SC-RCA is promising to be used as a low-cost, high specificity, and high-throughput detection method.

154.2 Materials and Methods

154.2.1 Materials

All oligonucleotides used as primers or adapters were synthesized and purified with HPLC at Sangon Biological Engineering Technology and Services Co. Ltd.

Table 154.1 Sequence of oligonucleotide used in this study

Name	Sequence (5′ → 3′)	Length (nt)
105 adp	TAATACGACTCACTATAGGTACAGTGAG	28
	CCTATAGTGAGTCGTATTATATTAGCACTGGG	32
271 adp	TAATACGACTCACTATAGGGCCACTGGT	28
	CCTATAGTGAGTCGTATTATATTTCCACTGAG	32
506 adp	TAATACGACTCACTATAGGCTCACTGAC	28
	CCTATAGTGAGTCGTATTATATTGCCAGTGGC	32
958 adp	TAATACGACTCACTATAGGAGCACTGCA	28
	CCTATAGTGAGTCGTATTATATTGGCACTGGC	32
105 P1	GGCAACTATGGATGA	15
105 P2	ATAACTACGATACGG	15
271 P1	GTAGCCGTAGTTAGG	15
271 P2	CAAGCAGCAGATTAC	15
506 P1	ACCTACACCGAACTG	15
506 P2	ACGCAGGAAAGAACA	15
958 P1	ACGAGTGGGTTACAT	15
958 P2	AGATGCGTAAGGAGA	15

(Shanghai, China). Their sequences were listed in Table 154.1. The phoshphorthioate primers were used to avoid the hydrolysis by the 3′-exonuclease activity of Phi29 DNA polymerase. The adapters designed with 9 nt sticky ends that were perfectly complementary with the digested DNA target. All the adapters used in this work were composed by mixing two single strand oligonucleotides together in buffer solution. The plasmid DNA pUC-18, employed as the DNA target, was purchased from New England Biolabs (Ipswich, MA, US). T4 DNA ligase, TspR I endonuclease, Phi29 DNA polymerase, and One Taq polymerase were also obtained from New England Biolabs. DNA ladder containing 1 kb–100 bp and deoxyribonucleotides (dNTPs) were purchased from Tiangen (Beijing, China). SYBR Green I and ethidium bromide nucleic dye were offered by Invitrogen (Beijing, China). Multi-functional DNA gel recovery kit was provided by Aidlab Biolab (Nanjing, China). Other chemicals employed were of analytical reagent grade and used without further purification. The high-purity deionized water (resistance > 18 MΩ* cm) was used in all instances.

154.2.2 Digestion of DNA with TspR I Endonuclease

For DNA digestion, 2 μL target DNA (plasmid pUC-18) was mixed with 5 U TspR I (0.1 U/μL, recognition site: 5′-NNCACSTGNN-3′) in 20 μL buffers [9]. The buffer (pH = 7.5) contained 20 mM Tris–acetate, 50 mM KAc, 10 mM $MgAc_2$, and 1 mM DTT. The reaction mixture was incubated at 65 °C for 2 h. To obtain the target DNA with different concentration, gradient dilution was applied and the diluted solution was stored at −18 °C for the following sensitivity assay.

154.2.3 Ligation of Hybridized DNA with T4 DNA Ligase

To circularize dsDNA molecules, the adapter with 9 nt cohesive ends that were perfectly complementary to that of the target was introduced. 1.0 μL adapter storage solution (10 nM/μL), 1.0 μL digest solution containing the target, 1.0 μL 10 × T4 DNA ligase buffer (pH = 7.5, 0.5 mM Tris–HCl, 0.1 mM $MgCl_2$, 0.1 mM DTT and 10 mM ATP), and 1.0 μL of T4 DNA ligase (1.0 U/μL) were mixed. High-purity deionized water was added to a final volume of 10 μL, followed by incubation at 25 °C for 25 min. After that, ligation reaction was terminated by heating at 65 °C for 10 min [10].

154.2.4 Amplification of the Ligated DNA with Phi29 DNA Polymerase

The above 10 μL of ligation solution was used to perform RCA reaction with the final volume of 20 μL consisting of 50 mM Tris–HCl (pH = 7.5), 10 mM $MgCl_2$, 10 mM $(NH_4)_2SO_4$, 4 mM DTT, 0.5 mM dNTP, 0.25 μM primer, and 5U Phi29 DNA polymerase (1.0 U/μL). Then, the mixture was incubated at 30 °C for 8 h. The reaction was terminated by heating the mixture at 65 °C in water bath for 10 min [11].

154.2.5 Digestion of Amplification Products with TspR I Endonuclease and Electrophoresis Analysis

Aliquots of 2 μL of amplification reaction were pipette and mixed with 0.5 μL (0.1 μL/U) TspR I and 2 μL 10 × NEB buffer 4 (pH = 7.9, 0.5 M KAc, 0.2 M Tris-Ac, 0.1 M $Mg(Ac)_2$, 10 mM DTT). The final volume was filled up to 20 μL by high-purity deionized water. The reactions were carried out at 65 °C for 2 h. All the digestion aliquots were subjected to polyacrylamide gel electrophoresis to evaluate the performance of SC-RCA.

154.3 Results and Discussion

154.3.1 Principle of SC-RCA

Self-Circularization RCA was developed to provide an effective method for detecting specific DNA target sequence in a solution. A simple scheme outlining

Fig. 154.1 Schematic illustration of the principle of SC-RCA

the SC-RCA was shown in Fig. 154.1. A digestion step is employed to generate a number of shorter fragments, including the target DNA fragment, with 9 nt sticky ends. Then a ligase is utilized to ligate the adaptor and the target DNA to form a double stranded circle with a gap. Phi29 DNA polymerase is then used to amplify the circle by RCA using the integral strand as the template and the open strand as the primer. The exponential amplification is achieved with the help of two primers complementary to the target sequence. Finally, the products consisting of tandem copies of dsDNA target were digested by restriction endonuclease (TspR I) at the cutting site as 5′-NNCASTGNN-3′. Hence, the target DNA meant to be replicated or detected is obtained with the augmentation of several magnitudes. However, if there are mismatches in sticky ends between the target and the adaptor DNA, ligation reaction will fail and no circular DNA will be produced for RCA.

T4 DNA ligase was exploited to perform the ligation reaction. The ligase features a high efficiency and low specificity, which means non-perfectly matched template-adapter could be ligated to form a unexpected circle [12]. Once the hybridization of the template and adapter was circularized, amplification was initiated by Phi29 DNA polymerase afterward. Hence, erroneous DNA sequences could be amplified unexpectedly. To eliminate the false-positive result mentioned above, two primers were introduced to the system to ignite exponential amplification. The primers are complementary to the target sequence away from the overhang region of the sticky ends. Therefore, the non-target circles only initiate a linear amplification generating fewer products than that of exponential amplification by several magnitudes [13]. Higher specificity can be expected consequently.

154.3.2 Amplification of the Single Fragment

Here, we used plasmid pUC-18 as a model target to check the feasibility of our strategy. There were 10 recognition sites on pUC-18 for TspR I digestion. After being cleaved by the endonuclease, 10 fragments with 9 nt sticky ends were generated and with the length ranging from 13 to 958 bp. The electrophoresis pattern of pUC-18 digested by TspR I was shown in Fig. 154.2. At first, the purified 271 bp fragment was chosen as the target DNA to be detected by SC-RCA. The fragment was separated by agarose electrophoresis and purified with Multi-functional DNA gel recovery kit. Concentration of the fragment was

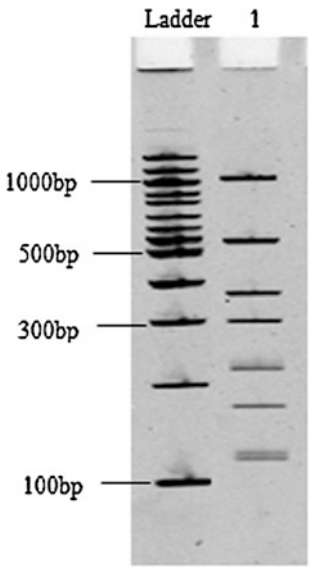

Fig. 154.2 Analysis of pUC-18 fragmentation by restriction enzyme TspR I. Lane 1: Digested fragments of pUC-18. The concentration of pUC-18 digestion reaction was 10 nM, and the reaction processed at 65 °C in water bath for 2 h. 6 μL digestion solution mixed with 1.2 μL loading buffer was loaded on 8 % PAGE. For electrophoresis, the voltage was set as 350 V and processed for 1.5 h

measured by Nano Drop NA analyzer. The result of the 271 bp fragment amplified by SC-RCA was shown in Fig. 154.3.

The products of SC-RCA, as shown in Fig. 154.3 lane 1, were in a ladder pattern and most of them were longer than 10 kb. The minimum band was 271 bp followed by the products with the length of integral multiples of 271 bp. From the size of the bands, it can be deduced that the products were typical RCA products which were the tandem repeats of the target sequence. The digested products exhibited as a neat, single band pattern which proved that the target DNA had been replicated efficiently by the protocol we presented.

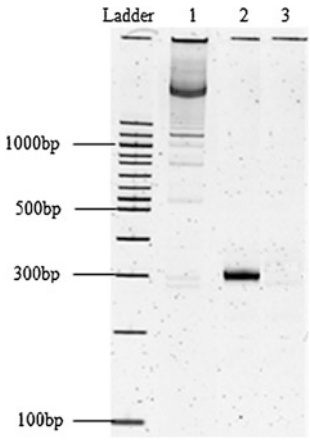

Fig. 154.3 Amplification of a single fragment by SC-RCA. Lane 1: SC-RCA products; Lane 2: SC-RCA products after digestion by TspR I; Lane 3: A negative control in the absence of T4 ligase. The concentration of adaptor and template was 10, 1.0 nM respectively

154.3.3 Amplification of One Specific Target from Multiple Fragments

In this part, SC-RCA was exploited to amplify a specific target among the multiple fragments created by TspR I digestion. To investigate the specificity of SC-RCA, 105, 271, 508, and 958 bp fragments were selected out of the 10 nascent fragments digested from pUC-18. Four types of adaptors and primers were elaborately designed in order to replicate each target mentioned above. As shown in Fig. 154.4, the amplification products with TspR I-cut templates appeared as a single clean band for four target fragments separately. Therefore, the results demonstrated that the method we presented here was not only applicable for replicating targets of various lengths with high specificity, but also can avoid nonspecific amplification that might be found in the operation of PCR [14].

To evaluate the sensitivity of this method, which is usually regarded as one of the most crucial parameters, different concentrations of the 271 bp target DNA were mixed with 10 nM adapter duplex respectively, in 10 μL of reaction buffer, and then was ligated and amplified according to the protocol described before. The electrophoresis results were shown in Fig. 154.5. As the concentration of template DNA decreased, the band intensity declined gradually. The band intensity decreased significantly when the target concentration hit to 1.0 fM, which indicated that diluted templates with about 600 mole/ml can be effectively amplified by means of SC-RCA. Hence, boasting the sensitivity like this, the method we proposed can be confidently applied in routine tests with general materials.

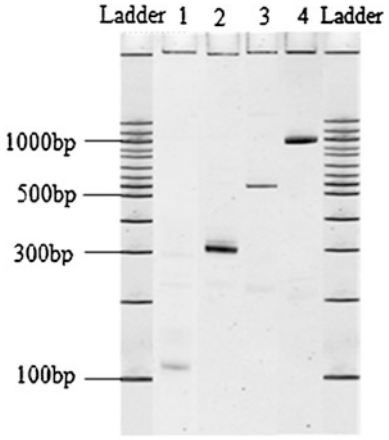

Fig. 154.4 Analysis of SC-RCA products with templates digested by TspR I. Lane 1: 105 bp; Lane 2: 271 bp; Lane 3: 508 bp; Lane 4: 958 bp. Concentration of the adaptors and the targets were 10, 1.0 nM, respectively

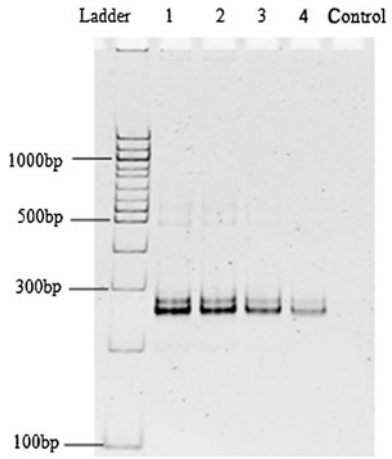

Fig. 154.5 The electrophoresis result of sensitivity of SC-RCA towards 271 bp target on the condition of multiple fragments. Lane 1: 1.0 pM; Lane 2: 100 fM; Lane 3:10 fM; Lane 4: 1 fM; Control: No T4 ligase. Concentration of 271 bp adaptor was 10 nM. The concentration of the DNA target was diluted from 1.0 pM to 1.0 fM

154.3.4 Comparison Between SC-RCA and PCR

As a modern detection and amplification method prevalently used worldwide, PCR is employed in most nucleic analysis tests for its stability and sensitivity [15]. Here, two amplification methods were compared in terms of specificity and sensitivity. As shown in Fig. 154.6, with the interference generated by other non-target fragment whose sticky ends shared the sequence in part with that of the target, 271 bp fragment replicated by SC-RCA manifested a desirable specificity

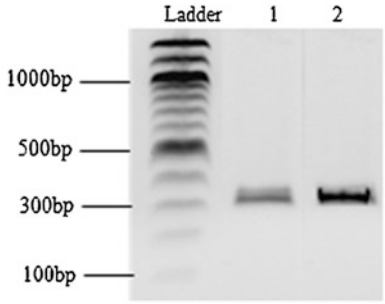

Fig. 154.6 Comparison between PCR and SC-RCA for amplifying target DNA. Lane 1: target amplified by PCR; Lane 2: target amplified by SC-RCA. Concentration of the template was 1 nM, and the protocol of PCR was referred to the literature with modification [18]. PCR procedure was as follow: initial denaturation performed at 94 °C for 30 s, annealing at 49 °C for 30 s, then primer elongation at 68 °C for 60 s. 30 cycles was employed. Finally the samples were incubated at 68 °C for another 5 min and terminated at 4 °C. 50 μL PCR reaction system (pH = 8.3) consisted of 1 μL template, 10 mM Tris–HCl, 50 mM KCl, 1.5 mM $MgCl_2$, 0.2 mM dNTPs, 0.2 μM primer, and 1.25 U One Taq DNA polymerase. Two primers are listed as follow: primer 1: 5′-atgaccaaaatcccttaacg-3′, primer 2: 5′-gtcttgagtccaacccgg-3′

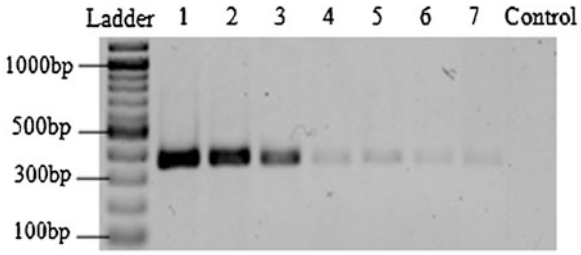

Fig. 154.7 The electrophoresis result demonstrating sensitivity of PCR for amplifying target DNA. Lane 1: 100 pM; Lane 2: 10 pM; Lane 3: 1 pM; Lane 4: 100 fM; Lane 5: 10 fM Lane 6: 1 fM; Lane 7: 100 aM; Control: no template

as much as that of PCR. However, since PCR relies on the precise thermal equipment, SC-RCA wins its edge for lower cost and easier procedure. For sensitivity of PCR, the detection limit of PCR toward the 271 bp target was also investigated (Fig. 154.7). The 358 bp PCR product contains the 271 bp target inside. Comparing to Fig. 154.5, PCR was able to detect 100 aM template target, which was one magnitude lower than that of SC-RCA. Distinct amplification mechanisms may mainly be responsible for the difference [16]. Nonetheless, as the specificity provided by SC-RCA is not only based on the 9-nt sticky ends but also enhanced by the added primers, there are reasons to believe that SC-RCA would reveal higher specificity than PCR when the test aliquots intermingle with tremendous DNA molecules sharing the sequence with the target [17].

154.4 Conclusions

In this work, we have developed a new method to detect and amplify target DNA with the digested plasmid fragment as a model. All the four fragments whose length ranging from 0.1 to 1.0 kb were successfully replicated with high sensitivity and specificity which can be mainly attributed to the specific ligase reaction and the robust amplifying capability of RCA. The detection limit has been decreased to 1.0 fM. The developed method holds some advantages over other techniques, such as simplicity and high specificity. Furthermore, comparing to PCR, SC-RCA can avoid complicated thermal cycling steps, heating in a period of time using a simple incubator is sufficient to amplify DNA to detectable levels [19]. Combining with the technology of DNA chip, the proposed protocol is promising to be easily extended to a high-throughput and automatic screening format in future applications [20].

Acknowledgments We are grateful for the financial support of the recruitment programs of "Wanren Plan", "Fund for Distinguished Young Scholars" of Shandong province, and "National Youth Qianren Plan".

References

1. Park SJ, Taton TA, Mirkin CA (2002) Array-based electrical detection of DNA with nanoparticle probes. Sci 295:1503–1506
2. Hatch A, Sano T, Misasi J et al (1999) Rolling circle amplification of DNA immobilized on solid surfaces and its application to multiplex mutation detection. Genet Anal 15:35–40
3. Nallur G, Luo CH, Fang LH et al (2001) Signal amplification by rolling circle amplification on DNA microarrays. Nucleic Acids Res 29:e118
4. Nilsson M, Gullberg M, Dahl F et al (2002) Real-time monitoring of rolling-circle amplification using a modified molecular beacon design. Nucleic Acids Res 30:e66
5. Zhang SB, Wu ZS, Shen GL et al (2009) A label-free strategy for SNP detection with high fidelity and sensitivity based on ligation-rolling circle amplification and intercalating of methylene blue. Biosens Bioelectron 24:3201–3207
6. Larsson C, Koch J, Nygren A et al (2004) In situ genotyping individual DNA molecules by target-primed rolling-circle amplification of padlock probes. Nat Methods 1:227–232
7. Zhang DY, Zhang WD, Li XP et al (2001) Detection of rare DNA targets by isothermal ramification amplification. Gene 274:209–216
8. Nilsson M, Malmgren H, Samiotaki M et al (1994) Padlock probes: circularizing oligonucleotides for localized DNA detection. Science 256:2085–2088
9. Truninger K, Witt H, Köck J et al (2002) Mutations of the serine protease inhibitor, Kazal Type 1 Gene, in patients with idiopathic chronic pancreatitis. Am J Gastroenterol 97:1133–1137
10. England TE, Gumport RI, Uhlenbeck OC (1977) Dinucleoside pyrophosphate are substrates for T4-induced RNA ligase. Proc Natl Acad Sci 74:4839–4842
11. Phillip SK, Denice KT, Kan VL (2002) Combinatorial multiplex assay format using electronic microchip arrays and its potential application in complex cancer diagnostics. Clin Chem 48:1851–1868
12. Kuhn H, Frank-Kamenetskii MD (2005) Template-independent ligation of single-stranded DNA by T4 DNA ligase. FEBS J 272:5991–6000
13. Lizardi PM, Huang X, Zhu Z et al (1998) Mutation detection and single-molecule counting using isothermal rolling-circle amplification. Nat Genet 19:225–232
14. Kwok S, Higuchi R (1989) Avoiding false positives with PCR. Nature 339:237–238
15. Angen O, Oliveira S, Ahrens P et al (2007) Development of an improved species specific pcr test for detection of *haemophilus parasuis*. Vet Microbiol 119:266–276
16. Demidov VV (2002) Rolling-circle amplification in DNA diagnostics: the power of simplicity. Expert Rev Mol Diagn 2:89–95
17. Gusev Y, Sparkowski J, Raghunathan A et al (2001) Rolling circle amplification: a new approach to increase sensitivity for immunohistochemistry and flow cytometry. Am J Pathol 159:63–69
18. Qu W, Jiang G, Cruz Y et al (1997) PCR detection of *human papillomavirus*: comparison between MY09/MY11 and GP5 +/GP6 + primer systems. J Clin Microbiol 35:1304–1310
19. Marquette CA, Blum LJ (2008) Electro-chemiluminescent biosensing. Anal Bioanal Chem 390:155–168
20. Su Q, Xing D, Zhou XM (2010) Magnetic beads based rolling circle amplification-electrochemiluminescence assay for highly sensitive detection of point mutation. Biosens Bioelectron 25:1615–1621

Chapter 155
Effect of Proteinase A Propeptide Deletion on its Enzyme Activity in *Saccharomyces cerevisiae*

Deguang Wu, Yefu Chen, Jun Lu, Yanan Qi, Cuiying Zhang and Dongguang Xiao

Abstract Two expression plasmids YCP-EP and YCP-54A respectively expressing the complete *PEP4* gene and the incomplete *PEP4* gene without the prosequence (encode the propeptide of proteinase A) from *Saccharomyces cerevisiae* W303-1A were constructed and transferred into *S. cerevisiae* W303-K22 (△*PEP4*). The yeast transformants WYCP-EP and WYCP-54A were obtained. Meanwhile, a mutant strain W54A deleted the prosequence of *PEP4* was obtained by homologous recombination. The proteinase A enzyme activities of the yeast transformants WYCP-EP, WYCP-54A and the mutant strain W54A were detected by fluorescent substrate, respectively. The results showed that only the strain WYCP-EP was able to produce the active proteinase A. Consequently, the results confirmed that the propeptide was required for formation of active mature proteinase A, and it provided the theoretical basis for the construction of genetic engineering strain with low-proteinase A by the deletion of prosequence.

Keywords *Saccharomyces cerevisiae* · Proteinase A · Propeptide · Expression plasmid · Enzyme activity

155.1 Introduction

Saccharomyces cerevisiae proteinase A (PrA, EC3.4.23.25) is a member of the aspartic proteinase superfamily, which is synthesized as a precursor (PreproPrA) of 405 amino acids encoded by *PEP4* gene [1]. The precursor consists of

D. Wu · Y. Chen · J. Lu · Y. Qi · C. Zhang · D. Xiao (✉)
Key Laboratory of Industrial Fermentation Microbiology, Ministry of Education, Tianjin Industrial Microbiology Key Laboratory, College of Biotechnology, Tianjin University of Science and Technology, 300457 Tianjin, People's Republic of China
e-mail: xiao99@tust.edu.cn

T.-C. Zhang et al. (eds.), *Proceedings of the 2012 International Conference on Applied Biotechnology (ICAB 2012)*, Lecture Notes in Electrical Engineering 251,
DOI: 10.1007/978-3-642-37925-3_155,

N-terminal signal peptide, followed by a propeptide (the prosequence of *PEP4* encoded) and the mature peptide. During the process of PrA mature, the 22 amino acids signal peptide is cleaved off in the endoplasmic reticulum (ER), and the zymogen proPrA was formed. The proPrA undergoes further carbohydrate modification in the Golgi complex, and subsequently an 54-amino-acid propeptide is cleaved to generate the mature PrA upon arrival in the vacuole [2]. However, when the culture condition goes against growth of yeast, such as nutritional deficiency, hyperosmolality, the proPrA will be conveyed to extracellular instead of being targeted to the vacuole [3] [Kondo 1995 #133]. Furthermore, the inactive proPrA will be matured to active PrA by automatically activation mechanism in vitro [4]. The active PrA can directly degrade foam proteins in beer, therefore, the extracellular mature PrA is the main reason that beer foam stability is decrease.

In recent years, seeking for the methods for decreasing the PrA content in draft beer has been the research focus in beer industry. Several research reported that the propeptide of PrA contained the sorting signal for targeting proPrA to the vacuole, however, the proPrA would be completely degraded in the ER in case of lacking the propeptide [5, 6]. Therefore, in this study, we researched the effect of PrA propeptide deletion (PrAΔpro) on its enzyme activity by monitoring the PrA enzyme activities of several constructed mutants with different *PEP4* genotypes. Our data provided the theoretical basis for the construction of genetic engineering strain with low-proteinase A by the deletion of prosequence.

155.2 Materials and Methods

155.2.1 Materials, Plasmids, and Strains

All Oligonucleotide primers used in this study are listed in Table 155.1.

Saccharomyces cerevisiae-Escherichia coli shutter vector YCP50 (AmpR URA3) was used for construction of expression plasmids. The complete *PEP4* gene was amplified from W303-1A [7] genomic DNA with primers DA-up and DB-down, and the PCR product was inserted into vector YCP50 to create the expression plasmid YCP-EP. Another expression plasmid YCP-54A, which contains the incomplete *PEP4* lacking the prosequence (pep4-23△76), was constructed as Fig. 155.1 described. The constructed recombinant plasmid pUC-ABK (Fig. 155.2), which contained A, B fragments from the upstream and downstream of the prosequence respectively and *KanMX* gene from pUG6, was used for the prosequence of *PEP4* deletion.

Escherichia coli strain DH5α was used for plasmid preparation and construction. S. cerevisiae W303-1A(Matα his3-11,15 leu2-3,112 trp1-1, ade2-1, ura3-1, can1-100)was used as the control for chromosomal expressing of wild-type PrA. Strain W303-K22 (△*pep4*), which derived from W303-1A deleted *PEP4* gene, was used for the expression of mutant forms of PrA in a △*pep4* strain background.

Table 155.1 PCR primers used in this study

Primer	Sequence(5′ → 3′)	Restriction site
DA-up	CGCGGATCCGAGAGAAGATGGTAGATACC	*Bam*H I
DA-down	AACTGCAGCAACTTGGTTGGCGCTGAC	*Pst* I
DB-up	AACTGCAGGTGGTCACGATGTTCCATTG	*Pst* I
DB-down	CGTGCATGCTTTTCGCTTCTGCTTACATTGC	*Sph* I
A-up	CCCAAGCTTCGCTGCTATTTATTCATTCCACC	*Hin*d III
A-down	GTGAAGCTTTGCAGCAACTTGGTTGGCGCT	*Hin*d III
B-up	CGAGCTCGGTGGTCACGATGTTCCAT	*Sac* I
B-down	CGAGCTCTGGTAGCCTCAGCGAAGTCT	*Sac* I
Kan-up	CGGGGTACCCAGCTGAAGCTTCGTACGC	*Kpn* I
Kan-down	CGGGGTACCCATAGGCCACTAGTGGATCTG	*Kpn* I
YZ1-up	GTTAGCTCACTCATTAGGCA	
YZ1-down	GACTTTTGCAGCAACTTGGT	
YZ2-up	GTTAGCTCACTCATTAGGCA	
YZ2-down	CGCTGCTATTTATTCATTCCACC	
YZ0-up	AGAAGCCTACCACGTAAG	
YZ0-down	GCTTCATGATCGTATTTAGAAT	

Note The restriction site introduced in each primer is indicated by an underline

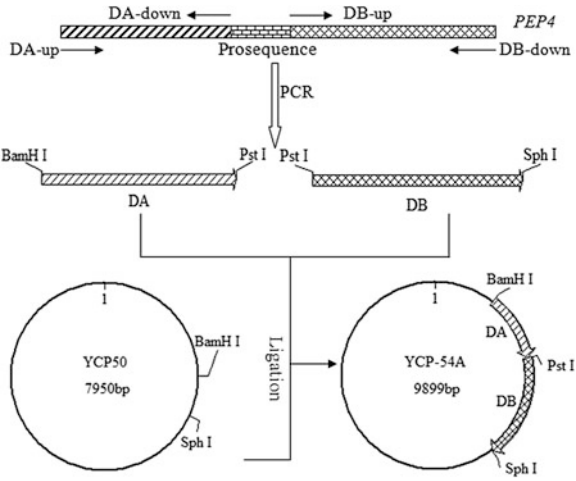

Fig. 155.1 Construction of expression plasmid YCP-54A

The yeast transformants WYCP-EP and WYCP-54A were constructed via transferring the expression plasmids YCP-EP and YCP-54A into W303-K22, respectively. The yeast transformant WYCP was constructed previously by transferring YCP50 into W303-K22 in our lab. The mutant strain W54A was constructed by homologous recombination. The recombinant cassette A-*KanMX*-B fragment was amplified via PCR from plasmid pUC-ABK and transformed into the parental strains W303-1A by the lithium acetate method. The W54A-K excised the *KanMX* gene was obtained by using the Cre-*loxP* recombination system [8, 9].

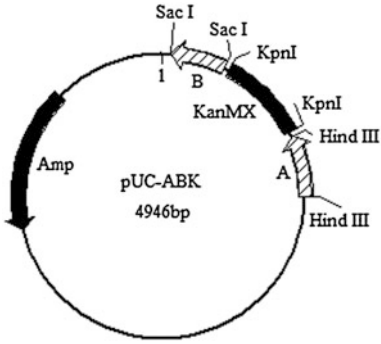

Fig. 155.2 Schematic diagram of recombinant plasmid pUC-ABK

155.2.2 Media and Cultivation Conditions

Escherichia coli strain DH5α was incubated in LB medium added ampicillin resistance at 37 °C for plasmid maintenance. Yeast strains were cultured in standard YEPD medium at 30 °C. The yeast recombinants were screened on YEPD plates additionally added 800 μg/mL G418. Yeast Synthetic Drop-Out Media Supplement without Uracil (Sigma USA) was used to screen the yeast transformants [7]. And YEPG medium (10 g/L yeast extract, 20 g/L peptone, and 20 g/L galactose) was used for Cre recombinase expression in yeast mutant strain.

155.2.3 Fermentation Assay and Analytical Methods

Fermentation assay was performed according to the method described by Hao [10]. PrA activity was assayed by a fluorescent method [11]. One unit of PrA will hydrolyze 1 mg of insulin chain B (oxidized) per minute at pH 6.0 (25 °C). Intracellular total proteins were measured by Bradford method [12]. Residual sugar was measured by Fehling reagent-Spectrophotometric method, and alcohol content was measured using Beer Analyzer.

155.3 Results and Discussions

155.3.1 Construction of Yeast Transformants WYCP-EP and WYCP-54A

According to the method described in the Materials and Methods section, two expression plasmids YCP-EP (expressing complete *PEP4*) and YCP-54A (expressing incomplete *PEP4* deleted prosequence) were successfully constructed

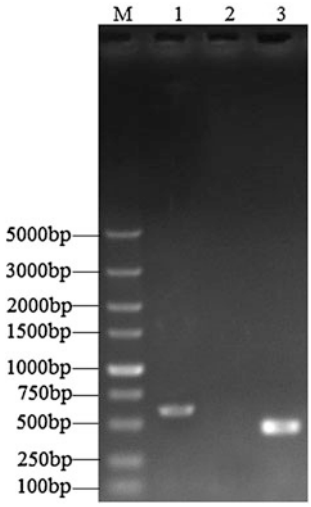

Fig. 155.3 PCR verification of yeast transformants. *M* marker DL 5000; *Lane 1,2,3* Respective PCR product from WYCP-EP, WYCP, WYCP-54A with primers YZ0-up/YZ0-down

and transferred into W303-K22 respectively, then two yeast transformants, WYCP-EP and WYCP-54A were obtained. In order to verify the two yeast transformants, compared with WYCP, the yeast plasmids of WYCP-EP and WYCP-54A were extracted and used as templates of PCR verification. The PCR verification was executed with primer pair YZ0-up/YZ0-down, which was located in the flank of the coding region of prosequence. The size of the PCR product from WYCP-54A should be less 162 bp than that of WYCP-EP and the WYCP has no PCR product. As shown in Fig. 155.3, the results indicated that we successfully constructed yeast transformants WYCP-EP and WYCP-54A.

155.3.2 Construction of PrA Propeptide Deletion Mutants

PrA propeptide deletion mutant W54A was constructed via homologous recombination. Two primer pairs YZ1-up/YZ1-down and YZ2-up/YZ2-down were designed to verify the deletion of prosequence of *PEP4* gene. Theoretically, the target 2.0 and 1.6 kb bands could be obtained from genome of W54A, but they could not be obtained from that of the parental strain W303-1A. Figure. 155.4 showed that the PCR products were consistent with expectation. Therefore, the results proved that the recombinant cassette A-*KanMX*-B fragment was successfully inserted into the locus of prosequence of *PEP4* and the prosequence was replaced by *KanMX*. In addition, the *KanMX* gene was excised from the mutant strain W54A, and another mutant strain W54A-K was obtained and identified via PCR (Fig. 155.4).

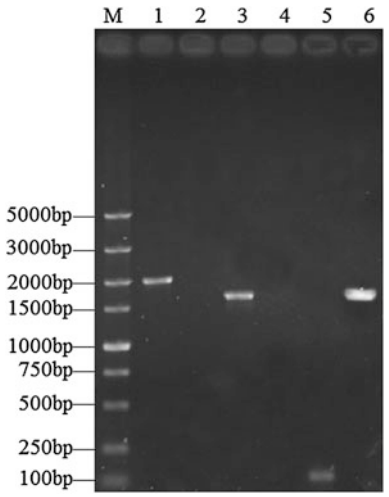

Fig. 155.4 PCR verification of the yeast recombinant strains. *M* marker DL 5000; *DNA templates* W54A (lane 1,3,6); W303-1A (lane 2,4); W54A-K (lane 5). *Primers* YZ1-up/YZ1-down (lane 1,2); YZ2-up/YZ2-down (lane 3,4); Kan-up/Kan-down (lane 5,6)

155.3.3 PrA Activity of Mutant Strains

The PrA activity of host strain W303-K22 and three yeast transformants (WYCP, WYCP-EP and WYCP-54A) cultivated in wort medium were measured. As illustrated in Table 155.2, taking the PrA activity of host strain W303-K22 and yeast transformant WYCP as the references, the obvious PrA activity (5.128 ± 0.02 × 10-5 U/mg) of the yeast transformant WYCP-EP (expressing complete PrA) was detected. By contrast, no PrA signal was detected in the yeast transformant WYCP-54A (expressing mutant PrAΔpro). The results indicated that the active PrA cannot be synthesized when the prosequence of *PEP4* is deleted and the propeptide is required for formation of active mature PrA.

Also, the same conclusion was suggested by monitoring the PrA enzyme activities of *PEP4* prosequence deletion mutants. The intracellular and extracellular PrA activity of two mutant strains (W54A and W54A-K) and the parental strain (W303-1A) were measured in the same wort medium. As shown in Table 155.3, the intracellular and extracellular PrA activity of the parental strain W303-1A were 12.308 × 10^{-5} and 12.208 × 10^{-5} U/mL, respectively. However,

Table 155.2 PrA activity of host strain and different yeast transformants

Strains	PrA construct in vector	Intracellular PrA activity[a](× 10^{-5} U/mg)
W303-K22	–	0.104 ± 0.002
WYCP	None	0.324 ± 0.005
WYCP-EP	PrA	5.128 ± 0.022
WYCP-54A	PrA△pro	0.639 ± 0.003

[a] The PrA activity in 1 mg intracellular total proteins was defined as the intracellular PrA activity (U PrA activity/mg)

Table 155.3 The intracellular and extracellular PrA activities of mutant strains and the parental strain

Strains	Genotype	Extracellular PrA[a] activity ($\times 10^{-5}$ U/mL)	Intracellular PrA activity ($\times 10^{-5}$ U/mg)
W303-1A	*PEP4*	12.208 ± 0.434	12.308 ± 0.272
W54A	*pep4*-23△76::*KanMX*	0.716 ± 0.006	0.347 ± 0.005
W54A-K	*pep4*-23△76::*loxP*	0.102 ± 0.005	0.431 ± 0.004

[a] The PrA activity in 1 mL fermentation liquor was defined as the extracellular PrA activity (U PrA activity/mL)

no PrA activities were found in the mutant strains W54A and W54A-K. Taking into account the results described above, we can draw an obvious conclusion that deletion of the prosequence of *PEP4* can significantly decrease the PrA activity of *S. cerevisiae*.

155.3.4 Fermentation Characteristics

In order to investigate the impact of the prosequence deletion on the fermentation performance, CO_2 reduction, ethanol and residual sugar of mutant strains were measured after the primary beer fermentation. As is shown in Table 155.4, compared to the parental strain, the CO_2 reduction of mutant strains remained stable. In addition, there were no significant differences for ethanol and residual between recombinant strains and the parental strain. Therefore, we can deduce that the entire leavening ability was almost the same either before or after prosequence of *PEP4* deleted. However, the reasons for this phenomenon may be that PrA can control the glycolytic enzymes expression in the direct or indirect manner [13] and the mutant PrA△pro can still activate the other necessary vacuolar hydrolyases such as PrB, CPY [14], so as to lead to the delay of cell metabolism.

Table 155.4 CO_2 reduction, ethanol and residual sugar of mutant strains and the parental strain

Strains	CO_2 reduction (g)	Ethanol (% vol)	Residual sugar (g/L)
W303-1A	1.18 ± 0.02	0.8 ± 0.06	42 ± 0.6
W54A	1.15 ± 0.01	0.7 ± 0.06	43 ± 1.0
W54A-K	1.14 ± 0.02	0.7 ± 0.06	42 ± 0.6

155.4 Conclusion

In this study, two expression yeast strains WYCP-EP and WYCP-54A and two deletion mutant strains W54A and W54A-K were constructed, and the fermentation assay was performed to investigate the impact of lacking of the propeptide of PrA on its enzyme activity. Our data suggested that deletion of the propeptide of PrA could significantly decrease the PrA activity and the decline trend was not influenced by the presence of the *KanMX* gene. Moreover, there were no significant differences in the fermentation characteristics between mutant strains and the parental strain. Therefore, our results provided the theoretical basis for the construction of genetic engineering strain with low-proteinase A by the deletion of prosequence.

Acknowledgments This work was financially supported by the National Natural Science Foundation of China (No. 31271916) and the Cheung Kong Scholars and Innovative Research Team Program in University of Ministry of Education, China (Grant No. IRT1166).

References

1. Teichert U, Mechler B, Muller H (1989) Lysosomal (vacuolar) proteases of yeast are essential catalysts for portein degradation, differentitation, and cell survival. J Biol Chem 264:16037–16045
2. Parr CL, Keates RAB, Bryksa BC et al (2007) The structure and function of *Saccharomyces cerevisiae* proteinase A. Yeast 24:467–480
3. Kondo H, Shibano Y, Fukui N et al (1995) Development of a novel and sensitive method for measurement of proteinase A in beer. Oxford University Press, 669-676
4. van den Hazel HB, Kielland-Brandt MC, Winther JR (1992) Autoactivation of proteinase A initiates activation of yeast vacuolar zymogens. Eur J Biochem 207:277–283
5. van den Hazel HB, Kielland-Brandt MC, Winther JR (1993) The propeptide is required for in vivo formation of stable active yeast proteinase A and can function even when not covalently linked to the mature region. J Biol Chem 268:18002–18007
6. van den Hazel HB, Kielland-Brandt MC, Winther JR (1995) Random substitution of large parts of the propeptide of yeast proteinase A. J Biol Chem 270:8602–8609
7. Izawa S, Ikeda K, Takahashi N et al (2007) Improvement of tolerance to freeze–thaw stress of baker's yeast by cultivation with soy peptides. Appl Microbiol Biotechnol 75:533–537
8. Güldener U, Heck S, Fiedler T et al (1996) A new efficient gene disruption cassette for repeated use in budding yeast. Nucleic Acids Res 24:2519–2524
9. Iwaki T, Takegawa K (2004) A set of *loxP* marker cassettes for Cre-mediated multiple gene disruption in *Schizosaccharomyces pombe*. Biosci Biotechnol Biochem 68:545–550
10. Hao X, Xiao DG, Zhang CY et al (2010) Influence of nutrients on proteinase A activity in draft beer during fermentation. Int J Food Sci Technol 45:1169–1174
11. Kondo H, Yomo H, Furukubo S et al (1999) Advanced method for measuring proteinase A in beer and application to brewing. J Inst Brew 105:293–300
12. Bradford MM (1976) A rapid and sensitive method for the quantitation of microgram quantities of protein utilizing the principle of protein-dye binding. Anal Biochem 72:248–254

13. Qi-he C, Xiao-jie L, Ming-liang F et al (2010) Effect of PrA encoding gene-*PEP4* deletion in industrial *S. cerevisiae* WZ65 on key enzymes in relation to the glycolytic pathway. Eur Food Res Technol 231:943–950
14. Klionsky DJ, Banta LM, Emr SD (1988) Intracellular sorting and processing of a yeast vacuolar hydrolase: proteinase A propeptide contains vacuolar targeting information. Mol Cell Biol 8:2105–2116

Chapter 156
Corncob Residue Pretreatment for 2,3-Butanediol Production by Simultaneous Saccharification and Fermentation

Xiaopei Peng, Cuiying Zhang, Yujie Tian, Xuewu Guo, Yanwen Liu and Dongguang Xiao

Abstract In order to utilize corncob residue in the production of 2,3-butanediol, a pretreatment method was carried out. Sodium hydroxide method was chosen from six different types of pretreatment for lignocellulosic materials. After the composition analysis and fermentation experiment of the treated residue, the condition of pretreatment was suggested (hydroxide concentration of 1.5 %, processing temperature at 80 °C, processing time of 3 h, solid-to-liquid ratio of 1:8). Comparison between the primary material and the treated residue was conducted, the results proved that the output of 2,3-butanediol and acetoin (20.35 g/L) with the treated material was 3.38 times of the yield with the unpretreated corncob residue (6.02 g/L). After 72 h SSF, sugar yield of the cellulose was 75.40 %.

Keywords 2,3-Butanediol · Corncob residue · Lignocellulose · Pretreatment · Simultaneous saccharification and fermentation

156.1 Introduction

2,3-Butanediol (2,3-BD) is a kind of transparent, odorless, and tasteless liquid. As an important platform chemical of the petroleum substitution theorem [1], its derivatives have a wide range of potential applications in many fields [2–5]. Recently, the production of 2,3-BD by microbial fermentation received increasing attention because of its economical efficiency [6–8]. However, the caring of the concentration of product and the neglecting of the raw material cost by most of the

X. Peng · C. Zhang (✉) · Y. Tian · X. Guo · Y. Liu · D. Xiao
Key Laboratory of Industrial Fermentation Microbiology, Ministry of Education, Tianjin Industrial Microbiology Key Laboratory, College of Biotechnology, Tianjin University of Science and Technology, Tianjin 300457, People's Republic of China
e-mail: cyzhangcy@tust.edu.cn

T.-C. Zhang et al. (eds.), *Proceedings of the 2012 International Conference on Applied Biotechnology (ICAB 2012)*, Lecture Notes in Electrical Engineering 251,
DOI: 10.1007/978-3-642-37925-3_156,

studies may be harmful to the commercial process of 2,3-BD product by microbial fermentation.

As an abundant lignocellulosic by-product in the main agricultural countries, corncob has certain positive benefits such as renewability, large storage, environment-friendly, and low cost [9–11]. The unusually high content (35–40 %, w/w) of hemicelluloses in corncob justifies it as an attractive feedstock for pentose-based biotransformation aimed at production of xylitol, bulk chemicals [12], and bioethanol [13]. However, the waste residue rich in cellulose is discarded or furnace-burned in many cases, this is a great waste of natural resources, and this may damage the environment because of the chemical reagent which reacts with the corncob. Therefore, it is significant to utilize this valuable cellulosic residue in an economical and environmental-friendly way.

In order to utilize the corncob residue by microbial fermentation, the cellulosic should be hydrolyzed to glucose by direct acting of cellulose [14–16]. However, most of the cellulose was wrapped by lignin or the compact structures of the corncob. Thus, some effectual and low-cost pretreatment methods to remove the obstacle of the enzymolysis are necessary [17]. Although several types of pretreatment of various lignocellulosic materials have been proposed in order to alter the structure of the lignocellulose matrix by removing lignin, hemicelluloses, or combinations, there is no pretreatment method fit for treating each kind of lignocellulosic material. Therefore, an appropriate pretreatment method toward corncob residue is a vital area of research.

In this study, corncob residue was used in 2,3-BD production. The aim of this work is to select and optimize a pretreatment method of corncob residue which could increase the yield of the 2,3-BD simultaneous saccharification and fermentation (SSF).

156.2 Materials and Methods

156.2.1 Materials and Pretreatment

Corncob residue from Longlive Biotechnology Co., LTD in Shandong Province was used as the raw material. Particles (after washing to pH7.0) ranged from 0.25 to 0.38 mm (40–60 mesh) were used in the experiments. The residue consisted of cellulose (66.19 %), lignin (16.60 %), hemicelluloses (4.76 %), and others (12.45 %).

Experiments were conducted in 250 mL flasks containing 10 g corncob residues which were treated with six different types of methods at 80 °C and a ratio 1:10 of weight of residues to volume sodium hydroxide solution for 2 h; other conditions of the six different types of pretreatment are shown in Table 156.1.

Table 156.1 Conditions of six different types of pretreatment

No.	Methods	Compound	Mass concentration (%)	pH
1.	Sulfuric acid process	Sulfuric acid	2	–
2.	Hydrochloric acid process	Hydrochloric acid	2	–
3.	Sodium hydroxide method	Sodium hydroxide	2	–
4.	Hydrocarbonylation process	Hydrogen peroxide	2	11
5.	Organic solvents process	Ethanol	60	11
6.	Combined process	Hydrogen peroxide and ethanol	2 and 60	11

"–" means not control

156.2.2 Culture Media

Seed culture medium with natural pH contained 2 % (w/v) glucose, 0.5 % (w/v) yeast extract, 0.2 % (w/v) ammonium sulfate, 0.1 % (w/v) sodium citrate, and 0.04 % (w/v) magnesium sulfate.

The medium used in SSF contained 10 % (w/v) corncob residue, 2 % (w/v) monopotassium phosphate, 0.5 % (w/v) dipotassium hydrogen phosphate, 1.5 % (w/v) corn steep liquor, 0.2 % (w/v) ammonium sulfate, 0.04 % (w/v) magnesium sulfate, and pH 4.8.

All the media were autoclaved at 115 °C for 20 min.

156.2.3 Microorganism and Fermentation Experiments

Klebsiella pneumonia strain CICC 10011 was obtained from the China Center of Industrial Culture Collection.

The activated strain was inoculated in 50 mL seed medium at 200 rpm and 37 °C for 12 h. Subsequently, 10 % seed culture was inoculated in fermentation medium. Furthermore, 40 FPIU cellulase/g residue were added, and the simultaneous saccharification and fermentations (SSFs) were conducted in 250 mL flasks with 50 mL working volume. All SSF experiments were carried out at 35 °C and 150 rpm. The resultant culture broth was withdrawn at a predetermined time of 36 h. Each experiment was conducted for 3 times.

156.2.4 Analytical Methods

The cellulose, hemicellulose, and lignin contents of corncob residue were analyzed by the methods described by Goering HK and Van Soest [18].

The liquid samples were analyzed by HPLC, equipped with RI detectors. 2,3-BD, and acetoin were analyzed using the refractive index detector and Aminex HPX-87H column at 65 °C with 5 mM H_2SO_4 as the mobile phase at 0.8 mL min^{-1} [19].

156.3 Results and Discussion

156.3.1 Method Selection

156.3.1.1 Effect of Different Types of Pretreatment

Six types of pretreatment (sulfuric acid process, hydrochloric acid process, sodium hydroxide method, hydrocarbonylation process, organic solvents process, and combined process of hydrocarbonylation and organic solvents) were conducted in the processing of the corncob residue for three times. The compositions of the materials after treatment were shown in Fig. 156.1. It was found that method 3 (sodium hydroxide method) resulted in lower lignin content (3.5 %) and higher amount of lignin removed (87.69 %) as compared to the other pretreatment compositions. It was observed that lignocelluloses became less compact after alkaline pretreatment due to the removal of lignin and the swell of cellulose [20]. Furthermore, it was noted that relaxing the structure enhanced enzymolysis. Thus, sodium hydroxide method was chosen from these six types of pretreatment.

156.3.1.2 Fermentation Experiment of Treated Samples

Due to the inhibition of cellulase in hydrolysis (the glucose would inhibit the action of cellulase), enzymolysis cannot demonstrate the real situation of SSF of 2,3-BD.Therefore, shake-flask fermentation experiments were conducted in order to prove the validity of the above selection. The residues, with equal weight cellulose, were inoculated in the medium for SSF. The result of SSF was shown in

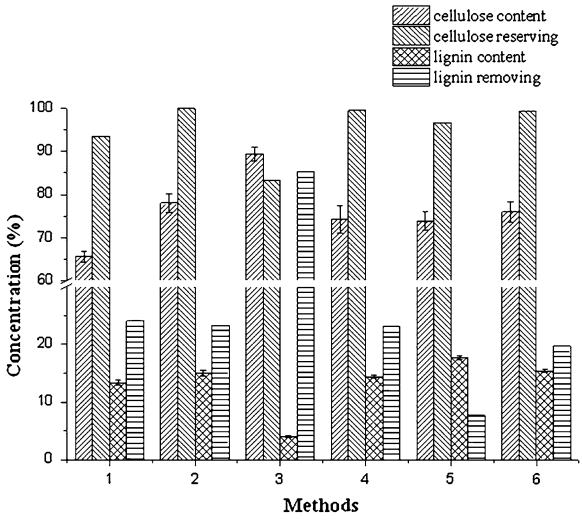

Fig. 156.1 Compositions of the treated materials

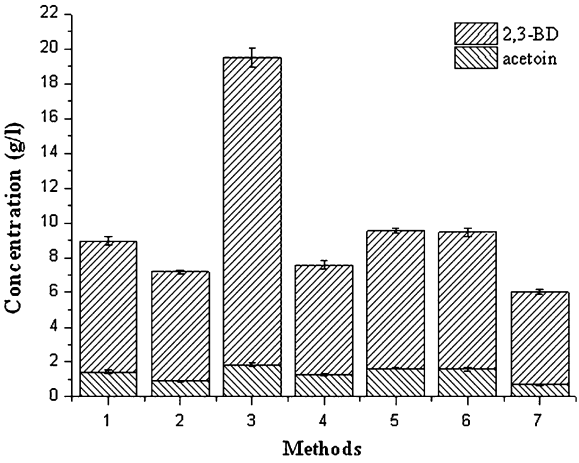

Fig. 156.2 Results of SSFs with residues treated with different methods. *1* sulfuric acid process, *2* hydrochloric acid process, *3* sodium hydroxide method, *4* hydrocarbonylation process, *5* organic solvents process, *6* combined process, *7* untreated

Fig. 156.2. It was clearly demonstrated that the output (19.468 g/L) of 2,3-BD and acetoin with alkali-treated residue was the greatest among the tested types. Thus, sodium hydroxide method was selected in the SSF of 2,3-BD.

156.3.2 Single Factor Experiments of Sodium Hydroxide Method

156.3.2.1 Effect of Sodium Hydroxide Concentration

The results generated by different sodium hydroxide concentrations are shown in Table 156.2. It was noted that with the increase in concentration of sodium hydroxide, there is a considerable decrease in lignin content and a dramatic increase in cellulose content. The decrease of lignin content does not continue significantly after concentration of alkali greater than 1.5 %.

156.3.2.2 Effect of Processing Temperature

Table 156.3 presents the effect of the processing temperature in sodium hydroxide pretreatment on cellulose and lignin. The results revealed that temperature had a

Table 156.2 Effect of sodium hydroxide concentration

Sodium hydroxide concentration (%)	Cellulose content (%)	Cellulose retention (%)	Lignin content (%)
0.5	79.75 ± 0.25	87.17	9.5 ± 0.2
1	85.05 ± 0.41	84.94	4.9 ± 0.1
1.5	87.74 ± 0.21	83.85	3.8 ± 0.1
2	89.69 ± 0.26	83.45	3.5 ± 0.1

Table 156.3 Effect of processing temperature

Processing temperature (°C)	Cellulose content (%)	Cellulose retention (%)	Lignin content (%)
40	81.54 ± 0.21	87.35	8.1 ± 0.2
60	84.1 ± 0.31	86.26	6.3 ± 0.2
80	87.74 ± 0.29	83.85	3.8 ± 0.1
100	84.15 ± 0.36	77.15	3.5 ± 0.1

great influence on alkali pretreatment. With the increase of temperature, the content of lignin decreased, but the incremental decreases markedly reduced at temperatures above 80 °C. In addition, the cellulose retention also reduced with increasing temperature. What was interesting was the fact at temperatures above 80 °C, the rate of cellulose retention dramatically decreased. This decrease resulted in the reduction of cellulose content (87.74 % at 80 °C and 84.15 % at 100 °C, the tendency of cellulose content was raised below 80 °C), which may be due to a faster decomposition of cellulose at high temperatures.

156.3.2.3 Effect of Processing Time

It is known that processing time is one of the important parameters in the pretreatment of lignocellulose. In this experiment, effect of processing time was studied. As the results shown in Table 156.4, the lignin content decreased to 3.7 % in 3 h, but the decrease was not obvious with longer processing time. In addition, the cellulose retention reduced continuously during the first 4 h, with the cellulose increasing only gradually in the first 2 h.

156.3.3 Orthogonal Optimization of Sodium Hydroxide Method

156.3.3.1 Design of the Orthogonal Test

After the single factor experiments of sodium hydroxide method, an orthogonal test for optimizing the alkali pretreatment was designed. The parameters studied in the single factor experiments (hydroxide concentration, processing temperature,

Table 156.4 Effect of processing time

Processing time (h)	Cellulose content (%)	Cellulose retention (%)	Lignin content (%)
1.	85.74 ± 0.42	85.45	4.7 ± 0.2
2.	87.74 ± 0.57	83.85	3.9 ± 0.1
3.	88.08 ± 0.13	83.24	3.7 ± 0.2
4.	88.21 ± 0.42	82.63	3.6 ± 0.1
5.	88.41 ± 0.28	82.57	3.6 ± 0.1

Table 156.5 Orthogonal experimental design of the pretreatment

No.	Sodium hydroxide concentration (%)	Processing temperature (°C)	Processing time (h)	Solid-to-liquid ratio (w/v)
1.	1	60	1	1:8
2.	1	80	2	1:10
3.	1	100	3	1:12
4.	1.5	60	2	1:12
5.	1.5	80	3	1:8
6.	1.5	100	1	1:10
7.	2	60	3	1:10
8.	2	80	1	1:12
9.	2	100	2	1:8

and processing time) were used as the factors of the orthogonal test. Furthermore, based on the influence on the dosage of the sodium hydroxide used in the pretreatment, solid-to-liquid ratio was also considered as an orthogonal factor. Therefore, an orthogonal test of 4 factors and 3 levels was designed (Table 156.5).

156.3.3.2 Results of the Orthogonal Test

With the orthogonal table, the test was conducted. Further investigations of the composition and the nature of fermentation were studied by composition analysis and SSF. The results are shown in Table 156.6. However, it is known that there was only one type of result that could be used in the analysis of orthogonal tests and thus how to analyze the results of the tests became a puzzle.

156.3.3.3 Analysis of the Results

A function E (shown in (1)) has been built for analyzing the results. With the function, the illustrative table (Table 156.7) was reached by orthogonal analysis. Thus 80 °C and 1:8 were chosen as the temperature and solid-to-liquid ratio for

Table 156.6 Results of the orthogonal test

No.	Cellulose content (%)	Cellulose retention (%)	Lignin content (%)	Concentration of product (g/l)
1.	87.13 ± 0.34	94.07	8.34 ± 0.1	15.347 ± 0.243
2.	88.01 ± 0.23	89.22	5.6 ± 0.1	18.769 ± 0.152
3.	88.67 ± 0.28	84.67	3.95 ± 0.1	20.071 ± 0.353
4.	88.32 ± 0.38	89.32	5.5 ± 0.2	18.869 ± 0.159
5.	85.92 ± 0.19	87	3.35 ± 0.1	20.334 ± 0.094
6.	83.63 ± 0.23	80.37	4.15 ± 0.2	19.956 ± 0.153
7.	85.65 ± 0.38	85.16	4.85 ± 0.1	19.455 ± 0.325
8.	87.19 ± 0.41	82.13	4.1 ± 0.1	19.985 ± 0.231
9.	80.57 ± 0.51	79.5	3.2 ± 0.1	20.379 ± 0.184

Table 156.7 Illustrative table of the orthogonal test

No.	Sodium hydroxide concentration (%)	Processing temperature (°C)	Processing time	Solid-to-liquid ratio (w/v)	E
1.	1	60	1 h	1:8	109.67
2.	1	80	2 h	1:10	125.94
3.	1	100	3 h	1:12	126.85
4.	1.5	60	2 h	1:12	126.31
5.	1.5	80	3 h	1:8	136.28
6.	1.5	100	1 h	1:10	126.94
7.	2	60	3 h	1:10	128.04
8.	2	80	1 h	1:12	124.61
9.	2	100	2 h	1:8	133.10
E.V.1*	120.820	121.340	120.407	126.350	–
E.V.2*	129.843	128.943	128.450	126.973	–
E.V.3*	128.583	128.963	130.390	125.923	–
E.D.#	9.023	7.623	9.983	1.050	–

E.V. * equalizing value; *E.D.* # extreme difference

economizing cost. 1.5 % was chosen easily as the sodium hydroxide concentration. Longer processing time resulted in a better impact, and 3 h was considered as the best processing time.

$$E = \frac{\mathrm{C} \times 50 \times \mathrm{Rc} \times 66.19\ \%}{5 \times \mathrm{Cc}} \tag{1}$$

E means the sum weight (g) of 2,3-BD and acetoin produced by SSF with the samples that were pretreated from unit mass (kg) of the untreated corncob residue. **C** stands for the concentration of the product in the zymotic fluid, **Rc** stands for the cellulose retention of the materials, **Cc** stands for the cellulose content of the stuff, **50** is the volume of the zymotic in each flask, **5** is the weight of treated or untreated corncob residues, **66.19** % is the cellulose content of the untreated raw stuff.

156.3.3.4 Result of the Pretreatment and SSF Experiment

The corncob residue after the optimized pretreatment was observed under a scanning electron microscope (enlargement ratio was 10,000 times). It is found that the change was large: the treated residue (Fig. 156.3a) had looser structure than the untreated one (Fig. 156.3b), and the cellulose was exposed from the embedding of the lignin after treatment. In order to prove the effect of these changes, a SSFs comparison between primary materials and pretreated residue was conducted. With the result shown in Fig. 156.4, it is proved that the output of 2,3-BD and acetoin (the precursor of 2,3-butanediol) (20.35 g/L) with the treated material was 3.38 times as the yield of the unpretreated corncob residue (6.02 g/L). This reflected that the pretreatment was remarkably useful to rise the hydrolysis speed and increase the output of 2,3-BD.

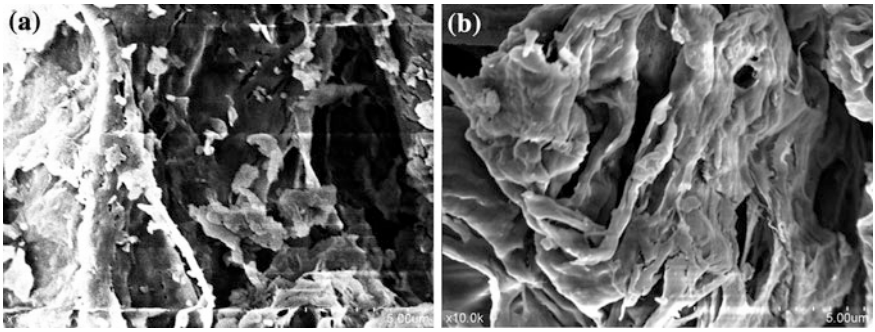

Fig. 156.3 Structures of the treated and untreated corncob residues (**a** is treated and **b** is untreated)

Fig. 156.4 Comparison between treated and untreated stuff

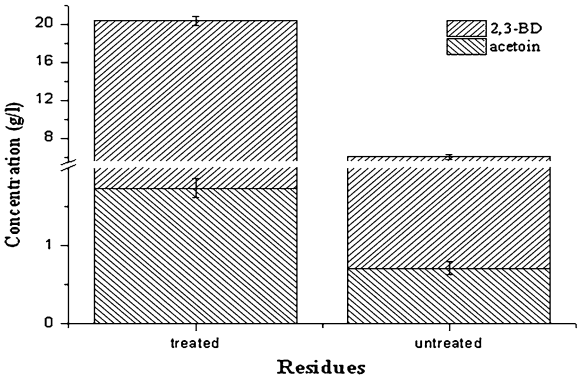

Aimed to find out the final production and the sugar yield, time course of SSF with treated materials was conducted (Fig. 156.5), the maximum yield (26.01 g/L) was got at 72 h, sugar yield of cellulose at this time was 75.40 %.

Fig. 156.5 Time course of SSFs with treated residue

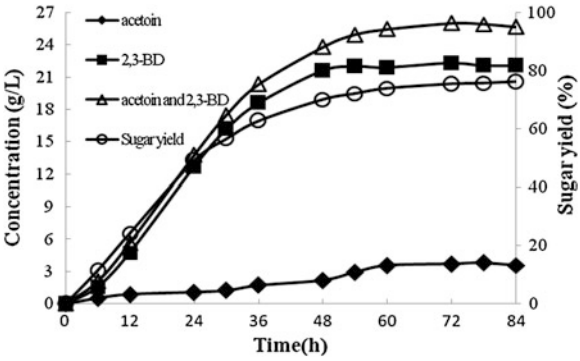

156.4 Conclusion

In conclusion, corncob residue is a feasible type of lignocelluloses for the production of 2,3-BD. Using the treated corncob residue by optimal sodium hydroxide method, 20.35 g/L 2,3-BD and acetoin were produced in 36 h with SSF, which is 3.38 times as the yield of raw stuff (6.02 g/L). The maximum yield (26.001 g/L) was got at 72 h, by this the sugar yield of cellulose was 75.40 %.

Acknowledgments This work was supported by program for the planning subject of "the twelfth five-year-plan" in National Science and Technology for the Rural Development in China (Grant No. 2012AA101805) and Science Foundation of Tianjin University of Science and Technology (Grant No. 20090401).

References

1. Syu MJ (2001) Biological production of 2,3-butanediol. Appl Microbiol Biotechnol 55:10–18
2. Palsson BO, Fathi-Afshar S, Rudd DF (1981) Biomass as a source of shemical feedstock: an economic evaluation. Science 213:513–517
3. Emerson RR, Flickinger MC, Tsao GT (1982) Kinetics of dehydration of aqueous 2,3-butanediol to methyl ethyl ketone. Ind Eng Chem Prod Res Dev 21:473–477
4. Garg SK, Jain A (1995) Fermentative production of 2,3-buanediol: a review. Bioresource Technol 2:103–109
5. Alam S, Capit F, Weigands WA et al (1990) Kinetics of 2,3-butanediol fermentation by *Bacillus amyloliquefaciens*: effect of initial substrate concentration and aeration. J Chem Technol Biot 47:71–84
6. Celińska E, Grajek W (2009) Biotechnological production of 2,3-butanediol-current state and prospects. Biotechnol Adv 27:715–725
7. Ji XJ, Huang H, Du J et al (2009) Development of an industrial medium for economical 2,3-butanediol production through co-fermentation of glucose and xylose by *Klebsiella oxytoca*. Bioresource Technol 100:5214–5218
8. Ji XJ, Huang H, Du J et al (2009) Enhanced 2,3-butanediol production by *Klebsiella oxytoca* using a two-stage agitation speed control strategy. Bioresource Technol 100:3410–3414
9. Kumar R, Singh S, Singh OV (2008) Bioconversion of lignocellulosic biomass: biochemical and molecular perspectives. J Ind Microbiol Biotechnol 35:377–391
10. Limayem A, Ricke SC (2012) Lignocellulosic biomass for bioethanol production: current perspectives, potential issues and future prospects. Prog Energy Combust 38:1–19
11. Mabee WE, McFarlane PN, Saddler JN (2011) Biomass availability for lignocellulosic ethanol production. Biomass Bioenergy 35:4519–4529
12. Hermann BG, Blok K, Patel MK (2007) Producing bio-based bulk chemicals using industrial biotechnology saves energy and combats climate change. Environ Sci Technol 41:7915–7921
13. Wyman CE (2007) What is (and is not) vital to advancing cellulosic ethanol. Trends Biotechnol 25:153–157
14. Prasad S, Singh A, Joshi HC (2007) Ethanol as an alternative fuel from agricultural, industrial and urban residues. Resour Conserv Recycl 50:1–39
15. Sun Y, Cheng J (2002) Hydrolysis of lignocellulosic materials for ethanol production: a review. Bioresource Technol 83:1–11
16. Cao Y, Tan H (2002) Effects of cellulose on the modification of cellulose. Carbohydr Res 337:1291–1296

17. Wyman CE (1999) Biomass ethanol: technical progress, opportunities, and commercial challenges. Annu Rev Energy Env 24:189–226
18. Goering HK, Van Soest PJ (1970) Forage fibre analysis. Agricultural Research Services, United States Department of Agriculture
19. Cheng KK, Liu Q, Zhang J et al (2010) Improved 2,3-butanediol production from corncob acid hydrolysate by fed-batch fermentation using *Klebsiella oxytoca*. Process Biochem 45:613–616
20. Cheng KK, Zhang J, Ping W et al (2008) Sugarcane bagasse mild alkaline/oxidative pretreatment for ethanol production by alkaline recycle process. Appl Biochem Biotechnol 151:43–50

Chapter 157
The Comparison on the Genotype of *idh-1* Between *Paralichthys olivaceus* and *Scophthalmus maximus*

Zhiyi Qiao, Shi Dong, Jinhui Sun, Yue Pei and Qi Wang

Abstract *Paralichthys olivaceus* and *Scophthalmus maximus* were two economic mariculture species in China. To study the relativity between the genotype of *idh-1* and the growth indices, 141 *Paralichthys olivaceus* from the culture stocks in Rongcheng and Yantai in Shandong province, Beidaihe in Hebei province and 60 *Scophthalmus maximus* from Hangu of Tianjin were investigated by the isozyme electrophoresis and specific dying and their biological indices. The results showed that the idh-loci of both species were polymorphic, but the genotype was quite different: there were three genotypes of *Paralichthys olivaceus* (AA, BB and AB, identical with the dimer of IDH); thus there were two genotypes of *Scophthalmus maximus* (A1, A2) with 53 and 7 individuals, respectively. By the statistical analysis of gene frequency, *Paralichthys olivaceus* showed the heterozygote surplus and genetic bias in Hardy–Weinberg equilibrium. The chi-test explained that only the loci of *idh-1* in Rongcheng expressed the significant bias in Hardy–Weinberg equilibrium, there were significant difference between the observational values of heterozygosity ($\overline{\text{Ho}}$) and Hardy–Weinberg expected heterozygosity ($\overline{\text{He}}$) ($P < 0.05$). From the relationship between locus and growth triats, we found that the heterozygote(AB) of *idh-1* have the growth dominance in comparison with homozygote (AA or BB). In the data of two groups of *Scophthalmus maximus*, the average value of the weight, length, and body height of the A2-individuals were all higher than those of A1. Compared to A1-individuals, the weight (group1)\height (group1 and 2) of A2-individuals have a significant difference($P < 0.01$). This result has provided reference for the molecular marker-assisted breeding of *Paralichthys olivaceus* and *Scophthalmus maximus*.

Z. Qiao · J. Sun · Y. Pei · Q. Wang
Tianjin Key Lab of AQUA-Ecology and Aquaculture, Tianjin Agricultural University, Tianjin 300384, People's Republic of China

S. Dong (✉)
College of Life Science, Tianjin Normal University, Tianjin 300387, People's Republic of China
e-mail: smkxxyds@mail.tjnu.edu.cn

T.-C. Zhang et al. (eds.), *Proceedings of the 2012 International Conference on Applied Biotechnology (ICAB 2012)*, Lecture Notes in Electrical Engineering 251,
DOI: 10.1007/978-3-642-37925-3_157,

Keywords *Paralichthys olivaceus* · *Scophthalmus maximus* · Idh-1 · Growth trait

157.1 Introduction

Japanese flounder, *Paralichthys olivaceus*, is widely distributed along the coast of Northeast Asia and is one of the most economically important marine species in the region. *P. olivaceus* is successfully cultured in Japan, China, and Korea. Like other aquaculture species, Japanese flounder is susceptible to several viruses, bacteria, and protozoan pathogens, and may also show pigmentation abnormalities, which decrease its market price [1]. Some economically important traits like disease resistance and growth are significantly associated with the genotype of *idh-1* [2–4].

Turbot, *Scophthalmus maximus*, is also a commercially important aquaculture species in China with 10-years' introduction from Britain. In recent years, infectious pathogens of the turbot have emerged. In particular, the bacterium Streptococcus iniae is responsible for major losses in many countries [5]. There is the relationship between the genotype of *idh-1* and growth trait [6].

IDH (E.C.1.1.1.42), which can catalyze the oxidation of isocitric acid to α-ketoglutaric acid in TCA cycle, is an important oxidoreductase in energy metabolism. The biocatalytic activities of IDH have an impact on the health and growth of fish directly or indirectly, and then influence the proportion of the gene phenotype in population. While Siyang [3] has found heterozygote surplus of 23 release groups of *Paralichthys olivaceus* in Japan, showing the selection advantage of heterozygote. Meanwhile, Feng [7] also found the significance bias in Hardy–Weinberg equilibrium in the analysis of the *idh-1* loci of the cultured stock of Japanese flounder, which shows the heterozygosis deletion. In the research of the *idh-1* of *Scophthalmus maximus*, we found the genetic deviation also [6]. This suggests that there may be an internal relationship between the genotype of *idh-1* and the health and the growth of flatfish.

In this paper, horizontal starch gel electrophoresis and specific dying of *idh-1* were employed to identify the gene phenotype of three groups of 141 *Paralichthys olivaceus* and two groups of *Scophthalmus maximus*, so as to find the molecular genetic marker of Bothidae by the comparison of their expressing features of *idh-1*.

157.2 Materials and Methods

Paralichthys olivaceus comes from three groups: 47 samples of the Rongcheng groups (280 days, the offspring of 27 wild parents from yellow sea) whose average weight is 26.66 ± 11.81; 41 samples of Beidaihe groups (70 days, the offspring of 200 wild parents from Bohai sea) whose average weight is 2.31 ± 0.91, and 40

Table 157.1 The dyeing reagent of IDH

Reagent	NADP (0.5 %)	PMS (1 %)	NBT (1 %)	Na3isocitrate (3 %)	Tris–HCl buffer (0.2 M pH 8.0)	D.W.
Dosage	9 mg	1.5 mg	3 mg	9 mg	15 ml	12 ml

samples of Yantai groups (110 days, the offspring of 120 wild parents from yellowi sea) whose average weight is 26.66 ± 11.8. The parents' sex ratio of three groups is about 2:1.

Sixty *Scophthalmus maximus* were randomly selected in different growth period of breeding stock, 30 individuals per group with the average weight of 10.61 ± 5.82 g (116 days) and 12.6 ± 28.20 g (165 days), respectively.

After the morphometry of every samples, they were put in the marked plastic bag and preserved at −20 °C. Separated the livers of the cryopreserved samples, then put on the dry agglutination plate, and covered with the filter paper of 5 × 5 mm.

The *idh-1* genotypes were determined by horizontal starch gel electrophoresis [8] and specificity dyeing technology. The gel of 11 % starch was prepared before one day and overnight at 4 °C.

Insert the filter papers which has absorbed the melting liquid into the gel on the second day, carry out the electrophoresis at 4 °Cin refrigerator (C-T, pH = 8.0 buffer), keep the constant current at 4 mA/cm^2 for about 4 h. Then cut the gel into slices with the thickness of 1 mm [8], dyeing and chromogenesis at 37 °C in dark, the formulation of dye solution is shown in Table 157.1. Then terminate reaction and decolorization by 0.7 % acetic acid. Finally, determine the genotype of *idh-1* and analyze the data by SPSS13.0.

157.3 Results

157.3.1 The Expression Character of idh-1

IDH is a dimer which is coded by two gene loci, *idh-1* and *idh-2*. Though their mobility is close, the tissue specificity and the enzyme activity are quite different. In two species, the *idh-1* activity of liver is the strongest and expressing polymorphism; while the *idh-2* express better in muscle and heart, expressing monomorphism (Fig. 157.1).

There are two alleles of *idh-1* in *P. olivaceus*: *a and *b, appears three genotypes: AA, AB, and BB (Fig. 157.2). In the *idh-1* detection of the *Scophthalmus maximus* of two period, we have gained clear pattern of phenotype of isozyme (Fig. 157.2): The phenotype is distinguished into two types: A1 and A2, the electrophoretic mobility of A2 is greater than A1. By the statistical analysis of the *idh-1* genotype of 60 *Scophthalmus maximus* samples, we find both phenotype

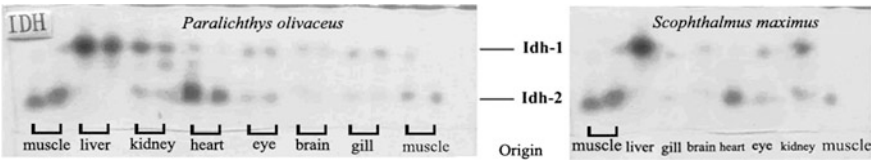

Fig. 157.1 The elcctrophoresis pattern of IDH in seven tissues of *P. olivaceus* and *Scophthalmus maximus*

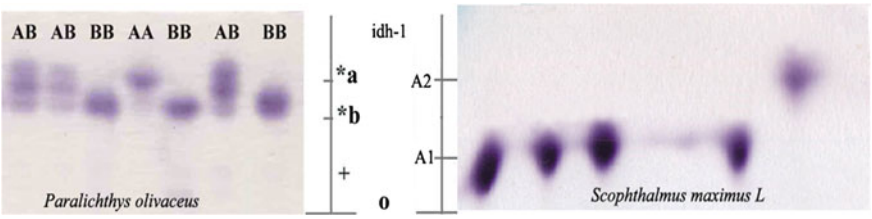

Fig. 157.2 The expression of the polymorphic of *Idh-1* in liver of *P. olivaceus* and *Scophthalmus maximus*

Table 157.2 The gene frequencies and other genetic indices of *P. olivaceus*

Indices	Groups		
	Rongcheng	Beidaihe	Yantai
Frequency of a	0.2449	0.3942	0.2750
Frequency of b	0.7551	0.6058	0.7250
Ho	0.490	0.558	0.450
He	0.370	0.478	0.399
d	0.324	0.168	0.129
Ne	72.5	62.5	45.9

Ho observed value of the heterozygosity of polymorphic loci
He expected value of the heterozygosity of polymorphic loci
d deviation indexes from Hardy–Weinberg equilibrum
Ne effective population size

appear in two groups (Table 157.2). The occurrence frequency of A1 is higher with 88.33 %, No heterozygous with three bands were observed.

157.3.2 The Character of the Genotype of idh-1

Table 157.2 shows that, the deviation indices from Hardy–Weinberg equilibrum (*d* value) of polymorphic locus of three groups of *P. olivaceus* are positive, i.e., there is the bias of Hardy–Weinberg equilibrium more or less, and is heterozygote

surplus. The number of effective population size (Ne) of population which is calculated from d value can reflect the degree of the deviation from Hardy–Weinberg equilibrum more clearly. When Ne value is higher than the sample number, means heterozygote surplus and heterozygosis deletion on the contrary. In our research, Rongcheng groups of *P. olivaceus* has a high degree of the heterozygote surplus of *idh-1* with the d value is 0.3240. Actually the Hardy–Weinberg equilibrum is a dynamic balance, the deviation within permitted is regard as coincidence.

The chi-test suggest that only the probability of the *P. olivaceus* of Rongcheng is significant difference ($0.01 < P < 0.05$) that fall short of Hardy–Weinberg equilibrum.

In the study of *Scophthalmus maximus*, we obtain two genotypes of homozygote, A1 and A2. The electrophoretic mobility of A2 is greater than A1. since isocitrate dehydrogenase (IDH) is dimer, every locus is controlled by a pair of alleles, there are three phenotype in general: the homozygous of allele A (AA); the homozygous of allele B (BB), and the heterozygous (AB). But the performance of *Scophthalmus maximus* is unusual, there must be a unique mechanism of the activity generation and the genetic patterns of IDH compared to *P. olivaceus*. The reason maybe that the dimer has no activity which consist of subunit-A and subunit-B, or the individual cannot hatch to survive who carries the AB gene, or there is other reasons hiding waiting for find.

157.3.3 The Relationship Between the Phenotype of idh-1 and Growth Indices

We have compared the weight of *P. olivaceus* to the different phenotypes (Table 157.3). Individuals of AB have the significant growth advantage than that of homozygous (BB) ($P < 0.05$). In addition, the growth advantage of heterozygous is displayed gradually by the growth of the fish.

From the results shown in Table 157.3, among two groups of *Scophthalmus maximus*, the average weight of the individuals with genotype A2 is higher than that of with genotype A1. Analyzing the data by SPSS 16.0, we find the *Scophthalmus maximus* with A2 has an obvious advantage than others (extremely significant difference, $P < 0.01$).

157.4 Discussion

To the *P. olivaceus*, Feng [7] also found the diversity of the IDH in liver of wild populations, but no heterozygote surplus. From Table 157.4, we can conclude that except Yantai groups, the Ho of the groups in this paper are higher than the wild

Table 157.3 The comparison of weight to the genotype of *idh-1* of two speices

Groups days	Genotypes	Individual number	Weight (g)
Rongcheng 280	AA	0	–
	BB	25	195.62 ± 65.23
	AB	24	217.46 ± 50.47
	Total	49	199.82 ± 65.97
Beidaihe 110	AA	6	2.63 ± 0.51
	BB	17	2.44 ± 0.88
	AB	29	2.40 ± 0.84
	Total	52	2.44 ± 0.81
Yantai 70	AA	2	24.40 ± 11.17
	BB	20	26.46 ± 13.09
	AB	18	27.12 ± 10.97
	Total	40	26.66 ± 11.81
Jia group	A1	27	10.18 ± 2.37
	A2	3	14.33 ± 1.15
Yi group	A1	26	12.15 ± 1.59
	A2	4	16.25 ± 0.55

Table 157.4 The comparison of heterozygote of the *idh-1* in 3 populations of *P. olivaceus*

	Youfeng Z[a]	Youfeng Y[b]	Rongcheng	Beidaihe	Yantai
Ho	0.4531	0.3461	0.4898	0.5577	0.4500
He	0.4998	0.4992	0.3700	0.4775	0.3988
d	−0.0934[c]	−0.3067[c]	0.3240	0.1679	0.1285

[a] *Z* the natural population in Feng [9]
[b] *Y* the wild population in Feng [9]
[c] calculated from the data of Feng [9]

groups of Feng [9]. But the data of He is just the opposite. The values of Feng [9] are all higher than that in our experiment. The *d* values of Feng [9]'s research are negative, which means heterozygous deficiency, while our conclusions is heterozygous surplus.

In Siyang [3]'s research, there were 19 groups that appear to be heterozygous surplus among the phenotype of *idh-1* of 23 groups of breeding *P. olivaceus* in Japan, that show the selective advantage of heterozygous. Suppose that the mortality of this 19 groups with heterozygous surplus is zero, namely the survival rate of heterozygous (AB) is 100 %, then the survival rate of homozygous of AA and BB are 69.2 and 75.2 %, respectively. In the aspects of body length, the values of 15 groups of heterozygous (AB) are higher than that of homozygous (BB), which reflect the correlation between survival rate/growing and the genotype of *idh-1*of the breeding groups.

Paralichthy solivaceus and *Scophthalmus maximus* both belong to Bothidae, but natural distribution in different area. Some reseachers has made great effort on the hybridization of this two speices to improve germplasm [11–13]. In our results,

there is great difference on the expression of IDH, it is mainly due to the genetic polymorphism. *Paralichthy solivaceus* is wild resources with higher genetic diversity, while *Scophthalmus maximus* is a introduction species with a serious degeneration by breeding in China [10]. This would provide reference to the breeding of Bothidae in the future.

References

1. Seikai T (2002) Flounder culture and its challenges in Asia. Rev Fish Sci 10:421–432
2. Siyang L, Ikeda M, Fojio Y (1997) Genetic features of natural and cultured populations in place (*Paralichthys olivaceus*). Tohoku J Agric Res 47(3–4):85–96
3. Siyang L, Ikeda M,Fujio Y (2000) Selective advantage of heterozygotes at the liver isocitrate dehydrogenase locus in the place. J Wuhan University (Nat Sci Ed) 46(4):495–499
4. Zhiyi Q, Shi D, Jinhui S, et al (2009) The research on the correlation between the genotype of *idh-1* and the lysozyme activity of *Paralichthys olivaceus*. J Tianjin Norm Univ (Nat Sci Ed) 1:35–38
5. Kitao T (1993) Streptococcal infections. In: Inglis V, Roberts, RJ, Bromage NR (eds) Bacterial diseases in fish. Blackwell, Oxford
6. Zhiyi Q, Shi D, Jinhui S et al (2012) Study on the genotype of *idh-1* and the correlation between its phenotype and biological characteristics of *Scophthalmus maximus* L.J. Anhui Agric Sci 2:127–130
7. Feng Y, Keling W, Jianhai X et al (1999) Biochemical genetic analysis of isozymes on the left-eyed flounder, *Paralichthys olivaceus* in the coastal waters of Shandong. Oceanologiaet Limnologia Sinica 30(2):127–133
8. Zhongren W (1996) Plant allozyme analysis. Sci Press, Beijing
9. Feng Y (2001) A preliminary study on the diversity of *Paralichthys olivaceus* populations and molecular phylogeny of Pleuronectiformes, Chin Academy Sci. Institute of Oceanology, DDDA
10. Shuming Z, Sifa L, Wanqi C (2000) Molecular genetic markers and variations of cultured *Paralichthys olivaceus* and *Scophthalmus maximus*. J Fishery Sci Chin 4:12–15
11. Dongdong X, Feng Y, Bao L et al (2010) Analysis of correlation between pairwise genetic distance of eight flatfishes and hybrid fitness. J Fisheries Chin 2:78–90
12. Aijun M (2011) The family selection of genetic manipulation and the nonlinear selection of flounder fish. In: Fisheries Soci academic annual meeting in 2011
13. Xinan W, Aijun M (2010) Progress of genetic improvement of flatfish. Marine Sci 07:12–15

Chapter 158
Production of Natural Chitosan from Xylose by *Actinomucor elegans* Culture

Xi Wang, Hua Zhao, Xin Feng and Jing Yang

Abstract The production of natural chitosan from xylose by *Actinomucor elegans* culture was investigated. The proportion of two main medium components (corn steep liquor and xylose) was optimized by response surface methodology. The optimal medium components were corn steep liquor 73.0 g/L, xylose 32.0 g/L, KH_2PO_4 2.0 g/L, $MgSO_4$ 2.0 g/L. Under the optimal conditions, the cultivation of *Actinomucor elegans* was carried out in a 250 mL flask containing 50 mL of medium which the initial pH value was 7.0 at 30 °C on a rotary shaker at 200 r/min, and the inoculum concentration was 6 %. The yield of chitosan reached 1.42 g/L after 48 h.

Keywords *Actinomucor elegans* · Chitosan · Cultivation · Xylose

158.1 Introduction

Chitosan is a linear hydrophilic polysaccharide of β-1, 4-glucosamine [1], and it is the only one natural alkaline polysaccharide discovered in the world until now [2]. It has the unique properties and physiological function, for example permeability, fiberizability, hygroscopicity, increasing viscosity, film property, adsorbability, antibiotic property, biocompatibility, moisture retention [3]. Due to its unique properties, chitosan has many practical applications especially in the agriculture, cosmetics, food, and pharmaceutical industries [4]. The traditional way for producing chitosan is extracting from shell waste of shrimp and crab [5]. During the process, the environmental pollution is increased and instability physico-chemical properties caused by using large amount of concentrated alkaline [6, 7].

X. Wang · H. Zhao (✉) · X. Feng · J. Yang
Key Laboratory of Industrial Microbiology, Ministry of Education,
College of Bioengineering, Tianjin University of Science and Technology,
Tianjin 300457, People's Republic of China
e-mail: zhaohua@tust.edu.cn

T.-C. Zhang et al. (eds.), *Proceedings of the 2012 International Conference on Applied Biotechnology (ICAB 2012)*, Lecture Notes in Electrical Engineering 251,
DOI: 10.1007/978-3-642-37925-3_158,

Chitosan is also an important component of the cell wall of certain fungi, particularly of those belonging to the class of Zygomycetes [8]. Thus huge amount of chitosan can be produced from fungal cell wall using fermentation technology, which could become the new alternatives in the current world.

Xylose takes the second position of most abundant carbohydrate polymer in nature world, following by the glucose, and it can reach 30 % of hydrolysate from lignocellulose [9]. It is one of the major components of lignocellulose [10] and it also can be the residual sugar from lignocellulose after production of ethanol. The process of transferring fuel in high yield from lignin and hemicellulose is a huge challenge in the current world's technology [11]. Xylose can be used to produce ethanol through the fermentation of some genetically engineered microorganism [12–16], but the result of this process was not very obvious. Thus, there will be a long way for it to be applicable in industry [12].

A large amount of microorganisms in nature are able to utilize xylose, including bacterium, fungus, and yeast [17]. Many of them are able to convert xylose to other products [18–21]. This essay aims to examine the potential of using xylose to produce chitosan by *Actinomucor elegans* fermentation. Moreover, it also provides a new idea for producing chitosan from lignocellulose.

158.2 Materials and Methods

158.2.1 Material

158.2.1.1 Microorganism

Actinomucor elegans TCCC45001 obtained from Culture Collection Tianjin University of Science and Technology was used in this study.

158.2.1.2 Medium

cant medium	PDA
Fermentation medium	the liquid was supplemented with xylose, corn syrup, 2.0 % $MgSO_4 \cdot 7H_2O$, 2.0 % KH_2PO_4

158.2.2 Methods

158.2.2.1 Fermentation Condition

The fermentation was carried out in a 250 mL flask containing 50 mL of medium in which the initial pH value was 7.0 at 30 °C on a rotary shaker at 200 r/min for 48 h. The flasks were inoculated with a spore suspension (10^6 spores/flask), which

was prepared by suspending the spores of the fungus in 0.9 % saline after its full growth in potato-dextrose agar plates at 30 °C for 3–7 days. The inoculum concentration of the fermentation medium was 6 % (v/v).

158.2.2.2 Mycelia Collection

At the end of fermentation, mycelia were filtrated by buchner funnel, and washed with distilled water, subsequently it was air-dried at 65 °C and weighed.

Chitosan Extraction

Chitosan was isolated from the dried mycelia as the following procedure [22]. Dried mycelia were dealt with 2 % NaOH (1:20, w/v) at 100 °C for 2 h. Alkali insoluble mass was thoroughly washed with water and dealt with 2 % acetic acid (w/v) at 60 °C for 3 h. This was centrifuged, then the supernatant was adjusted to pH 9.0 with NaOH to precipitate out chitosan. The precipitate was washed with chilled water, followed by ethanol and acetone and air-dried at 50 °C.

Method of Calculation

$$\text{Mycelium concentration} = \frac{M_1}{V} \times 100\,\%$$

M_1 is dry weight of mycelium (g); V is fermentation broth volume (L).

$$\text{Chitosan production} = \frac{M_2}{V} \times 100\%$$

M_2 is dry weight of chitosan (g); V is fermentation broth volume (L).

158.3 Results and Discussion

158.3.1 Optimization of The Addition of Xylose and Corn Steep Liquor with Response Surface Methodology

Medium composition has a great impact on chitosan production in fermentation processed by *Actinomucor elegans*. The fermentation medium contained xylose, corn steep liquor, and some inorganic salts. Xylose and corn steep liquor were the main ingredient among them, and their concentrations have great influence on cell growth and chitosan production, so the optimum components in medium were

Table 158.1 Levels and codes of factor

Factor (%)	Code	Coding standards				
		−1.41421	−1	0	1	+1.41421
Corn steep liquor	X_1	3.17	4	6	8	8.83
Xylose	X_2	1.59	2	3	4	4.41

Table 158.2 Test design and results of the central composite design

Experiment number	X_1	X_2	Production of chitosan (g/L)
1.	−1	−1	0.748
2.	−1	1	0.811
3.	1	−1	0.901
4.	1	1	0.918
5.	−1.41421	0	0.802
6.	+1.41421	0	0.966
7.	0	−1.41421	0.796
8.	0	1.41421	0.912
9.	0	0	0.964
10.	0	0	0.930
11.	0	0	0.981
12.	0	0	0.972
13.	0	0	0.967

$x_1 = (X_1 - 6.0)/2.0$, $x_2 = (X_2 - 3.0)/1.0$

determined with the response surface methodology. The chitosan production was taken as the response. According to the experimental results designed in Tables 158.1 and 158.2. Quadratic regression equation was built using SAS software. The regression equation was: $Y_1 = 0.9628 + 0.061492X_1 + 0.030506X_2 - 0.045525X_1X_1 - 0.0115X_1X_2 - 0.060525X_2X_2$. The results of the variance analysis and model credibility analysis of regression equation were shown in Tables 158.3 and 158.4.

As shown in Table 158.3, the quadratic regression model was significantly notable($p = 0.000174$) and the lack of fit was not notable ($p = 0.267065$), which indicated that the model fits better with the experiment, so it can be used to analyze and forecast the chitosan production. Model credibility analysis was shown in Table 158.4, in which the r-square, R^2 showed that the variability of the 95.23 % of chitosan yield could be explained by the model. The variation coefficient of Y was lower, $CV = 2.55903$, so the experimental operation was credible. In summary, the regression equation provided a suitable model for calculation of chitosan production.

Analyzed from the diagram and software, there were stable points in the regression equation. Stable point was the maximum point. The major factors which

Table 158.3 Variance analysis of regression equation

Siurce	DF	SS	MS	F	Prob > F
X_1	1	0.03025	0.03025	57.3407	0.000129
X_2	1	0.007445	0.007445	14.11269	0.007106
X_1X_1	1	0.014418	0.014418	27.32976	0.001215
X_1X_2	1	0.000529	0.000529	1.002764	0.349994
X_2X_2	1	0.025484	0.025484	48.3064	0.000221
Model	5	0.073728	0.014746	27.9517	0.000174
Linear	2	0.037694	0.018847	35.72653	0.000212
Qadratic	2	0.035505	0.017752	33.65133	0.000257
Cross product	1	0.000529	0.000529	1.002764	0.349994
Error	7	0.003693	0.000528		
Lack of fit	3	0.002182	0.000727	1.925684	0.267065
Pure Error	4	0.001511	0.000378		
Total	12	0.077421			

Table 158.4 Fit statistics for Y

Analysis items	Master Model
Mean	0.897538
R-square R^2	95.23 %
Adj. R-square R^2	91.82 %
RMSE	0.022968
CV	2.55903

corresponded to Maxima were x_1, x_2, The coded value was 0.65134, 0.19013, respectively. The best concentrations of xylose and corn steep liquor were 73.0 g/L and 32.0 g/L, now and the chitosan production could be 0.98 g/L (Fig. 158.1).

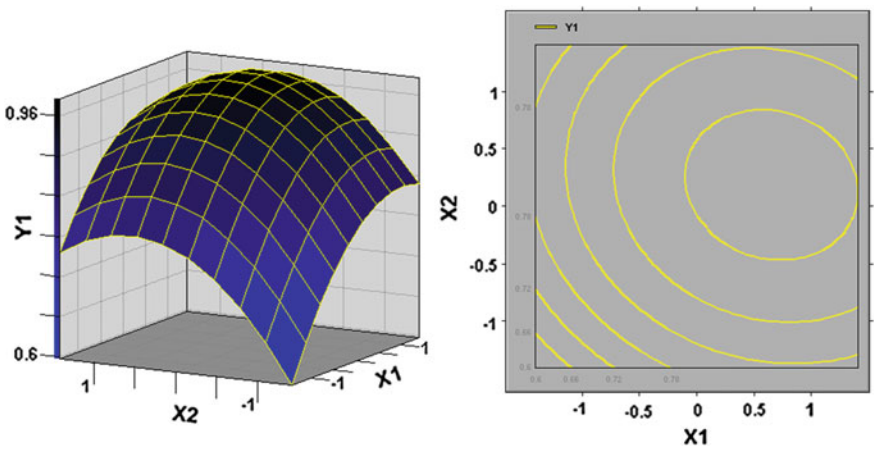

Fig. 158.1 Response surface stereograms and contour map

158.3.2 Optimization of Fermentation Condition

158.3.2.1 Effect of Initial pH on Chitosan Production

Initial pH was adjusted to different levels, and the fermentation temperature was controlled at 30 °C, the shaking speed was 150 r/min and the inoculum concentration was 4 %. The mycelium concentration and the chitosan production were tested after 48 h. The experimental results were shown in Fig. 158.2a.

As shown in Fig. 158.2a, the pH value had a significant effect on mycelium concentration and chitosan production in mycelium. When the pH of medium was controlled at 4.0–5.0, the mycelium concentration was the highest and the chitosan production was the highest too. However, pH value has greater effect on the degree of chitosan deacetylation. When the pH is neutral, the degree of chitosan deacetylation is the highest, because the deacetylase activity is the highest when pH is neutral. When pH value was 4.0–7.0, the chitosan production was about the same. So, the optimal pH of medium was 7.0.

158.3.2.2 Effect of Temperature on Production of Chitosan

Initial pH was adjusted to 7.0, shaking speed was 150 r/min, and the inoculum concentration was 6 %. At different fermentation temperatures, the mycelium concentration and chitosan production were determined after 48 h. The experimental results were shown in Fig. 158.2b.

As shown in Fig. 158.2b, temperature had a significant effect on mycelium concentration and chitosan production in mycelium after 48 h. Mycelium needs an optimal temperature range to grow vigorously. Optimal incubation temperature was 30 °C according to the experimental results.

158.3.2.3 Effect of Loaded Liquid on Chitosan Production

Initial pH was adjusted to 7.0, fermentation temperature was 30 °C, and shaking speed was 150 r/min, and the inoculum concentration was 4 %. Different loaded liquids were used and the mycelium concentration and the chitosan production were tested after 48 h respectively. The experimental results were shown in Fig. 158.2c.

As shown in Fig. 158.2c, when the liquid volume was 30 mL, the mycelium concentration was the highest, and when liquid volume was 50 mL, the chitosan production was about 30 mL. When the liquid volume was too small, the total yield of chitosan was low, and when liquid volume was too large, the dissolved oxygen, the medium production and the total chitosan production were also low. Above all, the optimal-loaded medium liquid was 50 mL/250 mL.

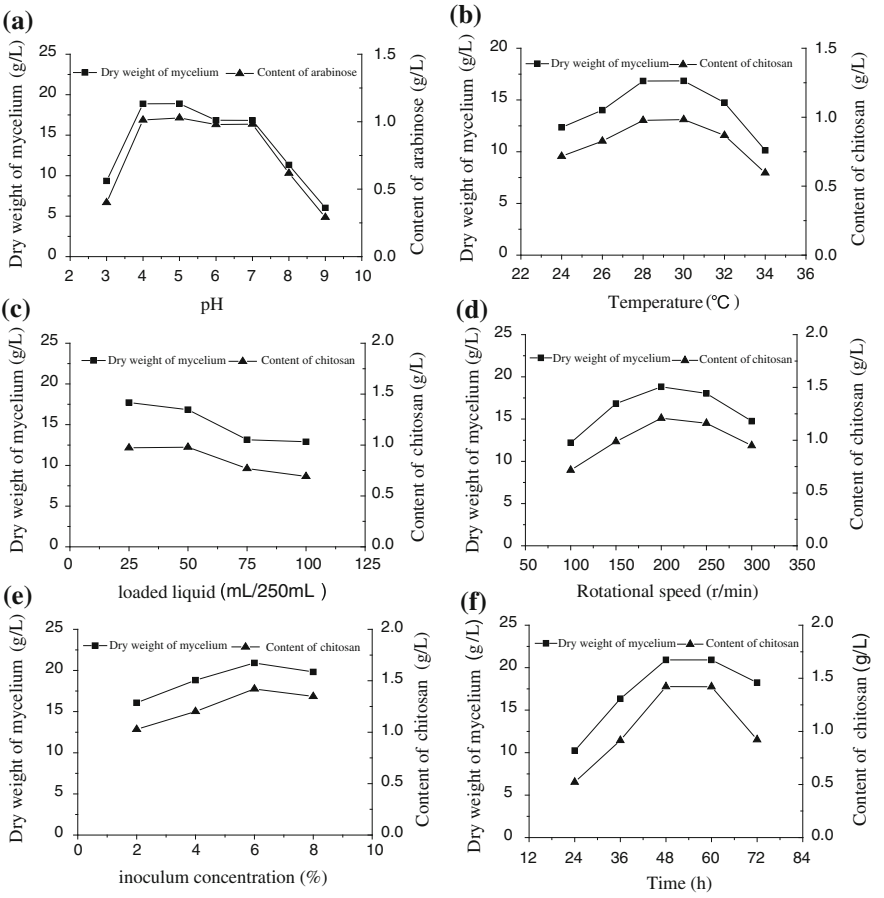

Fig. 158.2 Effect fermentation conditions on mycelium concentration and chitosan production

158.3.2.4 Effect of Shaking Speed on Chitosan Production

The initial pH was adjusted to 7.0 and the fermentation temperature was 30 °C. At different rotational speed, with the 4 % inoculum concentration, the determined mycelium concentration and the chitosan production were determined after 48 h, the experimental results were shown in Fig. 158.2d.

As shown in Fig. 158.2d, with the increasing speed, the dissolved oxygen increased and the mycelium was also increased. When the rotational speed was 200 r/min, the mycelium concentration and the chitosan production were the maximum. However, if the speed was too large, the mycelium will be destroyed. So, the optimal shaking speed of medium was 200 r/min.

158.3.2.5 Effect of the Inoculum Concentration on Chitosan Production

The initial pH was adjusted to 7.0. The fermentation temperature was 30 °C and the shaking speed was 200 r/min. With different inoculum concentrations, the mycelium concentration and the chitosan production were determined after 48 h, the experimental results were shown in Fig. 158.2e.

As shown in Fig. 158.2e, when the inoculum concentration was 6 %, the mycelium and the chitosan production reached the maximum. When the inoculum concentration was too large, the chitosan production was decreased. The reason may be that the content of sugar in the substrate could not meet the mycelium growth needs so that the nutrients would be premature failure. Above all, the inoculum concentration was confirmed as 6 %.

158.3.2.6 Effect of The Culture Time on Chitosan Production

The initial pH was adjusted to 7.0, and the fermentation temperature was 30 °C. The shaking speed was 200 r/min and the inoculum concentration was 6 %. The mycelium concentration and the chitosan production were determined after different times. The experimental results were shown in Fig. 158.2f.

As shown in Fig. 158.2f, the mycelium concentration and the chitosan production were both changed. Mycelium bloomed in 24 to 48 h. The mycelium concentration increased slowly and began to decline after 48 h, and the chitosan production was also falling. The reason may be that the cell wall of mycelium autolyzed gradually with the extending incubation time. The optimal culture time was 48 h according to the experimental result.

158.4 Conclusion

The proportion of two main medium components (corn steep liquor and xylose) was optimized by response surface methodology. The optimal medium components were 73.0 g/L of corn steep liquor, 32.0 g/L of xylose, 2.0 g/L of KH_2PO_4, and 2.0 g/L of $MgSO_4$. The fermentation conditions were optimized, and the optimal conditions were 7.0 of pH, 30 °C of temperature, 50 mL/250 mL of loaded liquid, 200 r/min of shaking speed, 6 % of inoculum concentration, 48 h of fermentation time. The chitosan production reached to 1.42 g/L with the optimized medium and fermentation conditions, which indicated that the potential use of xylose for the chitosan production by *Actinomucor elegans* was promising.

References

1. Mario FD, Rapana P, Tomati U et al (2008) Chitin and chitosan from basidiomycetes. Int J Biol Macromol 43(1):8–12
2. Tharanathan RN, Kittur FS (2003) Chitin-the undisputed biornolecule of grit potential. Crit Rev Food Sci 43(1):61–87
3. Kumar MNVR (2000) A review of chitin and chitosan applications. React Funct Polym 46(1):1–27
4. Göksungur Y (2004) Optimization of the production of chitosan from beet molasses by response surface methodology. J Chem Technol Biot 79(1):974–981
5. Wu J, Liu Q, Gan G (2008) Development situation of the production of chitosan by fermentation. Biotechnology 18(4):93–95
6. Chatterjee S, Adhya M, Guha AK et al (2005) Chitosan from Mucor rouxii: production and physico-chemical characterization. Process Biochem 40(1):395–400
7. Synowiecki J, Al-Khateeb NAAQ (1997) Mycelia of Mucor rouxii as a source of chitin and chitosan. Food Chem 60(4):605–610
8. Nwe N, Stevens WF (2004) Effect of urea on fungal chitosan production in solid substrate fermentation. Process Biochem 39(11):1639–1642
9. Xiong M, Chen G, Barford J (2011) Alteration of xylose reductase coenzyme preference to improve ethanol production by *Saccharomyces cerevisiae* from high xylose concentrations. Bioresour Technol 102(19):9206–9215
10. Pang Z, Liang J, Huang R (2011) Fermentation of xylose into ethanol by a new fungus strain *Pestalotiopsis sp.* XE-1. J Ind Microbiol 38(8):927–933
11. Zhang X, Tu M, Paice MG (2011) Routes to potential bioproducts from lignocellulosic biomass lignin and hemicelluloses. Bioenergy Res 4(4):246–257
12. Hong J, Zhang M, Liu C et al (2005) Progress in Metabolic Enineering of xylose—utilizing recombinant strains to produce ethanol. Food Ferment Ind 31(1):114–118
13. Asghari A, Bothast RJ, Doran JB et al (1996) Ethanol production from hemicellulose hydrolysates of agricultural residues using genetically engineered Escherichia coil strain Koll. J Ind Microbiol Biotechnol 16(1):42–47
14. Yang X, Peng Y (2006) Progress and Prospect of xylose-fementation study. Plant Fiber Sci China 28(5):262–266
15. Tanino T, Hotta A, Ito T et al (2010) Construction of a xylose-metabolizing yeast by genome integration of xylose isomerase gene and investigation of the effect of xylitol on fermentation. Appl Microbiol Biotechnol 88(5):1215–1221
16. Kato H, Suyama Yamada HR et al (2012) Improvements in ethanol production from xylose by mating recombinant xylose-fermenting *Saccharomyces cerevisiae* strains. Appl Microbiol Biotechnol 94(6):1585–1592
17. Wang J, An M (2007) Research progress in microorganisms of fementing xylose. Chem Bioeng 24(11):1–4
18. Wu C, Han J (2007) Research progress on xylitol production fermentated by microbiology from hemicellulosic hydroysate. China Food Addit 3:110–114
19. Liu H, Wang W, Feng G (2009) Study on single cell protein fermentation of corncobs hydrolysate by Sacchromyces cerevisiae. Food Sci Technol 34(6):48–51
20. Tai C, Li S, Xu Q et al (2010) Chitosan production from hemicellulose hydrolysate of corn straw: impact of degradation products on Rhizopus oryzae growth and chitosan fermentation. Lett Appl Microbiol 51(3):278–284
21. Zamani A, Edebo L, Sjostrom B et al (2010) Extraction and precipitation of chitosan from cell wall of zygomycetes fungi by dilute sulfuric acid. Biomacromolecules 8(12):3786–3790
22. Liu Z, Zhao H, Chu N et al (2010) Effects of the Fermentative Culture Medium on Production of Chitosan from *Actinomucor elegans*. J Tianjin Univ Sci Technol 25(2):13–17

Chapter 159
Inhibition of α-Amylase Activities by Extracts of Chinese Yam

Sai Qu, Liming Zhang, Xiaobian Zhang and Zhengjun Li

Abstract In order to search for new α-amylase inhibitors from Chinese Yam (*Dioscorea opposita* Thunb.), the extracts of alkali-soluble crude polysaccharides (ACP), water-soluble crude polysaccharides (WCP), total saponins, and flavones were isolated, and their inhibitory effects on α-amylase were evaluated. The experimental results show that the saponins and flavones had a marked inhibition effect on α-amylase, however, the ACP and WCP exhibited weakly inhibitory activities. The kinetic analysis indicates that the inhibition type of these extracts on α-amylase was competitive, and the enzyme-substrate apparent dissociation constant (Km') of acarbose (the control), WCP, saponins, and flavones is 118.86, 32.46, 79.23, 49.51 mg/ml, respectively.

Keywords Chinese yam · α-amylase · Inhibitory activitiy · Enzyme reaction kinetics

159.1 Introduction

At present, management of the blood glucose level is a critical strategy in the control of diabetes complications [1]. The drugs for diabetes include sulfonylureas and biguanides [2]. Inhibition of α-amylase could delay carbohydrate digestion and prolong overall carbohydrate digestion time, causing a reduction in the rate of glucose absorption and consequently reducing the postprandial plasma glucose

L. Zhang (✉)
Key Laboratory of Industrial Fermentation Microbiology, Ministry of Education, Tianjin University of Science and Technology, Tianjin 300457, People's Republic of China
e-mail: zhm@tust.edu.cn

S. Qu · L. Zhang · X. Zhang · Z. Li
College of Biological Engineering, Tianjin University of Science and Technology, Tianjin 300457, People's Republic of China

T.-C. Zhang et al. (eds.), *Proceedings of the 2012 International Conference on Applied Biotechnology (ICAB 2012)*, Lecture Notes in Electrical Engineering 251,
DOI: 10.1007/978-3-642-37925-3_159,

rise, therefore inhibitors of α-amylase play a significant role in the therapy as chemotherapeutic agents for Noninsulin-dependent diabetes mellitus (NIDDM).

Yam (*Dioscorea species*) is a member of the monocotyledonous family *Dioscoreaceae*. In China, the cultivation of yam has a long history for both edible and medical purpose [3]. Huai Shan Yao has been used for more than 2000 years in traditional Chinese medicine for the treatment of diabetes, diarrhea, asthma, and other ailments [4]. Of special note is the remedy for diabetes by Huai Shan Yao which has been consistently used since being recorded in the earliest Chinese medicinal documents Shen Nong Ben Cao Jing. Recent studies revealed that Huai Shan Yao has insulin sensitivity associated with the regulation of GLUT4 (glucose transporter type 4) expression [5]. In the present study, the inhibitory activities of polysaccharide, saponins, flavones on α-amylase were assayed. Following the tracks of α-amylase inhibition, polysaccharide, saponins, flavones with considerable inhibition were isolated and their activity were measured. After that, the inhibition type was determined by data analysis of enzyme reaction kinetics.

159.2 Materials and Methods

159.2.1 Materials

Plant sample of Chinese Yam was obtained from Anguo city, Hebei province, China. Both portions of yam were washed before sun drying and then milled to be obtained in a powder flour form. Chemicals and reagents used such as soluble starch, Hog pancreatic α-amylase, were procured from Sigma-Aldrich Chemical Co. (St. Louis. MO). All others are analytical reagent.

159.2.2 Extraction of Water-Soluble Crude Polysaccharide

The dried yam powder (100 g) was extracted with distilled water (1000 ml) at 70 °C water for 3 h, followed by a centrifugation (5000 g, 15 min). The water extracts were collected, and the residues were extracted again for three cycles. The combined extracts were pooled, and then condensed to about 200 mL under a reduced pressure. Subsequently, 4 volume of 95 % alcohol was added slowly by stirring to precipitate the polysaccharides. After deproteinization by Sevag method and lyophilization, the water-soluble crude polysaccharides (WCP) were obtained. The contents of WCP were analyzed by the phenol–sulfuric acid assay [6]. The result shows the yield of WCP was 12.68 %.

159.2.3 Extraction of Alkali-Soluble Crude Polysaccharide

The dried extracted residues of yam were suspended in $NaHCO_3$ solution (pH = 9.5) to extract the alkali-soluble crude polysaccharides (ACP). The residues were extracted at 70 °C for 3 h thrice. After that, the suspension was neutralized with citric acid. The supernatant containing ACP were concentrated and precipitated with 95 % EtOH (1:4, v/v) at 4 °C for overnight. The precipitate was collected by centrifugation and deproteinated by Sevag method [7]. Finally the supernatant was lyophilized to give ACP. The contents of ACP were analyzed by the phenol–sulfuric acid assay [6]. The result shows the yield of WCP was 13.09 %.

159.2.4 Extraction of Total Saponins

The yam flour was extracted via refluxing with different concentrations of ethanol (50, 60, 70, 80, 95 %), while other extraction parameters were constant (liquid-to-material ratio 10:1, extraction time 3 h, and extracted three times). The extracts were filtered and filtrates were evaporated to dryness using vacuum evaporator. The residue was treated with n-butyl alcohol saturated by water, then the resulting solution employed to degrease the materials by petroleum ether and deproteinated. Finally, the supernatant was lyophilized to give total saponins [8]. The contents were analyzed by the perchloric acid assay [9]. The results reviewed that the saponins yield ranged from 3.6 to 16.38 % with the increasing ethanol concentration. The highest yield of saponins was 16.38 % obtained at 70 % ethanol.

159.2.5 Extraction of Total Flavones

The dried powder of yam (100 g) was extracted with 95 % EtOH (1.5 L) for 3 h at 95 °C. After extraction, the sample was filtered and the filtrate was evaporated to dryness in a rotary vacuum evaporator (≤45 °C). The residue was degreased by petroleum ether and deproteinated. Finally the extracts were lyophilized to give yam flavones. The contents of flavones were analyzed by the sodium nitrite-aluminum nitrate-sodium hydroxide assay [10]. According to the data, the yield of flavones was 1.56 %.

159.2.6 Assay of α-Amylase Inhibitor Activity

The α-amylase inhibitor activity was measured by quantifying the reducing starch and described by improving iodine colorimetry [11]. The reaction mixture in a total volume of 20 ml contained 1 ml α-amylase enzyme which prepared fresh by dissolving 10 mg α-amylase (porcine pancreatic α-amylase) in 10 ml PBS, 1 ml suitably diluted α-amylase inhibitor, 15 ml 1 % starch solution and 3 ml buffer. The enzyme and inhibitor were first preincubated for 20 min at 50 °C before adding the substrate and buffer. In control, α-amylase inhibitor was replaced with equivalent volume of buffer. The blank contained equal volume of buffer instead of α-amylase enzyme and all other reagents. The reaction was stopped after 5 min, then 1 ml reaction mixture were pipetted into a tube which contents 5 ml 0.1 M iodine solution and 0.5 ml 0.5 M hydrochloride. The absorbance of the color developed was measured against the blank at 660 nm using UV/VIS Spectrophotometer [12].

One unit amylase activity was defined as the decrement of the starch under assay conditions by 1 ml amylase in 1 min. One unit of α-amylase inhibitor activity was defined as the reduction in amylase activity [13].

The percentage of inhibition ratio (IR) was determined according to the following equation:

$$\text{Inhibition Ratio } (\%) = \frac{U(0) - U(\text{i})}{U(0)} \times 100$$

where U (0) is the α-amylase activity after reaction without sample. U (i) is the α-amylase activity with sample.

159.2.7 Enzymatic Reaction Kinetics Analysis

To determine the nature of inhibition, α-amylase activity was measured at varying substrate concentration in the absence and presence of the fixed inhibitor concentrations in the reaction mixture and Lineweaver-Burk plot was plotted. The Km and Km' (enzyme-substrate apparent dissociation constant) value was determined from the plot as described by Lineweaver-Burk plot [14].

159.3 Results and Discussion

159.3.1 α-Amylase Inhibitory Activities of Yam Extracts

To determine the inhibitory potency of α-amylase inhibitor with the modified iodine Ultraviolet Spectrophotometry method, we compared the effect of different yam extracts at the series concentration of 0–50 mg/ml. In the present research, acarbose (a commercially available α-amylase inhibitor) was employed as the model compound for the evaluation of our method [15]. The ability of yam extraction to inhibit α-amylase activity in vitro was investigated and the result is presented in Figs. 159.1 and 159.2. It can be seen from Fig. 159.1 that the α-amylase inhibitory activities increased with the gradually enhanced concentration of inhibitor in the solvent. Totally speaking, the IR of saponins was between 7.33 % and 86.97 %. The percentage of inhibition of flavones was up to 78.45 % and the acarbose was to 99 %. As shown in Fig. 159.2, The polysaccharides of water extraction and alkali extraction had a few inhibition effects on α-amylase. When 50 mg/ml polyaccharides inhibitor was added into assay mixture, the IR of α-amylase activity was found to be 43 %. After that, no increase inhibition was observed.

159.3.2 Kinetic Parameters and the Type of Inhibition

We obtained Km of the reaction on the basis of the optimal conditions. The α-amylase solution was diluted at 100 U/mL. Five different concentrations of soluble starch were used, ranging from 2.5 to 30 mg/ml. Through the data shown in Fig. 159.3, the slope and intercept of Lineweaver-Burk plot was calculated, then the Km value for α-amylase was determined to be 25.68 mg/ml by michaelis–menten equation [16].

In the present research, acarbose was employed as the model compound for the evaluation of our method. A series of experiments were carried out in varied

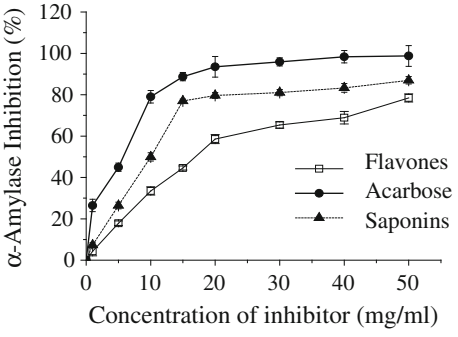

Fig. 159.1 Inhibitory activities of flavones, saponins, and acarbose

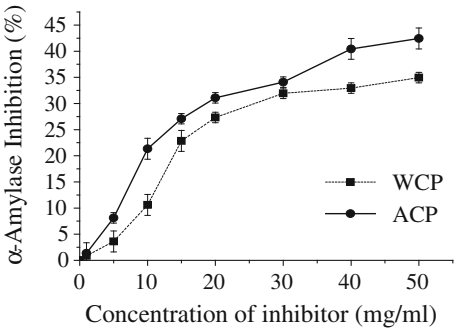

Fig. 159.2 Inhibitory activities of polysaccharides

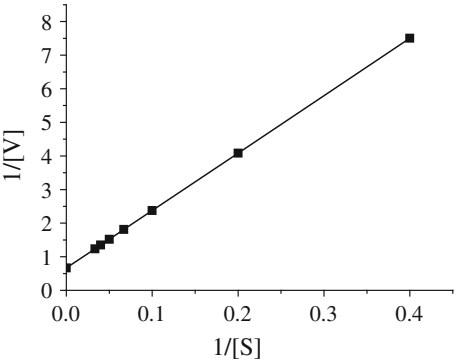

Fig. 159.3 Lineweaver-Burk plots of α-amylase assay

concentrations of soluble starch ranging from 2.5 mg/ml to 30 mg/ml at certain concentrations of yam extracts and acarbose. The data from these experiments were plotted by the method of Lineweaver-Burk [17]. Lineweaver-Burk plot was obtained as shown in Fig. 159.4. When the data were plotted by the method of Lineweaver-Burk, the intercept on axis of ordinates was the same in the presence or absence of yam extracts, clearly indicating that the inhibition was the competitive type [18]. Furthermore, the characteristic of inhibitory kinetics of yam extracts was also investigated (see Table 159.1) in the same way [19]. After the calculation by michaelis–menten equation, the Km' of acarbose (the control), WCP, saponins, and flavones is 118.86, 32.46, 79.23, 49.51 mg/ml, respectively.

According to the knowledge of enzyme reaction kinetics, the Km' value are directly related to the firmness of enzyme-substrate, and Km' value increased with the weakly binding of enzyme-substrate [20], so the inhibitory activity increase with an increased Km'value [21]. As the data revealed in Table 159.1, all Km'values were higher than Km value. This date validated the conclusion that yam extracts have inhibition effects on α-amylase. From analyzing the data in Fig. 159.4, a decreasing order of the inhibitory activity was confirmed: saponins > flavones > polysaccharides.

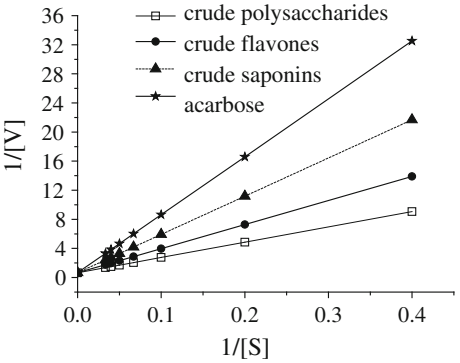

Fig. 159.4 Lineweaver-Burk plots of yam extracts and acarbose

Table 159.1 Enzyme-substrate apparent dissociation constant (Km')

Samples	Apparent dissociation constant of enzyme-substrate (Km' mg/ml)
Acarbose	118.86
Saponins	79.23
Flavones	49.51
WCP	32.46

159.4 Conclusion

The extracts of Chinese Yam showed considerable α-amylase inhibitory activity. The saponins exhibited remarkable competitive inhibitory activities against α-amylase and the inhibition ratio reach to 86.97 %. The percentage of inhibition of flavones was up to 78.45 %. From the michaelis–menten equation, the Km' value of acarbose, WCP, saponins, and flavones is 118.86, 32.46, 79.23, 49.51 mg/ml, respectively. We believe that our results have shown Chinese Yam to be a new source of α-amylase inhibitors, which may give some scientific evidences for Chinese conventional therapy of diabetes by Huai Shan Yao. The extracts could be used as lead compounds for drug screening, and might enable the preparation of new α-amylase inhibitors as functional food ingredients in the prevention and treatment of type-II diabetes and obesity.

Acknowledgments This work was financially supported by the Applied Foundation & Leading Technology Research Program of Tianjin (Grant No. 08JCZDJC15300).

References

1. Kwon YI, Apostolidis E, Kim YC et al (2007) Health benefits of traditional corn, beans and pumpkin: in vitro studies for hyperglycemia and hypertension management. J Med Food 10:266–275
2. Vandelaar FA, Lucassen PL, Akkermans RP et al (2005) alpha-Glucosidase inhibitors for type 2 diabetes mellitus. Cochrane Database Syst Rev, CD 003639

3. Farombi EO, Britton G, Emerole GO (2000) Evaluation of the antioxidant activity and partial characterization of extracts from browned yam flour diet. Food Res Int 33:493–499
4. Zava DT, Dollbaum CM, Blen M (1999) Estrogen and progestin bioactivity of foods, herbs and spices. In: Proceedings of the society for experimental biology and medine, vol 217. pp 369–378
5. McEwan R, Madivha RP, Djarova T et al (2010) Alpha-amylase inhibitor of amadumbe (*Colocasia esculenta*): isolation, purification and selectivity toward a-amylases from various sources. Afr J Biochem Res 4:220–224
6. Vilkas E, Radjabi-Nassab F (1986) The glucomannan system from Aloe vahombe (liliaceae). III. Comparative studies on the glucomannan components isolated from the leaves. Biochimie 68:1123–1127
7. Hilz H, Bakx EJ, Schols HA (2005) Cell wall polysaccharides in black currants and bilberries—characterisation in berries, juice, and press cake. Carbohydr Polym 59:477–488
8. Liu YW, Shang HF, Wang HF et al (2007) Immunomodulatory activity of dioscorin, the storage protein of yam (*Dioscorea alata* cv. Tainong No.1) tuber. Food Chem Toxicol 45:2312–2318
9. Hou WC, Chen HJ, Lin YH (1999) Dioscorin, the major tuber storage protein of yam (*Dioscorea batatas* Decne), with dehydro-ascorbate reductase and monodehydroascorbate reductase activities. Plant Sci 49:151–156
10. Lamien CE, Romito M, Millogo J et al (2005) Determination of the total phenolic, flavonoid and proline contents in B urkina Fasan honey, as well as their radical scavenging activity. Food Chem 91:571–577
11. Bandna K (2012) α-Amylase inhibitor in local Himalyan collections of Colocasia: isolation, purification, characterization and selectivity towards α-amylases from various sources. Pestic Biochem Phys 103:49–55
12. Akissoe N, Mestres C, Hounhouigan J et al (2005) Biochemical origin of browning during the processing of fresh yam (*Dioscorea* spp.) into dried product. J Agr Food Chem 53:2552–2557
13. Matsuura H, Asakawa C, Kurimoto M et al (2002) α-Glucosidase inhibitor from the seeds of balsam pear and the fruit bodies of Grifola frondosa. Biosci Biotech Biochem 66:1576–1578
14. Kanie Y, Kanie O (2002) Electrophoretically mediated microscale reaction of glycosi-das: kinetic analysis of some glycosidas at the nanoliter scale. Carbohydr Res 337:1757–1762
15. Lin JT, Yang DJ (2008) Determination of steroidal saponins in different organs of yam (*Dioscorea pseudojaponica Yamamoto*). Food Chem 108:1068–1074
16. Ibrahim AR, Abul-Hajj YJ (1990) Microbiological transformation of flavone and isoflavone. Xenobiotica 20:363–373
17. Khan RA, Khan MR (2012) Assessment of flavonoids contents and in vitro antioxidant activity of Launaea procumbens. Chem Cent J 6(1):43–44
18. Jiao L, Xia LL, Jiang P et al (2009) Characterization and anti-tumor activity of alkali-extracted polysaccharide from *Enteromorpha intestinalis*. Int Immunopharmacology 9:324–329
19. Nickavar B, Yousefian N (2009) Inhibitory effects of six Allium species on α-amylase enzyme activity. Iran J Pharm Res 8(1):53–57
20. Wang J, Zhu XH, Qin WH (1998) Adverse reaction and tolerance of acarbose. Chin J New Drugs Clin Rem 17:190–191
21. Lan P, Gao Y, Wang L et al (2010) Screening of glucosidase inhibitors from Chinese herbal medicines. Agr Jilin 05:138–142

Chapter 160
VvpGLT, a Grapevine Gene Encoding for a Plastidic Localized Glucose Transporter

Lei Zeng, Yanjie Yi, Huaijian Tang and Jinshui Wang

Abstract Glucose transporters mediate the membrane transport of a variable range of glucose, which play a crucial role in sugar distribution throughout the plant. To investigate the significance of glucose transporters during grapevine (*Vitis vinifera* L.) fruit development, a cDNA clone of a putative glucose transporter gene *VvpGLT* was isolated by screening the grapevine cDNA library. Phylogenetic comparison of the amino acid sequences showed the highest similarity to the *AtpGLcT* gene from *Arabidopsis thaliana*. The 1,629 bp *VvpGLT* cDNA clone was heterologously expressed in yeast resulting that *VvpGLT* was able to work as a glucose transporter in *Saccharomyces cerevisiae*, suggesting that *VvpGLT* is a gene that encodes for a glucose transporter. Induction of VvpGLT-GFP fusion protein expression in transgenic yeast and VvpGLT-GFP transient expression in onion epidermal cells revealed its plastidic localization. Based on the above analyses of VvpGLT, this is the first report of a functional plastidic localized glucose transporter in grapevine.

Keywords Glucose transporter · Grapevine · Heterologous expression · Subcellular localization

L. Zeng (✉) · Y. Yi · J. Wang
College of Bioengineering, Henan University of Technology,
Zhengzhou 450001, People's Republic of China
e-mail: zenglei718@163.com

H. Tang
College of Food Science and Technology, Henan University of Technology,
Zhengzhou 450001, People's Republic of China

T.-C. Zhang et al. (eds.), *Proceedings of the 2012 International Conference on Applied Biotechnology (ICAB 2012)*, Lecture Notes in Electrical Engineering 251,
DOI: 10.1007/978-3-642-37925-3_160,

160.1 Introduction

In higher plants, sugars are essential for plants, as building blocks for biomacromolecule, as osmotic regulators for cell enlargement, as regulatory signals for different signal-transduction pathways, as basic materials for various anabolic and catabolic reactions. In grape berries and other fruits, sugar content is one of the most important criteria for commercial quality. Sugars particularly contribute to grape berry and wine sensory properties such as color and flavor. Thus, the adequate production, storage, transport, and regulation of sugars in fruits have attracted close attentions.

Sugars are synthesized in the photosynthetic mesophyll cells of the leaves and then moved through the long-distance vascular system into the reproductive organs and storage and developing tissues like as roots, seeds, and flowers for their nutrition. The assimilate distribution between source and sink tissues recognized as a major determinant in crop yield involves several transport steps across membranes. Sugar transporters controlling photoassimilate partitioning within cells and among organs, play key roles in phloem apoplastic loading, transport, and unloading [1, 2].

Sugar transporter genes reported to date belong to a large gene family, known as the major facilitator superfamily (MFS). Two main subfamilies of the MSF are the disaccharide (or sucrose), transporters (DSTs), and the monosaccharide (or hexose) transporters (MSTs). Whereas DSTs appear to be specific for plants, the plant MSTs show the strongest homology to other eukaryotes and prokaryotes MSTs. Sugar transporters share little homology at the amino acid level, although they contain 12 putative transmembrane α-helices and a central hydrophilic region [3]. Sugar transporters can be identified based on sequence homology, functional similarity, and predicted topology models [4, 5]. DSTs and MSTs are responsible for coordination of sugar transport in various tissues at different stages of development and under varying environmental conditions [6].

In many plants, MSTs mediate the transport of a wide range of monosaccharides including glucose, fructose, maltose, raffinose, and sugar alcohols. In Arabidopsis for example, 53 putative monosaccharide transporter genes belonging to seven different subfamilies have been identified [7]. In addition to transport across the plasma membrane, monosaccharides are also transported across organelle membranes, such as the inner plastid envelope [8] and tonoplast [9]. MSTs on the Golgi apparatus have also been reported [10]. The grapevine genome encodes a total of 59 MST genes that group into the seven known subfamilies as defined by the *Arabidopsis* clades [11]. The localization of a few of these transporters are known but, to date, nothing is known about their exact physiological functions.

To understand the mechanisms of source-sink regulation in grapevines and to manipulate complicated mutual effect, it is significant that the potential membrane transport processes are thoroughly characterized. In this chapter, we functionally analyzed a candidate for the glucose transporter of the plastid inner envelope membrane from grape berries.

160.2 Materials and Methods

160.2.1 Plant Material

Grape (*Vitis vinifera* L. cv. Riesling) berries were harvested from the Sino-French Demonstration Farm, Huailai, China, in 2011. Eight to ten randomly selected bunches were sampled and transported to the laboratory at approximately 4 °C, then the berries were peeled and seeded, immediately frozen in liquid nitrogen, and stored at −80 °C for further analysis.

160.2.2 Grape Berry cDNA Library Construction

Total RNA of grape berries collected 45 days after flowering was isolated as described by Davies and Robinson [12]. RNA was then treated with RNase-free DNase I (Takara). The purity and quality of the RNA were checked by gel electrophoresis and $OD_{260/280}$ ratio. First-stranded cDNA was synthesized with a SuperScript RT-PCR kit (Invitrogen), and used for candidate sugar transporter cDNA cloning.

160.2.3 Cloning and Sequence Analysis of VvpGLT *Gene*

The cDNA fragment of *VvpGLT* was cloned by PCR using specific primers VvpGLT-F1 and VvPGLT-R1 (Table 160.1) from the aforementioned cDNA library. The PCR products were subcloned into the pMD19T simple vector (Takara) for amplification and sequencing.

Sequence analysis was performed on the BLAST server (http://www.ncbi.nlm.nih.gov/blast/Blast.cgi). A phylogenetic tree showing the relationships between VvpGLT and sugar transporters from *A. thaliana* and other organisms was

Table 160.1 Primers used for cloning and expression

Primer pairs	Primer sequence (5′-3′)
VvpGLT-F1	CCGCTCGAGATGCAAACTTCGACATA
VvPGLT-R1	GATGCCGCGGTTAAGTTGCAGGGTTA
VvpGLT-F2	ATGGGTACCATGCAAACTTCGACATA
VvpGLT-R2	CGCGGATCCAGTTGCAGGGTTAAGA
VvHT1F	CCGAGCTCATGCCGGCTGTCGGAGGCT
VvHT1R	CGCGGATCCTACATTCTTAACAGGGTAGT
VvpGLT-S	TCCCCGCGGATGCAAACTTCGACATA
VvpGLT-A	CGCGGATCCAGTTGCAGGGTTAAGA

constructed by aligning amino acid sequences with the program ClustalW (http://www.ebi.ac.uk/Tools/clustalw2/index.html). An unrooted tree was constructed and viewed using TreeView (http://taxonomy.zoology.gla.ac.uk/rod/treeview.html). Putative signal peptides were predicted using SignalP 3.0 [13], and transmembrane helices were predicted with the TMHMM Server v. 2.0 [14].

160.2.4 Plasmid Construction for Yeast Expression

VvpGLT cDNA was excised from the pMD19T-VvpGLT construct by XhoI/SacII digestion and inserted into the corresponding restriction sites of the pDR195 yeast shuttle vector [15]. The pDR195-VvpGLT construct was confirmed by DNA sequencing.

The pYES2 (Invitrogen) shuttle vector, which allows expression of full-length cDNA under control of the inducible yeast GAL1 promoter, was modified to yield the plasmid pYES2-GFP which contains the full-length GFP ORF downstream of the multiple cloning site [16] and used to express VvpGLT-GFP fusion proteins in yeast. The *VvpGLT* coding sequence was amplified using primers VvpGLT-F2 and VvpGLT-R2 (Table 160.1), which introduced BamHI sites at the N-terminal end and KpnI sites at the C-terminal end of the VvpGLT ORF and replaced the stop codon of the original VvpGLT ORF. This modified *VvpGLT* sequence was subcloned in-frame to the 5′ end of GFP, yielding the plasmid pYES2-VvpGLT-GFP. As a positive control, *VvHT1* cDNA (GenBank accession number AJ001061) was cloned upstream of GFP using the primer pair VvHT1F and VvHT1R (Table 160.1), yielding the plasmid pYES2-VvHT1-GFP. All of the constructs were validated by DNA sequencing.

160.2.5 Transformation into Glucose-Transport-Deficient Yeast

The pDR195-VvpGLT plasmid was used to transform *Saccharomyces cerevisiae* strain EBY.VW4000 by the lithium acetate method [17]. Transformants were selected on solid yeast nitrogen base (YNB) medium minus uracil and containing 2 % maltose. The fast-growing colonies were selected and verified by PCR after incubation for 3 days at 30 °C. Positive clones were replica-plated onto the same medium containing 2 % glucose instead of maltose, and the growth phenotype on glucose medium was assessed after 7 days at 30 °C. Cells transformed with the empty pDR195 vector were used as controls.

For in vivo localization of VvpGLT, the EBY.VW4000 yeast strain was transformed with the pYES2-VvpGLT-GFP plasmid, and in parallel, pYES2-VvHT1-GFP was transformed as additional controls. Transformants were selected

and verified as described above. Fast-growing colonies were picked and incubated in liquid YNB medium lacking uracil and containing 2 % maltose as the carbon source. The transformed yeast cells were washed with physiological saline, induced by the addition of 2 % galactose, and incubated at 30 °C for 12 h. The cells were observed by fluorescence microscopy (Nikon, Eclipse TE2000-E) at an excitation wavelength of 488 nm.

160.2.6 Transient Expression of VvpGLT-GFP Fusion Protein

The pEZS-NL shuttle vector was used transiently to express VvpGLT-GFP fusion proteins in onion epidermal strips. Full-length *VvpGLT* cDNA was amplified by PCR with gene-specific primers VvpGLT-S and VvpGLT-A (Table 160.1), and cloned upstream of in-frame with the GFP reporter gene to produce the VvpGLT-GFP fusion protein under control of the Cauliflower Mosaic Virus (CaMV) 35S promoter. Transient expression of the VvpGLT-GFP fusion protein in onion epidermal cells was conducted as described by Hayes and others [18]. Plasmolyzed onion epidermal cells were obtained by treatment with 5 % NaCl before observation.

160.3 Results and Discussion

160.3.1 Cloning of VvpGLT *cDNA Sequence*

VvpGLT has a 1,629 bp ORF potentially encoding a 542-aa protein, with a calculated molecular mass of 57.3 kDa and an isoelectric point at pH 9.6. Phylogenetic analysis of predicted VvHTs other *V. vinifera* MSTs and DSTs distributed them into different clades [16]. Analysis of the deduced amino acid sequences by TMHMM revealed the presence of 10 membrane-spanning domains with a large central hydrophilic loop between transmembrane domains 5 and 6 (Fig. 160.1). This topological model is consistent with the structures proposed for the MSTs and DSTs identified to date in microbes, mammals, and plants.

According to SignalP analysis, VvpGLT may not contain a signal peptide. Thus, it was unlikely to be exposed to the N-glycosylation machinery and may not be glycosylated (in vivo) even though it contain potential motif (asparagines residue 43). Sugar transporter signatures, including GRK motifs in loops 7, and in particular motifs corresponding to the PESPR/PETKGR motif after helices 5 and 10, were all present in the predicted amino acid sequences of the VvpGLT.

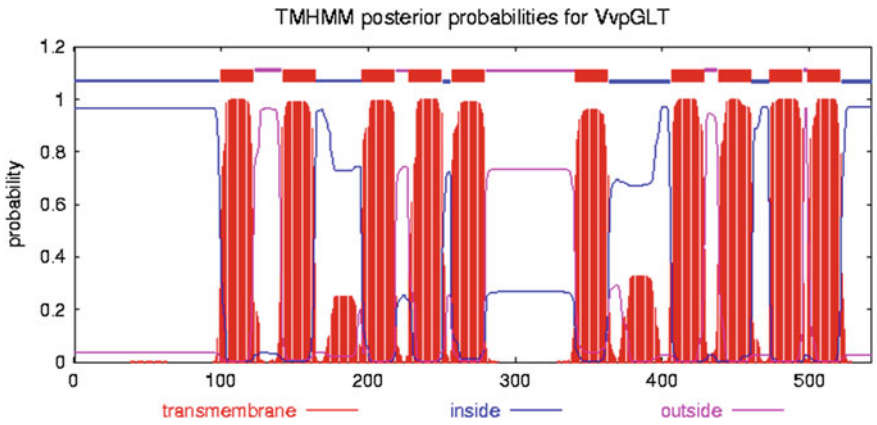

Fig. 160.1 Hydropathy profile and membrane-spanning model of VvpGLT

160.3.2 Heterologous Expression of VvpGLT *in Yeast*

To assess the physiological functionality of *VvpGLT*, we expressed VvpGLT in the yeast strain EBY.VW4000. This strain is completely lacking in glucose uptake due to concurrent knockout of endogenous hexose transporters, and can grow only on medium containing maltose as the carbon source. The pDR195-VvpGLT and pDR195 constructs were used for the transformation. URA^+ transformants were selected on maltose as a permissive carbon source and subsequently replica-plated onto synthetic medium containing 2 % glucose as the sole carbon source. pDR195-VvpGLT-positive transformants showed partially restored growth on glucose, whereas the transformants containing pDR195 were unable to form visible colonies on glucose medium (Fig. 160.2a).

To determine its possible subcellular localization, GFP-tagged VvpGLT was expressed in the mutant *hxt*-null yeast strain. Transformed cells containing pYES2-VvpGLT-GFP were cultured separately in selective medium containing maltose, with gene expression under the control of the GAL1 promoter. Distribution of the fusion proteins in the living cells was examined by fluorescence microscopy. A strong green fluorescent signal was observed after galactose induction, whereas the signal in cells without galactose induction was very weak (data not shown). As shown in Fig. 160. 2b, the fluorescence pattern of cells expressing pYES2-VvpGLT-GFP was significantly different from that of cells expressing pYES2-HT1-GFP, in the former, bright fluorescence was concentrated in the internal structures, which resembled plastids, suggesting that VvpGLT might be a plastidic localized transporter. In contrast, the fluorescence in cells expressing pYES2-HT1-GFP was predominantly localized at the cell periphery (Fig. 160.2c), which is consistent with the plasma membrane localization reported by Vignault and others [19].

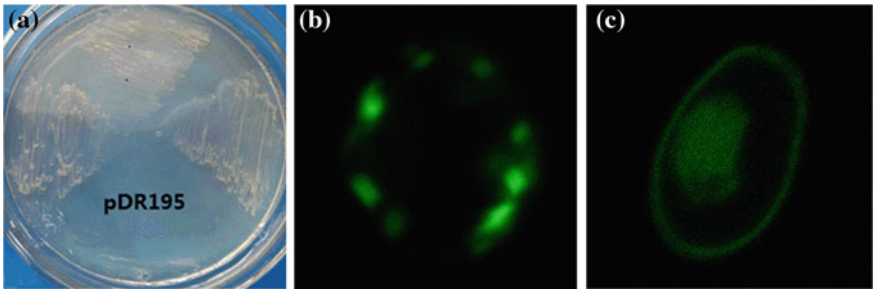

Fig. 160.2 Functional expression of *VvpGLT* cDNA in the *S. cerevisiae* EBY.VW4000 mutant defective in hexose uptake. **a** Growth phenotype of the mutant complemented by the empty vector (pDR195) and the vector carrying VvpGLT (pDR195-VvpGLT) on medium containing 2 % glucose as the sole carbon source. **b** Subcellular localization of VvpGLT-GFP fusion protein in transgenic yeast, dark-field image of yeast cell expressing the VvpGLT-GFP fusion construct, fluorescence signal resemble plastid structures. **c** Subcellular localization of VvHT1-GFP fusion protein in transgenic yeast, dark-field image of yeast cells expressing the VvHT1-GFP fusion construct, fluorescence signal is strong in the yeast plasma membrane

160.3.3 Subcellular Localization of VvpGLT Protein in Planta

To investigate the subcellular localization of VvpGLT in planta, the *VvpGLT* ORF was cloned upstream of, and in-frame with, the GFP reporter gene to produce a VvpGLT-GFP fusion protein, under control of the cauliflower mosaic virus (CaMV) 35S promoter. The construct, together with a construct containing native, non-targeted GFP, were bombarded into onion epidermal cells and the cellular localization of the fusion proteins determined by confocal microscopy. No fluorescence was observed in the plasma membrane, but clear fluorescence of the fusion protein was found in the inner layer of bombarded cells (Fig. 160.3), labeling the plastid and not the plasma membrane.

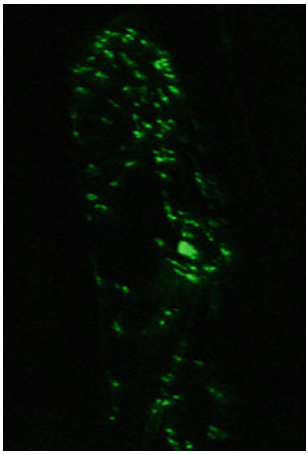

Fig. 160.3 Analysis of the cellular targeting of VvpGLT-GFP fusion protein in onion epidermal cells

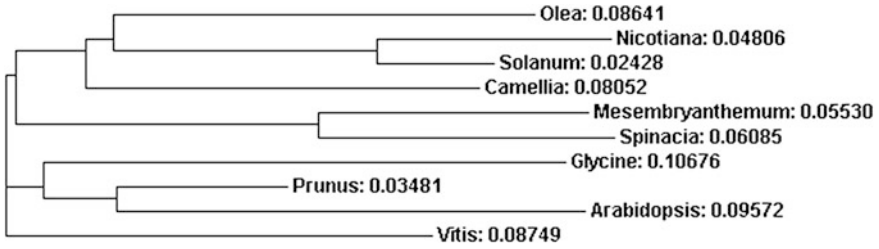

Fig. 160.4 Unrooted phylogenetic tree showing comparison of VvpGLT from grapevine and other organisms. Multiple sequence alignment was performed with Clustalx. The sequences were retrieved from the NCBI with the following accession numbers: *Vitis* (VvpGT1:AY608701), *Olea europaea* (AAK62031), *Camellia sinensis* (AFP19448), *Glycine max* (XP_003541360), *Mesembryanthemum crystallinum* (AF286906), *Nicotiana tabacum* (AF215852), *Spinacia oleracea* (AF215851), *Prunus armeniaca* (AAB88879), *Arabidopsis thaliana* (CAC01856), *Solanum tuberosum* (AF215853)

160.4 Conclusion

Although several MSTs and DSTs have been functionally characterized and localized at the cellular level in grapevine, none have been functional plastidic localized sugar transporters. Here we describe the functional characterization and subcellular localization of VvpGLT, a member of the *V. vinifera* MST family.

Searching GenBank with predicted amino acid sequences revealed a high similarity of VvpGLT with other sugar transporters (Fig. 160. 4). Our in silico analyses revealed that VvpGLT contains amino acid motifs which are conserved among members of the MFS and the amino acid signatures of typical sugar transporters.

Although sequence homologies enable the assignment of putative functions to unknown genes, the actual transport function of VvpGLT needed to be tested precisely by homologous or heterologous expression. Yeast growth experiments provide important evidence for the functionality of cloned gene. We further analyzed the intracellular localization of VvpGLT in the *hxt*-null yeast mutant strain EBY.VW4000 and in onion epidermis cells. The VvpGLT-GFP fusion protein localized preferentially to the plastid envelope membrane and not the plasma membrane.

In conclusion, the *VvpGLT* gene was cloned from grape berries. The sugar transporter function of VvpGLT was confirmed by heterologous expression in yeast, which also localized the transporter protein to the plastid. Transient expression in onion epidermis supported its role as a plastid transporter. The detailed roles of VvpGLT in berry development, sugar accumulation, and its upstream regulation await further investigation.

Acknowledgments This work was financially supported by the Doctor Foundation of Henan University of Technology (2011BS057) and the Key Research Project of the Education Department Henan Province (12B180005).

References

1. Riesmeier JW, Hirner B, Frommer WB (1993) Potato sucrose transporter expression in minor veins indicates a role in phloem loading. Plant Cell 5:1591–1598
2. Gottwald JR, Krysan PJ, Young JC et al (2000) Genetic evidence for the in planta role of phloem-specific plasma membrane sucrose transporters. Proc Natl Acad Sci USA 97:13979–13984
3. Marger MD, Saier MH Jr (1993) A major superfamily of transmembrane facilitators that catalyse uniport, symport and antiport. Trends Biochem Sci 18:13–20
4. Maiden M, Davis EO, Baldwin S et al (1987) Mammalian and bacterial sugar porters are homologous. Nature 325:641–643
5. Griffith JK, Baker ME, Rouch DA et al (1992) Membrane transport proteins: implications of sequence comparisons. Curr Opin Cell Biol 4:684–695
6. Szenthe A, Schäfer H, Hauf J et al (2007) Characterisation and expression of monosaccharide transporters in lupins, *Lupinus polyphyllus* and *L. albus*. J Plant Res 120:697–705
7. Buttner M (2007) The monosaccharide transporter(-like) gene family in Arabidopsis. FEBS Lett 581:2318–2324
8. Weber A, Servaites JC, Geiger DR et al (2000) Identification, purification, and molecular cloning of a putative plastidic glucose translocator. Plant Cell 12:787–802
9. Wormit A, Trentmann O, Feifer I et al (2006) Molecular identification and physiological characterization of a novel monosaccharide transporter from Arabidopsis involved in vacuolar sugar transport. Plant Cell 18:3476–3490
10. Wang HX, Weerasinghe RR, Perdue TD et al (2006) A Golgi-localized hexose transporter is involved in heterotrimeric g protein-mediated early development in Arabidopsis. Mol Biol Cell 17:4257–4269
11. Agasse A, Vignault C, Kappel C et al (2009) Sugar transport and sugar sensing in grape. In: Roubelakis-Angelakis KA (ed) Grapevine molecular physiology and biotechnology, 2nd edn. Springer, New York
12. Davies C, Robinson SP (1996) Sugar accumulation in grape berries-cloning of two putative vacuolar invertase cDNAs and their expression in grapevine tissues. Plant Physiol 111:275–283
13. Bendtsen JD, Nielsen H, von Heijne G et al (2004) Improved prediction of signal peptides: SignalP 3.0. J Mol Biol 340:783–795
14. Krogh A, Larsson B, von Heijne G et al (2001) Predicting transmembrane protein topology with a Hidden Markov Model: application to complete genomes. J Mol Biol 305:567–580
15. Rentsch D, Laloi M, Rouhara I et al (1995) NTR1 encodes a high affinity oligopeptide transporter in *Arabidopsis*. FEBS Lett 370:264–268
16. Zeng L, Wang Z, Vainstein A et al (2011) Cloning, Localization, and Expression Analysis of a New Tonoplast Monosaccharide Transporter from *Vitis vinifera* L. J Plant Growth Regul 30:199–212
17. Gietz D, Jean AS, Woods RA et al (1992) Improved method for high efficiency transformation of intact yeast cells. Nucleic Acids Res 20:1425
18. Hayes MA, Davies C, Dry IB (2007) Isolation, functional characterization, and expression analysis of grapevine (*Vitis vinifera* L.) hexose transporters: differential roles in sink and source tissues. J Exp Bot 58:1985–1997
19. Vignault C, Vachaud M, Cakir B et al (2005) VvHT1 encodes a monosaccharide transporter expressed in the conducting complex of the grape berry phloem. J Exp Bot 56:1409–1418

Chapter 161
Preparation and Characterization of New GA Carboxylic Acid Derivatives

Caiju Zhou, Yong-En Guo, Laitao Zhang, Baoguo Wang, Longjiang Chen and Tong-Cun Zhang

Abstract Gambogic acid (GA) shows important biological activities for carcinoma cells, such as selectively inducing apoptosis and differentiation, inhibiting proliferation and transference, inversing multiple drug resistance (MDR). However, its aqueous solubility is so low that its oral bioavailability is not as good as those marketed antitumor chemical drugs. In this paper, two GA derivatives with better aqueous solubility were designed and prepared. Among them N,N-bis-(β-hydroxyethyl) GA carboxamide was synthesized by DCC-HOBt catalyzed coupling reaction between GA and diethanolamine, and monoester of succinic acid by GA esterification with methyl succinyl chloride followed by mild hydrolysis with lithium hydroxide. The structures of these two target compounds and one intermediate were characterized by ESI–MS and ^{1}H NMR spectra after their purification. These studies are of great significance for us to develop GA chemical entities with effective potency to treat cancers.

Keywords Gambogic acid · Derivatives · Antitumor · Aqueous solubility · Prepare · Characterize

161.1 Introduction

Chemotherapy is one of the most extensively studied methods in antitumor therapies. Medicinal herbs are main sources of new drugs. More than half of the new chemicals approved between 1982 and 2002 were derived directly or indirectly

C. Zhou · T. Zhang
Key Laboratory of Industrial Fermentation Microbiology, Ministry of Education, College of Biotechnology, Tianjin University of Science and Technology, Tianjin 300457, people's Republic of China

Y.-E. Guo (✉) · L. Zhang · B. Wang · L. Chen
Pharmacy College, Jining Medical College, Rizhao 276826, people's Republic of China
e-mail: gyezcj@yahoo.com.cn

T.-C. Zhang et al. (eds.), *Proceedings of the 2012 International Conference on Applied Biotechnology (ICAB 2012)*, Lecture Notes in Electrical Engineering 251,
DOI: 10.1007/978-3-642-37925-3_161,

from natural products [1]. Gambogic acid (GA) and other active compounds have been isolated from Chinese medicinal herbs and tested for anticancer effects. GA has demonstrated its potential as an excellent cytotoxic agent against a variety of malignant tumors, including glioblastoma, and cancers of the breast, lung, and liver [2–9].

161.2 Materials and Methods

161.2.1 Materials

The ^{1}H NMR spectra were recorded on a Bruker ARX-300 spectrometer. Proton chemical shifts (δ) were reported in ppm downfield from tetramethylsilane (TMS). Mass spectra were obtained on an Agilent 1946A-MSD (ESIMS). All chemical reagents used were of analytical grade. GA was purified from gamboge supplied by Huashen Pharmaceutical Co., Bozhou, and methyl succinyl chloride prepared from succinic anhydride [10].

161.2.2 Methods [11, 12]

161.2.2.1 N, N-Bis(2-hydroxyethyl) GA Carboxamide (1)

To the mixture of gambolic acid (0.30 g, 0.48 mmol), dicyclohexylcarbodiimide (DCC, 0.12 g, 0.58 mmol), and 1-hydroxybenzotriazole (HOBt, 80 mg, 0.59 mmol) in THF (6.0 mL) stirred at rt, was added diethanolamine (50 mg, 0.48 mmol) in THF (1.0 mL). Stirring at rt continued for an additional 7.5 h, until GA disappeared by TLC detection on precoated silica gel G plates (petroleum ether-acetone, v/v 2:1). After the reaction mixture was concentrated at vacuum, the residue was mixed with icy water (1 mL), and extracted with dichloromethane (3 × 3 mL). The organic solutions were combined, and dried over anhydrous magnesium sulfate. After the drying agent was removed by filtration, the filtrate was concentrated under reduced pressure, and the residue was purified by flash column chromatography (silica gel, petroleum ether-EtOAc, v/v 3:1 to 1:1) to yield compound **1** (0.26 g, 76 %) as a wax.

161.2.2.2 GA-6-$CO_2(CH_2)_2CO_2H$

GA-6-$CO_2(CH_2)_2CO_2Me$ (2)

To the stirred solution of gambolic acid (0.10 g, 0.16 mmol) and triethylamin (32.2 mg, 0.32 mmol) in anhydrous dichloromethane (3.0 mL) cooled in an icy water bath, was added methyl succinyl chloride (35.9 mg, 0.24 mmol) in dichloromethane (2.0 mL). Stirring at rt continued for an additional 18 h, until GA disappeared by TLC detection on precoated silica gel G plates (petroleum ether-methanol-ethyl acetate, v/v 60:4:20). The same treatment procedure in compound **1** preparation was carried out, and the residue was purified by silica gel chromatography with petroleum ether- EtOAc (v/v 3:1) as the eluent to get compound **2** (83 mg, 70 %) as a yellow oil.

GA-6-$CO_2(CH_2)_2CO_2H$ (3)

To the solution of GA-6-$CO_2(CH_2)_2CO_2Me$ (0.28 g, 0.38 mmol) dissolved in ethanol(2.0 mL)and THF(2.0 mL),was added aqueous lithium hydroxide (3.0 mol/mL, 0.60 mL, 1.8 mmol). The mixture was stirred at 38–40 °C for 6 h, until GA-6-$CO_2(CH_2)_2CO_2Me$ disappeared by TLC detection on precoated silica gel G plates (petroleum ether-ethyl acetate–methanol, v/v 6:3:1). When the mixture was acidified to pH 2 with 3 mol/L hydrochloric acid, some solid appeared. The similar treatment procedure in compound **1** synthesis was carried out again, and the residue was purified by column chromatography (silica gel) with petroleum ether-EtOAc –AcOH (v/v 2:1:0.1) as the eluent to yield compound **3** (0.18 g, 66 %) as a yellow wax.

161.3 Results and Discussion

3.1 More aqueously soluble N,N-bis(β-hydroxylethyl) GA carboxamide (**1**) by means of DCC-HOBt catalyzed coupling reaction of GA with diethanolamine (as shown in Scheme 161.1) [13].

Compound **1:** ^{1}H NMR ($CDCl_3$, 300 MHz) δ: 12.67 (s, 1H, 6-OH), 7.53 (d, J = 6.9 Hz, 1H, 10-H), 6.67 (d, J = 10.2 Hz, 1H, 4-H), 6.12–6.16 (m, 1H, 27-H), 5.38 (d, J = 10.2 Hz, 1H, 3-H), 5.07–5.09 (m, 1H, 37-H), 3.81 (t, J = 1.0 Hz, 4H, 2C$\underline{H}_2$OH), 3.50–3.51 (m, 1H, 11-H), 3.24–3.28 (m, 1H, 31a-H), 3.14–3.18 (m, 1H, 31b-H), 3.13 (t, J = 1.0 Hz, 4H, 2NCH_2), 2.98 (d, J = 7.3 Hz, 2H, 26-H), 2.81–2.84 (m, 1H, 32-H), 2.52 (d, J = 9.0 Hz, 1H, 22-H), 2.32–2.30 (m, 1H, 21a-H), 2.05–2.07 (m, 2H, 36-H), 1.94 (s, 3H, 34-H), 1.76 (s, 3H, 35-H), 1.68 (s, 3H, 29-H), 1.66 (t, J = 8.6 Hz, 2H, 20-H), 1.63 (s, 3H, 39-H), 1.48 (s, 3H, 35-H), 1.42

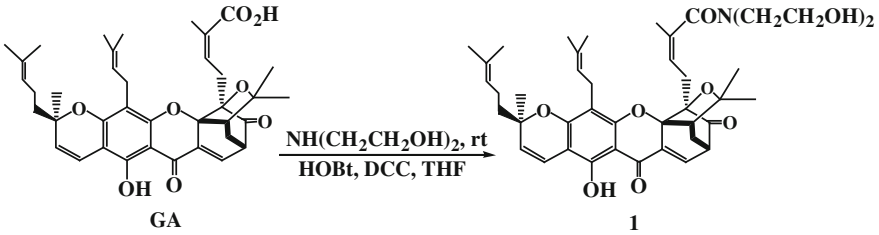

Scheme 161.1 The synthetic route for compound 1

(s, 3H, 40-H), 1.35–1.38 (m, 1H, 21b-H), 1.29–1.33 (m, 3H, 24-H), 1.27 (s, 3H, 19-H). ESI–MS: m/z 717 $[M + 2H]^+$, 715 $[M]^+$.

GA monoester of succinic acid (**2**) was obtained by esterification of GA with methyl succinyl chloride, followed by mild hydrolysis with lithium hydroxide in THF-EtOH-H_2O (as shown in Scheme 161.2) [14].

Compound 2: ^{1}H NMR (CDCl3, 300 MHz) δ: 7.53 (d, J = 6.9 Hz, 1H, 10-H), 6.67 (d, J = 10.2 Hz, 1H, 4-H), 6.12–6.16 (m, 1H, 27-H), 5.38 (d, J = 10.2 Hz, 1H, 3-H), 5.07–5.09 (m, 1H, 37-H), 4.10 (s, CO2CH3), 3.50–3.51 (m, 1H, 11-H), 3.24–3.28 (m, 1H, 31a-H), 3.14–3.18 (m, 1H, 31b-H), 2.98 (d, J = 7.3 Hz, 2H, 26-H), 2.81–2.84 (m, 1H, 32-H), 2.63 [m, 4H, (CH2)2CO2], 2.52 (d, J = 9.0 Hz, 1H, 22-H), 2.32–2.30 (m, 1H, 21a-H), 2.05–2.07 (m, 2H, 36-H), 1.94 (s, 3H, 34-H), 1.76 (s, 3H, 35-H), 1.68 (s, 3H, 29-H), 1.66 (t, J = 8.7 Hz, 2H, 20-H), 1.63 (s, 3H, 39-H), 1.48 (s, 3H, 35-H), 1.42 (s, 3H, 40-H), 1.35–1.38 (m, 1H, 21b-H), 1.29–1.33 (m, 3H, 24-H), 1.27 (s, 3H, 19-H). ESI–MS: m/z 744 $[M + 2H]^+$, 742 $[M]^+$.

Compound 3: ^{1}H NMR (CDCl3, 300 MHz) δ: 11.00 (s, 1H, CO2H), 7.53 (d, J = 6.9 Hz, 1H, 10-H), 6.67 (d, J = 10.2 Hz, 1H, 4-H), 6.12–6.16 (m, 1H, 27-H), 5.38 (d, J = 10.2 Hz, 1H, 3-H), 5.07–5.09 (m, 1H, 37-H), 3.50–3.51 (m, 1H, 11-H), 3.24–3.28 (m, 1H, 31a-H), 3.14–3.18 (m, 1H, 31b-H), 2.98 (d, J = 7.3 Hz, 2H, 26-H), 2.81–2.84 (m, 1H, 32-H), 2.65 [m, 4H, (CH2)2CO2], 2.52 (d, J = 9.0 Hz, 1H, 22-H), 2.32–2.30 (m, 1H, 21a-H), 2.05–2.07 (m, 2H, 36-H), 1.94 (s, 3H, 34-H), 1.76 (s, 3H, 35-H), 1.68 (s, 3H, 29-H), 1.66 (t, J = 8.8 Hz, 2H, 20-H), 1.63 (s, 3H, 39-H), 1.48 (s, 3H, 35-H), 1.42 (s, 3H, 40-H), 1.35–1.38 (m, 1H, 21b-H),

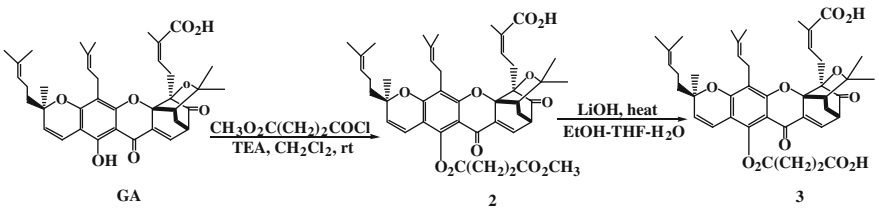

Scheme 161.2 The synthetic route for compound 3

1.29–1.33 (m, 3H, 24-H), 1.27 (s, 3H, 19-H). ESI–MS: m/z 730 $[M + 2H]^+$, 728 $[M]^+$.

The phenolic hydroxyl in GA is not reactive enough to get this monoester from GA's direct reaction with succinic anhydride catalyzed by NaOBu-t.

3.2 GA was stable when dissolved in acetone, acetonitrile, chloroform or dichloromethane, so the latter was chosen as the reaction solvent.

3.3 Usually α, β-unsaturated ketone in GA reacts easily with secondary amines in Michael addition manner. To avoid this side reaction only after more reactive intermediate was formed from GA, DCC, and HOBt, diethanolamine was added in icy water. Derivative **1** was obtained in 76 % of yield, and only small quantity of side product was detected by TLC with petroleum ether-EtOAc (v/v 2:1) as developing solvent.

3.4 Solubility and lipophilicity are among the important factors affecting drugs' absorption, distribution, metabolism, and elimination, destined by their molecular scaffolds and/or side chains apart from pharmacophore. After their chemical structure characterization, both target compounds will be evaluated soon for their expected improved aqueous solubility, absorption, cell membraneous permeability, and inhibitory activity against HCC cell proliferation. The goal of our GA anticancer agent design is to make pharmacodynamics, pharmacokinetics, and physicochemical properties in optimal match. The structure modification on C-30 and C-6 not only increases these derivatives' aqueous solubility, but also may contribute to their antitumor target orientation.

3.5 As one of the most important factors in GA derivatives preparation, reaction temperature is preferred to be controlled at 35 ~ 40 °C, so that reaction rate was accelerated while side reactions or GA degradation at higher temperature was suppressed.

161.4 Conclusion

From gambogic acid its two target derivatives and one intermediate were prepared, and their structures confirmed by ^{1}H NMR and ESI–MS techniques.

Acknowledgments This research was supported by Jining Medicinal College Program for Senior Talents Enrollment, China and the SME Technology Innovation Fund, China (Project No. 10C26211200209).

References

1. Newman DJ, Cragg GM, Snader KM (2003) Natural products as sources of new drugs over the period 1981-2002. J Nat Prod 66:1022–1037
2. Qiang L, Yang Y, You QD et al (2008) Inhibition of glioblastoma growth and angiogenesis by gambogic acid: an in vitro and in vivo study. Biochem Pharmacol 75:1083–1092
3. Qi Q, Gu H, Yang Y et al (2008) Involvement of matrix metalloproteinase 2 and 9 in gambogic acid induced suppression of MDA-MB-435 human breast carcinoma cell lung metastasis. J Mol Med 86:1367–1377
4. Wang X, Chen Y, Han QB et al (2009) Proteomic identification of molecular targets of gambogic acid: role of stathmin in hepatocellular carcinoma. Proteomics 9:242–253
5. Kasibhatla S, Jessen KA, Maliartchouk S et al (2005) A role for transferrin receptor in triggering apoptosis when targeted with gambogic acid. Proc Natl Acad Sci USA 102:12095–12100
6. Pandey MK, Sung B, Ahn KS et al (2007) Gambogic acid, a novel ligand for transferrin receptor, potentiates TNF-induced apoptosis through modulation of the nuclear factor-kappaB signaling pathway. Blood 110:3517–3525
7. Qin Y, Meng L, Hu C et al (2007) Gambogic acid inhibits the catalytic activity of human topoisomerase IIalpha by binding to its ATPase domain. Mol Cancer Ther 6:2429–2440
8. Zhao J, Qi Q, Yang Y et al (2008) Inhibition of alpha(4) integrin mediated adhesion was involved in the reduction of B16-F10 melanoma cells lung colonization in C57BL/6 mice treated with gambogic acid. Eur J Pharmacol 589:127–131
9. Zhou ZT, Wang JW (2007) Phase I human tolerability trial of gambogic acid. Chin J New Drugs 16:79–83
10. Sun Yaoran Mu, Wei Chang Ming (2010) Study on synthesis of monoester succinyl chlorides. J hijiazhuang Univ 12:21–24
11. Hou XF, Chu ZS, Yang Q et al (2012) Synthesis of N-benzyl kurarinol gambogate. Guangzhou Chem Ind 40:85–86
12. Han QB, Cheng SS, Tai J (2005) Stability and cytotoxicity of gambogic acid and its derivative, gambogoic acid. Biol Pharm Bull 28:2335–2337
13. Zhang HZ, Kasibhatla S, Wang Y et al (2004) Discovery, characterization and SAR of gambogic acid as a potent apoptosis inducer by a HTS assay. Bioorg Med Chem 12:309–317
14. Dahiya R, Kumar A, Yadav R (2008) Synthesis and biological activity of peptide derivatives of iodoquinazolinones/nitroimidazoles. Molecules 13:958–976

Chapter 162
Separation and Purification of Hyaluronic Acid from Fermentation Broth

Yunshuang Wang, Jian Zhang and Hao Liu

Abstract The objective of this research was to compare different methods for the separation and purification of hyaluronic acid from *Streptococcus zooepidemicus* ATCC39920 for their ease of use and reliability. The most appropriate conditions of pretreatment stage were heated to 70 °C for 1 h and kept at room temperature for 5 h. The fermented broth was diluted with the equal volume deionized water. Ten milligrams chitosan was slowly added to 1 L of solution with stirring for 30 min, followed by the addition 20 g diatomaceous earth-type filter aid. The mixture was stirring for 1 h. Then, the mixture was filtrated with diatomite, microfiltration (MF) membranes (5 μm in pore diameter), and ultrafiltration (UF) membranes (MWCO 50KD) to achieve the separation stage.The retentate was washed by the equal volume deionized water and when the volume concentration ratio (VCR) reached 4, the UF stage ended. Finally, the purification procedure adopted Sevag process to remove protein. The overall yield of HA could reach 62.53 % and the removal rate of protein could reach 95.22 %.

Keywords Hyaluronic acid · Fermentation broth · Pretreatment process · Separation process

162.1 Introduction

Hyaluronic acid (HA), is a high-molecular weight linear polysaccharide, composed of *D*-glucuronic acid and *N*-acetylglucosamine linked alternately by β-(1-3)- and β-(1-4)-glycosidic bonds. HA is typically found in the connective tissues of animals as well as in the capsules of streptococcal bacteria. The highest content of

Y. Wang · J. Zhang · H. Liu (✉)
Key Laboratory of Industrial Microbiology, Ministry of Education, Tianjin University of Science and Technology, Tianjin 300457, People's Republic of China
e-mail: wys0924@126.com

T.-C. Zhang et al. (eds.), *Proceedings of the 2012 International Conference on Applied Biotechnology (ICAB 2012)*, Lecture Notes in Electrical Engineering 251,
DOI: 10.1007/978-3-642-37925-3_162,

HA is found in rooster combs. Its molecular mass in human normal synovial fluid has been estimated to be 6–7 $\times$ 10^6 and in rheumatoid fluid 3–5 $\times$ 10^6 Dalton [1].

Traditionally, HA has been extracted from bovine eyes and rooster combs [2]. However due to limited tissue sources, risks of viral infection and high cost, HA production from microbial sources through the fermentation process has received increased attention especially when using the gram-positive bacterium *Streptococcus zooepidemicus* [3–7].

The separation and purification of HA involves the precipitation of HA from fermentation broth by repeatedly using large amounts of organic solvents such as ethanol, acetone, isopropanol, etc. [8–12]. However, the process is complicated and time-consuming, which leads to high cost. In order to improve the efficiency of the purification of HA a better understanding of each steps in the purification process is needed.

The purpose of this study was to compare different methods for the separation and purification of HA from *S. zooepidemicus* ATCC39920 for their ease of use and reliability. The yield of HA, the removal of protein and the transmittance of solution has been chosen to evaluate the step of the purification methods. The result presented can be used as a guide for the choice of purification method of HA from fermentation broth.

162.2 Materials and Methods

162.2.1 Bacterial Strain and Media

For the experiment, the broth used was produced by fermentation with *S. zooepidemicus* ATCC39920 (from College of Bioengineering, Tianjin University of Science and Technology).

The medium for seed culture contained (in g L^{-1} distilled water): glucose, 2.5; soy peptone, 3; tryptone, 17; K_2HPO_4, 2.5; NaCl, 5. After inoculum, the medium was incubated at 37 °C in a reciprocal shaker at 200 rpm for 12 h [13].

The production of HA was carried out in a 5 L fermentor (Biostat Aplus, Germany) with a working volume of 3 L. The fermentation medium contained (in g L^{-1} distilled water): sucrose, 50; yeast extract, 3.5; casein peptone, 10; K_2HPO_4, 2; NaCl, 1.5; $MgSO_4{\cdot}7H_2O$, 0.4. The fermentor was operated at 37 °C under shaking conditions at 400 rpm for 28 h at 2 vvm aeration [14].

162.2.2 Methods

162.2.2.1 General Separation and Purification Process

Figure 162.1 shows the general purification process of HA. Generally, the purification process included three steps, pretreatment procedure, separation procedure and purification procedure.

162.2.2.2 Pretreatment Procedure

Three pretreatment procedure including acidification, heating and dilution were treated to compare. Detailed methods see below.

1. Acidification: ① The fermentation broth was adjusted to a pH of about 4.5 with trichloroacetic acid and then rest for 1 h. ② The solution was readjusted to a pH of about 6 with NaOH and then rest for 5 h. ③ The solution was diluted with the equal volume deionized water.
2. Heating process: ① The fermentation broth was heated to 70 °C for 1 h. ② The solution was kept at room temperature for 5 h. ③ The solution was diluted with the equal volume deionized water.
3. Dilution process was that fermentation broth was diluted with the equal volume of deionized water directly.

Then, add 10 mg of chitosan to every 1 L of solution which were treated with three methods with stirring for 30 min. After that, add 20 g of diatomaceous earth-type filter aid to per liter of solutions with stirring for 1 h. The mixture was filtered by buchner funnel and filtrate was carried out with 5 μm in a continuous diafiltration mode. HA was recovered in the permeate solution.

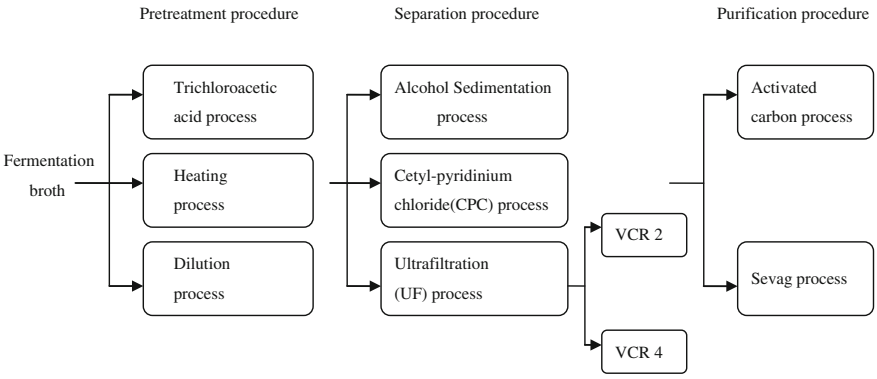

Fig. 162.1 The flow chart of experiment

162.2.2.3 Separation Procedure

The fermentation broth was investigated to determine the suitable operating condition for the good pretreatment process. Then pretreatment fermentation broth was treated, respectively, with alcohol sedimentation, cetyl-pyridinium chloride (CPC), and ultrafiltration (UF).

1. Alcohol sedimentation process: The HA solution was precipitated from the fermentation mixture by addition of 2 volumes of absolute ethanol and the mixture was kept at 4 °C for 1 h. Then the precipitate was separated by centrifugation and redissolved in pure water.
2. Cetylpyridinium chloride process: A 4 % solution of CPC was added to the pretreatment fermentation broth. The amount of CPC added is 2 times in weight than HA and the mixture was kept at 4 °C for 1 h. The precipitated cetylpyridinium salt was separated by centrifugation, and then redissolved in 2 M sodium chloride.
3. Ultrafiltration process: The experimental run was stopped upon achieving the desired volume concentration ratio (VCR). The UF processing used ultrafiltration membranes (MWCO 50KD) with pure water as diafiltrate. The transmembrane pressure (TMP) for UF was determined to be 0.1 MPa under different operation modes. HA product was collected from the retentate of UF. To investigate the effects of different operation modes on the performance of UF, two operation modes were examined, including ① UF stage ended when VCR reached 2. ② The equal volume deionized water was added to the retentate and made VCR reached to 4, after the process of UF was ended.

162.2.2.4 Purification Procedure

Activated charcoal process: The solution was treated with 10 g L^{-1} of activated charcoal and the mixture was shook in a reciprocal shaker at 200 rpm for 3 h.

Sevag process: The solution was treated with a quarter of the volume chloroform-normal butanol (volume ratio is 4:1), and shook fully for 30 min. Then, water phase and organic phase were separated by centrifugation. Water phase was collected and added a quarter of the volume chloroform-normal butanol, repeated many times.

162.2.3 Analytical Methods

The analysis of HA concentration, the raw fermentation broth sample was treated with the equal volume of 0.1 % (w/v) sodium dodecyl sulfate for 10 min to liberate the capsular HA and to facilitate the separation of the cells [15]. After the

cells were removed by High speed refrigerated centrifuge (CR 22G, Hitachi, Japan) at 12,000 rpm for 15 min, the supernatant was then subjected to HA precipitation by mixing it with three volumes of ethanol. The precipitate was collected by centrifugation at 5,000 rpm for 15 min, redissolved in deionized water, and analyzed for the HA concentration by the method of Bitter and Muir [16]. The optical density was measured at 530 nm by spectrophotometer (TU-1810, Purkinje General, China) with D-glucuronic acid used as the standard.

The concentration of protein was measured by the Bradford protein assay using BSA (bovine serum albumin) as standard.

The transmittance of solution was determined by spectrophotometer at 600 nm, and the transmittance of pure water was 100.

162.2.4 Calculation Methods

162.2.4.1 Symbol Meaning

C_0 HA concentration in raw fermentation broth (g L^{-1})
$C_{i,HA}$ HA concentration in treated fermentation broth (g L^{-1})
C_p Protein concentration in raw fermentation broth (μg mL^{-1})
$C_{i,p}$ Protein concentration in treated fermentation broth (μg mL^{-1})
V_o Raw fermentation broth volume (mL)
V_i Treated fermentation broth volume (mL)
Y_i The yield of HA in different processes
R_i The removal of protein in different processes

162.2.4.2 Equations

During the experiments, the yield of HA in different processes was calculated by using the following equations.

$$Y_i = \frac{C_{i,HA} \times V_i}{C_o \times V_o} \times 100\,\% \tag{1}$$

The removal of protein in different processes:

$$R_i = \frac{C_p \times V_o - C_{i,p} \times V_i}{C_p \times V_o} \times 100\,\% \tag{2}$$

162.3 Results and Discussion

162.3.1 Comparison of Different Pretreatment Procedures

Sterilization and degerming were considered first in the downstream process. In this section, the study compared the removal of protein impurities, the transmittance of solution at 600 nm, and the yield of HA after fermentation broth was treated with three pretreatment procedure methods. The data was shown in Table 162.1.

As can be seen in Table 162.1, trichloroacetic acid process should be eliminated due to its low yield of HA (69.59 %). The yield of HA (92.46 %) by heating process was the highest in three pretreatment processes. What's more, heating process had an obvious advantage on the transmittance of solution when compared with dilution process. Moreover, heating process without adding other substances will not contaminate environment potentially and lead to low cost. Therefore, heating process was more suitable for the pretreatment procedure.

162.3.2 Separation Procedures

The separation and purification of HA is one of the keys in HA production, and the method of separation and purification not only affect the quality of products, but also the cost of production. In this section, after fermentation broth was treated with three separation procedure methods, the removal of protein impurities, the transmittance of solution, and the yield of HA were determined. The data was shown in Table 162.2.

The experimental data of separation procedure under the four conditions were shown in Table 162.2. The CPC process and alcohol sedimentation process were lower than UF process in the content of HA. In UF process, the VCR 4 process showed higher the yield of HA and the removal of protein about 7.78 % and 39.87 % than the VCR 2 process, respectively. In addition, the transmittance of the solution of the VCR 4 process was higher, which showed lower impurity and pigment. In order to realize high degrees of yield and purification during HA

Table 162.1 The comparison of three pretreatment procedures

Operating mode	HA		Protein		T_{600nm}
	$C_{i,HA}$	Y_i	$C_{i,p}$	R_i	
Raw fermentation broth	4.11	100	3.16	0	41.52
Trichloroacetic acid process	2.86	69.59	2.32	26.58	92.88
Heating process	3.80	92.46	2.96	6.33	94.13
Dilution process	3.34	81.27	3.04	3.80	69.63

Table 162.2 The comparison of three methods for separation procedure

Operating mode		HA		Protein		T_{600nm}
		$C_{i,HA}$	Y_i	$C_{i,p}$	R_i	
Raw fermentation broth		4.11	100	3.16	0	41.52
Alcohol sedimentation process		1.50	36.50	1.87	40.82	96.26
Cetylpyridinium chloride (CPC) process		1.85	45.01	1.2	62.03	13.95
Ultrafiltration (UF) process	VCR 2	2.53	61.56	2.5	20.89	95.57
	VCR 4	2.85	69.34	1.24	60.76	97.25

Table 162.3 The comparison of two methods for purification procedure

Operating mode	HA		Protein		T_{600nm}
	$C_{i,HA}$	Y_i	$C_{i,p}$	R_i	
Raw fermentation broth	4.11	100	3.16	0	41.52
Activated charcoal process	2.41	58.64	0.222	92.97	68.46
Sevag process	2.57	62.53	0.151	95.22	99.13

separation, the VCR 4 process was adopted to effectively recover HA and washed out more small soluble molecules.

162.3.3 Purification Procedures

In this section, the main objective was to remove protein. The data of the two different methods were shown in Table 162.3.

As shown in Table 162.3, Sevag process had an obvious advantage of higher transmittance at 600 nm. What's more, the yield of HA (62.53 %) and the removal of protein (95.22 %) by Sevag process was slightly lower than the activated charcoal process, which were 58.64 % and 92.97 %, respectively. Therefore, Sevag process was more favorable to purification procedure.

162.4 Conclusions

The optimal procedure for purification was as follows: the fermentation broth was heated for 1 h at 70 °C and then kept at room temperature for 5 h and diluted with the equal volume deionized water. Ten milligrams of chitosan per liter of solution were added slowly to the fermentation broth by stirring for 30 min, 20 g L^{-1} of diatomaceous earth-type filter aid were added to the solution with stirring for 1 h. The mixture was filtered by buchner funnel and the filtrate was carried out with 5 μm in a continuous diafiltration mode. Then the filtrate used UF and the retentate

was washed with the equal volume of deionized water. The UF process did not finish until VCR was four. Finally, the Sevag process was used to remove protein in the purification procedure. The overall yield of HA could reach 62.53% and the overall removal rate of protein could reach 95.22 %.

Acknowledgments This work was supported by 7th Singapore–China JRP (no. 2011DFA31280), the Nation Science Foundation of China (no. 31101275), and a research grant (no. 20100207) from Tianjin University of Science and Technology, China.

References

1. Torvard C, Laurent U, Laurent BG et al (1996) The structure and function of hyaluronan: an overview. Immunol Cell Biol 74:A1–A7
2. Schiraldi C, Gatta AL, Rosa MD (2010) Biotechnological production and application of hyaluronan. Biopolymers 20:387–412
3. Huang WC, Chen TL, Wu WT (2010) Process for purifying medical grade hyaluronic acid. US20100137579A1
4. Ellwood DC, Evans CGT, Dunn GM et al (1995) Production of hyaluronic acid. US005411874
5. Romeo A, Lorenzi S, Padua (1996) Procedure for the purification of hyaluronic acid and fraction of pure hyaluronic acid for ophthalmic use. US005559104A
6. Miyamori T, Numazawa R, Sakimae A et al (1989) Method of producing hyaluronic acid. US4885244
7. Silhankova L, Demnerova K, Kralova B et al (1992) Hyaluronic acid preparation by fermentation of mutant strain of Streptococcus zooepidemicus. CS8904067-A2
8. Kendall FE, Heidelberger M, Dawson MH (1937) A serologically inactive polysaccharide elaborated by mucoid strains of group A hemolytic streptococcus. J Biol Chem 118:61
9. Cifonelli JA, Mayeda M (1957) The purificstion hyaluronic acid by the use of carcoal. Acta Bioch Bioph Sin 24:397–400
10. Brain MD, Esq M, O'Connell et al (2002) Method for purifying high molecular weight hyaluronic acid. US2002/0120132 A1
11. Stock AH, Lynn RJ (1961) Preparation and properties of partially purified erythrogenic toxin B of group A streptococci. J Immunol 86:561–566
12. Thonard JC, Migliore SA, Blustein R (1964) Isolation of hyaluronic acid from broth cultures of streptococci. J Biol Chem 239(3):726–728
13. Chen SJ, Chen JL, Huang WC et al (2009) Fermentation process development for hyaluronic acid production by *Streptococcus zooepidemicus* ATCC 39920. Korean J Chem Eng 26(2):428–432
14. Rangaswamy V, Jain D (2008) An efficient process for production and purification of hyaluronic acid from *Streptococcus equi* subsp. *zooepidemicus*. Biotechnol Lett 30:493–496
15. Chong BF, Nielsen LK (2003) Aerobic cultivation of *Streptococcus zooepidemicus* and the role of NADH oxidase. Biochem Eng J, pp 153–162
16. Bitter T, Muir HM (1962) A modified uronic acid carbazole reaction. Anal Biochem 4:330–334

Chapter 163
In Vitro Cytotoxicity of the Bile Acids and Bile Acid Derivatives

Xiangzheng Hu, Hongjian Zhou, Guangzhen Song, Anjun Liu and Lixia Wang

Abstract Polymeric dental resin materials are known to leach cytotoxic unreacted monomers and degradation products. In this study, methacrylic derivatives of bile acids have been synthesized for use as monomers in dental composites, their in vitro cytotoxicity and bile acids toward NIH3T3 fibroblasts has been evaluated by colorimetric MTT assay and compared with that of the common dental monomers BisGMA and TEGDMA. The results show that bile acids and their derivatives can induce mitochondrial dysfunction at similar or higher concentrations than the commercial dental monomers. Certain monomers did not influence colorimetric absorbance in MTT assay against the normal control over their entire range of solubility.

Keywords Bile acid derivative · Cytotoxicity · MTT colorimetric method · Synthesis

163.1 Introduction

Biocompatibility is one of important problems that should be considered for the preparation and use of biomaterials. The use of compounds of natural origin offers the advantage of improved biocompatibility. Bile acids (cholic acid, chenodeoxycholic acid, deoxycholic acid, and ursodeoxycholic acid, etc) and their derivatives are currently used for biomedical and biomaterial applications [1, 2].

X. Hu · H. Zhou · G. Song · A. Liu · L. Wang
College of Food Engineering and Biotechnology, Tianjin University of Science and Technology, Tianjin 300457, People's Republic of China

X. Hu (✉)
College of Science, Tianjin University of Science and Technology, Tianjin 300457, People's Republic of China
e-mail: huxzh@tust.edu.cn

T.-C. Zhang et al. (eds.), *Proceedings of the 2012 International Conference on Applied Biotechnology (ICAB 2012)*, Lecture Notes in Electrical Engineering 251,
DOI: 10.1007/978-3-642-37925-3_163,

Methacrylate monomers derived from bile acids have been proposed as monomers for composite dental fillings [3, 4]. Polymeric biomaterials with bile acid groups have attracted significant attention because their degradation is expected to lead to the release of endogenous compounds and to improve their physical properties [4–7]. The objective of this study is to evaluate the in vitro cytotoxicity of bile acids as well as their (meth)acrylate derivatives. This study places particular emphasis on comparing the cytotoxicity of these compounds to the common dental monomers 2,2-bis(4-(2-hydroxy-3-meth-acryloxypropoxy) phenyl)propane (Bis-GMA) and triethylglycol dimethacrylate (TEGDMA). The structures of all the compounds are listed in Fig. 163.1.

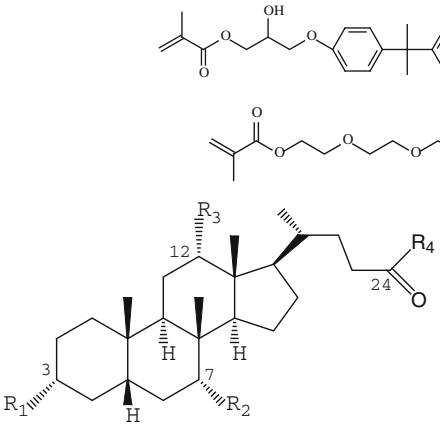

	R1	R2	R3	R4
3	HO^-	HO^-	HO^-	HO^-
4	HO^-	HO^-	H^-	HO^-
5	HO^-	¦ÂHO$^-$	H^-	HO^-
6	HO^-	H^-	HO^-	HO^-
7	HO^-	H^-	H^-	HO^-
8	HO^-	HO^-	HO^-	H_3CO^-
9	MO^-	HO^-	HO^-	H_3CO^-
10	MO^-	HO^-	MO^-	H_3CO^-
11	MO^-	MO^-	MO^-	H_3CO^-
12	HO^-	HO^-	HO^-	$HOCH_2CH_2O^-$
13	HO^-	HO^-	HO^-	$MOCH_2CH_2O^-$
14	MO^-	HO^-	HO^-	$MOCH_2CH_2O^-$
15	MO^-	HO^-	MO^-	$MOCH_2CH_2O^-$
16	MO^-	MO^-	MO^-	$MOCH_2CH_2O^-$
17	HO^-	HO^-	HO^-	$HO(CH_2)_4O^-$
18	HO^-	HO^-	HO^-	$HO(CH_2)_6O^-$
19	HO^-	HO^-	HO^-	$CH_3CH_2O^-$
20	HO^-	HO^-	HO^-	$CH_3(CH_2)_3O^-$
21	MO^-	HO^-	SO^-	$MOCH_2CH_2O^-$

Fig. 163.1 Chemical structures of the commercial monomers, bile acids, and bile acid derivatives

163.2 Materials and Methods

163.2.1 Materials and Equipments

Cholic acid was purchased from (An hui Kebao Company, China), Chenodeoxycholic acid, ursodeoxycholic acid, deoxycholic acid, lithocholic acid were prepared in our laboratory. BisGMA,TEGDMA were purchased from PolyScience (PolyScience Company, USA). 3-(4,5-dimethyl-2-thiazoly)-2,5-diphenyl-2H tetrazolium bromide(MTT) was obtained from Sigma (Sigma Chemical Company, USA). Dimethy l sulfoxide (DMSO) was from Amresco (Amresco Company, USA). Dolbecco's modification of Eagle's Medium (DMEM), EDTA- trypsin,penicillin and streptomycin,Hanks-balanced salt solution,fetal bovine serum were purchased from Gibco (Gibco Company, USA). Other regents and solvents were purchased from Tianjin Chemicals Company, China. Methacryloyl chloride (MAC) was prepared from methacrylic acid and benzoyl chloride. The solvents were all redistilled prior to use.

Cell strain: Mouse fibroblast cell line NIH3T3 was received from College of Biotechnology of Tianjin University of Science and Technology as a gift.

ELISA instrument (Bio-Rad Laboratories, USA), pipettes (Thermo Electron Corporation, USA), inverted phase contrast microscope (Nikon Corporation, Japan), BCM-1000A biological clean bench (Air tech Company, China), 2123TC water-jacketed CO_2 incubator (Shellab, USA). NMR spectra were recorded at 23 °C on a Bruker AMX-400 operating at 400.13 MHz for ^1H in deuterochloroform, which also served as an internal reference.

163.2.2 Synthesis of Bile Acid Derivatives

(1) Compounds 8–18 were synthesized according to the procedure published in literature [5–7].

(2) Synthesis of 19

This compound was synthesized with modified procedure from literature [5]. A solution of cholic acid (10.0 g) in 100 mL ethanol was acidified with concentrated hydrochloric acid to keep pH 3–4. The mixture was stirred at approximately 60 °C for 5 h and then was poured into 150 mL cool water to precipitate the solid. The product was filtered and washed with water, 5 % Na_2CO_3 aqueous solution and water. The product was obtained by recrystallization from ethyl acetate and got white powder solid 8.9 g, yield:89 %. m.p.: 161.4–162.7 °C. IR(cm^{-1}): 3337.9, 2938.9, 2859.7, 1738.6, 1445.5, 1375.7, 1256.0, 1179.5, 1089.5, 1044.2, 980.2, 910.1. ^1H NMR(400.13 MHz,$CDCl_3$):δ/ppm = 0.72 (s, 3H, 18-H_3), 0. 92 (s, 3H, 19-H_3), 1.00 (d, 3H, 21-H_3), 3.49 (m, 1H, 3α-H), 3.88 (s, 1H, 7α-H), 4.01 (s, 1H, 12α-H), 4.15 (s, 3H, $COOCH_2C\underline{H}_3$), 4.17 (s, 2H, $COOC\underline{H}_2CH_3$).

(3) Synthesis of 20

Compound 20 was synthesized with the same procedure as described for 19, with n-butyl alcohol instead ethanol.yield:82 %. m.p.: 132.7–133.4 °C. IR(cm^{-1}): 3399.7, 2936.2, 2867.8, 1735.8, 1465.9, 1377.2, 1251.1, 1180.0, 1078.8, 1046.0, 980.9, 913.1. ^{1}H NMR(400.13 MHz,$CDCl_3$):δ/ppm = 0.72 (s, 3H, 18-H_3), 0. 93 (d, 3H, 19-H_3), 1.01 (d, 3H, 21-H_3), 3.48 (m, 1H, 3α-H), 3.88 (s, 1H, 7α-H), 4.01 (s, 1H, 12α-H), 4.09 (s, 6H, $COO(C\underline{H}_2)_3CH_3$).

(4) Synthesis of 21

To an ice-cooled vigorous-stirred solution of 14(1.0 g, 1.70 mmol) in dry $CHCl_2$(25 mL), with 4-dimethylaminopyridine (DMAP, 0.08 g, 0.65 mmol) as catalyst and Et_3N (0.5 g, 4.81 mmol), methanesulfonyl chloride (0.58 g, 5.10 mmol) in $CHCl_2$ (10 mL) is slowly added dropwise under nitrogen atmosphere. The mixture was ice-cooled for 0.5 h, then left at room temperature for 24 h. The mixture was washed successively with brine, 5 % aqueous $NaHCO_3$ and brine. After drying the organic layer over anhydrous Mg_2SO_4 and evaporating the solvent under reduced pressure, the crude product was purified by column chromatography (silica gel, ethylacetate/petroleum ether = 2/1, ethylacetate, ethylacetate/ethanol = 10/1 as the eluent). IR(cm^{-1}): 3548.6, 3103.7, 2956.3, 2874.6, 1888.5, 1735.6, 1637.1, 1451.7, 1375.7, 1247.0, 1174.6, 1042.6, 961.8, 916.8. ^{1}H NMR(400.13 MHz, $CDCl_3$):δ/ppm = 0.60 (s, 3H, 18-H_3), 0. 88 (s, 3H, 19-H_3), 1.00 (d, 3H, 21-H_3), 1.93 (s, 3H, $C(C\underline{H}_3) = CH_2$), 1.97 (s, 3H, $C(C\underline{H}_3) = CH_2$), 2.42(s, 3H, $OSO_2C\underline{H}_3$), 4.10 (s, 1H, 7α-H), 4.36 (s, 4H, $COOC\underline{H}_2C\underline{H}_2OCO$), 4.79 (d, 1H, 3$\alpha$-H), 5.14(d, 1H, 12$\alpha$-H), 5.53 (s, 1H, $C(CH_3) = C\underline{H}$), 5.62 (s, 1H, $C(CH_3) = C\underline{H}$), 6.10 (s, 1H, $C(CH_3) = C\underline{H}$), 6.16 (s, 1H, $C(CH_3) = C\underline{H}$); MS: m/z = 666.24(M^+).

163.2.3 Cytotoxicity Test

Cytotoxicity of the molecules was measured by the 3-(4,5-dimethyl-2-thiazoly)-2,5-diphenyl-2H tetrazolium bromide (MTT) assay using NIH3T3 fibroblasts. These molecules were initially dissolved in DMSO which served as carrier for distribution into the wells and then diluted in cell culture medium. The cells (1×10^4/well) were maintained in Dulbecco's modified Eagle's medium (DMEM) supplemented with 10 vol % fetal bovine serum (FBS),100 U/ml penicillin and 100 μg/ml streptomycin. Monolayers of exponentially growing NIH3T3 fibroblasts were then incubated in the 96-well plate with the individual molecule to be tested at 37 °C in a humidified atmosphere of 5 % CO_2 for 24 h. The concentration of DMSO was always 1 vol % of the total volume of culture medium. Cells treated with 1 vol % DMSO served as controls. After removing the medium, cells were washed with phosphate-buffered saline (PBS), then 20 μl of MTT solution (5 mg of MTT/ml PBS) were added to each well. After 4 h of incubation,

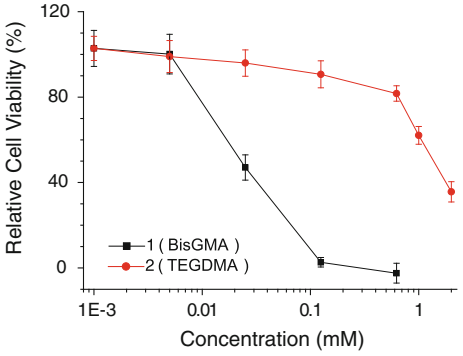

Fig. 163.2 Dose-response profiles obtained for the commercialmonomers Bis-GMA and TEGDMA

200 μl DMSO was added to each well to dissolve the reduced MTT. The optical densities of formazan production were measured at 490 nm. All experiments were performed in triplicate. Relative cell viability at each concentration and for each analyte was measured fifteen times (three times each on five different microplates). The IC_{50} value was obtained from the dose-response curves shown in Figs. 163.2, 163.3, 163.4, 163.5, 163.6, 163.7.

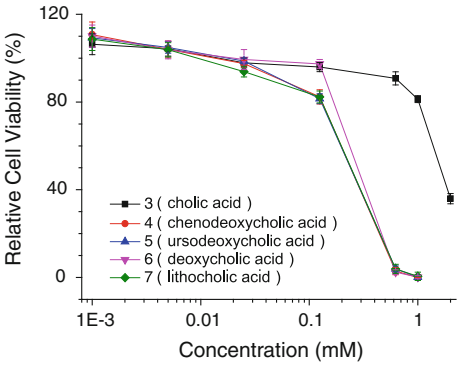

Fig. 163.3 Dose-response profiles of bile acids

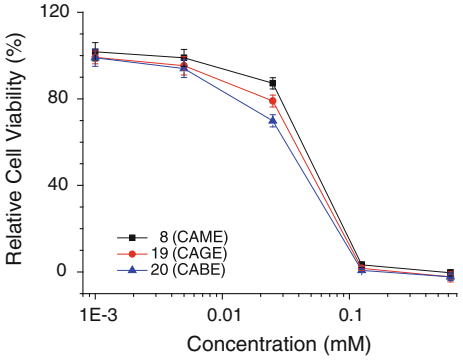

Fig. 163.4 Dose-response profiles of bile acid esters (methyl, ethyl, and butyl esters)

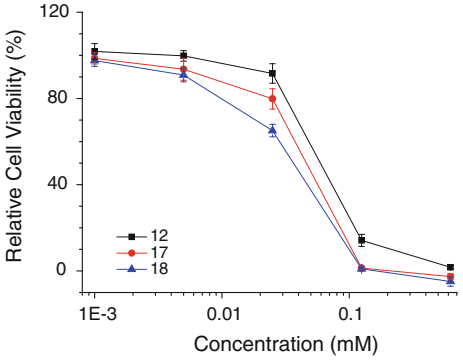

Fig. 163.5 Dose-response profiles of bile acid esters (ethylene glycol, butanediol, hexanediol esters)

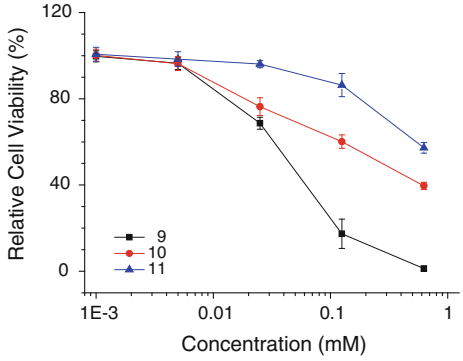

Fig. 163.6 Dose-response profiles of methyl cholate with mono-, di-, tri-methacrylate

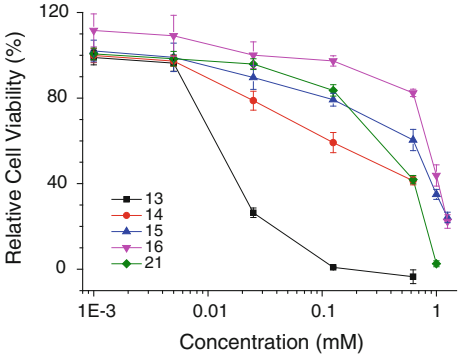

Fig. 163.7 Dose-response profiles of 2′-Hydroxyethyl cholate mono-, di-, tri-, tetra-methacrylate, and mono-methylsulfonyl

Statistical comparison of IC_{50} values was performed by one-way ANOVA followed by pairwise comparison of means using Dunnett's T3 post hoc test, with the use of SPSS 19.0 software.

163.3 Results and Discussion

Two types of cells can be used for in vitro cytotoxicity test: primary cell lines (such as pulp tissue fibroblasts and gingival tissue fibroblast) and built cell lines (such as of L929, 3T3, and cancer cells, etc.). Previous results showed that there was no obvious difference between primary gingival tissue fibroblasts and L-929 cells for cytotoxicity test [8]. In vitro cytotoxicity assay, dental pulp cells were more sensitive to dimethyl acrylic resin than odontoblasts [9].

NIH3T3 fibroblasts were exposed to increasing concentrations of the molecules, and the cytotoxic activities were analyzed by MTT. Cell line and cytotoxicity assay were selected based on their extensive precedence for evaluating the cytotoxicity [10, 11]. All molecules exhibited a dose-dependent effect, dose-response profiles were measured for each analyte (Figs. 163.2, 163.3, 163.4, 163.5, 163.6, 163.7), and the results of those cytotoxicities indicated by IC_{50} (concentration which inhibited 50 % cell growth relative to the controls). The results of these assays are presented in Table 163.1. The IC_{50} values of commercial monomers BisGMA and TEGDMA has been reported in previous literature [7, 12–14].

163.3.1 Cytotoxicity of Bile Acids and Bile Acid Alcohol Esters

The cytotoxicity of bile acids can induce hepatocyte death. The reduction of relative cell viability is depending on bile acid concentration. Bile acids accumulation in the liver during cholestasis is believed to be the reason of hepatocellular necrosis and apoptosis in part through induction of mitochondrial

Table 163.1 Comparison of the cytotoxicity (IC_{50})

Compound	IC_{50} (mM)	Compound	IC_{50} (mM)
1(BisGMA)	0.025 ± 0.002^{i}	13	0.017 ± 0.001^{j}
2(TEGDMA)	1.462 ± 0.076^{b}	14	$0.280 \pm 0.048^{d,e}$
3(cholic acid)	1.720 ± 0.071^{a}	15	>1
4(chenodeoxycholic acid)	0.216 ± 0.016^{e}	16	>1
5(ursodeoxycholic acid)	0.216 ± 0.011^{e}	17	0.041 ± 0.002^{g}
6(deoxycholic acid)	0.231 ± 0.010^{e}	18	0.033 ± 0.001^{h}
7(lithocholic acid)	0.232 ± 0.021^{e}	19	$0.041 \pm 0.002^{g,h}$
8	0.048 ± 0.004^{g}	20	0.034 ± 0.001^{h}
9	$0.046 \pm 0.007^{g,h,i}$	21	0.385 ± 0.009^{d}
10	0.262 ± 0.034^{e}		
11	0.648 ± 0.009^{c}		
12	0.066 ± 0.005^{f}		

All values displayed as mean ± S.D. Superscript letters denote equivalent means determined by pairwise comparison (Dunnett T3, $p < 0.05$

permeability transition (MPT) and mitochondrial generation of oxidative stress [15–20].

Bile acids, include chenodeoxycholic acid, ursodeoxycholic acid, deoxycholic acid, lithocholic acid have lower cytotoxicity than their ester derivatives (Figs. 163.3, 163.4). Cholic acid has much lower cytotoxicity than chenodeoxycholic acid, ursodeoxycholic acid, deoxycholic acid, and lithocholic acid (Fig. 163.3), which proved that the natural products have better cell compatibility. The cytotoxicity of bile acid esters became higher with their molecular weight increasing (Figs. 163.4, 163.5).

163.3.2 Cytotoxicity of Bile Acid Ester Derivatives

The cholic acid derivative 9 have similar cytotoxicity as its precursor 8, the cytotoxicity of 13 was higher than its precursor 12 and commercial monomers BisGMA(1). These seemingly contradictory trends are an indication that the mechanism of mitochondrial dysfunction caused by bile acids is relatively structure specific and modifications on different positions of these compounds may influence cytotoxicity. The cytotoxicity of bile acid esters derivatives became lower with the methacrylate group increasing (Figs. 163.6, 163.7). Especially, 15 and 16 even have not exhibited any cytotoxic response over their range of solubility. Figure 163.7 shows that the cytotoxicity of 15 (methacrylate on position 12) was higher than 21 (mesylate on position 12), which indicates that different reactive groups in the same reaction site of the steroidal backbone can lead to different cytotoxicity.

163.3.3 Synthesis of Bile Acid Derivatives

Literature reported that the reactive activity of three hydroxyl groups on bile acid steroidal skeleton is C3 > C12 > C7 [5]. Compounds 8–18 were synthesized by the use of a procedure as described in the literature. Compound 21 was synthesized

Table 163.2 Effect on productivity of feeding ratio between sulfonyl chloride and compound 14

N(sulfoyl chloride/14)	Response time/h	Yield/%
1.5	12	45–55
1.5	24	45–55
2.5	12	65–75
2.5	24	65–75
3.5	12	40–50
3.5	24	40–50
4.5	12	<10

by the use of a procedure as front description. Reaction conditions in Table 163.2 were used, the results are shown in Table 163.2 . Table 163.2 shows that 21 can be obtained by controlling the ratio of sulfonyl chloride and compound 14.

163.4 Conclusion

Cholic acid derivatives with di-, tri-, and tetra-methacrylate groups indicate lower cytotoxicity than the commercial dental monomers BisGMA, and higher cytotoxicity than diluent TEGDMA. Especially, cholic acid derivative with tri-, tetra-methacrylate group did not affect cell viability over their entire range of solubility. The mono-methacrylate derivative of bile acid with methacrylate group on C3 position has comparable cytotoxicity to BisGMA, while mono-methacrylate derivative of bile acid with methacrylate group on position 24 has higher cytotoxicity than BisGMA. Methyl sulfonyl could reduce the cytotoxicity, and its effect is more obvious than methyl acryloyl. The cholic acid is significantly less cytotoxic than other natural bile acids and BisGMA,TEGDMA. These results verify the feasibility and safety of polymeric materials based on bile acid derivatives for biomedical applications. However, it is also necessary to perform more extensive evaluation of the mechanism underlying cell lysis and the exact nature of the biodegradation compounds produced for these molecules.

Acknowledgments Financial support from the Science and Technology Project of Tianjin (No. 10JCZDJC22500, ZXCXSY10100) is gratefully acknowledged.

References

1. Virtanen E, Kolehmainen E (2004) Use of bile acids in pharmacological and supramolecular applications. Eur J Org Chem 16:3385–3399
2. Denike JK (1994) Preparation of new polymers from bile acid derivatives. Macromol Rapid Commun 15:459–465
3. Zhu XX, Nichifor M (2002) Polymeric materials containing bile acids. Acc Chem Res 35:539–546
4. Gouin S, Zhu XX, Lehnert S (2000) New polyanhydrides made from a bile acid dimer and sebacic acid: synthesis, characterization, and degradation. Macromolecules 33:5379–5383
5. Hu X, Zhang X, Wang Z et al (2005) Swelling and wettability of light-cured methacrylate-based dental resins prepared from cholic acid. Chin J React Polym 14:35–43
6. Hu X, Zhang Z, Zhang X et al (2005) Selective acylation of cholic acid derivatives with multiple methacrylate groups. Steroids 70:531–537
7. Gauthier MA, Simard P, Zhang Z et al (2007) Bile acids as constituents for dental composites: in vitro cytotoxicity of (meth)acrylate and other ester derivatives of bile acids. J R Soc Interface 4:1145–1150
8. Franz AKF, Skolka A (2007) Cytotoxicity of resin composites as a function of interface area. Dent Mater 23:1438–1446

9. Bolande JMM, Carnesd L (2006) In vitro cytotoxicity of a remineralizing resin-based calcium phosphate cement. Dent Mater 22:338–345
10. Issa Y, Watts DC, Brunton PA et al (2004) Resin composite monomers alter MTT and LDH activity of human gingival fibroblasts in vitro. Dent Mater 20:12–20
11. Al-Hiyasat AS, Darmani H, Milhem MM (2005) Cytotoxicity evaluation of dental resin composites and their flowable derivatives. Clin Oral Investig 9:21–25
12. Stanislawski L, Lefeuvre M, Bourd K et al (2003) TEGDMA-induced toxicity in human fibroblasts is associated with early and drastic glutathione depletion with subsequent production of oxygen reactive species. J Biomed Mater Res, Part A 66:476–482
13. Geurtsen W, Lehmann F, Spahl W et al (1998) Cytotoxicity of 35 dental resin composite monomers/additives in permanent 3T3 and three human primary fibroblast cultures. J Biomed Mater Res 41:474–480
14. Emmler J, Seiss M, Kreppel H et al (2008) Cytotoxicity of the dental composite component TEGDMA and selected metabolic by-products in human pulmonary cells. Dent Mater 24:1670–1675
15. Rolo AP, Oliveira PJ, Moreno AJ et al (2000) Bile acids affect liver mitochondrial bioenergetics: possible relevance for cholestasis therapy. Toxicol Sci 57:177–185
16. Rolo AP, Oliveira PJ, Moreno AJM et al (2001) Chenodeoxycholate is a potent inducer of the permeability transition pore in rat liver mitochondria. Biosci Rep 21:73–80
17. Rolo AP, Palmeira CM, Holy JM et al (2004) Role of mitochondrial dysfunction in combined bile acid-induced cytotoxicity: the switch between apoptosis and necrosis. Toxicol Sci 79:196–204
18. Boland EJ, MacDougall M, Carnes DL et al (2006) In vitro cytotoxicity of a remineralizing resin-based calcium phosphate cement. Dent Mater 22:338–345
19. Ceryak S, Bouscarel B, Malavolti M et al (1998) Extrahepatic deposition and cytotoxicity of lithocholic acid: studies in two hamster models of hepatic failure and in cultured human fibroblasts. Hepatology 27:546–556
20. Sokol RJ, Dahl R, Devereaux MW et al (2005) Human hepatic mitochondria generate reactive oxygen species and undergo the permeability transition in response to hydrophobic bile acids. J Pediatr Gastroenterol Nutr 41:235–243

Chapter 164
Studying on Extraction of Betulin from the White Birch and Synthesis of Betulinic Acid

Tong-Cun Zhang, Weiwei Xu, Nan Wang, Xuegang Luo, Jing Wang and Xiangzheng Hu

Abstract Betulin and betulinic acid are natural product with antitumor and anti-HIV-1 activity. Betulin can be got by chemical extraction from a lot of plants. Betulinic acid can be synthesized from betulin. In order to get high biological activity compounds with antitumor and anti-HIV-1 activity from the bark of the white birch, the extraction and purification method of betulin was studied; the optimized extraction and purification condition was obtained. The two-step synthetic routes of betulinic acid from betulin were discussed. Betulinic acid was synthesized by oxidizing betulin with Jones reagent, followed by selective reduction with $NaBH_4$. IR, HPLC–MS, H^1-NMR were used to identify the structure of betulin and betulinic acid.

Keywords Betulin · Extraction · Betulinic acid · Synthesis

164.1 Introduction

Cancer and AIDS have been the most important diseases leading to death nowadays. But most of the commonly used medicines of anti-HIV or anticancer are proved to have many limitations in clinical application, especially toxic side effect and drug-resistance. Therefore, the development of medicine with perfect anticancer and anti-HIV effect is needed.

T.-C. Zhang · W. Xu · N. Wang · X. Luo · J. Wang · X. Hu (✉)
College of Biological Engineering, Tianjin University of Science and Technology, Tianjin 300457, People's Republic of China
e-mail: huxzh@tust.edu.cn

X. Hu
College of Science, Tianjin University of Science and Technology, Tianjin 300457, People's Republic of China

T.-C. Zhang et al. (eds.), *Proceedings of the 2012 International Conference on Applied Biotechnology (ICAB 2012)*, Lecture Notes in Electrical Engineering 251,
DOI: 10.1007/978-3-642-37925-3_164,

Betulin exists in various plant resources, especially in the white birch bark. Betulin is a kind of bioactive substance with diverse biological activities, such as anti-inflammatory, antitumor, anti-HIV [1], which can be widely applied in food, cosmetic, and pharmaceutical fields. Betulin, as an important intermediate of medicine, can be obtained by extraction with organic solvent from the white birch bark [2].

Betulinic acid has antitumor, anti-HIV-1 and anti-inflammatory activities [3, 4], especially has an excellent effect on melanoma. As a potential precursor medicine of antitumor or anti-HIV, it has drawn the attention of researchers and investors. Betulin and betulinic acid have become a hotspot because of their excellent biological properties and good selectivity, low toxicity, and less side effects [5–8].

164.2 Materials and Methods

164.2.1 Materials, Reagents, Instruments

The white birch bark was collected in summer, Heilongjiang Province (2008–2009), in China. The birch bark was shattered to 60 meshes and immediately dried at 60 °C and stored in a dry and dark place.

Methanol, acetonitrile, ethanol, methanol, chloroform (Chl.), isopropyl alcohol (IPA), petroleum ether (B.P.: 60–90 °C, PE), ethyl acetate (EA), tetrahydrofuran (THF), and $NaBH_4$ are all of analytical grade.

H^1-NMR spectra are recorded on Bruker AM-400 NMR spectrometer in deuterated chloroform. HPLC spectra are recorded on Hitachi D–2000 spectrometers with UV detector. And Mass Detector is Waters 3,100; IR spectrometer is PerkinElmer spectrum65.

164.2.2 Methods

164.2.2.1 The Extraction and Purification of Betulin

The birch bark (100 g) with ethanol/IPA (10/1, V/V, 1,100 mL) was refluxed for 6 h in a Soxhlet's extractor; solvent was kept overnight at 0 °C. The precipitate was separated by filtration, washed on the filter with cold ethanol and then dried in vacuum drying oven.

In order to determine the optimum purification conditions for betulin, the solvents (A), solid–liquid ratio (B), and recrystallization times (C) were evaluated. And in every factor, we have chosen 3 levels to take the orthogonal design test (Table 164.1). Record every yield of crystal and determine the purity of betulin.

Table 164.1 Levels and factors in orthogonal design test of extraction of betulin

Level	Factor		
	A	B (V/V)	C
1	IPA/PE (10/1,V/V)	1/20	1
2	Chl./Methanol (1/1,V/V)	1/30	2
3	IPA/Methanol (3/1,V/V)	1/40	3

The optimal recrystallization process was determined based on both the yield of crystal (40 %) and the purity of betulin (60 %) as the combined value.

164.2.2.2 Synthesis and Purification of Betulinic Acid

A. Synthesis and Purification of Betulonic Acid

Freshly prepared Jones solution (2.3 mL) was added to a solution with betulin (1.0 g, 2.26 mmol) in acetone (100 mL) at 0 °C and the mixture were stirred at 0 °C. The course of the reaction was confirmed by TLC. After the reaction, the solvent was quenched with methanol (25 mL), stirred for 5 min, and added 40 mL H_2O. All the solid impurities in mixture were filtered out. After removing the organic solvent by reduced pressure distillation, the aqueous residue was extracted twice with ethyl acetate (40 mL). The organic layer was washed (H_2O, brine), dried ($MgSO_4$), and filtered. The solvent was removed in vacuum. The residue was column chromatographed over silica gel (200–300 mesh) using PE/EA (8/1) to obtain betulonic acid.

B. Synthesis and Purification of Betulinic Acid

$NaBH_4$ (0.227 g, 6 mmol) was gradually added to a solution with betulonic acid (0.90 g, 2 mmol) in THF (20 mL) at 0 °C and the mixture were stirred at 0 °C. The course of the reaction is confirmed by TLC. The reaction was quenched with HCl solution (3 mL, 2 mol/L). The solution was diluted with ethyl acetate (60 mL). The organic layer was washed (H_2O, brine), dried ($MgSO_4$), and filtered. The solvent was removed in vacuum to obtain crude betulinic acid. The crude betulinic acid was column chromatographed over silica gel (200–300 mesh) using PE/EA (6/1) to obtain betulinic acid.

164.2.2.3 Identification of the Chemical Structure and Purity of Betulin and Betulinic Acid

(1) Identification of the chemical structure

The chemical structure of betulin and betulinic acid was confirmed by IR, HPLC–MS,and H^1-NMR.

The HPLC analysis was carried out by VenusilC8 (4.6 × 250 mm). The mobile phase was methanol/acetonitrile/H_2O (45/45/10, V/V). The flow rate and injection volume were 1.0 mL/min and 10 μL. Betulin and betulinic acid were quantified, respectively, by UV detector at $\lambda = 210$ nm. All chromatographic operations were carried out at 30 °C [9, 10].

The MS conditions: The ion source is ESI (betulinic acid); the ion mode is negative; the scanning cover is 50–1000 u, the scanning mode is full scanning, the flow of desolvation gas is 700 L/h, the temperature of desolvation gas is 350 °C, the temperature of ion source is 150 °C.

(2) Determination of the purity of betulin and betulinic acid
A. The HPLC Conditions

The HPLC analysis was carried out by VenusilC8 (4.6 mm × 250 mm). The mobile phase was methanol/acetonitrile/H_2O (45/45/10, V/V). The flow rate and injection volume were 1.0 ml/min and 10 μL. Betulin and betulinic acid were quantified by UV detector at $\lambda = 210$ nm, respectively. All chromatographic operations were carried out at ambient temperature.

B. Preparation of Sample Solution

Accurately weighed equivalent to 2.0 mg of betulin or betulinic acid were dissolved with methanol/acetonitrile/H_2O (45/45/10, V/V, 1 mL). And then the solution was filtered through a membrane filter ($\varphi = 0.45$ μm).

C. The preparation of the blank reference solution

The blank reference solution were methanol/acetonitrile/H_2O (45/45/10, V/V) at the same conditions.

164.3 Results and Discussion

164.3.1 Results

164.3.1.1 The optimization process of the extraction and purification of betulin

The white birch bark (60 mesh, 100 g) with ethanol/IPA (10:1, V/V, 1100 mL) was refluxed for 6 h at 78 °C to give the crude betulin (34.7 g).

The orthogonal design test result of betulin purification is shown in Table 164.2.

According to the data (K1, K2, and K3) in Table 164.1, the effect of solvent, solid–liquid ratio, and recrystallization times on betulin quality were shown in Fig. 164.1.

Table 164.2 The result of the orthogonal design test of betulin purification

Ordinal	Factor			Result		
	A	B	C	Yield of crystal (%)	Purity (%)	Combined value (%)
1	1	1	1	57.5	54.18	55.51
2	1	2	2	38.9	89.02	68.97
3	1	3	3	20.8	96.65	66.31
4	2	1	2	40.4	71.04	58.78
5	2	2	3	27.2	95.60	68.24
6	2	3	1	63.4	67.02	64.37
7	3	1	3	20.2	96.40	65.92
8	3	2	1	71.7	66.38	68.51
9	3	3	2	45.1	76.24	63.78
K1	63.60 %	60.07 %	62.80 %			
K2	63.80 %	68.57 %	63.85 %			
K3	66.07 %	64.82 %	66.82 %			
R	2.47 %	8.50 %	4.03 %			

The combined value is derived from the yield of crystal (40 %) and the purity of betulin (60 %)

The optimum recrystallization condition is: the solvent is IPA/methanol (3/1, V/V), the solid–liquid ratio is 1/30 (g/mL) and the recrystallization time is 3 times.

164.3.1.2 The chemical structure and purity of betulin and betulinic acid

(1) The chemical structure of betulin and betulinic acid

The chemical structures of the betulinic acid and the betulin have been determined by H^1-NMR (Fig. 164.2a, b), respectively. IR (Fig. 164.3a, b) was used to identify the results. HPLC–MS spectrum of betulinic acid was carried out too (Fig. 164.4).

(2) The purity of betulin and betulinic acid

The HPLC spectrum showed that the purity of crude betulin is 50.56 % with a yield of 34.7 %. By the optimum recrystallization process, the purity of betulin is 95.2 % (Fig. 164.5a); yield of crystal is 20.8 %; and the purity of betulinic acid is 96.2 % (Fig. 164.5b) with a yield of 78.6 %.

164.3.2 Discussion

Betulin and betulinic acid possess antitumor, anti-HIV, and other biological properties. In the past decade, betulin, betulinic acid, and their derivatives have drawn the attention of researchers because of their excellent biological properties [11]. High quality betulin and betulinic acid have a huge market value.

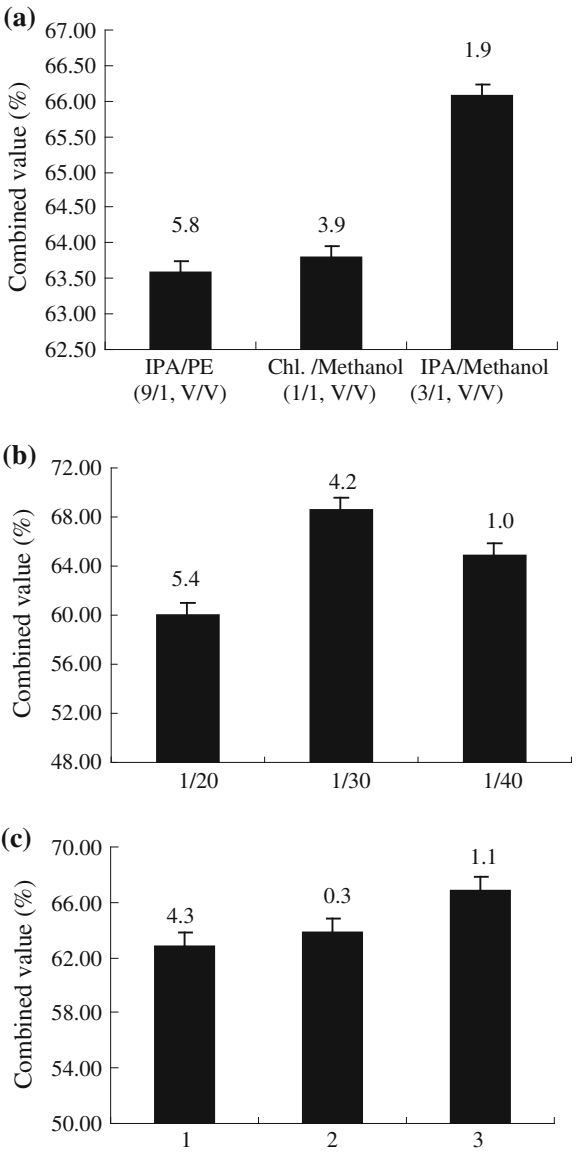

Fig. 164.1 The effect of the purification factor on betulin quality. **a** The effect of the solvent. **b** The effect of the solid–liquid ratio. **c** The effect of the recrystallization times. The combined value is derived from the yield of crystal (40 %) and the purity of betulin (60 %)

The commonly used organic-solvents, such as chloroform, methanol [12], methylbenzene [13], ethanol, dichloromethane, and diethyl ether [14], are ineffective for the extraction and purification of betulin. The experimental results showed: mixed-solvent ethanol/IPA is effective extraction solvent, which can improve the extraction yield as well as the purity of betulin. In this study, the orthogonal design test was used to optimize the recrystallization technology.

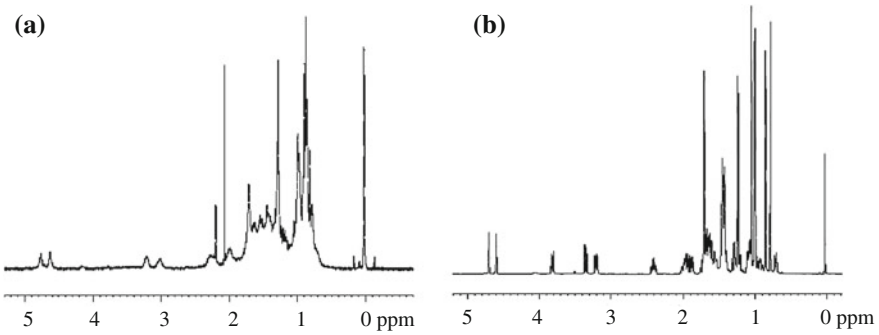

Fig. 164.2 **a** The H^1-NMR spectrum of betulinic acid. **b** The H^1-NMR spectrum of betulin

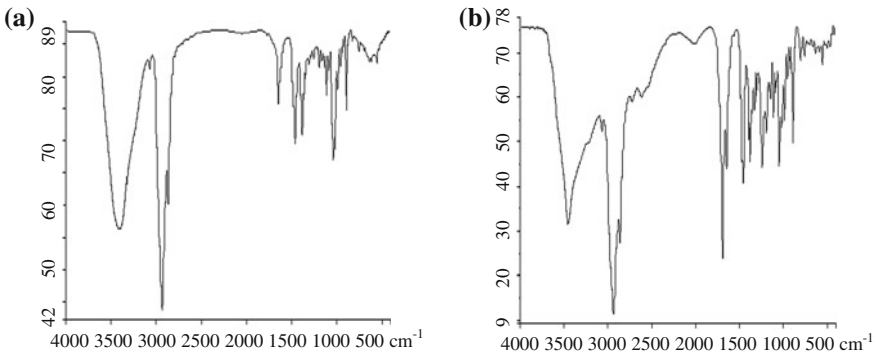

Fig. 164.3 **a** The IR spectrum of betulin. **b** The IR spectrum of betulinic acid

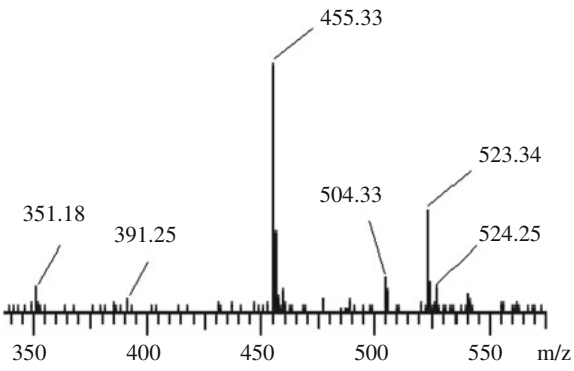

Fig. 164.4 The MS spectrum of betulinic acid

Betulinic acid can be obtained by extraction from plants and chemical synthesis [15–17]. But it is difficult to obtain betulinic acid by the method of extraction because of its very low content in plants [18]. Several kinds of synthesis methods

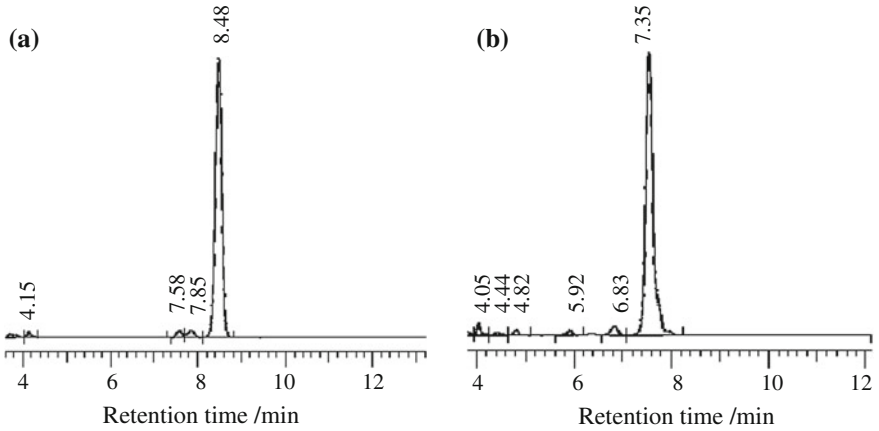

Fig. 164.5 **a** The HPLC spectrum of betulin. **b** The HPLC spectrum of betulinic acid

can be used to obtain betulinic acid [19, 20]. Semi-synthesis method by two-step synthesis with betulin as raw material is the most effective one. To this method, the betulin was oxidized by Jones reagent at first, followed by a reduction with $NaBH_4$ to afford crude betulinic acid of 73.4 % yield. The crude betulinic acid was purified by column chromatographed over silica gel (200–300 mesh) using PE/EA (6/1) to obtain 96.2 % betulinic acid (HPLC data) with a yield of 84.0 %.

164.4 Conclusion

Betulin was obtained from the white birch bark with ethanol/IPA as extraction solvent. Betulinic acid was prepared from betulin with two-step method. The optimal process and conditions were determined for the extraction of betulin and synthesis of betulinic acid. The betulin extraction method developed in this report may bring huge potential value for the development of new antitumor and anti-HIV-1 drug.

Acknowledgments Financial support from the Science and Technology Project of Tianjin (No. 10JCZDJC22500,10ZXCXSY10100) is gratefully acknowledged.

References

1. Fan GZ, Zhan YZ (2008) Advances in studies on betulin. Chin Tradit Herbal Drugs 39:1591–1594
2. Flekhter OB, Nigmatullina LR, Baltina LA et al (2002) Synthesis of betulinic acid from betulin extract and study of the antiviral and antiulcer activity of some related terpenoids. Pharm Chem J 36:484–487

3. Robert HC, Samir AK (2004) Chemistry, biological activity and chemotherapeutic potential of betulinic acid for the prevention and treatment of cancer and HIV infection. Med Res Rev 24:90–114
4. Toshihiro F, Yoshiki K, Robert E et al (1994) Anti-AIDS agents betulinic acid and platonic acid as anti-HIV principles from Syzigium Claviflorum, and the anti-HIV activity of structurally related triterpenoids. J Nat Prod 57:243–247
5. Darrick SHLK, Chen ZD, Nguyen VT et al (1997) A concise semi-synthetic approach to betulinic acid from betulin. Synth Commun 27:1607–1612
6. Csuk R, Schmuck K, schäfer R (2006) An practical synthesis of betulinic acid. Tetrahedron Lett 47:8769–8770
7. Pichettea A, Liu HY, Christian R et al (2004) Selective oxidation of betulin for the preparation of betulinic acid, an antitumoral compound. Synth Commun 34:3925–3937
8. Liu J, Zhang HF, He GQ et al (2009) Research progress and foreground of betulin and betulinic acid. Sci Technol Food Indus 30:360–366
9. Zhao GL, Yan WD, Dan C (2007) Simultaneous determination of betulin and betulinic acid in white birch using RP-HPLC. J Pharm Biomed 43:956–962
10. Zhang Z, Sun H (2004) Determination of betulin content from bark of Betula Platyphylla Suk by HPLC. Chem Indus For Prod 24:61–63
11. Cichewicz RH, Kouzi SA (2004) Chemistry, biological activity and chemotherapeutic potential of betulinic acid for the prevention and treatment of cancer and HIV infection. Med Res Rev 24:90–114
12. Yi JE, Wen LX, Yuan LY et al (2010) Study on extraction of betulin from white birch and synthesis of betulinic acid. J Hunan Agric Univ (Nat Sci) 36:574–580
13. Han SY, Fang GZ, Li SS et al (2005) Separation and purification of betulin by tetrahydrofuran-benzene extraction. Chem Indus For Prod 25:129–132
14. Wang SF, Zhang MG, Li YP (2007) Study on extraction and purification of betulin from birch bark. Chem Indus For Prod 27:22–26
15. Lai L, Yang X, Yang G et al (2006) Orthogonal test for optimizing extraction technique of betulinic acid in Semen Ziziphi Spinosae. Chin Tradit Herbal Drugs 4:532–534
16. Prakash Chaturvedula VS, Schilling JK, Johnson RK et al (2006) New cytotoxic lupane triterpenoids from the twigs of coussarea paniculata. J Nat Prod 66:4533–4541
17. Klaus W, Hartmut S (1995) Dodeca acetyl prodelphinidin B3 from the dried leaves of ziziphus spina-christ. Phytochemistry 38:505–507
18. Margaret MO, Bentley MD, Campbell CS et al (1988) Betulin and lupeol in bark from four white barked birches. Phytochemistry 27:2175–2176
19. Gaudet D, Pichette A. Process for preparing natural product derivatives from plants in a single step. US: 6280778
20. Krasutsky PA, Kolomitsyna O. Methods of manufacturing bioactive 3-esters of betulinic aldehyde and betulinic acid. WO. Patent 2006105356

Chapter 165
Research on the Optimum Conditions and the Effect of Antioxidant Peptide from Scallop Protein

Yuan Liu, Jian Wang, Zhisheng Zhang and Jie Wang

Abstract *Bay scallop* and *Japanese scallop* were chosen for enzymatic hydrolysis by neutral protease, alkaline protease, and papain, and the enzymolysis technology of scallop protein was optimized to obtain antioxidant peptide. The effect of kinds of scallop and enzyme, enzyme quantity, temperature, and the ratio of solid to liquid on the degree of hydrolysis (DH) and the free radical scavenging activity was studied. On the basis of single factor experiment, orthogonal experiment of $L_9(3^4)$ was used to optimize the technical parameters. The results indicated that the optimal hydrolytic conditions were as follows: using Bay scallop as the material, the enzyme quantity of the Neutral Protease was 3.25 % ([E]/[S]), temperature was 40 °C, and the ratio of solid to liquid was 1:2.5. Under this condition, the DH was 45.91 %, and the scavenging rate of DPPH radical and superoxide anion radical were 91.90 % and 79.72 % respectively.

Keywords DPPH radical · Antioxidant peptide · Scallop · Superoxide anion

165.1 Introduction

Because of the shortage of terrestrial resources, much attention is increasingly paid to find the novel active material from marine organism. Therefore, more and more active material has been gradually found from marine shellfish. Polypeptide from chlamys farreri (PCF) is a water-soluble polypeptide isolated first from chlamys

Y. Liu · Z. Zhang · J. Wang (✉)
College of Food Science and Technology, Agriculture University of Hebei, Baoding 071000, People's Republic of China
e-mail: wj591010@163.com

Y. Liu · J. Wang
Department of Food Science, Hebei North University, Zhangjiakou 075000, People's Republic of China

T.-C. Zhang et al. (eds.), *Proceedings of the 2012 International Conference on Applied Biotechnology (ICAB 2012)*, Lecture Notes in Electrical Engineering 251,
DOI: 10.1007/978-3-642-37925-3_165,

farreri. The study of cultured cells has found that PCF can efficiently remove oxygen free radicals produced by chemical systems [1], inhibit the oxidative stress of UVA on Hela epithelial cells [2], the oxidative stress of UVB on fibroblasts [3], obviously relieve the damage effects of UVA and UVB on the skin of km mutant hairless mice [4], increase the immunologic cellular activity, relieve the oxidative stress of thymocyte, inhibit thymocyte apoptosis [5], and avoid the immune cells damaged by ultraviolet and (60)Co radiation, and so on [6, 7]. So PCF, as a new natural antioxidant, is of great exploitation value.

Presently, many kinds of polypeptides with antioxidant activity have been extracted from different proteins [8, 9]. In this research, Scallop was chosen for enzymatic hydrolysis by protease to obtain antioxidant peptide. On the basis of screening experiment and single factor experiment, the technical parameters were optimized by orthogonal experiment, and the antioxidant obtained was used for antioxidation test in order to provide the theory basis for further study of the properties of antioxidant peptide from scallop protein.

165.2 Materials and Methods

165.2.1 Technologic Progress of the Preparation of Antioxidant Peptide from Scallop Protein

Fresh Scallop → removal of visceral → cleaning → preparation of meat emulsion → mixing with water according to a certain proportion → adjusting pH → isothermal enzymatic hydrolysis for 4 h according to different enzyme quantity and temperature → killing enzyme by boiling water bath for 10 min → centrifugation (10,000 $r \cdot min^{-1}$) for 30 min after cooling → collecting the supernatant → antioxidant peptide.

165.2.2 Design for Screening Kinds of Scallop and Enzyme

Three portions were taken, respectively, from the meat emulsion (the ratio of solid to liquid being 1:5) of Bay scallop and Japanese scallop. Each of them was separately added by neutral protease, alkaline protease, and papain ([E]/[S] = 1.2 %). Then the hydrolysis temperature and pH were adjusted to make each hydrolysate hydrolyzed for 4 h under the optimum conditions. The DH and free radical scavenging activity of the antioxidant peptide obtained were determined to screen kinds of scallop and enzyme.

165.2.3 Single Factor Design for Enzymatic Hydrolysis Conditions

165.2.3.1 Effect of Enzyme Quantity on the DH and Free Radical Scavenging Activity

Eight portions of meat emulsion of scallop (the ratio of solid to liquid 1:5) were added by protease selected according to the enzyme quantity ([E]/[S]) 0.5 %, 1.0 %, 1.5 %, 2.0 %, 2.5 %, 3.0 %, 3.5 %, 4.0 %, respectively. Then the hydrolysis temperature and pH were adjusted to make each portion of hydrolysate hydrolyzed for 4 h under the optimum conditions. Eventually, the DH and free radical scavenging activity were determined.

165.2.3.2 Effects of the Ratio of Solid to Liquid on the DH and Free Radical Scavenging Activity

Eight portions of meat emulsion of scallop were well mixed with water according to the ratio of solid to liquid 1:1, 1:2, 1:3, 1:4, 1:5, 1:6, 1:7, 1:8, and then added by protease according to the proportion selected, respectively. Then the hydrolysis temperature and pH were adjusted to make each hydrolysate hydrolyzed for 4 h under optimum conditions. Then, the DH and free radical scavenging activity were determined.

165.2.3.3 Effect of Temperature on the DH and Free Radical Scavenging Activity

Five portions of meat emulsion of scallop (treated according to the ratio of solid to liquid and enzyme quantity selected) were adjusted to the optimum pH, and then hydrolyzed for 4 h under 25, 30, 35, 40, 45 °C. Finally, the DH and free radical scavenging activity were determined.

165.2.4 Orthogonal Design for Enzymatic Hydrolysis Conditions

According to the principle of orthogonal experiment of $L_9(3^4)$, the technological parameters were optimized by three factors and three levels of orthorhombic methods. The DH was selected as index, and enzyme quantity, the ratio of solid to liquid and temperature as contributing factors.

165.2.5 Determination of the DH

Total nitrogen content: by micro-kjeldahl method [10].

Ammonia nitrogen content: by formaldehyde value method (GB/T5009.39-2003).

The DH was determined by the following formula (1):

$$\mathrm{DH}\,(\%) = \frac{\text{The weight of ammonia nitrogen}}{\text{The weight of total nitrogen}} \times 100 \qquad (1)$$

165.2.6 Determination of the Scavenging Rate of DPPH Radical

The method was improved on the basis of Ref. [11]. The sample of 0.5 mL, 0.5 mL distilled water, and 0.5 mL DPPH-ethanol solution of 0.2 mmol L^{-1} was successively added to the tube and well mixed, and then the reaction occurred in the dark at room temperature for 20 min. At last, the absorbance (A_s) at 517 nm was determined. In the blank group, DPPH- ethanol solution was replaced by 0.5 mL ethanol and the absorbance was A_x. In the control group, the sample was replaced by 0.5 mL distilled water and the absorbance was A_0, and distilled water and ethanol of the same volume were used for zero adjusting. The scavenging rate of DPPH radical was calculated by the following formula (2).

$$\text{Scavenging rate of DPPH radical}\,(\%) = 1 - \frac{(A_s - A_x)}{A_0} \times 100 \qquad (2)$$

A_0: the absorbance of control group; A_s: the absorbance of sampling group; A_x: the absorbance of blank group

165.2.7 Determination of the Scavenging Rate of Superoxide Anion Radical

The method was improved on the basis of Ref. [12]. 2.4 mL Tris–HCl buffer (pH 8.2) of 0.05 mol/L was used as water bath heated for 20 min at 25 °C, and then mixed with 0.3 mL pyrogallol solution (4 mmol L-1) preheated and the sample solution with different concentrations. The reaction occurred at 25 °C for 4 min, and was stopped by one drop of HCl (10 mmol L-1), and the absorbance was

determined at 325 nm. The test was repeated thrice and the mean value was calculated, as in (3).

$$\text{Scavenging rate of } O_2^- \cdot (\%) = (A_0 - (A_s - A_x))/A_0 \times 100 \quad (3)$$

A_0 The absorbance without the sample solution.
A_s The absorbance with the sample solution.
A_x The absorbance of the sample solution without the pyrogallol solution.

165.3 Results and Discussion

165.3.1 Screening of Kinds of Scallop and Enzyme

Table 165.1 shows that by using *Bay scallop* and neutral protease for enzymatic hydrolysis, the antioxidant peptide obtained had the highest DH and the strongest scavenging rate of DPPH radical and superoxide anion radical. It was possibly related to the type of enzyme and the amino acid composition of the scallop.

Enzyme can be divided into endopeptidase and exopeptidase according to the different action sites. Compared with endopeptidase mainly acting on the middle peptide bond of protein, the exopeptidase mainly acts on free amino and c-terminal and then gradually degradates amino acid residues. Neutral protease and alkaline protease selected in the study were both endopeptidase, and alkaline protease had a wide range of hydrolysis [13], while the papain mainly plays the role of exopeptidase in hydrolysis [14]. Now the research reports on protease cleavage site are few. Zhao et al. [15] deduced the cleavage site of neutral protease and alkaline protease for sodium caseinate by the High Performance Liquid Chromatography. They found that neutral protease had a wide range of cleavage sites when it

Table 165.1 Effect of species of scallop and enzyme on enzymatic hydrolysis

		DH (%)	Scavenging rate of DPPH radical (%)	Scavenging rate of superoxide anion radical (%)
Bay scallop	papain	$36.62 \pm 3.90^{\text{※※}}$	$60.39 \pm 7.24^{\text{※※}}$	$52.84 \pm 7.24^{\text{※※}}$
	alkaline protease	$34.92 \pm 1.47^{\text{※※#}}$	$35.12 \pm 7.49^{\text{#}}$	$51.85 \pm 7.49^{\text{※※#}}$
	neutral protease	$45.99 \pm 5.11^{\text{※#}}$	$80.10 \pm 8.14^{\text{※}}$	$64.68 \pm 8.14^{\text{※#}}$
Japanese scallop	papain	$23.01 \pm 3.4^{\text{※※}}$	$66.17 \pm 1.77^{\text{※#}}$	$33.69 \pm 4.40^{\text{※※}}$
	alkaline protease	$21.53 \pm 2.57^{\text{※※#}}$	$43.95 \pm 5.43^{\text{※※}}$	$29.60 \pm 5.87^{\text{※※#}}$
	neutral protease	$40.09 \pm 1.29^{\text{※#}}$	$68.84 \pm 7.04^{\text{※}}$	$55.22 \pm 7.50^{\text{※#}}$

Note There was significant difference between those whose shoulder markers in the same column were different ($p < 0.05$), while there was no obvious difference between those whose shoulder markers were the same

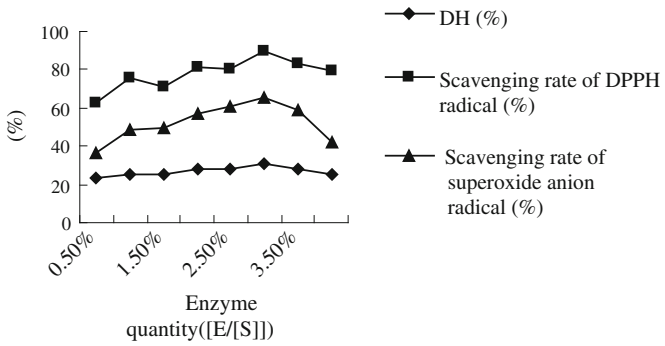

Fig. 165.1 Effect of enzyme quantity on enzymatic hydrolysis

hydrolyzed sodium caseinate because it could hydrolyze many amino acid residues, such as –Val, -Phe, -Cys, -Leu, -Tyr, -Trp, -Ile, -Lys, -Gly, etc. Besides, Bay scallop is rich in Tyr, Lys, Gly, and other amino acids compared with Japanese scallop [16]. Therefore, neutral protease had stronger hydrolytic capability when the hydrolysis on Bay scallop was carried out.

165.3.2 Effects of Enzyme Quantity on the DH and Free Radical Scavenging Activity

As shown in Fig. 165.1, when enzyme quantity ([S]/[E]) was at 0.50 %～4.0 %, the DH was higher slowly with the increase in enzyme quantity, and reached its maximum of 30.66 % at 3.0 %, and then decreased slowly with the unceasing increase in enzyme quantity. Hydrolysis efficiency generally could be improved with the increase in enzyme quantity when the substrate concentration was saturable, but when the ratio of solid to liquid in the test was 1:5, it obviously did not reach the saturated concentration, so the DH increased first and then decreased.

Enhanced with the increase in enzyme quantity, the scavenging activity of DPPH radical and superoxide anion radical both gradually, respectively, reached their maximum 89.75 % and 65.12 % at 3.0 %, and then decreased with the unceasing increase in enzyme quantity, possibly because the radical scavenging activity of polypeptide from enzymatic hydrolysis was lost when the polypeptide was hydrolyzed with the enzymatic hydrolysis.

165.3.3 Effects of the Ratio of Solid to Liquid on the DH and Free Radical Scavenging Activity

As shown in Fig. 165.2, when the ratio of solid to liquid was at 1:1～1:8, the DH increased rapidly and then decreased slowly, and reached its maximum of 33.22 %

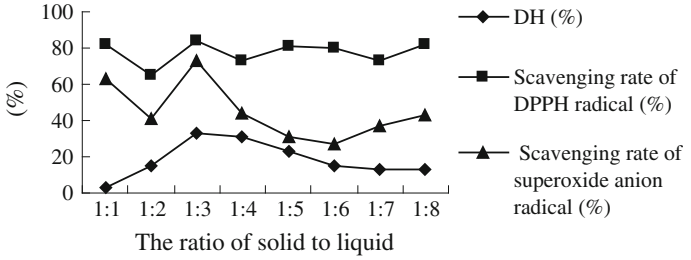

Fig. 165.2 Effect of the ratio of solid to liquid on enzymatic hydrolysis

at 1:3, the scavenging rate of DPPH radical increased first and then decreased, but the change was not clear, and it reached its maximum of 84.48 % at 1:3; the change range of the scavenging rate of superoxide anion radical was much more obvious, and the ratio of solid to liquid increased suddenly to its maximum of 73.28 %, and then decreased rapidly. Because the substrate concentration was too high at first result in excess substrate aggregating on the surface of enzyme, it formed an inactive intermediate which inhibited the enzymatic hydrolysis [17]; when the ratio of solid to liquid was at 1:3, the substrate concentration was moderate, which was beneficial for occupying the active center of enzyme, enhancing the amount of sensitive peptide bond, accelerating the reaction rate [18–20], and getting the target product with free radical scavenging activity. The substrate concentration and hydrolysis efficiency gradually decreased with the increase in the ratio of solid to liquid.

165.3.4 Effects of Temperature on the DH and Free Radical Scavenging Activity

From Fig. 165.3 it is seen that the DH was the highest and the scavenging activity of DPPH radical and superoxide anion radical was the strongest at 40 °C. It was possibly connected with the neutral protease in the test whose optimum temperature was 40 °C. When the temperature was higher or lower than it, the enzyme activity and reaction rate were affected, and the radical scavenging activity decreased.

165.3.5 Orthogonal Experiment of $L_9(3^4)$

On the basis of the above single factor experiment, according to the principle of orthogonal experiment of $L_9(3^4)$, the technological parameters were optimized by

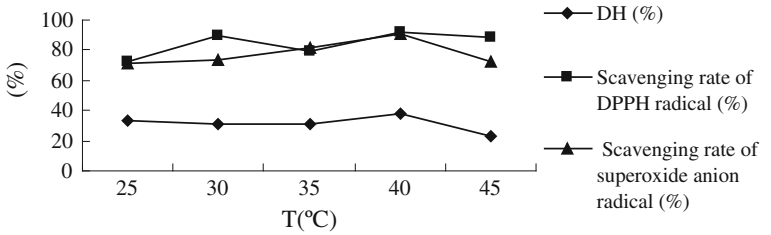

Fig. 165.3 Effect of temperature on enzymatic hydrolysis

Table 165.2 The factors and levels of orthogonal experiment

Level	Enzyme quantity ([E]/[S]) (%)	The ratio of solid to liquid	Temperature (°C)
1	2.75	1:2.5	37
2	3.0	1:3	40
3	3.25	1:3.5	43

three factors and three levels of orthorhombic methods. The DH was selected as index, and enzyme quantity, the ratio of solid to liquid and temperature as contributing factors. The specific factors and levels are as follows (Table 165.2), and the results are shown in Table 165.3.

On the basis of single factor experiment, the results of orthogonal experiment of $L_9(3^4)$ are shown in Table 3. According to the magnitude of extreme difference of

Table 165.3 $L_9(3^4)$ orthogonal design and results

No.	Factors				DH (%)
	A	B	C	Null columns	
I	1	1	1	1	35.77
II	1	2	2	2	43.44
III	1	3	3	3	10.22
IV	2	1	2	3	45.99
V	2	2	3	1	38.33
VI	2	3	1	2	15.33
VIII	3	1	3	2	43.44
IX	3	2	1	3	33.22
X	3	3	2	1	40.88
K1	89.43	125.20	84.32		
K2	99.65	114.99	130.31		
K3	117.54	66.43	91.99		
k_1	29.81	41.73	28.11		
k_2	33.22	38.33	43.44		
k_3	39.18	22.14	30.66		
R	9.37	19.59	15.33		
Optimization levels	A3	B1	C2		

the three factors, their descending sequence was the ratio of solid to liquid, the temperature, and enzyme quantity. The best optimal combination was A3 B1 C2, that is, enzyme quantity ([E]/[S]) 3.25 %, the temperature 40 °C and the ratio of solid to liquid (W/V)1:2.5. On this basis the verification experiment was conducted and repeated thrice. The mean value of the DH was 45.91 %, and the scavenging rate of DPPH radical and superoxide anion radical were 91.90 % and 79.72 %, respectively. This shows that the antioxidant peptide with higher radical scavenging activity can be obtained by using optimized technical parameters.

165.4 Conclusion

(1) By comparing the effects of kinds of scallop and enzyme on the DH and radical scavenging activity of the antioxidant peptide obtained, *Bay scallop* and neutral protease were chosen for enzymatic hydrolysis.
(2) Through single factor experiment, the DH was the highest and radical scavenging activity was the strongest when enzyme quantity ([E]/[S]), the ratio of solid to liquid (W/V), and temperature were 3.0 %, 1:3 and 40 °C, respectively.
(3) Three factors of enzyme quantity, temperature, and ratio of solid to liquid were optimized by orthogonal experiment. The optimal hydrolytic conditions were as follows: enzyme quantity ([E]/[S]) 3.25 %, the ratio of solid to liquid (W/V) 1:2.5, temperature 40 °C. Under these conditions, the DH was 45.91 % and the scavenging activity of DPPH radical and superoxide anion radical were 91.90 % and 79.72 %. This indicates that the antioxidant peptide obtained had strong scavenging activity of DPPH radical and superoxide anion radical.

References

1. Wang CB, He MQ, Qin SZ et al (1998) An tioxidative effect of polypeptides from the chlamys farreri in vitro. Chin J Mar Drugs 17:15–17
2. Yao RY, Wang CB (2002) Protctive effect of polypeptide from Chlamys farreri on HeLa cells damaged by ultraviolet A. Acta Pharmacol Sin 23:1018–1022
3. Ding BX, Wang CB (2003) Inhibitory effect of polypeptide from Chlamys farreri on UVB-induced apoptosis and DNA damage in normal human dermal fibroblasts in vitro. Acta Pharmacol Sin 24:1006–1010
4. Wang CB, Yao RY, Liu ZT et al (2002) Protective effects of polypeptide from Chlamys farreri on hairless mice damaged by ultraviolet A. Acta Pharmacol Sin 23:813–818
5. Che YL, Sun M, Ouyang WQ et al (2004) Effects of polypeptide from Chlamys farreri on apoptosis of thymocytes induced by oxidative damage. Mar Fish Res 25:33–38
6. Liu XP, Wang YZ, Han YT et al (2001) Efeect of polypeptides from Chlamys farrerion the proliferation of immune cells and its protection against ultraviolet in vitro. Oceanol Et Limnol Sin 32:414–419

7. Wang YZ, Liu XP, Yao RY et al (2001) The effects of PCF on the activity and recoveration of thymocytes irradiated by ^{60}Co. Chin J Mar Drugs 84:20–24
8. Bao B, Deligersang XuQ (2004) Advances in study on antioxidative peptide. J Inner Mong Instit Agric Anim Hus 25:121–124
9. Korhonen H, Pihlanto A (2006) Bioactive peptides: production and functionality. Int Dairy J 16:945–960
10. Ning ZX (1998) Handbook of Food Component Analysis. Chin Light Indus Press, Beijing
11. Wu YY, Tian Q, Shang J et al (2011) Study on character and application of pinctada fucata antioxidant peptide. Sci technol Food indus 32(123–126):130
12. Tong HJ, Zhang ZS, Wang O et al (2011) Study on the water extraction process of polysaccharides from argopectens irradias. J Agric Univ Hebei 34:85
13. Yu MJ, Ma MH, Wan JR (2005) Study on the reaction conditions of the hydrolysis of porcine blood by combinative enzyme. Food Sci Technol 26(96–98):101
14. Wang T, Zeng QZ, Xie ZF (2003) Studies on the technics of enzymatic hydrolysis of protein in scallop skirts by using endoenzymes and exopetidases. J Dal Fish Univ 18:125–129
15. Zhao MM, Zhao YL (2005) Analysis of amino acid composition of sodium caseina hydrolyte. Food Sci 26:115–117
16. Li N (2011) The amino acids, fatty acids and heavy metals content analysis of the shellfish and its product quality evaluation. Agric Univ Hebei, Baoding, China (in Chinese)
17. Peng ZY (2009) Introduction to enzymology. Chin Light Indus Press, Beijing
18. Wang L, Ye KN (2006) Enzymatic hydrolysis of aquatic proteins:A Review. Food Sci 27:807–812
19. Xu X, He JY, Liu GY et al (2011) Process eonditions optimization for antioxidant peptide preparation from small yellow croaker by response surface methodology. Food Sci 32:165–170
20. Zhou XS, Zhao MM, Lin WF et al (2006) Enzymatic hydrolysis of chicken protein by alcalase and scavenging activity of resulted hydrolysates on free radicals. J South Chin Univ Technol (Natural Science Edition) 34:117–122

Chapter 166
Tracing the Origin of Pigment in Broilers by Stable Nitrogen and Carbon Isotopes Analysis

Huiwen Wang, Fengmei Sun and Shuming Yang

Abstract A trial was carried on to tracing the origin of pigment in broilers with different contents of maize and different concentration of carophyll red in ration. About 320 broilers of AA were fed on basic diets with different contents of maize and basic diets with different concentration of carophyll red for 21 days, respectively, and then fed on the changed basic diets for 21 days. The results showed that the maize contents and the concentration of carophyll red had significant influence on the foot and skin color ($p < 0.05$). The $\delta^{13}C$ values in muscles were significantly affected by maize contents ($p < 0.05$), however, the $\delta^{15}N$ values of chicken had no obvious rules. It is confirmed that the origin of pigment in broilers was inferred by analyzing the $\delta^{13}C$ values and $\delta^{15}N$ values, and the stable isotope mass spectrometry technique was confirmed to be an effective tool in tracing the animal products.

Keywords Broilers · Pigment · Stable isotopes · Trace

H. Wang (✉)
Department of Animal Science of Hebei North University, Zhangjiakou 075131, People's Republic of China
e-mail: wanghuiwen04@163.com

F. Sun
Department of Food Science of Hebei North University, Zhangjiakou 075131, People's Republic of China

S. Yang
Institute of Quality Standard and Testing Technology for Agro-Product, Chinese Academy of Agricultural Science, Beijing 100081, People's Republic of China

T.-C. Zhang et al. (eds.), *Proceedings of the 2012 International Conference on Applied Biotechnology (ICAB 2012)*, Lecture Notes in Electrical Engineering 251,
DOI: 10.1007/978-3-642-37925-3_166,

166.1 Introduction

In recent years, organic or natural agricultural foods are more and more popular in China. Comparing with ordinary products, these organic or natural foods are sold at higher price. Sometimes the labels are only way to distinguish them, it is necessary to make another way to check them.

Carophyll red is a kind of artificial pigment that can legally used to improve skin or yolk color with maximum usage up to 30 mg/kg of diet in China, since some customers like yellow skin broiler and eggs with red yolk. But some customers do not like the charming products from chicken fed on artificial pigment, they prefer the products from chicken fed on natural pigments such as maize, chili powder, or alfalfa meal.

In the past 30 years, the analysis of naturally occurring variations on the abundance of stable isotopes has been increasingly used in the physiological and metabolism research [1], and has also helped to reconstruct the dietary of animals through the analysis of different tissues [2]. The ratios of stable isotopes of bio-elements, such as H, O, C, and N have been used to test the authenticity and geographical origin of several products such as fruit juice [3–7], honey [8–10], wines [11, 12], vegetable oils [13], and milk products [14, 15]. Piasentier et al. [16] demonstrated that it was possible to certify the food regimen of lamb by analyzing carbon and nitrogen isotope levels in muscle and fat by mass spectrometry.

The objective of this study was to trace the origin of pigment in broilers by nitrogen and carbon isotope analysis.

166.2 Materials and Methods

About 320 one-day-old broilers of AA were raised until 42 days old under similar condition and standard management procedures, feed and water were supplied ad libitum (Table 166.1).

The broilers were assigned to eight treatments with four replicates according to a completely randomized experimental design. The broilers were divided into two

Table 166.1 Experimental design

Group 1	Day 1–21 (Initial period)	Day 22–42 (Final period)
Treatment 1	Basic diets	Basic diets
Treatment 2	Basic diets + 15 mg/kg carophyll red	Basic diets
Treatment 3	Basic diets + 30 mg/kg carophyll red	Basic diets
Treatment 4	Basic diets + 60 mg/kg carophyll red	Basic diets
Treatment 5	Basic diets including 10 % maize	Basic diets including 70 % maize
Treatment 6	Basic diets including 30 % maize	Basic diets including 30 % maize
Treatment 7	Basic diets including 50 % maize	Basic diets including 50 % maize
Treatment 8	Basic diets including 70 % maize	Basic diets including 10 % maize

groups and the experiment was divided into two periods. Four diets with different concentration of carophyll red and four diets with different contents of maize had been fed to these broilers.

On day 21 and 42, 12 samples of each treatment approximately 30 g were collected from breast muscle. At the same time, the color of chicken skin was tested by a Roche Color Fan. After handling, the muscle samples were determined by stable isotope mass spectrometry for $^{13}C/^{12}C$ and $^{15}N/^{14}N$. The samples were weighed into tin capsules and introduced by means of an autosampler into the elemental analyser, where, in the presence of oxygen and copper oxide, they were quantitatively combusted to CO_2 and NO_x, the latter was then reduced to N_2 with copper. The gases formed were separated in a gas chromatograph column and analyzed in an isotope ratio mass spectrometer (Delta S- Finnigan MAT, Bremen, Germany).

Isotope ratio values were expressed as delta per thousand (δ ‰) in relation to Pee Dee Belemnite (PDB) international standards for $\delta^{13}C$ and atmospheric air for $\delta^{15}N$, according to the following equation:

$$\delta\%_{oo(\text{sample, standard})} = \left[\left(R_{\text{sample}} - R_{\text{standard}}\right)/R_{\text{standard}}\right] \times 1000 \quad (1)$$

where R represents the ratio between the least and most abundant isotopes, in particular $^{13}C/^{12}C$ and $^{15}N/^{14}N$. Each sample was analyzed twice and the values were averaged. Results were statistically analyzed by SAS.

166.3 Result and Discussion

The RCF values of initial and final period of each treatment are shown in Table 166.2, the result of isotopic analysis for $\delta^{13}C$ and $\delta^{15}N$ of breast muscle samples of each treatment are shown in Tables 166.3 and 166.4.

Hobson and Clark [17] reported that the choice of tissue type for isotopic analysis depended on the speed at which different tissues reflected the isotopic signature. Therefore, it depends on the metabolism rate of the tissue. Since the turnover rate in breast muscle of growing broiler chickens is very high and 99 % of

Table 166.2 Effect of group 1 and group 2 on RCF values

Group 1	RCF values		Group 2	RCF values	
	Initial period	Final period		Initial period	Final period
Treatment 1	$3.17^{ef} \pm 0.75$	$3.50^{def} \pm 1.05$	Treatment 5	$2.58^{ef} \pm 0.80$	$5.42^{b} \pm 0.80$
Treatment 2	$3.67^{cde} \pm 0.82$	$3.50^{def} \pm 0.82$	Treatment 6	$3.00^{ef} \pm 0.63$	$3.50^{def} \pm 0.55$
Treatment 3	$4.33^{bcd} \pm 0.82$	$3.33^{def} \pm 1.03$	Treatment 7	$4.67^{bc} \pm 1.03$	$4.92^{b} \pm 0.80$
Treatment 4	$4.67^{bc} \pm 1.03$	$3.58^{cde} \pm 0.80$	Treatment 8	$7.75^{a} \pm 0.76$	$2.42^{f} \pm 0.92$

Notes Means with different superscripts are differ significantly ($P < 0.05$), same superscripts are differ insignificantly ($P > 0.05$)

Table 166.3 Effect of different levels of carophyll red on $\delta^{13}C$ values and $\delta^{15}N$ values

Group 1	$\delta^{13}C$ values (‰)		$\delta^{15}N$ values (‰)	
	Initial period	Final period	Initial period	Final period
Treatment 1	$-19.75^{ij} \pm 0.33$	$-19.23^{fghi} \pm 0.20$	$2.99^{e} \pm 0.26$	$4.09^{bc} \pm 0.30$
Treatment 2	$-19.32^{ghi} \pm 0.38$	$-19.17^{fgh} \pm 0.21$	$2.88^{e} \pm 0.12$	$4.05^{bc} \pm 0.13$
Treatment 3	$-19.70^{hij} \pm 0.32$	$-18.90^{efg} \pm 0.28$	$2.87^{e} \pm 0.23$	$4.22^{b} \pm 0.13$
Treatment 4	$-19.99^{j} \pm 0.39$	$-19.36^{ghi} \pm 0.31$	$2.90^{e} \pm 0.26$	$3.98^{bc} \pm 0.21$

Notes Means with different superscripts are differ significantly ($P < 0.05$), same superscripts are differ insignificantly ($P > 0.05$)

Table 166.4 Effect of different levels of maize on $\delta^{13}C$ values and $\delta^{15}N$ values

Group 2	$\delta^{13}C$ values (‰)		$\delta^{15}N$ values (‰)	
	Initial period	Final period	Initial period	Final period
Treatment 5	$-21.41^{k} \pm 0.57$	$-17.29^{b} \pm 0.55$	$3.45^{d} \pm 0.16$	$4.73^{a} \pm 0.17$
Treatment 6	$-19.99^{j} \pm 0.46$	$-18.75^{def} \pm 0.27$	$3.33^{d} \pm 0.27$	$4.26^{b} \pm 0.20$
Treatment 7	$-18.51^{de} \pm 0.36$	$-17.98^{c} \pm 0.32$	$2.72^{e} \pm 0.22$	$3.98^{bc} \pm 0.15$
Treatment 8	$-16.61^{a} \pm 0.48$	$-18.29^{cd} \pm 0.89$	$3.86^{c} \pm 0.35$	$4.68^{a} \pm 0.15$

Notes Means with different superscripts are differ significantly ($P < 0.05$), same superscripts are differ insignificantly ($P > 0.05$)

the tissue carbon is replaced in approximately 17 days, the isotopic signature should safely represent the diets given to broilers. Therefore, breast muscle was chosen for analysis due to the higher commercial value of this cut, the low fat levels in the tissue, and mainly the higher turnover rate.

The Table 166.4 shows: with the increasing level of carophyll red and maize, the RCF values increased correspondingly, and when carophyll red was removed or the levels of maize decreased, the RCF values decreased too (Figs. 166.1 and 166.2). It explains all carophyll red and maize could improve the products' color, but maize is a C_4 plant that has higher ^{13}C content than most of C_3 plant, while carophyll red is only a kind of artificial pigment that has no influence to poultry products. So, the improved color products with increased $\delta^{13}C$ values are caused by high levels of maize, conversely, the products are caused by carophyll red.

The $\delta^{15}N$ values of each treatment have no significant difference during the initial period in group 1, but its have significant difference between initial and final period ($p > 0.05$, Figs. 166.1 and 166.2). Delgado and Garcia [18] reported the $\delta^{15}N$ values are influenced by the protein of animal origin. So, the high $\delta^{15}N$ values in final period are related to the high content of fish meal of this study. The $\delta^{15}N$ values have no distinct rule in group 2. Kornexl et al. [19] and Rossmann et al. [20] owed the changed $\delta^{15}N$ values of animal products to the environmental factor, so the unsteady $\delta^{15}N$ values in group 2 may be caused by temperature, humidity, soil, and agricultural practice.

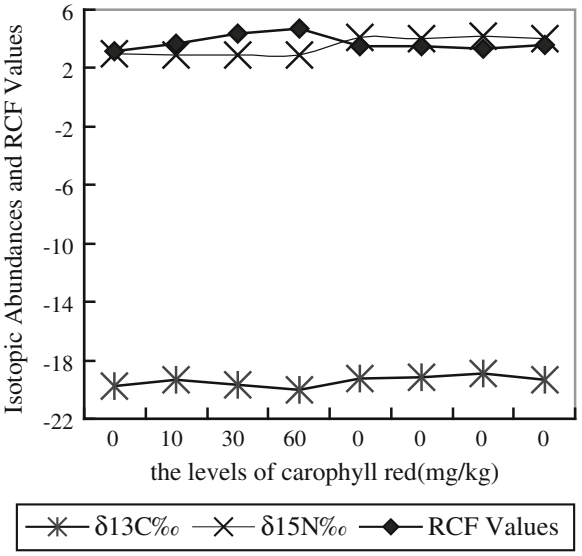

Fig. 166.1 Effect of adding pigment on δ^{13}C ‰ values and δ^{15}N ‰ values

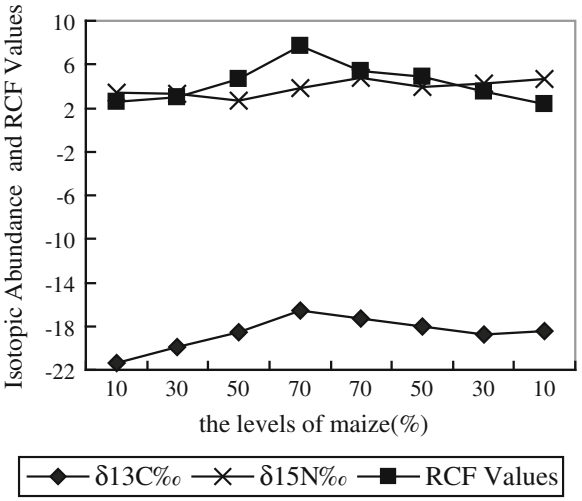

Fig. 166.2 Effect of maize on δ^{13}C ‰ values and δ^{15}N ‰ values

166.4 Conclusion

In maize diets, the RCF of leg and body skin and the δ^{13}C values are positively dependent on maize contents of diets. If carophyll red is used, the δ^{13}C values of chicken meat with golden skin (RCF6 $\pm$ 1)is less than -18 ‰. This study shows important difference in δ^{13}C values of the breast chicken and indicates the analysis of carbon and nitrogen stable isotopes might be used as a reliable evaluation tool for certification of qualified products from those unqualified products caused by carophyll red.

References

1. Gannes LZ, Del-Rio CM, Koch P (1998) Natural abundance variations in stable isotopes and their potential uses in animal physiological ecology. Comp Biochem Physiol 119:725–737
2. DeNiro MJ, Epstein S (1978) Influence of diet on the distribution of carbon isotopes in animals. Geochim Cosmochim Acta 42:495–506
3. Bricout J, Koziet J (1987) Control of the authenticity of orange juice by isotopic analysis. J Agric Chem 35:758–760
4. Bricout J, Koziet J (1985) Detection of the addition of sugar to orange juice by isotopic analysis. Sci de l'Alimentation 5:197–204
5. Camin F, Versini G, Gagliano G et al (2001) Regional origin assignment of italian orange juices by multielement and multicompound stable isotope ratio analysis. 6th international symposium on food authenticity and safety, Nantes, France
6. Kornexl BE, Rossmann A, Schmidt H (1995) Improving fruit juice origin assignment by combined carbon and nitrogen stable isotope ratio determination in pulps. Z Leben Unters Forsch A 202:5–59
7. Rossmann A, Rieth W, Schmidt HL (1994) Stable isotope ratio determination and its combination with conventional analyses (RSK values) for fruit juice authenticity control. In: Nagy S (ed) Methods to detect adulteration of fruit juice beverages. Agscience. Inc., Anburndale, Florida, vol 1, pp 28–40
8. Brookes ST, Barrie A, Davies JE (1991) A rapid $^{13}C/^{12}C$ test for determination of corn-syrups in honey. J Assoc Off Anal Chem 74:627–629
9. Giraudon S, Danzart M, Merle MH (2000) Deuterium nuclear magnetic resonance spectroscopy and stable carbon isotope ratio analysis/mass spectrometry of certain monofloral honeys. J Assoc Off Anal Chem 83:1401–1409
10. White JW, Winters K, Martin P et al (1998) Stable carbon isotope ratio analysis of honey: validation of internal standard procedure for worldwide application. J Assoc Off Anal Chem 81:610–619
11. Martin GJ, Guillou C, Martin ML et al (1988) Natural factors of isotope fractionation and the characterization of wines. J Agric Food Chem 36:316–322
12. Versini G, Monetti A, Reniero F (1997) Monitoring authenticity and regional origin of wines by natural stable isotope ratios analysis. In: Watkins TR (ed) Proceedings of the ACS symposium. Wine: nutritional and therapeutic benefits, ACS symposium series, vol 661, pp 113–130
13. Kelly S, Parker I, Sharman M et al (1997) Assessing the authenticity of single seed vegetable oils using fatty acid stable carbon isotope ratios ($^{13}C/^{12}C$). Food Chem 59:181–186
14. Manca G, Camin F, Coloru G et al (2001) Characterisation of the geographical origin of Pecorino Sardo cheese by casein stable isotope ($^{13}C/^{12}C$ and $^{15}N/^{14}N$) ratios and free amino acid ratios. J Agric Food Chem 49:1404–1409
15. Manca G, Franco MA, Versini G et al (2006) Correlation between multielement stable isotope ratio and geographical origin in Peretta cows'milk cheese. J Dairy Sci 89:831–839
16. Piasentier E, Valusso R, Camin F et al (2003) Stable isotope ratio analysis for authentication of lamb meat. Meat Sci 64:239–247
17. Hobson KA, Clark RG (1992) Assessing avian diets using stable isotopes I: turnover of ^{13}C in tissues. Condor 94:181–188
18. Delgado A, Garcia N (2001) $\delta^{15}N$ and $\delta^{13}C$ analysis to identify cattle fed on feed containing animal protein: a safety/quality index in meat, milk and cheese. 6th international symposium on food authenticity and safety, Nantes, France
19. Kornexl BE, Werner T, Rossmann A (1997) Measurement of stable isotope abundances in milk and milk ingredients—a possible tool for origin assignment and quality control. Z Leben Unters Forsch A 205:19–24
20. Rossmann A, Kornexl BE, Versini G (1998) Origin assignment of milk from alpine regions by multi-element stable isotope ratio analysis (Sira). J Food Sci Nutr 1:9–21

Chapter 167
Vascular Endothelial Growth Factor Induces Bone Marrow-Derived Mesenchymal Stem Cells Differentiation into Endothelial Cells

Nan Wang, Rui Zhang, Shuijing Wang, Jianjie du, Yanyang Tang and Tong-Cun Zhang

Abstract Mesenchymal stem cells (MSCs) are pluripotent progenitors and can differentiate into a variety of cell types, including osteoblasts, chondrocytes, and adipocytes. Vascular endothelial growth factor (VEGF) has been shown to stimulate endothelial cell mitogenesis and migrations. To investigate whether VEGF could induce rat bone marrow-derived MSCs differentiation into endothelial cells, we isolated and cultured rat bone marrow-derived MSCs from the femur of the Sprague–Dawley rats. MSCs were treated with VEGF for 2, 4, 7 days. The cellular morphology changes of MSCs were observed under phase contrast microscope. Then we tested the expression of endothelial cell markers VEGF receptor fms-related tyrosine kinase 1 (Flt-1) by reverse-transcription PCR (RT-PCR), western blot, and immunofluorescence technology. Our results showed that the expression levels of Flt-1 were significantly increased in time-dependent manner. The above results show that VEGF can induce mesenchymal stem cells differentiation into endothelial cells. The data provides the basis of constructing tissue engineering vascular.

Keywords Mesenchymal stem cells · Vascular endothelial growth factor · Endothelial cells · Differentiation

167.1 Introduction

Mesenchymal stem cell [1] (MSCs) are pluripotent progenitors that can differentiate into a variety of cell types, including osteoblasts, chondrocytes, and adipocytes. The ability of mesenchymal stem cells (MSCs) to differentiate into

N. Wang · R. Zhang · S. Wang · J. du · Y. Tang · T.-C. Zhang (✉)
A Key Laboratory of Industrial Microbiology, Ministry of Education and Tianjin City, College of Biotechnology, Tianjin University of Science and Technology, Tianjin 300457, People's Republic of China
e-mail: tony@tust.edu.cn

T.-C. Zhang et al. (eds.), *Proceedings of the 2012 International Conference on Applied Biotechnology (ICAB 2012)*, Lecture Notes in Electrical Engineering 251,
DOI: 10.1007/978-3-642-37925-3_167,

endothelial cells was recently demonstrated. Oswald et al. reported the differentiation of expanded adult human MSCs into cells with phenotypic and functional features of endothelial cells [2]. The differentiated MSCs provide new options for engineering of artificial tissues based on autologous MSCs and vascularized engineered tissues [3].

Vascular endothelial growth factor (VEGF), a vasculogenic factor [4], is an important signaling protein involved in both vasculogenesis (the formation of the circulatory system) and angiogenesis (the growth of blood vessels from pre-existing vasculature). As its name implies, VEGF activity is restricted mainly to cells of the vascular endothelium, although it does have effects on a limited number of other cell types [5, 6]. In vitro, VEGF has been shown to stimulate endothelial cell mitogenesis and cell migration. VEGF also enhances microvascular permeability and is sometimes referred to as vascular permeability factor [7, 8]. All members of the VEGF family stimulate cellular responses by binding to tyrosine kinase receptors (the VEGFRs) on the cell surface, causing them to dimerize and become activated through transphosphorylation. VEGF receptors fms-related tyrosine kinase 1 (Flt-1) [9] and the kinase insert domain receptor (KDR) [10] have an extracellular portion consisting of 7 immunoglobulin-like domains, a single transmembrane spanning region and an intracellular portion containing a split tyrosine kinase domain.

VEGF-A binds to VEGFR-1 (Flt-1) and VEGFR-2 (KDR/Flk-1). VEGFR-2 appears to mediate almost all of the known cellular responses to VEGF. The function of VEGFR-1 is less well defined, although it is thought to modulate VEGFR-2 signaling. Another function of VEGFR-1 is to act as a dummy/decoy receptor, sequestering VEGF from VEGFR-2 binding (this appears to be particularly important during vasculogenesis in the embryo).

The aim of our study is to investigate whether VEGF could induce rat bone marrow-derived MSCs differentiation into endothelial cells. It has the vital significance to cell transplantation for clinical treatment.

167.2 Materials and Methods

167.2.1 Cell Culture

Bone marrow-derived MSCs were isolated from the femurs and tibias of male Sprague—Dawley rats (weight 90–100 g) with the method published by our previous study [11, 12]. Bovine serum (FBS, PAA) at 37 °C in humified air with 5 % CO2. COS-7 cells (ATCC) were cultured in DMEM containing 10 % FBS, penicillin (100 U/mL) and streptomycin (100 U/mL).

167.2.2 Immunocytochemistry Assay

Immunocytochemistry assays were performed as described previously [13, 14]. The cells aftertreatment were fixed in 4 % paraformaldehyde for 15 min, and then blocked with normal goat serum for 30 min at room temperature (RT). Then, rabbit monoclonal antibody of Flt1 (1:500 dilution, Sigma) were added and incubated in a humid chamber over night. After washing with phosphate buffered saline (PBS) thrice, cells were incubated with appropriate secondary antibodies (fluorescein isothiocyanate (FITC)-goat anti-mouse IgG, Santa Cruz) for 50 min at 37 °C. After washing with PBS, the samples were observed under laser scanning confocal microscope (OLYMPUS, Japan). DAPI stain (blue) highlights the total nuclei.

167.2.3 Semi-Quantitative Reverse-Transcription Polymerase Chain Reaction

Semi-quantitative RT-PCR analysis was carried out as described previously [15, 16]. Briefly, total cellular RNA was extracted from cultured cells with Trizol reagent (Invitrogen) and reverse-transcribed using M-MLV reverse transcriptase (Promega) according to the manufacturer's instructions. The thermal cycle profile was as follows: denaturation for 30 s at 95 °C, annealing for 45 s at 52 °C about Flt-1 and 54 °C about GAPDH depending on the primers used, and extension for 45 s at 72 °C. For semi-quantitative assessment of expression levels, each PCR reaction was carried out for 28 cycles. PCR products were visualized on 2 % agarose gels stained with ethidium bromide under UV transillumination. Glyceraldehyde-3-phosphate dehydrogenase (GAPDH) was used as an internal control to show equal loading of the cDNA samples. The PCR primer sequences are as follows: GAPDH: forward-5′ATTCAACGGCACAGTCAAGG3′, reverse-5′GCAGAAGGGGCGGAGATGA3′; Flt-1: forward-5′CGGAGAAATCTGCTCGCTAT3′; reverse-5′CTTGGAAGGGACGACACG3′.

167.2.4 Western Blotting

Western Blotting was performed as described previously [17, 18]. The total protein of the cells was prepared using extraction buffer composed of PBS containing 0.5 % Triton X-100, EDTA, phenylmethylsulfonyl fluoride (PMSF), and complete protease inhibitors (Roche). The concentration of each protein lysate was determined by BCATM protein assay kit (Thermo). Equal amount of total protein was loaded on 12 % sodium dodecylsulfate polyacrylamide gel. Then samples were transferred to NC membranes and blocked for 60 min at RT in 5 % skim milk

powder (wt/vol) in PBS. The membranes were immunoblotted with mouse anti-rat β-actin (1:250 dilution, Santa Cruz) and rabbit anti-rat Flt1 (1:1,000 dilution, Abcam) antibodies overnight at 4 °C, and then incubated with IRDyeTM-800 conjugated anti-rabbit secondary antibodies (Li-COR) for 30 min at RT. The specific proteins were visualized by OdysseyTM Infrared Imaging System (Gene Company). β-actin expression was used as an internal control to show equal loading of the protein samples.

167.3 Results and Discussion

167.3.1 The Morphological Changes of MSCs Treated with VEGF

To investigate whether VEGF was able to induce differentiation of rat bone marrow-derived MSCs to endothelial cells, we used 50 ng/mL VEGF to stimulate MSCs for 2d, 4d and 7d. Endothelial phenotype was evident in VEGF-treated cells, while no obvious morphological changes were observed in those untreated cells (Fig. 167.1). MSCs in the control group were applanation, fusiform or polygon, and the cells in VEGF-treated groups became into colony, ellipse and arranged like pebble 7 days later.

167.3.2 The Expression of Flt-1 is Upregulated in VEGF-Treated MSCs Confirmed by Immunocytochemistry Analysis

To address the endothelial potential of MSCs, bone marrow-derived MSCs were treated with 50 ng/ml VEGF for 2d, 4d and 7d, and the expression of Flt-1 was estimated by immunocytochemistry. DAPI stained the nuclear in blue, and Flt1 stained in green. As shown in Fig. 167.2, MSCs stimulated with VEGF exhibit strong positive Flt expression, while MSCs in the control group have low expression. The results showed that the upregulation of endothelial cell marker Flt-1 expression was detected in MSCs treated with VEGF.

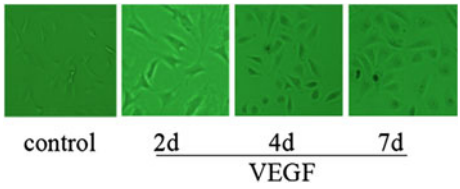

Fig. 167.1 The morphological changes of MSCs treated with VEGF at 2d, 4d and 7d in RMSC

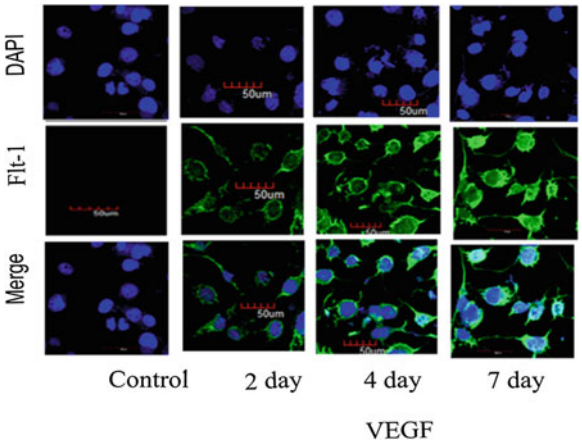

Fig. 167.2 Immunocytochemistry analysis Flt-1 expression by VEGF for 2d, 4d and 7d in RMSC

167.3.3 The mRNA Levels of Flt-1 are Increased in VEGF-Treated MSCs

To investigate the mRNA level changes of Flt-1 in MSCs differentiation, we tested the mRNA levels of Flt-1 by RT-PCR. As shown in Fig. 167.3a, VEGF increased the mRNA levels of endothelial cell markers Flt-1 in time-dependent manner. The intensity of PCR products on the agarose gel image was quantified using Biorad software and was plotted using Microsoft Excel. Data were shown as relative expression level after being normalized by GAPDH. Error bars represent the mean (±SE) of three independent experiments performed in triplicate. The chart showed that compared with no VEGF treatment, VEGF stimulation significantly upregulated Flt-1 mRNA levels (Fig. 167.3b).

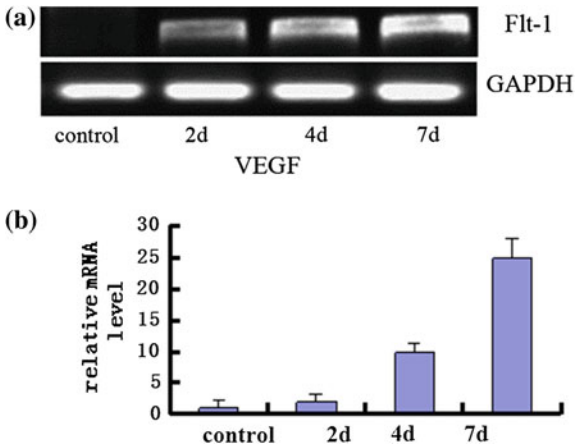

Fig. 167.3 The mRNA levels of Flt-1 in VEGF-treated MSCs at 2d, 4d, 7d. **a** The mRNA levels of Flt-1 by RT-PCR. **b** The relative quantity of Flt-1 mRNA levels depicted as a bar chart

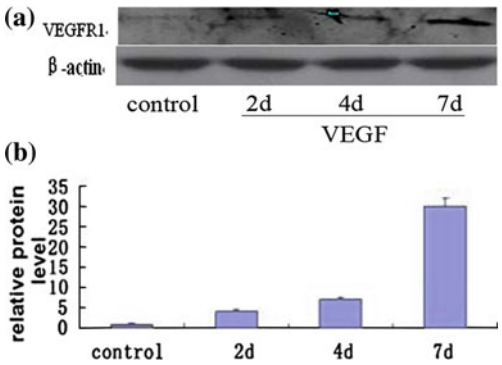

Fig. 167.4 Western blot assay detected Flt-1 expression in MSCs treated with VEGF at 2d, 4d and 7d. **a** The bands of Flt-1 protein by western blot assay. **b** The relative quantity of Flt-1 protein depicted as a bar chart

167.3.4 Western Blot Analysis Confirmed that the Expression of Flt-1 Increased in VEGF-Treated MSCs

We next detected the expression of Flt-1 in MSCs with or without VEGF by western blotting. As shown in Fig. 167.4a, with the VEGF-treated time prolonged, the expression of Flt-1 protein markedly rised in MSCs. The data in Fig. 167.4b showed relative expression level of Flt-1 after being normalized by β-actin. The results indicated that endothelial cell marker Flt-1 protein expression was upregulated in VEGF-treated mesenchymal stem cells.

167.4 Conclusion

To investigate whether VEGF can induce rat bone marrow-derived mesenchymal stem cells differentiation to endothelial cells, we did the above experiments. The cellular morphology changes of MSCs were observed under phase contrast microscope. MSCs treated with VEGF showed endothelial phenotype feature. Then we tested the expression of Flt-1 by RT-PCR, western blot and immunofluorescence. Results showed that the expression levels of Flt-1 were significantly increased in time-dependent manner. The above results show that VEGF can induce rat bone marrow-derived mesenchymal stem cells differentiation into endothelial cells. The data provides the basis of constructing tissue engineering vascular [19, 20].

Acknowledgments This work was financially supported by National Natural Science Foundation of China (31171303), Program for Changjiang Scholars and Innovative Research Team in University of Ministry of Education of China (IRT1166) and the Key Project of Chinese Ministry of Education (212010).

References

1. Pittenger MF, Mackay AM, Beck SC et al (1999) Multilineage potential of adult human mesenchymal stem cells. Science 284:143–147
2. Tischer E, Mitchell R, Hartman T et al (1991) The human gene for vascular endothelial growth factor. Multiple protein forms are encode through alternative exon splicing. J Biol Chem 266:11947–11954
3. Peters KG, De Vries C, Williams T et al (1993) Vascular endothelial growth factor receptor expression during embryogenesis and tissue repair suggests a role in endothelial differentiation and blood vessel growth. Proc Natl Acad Sci U S A 90:8915–8919
4. Vincenti V, Cassano C, Rocchi M et al (1996) Assignment of the vascular endothelial growth factor gene to human chromosome 6p21.3. Circulation 93:1493–1495
5. Wei MH, Popescu NC, Lerman MI et al (1996) Localization of the human vascular endothelial growth factor gene, VEGF, at chromosome 6p12. Hum Genet 97:794–797
6. ElAssal ON, Yamanoi A, Soda Y et al (1998) Clinical significance of microvessel density and vascular endothelial growth factor expression in hepatocellular carcinoma and surrounding liver: possible involvement of vascular endothelial growth factor in the angiogenesis of cirrhotic liver. Hepatology 27:1554–1562
7. Cornali E, Zietz C, Benelli R et al (1996) Vascular growth factor regulate angiogenesis and vascular permeability in Kaposi's sarcoma. Am J Pathol 149:1851–1869
8. Shweiki D, Itin A, Neufeld G et al (1993) Patterns of expression of vascular endothelial growth factor (VEGF) and VEGF receptors in mice suggest a role in hormonally regulated angiogenesis. J Clin Invest 91:2235–2243
9. Fong GH, Rossant J, Gertsenstein M et al (1995) Role of the Flt-1 receptor tyrosine kinase in regulating the assembly of vascular endothelium. Nature 376:66–70
10. Kaipainen A, Korhonen J, Pajusola K et al (1993) The related Flt4, Flt1, and KDR receptor tyrosine kinases show distinct expression patterns in human fetal endothelial cells. J Exp Med 178:2077–2208
11. Wang N, Ren GD, Zhou Z et al (2012) Cooperation of myocardin and Smad2 in inducing differentiation of mesenchymal stem cells into smooth muscle cells. IUBMB Life 64(4):331–339
12. Mise M, Arii S, Higashituji H et al (1996) Clinical significance of vascular endothelial growth factor gene expression in liver tumor. Hepatology 23:455–464
13. Chow NH, Hsu PI, Lin XZ et al (1997) Expression of vascular endothelial growth factor in normal liver and hepatocellular carcinoma: an immunohistochemical study. Hum Pathol 28:698–703
14. Xiang Y, Zheng Q, Jia B et al (2007) Ex vivo expansion, adipogenesis and neurogenesis of cryopreserved human bone marrow mesenchymal stem cells. Cell Biol Int 31:444–450. doi: 10.1016/j.cellbi.2006.11.012; S1065-6995(06)00271-X[pii]
15. Gospodarowicz D et al (1976) Humoral control of cell proliferation: the role of fibroblast growth factor in regeneration, angiogenesis, wound healing, and neoplastic growth. Prog Clin Biol Res 9:1–19
16. Rogers MS, Rohan RM, Birsner AE et al (2004) Genetic loci that control the angiogenic response to basic fibroblast growth factor. Faseb J 18:1050–1059
17. Rogers MS, Rohan RM, Birsner AE et al (2003) Genetic loci that control vascular endothelial growth factor-induced angiogenesis. Faseb J 17:2112–2114

18. Shaked Y, Bertolini F, Man S et al (2005) Genetic heterogeneity of the vasculogenic phenotype parallels angiogenesis. Implications for cellular surrogate marker analysis of antiangiogenesis. Cancer Cell 7:101–111
19. Carmeliet P et al (1999) Targeted deficiency or cytosolic truncation of the VE-cadherin gene in mice impairs VEGF-mediated endothelial survival and angiogenesis. Cell 98:147–157
20. Gerhardt H, Golding M, Fruttiger M et al (2003) VEGF guides angiogenic sprouting utilizing endothelial tip cell filopodia. J Cell Biol 161(6):1163–1177

Chapter 168
Fasting Effects on the Content of Liver and Muscle Glycogen in Sparrow

Xingjun Xu, Shuli Shao, Huaiyong Li, Ziqiang Wang, Guangjun Zhang, Chenyang Jin, Yabo Sun and Shijie Zhao

Abstract Glycogen is an important energy source of animals. In this study, we tested the effects of hunger domestication in baby mass, basal metabolic rate (BMR), and the content of liver glycogen and muscle glycogen. The sparrows were divided into the control group, the fasting group I, the fasting group II, the fasting group III, and the fasting group IV, respectively. After hunger domestication, baby mass was determined with a Sartorius balance, BMR was measured using the closed-circuit respirometer, the contents of liver and muscle glycogen were determined by the anthrone method. The results showed that the content of liver glycogen was higher than muscle glycogen in control group. The content of liver and muscle glycogen decreased significantly after fasting ($p < 0.01$).

Keywords Sparrows · Liver glycogen · Muscle glycogen · Hunger domestication

168.1 Introduction

Energy balance between ingestion and consumption is very important to animal's survival, growth, and reproduction. The energy reserves of the animals include direct energy substances in blood sugar, liver glycogen, muscle glycogen, and indirect energy material fat [1]. Glycogen, a storage form is important for animals to obtain energy for survival [2]. Sparrow is the common birds in the north, there are many research about it, but, up to now, the reports about the content of liver

X. Xu · H. Li · Z. Wang · G. Zhang · C. Jin · Y. Sun · S. Zhao
College of Life Science, Agriculture and Forestry,
Qiqihar University, Qiqihar 161006, People's Republic of China

S. Shao (✉)
College of Life Science, Qiqihar University, 30 Wenhua Street,
Qiqihar 161006, Hei Longjiang Province, China
e-mail: shshl32@163.com

T.-C. Zhang et al. (eds.), *Proceedings of the 2012 International Conference on Applied Biotechnology (ICAB 2012)*, Lecture Notes in Electrical Engineering 251,
DOI: 10.1007/978-3-642-37925-3_168,

and muscle glycogen of sparrow under hunger environmental conditions are little. Therefore, determination the content of liver and muscle glycogen of the sparrow in vivo has important theoretical significance and practical value for small birds energy balance.

168.2 Materials and Methods

168.2.1 Animals

Tree sparrows were live-trapped in Zhalong National Nature Reserve, Qiqihar City, Hei Longjiang Province (123° 47′ ~124° 37′ E, 46° 52′ ~47° 32′ N). The mean body mass of sparrows were 20.2 ± 0.5 g. Birds were transported to the laboratory and caged (50 × 30 × 20 cm) under natural photoperiod and room temperature. Food and water were supplied *ad lib*. After one week of adaptive feeding, sparrows were divided into five groups: control groups, fasting 1d, fasting 2d, fasting 3d, fasting 4d, respectively.

168.2.2 Determination of Body Mass

Body mass to the nearest 0.01 g was determined before experiment and after experiment with a Sartorius balance (model BS210).

168.2.3 Metabolic Trials

Oxygen consumption was measured using the closed-circuit respirometer according to Grecki [3]. Temperatures inside the animal chambers in a water bath were measured and maintained constant to ± 0.5 °C. The volume of the metabolic chamber was 3.6 L. The metabolic rates were measured at 25 °C and each trial lasted for 60 min after the animals had been in the metabolic chamber for about 1 h to stabilize its environment. Food was withheld 4 h to minimize the specific dynamic action before each test. H_2O and CO_2 were absorbed by silica gel and KOH. Records of oxygen consumption due to animal's activity in the chamber were discarded when computing the metabolic rate of each individual. The recording interval of O_2 consumption was 5 min. Two consecutive, stable and minimum readings were used to calculate metabolic rates. We used 20.08 J/ml O_2 to convert oxygen consumption to heat production and corrected to STP conditions [4–6].

168.2.4 Determination of Liver and Muscle Glycogen Content

After measurements, the animals were killed by decapitation and their liver and muscle were dissected out. Pieces of the liver and muscle (about 0.5 g) were isolated and added 5 % trichloroacetic acid solution (2 mL). Homogenization of the material for analysis was performed with Cole-Parmer 4,710 ultrasonic homogenizer for a period of 10–15 s room temperature. Food and water were supplied *ad lib*. After one week of adaptive feeding, sparrows were divided into five groups: control groups, fasting 1d, fasting 2d, fasting 3d, fasting 4d, respectively. The whole procedure was performed at a temperature of 0–4 °C (on ice). The glycogen content was determined by the anthrone method [7].

168.2.5 Determination of Body Fat

Body fat content was determined by Soxhlet extraction method [8]. Body fat content (%) = $(W_1 - W_2)/W \times 100$ %; Individual moisture content (%) = $(W - W_1)/W \times 100$ % (W_1: carcass dry mass; W_2: fat-free carcass dry mass after extraction; W: individual mass).

168.2.6 Statistics

The data were analyzed using SPSS package (16.0 version). Differences among groups were determined by One-Way ANOVA. All results were expressed as mean ±SD. Least significant difference (LSD) was used for statistical analysis of different groups, and $p < 0.05$ was taken to be statistically significant.

168.3 Results

168.3.1 Body Mass and Basal Metabolic Rate (BMR)

The mean masses of sparrows had no significant difference among the control groups and experimental groups ($p > 0.05$) (Table 168.1). After hunger domestication, the masses loss 2.50 g after 1d; 6.30 g after 2d; 6.70 g after 3d; 7.10 g after 4d; with the extension of the starvation, the weight reduced significantly ($p < 0.05$). Mass of sparrows increased 0.6 g in the control group after 4d ($p < 0.05$). Compared with the control group, the mass of the 1d group of sparrows decreased less than the 2d group, 2d, 3d, 4d group decreased to a larger extent.

Results from 2d to 4d group gave a slightly lower mass between groups, but the change in magnitude of the difference was not significant ($p > 0.05$). In the beginning of domestication, the body fat between the control group and experimental group sparrow had no significant difference. After domestication the sparrows body fat of four groups were decreased significantly ($p < 0.05$). The body fat of 3d and 4d group was lower than of 1d and 2d group, and body fat content of sparrows in the two groups did not differ significantly ($p > 0.05$). The BMR of sparrows in domesticated groups did not change significantly ($p > 0.05$).

168.3.2 Content of Glycogen

The content of liver glycogen differed among groups ($F = 575.493$, $p < 0.05$), the values decreased significantly within 1d and decreased slightly and slowly after 2d (Table 168.2). It was found that the content of muscle glycogen was lower than liver glycogen in the control group, and the content of both liver glycogen and muscle glycogen differed among groups ($F = 76.383$, $p < 0.05$). Compared with control groups, there was no difference after fasting 1d ($p > 0.05$), the values decreased significantly after 2d ($p < 0.01$), the differences of muscle glycogen content of sparrows among the other three groups were not significant ($p > 0.05$) (Table 168.2).

Table 168.1 The influence of sparrow's masses, body fat and BMR by fasting

Project	Control group	1d	2d	3d	4d
n	8	8	8	8	8
Early masses (g)	20.22 ± 0.51	21.74 ± 0.93	21.49 ± 0.20	21.35 ± 0.42	21.61 ± 0.47
Final masses (g)	20.85 ± 0.55	19.26 ± 1.63	15.19 ± 0.36	14.62 ± 0.44	14.50 ± 0.23
Masses change (g)	+0.57	−2.48	−6.30	−6.73	−7.11
Body fat content (%)	14.84 ± 1.28	8.76 ± 0.63	9.48 ± 0.50	7.14 ± 0.17	7.01 ± 0.13
BMR ($mLO_2/g{\cdot}h$)	5.67 ± 0.33	5.96 ± 0.60	6.20 ± 0.85	6.49 ± 0.89	5.58 ± 0.42

Table 168.2 The influence of sparrow's glycogen content by fasting

Project	Control group	1d	2d	3d	4d
n	8	8	8	8	8
Liver glycogen (%)	1.508 ± 0.04	0.305 ± 0.03**	0.128 ± 0.01**[a]	0.102 ± 0.01**[a]	0.072 ± 0.01**[a]
Muscle glycogen (%)	0.569 ± 0.02	0.486 ± 0.47*	0.139 ± 0.12**[a]	0.146 ± 0.16**[a]	0.083 ± 0.01**[a]

* $P < 0.05$, ** $P < 0.01$, compare with control group

[a] $P < 0.01$, compare with 1d group

168.4 Discussion

This study showed that the content of liver and muscle glycogen of sparrow would have been reduced gradually after fasting. The content of hephormone and muscle glycogen was affected significantly in the hunger domestication on the sparrow because of no direct source of energy for the sparrow in fasting conditions. In order to provide normal life activities of the energy required to sustain life, the body burns liver and muscle glycogen for energy [9]. The content of liver glycogen was more than the muscle glycogen, but the content of liver glycogen was reduced more significantly than muscle glycogen [10]. The reason was that the liver could directly improve energy, but muscle glycogen need to become liver glycogen to improve energy; the decline amplitude of liver glycogen and muscle glycogen of 1d group was larger than 2d, 3d, and 4d group, the changes of 2d, 3d, and 4d group was not significant. As an important energy source for the body, glycogen was metabolized after feed, and the next day, sparrow made a corresponding adjustment in order to adapt to this change. After fasting, the content of glycogen of sparrows and body mass was positively correlated, this may be due to the sparrow of higher mass stores more glycogen. The regulation of animal mass depends on the balance of energy intake and energy expenditure, weight change can reflect some adaptability adjustment due to the influence of the change of the nutrition and the environment, furthermore, the change of animal mass had an important effect on the animal physiology, morphology, and behavior.

Basal metabolic rate (BMR) is the rate of energy transformation in a rested, awake, and fasted state in the absence of thermal stress and is the smallest thermogenetic unit of animals maintaining normally physiological function. The use of BMR as an index of energy expenditure has received a great deal of attention from environmental physiologists, ecophysiologists, and comparative physiologists [11]. In this study, basal metabolic rate had no significant change, probably because when hungry sparrows lack the direct source of energy, the body had been at the lowest level of energy consumption [10].

168.5 Conclusion

The content of both liver glycogen and muscle glycogen decreased significantly after fasting, and the content of liver glycogen was higher than muscle glycogen. Tree sparrows could deplete the body's energy reserves and reducing the basis of energy consumption to ease the pressure to survive. This was one of animal's survival strategies.

Acknowledgments This work was financially supported by the science and technology research project from Hei Longjiang Education Department (No. 11541387), and the program for young teachers scientific research in Qiqihar university (2011 k-M38).

References

1. Swanson DL (2001) Are summit metabolism and thermogenic endurance correlated in winter acclimatized passerine birds? J Comp Physiol B 171:475–481
2. Ribeiro LF, Teixeira IP, Aparecidoda SG et al (2012) Effects of swimming training on tissue glycogen content in experimental thyrotoxic rats. Can J Physiol Pharmacol 90(5):587–593
3. Górecki A (1975) Kalabukhov-Skvortsov respirometer and resting metabolic rate measurement. In: Grodziński W, Klekowski RZ, Duncan A (eds) Methods for ecological bioenergetics. Blackwell Scientific, Oxford, pp 309–313
4. Maldonado K, Bozinovic F, Cavieres G et al (2012) Phenotypic flexibility in basal metabolic rate is associated with rainfall variability among populations of rufous-collared sparrow. Zoology(Jena) 115(2):128–133
5. Gentili GB, Tesi V, Linari M et al (2002) A versatile microwave plethysmograph for the monitoring of physiological parameters. IEEE Trans Biomed Eng 49(10):1204–1210
6. Ksiazek A, Konarzewski M (2012) Effect of dietary restriction on immune response of laboratory mice divergently selected for basal metabolic rate. Physiol Biochem Zool 85(1):51–61
7. Lovegrove BG, Perrin MR, Brown M (2011) The allometry of parrot BMR: seasonal data for the Greater Vasa Parrot, Coracopsis vasa, from Madagascar. J Comp Physiol B 181(8):1075–1087
8. Virot M, Tomao V, Colnagui G et al (2007) New microwave-integrated Soxhlet extraction. An advantageous tool for the extraction of lipids from food products. J Chromatogr A7 1174(1–2):138–144
9. Prestes J, Leite RD, Pereira GB et al (2012) Resistance training and glycogen content in ovariectomized rats. Int J Sports Med 33(7):550–554
10. Mauricio DM, Olivia VM, Adrián BR et al (2010) Daytime food restriction alters liver glycogen triacylglycerols, and cell size. A histochemica morphometric, and ultrastructural study. Comp Hepatol 9:5–14
11. Montgomery MK, Hulbert AJ, Buttemer WA (2012) Metabolic rate and membrane fatty acid composition in birds: a comparison between long-living parrots and short-living fowl. J Comp Physiol B 182(1):127–137

Chapter 169
Antibacterial Activity of Polyprenols and Other Lipids from *Ginkgo biloba* L. Leaves

Ran Tao, Chengzhang Wang and Zhenwu Kong

Abstract Polyprenols are new effective lipids separated from *Ginkgo biloba* L. leaves. In this paper, the light and heavy distillates were prepared from ginkgo lipids by extraction with petroleum ether, saponification, and molecular distillation. And then the seven known compounds: β-sitosterol acetate (1), palmitamide (2), glyceryl tripalmitate (3), β-sitosterol-3-O-β-D-glucopyranoside (4), β-sitosterol (5), stigmasterol (6), ergosterol (7), and polyprenols were isolated by chromatograph from lipids of *Ginkgo biloba* L. leaves. In the meantime, the antibacterial activity of light and heavy distillates, seven compounds and polyprenols was assessed against three pathogenic strains (*Staphylococcus aureus*, *Escherichia coli*, and *Bacillus subtilis*) employing disc-diffusion and broth-dilution assays. The heavy distillates showed the highest activity (zone of inhibition of 14–17 mm) followed by the light distillates (13–15 mm), polyprenols (12–14 mm), β-sitosterol (5) (10–14 mm), palmitamide (2) (11–13 mm), β-sitosterol-3-O-β-D-glucopyranoside (4) (10–13 mm), β-sitosterol acetate (1) (10–12 mm), stigmasterol (6), and ergosterol (7) (9–10 mm), glyceryl tripalmitate (3) (10 mm) at 500 μg/mL. MIC and MBC values for the bacteria sensitive to polyprenols were in the range of 31.3–62.5 μg/mL and 125 μg/mL. It can be inferred polyprenols which have synergistic inhibitory effect with other lipids.

Keywords *Ginkgo biloba* · Lipids · Polyprenols · Antibacterial activity

R. Tao · C. Wang (✉) · Z. Kong
Institute of Chemical Industry of Forest Products, CAF, Nanjing 210042,
People's Republic of China
e-mail: wangczlhs@sina.com

T.-C. Zhang et al. (eds.), *Proceedings of the 2012 International Conference on Applied Biotechnology (ICAB 2012)*, Lecture Notes in Electrical Engineering 251,
DOI: 10.1007/978-3-642-37925-3_169,

169.1 Introduction

Ginkgo biloba L. an endemic gymnospermous plant in china, is considered as a living fossil due to its survival over 180 millions of years. *Ginkgo biloba* L. leaves (GBL), as traditional chinese medicine, are commonly used in clinical. It was reported in the best-known chinese herbal, Shen Nong Ben Cao Jing (2800 BC) [1, 2]. GBL contain many kinds of bioactive components such as flavonoids, biflavones, proanthocyanidins, alkylphenols, carboxylic acids, polyprenols, and so on [2]. Ageta's study showed that ginkgo lipids mainly consisted of 10 % of fatty acids, 15 % of esters, 75 % of wax esters, aldehydes and long-chain alkanols [3]. Polyprenols, a kind of lipid from GBL, mainly existed in the form of acetates and were difficult to be separated from other lipid components. It was reported that non-saponifiable lipids of GBL contained terpenoids, polyprenols, sterols, chainlike alcohol (ketone, ester), and so on [4]. In the early 1970, Kircher [5] reported that the non-saponifiable fraction of GBL lipids was crystallized from alcohol-acetone and ethyl acetate to yield β-sitosterol. Thanh Thuy Nguyen Tu et al. used GC/MS to analyze the chemical composition of *Ginkgo biloba* L. external and internal leaves lipids and identify some components including several series of phenolic constituents and chain-like alcohol (ketone) [6]. *Ginkgo* polyprenols and chromatography of polyprenols in general were published at 2000 [7]. Wang et al. reported on studies separated of polyprenols enriched in heavy distillates from GBL by Molecular Short Distillation [4]. We reported recently on analysis of light distillates containing mainly volatile oil and chain-like alcohol (ketone, ester) separated by molecular distillation from non-saponifiable fraction of GBL based on Py-GC–MS [8]. Containing mainly sterols of the crystalline solids were separated from non-saponifiable fraction of GBL by saponification, extraction, refrigeration, and recrystallization [9]. However, there are still no systematic reports on the separation and purification of polyprenols and their co-existing lipids. On the basis of these studies, it is important to separate and identify main compounds of non-saponifiable lipids of GBL by chromatography and spectrometry for elucidating and studying further non-saponifiable lipids of GBL.

Biological activities of *Ginkgo* extracts and constituents were reported on defense against bacteria, insects, and fungi [10]. Sati et al. reported that hexane extracts of GBL had the function of defense against five animal and plant pathogenic strains [11]. A chloroform fraction that the active compounds were elucidated to be salicylic acids prepared from the sarcotesta of *Ginkgo* showed potent inhibitory activity against vancomycin-resistant *Enterococcus* (VRE) [12]. Therefore, we can conclude that fat-soluble components of GBL have the activity of defense against some specific types of bacteria. However, there are no evaluation of antibacterial activity of polyprenols and other lipids from GBL. Recently, we found that some components separated from non-saponifiable lipids of GBL had the antibacterial effect in vitro. In this study, we report that

polyprenols and other lipids are separated from non-saponifiable lipids of GBL by saponification, refrigeration, and chromatography. Besides, we report that the antibacterial effect of polyprenols and other lipids from GBL.

169.2 Materials and Methods

169.2.1 Materials

The dried GBL was collected in October 2011 from China's Jiangsu Province. This plant was identified and authenticated by Prof. WANG Cheng-zhang at the Institute of Chemical Industry of Forestry Products, CAF in China. Three bacteria (*Staphylococcus aureus* ATCC25923; *Escherichia coli*, NCTC12923; *Bacillus subtilis* NCTC10400) buyed from China General Microbiological Culture Collection Center (CGMCC) were used.

169.2.2 Extraction and Isolation

Air-dried and pulverized GBL (5 kg) were extracted 3 times with 15 L (total) petroleum ether (60–90 °C) for 24 h at 70 °C to give an extract (220 g) which was mixed with 2.5 L 5 % NaOH–EtOH for 2 h at room temperature, successively. The hydrolysate was extracted with 2.5 L petroleum ether for 3–4 times. The collected organic phases were washed with water to neutral and dried with anhydrous Na_2SO_4. The solvent was evaporated under vacuum to give the non-saponifiable lipid extract (110 g) which was dissolved in a solvent mixture (acetone:methanol = 85:15, V/V) for a solid–liquid ratio 1:6–1:8 (g/mL), then refrigerated for 2 h at −10 °C [4, 9, 13]. As a result, the frozen sediment (8 g) was generated by filtering quickly at low temperature from the refrigerated solution and the dissolved matters were concentrated to yield a product as brown oil (101 g).

The dissolved matters (101 g) were isolated by molecular distillation at feed temperature of 60 °C, distillation temperature of 280 °C, feed flow rate of 180 mL/h, scraper rate of 300 rpm, and operating pressure of 0.1–0.5 Pa to give the light distillates (LD) as yellow oil 21 g and the heavy distillates (HD) as dark brown oil 78 g. Polyprenols were further purified from a portion (10 g) of the heavy distillates by flash column chromatography (Merck, Kieselgel 60; 0.063–0.2 mm particle size; 6 × 80 cm), using petroleum ether (5 × 250 mL) and 1, 2, 3 % ethyl ether/petroleum ether (5 × 250 mL) as eluents [4, 13, 14]. The polyprenols (1.5 g, yielded) contents (over 95 %) in the samples were determined by HPLC using external standard method and the standard polyprenols (C_{75}–C_{105}) were purchased from Larodan Fine Chemical Co., Ltd, Sweden. HPLC measurement was performed at room temperature with Shimadzu SPD-10A instrument equipped with UV detector (210 nm) and a 5 μm Kromasil C18 ODS-1

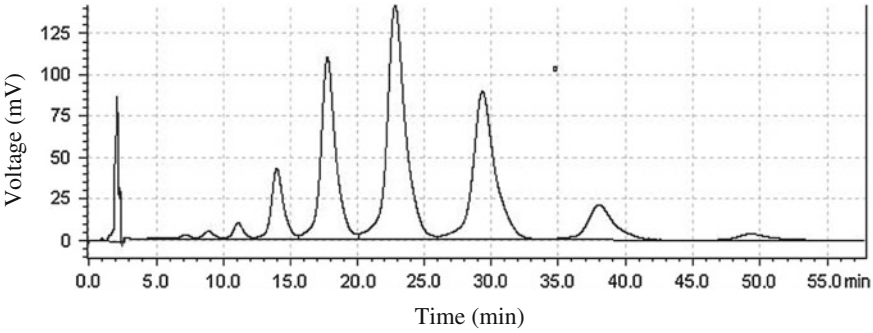

Fig. 169.1 Chromatogram of the polyprenols from *Ginkgo biloba* L. leaves

(150 × 4.6 mm) column, using a solvent mixture (isopropanol:methanol = 38:37, V/V) as the eluent at 1.0 mL/min (Fig. 169.1).

The frozen sediment (8 g) was dissolved in $CHCl_3$ (10 mL) and the $CHCl_3$ solution was subjected to silica gel (Merck, Kieselgel 60; 0.063–0.2 mm particle size; 6 × 80 cm) column chromatography. The fraction was eluted step by step with $CHCl_3$/MeOH (100:0–85:15 %, V/V) (10 × 150 mL). Fractions of similar composition determined by TLC analysis were pooled. The 100 % $CHCl_3$ portion was recrystallized from the 2-propanol to yield compound 1 (65 mg). The $CHCl_3$/MeOH (97:3 %, V/V) portion was recrystallized from anhydrous EtOH in order to generate compound 2 (40 mg). The $CHCl_3$/MeOH (95:5 %, V/V) portion was collected to yield compound 3 (30 mg). The $CHCl_3$/MeOH (90:10 %, V/V) portion was recrystallized from chloroform at low temperature to yield compound 4 (55 mg). The $CHCl_3$/MeOH (99:1 %, V/V) portion was subjected to gel permeation (GE, Sephadex LH-20; 1.5 × 80 cm) column chromatography, and eluted with $CHCl_3$/MeOH (50:50 %, V/V) (10 × 10 mL) in order to purify compounds 5 (6.6 g, cyclohexanone), 6 (35 mg, *n*-pentanol) and 7 (30 mg, Et_2O).

169.2.3 Determination of Antibacterial Activity

Antibacterial tests of selected bacteria were carried out using a disc-diffusion method [15]. A small sterile cotton swab was dipped into the 24-hour-old culture of bacteria and was inoculated by streaking the swab over the entire agar surface. After inoculation the plates were allowed to dry at room temperature in laminar chamber. The filter paper discs (6 mm) loaded with 100 μL of extract were placed on the surface of the agar plates. After 5 min the plates were incubated at 37 °C for 24 h. Gentamycin Sulfate (SigmaG3632, 100 mg) was used as positive control and the respective solvent as negative control. After 24 h of incubation, the diameter was observed for zone of inhibition, ZOI (measured in mm including disc size). All tests were performed in triplicate and observed values of ZOI are expressed as mean value with standard error of means (SEM).

169.2.4 Determination of Minimum Inhibitory Concentration and Minimum Bactericidal Concentration

Minimum inhibitory concentration (MIC) and Minimum bactericidal concentration (MBC) were determined using the broth-dilution method. MIC was performed at six concentrations of samples (250, 125, 62.5, 31.3, 15.6, 7.8 μg/mL) followed by serial dilution technique. All the wells showing no visible growth of strains were subcultured and incubated at 37 °C overnight. The highest dilution showing 100 % inhibition was recorded as MBC [11].

169.3 Results and Discussion

Totally seven known compounds were isolated from the different polar portion of the frozen sediment that collected from the non-saponifiable lipids of GBL by chromatography and the structures of the seven compounds were determined using spectroscopic techniques including ^{1}H and ^{13}C NMR according to the references: *β*-sitosterol acetate (1) [16], palmitamide (2) [17], glyceryl tripalmitate (3) [18, 19], *β*-sitosterol-3-O-*β*-D-glucopyranoside (4) [20], *β*-sitosterol (5) [21], stigmasterol (6), and ergosterol (7) [22] (Fig. 169.2).

The antibacterial activity of the light distillates (LD) and the heavy distillates (HD), seven compounds and polyprenols against bacteria were examined in this study and their potency were quantitatively assessed by ZOI (Table 169.1), MIC and MBC values (Table 169.2). The results from the diameters of inhibition zone showed from high to low were the heavy distillates (14–17 mm), the light distillates (13–15 mm), polyprenols (12–14 mm), *β*-sitosterol (5) (10–14 m), palmitamide (2) (11–13 mm), *β*-sitosterol-3-O-*β*-D-glucopyranoside (4) (10–13 mm), *β*-sitosterol acetate (1) (10–12 mm), stigmasterol (6), and ergosterol (7) (9–10 mm), glyceryl tripalmitate (3) (10 mm) at 500 μg/mL. The results indicated that the heavy distillates showed the highest activity among all the tested samples and inhibited the growth of all the bacterial strains (Table 169.1). MIC and MBC values for the bacteria sensitive to the heavy distillates were in the range of 15.6–31.3 μg/mL and 62.5–125 μg/mL, respectively (Table 169.2). The light distillates showed the second high activity, and the MIC values were in the range of 31.3–62.5 μg/mL and MBC were 62.5–250 μg/mL. MIC and MBC values for the bacteria sensitive to polyprenols were in the range of 31.3–62.5 μg/mL and 125 μg/mL. Glyceryl tripalmitate (3) was not active against *Staphylococcus aureus* and *Escherichia coli*. Stigmasterol (6) and ergosterol (7) was not active against *Bacillus subtilis.* All the samples were found less active than the used standard antibiotic gentamycin.

The non-saponifiable lipids of GBL were studied a little on its systematical isolation and antibacterial activity. Therefore, this study highlights for the first

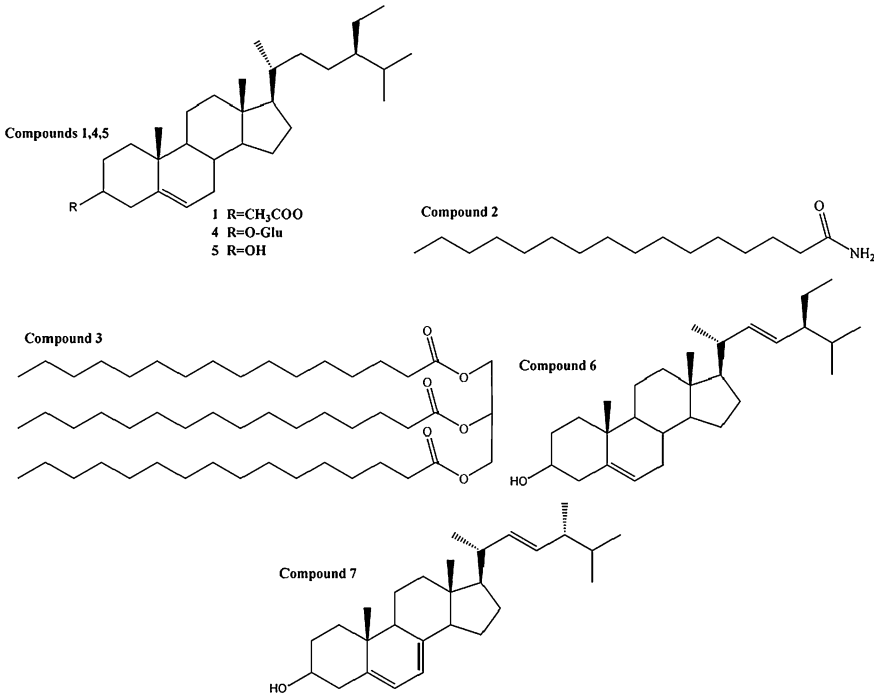

Fig. 169.2 Chemical structures of compounds 1–7 from *Ginkgo biloba* L. leaves

time the in vitro antibacterial activities of components separated from non-saponifiable lipids of GBL. This investigation supports that ethnobotanical uses of GBL relying on terpene trilactones and flavonoid glycosides, the active components of GBL might be responsible for their antibacterial activity [23]. In our previous study, it was reported on hepatoprotective and antitumor effects of GBL polyprenols in rats [14, 24, 25]. In this paper, this study supports new leads as there are no previous records on the antibacterial activity of polyprenols. Especially, the polyprenols are an important component [4] separated from the heavy distillates isolated by molecular distillation in the non-saponifiable lipids of GBL. And the heavy distillates had highest antibacterial activity in all samples of this study, except the positive control gentamycin. Therefore, it is of new implication to find out the other lipids having much more higher antibacterial activity than the polyprenols in the heavy distillates. It can also be inferred polyprenols that have synergistic inhibitory effect with other lipids.

Table 169.1 Zone of inhibition of different samples separated from *Ginkgo biloba*. L. leaves

	Diameter of inhibition zone (mm)[a]										
Bacteria	LD	HD	C1	C2	C3	C4	C5	C6	C7	Polyprenols	Gentamycin
Staphylococcus aureus	15 ± 0.9	17 ± 0.8	12 ± 0.4	13 ± 0	NA	13 ± 0.4	14 ± 0.6	9 ± 0.2	10 ± 0.4	14 ± 0.2	20 ± 0.6
Escherichia coli	14 ± 1.0	16 ± 0.6	11 ± 0.6	13 ± 0.2	NA	13 ± 0.2	13 ± 0.2	10 ± 0.2	9 ± 0.3	13 ± 0.6	21 ± 1.2
Bacillus subtilis	13 ± 0.3	14 ± 0.3	10 ± 1.0	11 ± 0.2	10 ± 0.9	10 ± 0.2	10 ± 0.3	NA	NA	12 ± 0.5	20 ± 0.4

[a] All the values are mean ± SEM of three determinations. LD: light distillates, HD: heavy distillates, C1: β-sitosterol acetate, C2: palmitamide, C3: glyceryl tripalmitate, C4: β-sitosterol-3-O-β-D-glucopyranoside, C5: β-sitosterol, C6: stigmasterol, C7: ergosterol, NA: not active

Table 169.2 Minimum inhibitory/bactericidal concentration (μg/mL) of different samples separated from *Ginkgo biloba*. L. leaves

	MIC and MBC values (μg/mL)									
Bacteria	LD	HD	C1	C2	C3	C4	C5	C6	C7	Polyprenols
Staphylococcus aureus	31.3	15.6	62.5	62.5	/	62.5	31.3	125	62.5	31.3
	125[a]	62.5[a]	250[a]	125[a]	/	125[a]	125[a]	250[a]	250[a]	125[a]
Escherichia coli	62.5	31.3	62.5	62.5	/	62.5	62.5	62.5	62.5	31.3
	125[a]	125[a]	250[a]	125[a]	/	250[a]	125[a]	250[a]	250[a]	125[a]
Bacillus subtilis	62.5	31.3	62.5	62.5	62.5	62.5	62.5	/	/	62.5
	250[a]	125[a]	250[a]	250[a]	250[a]	250[a]	250[a]	/	/	125[a]

[a] MBC values. LD: light distillates, HD: heavy distillates, C1: *β*-sitosterol acetate, C2: palmitamide, C3: glyceryl tripalmitate, C4: *β*-sitosterol-3-O-*β*-D-glucopyranoside, C5: *β*-sitosterol, C6: stigmasterol, C7: ergosterol

169.4 Conclusion

In this paper, the known compounds: *β*-sitosterol acetate (1), palmitamide (2), glyceryl tripalmitate (3) isolated and identified were reported first in all the components separated from GBL. The heavy distillates separated from GBL by molecular distillation showed the highest activity (zone of inhibition of 14–17 mm) in all samples of this study, except the positive control gentamycin. MIC and MBC values for the bacteria sensitive to polyprenols were in the range of 31.3–62.5 μg/mL and 125 μg/mL. Besides, this study can be inferred polyprenols that have synergistic inhibitory effect with other lipids. This study also provides new evidences as there are no previous reports on the antibacterial activity of non-saponifiable lipids including polyprenols from GBL against the pathogenic strains *Staphylococcus aureus*, *Escherichia coli*, and *Bacillus subtilis*. This study provides a new scientific basis for the ethnomedical use of GBL against bacterial diseases of animals and plants.

Acknowledgments The authors gratefully acknowledge the financial support by the National "Twelfth Five-Year" Plan for Science & Technology Support in China (No.2011BADB1B03).

References

1. Braquet P (1988) The ginkgolides from Chinese pharmacopeia to a new class of pharmacological agents: the antagonists of platelet activating factor. In: Braquet P (ed) Ginkgolides–Chemistry, biology, pharmacology and chemical perspectives, vol 1. Prous Science, Barcelona
2. Van Beek TA, Montoro P (2009) Chemical analysis and quality control of Ginkgo biloba leaves, extracts, and phytopharmaceuticals. J Chromatogr A 1216:2002–2032
3. Ageta H (1959) Chemical composition of the plants of the Coniferae and allied orders. XXVI, Studies on plant waxes. 13, Waxes from leaves of Ginkgo biloba and Ephedra gerardiana. J Pharm Soc Jpn 79:58–60

4. Wang CZ, Wang WL, Ye JZ et al (2008) Studies on separation of polyprenols from leaves of Ginkgo biloba L. by molecular short distillation. Chem Ind For Prod 28(3):23–27
5. Kircher HW (1970) β-sitosterol in Ginkgo biloba leaves. Phytochemistry 9:1879
6. Nguyen Tu TT, Derenne S, Largeau C et al (2001) Evolution of the chemical composition of Ginkgo biloba external and internal leaf lipids through senescence and litter formation. Org Geochem 32:45–55
7. Rezanka T, Votruba J (2001) Chromatography of long chain alcohols (polyprenols) from animal and plant sources. J Chromatogr A 936:95–110
8. Tao R, Wang CZ, Kong ZW (2012) Analysis of light distillates separated by molecular distillation from fat-soluble unsaponifiable matter of Ginkgo biloba leaves based on Py-GC–MS. Chem Ind For Prod 32(3):66–70
9. Wang CZ, Ye JZ, Zheng GY et al (2008) Studies on separation of sterols from Ginkgo biloba L. by molecular distillation and recrystallization. Chem Ind For Prod 28(2):43–47
10. Bombardelli E, Cristoni A, Morazzoni P (2000) Cosmetical uses of Ginkgo extracts and constituents. In: van Beek TA (ed) Ginkgo biloba. Harwood Academic Publishers, Singapore
11. Sati SC, Joshi S (2011) Antibacterial activities of Ginkgo biloba L. leaf extracts. Sci World J 11:2237–2242
12. Choi JG, Jeong SI, Ku CS et al (2009) Antibacterial activity of hydroxyalkenyl salicylic acids from sarcotesta of Ginkgo biloba against vancomycin-resistant Enterococcus. Fitoterapia 80:18–20
13. Wang CZ, Shen ZB, Tan WH et al (2004) Preparation and utilization of polyprenols and extractive from Ginkgo biloba L. leaves, Chinese Patent ZL01113696.0
14. Yang L, Wang CZ, Ye JZ et al (2011) Hepatoprotective effects of polyprenols from Ginkgo biloba L. leaves on CCl_4-induced hepatotoxicity in rats. Fitoterapia 82:834–840
15. Bauer AW, Kirby WM, Sherris JC et al (1966) Antibiotic susceptibility testing by a standardized single disk method. Am J Clin Pathol 45(4):493–496
16. Zhan Q, Wang Y, Li X et al (2009) Studies on the chemical constituents of petroleum ether extract of Lagerstroemia speciosa (Linn.) Pers leaves. Lishizhen Med Math Med Res 20(9):2125–2127
17. Lu LM, Song SJ, Xu SX et al (2001) Study on the chemical constituents of the ovum oil of Rana temporaria chensinensis David. Chin J Med chem 11(4):224–225
18. Alemany LB (2002) Using simple ^{13}C NMR linewidth and relaxation measurements to make detailed chemical shift assignments in triacylglycerols and related compounds. Chem Phys Lipids 120(1/2):33–44
19. Karaipekli A, Sari A, Bicer A et al (2010) Synthesis, thermal energy storage properties and thermal reliability of some fatty acid esters with glycerol as novel solid–liquid phase change materials. Sol Energy Mater Sol Cells 94(10):1711–1715
20. Sook KH, Hyun AJ, Hae YC et al (2006) In vitro peroxynitrite scavenging activity of 6-hydroxy kynurenic acid and other flavonoids from Gingko biloba yellow leaves. Arch Pharm Res 29(12):1074–1079
21. Kojim H, Sato N, Hatanoa A et al (1990) Sterol glucosides from Prunella vulgaris. Phytochemistry 29:2351–2355
22. Huang L, Cao Y, Xu H et al (2011) Separation and purification of ergosterol and stigmasterol in Anoectochilus roxburghii (wall) Lindl by high-speed counter-current chromatography. J Sep Sci 34(4):385–392
23. Singh B, Kaur P, Gopichand M et al (2008) Biology and chemistry of Ginkgo biloba. Fitoterapia 79(6):401–418
24. Wang CZ, Shen ZB (2003) The effects on transplanted Heps and EC tumors in mouse for polyprenols in combination with chemotherapeutic drugs. Chin J Biochem Pharm 24(3):113–115
25. Wang CZ, Shen ZB, Gao L (2003) Pharmacology of polyprenols from Ginkgo biloba L. leaves in combination with chemotherapeutic drugs on tumor. Chem Ind For Prod 23(3):15–18

Chapter 170
Effect of *Lactococcus lactis subsp.* on Production of Pigment and Citrinin by Monascus

Shichao Wang, Shuxin Zhao, Hongxia Mu, Fengyun Sun and Peng Chen

Abstract This study aimed at evaluation the effect of *Lactococcus lactis subsp.* TC-1 on production of pigment and citrinin by Monascus. 12 h fermented *Lactococcus lactis subsp.* TC-1 broth mixed with 24 h fermented *Monascus* FJ1 and FJ46, co-cultured for 96 h. Compared with the control, the result demonstrated that mixed culture could decrease the citrinin level dramatically, from 15.7 mg/kg to 1.3 mg/kg, and the red, orange, yellow pigment yield increased by 3.89, 2.22, 7.64 %, respectively. To study this phenomenon primarily, a series of experiments were carried out. Research revealed that, sodium lactate which exist in *Lactococcus lactis subsp.* TC-1 fermented broth play an important role. After mixed culture with sodium lactate, red, orange, yellow pigment yield increased by 130 %, 102 %, 46 % respectively, and citrinin yield decreased by 68 %.

Keywords Monascus · *Lactococcus lactis subsp* · Pigment · Citrinin · Mixed culture

170.1 Introduction

Red pigment is one of the most important color attributes for the acceptance of many types of food. Natural colorants derived from plants and microorganisms have recently gained popularity over synthetic coloring agents, which are potential carcinogens in some cases [1–3]. Pigments fermented by the fungi *Monascus sp*. have been traditionally used in Asia for coloring and securing a number of fermented foods [4–6]. Red yeast rice is produced by growing *Monascus sp*. on

S. Wang · S. Zhao (✉) · H. Mu · F. Sun · P. Chen
Key Laboratory of Industrial Microbiology, Ministry of Education, Tianjin Key Laboratory of Industrial Microbiology, School of Biotechnology, Tianjin University of Science and Technology, Tianjin 300457, China
e-mail: zsx999@tust.edu.cn

T.-C. Zhang et al. (eds.), *Proceedings of the 2012 International Conference on Applied Biotechnology (ICAB 2012)*, Lecture Notes in Electrical Engineering 251,
DOI: 10.1007/978-3-642-37925-3_170,

cooked rice to produce a red-colored product [7–9]. In China, monascus fermented product was also used as a Chinese medicine to strengthen the spleen, promote digestion, eliminate dampness and phlegm, promote blood circulation, and remove blood stasis [10, 11].

Besides pigments, most of *Monascus sp*. excretes a mycotoxin, citrinin, which rules out the use of the red pigments in various countries. Citrinin shows activity against bacteria, bacteriophages, sarcomas, protozoa, animal cells, and superior plant cells [12–14]. Citrinin has been known to be nephrotoxic, hepatotoxic, and carcinogenic to humans and animals. At present, the State Food and Drug Administration (SFDA) of China has enforced a limit of citrinin with level of 50 μg/kg in Red yeast rice-based functional foods [15]. Because of great concern about citrinin contamination, Japan has issued an advisory limit of 200 ppb; the current American Food and Drug Administration (FDA) action level of citrinin in agricultural products for sale is 20 ppb, and the European Union has a recommended a limit of 100 ppb [16].

Monascus pigment fermentations have been performed mainly in solid state cultures [17–19]. However, liquid state fermentation method features in large scale, higher degree of automation, and other significant advantages, so that much research has focused on liquid state fermentation [20]. There have been reports that improve many factors such as carbon and nitrogen sources, pH, and minerals that influence pigment and production in flask cultures [21]. In our laboratory, earlier research had mixed cultured monascus and the other strain, in this way, pigment production increased and excitation wavelength decreased.

The purpose of this work was to study the effect of *Lactococcus lactis subsp.* TC-1 on pigment and citrinin production of *Monascus*, and the mechanism of the action was also studied.

170.2 Materials and Methods

170.2.1 Material

Monascus stain: FJ1; *Lactococcus lactis subsp*. TC-1

170.2.2 Method

170.2.2.1 Cultivation

Seed Culture Preparation

Spore suspensions of *Monascus sp.* was prepared from actively growing plants in sterile distilled water. Spore suspension (1 ml) of FJ1 was inoculated to 250 ml

Erlenmeyer flasks containing 50 ml seed cultive medim (sucrose 1 %, peptone 0.3 %, K_2HPO_4 0.05 %, $MgSO_4$ 0.05 %, pH 5.7) and incubated at 35 °C for 24 h in a rotary shaker incubator at 160 r/min.

Monascus Fermentation

Prepared seed culture was transferred to the fermentation medium (rice powder 2 %, peptone 0.1 %, glucose 2 %, pH 5.8. 50mL in 250 mL Erlenmeyer flasks) and fermented for 5 days at 35 °C in a rotary shaker (160 r/min).

Lactococcus lactis subsp. TC-1 Fermentation

TC-1 was transferred to CM medium from stock culture and incubated at 30 °C for 12 h. And then 1 ml of seed culture was transferred to the CM medium (sucrose 1 %, peptone 1 %, yeast extract powder 1 %, K_2HPO_4 1 %, NaCl 0.2 %, $MgSO_4$ 0.02 %, pH 6.8. Fifty milli litre in 250 mL Erlenmeyer flasks) and static culture for 12 h at 30 °C.

Pretreatment of TC-1 Fermented Broth

The TC-1 fermented broth was centrifuged at 10,000 r/min for 10 min. The deposit washed with sterile water for three times and the supernatant filtered throw 0.22 μm filtration membrane before use. Heat treated the cell and supernatant to get the inactivated cell and supernatant. To separate the fermented supernatant, a 4000da hollow-fiber membrane was introduced, and the permeate and retentate filtered throw 0.22 μm filtration membrane before use.

Mixed Cultured of Different Treated TC-1 Fermented Broth and FJ1

After static culture for 12 h, 0.4 ml of TC-1 fermentation product was added to FJ1 fermented broth which was cultured for 24 h and co-cultured for 4 days at 35 °C in a rotary shaker (160 r/min).

170.2.2.2 Analytical Methods

Pigment Extraction and Analysis

Finely homogenized and ground sample 2 ml and 5 ml of absolute ethyl alcohol was placed in a tube with stopper, water bath (60 °C) for 1 h, and then the extract strained by a filter paper. The absorbance maxima of pigment extract was

measured by spectral analysis at 505, 465 and 410 nm to analyze the red and yellow pigments, respectively.

$$\text{Pigment production was expressed as a formula:Pigment production} = \frac{OD \times D \times V}{m} \quad (1)$$

V volume of fermented broth, ml.
D dilution.
m The biomass of V volume fermented broth, g.

Citrinin Determination

To make citrinin extraction, 2 ml broken mycelium suspension mixed with 4 ml absolute ethyl alcohol was placed in a water bath (60 °C) for 1 h,and then the fungal extracts filtered through a 0.22 μm hydrophobic membranes and analyzed for citrinin content by HPLC (Agilent 1,200 serious). A C18 column, 4.6 × 250 mm, i.d. 5 μm, was used as the analytical column (Agilent Eclipse XDB-C18). The mobile phase contained acetonitrile 35 %, nano water 65 % (pH 2.5), and the flow ratio was set at 1.5 ml/min, and citrinin was detected using a FLD detector set at excitation wavelength of 331 nm and emission wavelength 500 nm.

$$\text{Citrinin production was expressed as a formula:} C = \frac{C_0 \times D \times \mathrm{V}}{m} \quad (2)$$

C citrinin concentration, mg/kg.
D dilution.
C_0 citrinin concentration detect by HPLC, mg/L.
V volume of fermented broth, ml.
m The biomass of V volume fermented broth, ml.

Table 170.1 Effect of TC-1 on fermentation of FJ1

Strains	Pr/U/gD	Po/U/gD	Py/U/gD	Pc/mg/kg
FJ1	2574	1730	3304	15.7
L-FJ1	2605	1768	3557	1.3

L-FJ1: TC-1 mixed with FJ1, D: Dry mycelium, Pr, Po, Py, Pc: Production of red, orange and yellow pigment and citrinin

170.3 Results and Discussion

170.3.1 Effect of TC-1 on Fermentation of FJ1

Mixed cultured FJ1 and TC-1and the result were shown in Tables 170.1 and 170.2. As shown in the Table 170.2, the amount of pigment increased, and citrinin decreased distinctly.

170.3.2 Preliminary Study of the Effect that TC-1 Displayed in Fermentation of FJ1

170.3.2.1 The Effect of Supernatant

FJ1 fermentation broth added TC-1 fermented supernatant and inactive supernatant by heat treatment as a result, the amount of pigment production increased, and the citrinin production decreased (Table 170.3 and Fig. 170.1).

We can conclude from the results that certain components in the fermented supernatant increase the pigment production and decrease the citrinin production,and that compounds have heat resistance.

170.3.2.2 The Effect of Cell

Table 170.4 and Fig. 170.2 indicate co-cultured TC-1 cell and inactive cell by heat treatment with FJ1, respectively as preceding, the amount of pigment increased, and the citrinin increased.

Table 170.2 Effect of TC-1 on FJ1 pigment and citrinin production change ratio

Strains	Promotion ratio (%)			Inhibition ratio (%)
	Pr	Po	Py	Pc
FJ1	3.89	2.22	7.64	91.8

Table 170.3 Effect of different treated TC-1 fermented broth on FJ1 pigment and citrinin production change ratio

Additive	Promotion ratio (%)			Inhibition ratio (%)
	Pr	Po	Py	Pc
Fermented broth	8.2	2.5	12.1	75.4
Supernatant	29.7	60.5	29.3	68.8
Inactive supernatant	19.6	32.6	39.4	54.6

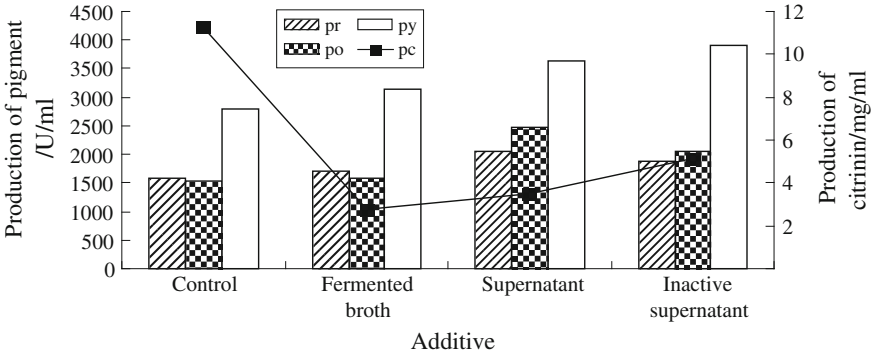

Fig. 170.1 The effect of different treated TC-1 fermented broth

Table 170.4 The effect of different treated TC-1 cell on FJ1 pigment and citrinin production change ratio

Additive	Promotion ratio (%)			Inhibition ratio (%)
	Pr	Po	Py	Pc
Fermented broth	25.2	13.8	28.3	40.6
Cell	12.6	25.1	0.05	−24.8
Inactive cell	3.2	−15.0	4.0	−11.6

170.3.2.3 The Effect of Different Components

Previous researches showed that, components decreased critrinin and increased pigments exist in TC-1 fermented supernatant. In further study, the main emphasis of our research focused on separation by ultrafiltration.

Effect of Different Size Molecules

In this experiment, added retentate and permeate separated from TC-1fermented supernant into FJ1 fermented broth. The amount of pigment increased, and the citrinin decreased, when mixed cultured with permeate. The retentate make the results adverse to that of permeate (Table 170.5 and Fig. 170.3).

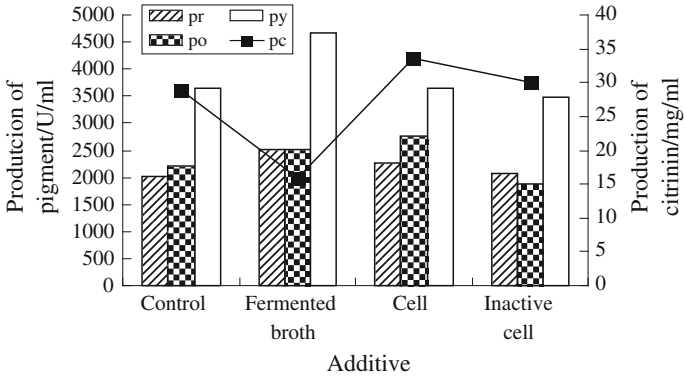

Fig. 170.2 The effect of different treated TC-1 cell

Table 170.5 The effect of composition of different size molecules on FJ1 pigment and citrinin production change ratio

Additive	Promotion ratio (%)		Inhibition ratio (%)	
	Pr	Po	Pr	Po
Permeate	31	23	23	51
Retentate	−18	−17	−2	−295

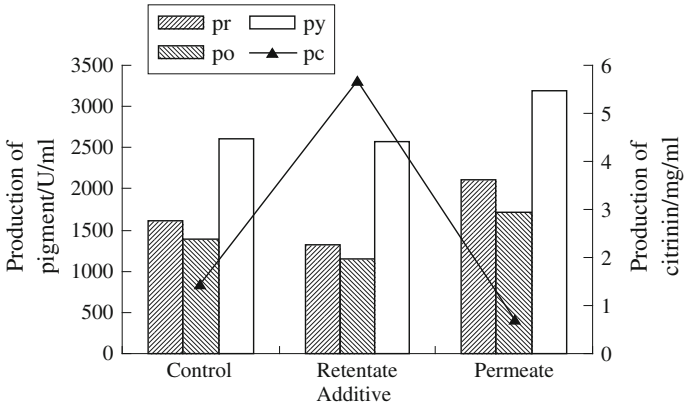

Fig. 170.3 The effect of composition of different size molecules

As we know, lactic acid and sodium lactate are important productions exit in Lactic acid bacteria fermentation broth. We surmised that the effects were caused by acetic acid and sodium lactate. Further study focused on the check of the surmise.

Table 170.6 The effect of lactic acid and sodium lactate on FJ1 pigment and citrinin production change ratio

Additive	Promotion ratio (%)			Inhibition ratio (%)
	Pr	Po	Py	Pc
Supernatant	109	84	39	59
Sodium lactate	130	102	46	68
Lactic acid	86	63	35	12

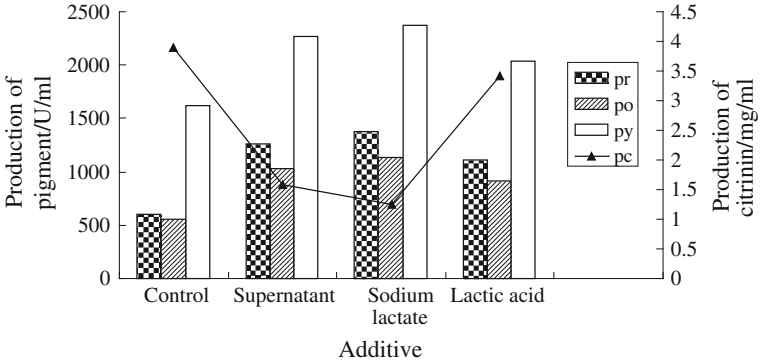

Fig. 170.4 The effect of lactic acid and sodium lactate

Effect of Lactic Acid and Sodium Lactate

In this experiment, Lactic acid and sodium lactate added into FJ1 fermentation broth as mentioned above.

According to Table 170.6 and Fig. 170.4 the amount of pigment increased, and the citrinin decreased, and the effect of sodium lactate superior to that of lactic acid.

170.4 Conclusions

Higher pigments production and lower critrinin production were achieved by mixed cultured *Lactococcus lactis subsp*. TC-1with *Monascus* FJ1. In this study, pigment production increased slightly, the critrinin decreased effectively. According to the study, sodium lactate, which produced by TC-1, played an important role in the procedure of increase in the pigment and decrease citrinin production. Further studies should be taken to investigate the mechanism of the action in detail.

References

1. Mapari SAS, Nielsen KF, Larsen TO et al (2005) Exploring fugal biodiversity for production of water-soluble pigments as potential natural food colorants. Curr Opin Biotechnol 16:231–238
2. Kongruang S (2011) Growth kinetics of biopigment production by Thai isolated Monascus purpureus in a stirred tank bioreactor. J Ind Microbiol Biotechnol 38:9–99
3. Vidyalakshmi P, Murugesh et al (2009) Stimulation of monascus pigments by intervention of different nitrogen sources. Glob J Biotechnol Biochem 1:25–28
4. Park HJ, Kim IS (2011) Antioxidant activities and anticancer effects of red yeast rice grown in the medium containing garlic. Food Sci Biotechnol 20(2):297–302
5. Lin CF (1973) Isolation and culture condition of Monascus sp. for the production of pigment in submerged culture. J Ferment Technol 51:407–414
6. Babitha S (2009) Microbial pigments. In: Singh nee' Nigam P, Pandey A (eds) Biotechnology for agro-industrial residues utilisation. Springer, Korea
7. Liu DC, Wu SW et al (2010) Effects of addition of anka rice on the qualities of low-nitrite Chinese sausages. Food Chem 11(8):245–250
8. Tseng YY, Chen MT et al (2000) Growth, pigments production and protease activity of Monascus purpureus as effect by salt, sodium nitrite, polyphosphate and various sugars. J Appl Microbiol 88:31–37
9. Huang Z, Xu Y, Zhang H et al (2011) Simultaneous determination of two Monascus metabolites in Red yeast rice by HPLC using fluorescence detection. Food Chem 27:1837–1841
10. Pattanagul P (2002) Using of vegetable oil, angkak, soy protein isolate and tapioca starch to improve the quality of sausages. Master's thesis, Chiang Mai University, Thailand
11. Pattanagul P, Pinthong R, Phianmongkhol A et al (2007) Review of angkak production (Monascus purpureus). Chiang Mai J Sci 34(3):319–328
12. Martin W, Lorkowski G, Creppy EE et al (1986) Action of citrinin on bacterial chromosomal and plasmid DNA in vivo and in vitro. Biotechnol Appl Microbiol 6:1273–1279
13. Blanc PJ, Loret MO, Goma G (1995) Production of citrinin by various species of Monascus. Biotechnol Lett 17:291–294
14. Fernanda S, Orozco B, Kilikian BV (2008) Effect of pH on citrinin and red pigments production by Monascus purpureus CCT3802. Microbiol Biotechnol 24:263–268
15. Li Y, Zhou YC, Yang MH et al (2012) Natural occurrence of citrinin in widely consumed traditional Chinese food Red yeast rice, medicinal plants and their related products. Food Chem 132:1040–1045
16. Shi YC, Pan TM (2011) Beneficial effects of Monascus purpureus NTU 568-fermented products: a review. Appl Microbiol Biotechnol 90:1207–1217
17. Lee CL, Wang JJ, Kuo SL et al (2006) Monascus fermentation of dioscorea for increasing the production of cholesterol-lowering agent-monacolin K and antiinXammation agent-monascin. Appl Microbiol Biotechnol 72:1254–1262
18. Babitha S, Soccol CR, Pandey A (2007) Solid-state fermentation for the production of Monascus pigments from jackfruit seed. Bioresour Technol 98:1554–1560
19. Lee CL, Hung HK, Wang JJ et al (2007) Improving the ratio of monacolin K and citrinin production of Monascus purpureus NTU568 under dioscorea medium through the mediation of pH value and ethanol addition. J Agric Food Chem 55:6493–6502
20. Lin CF (1973) Isolation and cultural condition of Monascus sp. for the production of pigment in a submerged culture. J Ferment Technol 51(4):07–14
21. Lee BK, Park NH, Piao HY et al (2001) Production of red pigments by Monascus purpureus in Submerged Culture. Biotechnol Bioprocess Eng 6:341–346

Chapter 171
Prediction of NH_4^+ Concentration During the Temperature Triggered Glutamate Fermentation Using At-Line Near-Infrared Spectroscopy

Jingbo Liang, Dalong Zhang, Xuan Guo, Qingyang Xu, Xixian Xie, Chenglin Zhang and Ning Chen

Abstract Near-infrared (NIR) spectroscopy, a rapid and nondestructive analytical technique, was applied to predict the NH_4^+ concentration of the culture broth from temperature triggered glutamate fermentation. NIR data of 164 samples of supernatant were analyzed by partial least squares (PLS) regression with several spectra preprocessing methods. The coefficient of determination (R^2), model root mean square error of calibration (RMSEC), and root-mean-square error of prediction (RMSEP) of the test calibration for NH_4^+ concentration were 0.9839, 4.34 and 4.62 mmol/l, respectively. These results suggested that the model had an accurate predictive capacity for NH_4^+ concentration. The proposed model provides a potential fast way for control and optimization of glutamate fermentation process.

Keywords Glutamate fermentation · NH_4^+ · Near-Infrared spectroscopy · Partial least squares

171.1 Introduction

Glutamate, mainly used as a flavoring agent, has become an important product for industrial exploitation of microbiology [1–3]. Since *Corynebacterium glutamicum* was selected for the glutamate producing bacterium by Kinoshita in 1957 [4], glutamate production is more than 1,500,000 tons per year worldwide [5]. Several strategies can induce glutamate overproduction, such as biotin limitation, addition of antibiotics (penicillin, ethambutol), detergents, or cerulenin (an inhibitor of the condensing enzyme of the fatty acid synthase complex), and temperature triggered [6–9]. In particular, when the temperature triggered strategy is used, the process is

J. Liang · D. Zhang · X. Guo · Q. Xu · X. Xie · C. Zhang · N. Chen (✉)
College of Biotechnology, Tianjin University of Science and Technology, Tianjin 300457, People's Republic of China
e-mail: ningch66@gmail.com

T.-C. Zhang et al. (eds.), *Proceedings of the 2012 International Conference on Applied Biotechnology (ICAB 2012)*, Lecture Notes in Electrical Engineering 251,
DOI: 10.1007/978-3-642-37925-3_171,

divided in two phases: (1) a first phase, where an optimal temperature is applied to the cell growth and (2) a second phase with a temperature shift for inducing glutamate overproduction [10].

In *Corynebacterium glutamicum*, glutamate is produced from 2-oxoglutarate amination as shown in Eq. (1), and thus NH_4^+ is rapidly exhausted during the process of glutamate production [11]. So ammonia is additionally and continuously added to enhance glutamate production during the fermentation process. While superfluous ammonia can lead to higher pH of fermentation broth and toxicity to the bacteria. So real time and exact monitoring of NH_4^+ concentration seems rather necessary.

$$2-\text{oxoglutarate} + NH_4^+ + \text{NADPH} + H^+ \overset{\text{glutamatedehydrogenase}}{\rightleftarrows} \text{glutamate} + H_2O + \text{NADP}^+ \quad (1)$$

In recent years, near-infrared (NIR) spectroscopy has increasingly been adopted as an analytical tool to detect targeted substance qualitatively and quantitatively in various fields including fermentation industry NH_4[12–20]. And it has even superseded some traditional methods for its unique advantages [21]: (1) it is a noninvasive, nondestructive characteristic; (2) it requires minimal sample without any addition preparation; (3) measurement and result delivery are quite fast and (4) a single spectrum allows several analytes to be determined simultaneously.

In this study, multivariate models were developed to quantify NH_4^+ concentration through the process of temperature triggered glutamate fermentation using at-line NIR spectroscopy and the partial least squares (PLS) regression. It will be of critical significance for the control fermentation process and instability of glutamate production.

171.2 Materials and Methods

171.2.1 Microorganism and Medium

The temperature triggered strain *Corynebacterium glutamicum* CN1021 used as glutamate-producing strain in this study was obtained from earlier work in our laboratory and stored at the Culture Collection of Tianjin University of Science and Technology.

The seed medium contained the following (per liter of water): glucose 30 g; corn steep liquor 40 ml; soybean protein hydrolysate 30 ml; vitamin B_1 0.6 mg; vitamin H 0.6 mg; KH_2PO_4 3 g; $MgSO_4$ 2 g; $MnSO_4$ 5 mg; $FeSO_4$ 5 mg; methionine 0.05 mg; and urea 5 g.

The medium for glutamate fermentation contained the following (per liter of water): glucose 50 g; beet molasses 40 g; corn steep liquor 40 ml; soybean protein

hydrolysate 20 ml; vitamin B_1 0.6 mg; vitamin H 0.6 mg; K_2HPO_4 4.5 g; $MgSO_4$ 2 g; $MnSO_4$ 30 mg; and $FeSO_4$ 30 mg.

The pH of both media was adjusted to 7.0 with 4 mol/l NaOH.

171.2.2 Process of Fermentation

A single colony of *Corynebacterium glutamicum* CN1021 was inoculate into a 1,000 ml baffled flask containing 100 ml of seed medium and cultivated at 32 °C, 200 rpm for 14 h. A 300 ml inoculum of this culture was transferred aseptically to a 5–l seed fermenter (Biotech-2002 Bioprocess controller, Baoxing, Shanghai, China) containing 3–l seed medium and cultivated at 33 °C for 14 h. The pH was adjusted to 7.0 with 25 % (v/v) ammonia during the whole cultivation period. The dissolved oxygen (DO) level was maintained at approximately 20 % saturation by adjusting the agitation and aeration rate.

Fed-batch fermentation was performed in 30–l jar fermenters (Biotech-2002 Bioprocess controller, Baoxing, Shanghai, China) containing 15 l of production medium with 20 % (v/v) inoculum size. In the process of glutamate fermentation, pH was maintained at 7.0 with 25 % (v/v) ammonia. The temperature of growth phase was kept at 33 °C and at 38.5 °C during the overproduction phase to provoke glutamate production. The DO level of growth phase and production phase was respectively maintained at approximately 20 and 10 % saturation by adjusting the agitation and aeration rate. When the initial glucose was depleted, 800 g/l glucose solution was fed into the fermenter to meet specific experimental requirement.

171.2.3 Sampling and Analytical Methods

For each microfermentation trial, samplings were carried out every hour during process of glutamate fermentation and a total of 164 samples from eight batches were obtained. Samples were centrifuged at 13,000xg for 2 min and supernatant were collected to determine NH_4^+ concentration by BioProfile 300A Nova (Nova Biomedical, Massachusetts, America).

171.2.4 NIR Spectra Acquisition and Preprocessing

The infrared spectra from 833–2,500 nm were obtained with a resolution of 8.0 cm^{-1} and an accumulation of 32 scans using a Bruker NIR Analyzer Tensor 37 spectrophotometer (Bruker Optics, Ettlingen, Germany).

The raw spectra were mathematically transformed and visualized using the software OPUS 7.0 (Bruker Optics, Ettlingen, Germany) with the aim to reduce the spectral variability associated with the physical characteristics of samples and the instrumental variability [22]. In order to achieve the best prediction performance, several spectral preprocessings were investigated followed by variable selection by different methods. The preprocessing methods include first derivative (1st), second derivative (2nd), standard normal variate (SNV), multivariate scatter correction (MSC), 1st + SNV and 1st + MSC.

171.2.5 Multivariate Calibration Model

The multivariate calibration model is a statistical tool that has been widely used in spectroscopy analysis [23]. Partial least squares regression (PLS) is a popular multivariate calibration technique for quantitative analysis of NIR spectral data [24]. The objective of this multivariate statistical technique to develop regression models is to establish a model for the analysis of unknown samples (determination of a physical or chemical property from the spectrum). Multivariate calibration model was developed using partial least square (PLS) regression with test set validation. The sampling was divided into calibration set and validation set. The selection of the number of latent variables (LVs) was due to the minimization of root-mean-square error of prediction (RMSEP) of the validation set, which reminded the predictive error obtained in the test set validation stage. PLS model was developed by OPUS 7.0 (Bruker Optics, Ettlingen, Germany). The RMSEP was calculated as Eq. (2):

$$\mathrm{RMSEP} = \sqrt{\frac{\sum_{i=1}^{n_p} \left(X_{pi} - \overline{X}_{pi}\right)^2}{n_p}} \tag{2}$$

in which n_p is the number of observations in the validation set and $\overline{X}_{pi}$ as well as X_{pi} is the measured and predicted values, respectively.

171.3 Results and Discussion

171.3.1 Chemical Analysis and NIR Spectra of Sample

The raw spectrum of samples by Bruker NIR Analyzer Tensor 37 spectrophotometer was shown in Fig. 171.1 and concentration of NH_4^+ from 164 collected samples during temperature triggered glutamate fermentation process was shown in Table 171.1. The NH_4^+ concentration of calibration set and validation set was

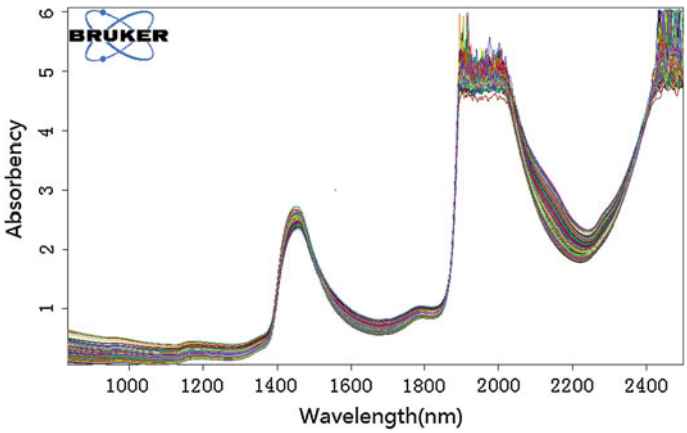

Fig. 171.1 NIR spectra of samples taken from glutamate fermentations

Table 171.1 Concentration of NH_4^+ collected from the fermentation broth

Constituent	NH_4^+	
Subsets	Calibration set	Validation set
Number of samples	131	33
Range (mmol/l)	4.21–135.86	9.49–127.09
Mean (mmol/l)	74.87	62.43
Standard deviation (mmol/l)	34.87	34.65

74.87 and 62.43 g/l, respectively. Of the determinations, the standard deviation of NH_4^+ concentration between calibration set and validation set was 34.87 and 34.65 g/l.

171.3.2 Development of a Multivariate Calibration Model

In order to establish multivariate calibration model, the fermentation broth samples were divided into the calibration set and validation set, which were selected randomly and equably by software (OPUS 7.0). In all, 131 samples were used for the calibration set, while the others 33 samples were used for the validation set (Table 171.1). Several spectral preprocessing methods were tested before the development of the multivariate calibration model (Sect. 171.2.5). The optimal preprocessing method was adopted by lowest RMSEP.

For the multivariate calibration model of NH_4^+ concentration, 1st + SNV (smoothing points 13) was identified as optimal preprocessing method. The main feature of the spectra was absorption bands at 2173.2–2353.8 nm, which was related to the combination tone of the N–H bond of NH_4^+. With the calibration

Table 171.2 Parameters of multivariate calibration models of NH_4^+ in the fermentation broth samples

Constituent	NH_4^+
Latent variables	3
Bands	2173.2–2353.8 nm
Spectra pre-processing	First derivative + SNV
RMSEC[a]	4.34
RMSEP[b]	4.62
True-prediction fitting equation	$y = 0.9391x + 4.3227$
Coefficient of determination	0.9839
Offset	−0.52
RPD[c]	7.43

[a] RMSEC: root-mean-square error of calibration
[b] RMSEP: root-mean-square error of prediction
[c] RPD: residual predictive deviation

model, the lowest RMSEP was 4.62 and LVs was 3 (Table 171.2 and Fig. 171.2). Figure 171.3 and Table 171.2 showed that true-prediction fitting equation and coefficient of determination (R^2) were $y = 0.9391x + 4.3227$ and 0.9839 between experimental value and predictive value in the test set validation.

Residual predictive deviation (RPD) was used to evaluate how well the calibration model could predict compositional data. The RPD was defined as the standard deviation (SD) of the population's reference values divided by the RMSEP for the NIRS calibrations. The relatively high RPD values indicated models to have greater power to predict the chemical composition. Generally, an RPD greater than three could be considered very well for prediction purposes [25]. The RPD of calibration model for NH_4^+ concentration was 7.43 (Table 171.2). The multivariate calibration model has the very strong predication ability of NH_4^+ concentration.

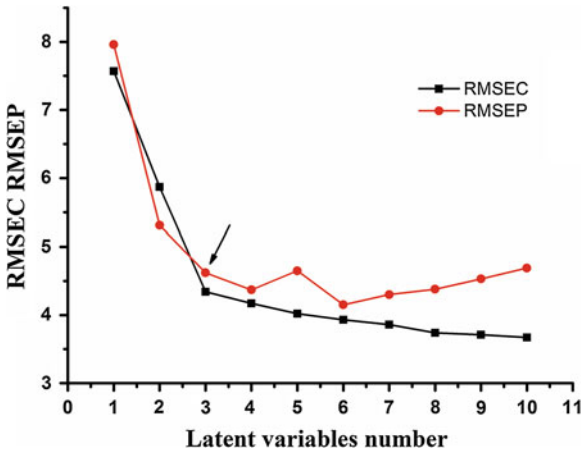

Fig. 171.2 RMSEE, RMSEP of NH_4^+ vs. latent variables number f determination by NIR

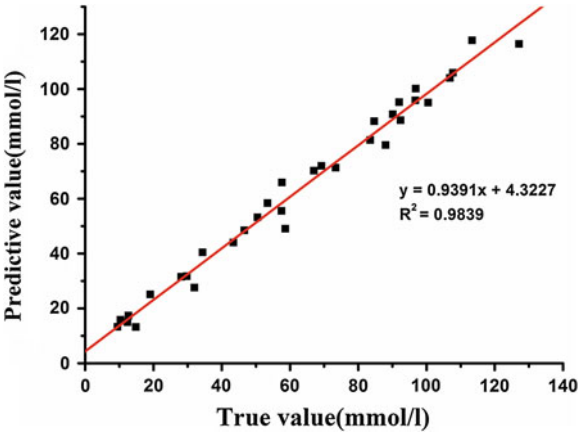

Fig. 171.3 Predictive value for NH_4^+ versus true value for validation set

171.4 Conclusion

NIR spectroscopy was widely used as a rapid, nondestructive method for determining various compounds simultaneously in fermentation industry. Comparing with the traditional chemical analysis, NIR spectroscopy and PLS model is a fast, versatile, cheap, and environmentally safe analytical method to predict compounds concentration. The results of this work demonstrate a good ability of NIR spectroscopy to predict NH_4^+ concentration in temperature triggered glutamate fermentation process. The model had well correlation of determination and low predictive errors. NIR spectroscopy has the potential to dramatically reduce analytical time and cost of monitoring significant compounds in glutamate during fermentation for both research and commercial production applications.

Acknowledgments This work was supported by Program for Changjiang Scholars and Innovative Research Team in University (IRT 1166), by Tianjin Research Program of science and technology (Grant No. 12ZCZDSY01900), national high technology research and development program (2013AA102106), and by national science and technology supporting program (2011BAC11BB03).

References

1. Nandakumar R, Yoshimune K, Wakayama M et al (2003) Microbial glutaminase: biochemistry, molecular approaches and applications in the food industry. J Mol Catal B-Enzym 23:87–100
2. Jyothi A, Sasikiran K, Nambisan B et al (2005) Optimisation of glutamic acid production from cassava starch factory residues using Brevibacterium divaricatum. Process Biochem 40:3576–3579
3. Kusumoto I (2001) Industrial production of L-glutamine. J Nutr 131:2552S–2555S
4. Kinoshita S (1985) Glutamic acid bacteria. In: Demain, Solomon (eds) Biology of industrial microorganisms. Wiley, London, pp 115–142

5. Shimizu H, Hirasawa T (2007) Production of glutamate and glutamate-related amino acids: molecular mechanism analysis and metabolic engineering. In: Wendisch Volker F (ed) Amino acid biosynthesis-pathways. Regulation and Metabolic Engineering, Wiley, pp 1–38
6. Momose H, Takagi T (1978) Glutamic acid production in biotin-rich media by temperature sensitive mutants of *Brevibacterium lactofermentum*, a novel fermentation process. Agr Biol Chem 42:1911–1917
7. Delaunay S, Gourdon P, Lapujade P et al (1999) An improved temperature-triggered process for glutamate production with *Corynebacterium glutamicum*. Enzyme Microb Tech 25:762–768
8. Eggeling L, Bott M (2005) Handbook of *Corynebacterium glutamicum*. CRC Press, Boca Raton, pp 439–463
9. Hashimoto KI, Kawasaki H, Akazawa K et al (2006) Changes in composition and content of mycolic acids in glutamate-overproducing *Corynebacterium glutamicum*. Biosci Biotech Biochem 70:22–30
10. Bokas D, Grattepanche F, Duportail G et al (2007) Cell envelope fluidity modification for an effective glutamate excretion in *Corynebacterium glutamicum* 2262. Appl Microbiol Biot 76:773–781
11. Tesch M, Eikmanns B J, Graaf AA et al (1998) Ammonia assimilation in *Corynebacterium glutamicum* and a glutamate dehydrogenase-deficient mutant. Biotech Lett 20:953–957
12. Nicolai BM, Beullens K, Bobelyn E et al (2007) Nondestructive measurement of fruit and vegetable quality by means of NIR spectroscopy: a review. Postharvest Biol Tec 46:99–118
13. Aït Kaddour A, Mondet M, Cuq B (2008) Application of two-dimensional cross-correlation spectroscopy to analyse infrared (MIR and NIR) spectra recorded during bread dough mixing. J Cereal Sci 48:678–685
14. Shiroma C, Rodriguez-Saona L (2009) Application of NIR and MIR spectroscopy in quality control of potato chips. J Food Compos Anal 22:596–605
15. Krämer K, Ebel S (2000) Application of NIR reflectance spectroscopy for the identification of pharmaceutical excipients. Anal Chim Acta 420:155–161
16. De Maesschalck R, Sanchez FC, Massart DL et al (1998) On-line monitoring of powder blending with near-infrared spectroscopy. Appl Spectrosc 52:725–731
17. Amigo J, Cruz JM, Bautista M et al (2008) Study of pharmaceutical samples by NIR chemical-image and multivariate analysis. Trac-Trend Anal Chem 27:696–713
18. Fernández-Novales J, López MI, Sánchez MT et al (2008) A feasibility study on the use of a miniature fiber optic NIR spectrometer for the prediction of volumic mass and reducing sugars in white wine fermentations. J Food Eng 89:325–329
19. Zeaiter M, Roger JM, Bellon-Maurel V (2006) Dynamic orthogonal projection. A new method to maintain the on-line robustness of multivariate calibrations. Application to NIR-based monitoring of wine fermentations. Chemometr Intell Lab 80:227–235
20. Yu HY, Niu XY, Lin HJ et al (2009) A feasibility study on on-line determination of rice wine composition by Vis–NIR spectroscopy and least-squares support vector machines. Food Chem 113:291–296
21. Blanco M, Villarroya I (2002) NIR spectroscopy: a rapid-response analytical tool. Trac-Trend Anal Chem 21:240–250
22. Puchert T, Holzhauer CV, Menezes JC et al (2011) A new PAT/QbD approach for the determination of blend homogeneity: combination of on-line NIRS analysis with PC scores distance analysis (PC-SDA). Eur J Pharm Biopharm 78:173–182
23. Thomas EV (2000) Adaptable multivariate calibration models for spectral applications. Anal Chem 72:2821–2827
24. Spiegelman CH, McShane MJ, Goetz MJ et al (1998) Theoretical justification of wavelength selection in PLS calibration: development of a new algorithm. Anal Chem 70:35–44
25. Cozzolino D, Kwiatkowski MJ, Parker M et al (2004) Prediction of phenolic compounds in red wine fermentations by visible and near infrared spectroscopy. Anal Chim Acta 513:73–80

Chapter 172
Studies on Protein Extraction from *Caragana korshinskii* Kom. Using Acetone Precipitation Method

Cheng Zhong, Zhao Zhou, Rui Wang, Peipei Han and Shiru Jia

Abstract *Caragana korhinskii* Kom is a desert shrub which belongs to genus Caragana. In this work, protein extraction from *C. Korshinskii* Kom using acetone precipitation method was investigated. Orthogonal experiments showed that the optimal extraction conditions were as follows: ratio of extraction buffer to tissue pounder 20:1, extraction time 7 h, ratio of acetone to supernatant 3.5:1. Sodium dodecyl sulfate polyacrylamide gel electrophoresis (SDS-PAGE) analysis indicated that five major bands and two large diffuse bands could be found. The approximate molecular weight for the extracted proteins ranged from 25 to 66.2 kDa.

Keywords *Caragana korshinskii* Kom. · Protein extraction · Orthogonal analysis · SDS-PAGE

172.1 Introduction

Protein has played a significant role in our daily life. It can satisfy not only our energy requirements but also the needs of a variety of amino acids. According to Food and Agriculture Organization Reports, protein consumption in many developing countries is even lower than the global protein average intake [1]. As protein with high quality can apply in human consumption as well as animal feed additive, protein extraction from biomass, and other resources would greatly reduce the threat of protein scarcity and certainly benefit the underdeveloped countries [2].

C. Zhong · Z. Zhou · R. Wang · P. Han · S. Jia (✉)
College of Biotechnology, Tianjin University of Science and Technology, Tianjin 300457, People's Republic of China
e-mail: jiashiru@tust.edu.cn

C. Zhong · Z. Zhou · R. Wang · P. Han · S. Jia
Key Laboratory of Industrial Fermentation Microbiology, Ministry of Education, Tianjin 300222, People's Republic of China

T.-C. Zhang et al. (eds.), *Proceedings of the 2012 International Conference on Applied Biotechnology (ICAB 2012)*, Lecture Notes in Electrical Engineering 251,
DOI: 10.1007/978-3-642-37925-3_172,

In 1763, Philip Caragana Fabricicus found the genus Caragana [3]. Since then, more than 100 Caragana species have already been discovered, of which 66 have been reported in China [4]. Moreover, numerous species cultured are often applied to dune-fixation, livestock forage and biological resources for energy as well as fiber production. In addition, more than 10 species have been used in traditional Chinese medicine for a long time [5]. As one species of the genus Caragana, *Caragana korshinskii* Kom. is long-lived grassland and desert shrub species [6] which is supposed to be an indicators of desertification in sandy land-scapes [7] and is widely used to improve regional eco-environments [8]. However, few data is available on protein of *C. korshiskii* Kom. and limits its application on food industry. Gao et al. [9] assessed the content of crude protein and crude fat in *C. korshinskii* Kom., and showed that the average content of crude protein was 18.65 % and crude protein in leaf was highest (24.84 %). Due to its high content of protein, *C. korshinskii* Kom. promises to be one potential protein resource.

In this work, acetone precipitation method was used for protein extraction from *C. korshinskii* Kom., and the optimal extraction condition was established. The isolated protein was investigated by SDS-PAGE in order to have a preliminary estimate of the molecular weight.

172.2 Materials and Methods

172.2.1 Material and Reagents

Unstained protein molecular weight maker was obtained from Fermentas. All chemicals used were analytical grade.

172.2.2 Plant Samples

C. korshinskii Kom. was obtained from Liang Cheng County of Inner Mongolia, China. Air-dried leaves and tissues were milled by a 20-mesh sieve and ground into powders in liquid nitrogen before stored at −20 °C.

172.2.3 Protein Extraction

Acetone precipitation method to extract protein from C. Korshinskii Kom. was preformed according to the method of Wu et al. [10] with some modifications.

For 1 g scale: 1 g tissue pounder with 0.1 g insoluble polyvinylpyrrolidone was ground in a mortar and a given ratio of extraction buffer [62.5 mmol· L^{-1} Tris-HCl

Table 172.1 Factors and levels for orthogonal test

Variable	Level		
	1	2	3
A: ratio of extraction buffer to tissue pounder (v/w)	1:15	1:20	1:25
B: extraction time (h)	5	6	7
C: ratio of acetone to supernatant (v/v)	2.5	3	3.5

(pH 6.8), 0.5 % (w/v) SDS, 10 % (v/v) glycerol, 5 % (v/v) β-mercaptoethanol] was added. The mixture was homogenized at 4 °C for a given time and centrifuged at 12,000 g for 20 min at 4 °C. The supernatant was transferred to a 50 mL centrifuge tubes preweighed and given volumes of cooled acetone (−20 °C) were added. Proteins were allowed to precipitate overnight at −20 °C, and were then collected by centrifugation at 12,000 g for 20 min at 4 °C. After discarding the supernatant, the precipitate was rinsed three times with cooled acetone (−20 °C) and dried under vacuum before stored at −80 °C.

172.2.4 Optimization of Protein Extraction

An orthogonal L9 $(3)^4$ design was used to optimize the extraction conditions. As shown in Table 172.1, nine experiments were carried out at the above three factors (ratio of extraction buffer to tissue pounder, extraction time, ratio of acetone to supernatant) with three different levels on the basis of single-factor test. The results were assessed by the protein extraction yield, which was defined as the protein content extracted to the tissue pounder (mg/g).

172.2.5 Protein Recovery

The acetone-precipitated extracts were dissolved in MilliQ water. The solution was measured by the Bradford method (1976) [11] to determine the protein concentration and stored at −80 °C for latter use.

172.2.6 Sodium Dodecyl Sulfate Polyacrylamide Gel Electrophoresis (SDS-PAGE)

SDS-PAGE was performed according to the method of Laemmli [12], using discontinuous polyacrylamide gels consisting of a 5 % stacking gel and a 12 % separation gel. Briefly, protein solution was diluted in 2 × loading buffer [12.5 % (v/v) 0.5 mol/L Tris-HCl (pH 6.8), 10 % (w/v) SDS, 10 % (v/v) glycerol, 5 %

(v/v) β-mercaptoethanol, 2.5 % (w/v) bromophenolblue], and was boiled for 5 min. 30–50 μg proteins were loaded per slot. The SDS-PAGE gel was run on electrophoresis apparatus (DYY-8C, Beijing Liuyi Instrument Factory, Beijing) at 80 V constant voltages for 45 min and at 110 V constant voltages for 60 min in stacking gel and separation gel respectively. At the end of electrophoresis, protein bands were been displayed after the gel was stained with Coomassie Brilliant Blue R-250 (Bio Basic Inc.), and the images were obtained by Infrared Imaging Systems (Obyssey, LI-COR, Inc.). Three independent replicates were preformed.

172.3 Results and Discussion

172.3.1 Effect of Ratio of Extraction Buffer to Tissue Pounder on Extraction Yield of Protein from C. korshinkii Kom

In this study, the influence of different ratio of extraction buffer to tissue pounder on extraction yield of protein was investigated. The extraction experiment was carried out at a fixed extraction time (4 h) and ratio of acetone to supernatant (2.5:1). As shown in Fig. 172.1, with increasing ratio of extraction buffer to tissue pounder from 5:1 to 20:1, the protein extraction yield varied from 5.7 to 85.1 mg/g. The maximum extraction yield (85.9 mg/g) was observed when the ratio of extraction buffer to tissue pounder (v/w) was 25:1.

172.3.2 Effect of Extraction Time on Extraction Yield of Protein from C. korshinskii Kom

In this study, the influence of different extraction time on extraction yield of protein was investigated. The extraction experiment was carried out at a fixed ratio of extraction buffer to tissue pounder (15:1) and ratio of acetone to supernatant

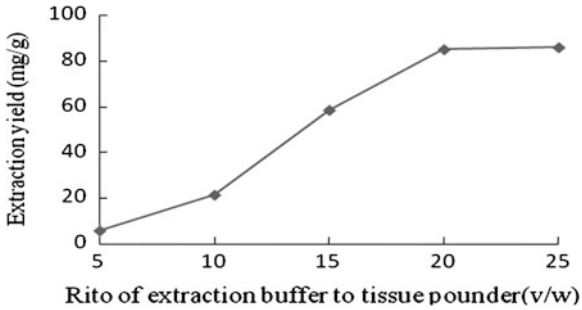

Fig. 172.1 Effect of different ratio of extraction buffer to tissue pounder on extraction yield

(3:1). Figure 172.2 showed that the extraction yield increased as the extraction time ranged from 3 to 6 h and then decreased at the extraction time of 7 h. The extraction yield reached the peak (62.3 mg/g) at the extraction time of 6 h.

172.3.3 Effect of Ratio of Acetone to Supernatant on Extraction Yield of Protein from C. korshinskii Kom

In this study, the influence of different ratio of acetone to supernatant on extraction yield of protein was investigated. The extraction experiment was carried out at a fixed ratio of extraction buffer to tissue pounder (15:1) and extraction time (4 h). Figure 172.3 showed the similar tendency as in Fig. 172.2 and the highest extraction yield (55.8 mg/g) was obtained when the ratio of acetone to supernatant was 3.5:1.

172.3.4 Orthogonal Analysis

Table 172.2 indicated that the highest extraction yield (110.87 mg/g) was obtained in ninth experiment and the optimum conditions were as follows the ratio of

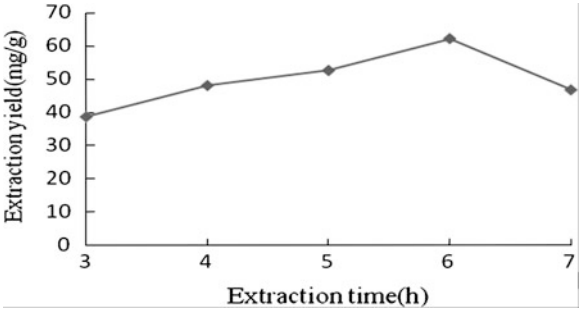

Fig. 172.2 Effect of different extraction time on extraction yield

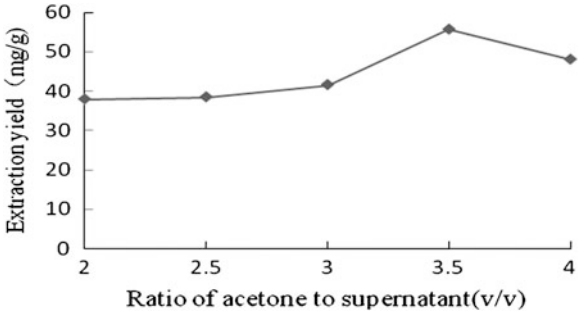

Fig. 172.3 Effect on different ratio of acetone to supernatant on extraction yield

Table 172.2 Orthogonal experiments

No.	A	B	C	Extraction yield (mg/g)
1	1	1	1	67.27
2	2	1	2	84.79
3	3	1	3	109.93
4	1	2	2	86.90
5	2	2	3	105.74
6	3	2	1	105.10
7	1	3	3	66.29
8	2	3	1	91.2
9	3	3	2	110.87
K1	87.330	73.487	87.857	
K2	99.247	93.910	94.187	
K3	89.453	108.633	93.987	
R	11.917	35.146	6.330	

extraction buffer to tissue pounder, extraction time and the ratio of acetone to supernatant was 20:1, 7 h and 3.5:1 according to K values. The influence of each factor on extraction yield increased in order: C < A < B according to R values.

172.3.5 SDS-PAGE Analysis

As shown in the Fig. 172.4, the separation of protein samples indicated five major bands ranging from 25 to 66.2 kDa in molecular weight could be detected and two large diffuse bands could be visualized between 14.4 and 25 kDa. The band with

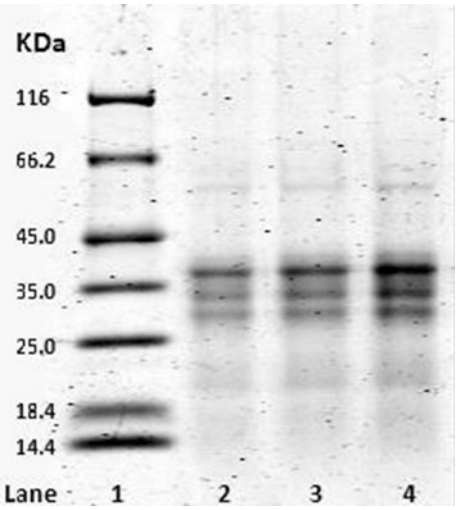

Fig. 172.4 SDS-PAGE analysis of protein from *C. Korshinskii Kom*. Lane 1 was 20μL molecular weight maker, and Lanes 2, 3, 4 were both protein solutions with loading buffer using different volume (20, 25, 30 μL respectively)

estimated molecular weight of 38 kDa and high abundance could be speculated to correspond to DREB2 owing to its characteristic that DREB2 can be highly expressed under adverse conditions, such as drought, high salt, or low temperature [13], and the molecular weight of DREB2 approximated 37 kDa according to its amino acid sequence [14, 15]. However, few research of *C. Korshinskii* Kom. has been focused on its proteomics so far. As a result, the other bands existed on the gel cannot be easily identified.

172.4 Conclusion

In this work, acetone precipitation method was used for protein extraction from *C. korshinskii* Kom. Orthogonal analysis indicated that the highest extraction yield would be obtained when the ratio of extraction buffer to tissue pounder, extraction time and the ratio of acetone to supernatant was 20:1, 7 h, 3.5:1 respectively, and extraction time had a significant effect on the extraction yield. SDS-PAGE analysis indicated that five major bands ranging from 25 to 66.2 kDa and two large diffuse bands ranging from 14.4 to 25 kDa existed in the protein of *C. korshinskii* Kom.

Acknowledgments The authors are grateful for the financial support from the Introduced Talent Start-up Fund (No. 20100413) of Tianjin University of Science and Technology.

References

1. http://www.fao.org/index_en.htm
2. Chiesa S, Gnansounou E (2010) Protein extraction from biomass in a bioethanol refinery—Possible dietary applications: Use as animal feed and potential extension to human consumption. Bioresour Technol 102:427–436
3. Polhill RM, Raven PH (1981) Advances in Legume Systematics. Kew Publishing, Britain
4. Niu XW (1988) Cultivation and Utilization of Peashrubs. Shanxi Science and Education press (in Chinese), Taiyuan
5. Meng QX, Niu Y, Niu XW et al (2009) Ethnobotany, phytochemistry and pharmacology of the genus Caragana used in traditional Chinese medicine. J Ethnopharmacol 124:350–368
6. Bian J, Peng F, Xu F et al (2009) Fractional isolation and structural characterization of hemicelluloses from *Caragana korshinskii*. Carbonhyd Polym 80:753–760
7. Schlesinger WH, Raikes JA, Hartley AE et al (1996) On the spatial pattern of soil nutrients in desert ecosystem. Ecology 77:364–374
8. Su YZ, Zhao HL (2003) Soil properties and plant species in an age sequence of Caragana microphylla plantations in the Horqin Sandy Land, north China. Ecol Eng 20:223–235
9. Gao YN, Chang JB, Zhou C (2011) Study on dynamic change of nutritive components in Ningtiao Caragana. Northern Environ 23:41–43 (in Chinese)
10. Wu QF, Li C, Ke L et al (2011) A high-efficiency, two-dimensional gel electrophoresis platform for mature leaves of grass pea (*Lathyrus sativus* L.). Acta Physiol Plant 33:2387–2397
11. Bradford MM (1976) A rapid and sensitive method for the quantitation of microgram of protein utilizing the principle of protein-dye binding. Anal Biochem 72:248–254

12. Laemmli UK (1970) Cleavage of structural proteins during the assembly of the head bacteriophage T4. Nature 227:680–685
13. Maizoi J, Shinozaki K, Yamaguchi-Shinozaki K (2012) AP2/ERF family transcription factors in plant abiotic stress responses. Biochim Biophys Acta 1819:86–96
14. http://www.ncbi.nlm.nih.gov/protein/290889451?report=graph
15. http://www.proteomics.com.cn/tools/mwcal/

Chapter 173
Signaling Pathways in Cardiac Hypertrophy

Man Li, Nan Wang, Wenjing Liu, Xin Zhi and Tong-Cun Zhang

Abstract In a number of pathological conditions such as hypertension, valvular disease, myocardial infarction, and cardiomyopathy, postnatal cardiomyocytes undergo cardiac hypertrophy. Cardiac hypertrophy is the heart's response to increased biomechanical stress, which is accompanied by activation of a fetal gene program, assembly of sarcomeres, and cellular enlargement. Prolonged hypertrophy is a major predictor of heart failure and sudden death. Identification of the signaling molecules is necessary for the development of therapeutic strategies to prevent or reverse the disease. Recent researches have found that there were different signaling pathways activated in cardiac hypertrophy, but the molecular mechanism of cardiac hypertrophy is not completely elucidated so far. In this review, we summarize recent insights into hypertrophic signaling pathways.

Keywords Hypertrophy · Signaling molecules · Signaling pathways

173.1 Introduction

Cardiac hypertrophy is an important phase in heart disease development. In a number of pathological conditions such as hypertension, valvular disease, myocardial infarction, and cardiomyopathy, postnatal cardiomyocytes undergo cardiac hypertrophy. Cardiac hypertrophy is the heart's response to increased biomechanical stress which is accompanied by activation of a fetal gene program,

M. Li · N. Wang · W. Liu · X. Zhi · T.-C. Zhang (✉)
Tianjin Key Laboratory of Industrial Microbiology, College of Biotechnology, Tianjin University of Science and Technology, Tianjin 300457, People's Republic of China
e-mail: tony@tust.edu.cn

M. Li · N. Wang · W. Liu · X. Zhi · T.-C. Zhang
Key Laboratory of Industrial Fermentation Microbiology, Ministry of Education, Tianjin 300457, People's Republic of China

T.-C. Zhang et al. (eds.), *Proceedings of the 2012 International Conference on Applied Biotechnology (ICAB 2012)*, Lecture Notes in Electrical Engineering 251,
DOI: 10.1007/978-3-642-37925-3_173,

assembly of sarcomeres, and cellular enlargement. Hypertrophic growth after acute and chronic stress may initially augment cardiac output, but prolonged hypertrophy is a major predictor of heart failure and sudden death [1]. During the past years, the signaling mechanisms leading to cardiac hypertrophy have been intensively investigated. There were different signaling pathways activated in cardiac hypertrophy, for example, mitogen-activated protein kinase (MAPK) signal transduction pathway, Ca^{2+} dependent signal transduction pathway, Phosphoinositide 3-kinase (PI3 K)/Akt signal transduction pathway, Janus kinase/signal transducer and activator of transcription (JAK/STAT) signal transduction pathway, etc. It is believed to be mediated by signaling molecules that transduce the stress signals from the environment into different cellular compartments. Specific transcription factors such as myocyte enhancer factor 2 MEF2, GATA4, nuclear factor of activated T cells NFAT, nuclear factor κb NFκB, Csx/Nkx2–5, serum response factor (SRF) and myocardin have been identified that play an important role in activating the fetal gene program, but the molecular mechanism of cardiac hypertrophy is not completely elucidated so far. In this review, we summarize recent insights into hypertrophic signaling pathways. Identification of the signaling molecules is necessary for the development of therapeutic strategies to prevent or reverse the disease.

173.2 Signaling Pathways in Cardiac Hypertrophy

At the cellular and molecular level, cardiac hypertrophy that happens includes three parts, extracellular stimulating signal, cells signal transduction and changes in gene expression. Different hypertrophic stimulus induces specific cardiac hypertrophy, which mainly depends on activating different signal transduction pathways. Nowadays many of the signaling pathways that have been implicated in the regulation of hypertrophy, including MAPK signal transduction pathway, Ca^{2+} dependent signal transduction pathway, PI3 K/Akt signal transduction pathway, JAK/STAT signal transduction pathway, Wnt signaling pathway and MicroRNAs, etc.

173.2.1 MAPK Signaling Pathway

The mitogen-activated protein kinase signal transduction pathway is now recognized as an important regulatory system in eukaryotic cells, which participates in the intracellular transmission of extracellular signals that control embryogenesis, cell differentiation, cell proliferation, and cell death. The MAPK cascades are generally sub-classified into three main branches, including extracellular signal-regulated kinases (ERKs), c-Jun N-terminal kinases (JNKs), and p38 s [2]. All MAPK pathways include three signaling levels, MAPKs are activated by the MAPK kinases (MKKs) that phosphorylate MAPKs at two sites, conserved

threonine and tyrosine residues. The MKKs are themselves phosphorylated and activated by serine/threonine kinases that function as MKK kinases (MKKKs).

At least five different ERK proteins have been identified in mammalian cells, ERK1–5. ERK1/2 are known to be activated in response to almost every stress- and agonist-induced hypertrophic stimulus. For example, in response to agonist stimulation or cell stretching, ERK1/2 become activated in cultured cardiomyocytes. Clerk etal reported that MEK1-ERK1/2 was required for sarcomeric organization induced by hypertrophic agonists [3]. Transgenic overexpression of an ERK kinase(MEK)1, a MAPK kinase that specifically activates ERK1/2, results in considerable cardiac hypertrophy [4]. The depletion of ERK was reported to downregulate PE-induced hypertrophic responses in cardiomyocytes.

Another member of the MAPK family, c-Jun N-terminal kinases (JNKs), is also activated in cultured cardiomyocytes by the growth promoters phenylephrine (PE) and endothelin-1 [5], which suggesting that it may contribute to the hypertrophic phenotype. But, there is no evidence that JNK activation fosters the sarcomeric organization that is an obligate feature of cardiac hypertrophy. So it is likely that JNK pathway alone may not be sufficient to support all of the main features associated with the hypertrophic growth program.

Similarly, previous studies have demonstrated that p38 is activated in cultured neonatal cardiomyocytes by hypertrophic stimulation and in mouse hearts in response to pressure overload. Four different p38 MAPK isoforms have been described, including p38 (or p38α), p38β, p38γ, and p38δ. MKK3 and MKK6 are the major upstream activators of p38 MAPK. Indeed, adenoviral-mediated gene transfer of activated MKK3 or MKK6 is sufficient to induce ANF expression and hypertrophy in cultured neonatal cardiomyocytes. Adenoviral-mediated gene transfer of a dominant-negative p38β MAPK blunted the hypertrophic response of neonatal cardiomyocytes [6], whereas the activation of p38α led to the induction of cardiomyocytes apoptosis. A current research suggests that choline prevents Ang II-induced cardiac hypertrophy through inhibition of reactive oxygen species (ROS)-mediated p38 MAPK activation [7]. These research results suggest that p38 pathway may contribute to the development of hypertrophy and the transition to heart failure. In a word, the ERKs, JNKs, and p38 s are critically involved in the regulation of signaling pathways, ultimately leading to cardiac hypertrophy.

173.2.2 Calcium-Dependent Signaling Pathway

Ca^{2+} is a major second messenger of signal out of cell and physiological and biochemical reaction in cell. A number of hypertrophic stimuli could increase intracellular Ca^{2+} levels and many reports suggest that Ca^{2+} is involved in the generation of cardiac hypertrophy. The molecular mechanism of Ca^{2+}-induced cardiac hypertrophy has not yet been elucidated clearly. The Ca^{2+}/calmodulin-dependent protein kinases (CaMKs) and the Ca^{2+}/calmodulin-dependent phosphatase (calcineurin) are critical transducers of Ca^{2+}signals.

CaMKs are serine/threonine kinases that are regulated by Ca^{2+} liganded calmodulin (CaM). The CaMK family consists of CaMKI, CaMKII, and CaMKIV, of which CaMKII is the predominant cardiac isoform. CaMKII can phosphorylate a range of substrates in response to increasing intracellular Ca^{2+} concentrations such as ryanodine receptors, phospholamban (PLB), sarcoplasmic reticular Ca^{2+} ATPase (SERCA), L-type Ca^{2+} channels, activating transcription factor-1, and cAMP response element-binding protein. The CaMKII subunits α, β, γ, and δ show different tissue distributions. The δ isoform of CaMKII predominates in the heart. Different splice variants of the δ isoform have different intracellular localization. CaMKIIδB localizes to the nucleus, whereas CaMKIIδC localizes to the cytoplasm, because of the δB isoform containing a nuclear localization signal (NLS) that is absent from δC. A growing body of evidence has suggested that Ca^{2+} signaling plays a critical role in the development of cardiac hypertrophy. Increased intracellular Ca^{2+} binds to calmodulin (CaM) and then CaMKII is activated by binding to Ca^{2+}/CaM and subsequent autophosphorylation. Activation of CaMKII regulates the phosphorylation of the histone deacetylases (HDACs), especially class II HDACs, which associate with MEF2 to repress MEF2-induced gene expression. Phosphorylation of HDACs by CaMKII leads to the release of MEF2 from HDACs into the nucleus and the activation of MEF2 downstream targets. Studies initiated in vitro experiments, extended to animal models and findings from humans suggest that CaMKII is a critical transducers of Ca^{2+} signals. To stimulate neonatal rat cardiomyocytes with interleukin-1 h can activate CaMKII and then regulate the expression of brain natriuretic peptide (BNP) that is another hypertrophic marker gene [8]. Transient expression of CaMKIIδB in neonatal rat cardiomyocytes-induced gene expression and resulted in an enhanced response to phenylephrine, as assessed by transcriptional activation of an ANF-luciferase reporter gene. Transgenic mice that overexpress CaMKIIδB, develop hypertrophy and dilated cardiomyopathy [9]. In addition, CaMKII expression is increased in human, mouse, and large animal models of heart failure, suggesting that CaMKII may be involved in the transformation from hypertrophy to heart failure.

The calcium/calmodulin-activated protein phosphatase calcineurin (PP2B) is activated by sustained elevations in intracellular calcium, which facilitates binding to nuclear factor of activated T cells (NFAT). NFAT transcription factors are downstream effectors of calcineurin and normally hyperphosphorylated in the cytoplasm. After calcineurin-mediated dephosphorylation, NFAT rapidly translocates to the nucleus and induces the transcription of genes. Activation of the calcineurin-NFAT pathway in the heart is sufficient to induce cardiac hypertrophy, for example, cardiac-specific activation of calcineurin induces a robust hypertrophic response in transgenic mice [10]. In vitro infection of cultured cardiomyocytes with an activated calcineurin similarly induced a hypertrophic response. Furthermore, Cardiac overexpression of a constitutively activated NFATc4 mutant protein resulted in cardiac hypertrophy in transgenic mice [10]. Studies using expression of a dominant-negative NFAT mutant protein in cultured cardiomyocytes [11] and genetic ablation of NFATc3 in mice [12] have indicated that NFAT proteins are essential mediators of cardiac hypertrophy. Recent data show that

TNF-α increases the expression of CaMKIIδB by 35.21 % and that of CaN by 22.22 % compared to control, indicating that the Ca^{2+}/CaMKII- and CaN-dependent signaling pathways are involved in cardiac hypertrophy induced by TNF-α [13].

173.2.3 JAK/STAT Signaling Pathway

The janus kinase/signal transducer and activator of transcription signal transduction pathway was first identified as a major intracellular signaling pathway linked to the activation of cytokine receptors and has been implicated in pressure overload induced cardiac hypertrophy and remodeling. Because it transmits information received from extracellular polypeptide signals directly to target genes in the nucleus without the interplay of second messengers, the JAK/STAT signaling pathway is regarded as a model for direct signal transduction. Ligand binding to the extracellular domain of cytokine receptors induces dimerization and tyrosine phosphorylation of Jaks. The Jaks, in turn, phosphorylate the receptor, which provides docking sites for STAT proteins. Once STATs are phosphorylated, they dimerize and translocate to the nucleus, where they interact with specific DNA sequences and transcription factors to induce or modulate the expression of a broad range of target genes.

The JAKs belong to the nonreceptor tyrosine kinase superfamily and the mammalian JAK family has four members, Tyk2, JAK1, JAK2, and JAK3. Among the four members, Tyk2, JAK1, and JAK2 are expressed in cardiomyocytes while JAK3 is mainly found in cells of haematopoietic origin. The mammalian STAT family consists of seven members, STAT1, STAT2, STAT3, STAT4, STAT5a, STAT5b, and STAT6. STAT proteins possess a conserved structural organization. They contain a tetramerization domain and a leucine-zipper-like domain at the N-terminus, a DNA-binding domain in the middle, an Src homology 3 (SH3)-like domain, an SH2 domain, and a transactivation domain at the C-terminal end. The SH2 domain is important for cytokine receptor binding and determines the selectivity of STAT binding to the various cytokine receptors. Between the SH2 domain and the C-terminus, approximately 700 residues from the N-terminus, are the tyrosine residues that are phosphorylated by the JAKs. Among the seven STAT proteins, STAT3 has been implicated in transduction of the cellular signals that are involved in development of cardiac hypertrophy. Transgenic mice with cardiac-specific overexpression of STAT3 exhibited marked ventricular hypertrophy with increased expression of atrial natriuretic factor (ANF), β-myosin heavy chain (MHC), and cardiotrophin-1 [14]. In addition, STAT3-mediated pathway plays a critical role in gp130-dependent cardiac hypertrophy confirmed by transfecting wild-type and mutated-type STAT3 cDNA to cardiomyocytes.

Various stimuli that are known to activate hypertrophic growth of cardiomyocytes have been demonstrated to activate JAK-STAT signaling in cultured cardiomyocytes or whole heart preparations. The transmembrane glycoprotein

gp130 is an upstream activator of the JAK/STAT pathway. Activation of the JAK/STAT pathway by overload was mediated by gp130, and at least cardiotrophin-1 (CT-1) and IL-6 were involved in activation of this pathway [15]. Moreover, mechanical stretch, pressure overload, and ANG II, which induce cardiac hypertrophy, have been shown to activate cardiac JAK/STAT signaling. The components of the Jak/STAT pathway activated by Ang II are Tyk2, Jak1, and Jak2 kinases, STAT1, STAT2, STAT3, STAT5A, and STAT6 proteins. In vitro, 20 % mechanical stretch of neonatal rat cardiomyocytes induces phosphorylation of Jak1, Jak2, Tyk2, STAT1, STAT3, and gp130. Similar phosphorylation patterns are seen in pressure-overloaded rat hearts in vivo. A new study has found that in the process of Ang II-induced cardiomyocyte hypertrophy, visfatin expression was increased mainly through the AT1-R-JAK/STAT pathway [16]. The evidence supports an important role of Jak/STAT signaling in the development of cardiac hypertrophy.

173.2.4 Wnt/Frizzled Pathway

Wnt signaling has important functions in stem cell biology, cardiac development and differentiation, angiogenesis, cardiac hypertrophy, cardiac failure, and aging. Wnt proteins are secreted proteins and in human, 19 Wnt proteins are known. They bind to receptors to activate intracellular signal transduction. The first and probably best-studied class of Wnt receptors is the frizzled family, and members of the frizzled family are widely expressed in the cardiovascular system as well as in other organs. Stimulation of the Wnt/Frizzled pathway activates the disheveled (Dvl) protein. Disheveled subsequently can inhibit glycogen synthase kinase-3β. The inhibition of glycogen synthase kinase-3β leads to an increased amount of β-catenin, which can act as a transcription factor for several hypertrophy-associated target genes, including the proto-oncogenes c-myc, c-fos and c-jun and cyclin D1 [17].

Glycogen synthase kinase-3β (GSK-3β) is one of the most powerful negative regulators that can antagonize the hypertrophic response. Hypertrophic stimuli lead to phosphorylation of GSK-3β at the Ser9 residue and inhibition of its activity. But Wnt signaling does not modulate the activity of GSK-3β by phosphorylation of its Ser9 residue; it has been proposed to disrupt the so-called β-catenin degradation complex [18], which results in the release of GSK-3β and accumulation of cytosolic β-catenin.

During the development of hypertrophy in the rat heart, frizzled-2 expression was found to be upregulated. Overexpression of β-catenin-induced hypertrophic growth both in vitro and in vivo [19]. In mice lacking the Disheveled-1 (Dvl-1) gene, an attenuated hypertrophic response upon pressure overload induced by aortic constriction was observed, demonstrating that an interruption of Wnt/frizzled signaling can attenuate the hypertrophic response [20]. These data indicate that interruption of Wnt/Frizzled pathway may provide novel therapeutic targets for antihypertrophic therapy.

173.2.5 MicroRNAs in Cardiac Hypertrophy

MicroRNAs (miRNAs) are endogenous, single-stranded molecules consisting of approximately 18–25 nucleotides that regulate target gene expression post transcriptionally. Many miRNAs are highly evolutionarily conserved and the human genome can encode up to 1000 miRNAs. miRNAs are transcribed as parts of longer molecules (pri-miRNAs) that are processed in the nucleus into hairpin RNAs by the RNase III-type enzyme Drosha. These pre-miRNAs are transported to the cytoplasm via exportin-5 and further processed by the ribonuclease Dicer. Mature miRNAs negatively regulate target gene expression through complementarity to target sequences in the 3′ untranslated region of target mRNAs by translational repression or degradation of bound RNA.

The role of miRNA has been implicated in various biological and pathological processes. Many studies have shown that miRNAs can control cardiac hypertrophy in vitro and in vivo. Cardiac-specific overexpression of miR-195 in mice causes an increase in left ventricular, wall size, upregulation of ANP, BNP and β-MHC, and reduced cardiac output [21] and overexpression of miR-214 in the cardiomyocytes also causes significant hypertrophy. In mice subjected to TAC, Akt-overexpressing transgenic mice or exercise-trained wild-type mice, miR-1 and miR-133 expressions were consistently downregulated. In vitro, transfection of cardiomyocytes with a miR-133-expressing viral vector blunted the hypertrophic response of cardiomyocytes stimulated with the hypertrophic agonist phenylephrine. miR-1, miR-133, miR-29, miR-30, and miR-150 have often been found to be downregulated whereas miR-21, miR-23a, miR-125, miR-195, and miR-199 have often been found to be upregulated with hypertrophy [22]. Several recent studies add new evidence to its role in cardiac hypertrophy. Both miRNA-142-3p and –5p are repressed by serum-derived growth factors in cultured cardiac myocytes, in models of cardiac hypertrophy in vivo and human cardiomyopathic hearts [23]. miR-221 regulated cardiomyocyte hypertrophy probably through down-regulation of p27, suggesting that miR-221 may be a new intervention target for cardiac hypertrophy [24]. Thus, it appears that miRNAs play multiple and essential roles in the regulation of cardiac hypertrophy.

173.2.6 PI3 K/Akt Signaling Pathway

Phosphoinositide3-kinase (PI3 K)/Akt signaling is mainly involved in physiological cardiac hypertrophy mediated by insulin-like growth factor-1 (IGF-1) and growth hormone (GH). The binding of IGF-1 to its receptor triggers the activation of several intracellular kinases, including PI3 K. PI3 K phosphorylates the membrane phospholipid phosphatidylinositol-4, 5-bisphosphate and recruits the protein kinase Akt (also known as PKB). Subsequently, Akt and its activator, 3-phosphoinositide–dependent protein kinase–1 (PDK1), translocate to the membrane, which leads to phosphorylation and activation of Akt.

The involvement of PI3 K/Akt signaling pathway in the control of physiological and pathological cardiac hypertrophy is well established. Over-expression of IGF-1 receptor leads to cardiac hypertrophy with enhanced cardiac function, while cardiac-specific deletion of the IGF-1 receptor blocks exercise-induced cardiac hypertrophy [25]. Transgenic mice that overexpress constitutively active PI3 K or dominant-negative PI3 K have larger or smaller hearts [26]. In addition, overexpression of activated Akt1 or Akt3 in the heart under the control of α-myosin heavy chain (α-MHC) promoter is sufficient to induce cardiac hypertrophy [27]. Akt1 gene-deleted mice weigh approximately 20 % less than wild-type animals and have a proportional reduction in size of all somatic tissues, including the heart. Cardiac-specific inducible Akt1-Tg mice develop adaptive or physiological hypertrophy following short-term induction but exhibit pathological hypertrophy and cardiomyopathy with longer periods of transgene induction. These data suggest that PI3 K/Akt signaling pathway contributes to the physiological and pathological cardiac hypertrophy.

173.3 Outlook

Clinical studies have demonstrated that cardiac hypertrophy is an independent risk factor of cardiac morbidity and mortality. Therefore, it is important to understand the mechanisms underlying the development of cardiac hypertrophy. The data summarized here elucidate many mechanisms that are involved in hypertrophy, including MAPK signal transduction pathway, Ca^{2+} dependent signal transduction pathway, PI3 K/Akt signaling pathway, JAK/STAT signal transduction pathway, Wnt signaling pathway and MicroRNAs, etc. But, whether these mechanisms apply to pathophysiological hypertrophy induced by mechanical stress in humans is still uncertain. Further investigation will be required to fully understand the mechanism of cardiac hypertrophy. Patients receive symptomatic treatment, and future biologically targeted therapy will depend on the discovery of new pathways that initiate, promote or potentially reverse the onset of cardiac hypertrophy.

Acknowledgments This work was financially supported by National Natural Science Foundation of China (No. 30970615, 31071126, 31171303), Program for Changjiang Scholars, Innovative Research Team in University of Ministry of Education of China (IRT1166), the Key Project of Chinese Ministry of Education (212010) and National Training Programs of Innovation and Entrepreneurship for Undergraduates (201210057011).

References

1. Lorell BH, Carabello BA (2000) Left ventricular hypertrophy: pathogenesis, detection, and prognosis. Circulation 102(4):470–479
2. Garrington TP, Johnson GL (1999) Organization and regulation of mitogen-activated protein kinase signaling pathways. Curr Opin Cell Biol 11(2):211–218

3. Clerk A, Michael A, Sugden PH (1998) Stimulation of the p38 mitogen-activated protein kinase pathway in neonatal rat ventricular myocytes by the G protein–coupled receptor agonists, endothelin-1 and phenylephrine: a role in cardiac myocyte hypertrophy? Cell Biol 142(2):523–535
4. Bueno OF, Witt SA, Tymitz KM (2000) The MEK1—ERK1/2 signaling pathway promotes compensated cardiac hypertrophy in transgenic mice. EMBO J 19(23):6341–6350
5. Bogoyevitch MA, Ketterman AJ, Sugden PH (1995) Cellular stresses differentially activate c-Jun N-terminal protein kinases and extracellular signal-regulated protein kinases in cultured ventricular myocytes. J Biol Chem 270(50):29710–29717
6. Wang Y, Huang S, Sah VP et al (1998) Cardiac muscle cell hypertrophy and apoptosis induced by distinct members of the p38 mitogen-activated protein kinase family. J Biol Chem 273(4):2161–2168
7. Wang S, Han HM, Pan ZW et al (2012) Choline inhibits angiotensin II-induced cardiac hypertrophy by intracellular calcium signal and p38 MAPK pathway. Naunyn Schmiedebergs Arch Pharmacol 385(8):823–831
8. He Q, LaPointe MC (2000) Interleukin-1beta regulates the human brain natriuretic peptide promoter via Ca^{2+}-dependent protein kinase pathways. Hypertension 35:292–296
9. Zhang T, Johnson EN, Gu Y et al (2002) The cardiac-specific nuclear δB isoform of Ca^{2+}/calmodulin-dependent protein kinase II induces hypertrophy and dilated cardiomyopathy associated with increased protein phosphatase 2A activity. Biol Chem 277(2):1261–1267
10. Molkentin JD, Lu JR, Antos CL et al (1998) A calcineurin-dependent transcriptional pathway for cardiac hypertrophy. Cell 93(2):215–228
11. van Rooij E, Doevendans PA, de Theije CC, Babiker FA, Molkentin JD, de Windt LJ (2002) Requirement of nuclear factor of activated T-cells (NFAT) in calcineurin mediated cardiomyocyte hypertrophy. Biol Chem 277:48617–48626
12. Wilkins BJ, Bueno OF, Braz JC et al (2002) Targeted disruption of NFATc3, but not NFATc4, reveals an intrinsic defect in calcineurin-mediated cardiac hypertrophic growth. Mol Cell Biol 22(21):7603–7613
13. Wang GJ, Wang HX, Yao YS, Guo LY, Liu P (2012) The role of Ca^2 +/calmodulin-dependent protein kinase II and calcineurin in TNF-α-induced myocardial hypertrophy. Braz J Med Biol Res 45: 264–272
14. Kunisada K, Negoro S, Tone E et al (2000) Signal transducer and activator of transcription 3 in the heart transduces not only a hypertrophic signal but a protective signal against doxorubicin-induced cardiomyopathy. Proc Natl Acad Sci U S A 97(1):315–319
15. Pan J, Fukuda K, Kodama H et al (1998) Involvement of gp130-mediated signaling in pressure overload-induced activation of the JAK/STAT pathway in rodent heart. Heart Vessels 13(4): 199–208
16. Chang L, Yang R, Wang M et al (2012) Angiotensin II type-1 receptor-JAK/STAT pathway mediates the induction of visfatin in angiotensin II-induced cardiomyocyte hypertrophy. Am J Med Sci 343(3):220–226
17. Reya T, Clevers H (2005) Wnt signalling in stem cells and cancer. Nature 434(7053):843–850
18. Gordon MD, Nusse R (2006) Wnt signaling: multiple pathways, multiple receptors, and multiple transcription factors. J Biol Chem 281(32):22429–22433
19. Haq S, Michael A, Andreucci M et al (2003) Stabilization of beta-catenin by a Wnt-independent mechanism regulates cardiomyocyte growth. Proc Natl Acad Sci USA 100(8):4610–4615
20. van de Schans VA, van den Borne SW, Strzelecka AE et al (2007) Interruption of Wnt signaling attenuates the onset of pressure overload-inducedcardiac hypertrophy. Hypertension 49(3):473–480
21. van Rooij E, Sutherland LB, Liu N et al (2006) A signature pattern of stress-responsive microRNAs that can evoke cardiac hypertrophy and heart failure. Proc Natl Acad Sci USA 103(48):18255–18260

22. Cheng Y, Ji R, Yue J et al (2007) MicroRNAs are aberrantly expressed in hypertrophic heart. Do they play a role in cardiac hypertrophy? Am J Pathol 170(6):1831–1840
23. Sharma S, Liu J, Wei J, Yuan H, Zhang T, Bishopric NH (2012) Repression of miR-142 by p300 and MAPK is required for survival signalling via gp130 during adaptive hypertrophy. EMBO Mol Med 4(7):617–632
24. Wang C, Wang S, Zhao P et al (2012) MiR-221 promotes cardiac hypertrophy in vitro through the modulation of p27 expression. J Cell Biochem 113(6):2040–2046
25. Kim J, Wende AR, Sena S et al (2008) Insulin-like growth factor I receptor signaling is required for exercise induced cardiac hypertrophy. Mol Endocrinol 22(11):2531–2543
26. Shioi T, Kang PM, Douglas PS, Hampe J, Yballe CM, Lawitts J, Cantley LC, Izumo S (2000) The conserved phosphoinositide 3-kinase pathway determines heart size in mice. EMBO J 19(11):2537–2548
27. Taniyama Y, Ito M, Douglas PS et al (2005) Akt3 overexpression in the heart results in progression from adaptive to maladaptive hypertrophy. J Mol Cell Cardiol 38(2):375–385

Chapter 174
Progress in Heparin-Functionalized Biomaterials

Yingfeng Wu, Juan Li, Feipeng Zhu and Hao Wang

Abstract The present article reviews the recent progress on heparin functionalization of biomaterials. Achievements in materials preparation based on physical adsorption coatings, covalent graft, and biomimetic microcarriers are included. All these heparin-containing materials have antithrombogenicity or can control the release of growth factors, which have been extensively investigated. However, the research in the near future will focus on construction of various systems to control the release of heparin affinitive growth factors.

Keywords Heparin · Growth factors · Functionalization · Biomaterials

174.1 Introduction

Heparin is a natural biologically relevant, highly anionic polysaccharide. The biological roles of this glycosaminoglycan (GAG) have been widely studied due to its importance in medicine and biomedical applications. Heparin is able to reversibly bind to many bioactive proteins, such as antithrombin III (AT-III), heparin interacting protein (HIP), and platelet factors (PF) [1]. In addition, heparin contains binding sites for many kinds of growth factors, such as basic fibroblast

Y. Wu
Department of Vascular Surgery, XuanWu Hospital, Capital Medical University, Beijing 100053, People's Republic of China

J. Li (✉)
Chinese Academy of Science, Institute of High Energy Physics, Beijing 100049, People's Republic of China
e-mail: lijuan@ihep.ac.cn

F. Zhu · H. Wang
School of Life Science and Technology, Beijing Institute of Technology, Beijing 100081, People's Republic of China

T.-C. Zhang et al. (eds.), *Proceedings of the 2012 International Conference on Applied Biotechnology (ICAB 2012)*, Lecture Notes in Electrical Engineering 251,
DOI: 10.1007/978-3-642-37925-3_174,

growth factor (bFGF) and vascular endothelial growth factor (VEGF) [2–4]. And heparin can promote the cell propagate, the tissue or organ repairs and regeneration [5]. In recent years, the heparin functionalization of biomaterials is paid great attention to, whose various techniques have been built up continuously, and these studies have displayed magnificent application prospect at tissue engineering fields [6, 7].

174.2 Structures and Bioactivity of Heparin

174.2.1 Structures of Heparin

Heparin was first purified and named in 1935, in the same year, heparin was applied to cure thrombotic diseases. Now, heparin is already considered one of the most effective, the most widely used anticoagulant medicines. Heparin molecular includes different length of acid mucopolysaccharide, mainly including two kinds of disaccharide units alternatively conjuncted mixture of D-glucosamine sulphate, D-iduronic acid sulphate, and D-glucuronic acid Fig. 174.1. The heparin molecular weight between 4 and 40 kDa [8]. Because there are variability of epimerization and sulfation during the process of biosynthesizes, most of heparin molecules are different among the microstructures. When the quantity of O-sulfation was more than that of N-sulfation in polysaccharide chain and most of glucosamine (about 80 %) were N-sulfation, the polysaccharide could be called heparin [9, 10].

174.2.2 Anticoagulation Function of Heparin

In the body, the cells contacting blood, like endothelial cells, can secrete sulfuric acid heparin, heparin, and other substances to keep the blood not solidify in circulating process. The content is very few in normal person's blood plasma, only

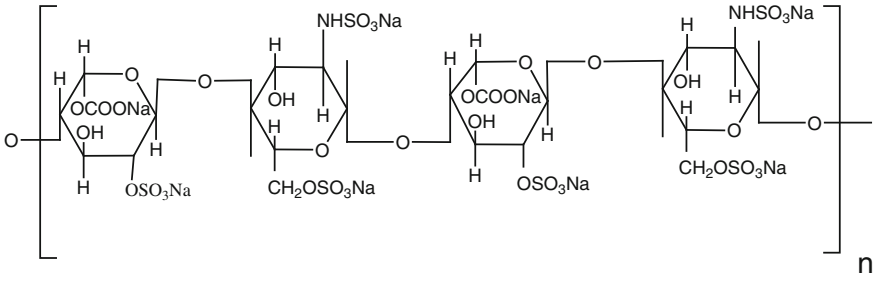

Fig. 174.1 The structure of heparin

0.09 mg/L. The heparin play anticoagulant function via AT III and the heparin cofactor (HC II) and the activated protein C inhibitors (APCI), and the AT III offered 80 % contributions [11, 12].

In the endogenous coagulation-anticoagulation system, the interaction was happened between heparin and vessel wall and heparin was adsorbed by the vascular endothelial, so the vessel wall is the main storage place of the heparin. After heparin adsorbed by the vascular endothelial, the release of endogenous amino-polysaccharide can be promote, and the injured vascular endothelial can recovery electric charge. The process can prevent blood platelets to attach on the surface of vessel wall and release the protein factor from platelets, then the anticoagulation effect can be reached. The heparin can also promote the vascular endothelial cells to release the tissue plasminogen activator (t-PA) and prevent blood from forming thrombus. Moreover, the heparin can make the negative charge of the blood cell surface and blood vessel wall increase, strengthen their repellency interaction, then change the blood viscosity, promote blood flow, and prevent blood from bolt formation [13].

174.2.3 The Nonanticoagulation Function of Heparin

The growth factors play the important roles to the cell multiplication, tissue or organ repair and regeneration, is one of the main aspects of the tissue engineering fields [14]. There are studies show that a lot of growth factors make more physiology functional via tying the heparin closely combined in the specific area in the extracellular matrix (ECM). The growth factors include the fibroblast growth factor (FGF) [15], the vascular endothelial growth factor (VEGF) [10, 16], conversion grows the transforming growth factor-β (TGF-β) [11, 17], the bone morphogenetic proteins (BMP) [18], the epidermal growth factor (EGF) [19, 20], the hepatocyte growth factor (HGF) [21], the nerve growth factor (NGF) [22], the platelet derived growth factor (PDGF) [23], and the insulin-like growth factor (IGF) [24]. In addition, some antibiotics are also heparin binding protein [25].

174.3 Heparinized Modification on the Surface of Biomaterials

174.3.1 Surface Coating of Heparin

The physical adsorption or coating is the most simple modification technique on the biomaterials surface. The coating of heparin on the surface of inert material can improve the blood compatibility of the biomaterial consumedly. With very strong negative electricity, heparin molecule chains can avoid bending or tangling with each other. After adsorption of heparin, the polymer materials would keep

good anticoagulant activity for some time [26]. In order to keep the activity of heparin, there are some researchers blended heparin with polymer materials such as polyurethane [27], while on the surface of the polymers mixed heparin, there are abundant reactive groups [28].

In order to increase the quantity and stability of heparin absorption on the material surface, some researchers take steps to get a multilayer composite materials: first, take the surface adsorption or covalence modification method to coat the polymer surface with substance such as protein [29] or chitosan [30]; then proceed the coating of heparin; finally, form multilayer composite materials, for examples, polycaprolactone [26], polyurethane [31], hydroxyapatite [30], polyethylene [32], polytetrafluoroethylene [29], and so on.

174.3.2 Covalence Modification of Heparin

The covalence modification is that covalent bonds connected between biomaterials and heparin moleculars, which can not only improve the use efficiency of heparin and the stability of heparin immobilization, but also unify the mechanical properties and anticoagulant activity of the materials.

The main steps of the covalent method is: first, preprocess the surface of polymer materials and make the surface have more groups which can react with heparins, then the groups on the surface can link heparin by covalent bonds [33, 34]. The linkage mainly takes advantage of the carboxyl and sulphur amino groups of heparin. The carboxamide linkage is one of the popular methods, which usually takes advantage of the reaction between the carboxyl or sulfonamide of heparin and the carboxyl or amino groups on the material surface by the EDC as a catalyst Fig. 174.2 [35]. With such a reaction, Wang et al. [36] immobilized heparin on the surface of poly (glutamic acid) with chitosan coating; Zhu et al. grafted heparin on the surface of polylactic acid films [37] and polytetrafluoroethylene artificial blood vessels [38] with azide chitosan coating. Figure 174.3 shows the reaction between chitosan and heparin. The other method is to graft the azide chitosan on the material surface firstly and then link heparin and chitosan [39]. Meanwhile, Aksoy et al. [31] took another method that immobilized heparin on the surface of polyurethane material after the surface has been previously oxidized and carboxylated, and they have verified the cell compatibility of the materials. Furthermore, some researches adopted O_2 plasma [40], NH_3 plasma [41], and the UV photosensitized reaction [35, 37] to preprocess the surface of

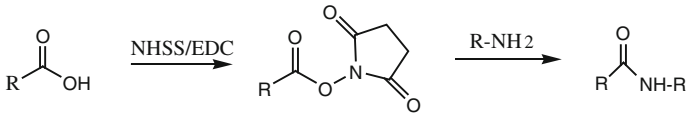

Fig. 174.2 Acylamine reaction catalyzed by EDC/NHSS

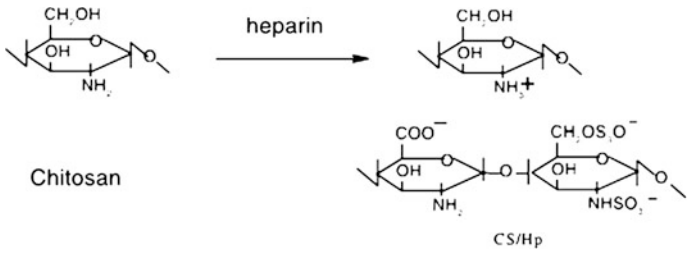

Fig. 174.3 Reaction of chitosan and heparin

polymer and metal materials to import active groups, which can be used to link the heparin molecules.

Under various reaction conditions, Marconi et al. [15] made the acrolyl chloride (AC) or the hexamethylene diisocyanate(HMDI) form covalence bonds with heparin molecules, with dibutyltin dilaurate as the catalyst in the reaction, and then heparin moleculars were immobilized on the surface of various compositions polyethylene (PE). The method can significantly prolong the coagulation time of materials.

Polymers are frequently used as media substance in the process of covalent modification on the surface of metal materials. Weng et al. [42] adopted the 3-amino-propyltriethoxylsilane as difunctional silane coupling agent to graft heparin on the surface of TiO2. Hou et al. [43] adopted the reaction between hydroxyl and hydroxyethyl groups catalyzed by APTES to form heparin covalence conjunction on the surface of Ti–O-N film. Chuang et al. [30] modified the stainless steel surface with poly ethylene glycol (PEG), and then immobilized heparin on the surface via ester bonds.

Because of the interaction on anticoagulation path of heparin and various affinitive factors, researchers also used the complex of heparin and anticoagulant cofactors to modify the material surface. Zhang et al. [44] adopted heparin and heparin affinity antithrombin to modify the material surface; Smith et al. [45] used heparin and fibrin thrombin to get anticoagulant surface. Our group [46] has previously reported the method that blend membranes of heparin and fibroin with low concentration heparin were prepared, and then aminogroups were imported to the surface of membranes by the plasma technique and AT-III were grafted to the aminogroups by cross-linking agents; finally, the anticoagulant materials with low toxic were gained. Besides the plasma technique, the methods of the ozone activation are also frequently applied to covalent modification of heparin [47].

174.4 Bionic Controlled Releasing of Heparin Vectors

Because the conformation of heparin will change by multisites immobilization on the material surface after covalent linkage of heparin, some activities of heparin will lose. Therefore the design of bionic controlled releasing of heparin vectors

emerged as the times require. The design of bionic controlled releasing vectors refers to the design which is according to the multiple action mechanism of the living cells, the intercellular or the biological activity substances (such as enzyme, protein and hormone, and so on). The design and the preparation of the suitable carries controlled the releasing of the biological activity substance. The aims which the effective stimulus cell to multiplicate, differentiate, the grown tissue regenerate of the design will be reached [48]. The microspheres, the hydrogel, the microcapsule, the micell, and some other vectors all are good control releasing carriers. These carriers can load or carry the biological activity substances in the structure of macromolecules, which can not only control the releasing also protect the biological active components. The interactions between heparin and many kinds of growth factors and the biological actions of each kind of growth factors can make dynamic balance in the releasing process. Therefore the heparin of controlled releasing carriers is a method which not only can gain the anticoagulant materials, but also prepare varieties of growth factors carriers simultaneously [49].

The tissue engineering hydrogel is a suitable carrier for growth factor [49], particularly situ hydrogel. And the situ cross-linking hydrogel refers to the hydrogel which was prepared by directly cross-linking in the raw materials solution including medicine. Because the molecular weight of the growth factors is low and the growth factors diffuse quickly in the hydrogel, the hydrogel cannot control their release and protect their activities exactly. Some studies discovered that binding heparin can make the growth factors sustained release and remain activities in the natural or artificial macromolecule hydrogels, for instance, alginate [50], chitosan [51], polyethylene glycol copolymer [52], collagen [53], and so on. The combination of heparin and hydrogels may use the negative charge on the heparin moleculars to form ionic bonds, and may also use–COOH,–OH, and so on active groups in the heparin member chain to form covalent bonds [49].

Recently, more and more researchers use the polymer which covalently grafted heparin for the hydrogel preparation [53]. Nilasaroya et al. [54] prepared PVA-heparin hydrogel by methyl acrylate suspension-arm connected heparin, and they discovered that the hydrogel not only has the anticoagulant activity, but also enhance the biological activity of FGF-2 when they evaluated the biocompatibility of the hydrogel. Tae et al. [55] exploited an injectable hydrogel through the copolymerizing of thiol heparin (Hep-SH) and poly(the ethylene glycol) diacrylate (PEG- DA). The hydrogel still has the activity to combine with the AT III and can embed to fiber cell. The fiber cell can propagate normally in the hydrogel. If fibrinogens are added in the hydrogel, the rate of cell proliferation can increase 5-fold higher. Tae et al. [52] also adopted the hydrazine heparin and PEG to make hydrogel and VEGF was used as a target heparin-affinity factor for controlled release. At last, the hydrogels were subcutaneous injected in the back of mice. The results show that near the injection sites, the density of the platelet endothelial cell adhesion molecule-1 significantly increased. Nakamura et al. [56] prepared hydrogels to load and carry FGF-2 by the 6-O-desulfurization heparin. In the experiments of subcutaneous implant hydrogels in rats, the hydrogel can significantly stimulate the formation of blood vessels and fibrous tissue. Choi et al. [57]

manufactured the hydrogel to load the human growth hormone (hGH) by the heparin Hep-SH and PEG. The hGH can be closely conglutinated with the hydrogels and the release of hGH can be controlled by the level of sulfhydryl heparin. The hGH was stable in the hydrogel and kept its good bioactivity after release.

174.5 Prospect

Heparin has good and stable anticoagulation functions; in particular, it has the abilities of high affinity and specific binding with various growth factors. Heparin-functional materials can improve the anticoagulant properties or the physiological activity of the growth factors, so heparin has a wide application prospects in the fields of biological materials and tissue engineering. Bionic controlled release system can avoid the side effects caused by its strong anticoagulant and the dose limitation. To set up the excellent performance of varieties "bionic" heparin functionalized controlled-release system will become a research hotspot in the coming years.

References

1. Yamaguchi N, Chae B, Zhang L et al (2005) Rheological characterization of polysaccharide-poly (ethylene glycol) star copolymer hydrogels. Biomacromolecules 6:1931–1935
2. Capila I, Linhardt R (2002) Heparin–protein interactions. Angew Chemint Ed 41:391–412
3. Forster M, Mulloy B (2006) Computational approaches to the identification of heparin-binding sites on the surfaces of proteins. Biochem Soc Trans 34:431–434
4. Chu C, Goerges A, Nugent M (2005) Identification of common and specific growth factor binding sites in heparan sulfate proteoglycans. Biochemistry 44:12203–12213
5. Jin K, Mao X, Guerra G, Jin L et al (2005) Heparin-binding epidermal growth factor-like growth factor stimulates cell proliferation in cerebral cortical cultures through phosphatidylinositol 3-kinase and mitogen-activated protein kinase. J Neurosci Res 81:497–505
6. Joung Y, Bae J, Park K (2008) Controlled release of heparin-binding growth factors using heparin-containing particulate systems for tissue regeneration. Expert Opin Drug Deliv 5:1173–1184
7. Zhu C, Ma L (2006) Medical macromolecule materials Beijing, 67–69
8. Li J, Liu X, Zhu B, Shao Y et al (2008) Alginate-templated microcapsules carrying heparin via layer-by-layer self-assembly. ICBBE, Shanghai, pp 1420–1424
9. Korir A, Larive C (2009) Advances in the separation, sensitive detection, and characterization of heparin and heparan sulfate. Anal Bioanal Chem 393:155–169
10. Mousa S (2005) Effect of low molecular weight heparin and different heparin molecular weight fractions on the activity of the matrix-degrading enzyme aggrecanase: structure-function relationship. J Cell Biochem 95:95–98
11. Vlodavsky I, Ilan N, Nadir Y et al (2007) Heparanase, heparin and the coagulation system in cancer progression. Thromb Res 120:S112–S120

12. Gupta V, Gowda L (2008) Conformational changes of ovine alpha-1-proteinase inhibitor: The influence of heparin binding. J Mol Struct 891:456–462
13. Mousa S, Liu R (2002) Effect of low molecular weight heparin and different heparin molecular weight fractions on aggrecanase activity: Structure-function relationship. Blood 100:93b–93b
14. Ori A, Wilkinson M, Fernig D (2008) The heparanome and regulation of cell function: structures, functions and challenges. Front Biosci 13:4309–4338
15. Harmer N (2007) The fibroblast growth factor (FGF)—FGF receptor complex: Progress towards the physiological state. Bioact Conformation I, Topic Curr Chem 272:83–116
16. Krilleke D, DeErkenez A, Schubert W et al (2007) Molecular mapping and functional characterization of the VEGF164 heparin-binding domain. J Biol Chem 282:28045–28056
17. Rider CC (2006) Heparin/heparan sulphate binding in the TGF-beta cytokine superfamily. Biochem Soc Trans 34:458–460
18. Khan S, Nelson M, Pan C et al (2008) Endogenous heparan sulfate and heparin modulate bone morphogenetic protein-4 signaling and activity. Am J Physiol Cell Physiol 294:C1387–C1397
19. Takazaki R, Shishido Y, Iwamoto R et al (2004) Suppression of the biological activities of the epidermal growth factor (EGF)-like domain by the heparin-binding domain of heparin-binding EGF-like growth factor. J Biol Chem 279:47335–47343
20. Mitchell C, Nivison M, Jackson L et al (2005) Heparin-binding epidermal growth factor-like growth factor links hepatocyte priming with cell cycle progression during liver regeneration. J Biol Chem 280:2562–2568
21. Sakiyama R, Fukuta K, Matsumoto K et al (2007) Stimulation of hepatocyte growth factor production by heparin-derived oligosaccharides. J Biochem 141:653–660
22. Ohta M, Suzuki Y, Chou H et al (2004) Novel heparin/alginate gel combined with basic fibroblast growth factor promotes nerve regeneration in rat sciatic nerve. J Biomed Mater Res Part A 71:661–668
23. Vercoutter-Edouart A, Dubreucq G, Vanhoecke B et al (2008) Enhancement of PDGF-BB mitogenic activity on human dermal fibroblasts by biospecific dextran derivatives. Biomaterials 29:2280–2292
24. Kuang Z, Yao S, Keizer D et al (2006) Structure, dynamics and heparin binding of the C-terminal domain of insulin-like growth factor-binding protein-2 (IGFBP-2). R.S J Mol Biol 364:690–704
25. Bastani B, Amin K, Herr A et al (2005) Prolonged stability of stored vancomycin, gentamicin, and heparin for use in the antibiotic-lock technique. ASAIO J 51:761–763
26. Liu L, Guo S, Chang J, Ning C et al (2008) Surface modification of polycaprolactone membrane via layer-by-layer deposition for promoting blood compatibility. J Biomed Mater Res Part B-Appl Biomater 87B:244–250
27. Lv Q, Cao C, Zhu H (2003) Novel solvent system for blending of polyurethane and heparin. Biomaterials 24:3915
28. Tang Y, Cao C, Ma X et al (2005) Mechanical properties and antithrombogenecity of blend membrane of silk fibroin. ASBM6:Adv Biomater, Key Eng Mater 6, 445–448
29. Vallieres K, Petitclerc E, Laroche G (2007) Covalent grafting of fibronectin onto plasma-treated PTFE: Influence of the conjugation strategy on fibronectin biological activity. Macromol Biosci 7:738–745
30. Sun F, Pang X, Zhitomirsky I (2009) Electrophoretic deposition of composite hydroxyapatite-chitosan-heparin coatings. J Mater Process Technol 209:1597–1660
31. Aksoy A, Hasirci V, Hasirci N (2008) Ce modification of polyurethanes with covalent immobilization of heparin. Macromol Symp 269:145–153
32. Ji J, Tan Q, Shen J (2004) Construction of albumin multilayer coating onto plasma treated poly (vinyl chloride) via electrostatic self-assembly. Polym Adv Technol 15:490–494
33. Foley P, Barthel C, Brausa H (2002) Effect of covalently bound heparin coating on patency and biocompatibility of long-term indwelling catheters in the rat jugular vein. Comp Med 52:243–248

34. Shi H, Mo X, He C et al (2008) Preparation, characterization and anticoagulant property of P(LLA-CL) nanofibrous scaffolds by heparinization. J Clin Rehabilitative Tissue Eng Res 12, 10–14
35. Murugesan S, Xie J, Linhardt R (2008) Immobilization of heparin: Approaches and applications. Curr Top Med Chem 8:80–100
36. Wang X, Li D, Wang W et al (2003) Covalent immobilization of chitosan and heparin on PLGA surface. Int J Biol Macromol 33:95
37. Zhu A, Zhang M, Wu J (2002) Covalent immobilization of chitosan/heparin complex with a photosensitive hetero-bifunctional crosslinking reagent on PLA surface. Biomaterials 23 4657–4665
38. Zhu A, Ming Z, Jian S (2005) Blood compatibility of chitosan/heparin complex surface modified ePTFE vascular graft. Appl Surf Sci 241:485–492
39. Lin W, Liu T, Yang M (2004) Hemocompatibility of polyacrylonitrile dialysis membrane immobilized with chitosan and heparin conjugate. Biomaterials 25:1947
40. Hasirci N, Aksoy E (2007) Synthesis and modifications of polyprethanes for biomedical purposes. High Perform Polym 19:621–637
41. Tan Q, Ji J, Zhao F et al (2005) Fabrication of thromboresistant multilayer thin film on plasma treated poly (vinyl chloride) surface. J Mater Sci Mater Med 16:687
42. Weng Y, Hou R, Xie D et al (2007) Covalent immobilization of heparin on anatase TiO2 films via chemical adsorbent phosphoric acid interface. Bioceram Key Eng Mater 192–1:865–868
43. Hou R, Weng Y, Wang J et al (2007) Study on covalent immobilization of heparin on ti-o-n surface and antithrombogenicity. J Inorgan Mater 22:996–1000
44. Zhang H, Zhao R, Chen Z et al (2005) QCM-FIA with PGMA coating for dynamic interaction study of heparin and antithrombin III.Biosens. Bioelectron 21:121–127
45. Smith L, Berry L, Chan A (2004) Reaction of fibrin-bound thrombin with a covalent antithrombin-heparin complex results in an anticoagulant surface. Blood 104, 512A–512A
46. Yang X, Wu K, Yu Q et al (2004) Immobilization of antithrombin-III on fibroin/heparin blend membrane and its anticoagulant performance. Trans Beijing Inst Technol 24:837–840
47. Hou C, Zhang W, Huo D et al (2003) Advances in the study on integrated mode of heparin and noumenon. Biomaterials 22:703–709
48. Anonymous (2006) Heparin coating as a preventive strategy to control catheter-associated urinary tract infections. Eur Urol Suppl 5:144–148
49. Ding S, Zheng G, Yin Y et al (2008) Heparin for growth factor delivery systems. Prog Chem 20:1998–2011
50. McLennan G, Johnson M, Stookey K et al (2000) Kinetics of release of heparin from alginate hydrogel. J.V.I.R 11, 1087–1094
51. Chandy T, Mooradian D, Rao G (1998) Chitosan polyethylene glycol alginate microcapsules for oral delivery of hirudin. J Appl Polym Sci 70:2143–2153
52. Tae G, Scatena M, Stayton P et al (2006) PEG-cross-linked heparin is an affinity hydrogel for sustained release of vascular endothelial growth factor. J Biomater Sci Polym Ed 17:187–197
53. Silva A, Richard C, Bessodes M et al (2009) Growth factor delivery approaches in hydrogels. Biomacromolecules 10:9–18
54. Nilasaroya A, Poole-Warren L, Whitelock J et al (2008) Structural and functional characterisation of poly (vinyl alcohol) and heparin hydrogels. Biomaterials 29:4658–4664
55. Tae G, Kim Y, Choi W, Kim et al (2007) Formation of a novel heparin-based hydrogel in the presence of heparin-binding biomolecules. Biomacromolecules 8:1979–1986
56. Nakamura S, Ishihara M, Obara K et al (2006) Controlled release of fibroblast growth factor-2 from an injectable 6-O-desulfated heparin hydrogel and subsequent effect on in vivo vascularization. J Biomed Mater Res Part A 78A:364–371
57. Choi W, Kim M, Tae G et al (2008) Sustained release of human growth hormone from heparin-based hydrogel. Biomacromolecules 9:1698–1704

Chapter 175
Identification of an Antifungal Bacillus Strain and Studies on Its Antifungal Active Ingredients

Yingde Shen, Ruibin Liu, Yuehua Chen and Jun Cai

Abstract Strain NK-2 which has broad spectrum of antifungal activity against eight kinds of phytopathogenic fungi was identified as *Bacillus amyloliquefaciens* by analysis of partial 16S rDNA, *gyrA* gene, and *rpoB* gene sequences. The crude protein, obtained from NK-2 culture, exhibited inhibitory activity on mycelial growth and conidial spore germination of *Fusarium oxysporum*. The crude proteins were further purified by Sephadex G-200 and the antifungal fraction was checked by SDS-PAGE. The putative active protein was then analyzed by Tandem mass spectrum. The result revealed that the target protein was high similar to protein YhfE from *B. amyloliquefaciens* FZB 42. Then we cloned the *yhfE* (GenBank accession:HM143898) from NK-2 genome and expressed it in *Escherichia coli* BL21. The purified recombinant YhfE protein could also inhibit the spore germination and mycelial growth of *F. oxysporum*. We have found for the first time, to our knowledge, that YhfE has antifungal activity.

Keywords Antifungal protein · *Bacillus amyloliquefaciens* · Mass spectrometry · YhfE

The authors Y. Shen and R. Liu contributed equally to this paper.

Y. Shen · Y. Chen · J. Cai (✉)
Key Laboratory of Molecular Microbiology and Technology, Ministry of Education, College of Life Science, Nankai University, Tianjin 300071, People's Republic of China
e-mail: caijun@nankai.edu.cn

R. Liu
Tianjin Taihe Pharmaceutical Co. Ltd., Tianjin 300270, People's Republic of China

T.-C. Zhang et al. (eds.), *Proceedings of the 2012 International Conference on Applied Biotechnology (ICAB 2012)*, Lecture Notes in Electrical Engineering 251,
DOI: 10.1007/978-3-642-37925-3_175,

175.1 Introduction

Bacillus amyloliquefaciens which is closely related to *Bacillus subtillis* has extensively been studied as biological control agents of plant pathogens, and it can produce a range of antimicrobial compounds, for example cyclic lipopeptides [1], polyketides [2], proteins, and so on. Many investigators have devoted their time and energy to search for the cyclic lipopeptides including iturins [3, 4], fengycins [5], and surfactines [5, 6]. Some bacterial antifungal proteins have also been isolated successfully from *B. amyloliquefaciens*, such as baciamin [7], *β*-Glucanase [8], and cellulose [9]. However, it is much less abundantly compared with that on bacterial antifungal peptides.

In this paper, strain NK-2 with broad antifungal spectrum was identified as *B. amyloliquefaciens* using methods of molecular biology [10–12]. In order to probe what substances were responsible for its antifungal activity, we analyzed the putative active protein by Tandem Mass Spectrometry (MS-MS). Fortunately, the protein could be found in database and had high similar to protein YhfE of *B. amyloliquefaciens* FZB 42. To verify its antifungal activity, *yhfE* gene from NK-2 genome was expressed in *E. coli 21* (DE3) and the recombinant protein was purified to test if it can control of the spore germination and mycelium growth of *F. oxysporum*. The results indicated that the recombinant protein did work. It is the first time, to our knowledge, that YhfE has antifungal activity.

175.2 Materials and Methods

175.2.1 Bacterial Strain, Fungi Strains, and Growth Conditions

NK-2 was cultivated in LB medium with shaking in 200 rpm at 30 °C. *E. coli* BL21(DE3) was cultivated in LB medium with shaking in 200 rpm in at 37 °C.

The fungi such as *Aspergillium niger*, *Botrytis cinerea, Fusarium graminearum*, *Fusarium oxysporum*, *Penicillium chrysogenum*, *Physalospora piricola*, *Rhizopus nigricans*, *Rhizoctonia solani* were incubated in a potato-dextrose agar (PDA) medium at 25 °C and stored in our laboratory.

175.2.2 Strain Identification

Strain NK-2 identification, including 16S rDNA, *gyrA* and *rpoB* sequence analysis and the neighbor joining phylogenetic tree construction, was performed as described previously [12].

175.2.3 Isolation and Analysis of Antifungal Protein from Strain NK-2

NK-2 was grown in 100 ml LB medium m for 72 h at 30 °C. Cell-free supernatant was precipitated by 65 % ammonium sulphate saturation and the precipitate was dissolved in 10 ml 25 mM Tris-HCl buffer (pH 7.20), and dialyzed extensively against the same buffer for 24 h to remove ammonium sulphate. Following dialyzation, the supernatant was concentrated with Millipore centrifugal filter with a 30 kDa cutoff, and the antifungal activity of crude proteins was tested against *F. oxysporum*. The concentrated antifungal crude protein was applied to a Sephadex G-200 column. The active-peak fractions were pooled and concentrated. Sodium dodecyl sulphate polyacrylamide gel electrophoresis (SDS-PAGE) was used to check the protein purity and to determine the molecular weight of the protein. After electrophoresis, the gel was stained in silver-stained method.

Tandem Mass Spectrometry (MS-MS) analysis was performed by Tianjin Biochip Corporation (Tianjin, China) to analyze the character of protein segment sequences and molecular weight of the antifungal compounds. The concentration of protein was assayed with the Bradford method.

175.2.4 Antifungal Activity

NK-2 was first screened for its ability to inhibit fungal growth on PDA plates using the dual culture technique [13], and eight sort of phytopathogenic fungi were tested. Antifungal activity of the crude protein and recombination protein against *F. oxysporum* including inhibited the growth of mycelium and spores were assayed according to the method of Roberts et al. [14]. Described simply, conidial suspension (20 μl) was mixed with 180 μl crude protein obtained from NK-2 culture or purified recombinant protein and added to the cylinder on PDA plate. For the control treatment, conidial suspension (20 μl) was mixed with 180 μl sterile Tris buffer was added to another cylinder. The plates were incubated at 30 °C for 72 h, and then inhibition of spore germination in the cylinders was judged by visual inspection. To test the ability of inhibiting fungal growth, the fungus *F. oxysporum* was grown in PDA for 2 days at 30 °C, then 200 μl crude proteins obtained from NK-2 culture or purified recombinant protein was added to the cylinder on PDA plate. The plates were incubated at 30 °C for 72 h.

175.2.5 Cloning and Expressing of yhfE from Strain NK-2

The putative antifungal protein gene *yhfE* was amplified using forward primer (GTAGGATCCGTGGCAAATATGAAAC) and reward primer (CTTGAGCTC TTATGCCATCGG). The amplified *yhfE* PCR products were extracted using Gel

Extraction kit (Bio Basic Inc., Markham Ontario, Canada). The *Bam*HI and *Sac*I fragments were recovered and cloned into the corresponding sites of the plasmid pET-28a (Novagen) and transformed into competent cells of *E. coli* BL21. The recombinant YhfE protein was induced by IPTG, purified by Ni-NTA affinity column. SDS-PAGE was performed to check the protein purity and to determine the molecular weight of the protein. After electrophoresis, gels were stained with Coomassie brilliant blue R-250.

175.3 Results

175.3.1 Identification of Strain NK-2

The 16S rDNA from NK-2 (Accession no. GU064894) were analyzed on the website (http://blast.ncbi.nlm.nih.gov/Blast.cgi), the sequence showed high similarities (100 % or 99 %) to *B. subtillis*, *B. amyloiquefaciens*, and *B. velezensis*.

The *gyrA* (Accession no. GU226662) sequence from strain NK-2 had 99 % or 98 % identity with the sequence of *B. amyloliquefaciens* and *B. velezensis*; while *rpoB* (accession no. GU226663) sequences from strain NK-2 had 100 % identity with *B. amyloliquefaciens* FZB42 and DSM7. The phylogenetic tree was constructed using concatenated *gyrA* and *rpoB* sequences of related members of the *Bacillus* genus revealed that strain NK-2 should be assigned to *B. amyloliquefaciens* rather than *B. velezensis* (Data not shown).

175.3.2 Antifungal Spectrum of Wild Strain NK-2

Antifungal activity of NK-2 toward eight fungi was observed. The result showed us that NK-2 exhibited a broad spectrum of antifungal activity against all tested plant pathogenic fungi (Fig. 175.1).

175.3.3 Isolation of Crude Protein, Purification, SDS-PAGE, and MS Analysis

A crude antifungal protein was obtained by adding ammonium sulphate to supernatant fluid of strain NK-2 to a final saturation of 65 % and displayed antifungal activity against *F. oxysporum.* Moreover, after ultrafiltration separation, the retentate of crude protein kept the activity while the filtrate did not. The crude protein was subsequently separated by gel filtration on a Sephadex G-200 column chromatography. The active fractions were further separated by SDS-PAGE. The protein with apparent molecular weight 42 kDa was supposed to be the putative

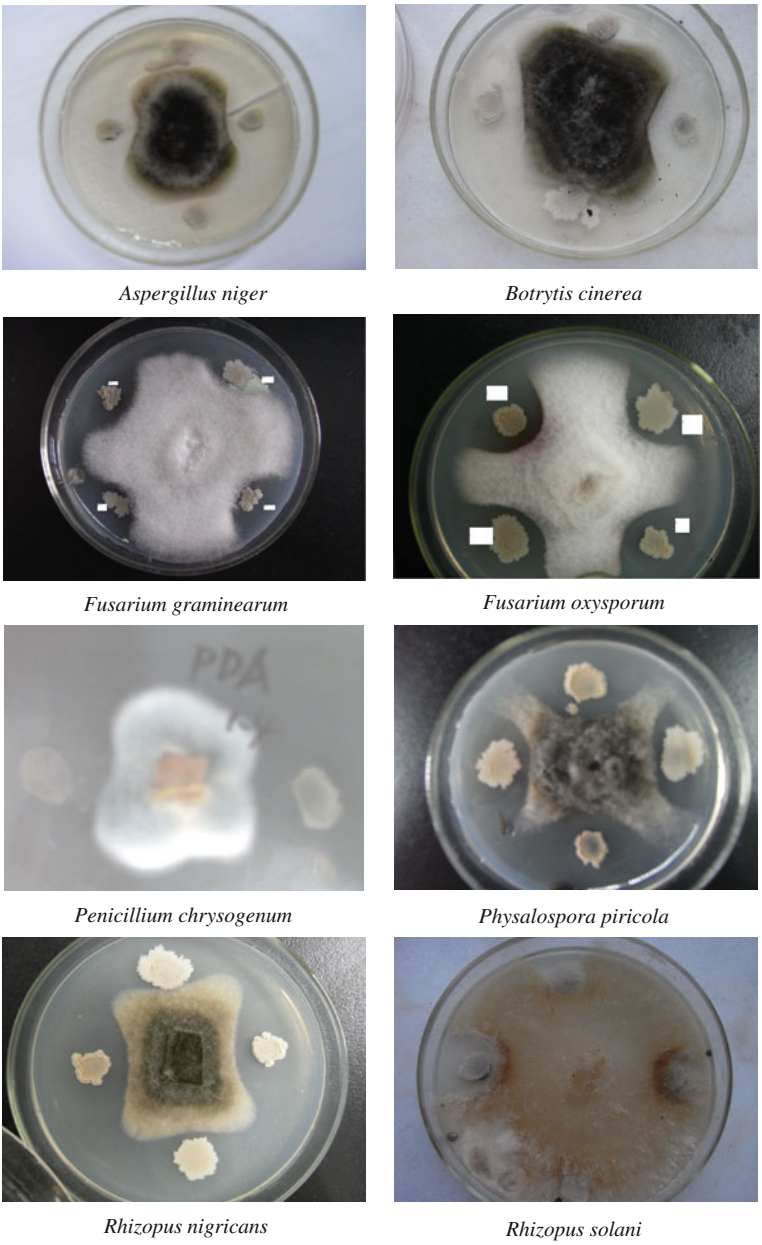

Fig. 175.1 The test of antifungal spectrum of NK-2 against eight phytopathogenic fungi

active protein (Fig. 175.2). MS-MS was utilized to identify the antifungal compounds. The result of mass spectrum revealed our target protein was similar to protein YhfE from *B. amyloliquefaciens FZB 42*.

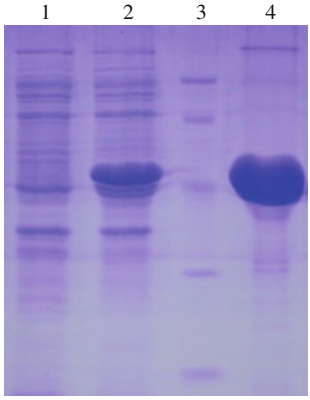

Fig. 175.2 SDS-PAGE analysis of the expression of the recombinant *yhfE*. *1* *E. coli* BL21 without *yhfE* in pET28 as control, *2* *E. coli* BL21 with *yhfE* in pET28, *3* protein marker, *4* the purified YhfE

175.3.4 Cloning, Expressing, and Bio-Activity of yhfE *Gene from Strain NK-2*

The *yfhE* from NK-2 genome was cloned and the sequencing result was submitted to GenBank (accession no. HM143898). And *yhfE* was expressed in *E. coli* BL21 with recombinant pET28(a+)-*yhfE* plasmid, then purified by Ni-NTA spin columns. SDS-PAGE was used to test the expression and purification of YhfE (Fig. 175.2). The bioassay demonstrated that the purified recombinant YhfE protein could also inhibit the spore germination and mycelium growth of *F. oxysporum* (Fig. 175.3).

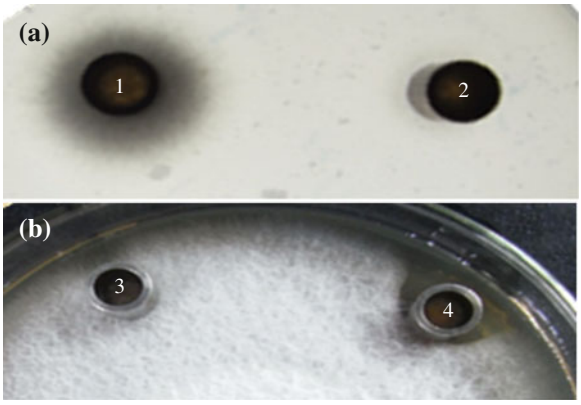

Fig. 175.3 Bioassay of the purified recombinant YhfE protein against *F. oxysporum*. *A* inhibition of spore germination, *B* inhibition of mycelium growth. *1*, *3:* Tris-HCl buffer, *2*, *4*: YhfE

175.4 Conclusion

The *16S rDNA* gene is usually used as a framework for modern bacterial classification, but it shows limited variation in classifying some closely related taxa [15]. In contrast, some protein-coding genes with higher mutation rates have been used successfully to differentiate taxa that cannot be identified using 16S rRNA sequences alone. For example, *gyrA* (codes for DNA gyrase subunit A) and *rpoB* (codes for DNA-directed RNA polymerase subunit beta) genes are useful for the rapid identification of *Bacillus subtilis* and allied taxa, especially organisms in these taxa that cannot be differentiated by using 16S rRNA analysis [12]. In this study, strain NK-2 showed 16S rDNA sequences almost identical to members of the *B. subtilis* group. Thus, the sequence data of *gyrA* and *rpoB* genes were used to distinguish NK-2 from other closely related taxa. It is obvious that the combined analysis of partial *gyrA* and *rpoB* gene sequences is a very efficient method for identifying *B. subtilis* and allied taxa, especially when these taxa cannot be differentiated using conventional phenotypic tests and 16S rDNA analysis.

Many researchers attempt to get the antifungal protein-coding genes by N-terminal amino acid sequencing, but these sequences often showed no significant homology with any known proteins in date base, suggesting that the purified protein may be novel one. So they usually could not get the genes with the method of N-terminal amino acid sequencing as a result.

It is very complicated and tedious in the process of protein purification. The primary purified protein is enough to satisfy the need of MS-MS which can avoid the time-consuming process of protein purification. The genome of *B. amyloliquefaciens* FZB42 has been sequenced for several years [1]. In light of the whole genome sequence information, we got the *yhfE* gene successfully from strain NK-2 on the basis of MS-MS analysis. Moreover, the purified recombinant YhfE protein could also inhibit the spore germination of *F. oxysporum.*

Acknowledgments This work was supported by the Development Program of China (863 Program) (No. 2011AA10A203), the National Natural Science Foundation of China grant (30971957), and Natural Science Foundation of Tianjin Science and Technology Commission (11JCYBJC08300, 12JCYBJC19800).

References

1. Koumoutsi A, Chen XH, Henne A et al (2004) Structural and functional characterization of gene clusters directing nonribosomal synthesis of bioactive cyclic lipopeptides in *Bacillus amyloliquefaciens* strain FZB42. J Bacteriol 186:1084–1096
2. Chen XH, Vater J, Piel J et al (2006) Structural and functional characterization of three polyketide synthase gene clusters in *Bacillus amyloliquefaciens* FZB42. J Bacteriol 188: 4024–4036
3. Arrebola E, Jacobs R, Korsten L (2010) Iturin A is the principal inhibitor in the biocontrol activity of *Bacillus amyloliquefaciens* PPCB004 against post-harvest fungal pathogens. J Appl Microbiol 108:386–395

4. Yu GY, Sinclair JB, Hartman GL et al (2002) Production of iturin A by *Bacillus amyloliquefaciens* suppressing *Rhizoctonia solani*. Soil Biol Biochem 34:955–963
5. Chen L, Wang N, Wang X et al (2010) Characterization of two anti-fungal lipopeptides produced by *Bacillus amyloliquefaciens* SH-B10. Bioresource Technol 101:8822–8827
6. Wang Y, Lu Z, Bie X et al (2010) Separation and extraction of antimicrobial lipopeptides produced by *Bacillus amyloliquefaciens* ES-2 with macroporous resin. Eur Food Res Technol 231:189–196
7. Wong JH, Hao J, Cao Z et al (2008) An antifungal protein from *Bacillus amyloliquefaciens*. J Appl Microbiol 105:1888–1898
8. Kim PI, Chung KC (2004) Production of an antifungal protein for control of *Colletotrichum lagenarium* by *Bacillus amyloliquefaciens* MET0908. FEMS Microbiol Lett 234:177–183
9. Lee YJ, Kim BK, Lee BH et al (2008) Purification and characterization of cellulase produced by *Bacillus amyoliquefaciens* DL-3 utilizing rice hull. Bioresource Technol 99:378–386
10. Fritze D (2004) Taxonomy of the genus Bacillus and related genera: the aerobic endospore-forming bacteria. Phytopathology 94:1245–1248
11. Porwal S, Lal S, Cheema S et al (2009) Phylogeny in aid of the present and novel microbial lineages: diversity in Bacillus. PLoS ONE 4(2):e4438
12. Xiao L, Xie CC, Cai J et al (2009) Identification and characterization of a chitinase-produced Bacillus showing significant antifungal activity. Curr Microbiol 58:528–533
13. Yoshida S, Hiradate S, Tsukamoto T et al (2001) Antimicrobial activity of culture filtrate of *Bacillus amyloliquefaciens* RC-2 isolated from mulberry leaves. Phytopathology 91:181–187
14. Roberts RG (1990) Post-harvest biological control of grey mold of apple by *Cryptococcus laurentii*. Phytopathology 80:526–530
15. Fox GE, Wisotzkey JD, Jurtshuk P (1992) How close is close: 16S rRNA sequence identity may not be sufficient to guarantee species identity. Int J Syst Bacteriol 42:166–170

Chapter 176
Enrichment of Flavonoids and Removal of Organic Acid by Treatment of Weak-Base Anion Resins

Yuping Zhao, Shuyang Sun, Zuli Sun, Wenguang Jiang, Jianrong Yang, Pu Song, Xiangping Zheng and Tiantian Tian

Abstract In the manufacture of flavonoids-enriched hawthorn juice, a high concentration of organic acids is the main problem. In order to produce high quality juice and facilitate its use in many food products, an investigation on the deacidification of Chinese hawthorn juice using an ion exchange process was initiated. Among the tested five resins, D301G was found to perform the best, allowing the production of hawthorn juice with the lowest acidity and highest content of flavonoids. After optimization, a temperature of 30 °C and a flow rate of 10 BV/h were selected, respectively. When one cycle of processing (23 BV) was finished, the physiochemical characteristics of combined juices were analyzed. It was found that over 55 % of initial acid was removed; the concentrated flavonoids reached 3.8 g/kg; and the sugars and minerals contained in the juice underwent negligible changes. Additionally, after regeneration of D301G with 20 cycles, the resin still possessed strong capacity to reduce organic acids and retain flavonoids. Therefore, the current investigation proved that an adsorption processing of hawthorn juice with weakly basic anion exchange resins enabled production of flavonoids-enriched juices with low amount of titratable acidity and without affecting sugars and minerals.

Keywords Hawthorn juice · Deacidification · Weak-base anion resin · Organic acids · Flavonoids

Y. Zhao (✉) · Z. Sun · J. Yang · P. Song · X. Zheng · T. Tian
Institute of Life Science, Yantai University, Shandong 264005, People's Republic of China
e-mail: water15689@163.com

S. Sun
School of Food Engineering, Ludong University, Shandong 264000, People's Republic of China

W. Jiang
International Journal of Food Science and Technology, Technology Center of Changyu Pioneer Wine Company Limited, Shandong 264000, People's Republic of China

T.-C. Zhang et al. (eds.), *Proceedings of the 2012 International Conference on Applied Biotechnology (ICAB 2012)*, Lecture Notes in Electrical Engineering 251,
DOI: 10.1007/978-3-642-37925-3_176,

176.1 Introduction

Crataegus pinnatifida Bge. Var. major N.E. Br. (*Rosaceae*), named Shanzha in China, is a tasteful and traditional fruit in China, which is widely distributed in the northeast and southwest areas of China, such as Liaoning, Hebei, Henan, and Shandong provinces. It is larger than the counterpart grown in European countries. Other than the taste and flavor that this fruit provides, it also exerts several pharmacological and clinical effects, such as anti-inflammatory, antiarrhythmic, and hypolipidemic effects. Many studies suggested that consumption of Shanzha showed benefits for cardiovascular functions, mainly due to the reduction of serum cholesterol. In addition, it has been documented that Shanzha also functions as an antioxidant, and one major of the active constituents showing marked antioxidative activity from Shanzha was identified as flavonoids [1].

Chinese hawthorn fruit has intense and special aromas, which makes it a desirable ingredient in the formulation of various food products, such as jam, confect, juice, canned food, vinegar, and wine. The fruits have also been used as a peptic agent in herbal medicine and recently as a local soft drink material for the diet. However, the content of organic acid in the dried Chinese hawthorn fruits can be up to 5 %, and thus only limited amounts of juice can be added to food products, because superfluous addition can decrease the food quality by introducing a strong taste of acidity. Adding of sweetening agents or simple neutralization by basic compounds are not suitable, since these methods affect the flavor and natural taste of juices and lead to poor palatability. Therefore, various processing aids such as calcium precipitation, ion exchange (IE), and electrodialysis (ED) were attempted to deacidify the hawthorn juices. Among these methods, the employment of IE process is based on the principle of physically entrapping organic materials in the matrix [2], by subjecting the juice to a column containing the resins. The method has the advantage of removing phenolic compounds, amino acids, and proteins present in juice [3, 4]. Particularly, a weak-base anion resin is preferred in the food industry for acid reduction because it does not exchange ions but adsorbs acids [4, 5, 11, 12]. Additionally, using weak-base anion resins includes another benefit of reduced requirement of regenerant [5]. However, one major drawback of the IE technique is that most minerals, which are important nutritional constituents in fruit juices, are exchanged. During recent years, IE technique has been intensively studied for deacidification in various kinds of juices, such as pear [3], grape [6], passion fruit [7, 8], and orange [4], and great achievements has been accomplished in these studies.

In the current paper, studies on the deacidification of Chinese hawthorn juice with a weak ion exchange resin are reported. The reduction of acidity was achieved by increasing the pH from 2.9 to 4.0. Then, the physicochemical and sensorial properties of juices treated were analyzed.

176.2 Materials and Methods

176.2.1 Preparation of Hawthorn Juice

Fruits of Chinese hawthorn, Crataegus pimmatifida Bge variety, obtained fresh from the local market (Hebei, China), were washed thoroughly in water, milled, and boiled at 100 °C for 5 min, followed by cooled to about 50 °C. Then, the mash was pressed by Universal Fruit Press HP 5000 (Bucher-Guyer), and a pectic enzyme preparation (16 U/ml) was added, followed by incubation at 50 °C for 4 h. Hawthorn juice was extracted from the incubated mass and centrifuged at 2200xg for 15 min. And the obtained juice was used for the following investigations.

176.2.2 Treatment of Resins and Operation of the Columns

Five resins, D301G, D301R, D392, D201-4, D101, provided by the Chemical Plant of NanKai University, were tested in the study. The matrix types of all resins are crosslinked-polystyrene. D101 is macroporous, while others are using primary, secondary, or tertiary amine as ligand. Resins (50 mL) were rinsed with water and allowed sufficient time to swell; then the resins were transferred to a glass column (1.8 × 28 cm). Before used, both the columns were regenerated with the requisite quantities of 5 % (w/v) hydrochloric acid and 4 % (w/v) sodium hydroxide, respectively, followed by washing down the column with distilled water. The hawthorn juice was pumped into the ion exchange column using a peristaltic pump (Masterflex, Cole-Parmer Instrument Company, Chicago, U.S.A.). And treated juice samples were individually collected at each BV. Three temperatures (20, 30, and 40 °C) and three flow rates (10 and 15 BV/h) were tested for the optimization of most suitable conditions.

176.2.3 Regeneration of Resins

Regeneration of the resins was carried out using 6 BV of 4 % NaOH, followed by washing with 7 BV of water at a flow rate of 10 ml/min. Then, the resins were rinsed with deionized water to get rid of excessive NaOH, and ready for next processing cycle.

176.2.4 Physical and Chemical Analysis of Juice

pH and titratable acidity were analyzed throughout the deacidification process. pH was measured using a Mettler-Toledo MP 220 pH meter (Mettler, Viroflay,

France). Titratable acidity was assayed by titration with 0.1 N NaOH and expressed as grams of citric acid per kg of juice. Total soluble solids of hawthorn juice were read off by refractometry with an Atago hand refractometer (model N-20, Atago Co., Tokyo, Japan). Total sugars were determined by the colorimetric method of DuBois et al. [9].

176.2.5 Minerals Analysis

Determination of minerals (Cu, Fe, Ca, Na, and K) was followed the procedure of Vivekanand [3], using a Varian atomic absorption spectrophotometer system (Spectra AA-400, Varian Inc., Palo Alto, Calif., U.S.A.). 2 ml juice sample was mixed with 1 mL hydrochloric acid and 250 μl solution containing 4 % (w/v) of cesium chloride and 8 % (w/v) of strontium chloride. And the volume was finally made up to 10 ml using milli-Q water.

176.2.6 Analysis of Organic Acids

Fruit juice (10 g) was diluted to 50 ml with K_2HPO_4 (0.01 mol/l, pH 2.6), and filtered through a 0.22-μm nylon filter. Then an aliquot of 20 μl was injected onto a HPLC system (KNAUER, Berlin, Germany), equipped with model K-1001 pump, thermostated column compartment model A-150 and a K-2501 UV detector (KNAUER, Berlin, Germany) with wavelength set to 210 nm. Chromatographic separation was performed on the column of Prontosil 120-10-C_{18}H (250 × 4.60 mm i.d., 10 μm) (KNAUER, Berlin, Germany), using 0.01 mol/l K_2HPO_4 (pH 2.6) as the mobile phase at a flow rate of 0.5 ml/min. The compounds were identified by their peak retention times.

176.2.7 Analysis of Flavonoids

Content of flavonoids in the juice was analyzed by the aluminum chloride colorimetric method of Chang et al. [10]. Briefly, an aliquot of 0.5 ml sample was separately mixed with 1.5 ml of 95 % ethanol, 0.1 ml of 10 % aluminum chloride, 0.1 ml of 1 M potassium acetate, and 2.8 ml of distilled water. The mixture was incubated at room temperature for 30 min, followed by absorbance recording at 415 nm on a Shimadzu UV-160A spectrophotometer (Kyoto, Japan).

176.2.8 Statistical Analysis

Statistical procedures were carried out using the SPSS version 13.0 statistical package for windows (SPSS Inc., Chicago, Illinois). Variations between treatments were evaluated using analysis of variance and means were separated based on least significant difference at 95 % confidence interval.

176.3 Results and Discussion

176.3.1 Selection of Resins

Before passing through ion exchange resins for deacidification, the initial compositions of hawthorn juice were analyzed (Table 176.1). The titratable acidity in respect to citric acid was 17.6 g/l, thus leading to an extreme low pH (2.9); citric acid was the predominant acid (83.5 %) among the tested four main organic acids including oxalic, tartaric, malic, and citric acids.

The physicochemical properties and sensorial analysis are good parameters to discriminate and select the resins. Complementary standard is the retention of useful substance. In the present study, acid elimination and flavonoids retention were both used as criteria. The more efficient resins should be the ones that provide the highest production of deacidified juice and retain the most quantity of flavonoids. After successively passing the column with 15 bed volume (BV), titratable acidity of deacidified juices from each column were analyzed. Result in Fig. 176.1 shows that the concentration of organic acids differed significantly after the treatment. Three weak anion ion exchange resins, i.e., D301G, D301R, and D392 exhibited more capability in deacidifying the juice, with the acid reduction percentage of 35.9, 16.5, and 26.1 % after 15 BV, respectively. Especially D301G, it yielded a total reduction of nearly 80 %. This result was different from that observed in the treated juices using strong basic exchange resins where organic

Table 176.1 Effect of ion exchange treatment on the chemical composition of hawthorn juice

Constituents	Fresh	After one cycle of treatment
Total soluble solids (g/kg)	15.5 ± 0.7	14.5 ± 0.6
Titrable acidity (g citric acid/kg)	17.6 ± 0.8	7.9 ± 0.3
pH	2.9 ± 0.1	4.1 ± 0.2
Total sugars (g/kg)	64.2 ± 3.3	63.3 ± 3.2
Flavonoids (g/kg)	7.2 ± 0.3	3.8 ± 0.1
Potassium (mg/kg)	3595 ± 146	3012 ± 129
Calcium (mg/kg)	2784 ± 113	2133 ± 101
Magnesium (mg/kg)	609 ± 30	505 ± 23
Sodium (mg/kg)	557 ± 22	581 ± 28

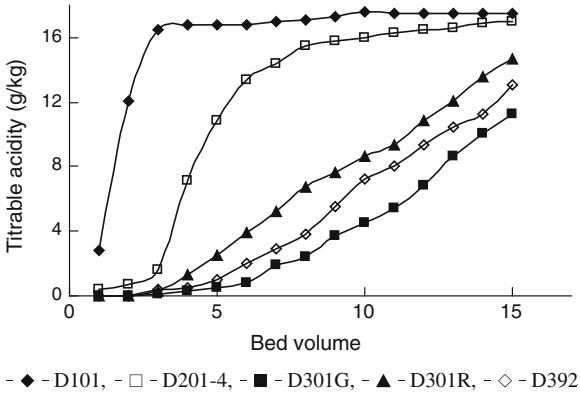

Fig. 176.1 Reduction in titratable acidity of juice after treatment with various resins

acids were removed only during initial bed volumes and increased to near initial levels after 5 bed volumes. D101 completely lose the deacidification capacity only after 3 BVs, and D102 was quickly saturated after 6 BV. In addition, it was reported that weak-base resins requires lower consumption of regeneration reagents for deacidification of juices other than presenting higher ion exchange capacities [11, 12]. Thus, these strong ion exchange resins were excluded from the following investigations. In the meantime, the second criterion for the retention of as much flavonoids as possible is also taken into account. It was found that the concentration of flavonoids after the treatment was quite similar among the processed juice. In particular, flavonoids in the obtained juice from D301G after 15 BV was retained up to 5.81, almost equal to 5.77 and 5.75 g/kg from the column of D392 and D301R, respectively. When experiments were ended after 15 BV, D301R resin was still effective in removing organic acids. Consequently, the most suitable resin for the deacidification of hawthorn juice is D301G.

176.3.2 Optimization of Flow Rate and Temperature During Resin Processing

When the resin was selected, important parameters affecting the acid removal efficiency were studied, i.e., flow rate and temperature. As seen in Fig. 176.2, at the beginning of the treatment, D301G resin adsorbed significant amount of organic acids at both flow rates, thus significantly reducing the titratable acidity of treated juice. However, the acid removal efficiency decreased slowly due to the gradual exhaustion of the adsorption capacity of the resin. At 8 BV, a more decrease of 11 % in acid reduction was observed when a smaller flow rate of 10 BV/h was employed compared to 15 BV/h. The amount of titratable acidity adsorbed decreased significantly toward the end of the processing cycle (22 BV), separate reductions of 3.7 and 1.4 % for 10 BV/h and 15 BV/h in the titratable acidity was achieved. In the determination of flavonoids retained in treated juice,

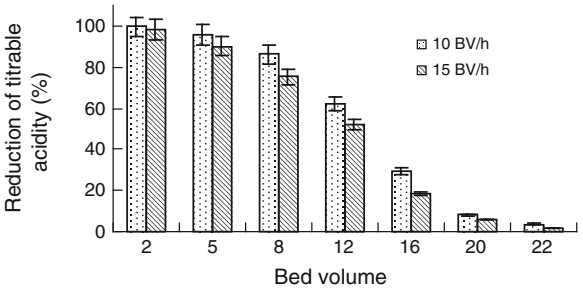

Fig. 176.2 Influence of the flow rate on the reduction of titrable acidity by D301G

an opposite trend was observed. This useful substance was eliminated more when processing at a lower flow rate, but the difference was quite negligible among the three flow rates tested. Therefore, the reduction of flow rate (10 BV/h) is recommendable in the treatment of hawthorn juice, which was in agreement with the conclusion that Vera et al. drew from their studies [8].

The effect of processing temperatures (20, 30, and 40 °C) on the adsorption capacity of resins was also studied. Treatment at a lower temperature (20 and 30 °C) appeared to exclude more acids. Processing at 40 °C was comparatively more easily saturated than that at 20 and 30 °C. However, there was a slight loss of flavonoids as a result of lower temperature, possibly due to treatment at lower temperatures favoring an entire interaction between the flavonoids present in the juice and the functional ligand contained in the resin. Thus, mild temperature (30 °C) was more effective in removing organic acids throughout all bed volumes.

176.3.3 pH, Titratable Acidity, and Total Soluble Solids

After the optimization of operating parameters, a breakthrough curve of D301G resin as a function of the volume of juice expressed in BV was presented in Fig. 176.3. Significant changes in the pH value of treated juice from the column

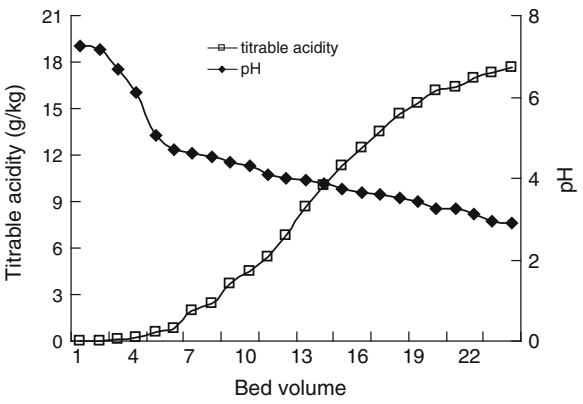

Fig. 176.3 Variations of pH and titrable acidity during the acidification process by D301G

were detected in the early column volumes (first and second BV), reaching a maximum of 7.25, but pH of juices from column decreased gradually and thereafter arrived 3.0 toward the end of the treatment, and the value decreased to its initial level after 23 BV because the resin was saturated. When all juice volume were combined, the final pH reached 4.1.

Figure 176.3 also shows the decline in the titratable acidity as a function of treated juice volume expressed in BV. At pH 4.0, the titratable acidity decreased about 62 % for the juices (12 BV). The reduction in the titratable acidity of treated juice was insignificantly affected toward the end of the processing, due to the exhaustion of the adsorption capacity of the resins. When all column volumes were combined, a total reduction of 55 % was achieved after a full processing cycle.

As for the parameter of total soluble solids, it was expected that this value in high acid juice should decrease along with the removal of acid. In our experiment, it was found that the value decreased significantly at the beginning of the treatment, probably because the resins adsorbed a large amount of organic acids. As the processing continued, total soluble solids in the treated juice remained essentially unchanged. Therefore, our observation was in agreement with the finding from Vera et al. [13] that the amount of total soluble solids was also depending on organic acid concentration.

176.3.4 Deacidification of Hawthorn Juice Using D301G

During the process of deacidification, four organic acids including oxalic, tartaric, malic, and citric acids were quantified by means of HPLC. It was observed that a significant reduction of over 95 % occurred in the concentration of malic acid in the treated juice from first to fifth BV. Tartaric acid content followed the same pattern (>92 %) as malic acid at first and second BV. However, obvious removal of oxalic acid in the treated juice was recorded only by first BV. In the meantime, significant decrease (98 %) took place in the content of citric acid from 1st to 4th BV, and insignificant reduction in the adsorption capacity of resins for citric acid was observed until 13th BV (95 % from 6th to 12th BV). At the end of the processing cycle, the resin was exhausted and acidity was essentially the same as the untreated juice. Based on these observations, it is speculated that citric acid behaved as the elution buffer for all other organic acids during the treatment, and all other organic acids were eluted before citric acid which was strongly absorbed by the resins. When the processing continued, citric acid was finally eluted, and the concentration of which was quite low in the treated hawthorn juice. Based on these results, it was calculated that one L of the resin could remove about 180 g of citric acids.

176.3.5 Retention of Flavonoids, Sugars, and Minerals

One key factor to be considered during the selection of a treatment process for juice is to avoid any losses of nutritional value [3]. As seen in Fig. 176.4, a marked reduction in the content of flavonoids in hawthorn juice from the early column volumes (first–fourth BV) was observed, resulting in a significant decrease of over 95 %. However, the flavonoids concentration of treated juice from the resin column showed a gradual decrease from the fifth BV on, but the loss was still more than 90 %. A marked improvement in flavonoids concentration was detected in the treated juice at seventh BV. Such increase indicated that the resin adsorbed a large amount of flavonoids present in the hawthorn juice and was gradually saturated. Consequently, after processing juice of 19 BV, juice entering column almost had few losses in the content of flavonoids. Thus, the resin maintained its high recovery efficiency on flavonoids throughout the rest processing cycle. When all column volumes were combined, there was a 47 % loss of flavonoids in the treated juice.

The total sugars originally contained in the juice were 64.2 g/kg. As the process continued, the amount of total sugars varied insignificantly, and the values measured at 10 and 20 BV were 65.6 and 64.4 g/kg, respectively. Similar observation was found at other BV, indicating that only small changes occurred in the sugar content. Therefore, the adsorption treatment appeared to have negligible effect on the content of total sugars in the hawthorn juice. Vivekanand et al. has reported similar results for pear juices using weak-base exchange resins [3].

The concentration of ions was analyzed in the deacidified juices until pH 4. Table 176.1 shows the content of the major ions after the resin treatment. The concentration of cations including potassium, magnesium, and calcium ions showed insignificant changes. In the meantime, a slight increase in the sodium concentration was observed in the treated juices. These results suggested little changes occurred in the mineral content after treatment, and insignificant loss took place during the deacidification process.

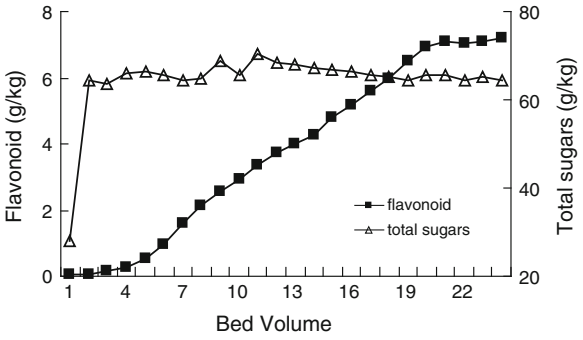

Fig. 176.4 Variations of total sugars and flavonoids during the acidification process by D301G

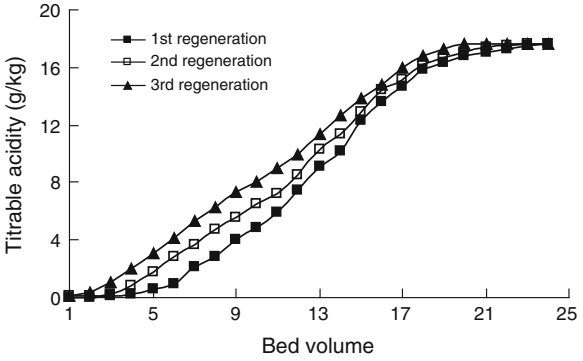

Fig. 176.5 Effect of regeneration on the acid removal capacity of D01G

176.3.6 Regeneration

The function of regeneration is to allow the mobility of resin particles and eliminate air pockets as well as resin fines that may have been formed during the processing cycle [3, 8, 14]. This also helps the redistribution of resins more compactly. Regeneration of resins allows repeated use of same matrix, thus decreasing the cost and improving process efficiency. In the current study, we found after five processing cycles (115 BV), the resin still possess strong capacity to deacidify high acidity juice. Figure 176.5 shows that the titratable acidity and pH of the combined volume from third regeneration was 8.8 g/kg and 3.9, respectively, quite similar to the values obtained from the first processing cycle (7.9 g/kg and 4.1). In addition, flavonoids were insignificantly affected when the resin was repeatedly used. The flavonoids content of the combined volume from 3rd regeneration was 5.1 g/kg, almost 1.4 times higher than that obtained from the first processing cycle. Moreover, from the 6th to 11th processing cycle, the treatment volume was reduced to 19 BV for each cycle, and the combined volume from these cycles reached the same level of acidity as values obtained from the previous five cycles, and simultaneously retained higher amount of flavonoids (5.4 g/kg). In the following treatment (12th–18th regeneration), the processing volume was continued to decrease to 16 BV, and it was found a similar acid removal efficiency (49 %) was attained, and higher levels of condensable flavonoids (6.1 g/kg) was achieved in treated juices at the end of the 19th processing cycle (386 BV). These data proved that resins of D301G can adsorb a large amount of organic acids and retained its deacidification capacity after repeated use.

176.4 Conclusion

The Chinese hawthorn juice contains high content of organic acids which limits its utilization in the formulation of many food products. Thus, a reduction of its acidity can improve the juice quality. In the present study, the removal of organic

acids was accomplished by an IE process using a weak-base ion exchange resin of D301G. Regarding the juice quality, the physicochemical analysis showed that the combined juice from the first processing cycle yielded a titratable acidity, pH and flavonoids concentration of 7.9, 4.1, and 3.8 g/kg under the operating conditions of 30 °C and 10 BV/h. The sugar concentration remained unchanged. In addition, the reduction of acidity led to a slight decrease in the amount of total soluble solids and insignificant influence of cations. These results demonstrate that the IE process is an efficient process to deacidify the Chinese hawthorn juice while retain the amount of flavonoids.

References

1. Kao ES et al (2007) Effects of polyphenols derived from fruit of crataegus pinnatifida on cell transformation, dermal edema and skin tumor formation by phorbol ester application. Food Chem Toxicol 45:1795–1804
2. Bhatia AK, Dang RL, Gaur GS (1979) Deacidification of apple juice by ion exchange resins. Indian Food Pack 33(1):15–20
3. Vivekanand SA, Iyer M (2003) Quality enhancement of UF-clarified pear juice using adsorbent and weakbase resins at different temperatures. J Food Sci 68(1):333–338
4. Couture R, Rouseff R (1992) Debittering and deacidifying sour orange (Citrus-aurantium) juice using neutral and anion-exchange resins. J Food Sci 57(2):380–384
5. Lue SJ, Chiang BH (1989) Deacidification of passion fruit juice by ultrafiltration and ion-exchange processes. Int J Food Sci Tech 24(4):395–401
6. Vibhakar S, Prabhaka JV, Bhatnaga Hc (1966) The clarification and deacidification of grape juice by ion-exchange resins. J Sci Food Agr 17(11):488–496
7. Calle EV et al (2002) Deacidification of the clarified passion fruit juice (P-edulis f. flavicarpa). Desalination 149(1–3):357–361
8. Vera E et al (2003) Comparison between different ion exchange resins for the deacidification of passion fruit juice. J Food Eng 57(2):199–207
9. DuBois M et al (1956) Colorimetric method for determination of sugars and related substances. Anal Chem 28(3):350–356
10. Chang CC et al (2002) Estimation of total flavonoid content in propolis by two complementary colorimetric methods. J Food Drug Anal 10(3):178–182
11. Johnson RL, Chandler BV (1985) Ion exchange and adsorbent resins for removal of acids and bitter principles from citrus juices. J Sci Food Agr 36(6):480–484
12. Johnson RL, Chandler BV (1986) Debittering and de-acidification of fruit juices. Food Technol Aust 38(7):294–297
13. Vera E et al (2007) Deacidification of clarified tropical fruit juices by electrodialysis. Part II. Characteristics of the deacidified juices. J Food Eng 78(4):1439–1445
14. Qu FX et al (2012) Study on the acsorption kinetics of organic acids and total flavonoids in hawthorn fruit juice. Sci Technol Food Ind 33(22):109–112

Chapter 177
Study on the Decolourization Methods of Crude Alkaline Protease

Hongbin Wang, Zhijia Lv, Jing Wang and Fuping Lu

Abstract In order to optimize the decolorization process of crude alkaline protease, the effects of the decolorization methods by active carbon, ultrafiltration, ammonium sulfate salting-out, and ultrafiltration-coupled salting-out were compared. The results showed that the activate carbon method had obvious effect on decolorization, while it could absorb a large number of enzymes and increase the loss of enzyme activity. The ultrafiltration method would cause enzyme denaturation and reduce enzymatic specific activity. The ammonium sulfate method had no influence on enzyme activity, but it had poor effect on decolorization. The ultrafiltration-coupled salting-out not only had little influence on enzyme activity and protein concentration but also had excellent effect of decolorization, the decolorization rate reached 91.99 %, the total activity decreased only 17 %, and the specific activity increased 28 %.

Keywords Decolorization · Alkaline protease · Ultrafiltration-coupled salting-out

177.1 Introduction

In recent years, the use of alkaline proteases as industrial catalysts has increased rapidly [1, 2]. Among all proteases, alkaline proteases are employed primarily as detergent additives. They account for approximately 40 % of the total worldwide enzyme market and this trend is expected to increase in future [3, 4]. There are many different ways to obtain alkaline proteases and the most common way is produced by alkaliphilic microorganisms. Microbial alkaline proteases have several advantages such as high catalytic activity, selectivity, and stability

H. Wang · Z. Lv · J. Wang · F. Lu (✉)
College of Biotechnology, Tianjin University of Science and Technology, Tianjin 300457, People's Republic of China
e-mail: lfp@tust.edu.cn

T.-C. Zhang et al. (eds.), *Proceedings of the 2012 International Conference on Applied Biotechnology (ICAB 2012)*, Lecture Notes in Electrical Engineering 251,
DOI: 10.1007/978-3-642-37925-3_177,

characteristics [5, 6]. However, there are lots of pigments in fermentation broth and the pigments increase the difficulty of separation and purification of alkaline proteases. Therefore, crude alkaline protease should be decolorized before purification [7, 8].

There are several methods for decolorization, such as active carbon absorption [9, 10], ammonium sulfate salting-out [11] and ultrafiltration [12, 13] method. Active carbon can absorb pigments efficiently and rapidly, but it can also absorb a large number of enzymes and increase the loss of enzyme activity. Ultrafiltration can isolate small-molecular pigments from fermentation broth efficiently and have obvious discolored effect. However, ultrafiltration may cause protein denaturation due to high shear and reduce enzymatic specific activity. Ammonium sulfate salting-out is the commonly used method for purification of protein [14], with high solubility and little effect on protein denaturation, but it has poor effect on decolorization [15]. In this paper, we combined ammonium sulfate salting-out and ultrafiltration method together for the decolorization of crude enzyme solutions containing alkaline proteases, which not only achieved obvious effect of decolorization but also reduced the loss of enzyme activity.

177.2 Materials and Methods

177.2.1 Materials

Crude alkaline proteases and active carbon ZX303 were purchased from Noao Sci & Tech Development Co., Ltd (Tianjin, China), tubular ultrafiltration membrane (MWCO 10 kD) was purchased from Motimo Tech Co.,Ltd (Tianjin, China). All other reagents were analytical grade.

177.2.2 Analysis Methods

177.2.2.1 Enzyme Activity Determination

Alkaline protease activity was determined by the modified method of Anson [16] using casein as the substrate dissolved in 50 mM borate buffer (pH 10.0). The proteolytic reaction was carried out at 0 °C for 20 min, and stopped with 10 % trichloroacetic acid. The mixture was kept at 0 °C for 10 min and centrifuged at 12,000 rpm for 2 min. To 1.0 mL supernatant 5.0 mL 0.5 M Na_2CO_3 solution and 1.0 mL threefold-diluted Folin–Ciocalteau reagent were added. After the reaction mixture had maintained for 20 min at 0 °C, the absorbance was measured at 680 nm.

177.2.2.2 Protein Concentration Determination

Protein concentration was determined by the method of Bradford [17]. Protein solution (0.1 mL) was pipetted into 12 × 100 mm test tubes. 1.0 mL coomassie brilliant blue G-250 reagent was added to the test tube and the contents mixed either by inversion or vortexing. The absorbance at 595 nm was measured after 2 min in 1 mL cuvettes against a reagent blank prepared from 0.1 mL of buffer and 1.0 mL of G-250 reagent.

177.2.2.3 Decolorization Rate Determination

The decolorization rate was determined using UV spectrophotometer (TU—1810) at 420 nm, which is the wavelength of maximum absorbance of alkaline protease solution. Decolorization rate has been evaluated using following Eq. (1).

$$\text{Decolorization } \% = [(\text{Initial absorbance} - \text{Observed absorbance})/\text{Initial absorbance}] \times 100 \quad (1)$$

The samples were centrifuged at 5,000 rpm for 15 min by using a centrifuge (CR−GIII).

177.2.2.4 Molecular-Weight Distribution Determination

The molecular weight distribution was determined by the method of Hiroaki Komatsu using high-performance gel permeation chromatography (HPGPC) [18].

177.2.3 Decolorization Methods

177.2.3.1 Preparation of Enzyme Solution

Crude alkaline protease (10 g) was dissolved in distilled water (100 mL), and the solution was kept at 0 °C and centrifuged at 5,000 rpm for 30 min. The decolorization of supernatant was kept at 0 °C and in natural pH.

177.2.3.2 Decolorization by Active Carbon

The crude enzyme solution (100 mL) was mixed with active carbon ZX303 at the concentration of 4 % (w/v) and stirred with a mechanical stirrer for 30 min. The mixture was centrifuged at 10,000 rpm for 10 min. All of the above operations were done at 0 °C and in natural pH.

177.2.3.3 Decolorization by Ultrafiltration

The crude enzyme solution (15 mL) was pipetted into 10 × 500 mm tubular ultrafiltration membrane at 0 °C and centrifuged at 10,000 rpm for 60 min. Distilled water was added to maintain the volume of enzyme solution. This experiment should be repeated twice.

177.2.3.4 Decolorization by Ammonium Sulfate Salting-Out

Crude enzyme solution (50 mL) was added solid ammonium sulfate (0–80 % saturation). The precipitate was discarded, and determinate the enzyme activity of the supernatant. According to the relationship between ammonium sulfate saturation and enzyme activity, the crude enzyme solution (50 mL) was fractionated with ammonium sulfate at 40 % saturation and the supernatant was fractionated with ammonium sulfate at 60 % saturation.

177.2.3.5 Decolorization by Ultrafiltration-Coupled Salting-Out

Crude enzyme solution (50 mL) was added to solid ammonium sulfate (40 % saturation), with stirring, over a 60-min period. The mixture was centrifuged at 10,000 rpm for 20 min. The precipitate was dissolved by distilled water (50 mL) and added solid ammonium sulfate (60 % saturation). Centrifuged at 10,000 rpm for 20 min and the supernatant was pipetted into 10 × 500 mm tubular ultrafiltration membrane. The mixture was centrifuged at 10,000 rpm for 60 min. All of the above operations were done at 0 °C.

177.3 Results and Discussion

177.3.1 Effect of Active Carbon

The effect of active carbon on decolorization was presented in Table 177.1. After treated by active carbon, the color of the enzyme solution changed obviously and the decolorization rate reached 76.65 %. However, the enzyme activity lost 58 % and the protein concentration lost 41.6 %. The result indicated that active carbon could absorb pigments efficiently, but it could also absorb alkaline protease and increase the loss of enzyme activity.

177.3.2 Effect of Ultrafiltration

Figures 177.1 and 177.2 showed the molecular weight distribution before and after ultrafiltration. Because of the principle of molecular sieve, the protein eluted at

Table 177.1 Effects of decolorization of the crude enzyme

Methods	Enzyme activity (U)	Protein concentration (mg)	Enzymatic specific activity (U/mg)	Decolorization rate (%)	Activity recovery (%)
Crude enzyme	41284.42	84.72	498.04	–	100
Active carbon	17373.33	49.47	351.12	76.65	42.08
Ultrafiltration	22071.35	71.64	308.25	60.84	53.46
Ammonium sulfate salting-out	40980.82	60.70	675.14	43.43	99.26
Ultrafiltration-coupled salting-out	33885.28	52.80	641.76	91.99	82.08

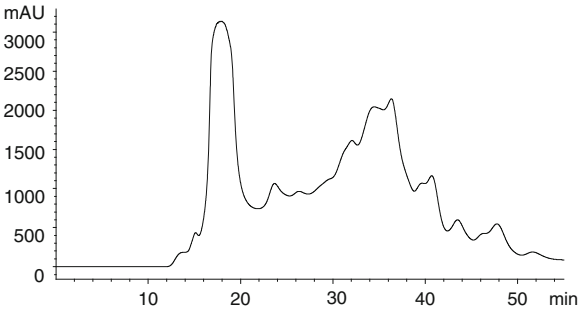

Fig. 177.1 Molecular weight distribution of the crude enzyme solution determined by HPGPC method

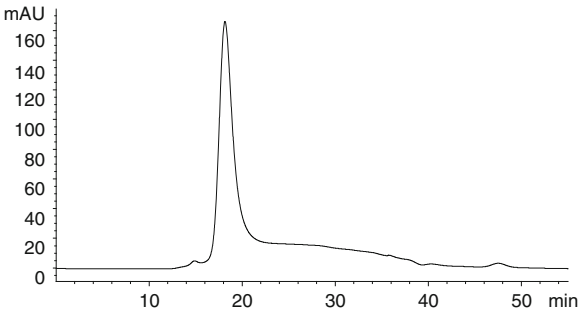

Fig. 177.2 Molecular weight distribution of the enzyme solution after ultrafiltration determined by HPGPC method

short retention time and the pigment eluted at long retention time. The result showed that a large number of pigments were isolated by ultrafiltration. Table 177.1 showed the effect of ultrafiltration. Decolorization rate reached 60.48 %, the enzyme activity lost 47 % and the protein concentration lost 38 %. This showed that the effect of ultrafiltration was not ideal.

177.3.3 Effect of Ammonium Sulfate Salting-Out

Figure 177.3 showed the relative activity of supernatant and precipitate at different gradient of ammonium sulfate (0–80 %). The change of relative activity of

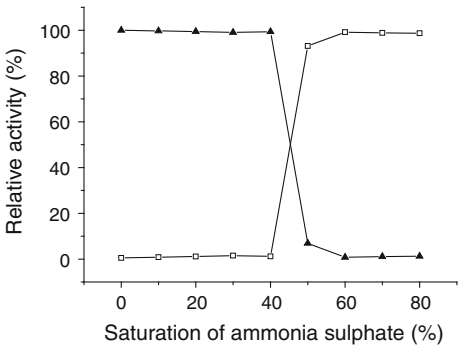

Fig. 177.3 Enzyme activity grads curve. ▲- the relative activity of supernatant, □- the relative activity of precipitate

supernatant was not obvious until the gradient reached 40 %. When the gradient reached 60 % there was no relative activity in supernatant. Therefore, hybrid protein could be precipitated by ammonium sulfate (40 % saturation) and alkaline protease could be separated by ammonium sulfate (60 % saturation). Table 177.1 showed the effect of ammonium sulfate salting-out, and the change of enzyme activity was not obvious and the enzymatic specific activity increased 35 %. This demonstrated that ammonium sulfate had no influence on enzyme activity. However, the ammonium sulfate salting-out had no significant effect on decolorization and the decolorization rate only reached 43 %.

177.3.4 Effect of Ultrafiltration-Coupled Salting-Out

The effect of ultrafiltration-coupled salting-out on decolorization was presented in Table 177.1. After treated by ultrafiltration-coupled salting-out, the color of the enzyme solution changed obviously and the decolorization rate reached 91.99 %, which was much more than 76.65 % obtained by active carbon. Meanwhile, the enzyme activity lost only 17 % and the enzymatic specific activity increased 28 %. The result indicates that the ultrafiltration-coupled salting-out method not only had little influence on enzyme activity and protein concentration but also had excellent effect of decolorization.

177.4 Conclusion

Active carbon has been widely used for decolorization of enzyme because of its well known high adsorptive power. However, the discolored effect of active carbon was limited because the enzyme activity loss depended on the concentration of active carbon and the action time with the absorbent [19, 20]. In this study, decolorization rate and the enzyme activity was used as monitoring indexes to

evaluate the discolored effect of crude alkaline proteases by active carbon absorption, ammonium sulfate salting-out, ultrafiltration, and ultrafiltration-coupled salting-out methods. The results showed that the discolored effect of ultrafiltration-coupled salting-out method was most obvious and the decolorization rate reached 91.99 %. On the other hand, ultrafiltration-coupled salting-out method had little effect on enzyme activity. Through the ultrafiltration-coupled salting-out method, the enzyme activity lost only 17 % and the enzymatic specific activity increased 28 %. In conclusion, the ultrafiltration-coupled salting-out method, which not only achieved obvious effect of decolorization but also reduced the loss of enzyme activity, was an ideal method for decolorization.

Acknowledgments This work was supported by the National High Technology Research and Development Program ('863' Plan) (2013AA102106 and 2011AA100905-4), the the Program for Changjiang Scholars and Innovative Research Team in University (IRT1166), and the National Natural Science Fund (31101219).

References

1. Anwar A, Saleemuddin M (1998) Alkaline proteases: a review. Bioresource Technol 64:175–183
2. Ellaiah P, Srinivasulu B, Adinarayana K (2002) A review on microbial alkaline proteases. J Sci Ind Res India 61:690–704
3. Prakasham RS, Rao CS, Sarma PN (2006) Green gram husk—an inexpensive substrate for alkaline protease production by *Bacillus sp* in solid-state fermentation. Bioresource Technol 97:1449–1454
4. Rao MB, Tanksale AM, Ghatge MS et al (1998) Molecular and biotechnological aspects of microbial proteases. Microbiol Mol Biol R 62:597–635
5. Gupta R, Beg QK, Lorenz P (2002) Bacterial alkaline proteases: molecular approaches and industrial applications. Appl Microbiol Biotechnol 59:15–32
6. Gupta R, Beg QK, Khan S et al (2002) An overview on fermentation, downstream processing and properties of microbial alkaline proteases. Appl Microbiol Biotechnol 60:381–395
7. Koo KB, Joo HS, Choi JW (2011) Decolorization method of crude alkaline protease preparation produced from an alkalophilic *Bacillus clausii*. Biotechnol Bioproc E 16:89–96
8. Kumar CG, Takagi H (1999) Microbial alkaline proteases: from a bioindustrial viewpoint. Biotechnol Adv 17:561–594
9. Shen ZM, Wang WH, Jia JP et al (2001) Degradation of dye solution by an activated carbon fiber electrode electrolysis system. J Hazard Mater 84:107–116
10. Lopez F, Medina F, Prodanov M et al (2003) Oxidation of activated carbon: application to vinegar decolorization. J Colloid Interf Sci 257:173–178
11. King TP (1972) Separation of proteins by ammonium sulfate gradient solubilization. Biochem 11:367–371
12. Hamachi M, Gupta BB, Ben Aim R (2003) Ultrafiltration: a means for decolorization of cane sugar solution. Sep Purif Technol 30:229–239
13. Simonic M (2009) Efficiency of ultrafiltration for the pre-treatment of dye-bath effluents. Desalination 245:701–707
14. Dennison C, Lovrien R (1997) Three phase partitioning: concentration and purification of proteins. Protein Expres Purif 11:149–161

15. Foster PR, Dunnill P, Lilly MD (1976) The kinetics of protein salting-out: precipitation of yeast enzymes by ammonium sulfate. Biotechnol Bioeng 18:545–580
16. Anson ML (1938) The estimation of pepsin, trypsin, papain, and cathepsin with hemoglobin. J Gen Physiol 22:79–89
17. Bradford MM (1976) A rapid and sensitive method for the quantitation of microgram quantities of protein utilizing the principle of protein-dye binding. Anal Biochem 72:248–254
18. Komatsu H, Takahata T, Tanaka M (1993) Determination of the molecular-weight distribution of low-molecular-weight heparins using high-performance gel permeation chromatography. Biol Pharm Bull 16:1189–1193
19. Kumar CG, Parrack P (2003) Activated charcoal: a versatile decolorization agent for the recovery and purification of alkaline protease. World J Microb Biotechnol 19:243–246
20. Aikat K, Bhattacharyya BC (2001) Regeneration of activated charcoal used in decolorization and purification of crude protease from *Rhizopus oryzae*. Biotechnol Lett 23:1915–1919

Chapter 178
Research Progress of the Polysaccharide O-Acetylated Pustulan-Type Glucans from *Umbilicariaceae lichens*

Junjie Sun, Xinli Wei and Jiangchun Wei

Abstract Polysaccharides from lichens have been studied for many years. The polysaccharide O-acetylated pustulan-type glucans have been found and reported in 56 species of Umbilicariaceae, such as *Umbilicaria angulata*, *U. caroliniana*, *U. Esculenta*, *U. hirsuta*, *U. polyphylla*, and *Lasallia papulosa* etc. All the polysaccharide obtained from the lichens showed a remarkable antitumour effect especially the O-acetylated pustulan-type glucans. The authors also give a prospect of the feasibility of research and development for such a polysaccharide from lichens.

Keywords *U. esculenta* · Structure · Antitumor activity · Bioactivities · Lichen-fungi

178.1 Introduction

Polysaccharides in lichens include lichenin, isolichenin, and pustulan [1]. Lichenin is a linear polymer united by the β-D-glucose combining with 1, 3 or 1, 4 glycosidic bonds, the molecular weight of which is ranging in $2 \times 10^4 - 6.2 \times 10^4$. The optical rotation is generally positive and relatively low [2–4]. Isolichenin is also a kind of linear polymer united by α-D-glucose combining with residues 1, 3

J. Sun · X. Wei (✉) · J. Wei (✉)
State Key Laboratory of Mycology, Institute of Microbiology, Chinese Academy of Sciences, Beijing 300457, People's Republic of China
e-mail: weixl@im.ac.cn

J. Wei
e-mail: weijc2004@126.com

J. Sun · J. Wei
College of Life Science, Shandong Agricultural University, Taian 271018, People's Republic of China

T.-C. Zhang et al. (eds.), *Proceedings of the 2012 International Conference on Applied Biotechnology (ICAB 2012)*, Lecture Notes in Electrical Engineering 251,
DOI: 10.1007/978-3-642-37925-3_178,

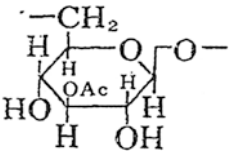

Fig. 178.1 The structure of β-1, 6 acetylated unit of pustulan [7]

or 1, 4 glycosidic bonds, which is first discovered in the lichens, its molecular weight is about 6×10^3 to 8×10^3, and its rotation is dextral [3, 5]. The pustulan is a kind of D-glucan, bonded by β-1, 6 glycosidic bonds, which is extracted from the *Umbilicariaceae lichens*. Each per number (about 10–15) of dextran monomers contains a monomer acetylated in the position C3 or C4 (Fig. 178.1) [6, 7]. Pustulan forms a gel in water, a property directly related to the degree of acetylation, and the level of acetylation is influenced by lichen species and the conditions under which the lichen has been stored [8].

178.2 Researches on Pustulan

Up to now, the polysaccharide O-acetylated pustulan-type glucans have been found and reported in 56 species of Umbilicariaceae, 47 of *Umbilicaria* and nine of *Lasallia*, apparently constant in the family [8]. The researches on the pustulan mainly focused on these two aspects: structure and bioactivities.

178.2.1 Researches on the Structure of Pustulan

It is for the first time that pustulan had been extracted from *Umbilicaria pustulata* (L.) Hoffm and *U. hirsuta* (Sw.) ACH. by Drake in 1943. He gave a speculation on the structure of pustulan that it was a kind of glucan combined with β-1, 6 glycosidic bonds [9]. The speculation was proved to be right by Lindberg and MacPherson until 1954 [10]. They confirmed that the pustulan indeed was glucan with β-1, 6 glycosidic bonds by the hydrolysis products of pustulan which are glucose, gentiobiose, and some kind of low molecular sugars and by the methods of degrading the fully methylated pustulan [11].

According to the results of Shibata's researches, pustulan has been found characteristically in the lichens of *Umbilicaria esculenta* (Miyoshi) Minks, *U. angulata* Tuck, *U. caroliniana* Tuck, *U. polyphylla* (L.) Baumg, and *Lasallia papulosa* (Ach.) Llano. It has also been shown that pustulan contains 2 % of O-acetyl groups which are characterized by their absorption at 1,735 and 1,250 cm^{-1} and removed by alkaline hydrolysis with 2 % aq. Na_2CO_3 at room temperature. The acetyl contents in pustulan were determined by gas chromatography after hydrosis, revealing 1 acetyl group for every 10–12 glucose units [1]. By the method of Bouveng [12], the

native polysaccharide swollen in dimethyl-formamide was treated with phenylisocynate to form a phenyl carbamate which was methylated by Kuhn's method and treated with $LiAIH_4$ to give a partially methylated glucan. The methyl ether in the 3-position of D-glucose was obtained by the hydrolysis of the partially methylated glucan to indicate, the acetyl group is attached to the 3-hydroxyl [12]. The molecular weight of pustulan has been determined by the equilibrium sedimentation method to be C.2000 (DP c.120) [13].

Shi isolated two kinds of water-soluble polysaccharides UV-2, UV-3 from *Umbilicaria vellea* (L.) Ach. in 1994. The results of the structure analysis proved that those polysaccharides were heteropolysaccharides with partially acetylated groups and multiple branches [14].

178.2.2 Researches on the Bioactivities of Pustulan

The scholars began to study the bioactivities of the pustulan since 1940s. The Japanese scholars are the pioneers. Shibata extracted a kind of β-1,6-glucan with partially acetylated groups from *U. esculenta* and *L. papulosa* and named the polysaccharide GE-3. The GE-3 has significant antitumor activity in vivo which is higher than those polysaccharides without acetylated [7, 15–19]. That β-1,6-D-glucan can inhibit the expression of HIV antigen on the Molt-4 (clone 8) cells remarkably, therefore it can inhibit the HIV virus. When some C3 positions of GE-3 get acetylated and then sulfated by $ClS0_3H$, the polysaccharides change into the sulfate derivatives GE-3-S which are inhibitors of HIV [20].

The domestic researches on pustulan started relatively later. In 1994, Shi isolated two kinds of water-soluble polysaccharides UV-2, UV-3. The results of pharmacological experiments on the UV-2 and UV-3 showed that the UV-2 has the function of strengthening the immune system and enhancing the phagocytic ability of peritoneal macrophage [14].

The Korean scholars also did similar researches on the extracts and polysaccharides from *U. esculenta* in recent years [21–23]. They found that the extracts from *U. esculenta* have the inhibitive ability to the thrombosis, glycosidases, and the formation of melanin. Kim used methanol to extract substances from *U. esculenta* and named it methanol extracts. He conducted the experiments of methanolic extract on platelet aggregation in vitro and pulmonary thrombosis in vivo. The extract showed concentration depending inhibitory effects on platelet aggregation induced by ADP, with IC_{50} value of 2.4 mg/mL. On the other hand, the extract did not show any fibrinolytic activity and alter coagulation parameters such as activated partial thromboplastin time (APTT), prothrombin time (PT), and thrombin time (TT) in rat platelet. These results suggested that the antithrombotic activity of *U. esculenta* extracts might be due to antiplatelet activity rather than anticoagulation activity [23]. The extracts also showed to reduce melanin formation in human melanoma cells which evidenced melanogenesis inhibitory effects via multiple routes [22]. Lee detected inhibitory activity of the extracts

from *U. esculenta* toward β-glucosidase. The extracts showed strong inhibition of disaccharide hydrolytic enzymes of mold and mammalian origin, but weak or no inhibition of polysaccharide hydrolytic enzymes except glucoamylase and laminarinase. Purified inhibitor was identified as 1-deoxynojirimycin (1, 5-dideoxy-1, 5-immino-D-glucitol) by NMR spectrometry. The purified inhibitor was identified as 1-deoxynojirimycin (1, 5-dideoxy-1, 5-immino-D-glucitol) by NMR spectrometry [23].

Kim evaluated the phenotype and functional maturation of dendritic cells (DCs) following treatment of extracted glucan (PUE) by flow cytometric analysis and cytokine production. As a mechanism of action, PUE increased phosphorylation of ERK, JNK, and p38 MAPKs, and enhanced nuclear translocation of NF-κB p50/p65 in DCs. The results indicate that PUE induced DC maturation via MAPK and NF-κB signaling pathways [24]. Indeed, the basic mechanism of the immunostimulatory, antitumor, antiinfection, and other therapeutic effects of glucans is thought to occur via the modulation of innate immunity including macrophage and dendritic cell (DC) function [25].

178.3 The Outlook and Prospect of Pustulan

The researches on the pustulan progressed slowly. One factor that contributes to the slow progress is the relatively slow growth of lichens in nature and the difficulty of artificial cultivation, the massive production, and industrialized application process of pustulan is yet to be developed. Study shows that most of lichen polysaccharides were produced by the mycobionts, and polysaccharides of photobionts gave a different character in comparison with those of intact lichens [1]. Therefore, it is the best way using the mycobionts to conduct the massive liquid culture and further fermentation for exploiting the industrial applications of the pustulan.

There also exist some other problems. The pretreatments and the solvents used for extraction might eventually affect the final structure of pustulan and other polysaccharides. For instance, methanol, which has commonly been used as one of the extraction solvents for removing lipids and coloring matter, might cause loss in the possible acetyl contents due to transesterification [6]. Consequently, how to pretreat and select the solvent for extraction is an important issue for the study of pustulan. Besides, the mechanism of the pustulan's antitumor activity is not very clear and the pharmacological mechanism still needs to be studied.

Most researches focus on the β-glucan, to which the most of bioactivities of the polysaccharides are related, while the pustulan from *Umbilicariaceae lichens* is β-glucan. Being as a kind of significant active lichen natural products, pustulan has remarkable antitumor activity with little toxic side effects and its sulfide derivatives having anti-HIV activity. Therefore, the research on the pustulan will be a hotspot in the lichen bioactivity researches. In order to well study the bioactivities of pustulan and clarify the pharmacological mechanism of the antitumor and

anti-HIV activity, etc., it would be very important to obtain plenty of artificial cultures of lichen-forming fungi. The research on the massive industrial production will broaden the prospect of the application of pustulan as drugs and health products.

References

1. Shibata S (1973) Polysaccharides of lichens. J Natl Sci Counc Sir Lanka 1:183–188
2. Berit SP, Elin SO, Kristin I (2002) Chromatography and electrophoresis in separation and characterization of polysaccharides from lichens. J Chromatogr A 967:163–171
3. Olafsdottir ES, IngoIfsdottir K (2001) Polysaccharides from lichens: structural characteristics and biological activity. Planta Med 3:199–208
4. Pang MF, Wang QL, Hu ZH (2011) Advances in studies on chemical constituents from lichen and their pharmacological effects. Chin Tradit Herbal Drugs 12:2571–2576
5. Zhang P, Fan SJ (2007) Review of the antibiotic from lichens and lichenan. Shandong Sci 2:41–44
6. KjØlberg O, Kvernheim AL (1984) Studies on the polysaccharides of lichens. II. The structure of water-soluble polysaccharides in *Umbilicaria pustulata* (L.) Hoffm. and *Umbilicaria spodochroa* (Ach.) Hoffm. Acta Chem Scand B 38:735–739
7. Nishikawa Y, Takeda T, Shibata S et al (1969) Polysaccharide of lichens and fungi.III. Further investigation on the structures and the antitumor activity of the polysaccharides from *Gyrophora esculenta* Miyoshi and *Lasallia papulosa* Llano. Chem Pharm Bull 9:1910–1916
8. Narui T, Sawada K, Culberson CF et al (1999) Pustulan-type polysaccharides as a constant character of the Umbilicariaceae (Lichenized Ascomycotina). The Bryologist 102:80–85
9. Drake B (1943) Biochem Z 313:388
10. Lindberg B, MacPherson J (1954) Acta Chem Scand 8:985
11. Hellerqviet CG, Lindberg B, Samuelson K (1968) Methylation analysis of Pustulan. Acta Chem Scand 22:2736
12. Bouveng HO (1961) Phenylisocyanate derivative of carbohydrates. Acta Chem Scand 15:96
13. Yphantis DA (1964) Biochem 3:297
14. Shi WY, Shang LJ, He W et al (1994) Isolation, purification and characterization of polysaccharies UV-2 and UV-3 from *Umbilicaria Vellea*. Acta Bota Sini 3:233–238
15. Huang J (2008) Study on extraction, isolation, structure analysis and radiation protection activity of polysaccharides from *Parmelia tinctorium*. Peking Union Medical College
16. Shibata S, Nishikawa Y, Takeda T et al (1968) Polysaccharide of lichens and fungi I. Antitumour active polysaccharide of *Gyrophora esculenta* Miyoshi and *Lasallia papulosa* (Ach. Llano). Chem Pharm Bull 12:2362–2369
17. Takeda T, Funatsu M, Shibata S et al (1972) Polysaccharides of lichens and fungi V. Antititumour active polysaccharides of lichens of *Evemia*. Chem Pharm Bull 11:2445–2449
18. Fukuoka F, Nakanishi M, Shibata S et al (1968) Polysaccharide of lichens and fungi. II. Antitumor activities on sarcoma-180 of the polysaccharide preparations from *Gyrophora esculenta* Miyoshi, *Cetraria Islandica* (L.) Ach. Var. Orientalis Asahina, and some other lichens. Gann 59:421
19. Nishikawa Y, Tanaka M, Shibata S et al (1970) Polysaccharide of lichens and fungi. IV. Antitumour active O-acetylated Pustulan-type glucans from the lichens of *Umbilicaria* species. Chem Pharm Bull 7:1431–1434
20. Hirabayashi K, Iwata S, Ito M et al (1989) Inhibitory effect of a Lichen polysaccharide sulfate, GE-3-S, on the replication of human immunodeficiency virus (HIV) in vitro. Chem Pharm Bull 9:2410

21. Kim MS, Lee KA (2006) Antithrombotic activity of Methanolic Extract of *Umbilicaria esculenta*. J Ethnopharmacol 105:342–345
22. Kim MS, Cho HB (2007) Melanogenesis inhibitory effects of methanolic extracts of *Umbilicaria esculenta* and *Usnea longissima*. J Microbiol 45:578–582
23. Lee KA, Kim MS (2000) Glucosidase inhibitor from *Umbilicaria esculenta*. Can J Microbiol 46:1077–1081
24. Hyung SK, Kim JY, Lee HK et al (2010) Dendritic cell activation by glucan isolated from *Umbilicaria Esculenta*. Immun Net 6:188–197
25. Schepetkin IA, Quinn MT (2006) Botanical polysaccharides: macrophage immunomodulation and therapeutic potential. Int Immunopharmacol 6:317–333

Chapter 179
Effects of UV-B Radiation and NaCl Stress on the Protein Expression in *Nostoc flagelliforme*

Lei Yang, Haifeng Yu and Hongxian Lv

Abstract To establish an efficient SDS-PAGE system to separate proteins of *Nostoc flagelliforme* cells, the protein extraction, sample volume, and other conditions were modified. The results showed that total proteins were extracted by using acetone as precipitator, the most appropriate sample volume was 30–45 μg, concentration of resolving gel was 12 %, when the protein moved to the resolving gel, the current was changed to 20 mA, With Coomassie brilliant blue staining, 13 clear protein bands appeared in SDS-PAGE gel. UV-B radiation affected the conformation of *Nostoc flagelliforme* proteins (33, 114, and 130 kDa protein), and salt stress induced 117 and 130 kDa protein, showing these proteins were important factors for the adaption to the corresponding adverse environment.

Keywords NaCl stress · *Nostoc flagelliforme* cells · SDS-PAGE · The protein extraction · UV-B

179.1 Introduction

Nostoc flagelliforme is a kind of terrestrial cyanobacterium which is edible and thrives in arid or semiarid areas [1]. Because of its living environment, *Nostoc flagelliforme* is often exposed to high solar radiation and high salt stress in their natural habitats [2]. It is so sensitive to environment that it's physiological and biochemical characteristics change in different habitats, which further leads to the change in the proteome of *Nostoc flagelliforme* cells. In recent years, researchers have paid more and more attention on the characteristics and physiological regulation ability under extreme environment [3–7]. It is an important aspect to

L. Yang · H. Yu (✉) · H. Lv
School of Food and Bioengineering, Shandong Polytechnic University, Jinan 250353, People's Republic of China
e-mail: yhf0831@yahoo.com.cn

T.-C. Zhang et al. (eds.), *Proceedings of the 2012 International Conference on Applied Biotechnology (ICAB 2012)*, Lecture Notes in Electrical Engineering 251,
DOI: 10.1007/978-3-642-37925-3_179,

explore the *Nostoc flagelliforme* protein and its gene expression differences in the protein level for the adversity adaption, which is related to the in-depth study of response mechanisms. However, there is little study on the mechanism of the *Nostoc flagelliforme* cells stress response in the proteome level.

SDS-PAGE is one of the most commonly used methods for protein detection. It is not only used to determine the relative molecular mass of proteins, but also for the separation and purification of proteins. At present, the method has been applied in analysis of proteins in salina, green Dunaliella algae, and other algae which could form specific proteins in the resilience environment [8, 9].

This work aimed to develop an efficient SDS-PAGE method for analyzing the total protein of Nostoc flagelliforme cells and exploring the response of *Nostoc flagelliforme* under UV radiation and salt stress at the protein level with the SDS-PAGE of conditions which has been developed.

179.2 Materials and Methods

179.2.1 Materials

The *Nostoc flagelliforme* was collected in the eastern side of the Helan Mountain in Yinchuan, Ningxia, China, in 2010, and had stored in dry conditions at room temperature for 26 months before getting used in experiments. Isolated and axenic cells were obtained according to previous methods [10]. Axenic cells were screened and cultured in BG-11_0 (free of nitrogen) medium. The cells were cultured in BG-11 medium in 500 mL shake-flask containing 200 mL medium at 25 °C under continuous illumination of 60 μmol photon $m^{-2}s^{-1}$ and were grown to its late growth phase as inoculums.

179.2.2 UV Treatment and NaCl Treatment

50 mL homogenized suspension of *Nostoc flagelliforme* cells from their exponential growth phase was used and irradiated under UV-B, using UV light meters to measure the UV irradiance. The culture suspension was placed in glass Petri dishes of 90 mm diameter over a magnetic stirrer and irradiated for 24 h.

Homogenized suspension of *Nostoc flagelliforme* cells from their exponential growth phase were cultured in BG-11_0 medium with NaCl at an initial concentration of 0.8 mol L^{-1} for 24 h in 500 mL shake-flask containing 200 mL medium at 25 °C under continuous illumination of 60 μmol photon $m^{-2}s^{-1}$.

Cultures maintained under continuous illumination of 60 μmol photon m^{-2} s^{-1} light intensity provided from fluorescent tubes were always treated as control.

179.2.3 Protein Extraction Methods

Direct extraction method: 30 mL homogenized suspension of *Nostoc flagelliforme* cells from their exponential growth phase was used and directly dissolved in 2 mL of cracking buffer [100 mg of sodium dodecyl sulfate (SDS), 0.1 mL of mercaptoethanol, 1.0 mL of glycerol, 2 mg of bromophenol blue, 2 mL of Tris–HCl buffer (0.05 mol L^{-1} pH 8.0)], grinded, centrifuged, and the supernatants were collected.

Acetone method: 30 mL of homogenized suspension of *Nostoc flagelliforme* cells from their exponential growth phase was used and suspended in 2 mL of phosphate buffer (0.05 mol L^{-1} pH = 7). After being grinded, processed suspension was kept to stand for 1 h, centrifuged at 5,000 rpm for 15 min and the supernatants were collected. The supernatants were placed at 4 °C for 4 h after the addition of 5 mL of precooling acetone, and then centrifuged at 5,000 rpm for 15 min. The precipitation was heated in boiling water bath for 3 min after the addition of 150 μL of cracking buffer, then centrifuged at 5,000 rpm for 15 min and then the supernatants were collected [11].

Trichloroacetic acid (TCA)-acetone method: 30 mL of homogenized suspension of *Nostoc flagelliforme* cells from their exponential growth phase was used and suspended in 2 mL of phosphate buffer (0.05 mol L^{-1} pH = 7), grinded broken, processed standing for 1 h, centrifuged at 5,000 rpm for 15 min, and the supernatants were collected. The supernatants were placed at 4 °C for 2 h after the addition of 5 mL of TCA, and then centrifuged at 5,000 rpm for 15 min. The precipitation was washed with acetone. The precipitation was heated in boiling water bath for 3 min after the addition of 150 μL of cracking buffer, then centrifuged at 5,000 rpm for 15 min and the supernatants were collected [12].

179.2.4 Protein Extraction Methods

The quantitative analysis of protein referred to the Bradford method [13].

179.2.5 Preparation of the Gel

The reagents: the Acr/Bis (30.0 g acrylamide, 0.8 g bis-acrylamide dissolved in 100 mL of distilled water); stacking gel buffer [5.98 g Tris dissolved in 48 mL of HCl (1 mol L^{-1}), and compensated to 100 mL with distilled water, pH = 6.7]; the resolving gel buffer (36.3 g Tris dissolved in 48 mL of HCl(1 mol L^{-1}), and compensated to 100 mL with distilled water, pH = 8.9); 10 % (w/v) SDS; 1 % (v/v) tetramethylethylenediamine (TEMED) solution; 10 % (m/v) ammonium persulfate solution.

10 % resolving gel [14], 12 % resolving gel [15], and 3 % stacking gel were prepared.

179.2.6 SDS-Page

Both electrophoresis tank (DYCZ-24D) and electrophoresis apparatus (DYY-8B) were purchased from Beijing Liuyi Instrument Limited Company. The staining was coomassie brilliant blue G-250 (0.1 % (w/v)) and the destaining solutions were methanol (10 % (v/v)) and acetic acid (10 % (v/v)).

Photograph of the gel was analyzed using 1D analysis software.

179.3 Results and Discussion

179.3.1 Comparison of Different Protein Extraction Methods

As shown in Fig. 179.1, the direct extraction method could get a higher protein content compared by the acetone method and the TCA-acetone method. However, the protein got by the direct extraction method could not be effectively separated by SDS-PAGE (Fig. 179.2). There are 7 and 11 protein bands were found in TCA-acetone extraction method and acetone method, respectively, so the direct extraction method was not suitable for SDS-PAGE. In contrast, less protein were obtained by acetone precipitation method and TCA method compared with direct extraction method. In addition, the number of protein bands which extracted by the acetone method were more than the TCA-acetone method. Therefore, the acetone method might be more suitable to *Nostoc flagelliforme* protein for SDS-PAGE.

Nostoc flagelliforme cells are rich in large quantities of polysaccharides and pigments [16] which have an important influence on the SDS-PAGE, so the removal of impurities from the extracted protein is the key to SDS-PAGE. The

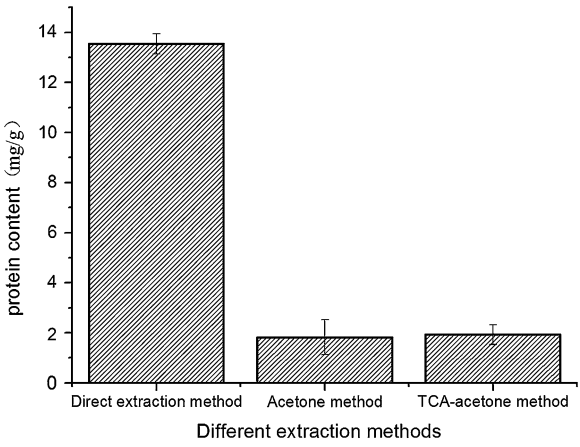

Fig. 179.1 Protein content with different extraction methods

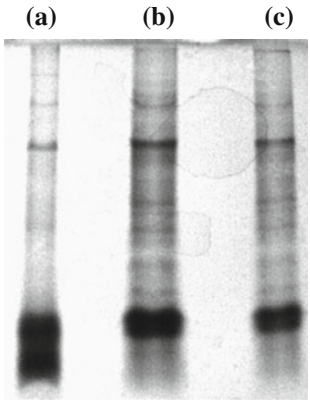

Fig. 179.2 SDS-PAGE images of *Nostoc flagelliforme* with different extraction methods. **a** direct dissolution method, **b** acetone method, **c** TCA method

protein sample extracted by the acetone method appeared to have more abundant and clearer electrophoresis bands in SDS-PAGE images.

179.3.2 Choice of Electrophoresis Conditions

The extraction by the acetone method was used for SDS-PAGE. Electrophoresis voltage and current was shown in Table 179.1. More and clearer electrophoretic bands were found under condition *a* (Fig. 179.3a). In addition, there was a darker connection strip in the bottom of images under condition *b* (Fig. 179.3b). Therefore, condition *a* was suitable to *Nostoc flagelliforme* protein for SDS-PAGE.

179.3.3 Sample Volume

The extraction by the acetone method was used for SDS-PAGE. SDS-PAGE was carried out under condition *a*.

The number of bands was 13 in 30–45 μg protein sample (Fig. 179.4). When the sample volume was greater than 45 μg, the high-abundant proteins would

Table 179.1 Conditions of SDS-PAGE

Electrophoresis conditions	Condition *a*			Condition *b*		
	Voltage (V)	Current (mA)	The concentrate (%)	Voltage (V)	Current (mA)	The concentrate (%)
Stacking gel	15	10	3	20	20	3
Resolving gel	29	20	12	40–80	40	10

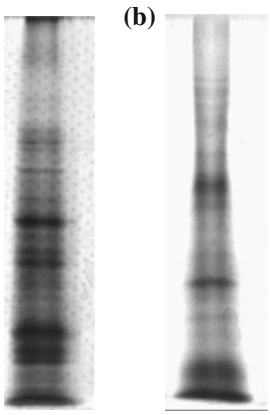

Fig. 179.3 SDS-PAGE images of *Nostoc flagelliforme* with different conditions

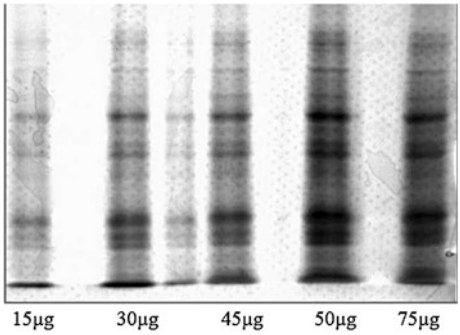

Fig. 179.4 SDS-PAGE images of *Nostoc flagelliforme* with different sample volume of the protein

cover the low-abundance proteins and when the sample volume was lower than 30 μg, some bands would be unclear or disappear. Therefore, the most appropriate sample volume was 30–45 μg.

179.3.4 SDS-PAGE Analysis of Protein in Nostoc flagelliforme *with UV-B and NaCl Stress*

Upon UV-B exposure for 24 h, certain proteins of *Nostoc flagelliforme*, especially, 15–33 kDa, were selectively repressed and a few others e.g., 33, 114, 130 kDa were overproduced, conferring protection to the cells from UV injury (Fig. 179.5). However, upon 0.8 mol L^{-1}NaCl stress for 24 h, most proteins of *Nostoc flagelliforme*, especially, 20–50 kDa, were selectively repressed. However, there are still a small number of proteins, such as the 130,117 kDa protein stress induced by salt. The changes of these proteins might account for stress resistance of *Nostoc flagelliforme*.

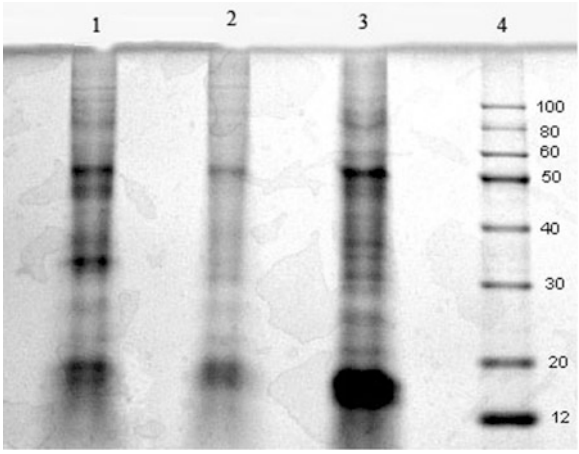

Fig. 179.5 SDS-PAGE analysis of protein in *Nostoc flagelliforme* with different stress. *1* UV-B treatment *2* NaCl treatment *3* Control *4* Marker

Tolerance of *Nostoc flagelliforme* to environmental stresses is attributed to the respond to physiological and metabolic processes, and the synthesis of proteins is an important mechanism for that. The cyanobacterium *Synechocystis sp.* showed a capability for de novo formation of D1 and D2 proteins, the key proteins in photosystem II (PSII) in response to UV stress [17]. The terrestrial cyanobacterium, *Tolypothrix byssoidea*, induced 43, 49, and 58 kDa proteins upon UV exposure, conferring protection to the organism to survive prolonged UV exposure [18]. The estuarine cyanobacterium *Lyngbya aestuarii* also induced 20 and 22 kDa proteins upon UV exposure [15], and the same situation also appeared in *Chlorococcum sp.* [19]. Moreover, SSPs (The proteins which preferentially synthesized during salt stress) has been studied in previous studies. The stress proteins of plants are predominantly of low molecular mass [20]. Jiang [8] reported that some protein of *Dunaliella viridis* in salinity stress by inducing increased expression, and these proteins included antioxidant protein, cytoplasmic cytoskeleton proteins, molecular chaperones, protein functions of the Calvin cycle, photosynthetic electron chain proteins and amino acid synthesis, protein synthesis enzymes and ion channel protein which were a variety of different biological function of proteins. In this study, UV-B radiation affected the conformation of *Nostoc flagelliforme* proteins, namely, 33,114, and 130 kDa protein, and salt stress induced 117 and 130 kDa protein, these proteins appeared as stress protein during adaptation to a changed environment.

179.4 Conclusions

The SDS-PAGE system of proteins of the *Nostoc flagelliforme* cells has been established. Total protein was extracted with acetone method, the most appropriate sample volume was 30–45 μg, concentration of resolving gel was 12 %, when the

protein went to the resolving gel, the current was changed to 20 mA, with Coomassie brilliant blue staining, 13 clear proteins bands appeared with SDS-PAGE. The *Nostoc flagelliforme* proteins, namely, 33, 114, and 130 kDa protein affected by UV-B, and 117 and 130 kDa protein induced by salt stress were discovered and these proteins appeared as stress responsive factors during adaptation to environment change.

Acknowledgments This work was supported by the National Natural Science Foundation of China (No.20806047; 20776112), China Postdoctoral Science Foundation (No.20090450116), and Excellent Middle Aged and Young Scientist Award Foundation of Shandong Province (No.BS2011SW029).

References

1. Gao K (1998) Chinese studies on the edible blue-green alga, *Nostoc flagelliforme*, a review. J Appl Phycol 10:37–49
2. Qian K, Zhu H, Chen S (1989) The ecological conditions for *Nostoc flagelliforme* and their analysis. Acta Phytoecologica et Geobotanica Sinca 13:97–104 (in Chinese)
3. Ye C, Gao K (2004) Photosynthetic response to salt of aquatic-living colonies of the terrestrial cyanobacterium *Nostoc flagelliforme*. J Appl Phycol 16:477–481
4. Ferroni L, Klisch M, Pancaldi S et al (2010) Complementary UV-absorption of Mycosporine-like amino acids and scytonemin is responsible for the UV-insensitivity of photosynthesis in *Nostoc flagelliforme*. Marine Drugs 8:106–121
5. Bi Y, Deng Z, Hu Z et al (2005) Response of *Nostoc flagelliforme* to salt stress. Acta Hydrob Sinica 29:125–129 (in Chinese)
6. He Y, Yu H, Yang L (2011) Assessment of salinity-induced lipid peroxidation and antioxidants of cyanobacterium *Nostoc flagelliforme*. J Qingdao Univ Sci Technol 32:626–629 (in Chinese)
7. Liang W, Jiao G, Zhou W et al (2011) Differential expression and gene cloning of peroxiredoxin from *Nostoc flagelliforme* subjected to dehydration and rehydration. Chin J Appl Environ Biol 17:666–672 (in Chinese)
8. Jiang W, Li Y, Sun H (2009) Halotolerance of *Dunaliella viridis* and the effects of hyperosmotic stress on its protein expression. Period Ocean Univ China 39:347–352 (in Chinese)
9. Wang X, Chai X, Wang X et al (2009) Growth and salt-induced proteins in alga *Dunaliella salina* at different salinities. Fish Sci 28:90–92 (in Chinese)
10. Su J, Jia S, Chen X, Yu H (2008) Morphology, cell growth, and polysaccharide production of *Nostoc flagelliforme* in liquid suspension culture at different agitation rates. J Appl Phycol 20:213–217
11. Gu R, Liu Q, Chen X, Jiang X (1999) Comparison and optimization of the methods on protein extraction and SDS-PAGE in woody plants. Chin Bulletin Bot 16:171–177 (in Chinese)
12. Liang W, Wang X, Jiao G et al (2009) Establishment and optimization of two-dimensional gal electrophoresis for proteone of *Nostoc flagelliforme*. Acta Bot Boreal 29:1550–1556
13. Bradford MM (1976) A rapid and sensitive method for the quantitation of microgram of protein utilizing the principle of protein-dye binding. Anal Biochem 72:248–254
14. Wang Z (2000) Studies oil taxonomy and mutants identification by protein SDS-PAGE in *Spiruliua*. J Zhejiang Uinv 26:583–587 (in Chinese)

15. Rath J, Adhikary SP (2007) Response of the estuarine cyanobacterium *Lyngbya aestuarii* to UV-B radiation. J Appl Phycol 19:529–536
16. Lin Y, Yu H, Xu P et al (2007) Extraction and physicochemical properties of *Nostoc flagelliform* polysaccharide. Mod Food Sci Technol 23:34–49 (in Chinese)
17. Vass I, Kirilovsky D, Perewoska I et al (2000) UV-B radiation induced exchange of the D1 reaction centre subunits produced from the *psbA2* and *psbA3* genes in the cyanobacterium *Synechocystis* sp. PCC 6803. Eur J Biochem 267:2640–2648
18. Adhikary SP (2003) Heat shock proteins in the terrestrial epilithic cyanobacterium *Tolypothrix byssoidea*. Biol Plant 47:125–128
19. Abo-Shady AM, El-Naggar AH, El-Sheekh MM et al (2008) Impact of UV-B radiation on antioxidant enzymes and protein electrophoretic pattern of the green alga *Chlorococcum sp*. Ann Microbiol 58:195–201
20. Chauhan VS, Singh B, Singh S et al (2011) Regulation of sodium influx in the NaCl-resistant ($NaCl^r$) mutant strain of the cyanobacterium *Anabaena variabilis*. Curr Microbiol 42:100–105

Chapter 180
Study on Antibacterial Activity of *Radix isatidis* Extracts and Preliminary Investigation of Their Antibacterial Mechanism

Lin Tian and Zhan Wang

Abstract The antibacterial mechanism of *Radix isatidis* extracts against *Escherichia coli* and *Bacillus subtilis* was investigated by determining the changes in electrical conductivity of bacterial suspension treated by *Radix isatidis* extracts, as well as the changes of phosphorus metabolism and protein expression. The results showed that the electrical conductivity of treated bacterial suspension was significantly increased, indicating that *Radix isatidis* extracts could damage the integrity of cell membrane. In addition, the consumption of phosphorus was decreased in the *Radix isatidis*-treated bacteria, which influenced the synthesis of important cellular components, such as phospholipid, energy metabolism. Coomassie brilliant blue G-250 colorimetric assay demonstrated that *Radix isatidis* extracts could block the expression of some proteins in bacterial cells.

Keywords Antibacterial mechanism · *Bacillus subtilis* · *Escherichia coli* · *Radix isatidis*

180.1 Introduction

Chemical preservatives are widely used in the food industry in recent years. Although it can effectively inhibit bacterial growth, chemical preservatives have some side effects, teratogenic, carcinogenic, or mutagenic effect to harm human health, as well as a threat to the natural environment. Therefore, people pay more attention to the research and development of easy to use, effective and nontoxic natural food preservatives [1, 2].

L. Tian (✉) · Z. Wang
Department of Basic Science, Tianjin Agricultural University, Tianjin 300384, People's Republic of China
e-mail: xiaolinzi2004_china@126.com

T.-C. Zhang et al. (eds.), *Proceedings of the 2012 International Conference on Applied Biotechnology (ICAB 2012)*, Lecture Notes in Electrical Engineering 251,
DOI: 10.1007/978-3-642-37925-3_180,

China is the birthplace of Chinese herbal medicine and the largest production country. Chinese herbal medicine attracted much of the world's attention because of its unique concept and effects on disease. Its effect and safety has been confirmed in the long history. Herbal medicine used as a food preservative, not only to avoid the toxic hazards of chemical preservatives, but also can give the food a unique flavor. Chinese herbal medicine as a welcomed and promising preservative has the following advantages: First, because it is a natural substance, it has no toxic side effects within the normal range of use; Second, it has multiple effects, such as health care, antibacterial, and disease prevention [3].

Radix Isatidis has been widely applied in the research and development of Chinese medicines. However, the research on *Radix Isatidis* antibacterial mechanism has not been found.

In this study, we investigated the antibacterial mechanism of *Radix Isatidis* extracts liquid against *Escherichia coli* and *Bacillus subtilis* in order to provide a theoretical support for its development into a new natural preservative or antibacterial agent.

180.2 Materials and Methods

180.2.1 Drugs and Instruments

180.2.1.1 Strains

Escherichia coli and *Bacillus subtilis*.

180.2.1.2 Medium

Nutrient Broth medium for *Escherichia coli*, NB medium supplemented with 15 g L^{-1} glucose for *Bacillus subtilis*.

180.2.1.3 Reagents

Reaction solution of Coomassie Brilliant Blue G-250 [4], 0.1 mol L^{-1} phosphate buffer.

180.2.2 Methods

180.2.2.1 Extracts Method of *Radix Isatidis*

Pulverized *Radix Isatidis* was decocted by boiling water for an hour, filtered, and set the volume to 30 mL. The concentration of *Radix Isatidis* was 1 g mL^{-1}.

180.2.2.2 Determination of the Antibacterial Activity of *Radix Isatidis* Extracts

The cultivation was realized by culturing the *Bacillus subtilis* in the Nutrient Broth medium supplemented with 15 g L^{-1} glucose at 37 °C with orbital shaking at 180 rpm for 12 h. The *Radix Isatidis* extracts was added into the broth in which the cell concentration is 10^4 CFU mL^{-1} obtained through diluted by appropriate medium.

The *Radix Isatidis* extracts was added into the broth. The mixture was incubated for 5, 10, 20, 30, 40, and 80 min, respectively. The 50 μL mixture was removed for culturing for 24 h.

180.2.2.3 Determination of Electrical Conductivity

5 mL *Radix Isatidis* extracts was added into the 5 mL broth which its concentration is 10^8 CFU mL^{-1} obtained through diluted by 0.1 mol L^{-1} phosphate buffer. The electrical conductivity was measured every 10 min [5].

180.2.2.4 Determination of Phosphate Metabolism

In our study, we used the method as reported before [6].

180.2.2.5 Determination of Soluble Protein Contents

In our study, we used coomassie brilliant blue G-250 staining method determining the soluble protein content as reported before [7].

180.3 Results and Discussion

180.3.1 Antibacterial Activity of Radix Isatidis *Extracts Against* Escherichia coli *and* Bacillus subtilis

As the results showed that (Fig. 180.1), *Radix Isatidis* extracts had antibacterial activity against *Escherichia coli* and *Bacillus subtilis*, but stronger against former. The antibacterial rate against *Bacillus subtilis* reached 33.8 % at 30 min, almost three times against *Escherichia coli*.

180.3.2 The Changes of Electrical Conductivity After Radix Isatidis *Extracts Treatment*

As Shown in Figs. 180.2 and 180.3, when the concentration of *Radix Isatidis* extracts was 0.01 g mL^{-1}, the conductivity of broth of the two strains treated by *Radix Isatidis* at different treatment time were higher than those of control, but showed a greater conductivity difference in the *Bacillus subtilis* with the control. When the concentration was 0.005 g mL^{-1}, the conductivity were higher than those of control with 75 min.

180.3.3 The Changes of Phosphate Metabolism After Radix Isatidis *Extracts Processing*

As shown in Figs. 180.4 and 180.5, compared with the control, the phosphorus consumption gradually reduced after treatment by *Radix Isatidis* extracts which showed that *Radix Isatidis* extracts not only can damage the cell membrane, but also can affect phosphate metabolism.

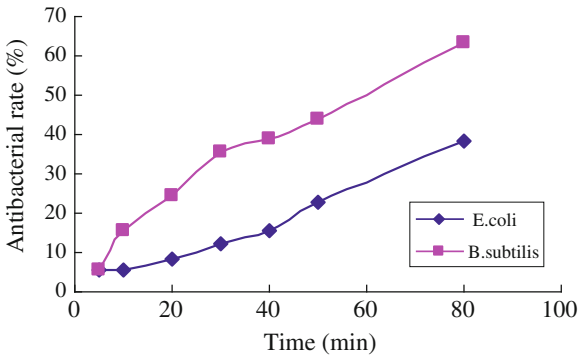

Fig. 180.1 Antibacterial rate of *Radix Isatidis* extracts against *Escherichia coli* and *Bacillus subtilis*

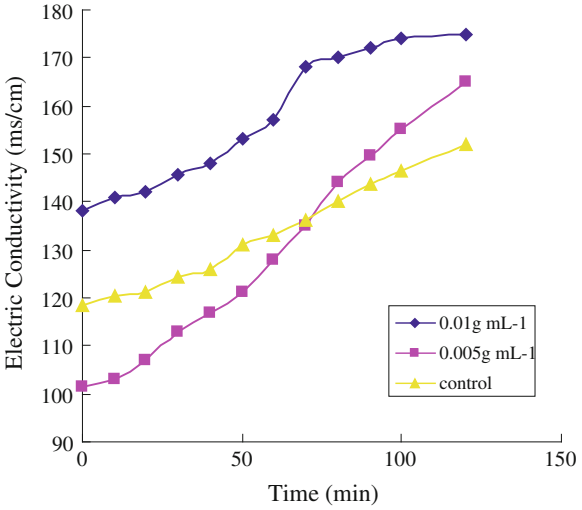

Fig. 180.2 Electrical conductivity of the broth of *Bacillus subtilis* treated by *Radix Isatidis* extracts

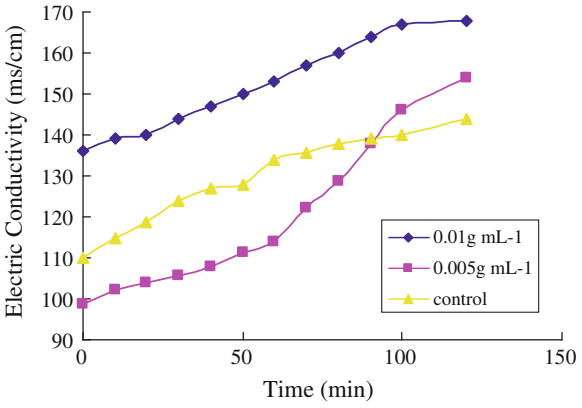

Fig. 180.3 Electrical conductivity of the broth of *Escherichia coli*. treated by *Radix Isatidis* extracts

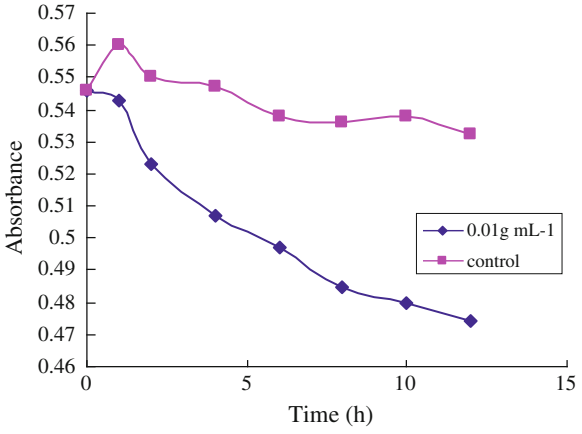

Fig. 180.4 Phosphorus content of the broth of *Bacillus subtilis* treated by *Radix Isatidis* extracts

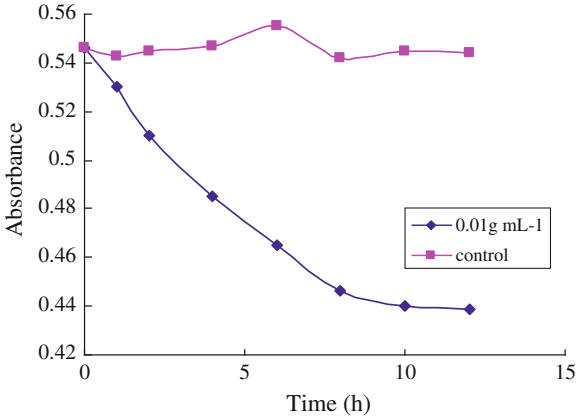

Fig. 180.5 Phosphorus content of the broth of *Escherichia coli*. treated by *Radix Isatidis* extracts

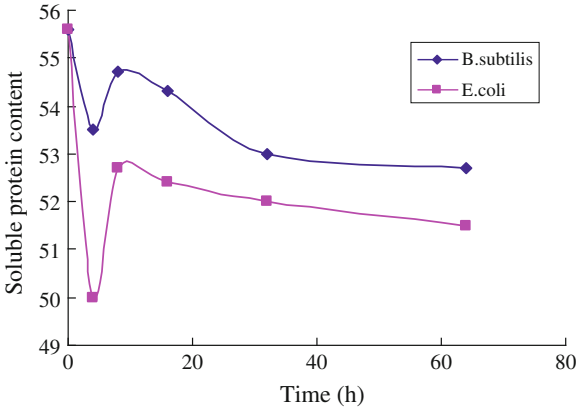

Fig. 180.6 Soluble protein content of the broth of *Escherichia coli*. and *Bacillus subtilis* treated by *Radix Isatidis* extracts

180.3.4 Changes in the Soluble Protein Content

As the results showed (Fig. 180.6) that, the soluble protein content showed a big difference with that of untreated control in less than 4 h, but achieve a balance after 32 h.

180.4 Discussion

180.4.1 Effects of Radix Isatidis Extracts on the Permeability of Cell Membrane

The cell membrane is a protective barrier for bacteria. When the cell membrane is destroyed, bacterial protection barrier is broken. So that its internal electrolyte is

leaked to the nutrient solution, and nutrient solution of electrical conductivity rises. Therefore, the changes in the broth electrical conductivity reflect the changes in the bacterial membrane permeability.

In our study, we found that the electrical conductivity continued to increase which indicated the cell membrane was definitely destroyed. And the higher concentration of *Radix Isatidis* extracts can damage the cell membrane faster compared with the lowers.

180.4.2 Effects of Radix Isatidis *Extracts on Bacterial Phosphate Metabolism*

Phosphorus, a trace element, is necessary for all organisms and an important component of nucleic acids, phospholipids, and glucose metabolism intermediates including microorganisms, so that it plays a central role in cellular energy metabolism. The bacteria use glucose through a series of the phosphorylation reaction, to provide the energy needed for the growth and reproduction. Therefore, consumption of phosphorus may reflect the metabolic function and the state of growth of the cell as a whole.

In our study, we found that the consumption of phosphorus continued to reduce indicate there was a continuous destruction in bacterial phosphate metabolism, and even the energy metabolism of the bacteria.

180.4.3 Effects of Radix Isatidis *Extracts on Protein Synthesis in Bacteria*

The protein is not only the structure and composition of the microorganism cells, but also catalyzes the intracellular biochemical reactions in the form of the enzyme. Therefore, the reduction of protein content may reflect that the *Radix Isatidis* extracts could inhibit or destruct the protein synthesis in bacteria, which indirectly led to the death of bacteria.

In addition, with the extension of reaction time, the effective and antibacterial component *Radix Isatidis* extracts damaged. Meanwhile, Protein contained in the liquid medium itself was consumed by the bacterial life activities. Therefore, protein contents reached equilibrium late in the experiment.

180.5 Conclusion

In conclusion, we demonstrate that the *Radix Isatidis* extracts could lead to the death of bacteria through destroying the structure of the cell membrane, affecting the bacterial phosphate metabolism and the synthesis and expression of bacterial protein.

Acknowledgments The research was supported by Tianjin Agricultural Sciences Research Development Fund evolution, the item No. is 2011N08.

References

1. Lu ZK (2003) Research progress of plant source of natural food preservatives. J Food Sci Technol 2003:94–98 (in chinese)
2. JP W(2009) New plant natural food preservations and antibacterial performance. J China Food Addit (in chinese), 2009:61–64
3. MH Research of inhibitory effect of chinese medicine. J Beijing Univ Tradit Chin Med (in chinese)
4. Chen Q (2009) *Radix Isatidis* pharmacological effects and clinical applications. J Chin Pharm Aff 2009:607–608 (in chinese)
5. Lu SX (2008) Study on the inhibitory effect of nisin and its bacteriostatic mechanism. J Chin Brewing 186:87–91 (in chinese)
6. Zhang XH, He J, Shen HM (2008) Cocklebur extract inhibition of *Botrytis cinerea* and Antibacterial Mechanism. J Pratacultural Sci 2008:99–104 (in chinese)
7. Zhai P (2006) *Musca domestica* inhibitory kinetics and its mechanism. J China Biotechnol 26:33–39 (in chinese)

Chapter 181
Optimization Research of Sufu by Enzymatic Accelerated Maturation

Jianming Wang, Feng Hu, Ping Li, Changsheng Qiao, Yuan Geng and Hengxing Yang

Abstract Sufu, one of the famous traditional fermented soybean curds, was fast manufactured by maturing acceleration using enzymes. The optimum condition of enzymatic hydrolysis sufu was determined by the single factor and orthogonal tests. Four single factor of important effect on content of peptide and DH were explored. The optimum condition was determined as enzyme dosage was fixed 0.01 %, substrate concentration of soya milk of 6.0 %, hydrolysis temperature 50 °C and hydrolysis time 5 h by orthogonal tests. Under these conditions, The resulted content of peptide was 106.4 mg/g(dry basis) and DH was 25.56 %.

Keywords Sufu · Enzyme ripening · Peptide · DH · Orthogonal experiment

181.1 Introduction

In Asian countries, soybean is consumed in many forms, including soymilk, tofu products, and fermented products such as miso, soy sauce, tempeh, and sufu. Sufu is a traditional fermented soybean curd originating in China [1]. It is a soft cheese like product with a spreadable creamy consistency, and it has been consumed

J. Wang · C. Qiao · Y. Geng · H. Yang
College of Food Engineering
and Biotechnology, Tianjin University of Science and Technology, Tianjin 300457,
People's Republic of China

F. Hu (✉)
College of Biotechnology, Tianjin University of Science and Technology, Tianjin 300457,
People's Republic of China
e-mail: hufengyx@126.com

P. Li
SGS-CSTC Standards Technical Services Company Limited, Tianjin 300457,
People's Republic of China

T.-C. Zhang et al. (eds.), *Proceedings of the 2012 International Conference on Applied Biotechnology (ICAB 2012)*, Lecture Notes in Electrical Engineering 251,
DOI: 10.1007/978-3-642-37925-3_181,

widely as an appetizer for centuries in China [2, 3]. There is a similar product called tofuyo in Okinawa, Japan. China has many different colors of sufu, such as red sufu, white sufu, and gray sufu, but red sufu is the most popular type due to its attractive color and fine flavor [4].

During sufu preparation, the changes in the chemical components, especially those related to the degradation of protein, It had been reported that most of the soybean proteins were degraded into peptides and amino acids in well-qualified sufu. Soybean peptides are a group of short chain peptides with 3–10 amino acid residues derived from soybean protein hydrolyzed. It should be considered not only as a nutrient but also as a functional factor to human health because of its various bioactivities such as immunostimulative, anti-hypertensive, and antithrombotic properties [5].

For the manufacture of traditional fermented sufu, pehtze was first prepared by growing a fungus such as Actinomutor, Mucor, or Rhizopus on tofu cubes. The prepared pehtze is then aged in a saline solution for ca 4–6 months [6]. It (The manufacture of traditional fermented sufu) was a long and complex process, semi-finished products occupied a large space, and it was difficult to expand production scale. As soybean proteins are precursors of many different bioactive peptides [7, 8], there are many studies on the production of soybean peptides by hydrolysis of soybean protein with commercial enzyme preparation [9]. And while during the manufacturing of enzyme ripened sufu, the salted tofu cubes are then ripened with enzyme for ca 4–6 weeks. Considering the lack of research on sufu prepared by enzyme ripening method, we have previously conducted a series of study to investigate some biochemical and physical changes during the hydrolyzed of enzyme-ripening sufu. It was found that hydrolytic enzymes catalyzed the hydrolysis protein.

The objectives of this work were: to study effects of different enzyme reaction conditions on enzymatic hydrolysis; to study the novel manufacture of sufu by enzymatic accelerated maturation was feasible, which had certain theoretical basis for enzymatic sufu instead of traditional sufu.

181.2 Materials and Methods

181.2.1 Reagents and Materials

Soybean was supplied by Tianjin Limin Flavoring Co., Ltd in China. Accelerzyme CPG (900 CPGU/g) was obtained from DSM Enzymes (Netherlands) Flavoring Co., Gly–Gly-Tyr-Arg was purchased from Sigma Company, Trichloroacetic acid (TCA), Formaldehyde, $CuSO_4 \cdot 5H_2O$, NaOH, H_2SO_4, K_2SO_4, were purchased from Tianjin Damao Chemical Reagent Factory. Actinomucor elegans was preserved the laboratory.

Actinomucor elegans was used topacked in the surface cover of sufu.

The chemical and reagents used in the experiment were of analytical or food grade quality. Preparation of pehtze (pizi) hydrolysates using enzymes.

Preparation of tofu used for sufu mainly follows the process technologies for commercial tofu except for slight differences in some steps. Pehtze (or pizi), fresh bean curd overgrown with mycelium of molds that was flattened by hand, in the same way as done in the traditional way, is produced by means of solid substrate fermentation [10]. Then, increased to right temperature, the enzyme began to work. After several hours, the index came to the standard, stopped hydrolyze. The enzymatic accelerate ripening sufu production flow is briefly outlined:

Soybean→soy milk→sterilization→agitating and adding→ingredients→adding enzymes→hydrolysis→enzyme denaturing→packaging→enzymatic accelerated maturation sufu

181.2.2 Sufu Sample Preparation

The inner yellow part of sufu was taken, frozen at −50 °C and freeze-dried in a chamber freeze-dryer. The freeze-dried parts were ground in a pulverizer and the resulting powders were used for peptide analysis.

181.2.3 Peptide Extraction

The sufu powder was extracted with 5 % TCA, solvent/sufu ratio 10:1 (w/v ratio) at 55 °C for 30 min. After extraction, the suspensions were centrifuged at 3,000 rpm for 10 min, and the supernatants were used.

181.2.4 Standard Curve

Gly–Gly-Tyr-Arg tetra-peptide was dissolved in 5 % of the TCA to solution of different concentrations. The standard curve of Gly–Gly-Tyr-Arg tetra-peptide was as follows: (Fig. 181.1).

Y is the OD value of the solution of different concentrations and X is the concentration of peptide in solution. There is positive correlation between X and Y, thus the greater the OD value, the greater the concentration of peptide.

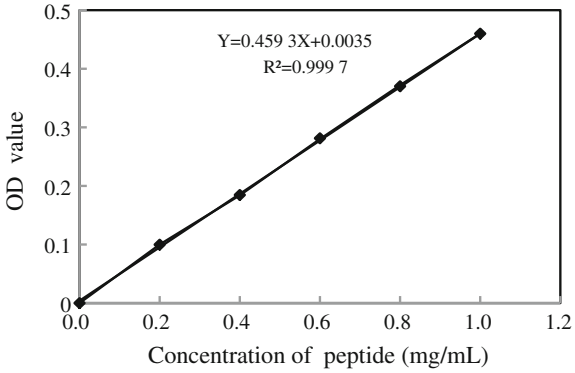

Fig. 181.1 Standard curve peptide

181.2.5 Measurement of Peptide

2.5 mL of supernatant added 2.5 mL of 10 % TCA solution, mixed on whirlpool hybrid instrument, then centrifuged at 4,000 rpm for 15 min. The supernatants were fully transferred to a 50 mL volumetric flask and the volume was completed with the extraction solvent to the mark. Take 6.0 mL of the above solution by adding 4.0 mL of the biuret reagent in another tube and mixed well. Then centrifuged at 2,000 rpm for 10 min. OD values were measured at the wavelength of 540 nm using ultraviolet-visible spectrophotometer. Each test included blank controls containing extraction solvent (without supernatant) and triplicate test amples. Then, quantitative analysis was done by using the standard curve of Gly–Gly-Tyr-Arg tetra-peptide.

181.2.6 DH

The DH is an important unit of measure in proteolysis. This unit is defined as the ratio between the bonds cleaved and the total peptide bonds present. It was determined by analyzing the number of amino groups by ninhydrin titration or formaldehyde titration [11]. The formaldehyde titration method was used here.

181.2.7 Experimental Design for Enzymic Hydrolyze

The process conditions for peptide and DH during enzymatic sufu production process were optimized by single-factor experiment design. And then, orthogonal test was used for further optimization of conditions.

181.3 Results and Discussion

181.3.1 Effect of Substrate Concentration on Content of Peptide and DH

Substrate concentration has been found to be the important factor besides temperature, time, enzyme dosage, and composition. Different substrate concentration will affect a reaction. Figure 181.2 shows effect results of different substrate concentration on content of peptide and DH of enzymatic sufu. As can be seen, the DH gradually increased when substrate concentration value increased. In addition, DH increased when substrate concentration changed from 4 to 6 %. The possible reason is that substrate concentration was used as reactant beneficial to hydrolysis reaction. However, over-substrate concentration led to too difficult touch of substrate and enzyme, which could be unbeneficial to an enzyme-catalyzed reaction.

The similar changes can also be seen in the content of peptide curve of Fig. 181.2. In the meantime, we observed that content of peptide increased quickly when substrate concentration changed from 4 to 6 %, and increased slowly after 6 %. According to these results and consideration of saving substrate for industrial point protease of view, we regarded the 6 % as reasonable substrate concentration for hydrolysis of enzymatic sufu.

(Enzyme dosage 0.01 %, hydrolysis temperature 50 °C and hydrolysis time 4 h and then measured the content of peptide and DH).

181.3.2 Effect of Hydrolysis Time on Content of Peptide and DH

Effect of different hydrolysis time on peptide and DH of enzymatic sufu were shown in Fig. 181.3. As can be seen, the peptide and DH gradually increased when the time increased. In the meantime, it was also found that peptide and DH

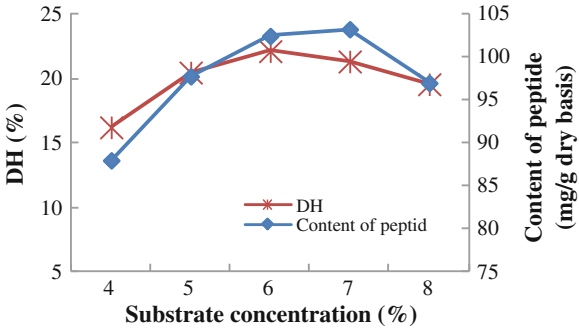

Fig. 181.2 Effect of substrate concentration on content of peptide and DH

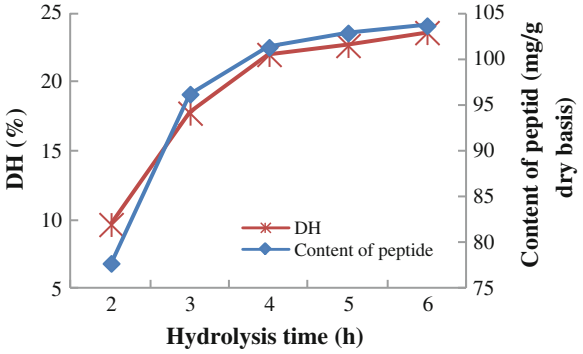

Fig. 181.3 Effect of hydrolysis time on content of peptide and DH

increased quickly as the time changed from 2 to 4 h, and increased slowly after 4 h. It is significant to consider saving time for industrial point protease of view. Therefore, 4 h was considered as a reasonable time for hydrolysis of enzymatic sufu.

(Enzyme dosage 0.01 %, substrate concentration 6.0 % and hydrolysis temperature 50 °C and then measured the content of peptide and DH).

181.3.3 Effect of Hydrolysis Temperature on Content of Peptide and DH

Different temperature will affect a reaction. Figure 181.4 shows effect of different temperature on peptide and DH of enzymatic sufu. As can be seen, the content of peptide and DH gradually increased when substrate concentration value increased. In addition, the content of peptide and DH increased when temperature changed from 40 to 50 %.The content of peptide and DH increased when temperature changed from 40 to 50 °C. When temperature was higher than 50 °C, the content of peptide and DH were decreased along with the increase of temperature of hydrolysis. The possible reason is that high temperature led to inactivation of some

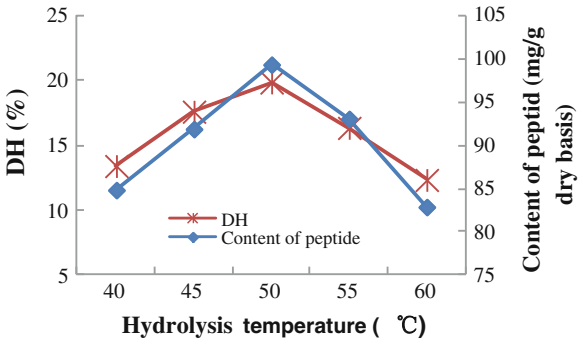

Fig. 181.4 Effect of hydrolysis temperature on content of peptide and DH

enzyme, which could be unbeneficial to an enzyme-catalyzed reaction. Therefore, 50 °C was the reasonable temperature for hydrolysis of enzymatic sufu.

(Enzyme dosage 0.01 %, substrate concentration 6.0 % and hydrolysis time 4 h and then measured the content of peptide and DH).

181.3.4 Effect of Enzyme Dosage on Content of Peptide and DH

Effect of different enzyme dosage on content of peptide and DH of enzymatic sufu were shown in Fig. 181.5. As can be seen, the content of peptide and DH gradually increased when the dosage increased. In the meantime, it was also found that content of peptide and DH increased quickly as the enzyme dosage changed from 0.005 to 0.01 %, and increased slowly after 0.01 %. In general, over broad ranges of enzyme and substrate relationship, there is an increase in the overall hydrolysis rate as the enzyme dosage is increased [12]. The actual specificity of the enzymes may be altered at a very high dosage and there is also a possibility of some reverse reactions. It is significant to consider this in the case of the production of protein hydrolysates intended for food industry. Therefore, 0.01 % was considered as a reasonable dosage for hydrolysis of enzymatic sufu.

(substrate concentration 6.0 % hydrolysis time 4 h and hydrolysis temperature 50 °C and then measured the content of peptide and DH).

181.3.5 Optimization of Hydrolysis Parameters

In this experiment, we took content of peptide and DH values produced in the process of hydrolysis as objective parameters. The enzyme dosage was fixed as 0.01 %. The Accelerzyme CPG was the enzyme used for this test. The influence of substrate concentration (A), hydrolysis time (B), and hydrolysis temperature (C) on the hydrolysis by enzyme was determined using one-factor experimental design

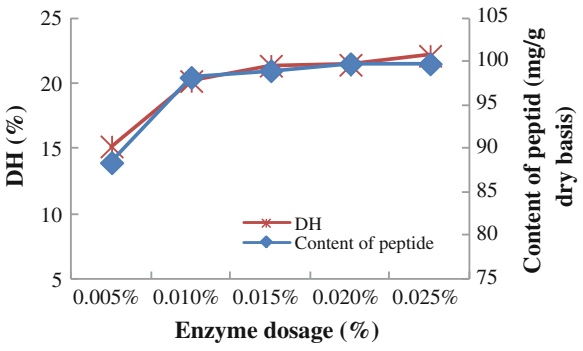

Fig. 181.5 Effect of enzyme dosage on content of peptide and DH

Table 181.1 Coded and real values for each variable of the orthogonal experimental design

Variables	Symbol	Coded levels		
		1	2	3
Substrate concentration (%)	A	5	6	7
Hydrolysis time (h)	B	3	4	5
Hydrolysis temperature (°C)	C	40	50	60

as mentioned in the previous section. Each variable was coded at three levels: 1, 2, and 3 (Table 181.1).

The observed values for content of peptide and DH at different combinations of the independent variables were shown in Table 181.2. The significance of the investigated factors and levels could be realized using the range (R) analysis method. As can be seen, the significance of factors for content of peptide followed the sequence: C > B > A. On the other hand, the sequence of impact of factors on the DH was C > B > A. In the light of content of peptide and DH values of hydrolysis, the best reaction condition was $A_2B_2C_3$. As can be seen from the ANOVA table (Table 181.3), among the independent variables for content of peptide that substrate concentration, hydrolysis time, and hydrolysis temperature had relatively significant effect ($p \leq 0.05$). And the significance of factors for DH was hydrolysis time. We confirmed the optimal hydrolysis condition was substrate concentration 6 %, hydrolysis time 5 h and hydrolysis temperature 50 °C. The enzyme dosage was fixed as 0.01 %. In the end, the maximum content of peptide can reached 106.4 mg/g(dry basis)and the maximum DH can reach 25.56 %.

Table 181.2 Orthogonal design for experimental design and actual results

Run	A	B	C	Content of peptide (mg/g)		DH (%)
1.	1	1	1	94.25		13.98
2.	1	2	2	103.27		21.66
3.	1	3	3	100.91		20.53
4.	2	1	2	104.44		24.43
5.	2	2	3	106.4		25.56
6.	2	3	1	91.9		15.42
7.	3	1	3	102.48		21.02
8.	3	2	1	93.86		17.03
9.	3	3	2	98.56		19.11
K	Content of peptide			DH		
	A	B	C	A	B	C
k_1	99.263	100.39	93.337	18.723	19.810	15.477
k_2	100.913	101.177	102.09	21.803	21.417	21.733
k_3	98.300	96.910	103.05	19.053	18.353	23.370
R	2.613	4.267	9.713	2.940	3.064	6.2893

Table 181.3 Analysis of variance (ANOVA) for the orthogonal experiment

Source	Content of peptide			Error	DH			Error
	A	B	C		A	B	C	
SS	10.48	30.934	171.891	0.41	17.158	14.087	87.069	2.95
Df	2	2	2	2	2	2	2	2
F ratio	25.561	75.449	419.246		5.808	4.769	29.475	
F threshold	19	19	19		19	19	19	
	*	*	*				*	

* Significant at $p \leq 0.05$

181.4 Conclusion

This research provided the optimal condition for hydrolysis sufu using enzyme. Content of peptide and DH (hydrolysis degree) were determined as screen indictor. The preliminary study confirmed that substrate concentration, hydrolysis time, hydrolysis temperature, and enzyme dosage were the main factors for content of peptide and DH. Through the orthogonal experimental design, we confirmed the optimal hydrolysis condition was substrate concentration 6 %, hydrolysis time 5 h, and hydrolysis temperature 50 °C. The enzyme dosage was fixed as 0.01 %. The maximum content of peptide can reached 106.4 mg/g(dry basis)and the maximum DH can reach 25.56 %. Therefore, the research showed novel manufacture of sufu by enzymatic accelerated maturation was feasible, which had certain theoretical basis for enzymatic sufu instead of traditional sufu.

Acknowledgments This work was part of the project (06YFSZSF05300) funded by Tianjin Key Technology R & D Program, Tianjin, P.R. China in 2011.

References

1. Steinkraus KH (1996) Chinese sufu handbook of indigenous fermented foods. Marcel Dekker, New York, pp 633–641
2. Zhang GY, Shi YG (1993) A review of sufu production in China. Food Ferm Indu 6:72–74
3. Han BZ, Beumer RR, Rombouts FM et al (2001) Microbiological safety and quantity of commercial sufu-a Chinese fermented soybean food. Food Cont 12:541–547
4. Han BZ, Rombouts FM, Nout MJR (2003) Review: sufu-a Chinese fermented soybean food. Int J Food Sci 81:17–34
5. Okamoto A, Hanagata H, Kawamura Y et al (1995) Anti-hypertensive substances in fermented soybean natto. J Plant Food Hum Nutr 47:39–47
6. Hesseltine CW, Wang HL (1967) Traditional fermented foods. J Biotech Bioe 9:275–288
7. Shin ZI, Yu R, Park SA et al (2001) His–His-Leu a angiotensin converting enzyme inhibitory peptide derived from Korean soybean paste, exerts antihypertensive activity in vivo. J Agric Food Chem 49:3004–3009
8. Wu JP, Ding XL (2001) Hypotensive and physiological effect of angiotensin converting enzyme inhibitory peptides derived from soybean on spontaneously hypertensive rats. J Agric Food Chem 49:501–506

9. Nielsen PM, Petrsen D, Dambmann C (2001) Improved method for determining food protein degree of hydrolysis. J Food Sci 66:642–646
10. Chou CC, Ho FM, Tsai CS (1988) Effects of temperature and relative humidity on the growth and enzyme production by Actinomucor Taiwanensis during sufu pehtze preparation. Appl Environ Microb 54:688–692
11. Uhlig GH (1998) Industrial enzymes and their applications. Wiley, New York
12. Godfrey T, West S (1996) Industrial enzymology. Stockton Press, New York

Chapter 182
Optimization of the Electroporation Conditions for DNA Transformation of *Staphylococcus carnosus*

Qiang Gao, Mengxiao Wang, Changyan Yu, Lin Huang, Xiu Zheng and Yan Zhu

Abstract In this paper, the optimization of electroporation method for *Staphylococcus carnosus* is investigated. The various factors for electrotransformation are evaluated, including bacterial growth phase, electroporation parameters, pBT2 plasmid DNA concentration and structure, the effect of protoplast or other cell wall-weakening treatments, and the prepulse incubation temperatures, etc. The primary optimized electroporation method is consisted of 60 μL electrocompetent cells and 800–1,000 ng plasmid DNA using the electroporation parameters of 21 kV cm^{-1} field strength, 50 Ω resistance, and 25 μF capacitance by a Bio-Rad Gene Pulser Xcell^{TM} system. Using this optimized method, three different plasmids (pBT2, pCX19, and pTX15) are successfully transformed into *S. carnosus*, and the transformation efficiencies are stationary at around 1×10^3 transformants per μg plasmid DNA. Our results indicate that this electroporation method can be generally applied for foreign DNA transformation into *S. carnosus* host.

Keywords Electroporation · *Staphylococcus carnosus* · Plasmid · Electrocompetent cells

Q. Gao (✉) · M. Wang · C. Yu · L. Huang
Key Laboratory of Industrial Fermentation Microbiology of Ministry of Education, Tianjin Key Laboratory of Industrial Microbiology, College of Biotechnology, Tianjin University of Science and Technology, Tianjin 300457, People's Republic of China
e-mail: gaoqiang@tust.edu.cn

X. Zheng · Y. Zhu
The Logistic Service Group, Tianjin University of Science and Technology, Tianjin 300457, People's Republic of China

T.-C. Zhang et al. (eds.), *Proceedings of the 2012 International Conference on Applied Biotechnology (ICAB 2012)*, Lecture Notes in Electrical Engineering 251,
DOI: 10.1007/978-3-642-37925-3_182,

182.1 Introduction

As a non-pathogenic and Gram-positive bacterium, *Staphylococcus carnosus* is the only one bacterium fully recognized as food-grade GRAS (generally regarded as safe) in *Staphylococci* family [1, 2]. This microorganism plays an important role in the ripening of dry sausages and hams, and it has been used as a starter culture for dry meat manufacture in Europe since 1950s. Furthermore, due to the above significance, *S. carnosus* has been developed as a bacterial host system for foreign protein expression and cell surface display for decades [2].

The transformation step is of key importance for successful genetic manipulation. In general, electroporation is a mechanical method which transfers polar DNA molecules directly into the host cell with the aid of the high-voltage pulse lasted a few microseconds to a millisecond. Moreover, the advantages of this method are effective, rapid, and at low cost. Since the electroporation-mediated transformation of *Staphylococcus aureus* and *S. epidermidis* are quite successful [3], it would be preferable if the efficient transformation of *S. carnosus* by electroporation would be ubiquitously achieved. Löfblom et al. [4] also reported the electroporation-mediated transformation for the protein surface display in *S. carnosus* with a shuttle plasmid.

Since only one plasmid is reported for the transformation into *S. carnosus* by electroporation before, in this study, we attempt to optimize a popular electroporation method of foreign DNA transformation for *S. carnosus* using three different plasmids, pBT2, pCX19, and pTX15.

182.2 Materials and Methods

182.2.1 Bacteria, Plasmids, and Cultivation

Escherichia coli DH5α is cultivated in LB medium, and *Staphylococcus carnosus* TM300 is grown in B2 medium, which is also used as the recovery medium after pulse. Plasmids pBT2, pCX19, and pTX15 are used for the determination of the efficiencies of DNA electrotransformation [2, 3]. Self-prepared TBAB or DM-3 medium is used to select transformants [5]. Cell growth is measured using optical density at 578 nm (OD_{578}).

The DNA of *E. coli-Staphylococci* shuttle plasmid pBT2 is extracted from *E. coli* host using Tiangen pure midi plasmid kit (Tiangen Biotech Co. Ltd., Beijing, China). Plasmid DNAs of pCX19 and pTX15 are, respectively, prepared from *S. carnosus* TM300 host by the same kit, except an additional lysostaphin incubation step for the cell wall degradation.

182.2.2 Preparation of Electrocompetent Cells and Electroporation

Cell competence means the physiological state of a cell which easily absorbs exogenous DNA. Here, the electrocompetent cell preparation and electroporation procedure are mainly based on the method of Löfblom et al. [4] with some modification. Briefly, a colony of *S. carnosus* TM300 is inoculated into 50 mL B2 broth in a 250-mL flask and shaken at 150 rpm and 37 °C for 12 h. The seed culture is diluted into 100 mL B2 broth to an initial OD_{578} of about 0.5 in a 500-mL flask and cultivated as above. When OD_{578} reaches about 0.6, the culture is placed on ice for 10 min, then the cells are harvested by centrifugation at 5,000 x*g* and 4 °C for 10 min. The cells are washed three times with ice-cold sterile water and twice with ice-cold sterile 10 % (w/v) glycerol, subsequently resuspended with 400 μL sterile ice-cold 10 % (w/v) glycerol. Finally, the electrocompetent cell suspension is divided into 60 μL aliquot and reserved at −70 °C up to 6 months.

A certain amount of plasmid DNA is added to a 60-μL electrocompetent cell preparation for electroporation. The electroporation procedure is performed using a Bio-Rad Gene Pulser Xcell™ apparatus (Bio-Rad Laboratories, Hercules, CA, USA) and a Bio-Rad 1-mm electrode-gap cuvette. After pulse, the cells are transferred into 1 mL B2 medium and cultivated at 30 °C and 150 rpm for 2 h. Then 200 μL of cell suspension are spread on TBAB plates containing a corresponding antibiotic. After 24 h incubation, transformants emerge and are used for further experiments.

182.2.3 Cell Wall Weakening Treatment

S. carnosus TM300 protoplast is prepared according to the Ref. [6]. Alternatively, lysostaphin is added in the 60-μL electrocompetent cell preparation at the final concentration of 50 μg mL^{-1} and incubated at 37 °C for 30 min for cell wall weakening treatment [7, 8]. The subsequent electroporation is operated in the optimized condition.

182.3 Results and Discussion

182.3.1 Determination of S. carnosus *Growth Phase*

The growth curve of *S. carnosus* TM300 is first determined, since it is crucial for the relationship between growth state of the bacterium and transformation efficiency. During the first 8 h inoculation, cell growth is slow since the bacterium is adapting

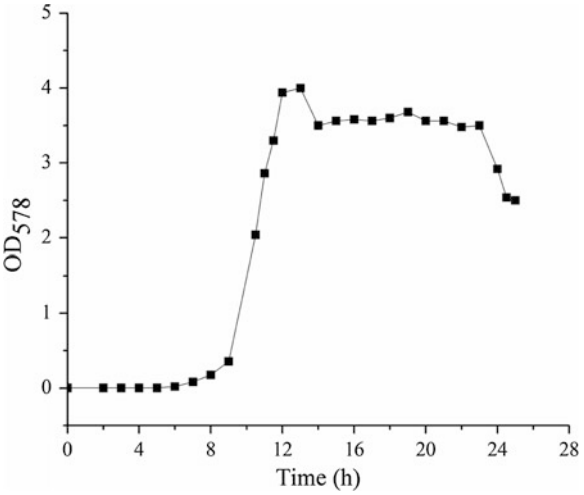

Fig. 182.1 Growth curve of *S. carnosus* TM300 in B2 medium

to the new environment. The next 2 h appears the logarithmic phase with the vitality of the bacterium. After 14 h cultivation, it goes into stationary phase (Fig. 182.1). So the culture time is chosen between 11 and 13 h for seed incubation.

182.3.2 Optimization of Electroporation Parameters

Electrical parameters are of the overall most importance for successful electroporation-mediated transformation of various bacteria [2–8]. To simplify the optimization procedure, a fixed field strength of 21 kV cm^{-1} is used in this paper for electroporation according to the Ref. [4]. Thus, for the Bio-Rad Gene Pulser Xcell^{TM} used here, the parameter optimization only focuses on capacitance and resistance. First, we compare the electrotransformation efficiency at capacitance of 25 and 50 μF for electroporation at the resistance of 100 Ω. The results exhibit that 1.1×10^2 recombinants per μg pBT2 plasmid DNA are obtained at 25 μF capacitance, but no transformants available at 50 μF. Hence, capacitance of 25 μF is chosen for further optimization of the resistance parameter. Finally, the resistance is optimized from the range of 50–200 Ω. Figure 182.2 illustrates that the pulse at 50 Ω resistance with accompanied 1.3 ms conferred the best transformation efficiency, i.e., about 2.8- and 40-fold increase when compared to those at 100 and 150 Ω, respectively. Accordingly, the optimized parameters for *S. carnosus* electrotransformation are the combination of 21 kV cm^{-1} field strength, 25 μF capacitance, and 50 Ω resistance.

In addition, twice pulses just yield a couple of transformants compared with single pulse of 1.03×10^3 transformants for the same batch electrotransformation at the optimized electroporation conditions. Thus only single pulse is applied in the following electrotransformation experiments.

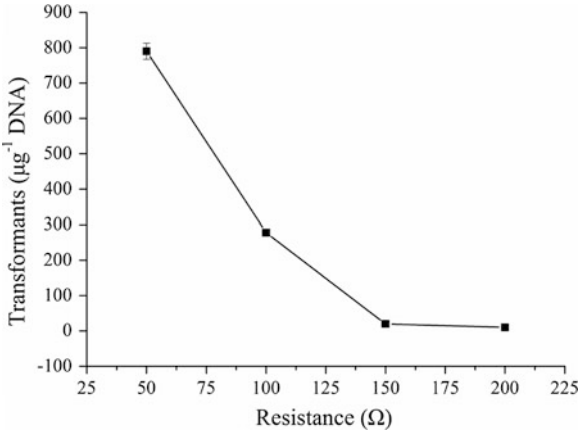

Fig. 182.2 Optimization of the relationship between resistance and transformation efficiency ($n = 3$)

182.3.3 Effect of Plasmid DNA Concentration and Plasmid Structure

In this study, when the amount of plasmid pBT2 DNA is increased, the transformation efficiency first rises, but drops with over 1,000 ng plasmid DNA under the optimal electrical parameter settings, e.g., the electrotransformation efficiency with 800–1,000 ng DNA is around 1.1-fold and 10-fold improvement as compared to those with 1,200 ng and 600 ng DNA, respectively (Fig. 182.3). Therefore, the optimal amount of plasmid DNA is 800–1,000 ng in the 60-μL electrocompetent cell preparation.

Conley and Saunders [9] reported the successful transformation of *E. coli* by linearized pBR322 plasmid DNA. Here, the unique *Bam*HI site in pBT2 is used to

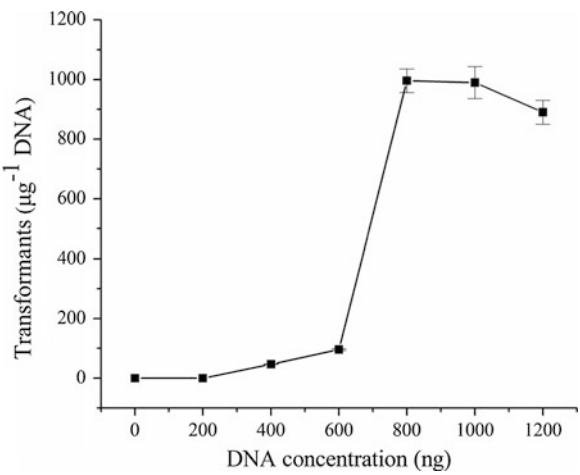

Fig. 182.3 Effect of pBT2 plasmid DNA concentration on transformation efficiency ($n = 3$)

linearize this plasmid. Under the optimized electroporation conditions, linearized plasmid pBT2 DNA is attempted to be transformed into *S. carnosus* electrocompetent cells, but no transformants formed. Hence, the linearized plasmid seems not to be re-circularized in *S. carnosus* as contrast in *E. coli*. This is in agreement with the outcomes in *S. epidermidis* by Augustin and Götz [2], and the reason might be due to the strong restriction enzyme system in *S. carnosus* [4].

182.3.4 Effect of Plasmid Source and Size on Electrotransformation

The plasmid DNA of heterologous source often decreases the electroporation efficiency, but that of homologous source does not [10]. In this paper, to establish a general-purpose electrotransformation protocol for *S. carnosus*, three plasmids extracted from different bacterial hosts, pBT2 from *E. coli*, pCX19 and pTX15 from *S. carnosus*, are successfully transformed into *S. carnosus* TM300 host. In brief, plasmid pBT2 is pulsed with *S. carnous* competent cells by heating at 56 °C for 2 min to temporary inactivate the host restriction system, but pTX19 and pTX15 not [4]. Our results reveal that there are no significant differences of electrotransformation efficiency between the heterologous and homologous sources of plasmid DNA, which is convenient for the gene manipulation using shuttle vector (e.g., plasmid pBT2) in an intermediate host, such as *E. coli*. Furthermore, in spite of the larger size of pTX15 than those of pBT2 and pCX19, all the transformation efficiencies are around 1×10^3 transformants per μg plasmid DNA (Table 182.1). Thus, the size and source of the tested plasmid exhibit no decisive influence for the electrotransformation by this method.

182.3.5 Effect of Prepulse Incubation Temperature on Electrotransformation

Since the prepulse incubation temperature is important for transformation frequency [2, 3, 11, 12], for some bacteria such as *E. coli*, the pulser cuvette containing the cells and plasmid DNA is placed on ice before electroporation for a better transformation efficiency [13]. However, no obvious difference is observed

Table 182.1 Transformation efficiencies in the optimized condition

Plasmids	Transformation efficiency (CFU/per μg plasmid DNA)
pBT2	1.03×10^3
pCX19	9.9×10^2
pTX15	9.8×10^2

between prepulse incubation on ice for 10 min and direct pulse in our procedure (data not shown). This is in agreement with the outcomes of Löfblom et al. [4].

182.3.6 Comparison of Wall-Weakening Treatments

Owing to the much thicker peptidoglycan barriers, Gram-positive bacteria usually show lower transformation efficiency than Gram-negative bacteria. Thus, for the efforts to weaken such cell walls, specific enzymes, like lysostaphin and mutanolysin, have been used to weaken such physical barriers and thus to enhance the electrotransformation efficiencies of Gram-positive bacteria. For example, Scott and Rood [7] evaluated the electroporation transformation of lysostaphin-treated *Clostridium perfringens*, Rattanachaikunsopon and Phumkhachorn [8] used mutanolysin to disrupt the cell walls of some Gram-positive bacteria before successful transformation. Here, a direct protoplast electrotransformation of *S. carnosus* TM300 is conducted in the optimized condition, but no transformants are formed. Another evaluation is also carried out with the wall-weakened cells by lysostaphin, the efficiency of electrotransformation results in only obtaining 3 transformants per μg plasmid DNA, and when cultured on TBAB agar plates for 72 h, but is merely increased up to 12 transformants per μg plasmid DNA on DM-3 medium. Nonetheless, it is still much less efficient and more time-consuming as compared to the direct electroporation to the intact cells. Hence, the cell wall-weakening treatment demonstrates helplessness for efficient electrotransformation of *S. carnosus* under the given conditions.

182.4 Conclusion

Electroporation is a rapid and efficient method for bacterial DNA transformation as compared to other traditional methods, such as conjugation, etc. Using this protocol, lots of successful DNA transformation have been achieved for further research in many bacteria, which are impossible using traditional methods. However, successful electrotransformation involves many aspects, including bacterial age, medium components of incubation and recovery media, cultivation manner, composition of wash buffer, preparation procedure of competent cells, vector DNA concentration and source, electrical parameters, pre- and after pulse treatments, and even more. To obtain the high transformation efficiency, the electroporation for each detailed strain and plasmid might be more or less remodified based on the known protocol.

In this paper, we have a primary optimized general electroporation method for plasmid DNA transformation of *S. carnosus* using a Bio-Rad Gene Pulser Xcell™ apparatus and a Bio-Rad 1-mm gap cuvette. During the optimization process, we find that the plasmid DNA concentration is one of the key factors to determine the

transformation efficiency. In general, for the prepared competent cells, the efficiency increases with the increased plasmid DNA concentration. However, excessive DNA results in a slight decrease in transformation (Fig. 182.3), which can be referred to the saturation of plasmid DNA to the given cells. Another key factor for the efficient electrotransformation is the electroporation parameter settings by the combination of field strength, resistance, and capacitance, which depend on the specific pulser model. Therefore, the optimization of electrotransformation ought to be modified for each strain and plasmid based on the reported protocol.

The inherent properties of the host strain also decide the final transformation efficiency. This is owing to the restriction enzyme machinery of the host cells, which greatly decreases the transformation efficiency when compared to the restriction deficient host or using heterologous plasmid DNA. To overcome this problem, the heat-induction protocol has been developed for the temporary inactivation of the host restriction system [4, 10, 13]. In our experiment, the transformation efficiency is very similar by using either heterologous plasmid DNA with heat-induced host cells or homologous plasmid DNA with none heat-treated cells, which indicates that the restriction system exists in *S. carnosus* cells, and heat induction of the host cells is an efficient method to improvement the transformation efficiency. Also, the failure of electrotransformation using linearized plasmid DNA also confirms this conclusion.

Finally, the electrotransformation efficiency achieved about 1×10^3 transformants per μg plasmid DNA. For the reason of lower efficiency here compared to that by Löfblom et al. [4], it is probably due to the different plasmids and less DNA amounts used here. Nevertheless, three different plasmids from either homologous or heterologous source are successfully transformed into *S. carnosus* TM300 with enough transformants using the optimized method described here, thus this procedure can be routinely used to insert a foreign gene into *S. carnosus* host in the conventional molecular biology research.

Acknowledgments We cordially thank Professor Dr. Friedrich Götz (Eberhard-Karls-Universitaet, Tuebingen, Germany) for generously providing *S. carnosus* TM300 strain and plasmids pBT2, pCX19 and pTX15. This work is financially supported by National 973 Program of China (2011CB707401 and 2013CB734004), National 863 Program of China (2012AA021302), the Key Project for Innovative Research of Tianjin Binhai New Area of China (2011-BK120014) and National Science Foundation of China (31101275).

References

1. Schleifer KH, Fischer U (1982) Description of a new species of the genus *Staphylococcus*: *Staphylococcus carnosus*. Int Syst Bacteriol 32:153–156
2. Augustin J, Götz F (1990) Transformation of *Staphylococcus epidermidis* and other staphylococcal species with plasmid DNA by electroporation. FEMS Microbiol Lett 54:203–207

3. Schenk S, Laddaga RA (1992) Improved method for electroporation of *Staphylococcus aureus*. FEMS Microbiol Lett 73:133–138
4. Löfblom J, Kronqvist N, Uhlén M et al (2006) Optimization of electroporation mediated transformation: *Staphylococcus carnosus* as model organism. J Appl Microbiol 102:736–747
5. Chang S, Cohen SN (1979) High frequency transformation of *Bacillus subtilis* protoplasts by plasmid DNA. Mol Genet Genomics 168:111–115
6. Götz F, Schumacher B (1987) Improvements of protoplast transformation in *Staphylococcus carnosus*. FEMS Microbiol Lett 40:285–288
7. Scott PT, Rood JI (1989) Electroporation-mediated transformation of lysostaphin-treated *Clostridium perfringens*. Gene 82:327–333
8. Rattanachaikunsopon P, Phumkhachorn P (2009) Glass bead transformation method for Gram-positive bacteria. Braz J Microbiol 40:923–926
9. Conley EC, Saunders JR (1984) Recombination-dependent recircularization of linearized pBR322 plasmid DNA following transformation of *Escherichia coli*. Mol Genet Genomics 194:211–218
10. Van de Rest ME, Lange C, Molenaar DA (1999) Heat shock following electroporation induces highly efficient transformation of *Corynebacterium glutamicum* with xenogeneic plasmid DNA. Appl Microbiol Biotech 52:541–545
11. Bringel F, Hubert JC (1990) Optimized transformation by electroporation of *Lactobacillus plantarum* strains with plasmid vectors. Appl Microbiol Biotech 33:664–670
12. Lechner M, Märkl H, Götz F (1988) Lipase production of *Staphylococcus carnosus* in a dialysis fermentor. Appl Microbiol Biotech 28:345–349
13. Edwards RA, Helm RA, Maloy SR (1999) Increasing DNA transfer efficiency by temporary inactivation of host restriction. Biotechniques 26:892–898

Chapter 183
Neutralization of the Residual Alkaline Solution of Chitosan with CO_2 Gas

Ainan Guo, Shiru Jia, Yujie Dai, Peipei Han, Guojuan Xu, Xintong Zheng and Yanyan Li

Abstract Chitin is converted into chitosan by deacetylation in concentrated sodium hydroxide. Therefore, there is residual lye attached to the surface of chitosan that should be neutralized. In this study, CO_2 was used to neutralize the residual alkali under different pressures, instead of washing with water. The results demonstrated that the neutralization of NaOH residue with CO_2 for the process of deacetylation of chitin is advantageous over the water-washing method. It only took 1 h to neutralize NaOH under 4 MPa and 100 rpm/min, which saved much time compared with 5 h of the water-washing method. In addition, the consumption of water was one fifth that of water-washing method, thus it could save about 80 % of water. Loss rate of chitosan after neutralization was less than half of washing. On the whole, it reduced the consumption of time, manpower, water resource, and cost. It was easy and simple to handle and facilitated the large-scale production.

Keywords Chitosan · Deacetylation · Residual lye · CO_2 gas · Neutral pH

183.1 Introduction

Besides cellulose, chitin is the most abundant natural organic compound on the earth [1, 2]. It is not only the major component of the carapaces, crusts, and shells of crustaceans such as shrimps, crabs helminths, and insects, but also an ingredient of cell walls in fungi and yeast [3, 4]. Chitin is a linear polymer consisting mainly of β-(1,4)-linked 2-acetamido-2-deoxy-β-D-glucopyranose units and partially of β-

A. Guo · S. Jia (✉) · Y. Dai · P. Han · G. Xu · X. Zheng · Y. Li
College of Biotechnology, Tianjin University of Science and Technology, Tianjin 300457, People's Republic of China
e-mail: jiashiru@tust.edu.cn

T.-C. Zhang et al. (eds.), *Proceedings of the 2012 International Conference on Applied Biotechnology (ICAB 2012)*, Lecture Notes in Electrical Engineering 251,
DOI: 10.1007/978-3-642-37925-3_183,

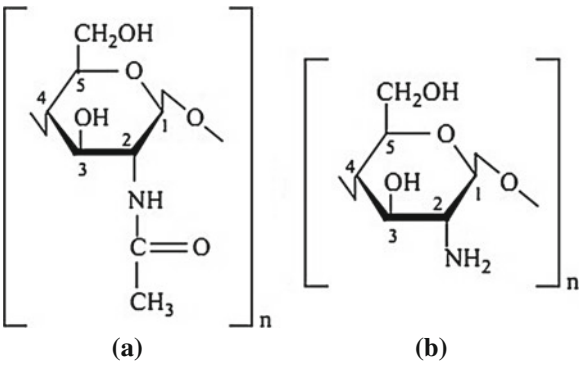

Fig. 183.1 The chemical structures of chitin (**a**) and chitosan (**b**)

(1,4)-linked 2-amino-2-deoxy- β-D-glucopyranose. Therefore, chitin is insoluble in water and common organic solvents and it only dissolves in specific solvents such as N,N-dimethylacetamide (DMAc)-LiCl, hexafluoroacetone, or hexafluoro-2-propanol [5–7].

When the degree of deacetylation (DDA) of chitin reaches more than 50 %, it becomes soluble in acidic aqueous solutions and is called chitosan [8]. Chitosan is one of the vast, renewable, nontoxic, and biodegradable carbohydrate polymers [9]. It is the only cationic alkaline polysaccharose so that it has been widely used in food, pharmaceutics, biomaterials, cosmetics, textiles, and environmental protection industries [3, 10–15]. The chemical structures of chitin and chitosan are shown in Fig. 183.1 [16].

There are three steps in the preparation of chitosan, and that is, demineralization, deproteinization, and deacetylation [17]. In traditional technology, concentrated solution of NaOH is usually used for the deacetylation, which is necessary in the preparation process of chitosan, and a lot of alkaline waste water is generated in this process [18]. Furthermore, there is residual lye attached to the surface of chitosan that should be neutralized to facilitate subsequent operations. In conventional process, distilled water is normally used to wash off the residual lye attached to chitosan, which costs a lot of water and time [19, 20]. Chitosan is insoluble in water and alkaline solution, but soluble in dilute acid solution, so acid solution can not be directly added to neutralize residual lye [21]. Therefore, it is significant to find a better way to remove residual lye instead of washing.

In this study, a new way was applied to solve these problems, which was to neutralize the residual alkaline solution from the deacetylation process with CO_2 gas until chitosan became neutral pH.

183.2 Materials and Methods

183.2.1 Materials

All of the reagents used were of analytical purity, and the distilled water was used for all reagent solution. Chitin was isolated from fly pupal derived from Agricultural and Sideline Products Purchasing Station of Puyang (China). The high pressure reactor was purchased from Petroleum Scientific Research Instrument Factory of Haian County (China).

183.2.2 Extraction of Chitin

Demineralization: 5 % HCl dilute solution with the weight ratio of 1:10 to fly pupal was used to remove the mineral substances, especially Ca^{2+}. Raw materials were crushed and heated for 2 h in boiling water bath together with dilute HCl solution. Then the resulting solid was washed to neutral pH with distilled water.

Deproteinization: Deproteinization of chitin was carried out using 5 % NaOH solution with the weight ratio of 1:10 to fly pupal, and heating for 2 h in boiling water bath. Then the resulting solid was washed with distilled water until neutral pH.

183.2.3 Preparation of Chitosan

The chemical reaction for the preparation of chitosan was given as follows:

$$(\mathrm{R-NHCOCH_3})n + x\mathrm{NaOH} \rightarrow (\mathrm{R-NHCOCH_3})n - x + (\mathrm{R-NH_2})x + x\mathrm{CH_3COONa} \quad (1)$$

50 % NaOH solution with ten times of the chitin weight was added to chitin treated as the method described above, and then heated for 2 h in boiling water bath. The mixture was separated by centrifuge, and supernatant lye was prepared for next deproteinization, the resulting solid was chitosan.

183.2.4 Neutralization of the Residual NaOH

A small fraction of distilled water was added to chitosan to create a liquid environment to avoid solid Na_2CO_3 generated from neutralization attaching to the surface of chitosan. After measuring pH and conductivity of the samples, CO_2 was

introduced into the high pressure reactor and kept the pressures of 1, 2, 3, and 4 MPa, respectively and the stirring speed was 100 rpm/min. The pH and conductivity of samples were measured again after the introduction of CO_2 for a certain period of time until chitosan got to neutral pH. Na_2CO_3 and $NaHCO_3$ were generated from neutralization reaction, which resulted in the increase of conductivity. Therefore, the solid was washed with distilled water until conductivity was steady, which meant that Na_2CO_3 and $NaHCO_3$ were almost removed, and the consumption of water was calculated. Then chitosan was dried by lyophilization to the constant weight.

Distilled water was used to wash NaOH in the control group. Relevant parameters of two methods were compared. All the results presented were the mean value of three replicates.

183.3 Results and Discussion

183.3.1 Washing Times and Water Consumption of the Control Group

Traditionally, concentrated NaOH solution is usually used for the deacetylation of chitin, and there is residual lye attached to the surface of chitosan. Therefore, distilled water is used to remove NaOH. In this study, pH and conductivity were used to monitor the NaOH remnants of the control group (shown in Fig. 183.2). pH and conductivity of samples decreased as the increase of washing times. The pH and the conductivity of samples were close to that of distilled water after 15 times of washing. Finally, the conductivity of distilled water was 7.17 and 0.447 mS/cm, respectively. The total consumption of water was 3,200 mL and a

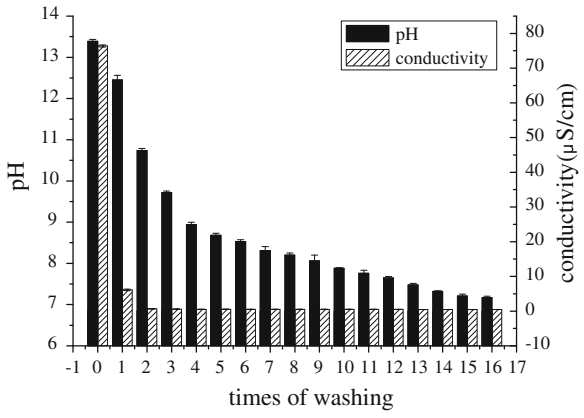

Fig. 183.2 Changes of pH and conductivity of the control group by distilled water washing

large number of alkaline waste water needed to deal with. In addition, a part of samples were lost in the process of washing for many times.

183.3.2 NaOH Neutralization of Treatment Groups Under Different Pressures

In treatment groups, CO_2 was introduced to neutralize NaOH. The pH and treatment time under different pressures were shown in Table 183.1. It can be seen that the reaction velocity raised and the neutralization time reduced with pressure increasing. It only took 1 h under 4 MPa and 100 rpm/min when samples became neutral pH, which saved a lot of time compared with 5 h of the washing method.

183.3.3 Washing Times and Water Consumption of the Treatment Groups

Figure 183.3 presented the change of conductivity of treatment groups (neutralized under different pressures) with washing times. It showed that the conductivity of samples declined after neutralization with CO_2, because OH^- was neutralized by CO_2. However, HCO_3^- and CO_3^{2-} were produced in neutralization so that the conductivity was still higher. These anions and some cations (for example, Na^+) should be washed off and the conductivity was monitored as the indicating factor of the washing effect. The conductivity significantly declined with washing times and was close to that of distilled water, which implied that there are nearly no carbonate left for the prepared chitosan. It only cost about 600 mL water, which was much less than that of the control group. The conductivities under different pressures were similar.

Table 183.1 The pH and time of treatment groups under different pressures

	Pressure (MPa)	Time (h)	Stirring speed (rpm/min)	Original pH	Final pH
Group 1	1	2.5 ± 0.141	100	13.47 ± 0.014	7.17 ± 0.016
Group 2	2	2.0 ± 0.106	100	13.52 ± 0.035	7.12 ± 0.050
Group 3	3	1.5 ± 0.086	100	13.42 ± 0.031	7.18 ± 0.028
Group 4	4	1.0 ± 0.099	100	13.49 ± 0.028	7.15 ± 0.042

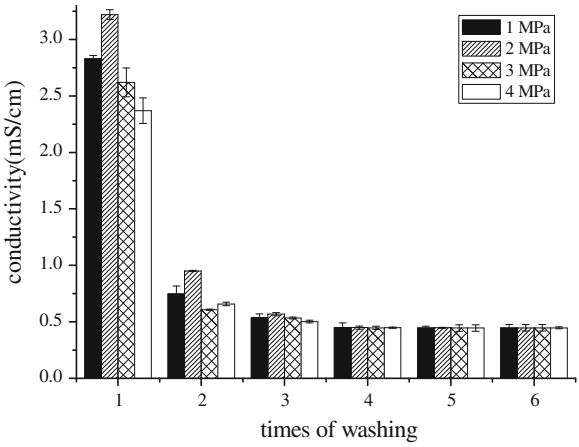

Fig. 183.3 The change of the conductivity of treatment groups with washing times

183.3.4 Effect of Two Methods on Chitosan Loss Rate

As shown in Fig. 183.4, chitosan loss rate of the control group (0 MPa) was compared with that of treatment groups (1–4 MPa). In the control group, it needed to wash samples and separate the solid chitosan from the mixture time and time, which resulted in the loss of samples. A part of chitosan was lost in the process.

In the control group, loss rate of chitosan was over 50 % while it was about 25 % for the treatment groups under 1, 2, 3, and 4 MPa, respectively and it was less than half of the control group. The yield of chitosan was less influenced by different pressures.

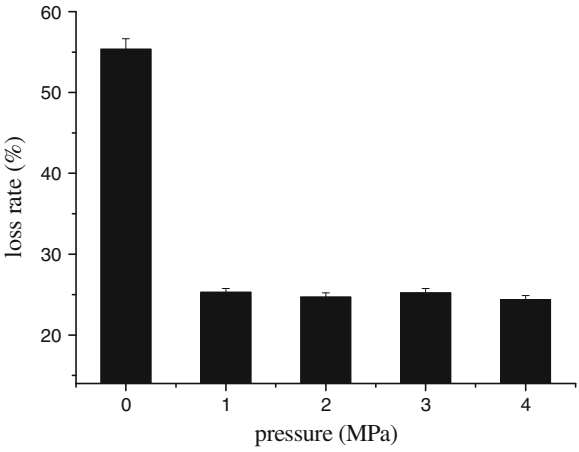

Fig. 183.4 Chitosan loss rate of the control group (0 MPa) and treatment groups (1–4 MPa)

183.4 Conclusion

This study demonstrated that the neutralization of NaOH residue with CO_2 for the process of deacetylation of chitin was advantageous over the water-washing method. It only took 1 h to neutralize the chitosan under 4 MPa and 100 rpm/min, which made much time saved compared with 5 h of the water-washing method. In addition, the consumption of water was only one fifth that of water-washing method, thus it could save about 80 % of water. Loss rate of chitosan after neutralization was less than half of water-washing method. On the whole, it reduced the consumption of time, manpower, water resource, and cost. It was easy and simple to handle and facilitated the large-scale production. It provided us with a sustainable developing way of the chitosan preparation that not only improved the economic development in a benign direction, but also protected the environment.

Acknowledgments This work was supported by program for Changjiang Scholars and Innovative Research Team in University (IRT1166).

References

1. Muzzarelli RAA, Jeuniaux C, Gooday GW (1986) Chitin in nature and technology. Plenum Publishing Corporation, New York
2. Roberts GAF (1992) Chitin chemistry. Macmillan Press, London, pp 85–91
3. Rinaudo M (2006) Chitin and chitosan: properties and application. Prog Polym Sci 31:603–632
4. Bowman SM, Free SJ (2006) The structure and synthesis of the fungal cell wall. BioEssays 28:799–808
5. Jolanta KC, Małgorzata K, Zbigniew B et al (2010) Application of spectroscopic methods for structural analysis of chitin and chitosan. Mar Drugs 8:1567–1636. doi:10.3390/md8051567
6. Austin PR (1988) Chitin solutions and purification of chitin. Methods Enzymol 161:403–407
7. Kurita K (2001) Controlled functionalization of the polysaccharide chitin. Prog Polym Sci 26:1921–1971
8. Al Sagheer FA, Al-Sughayer MA, Muslima S et al (2009) Extraction and characterization of chitin and chitosan from marine sources in Arabian Gulf. Carbohyd Polym 77:410–419
9. Marguerite R (2006) Chitin and chitosan: properties and applications. Prog Polym Sci 31:603–632
10. Wu Y, Pingjia Y, Yuanan W et al (2008) An innovative method for preparation of acid-free-water-soluble low-molecular-weight chitosan (AFWSLMWC). Food Chem 108:1082–1087
11. Shahidi F, Arachchi JKV, Jeon YJ (1999) Food applications of chitin and chitosans. Trends Food Sci Tech 10:37–51
12. George M, Abraham TE (2006) Polyionic hydrocolloids for the intestinal delivery of protein drugs: Alginate and chitosan—a review. J Control Release 114:1–14
13. Khor E, Lim LY (2003) Implantable applications of chitin and chitosan. Biomaterials 24:2339–2349
14. Knorr D (1991) Recovery and utilization of chitin and chitosan in food processing waste management. Food Technol-Chicago 45:114–122

15. Rashidova SSh, Milusheva RYu, Voropaeva NL et al (2004) Isolation of chitin from a variety of raw materials, modification of the material, and interaction its derivatives with metal ions. Chromatographia 59:783–786
16. Paulino Alexandre T, Simionato Julliana I, Garcia Juliana C et al (2006) Characterization of chitosan and chitin produced from silkworm crysalides. Carbohyd Polym 64:98–103
17. Domard A (2011) A perspective on 30 years research on chitin and chitosan. Carbohyd Polym 84:696–703
18. Chang KL, Tsai G, Lee J et al (1997) Heterogeneous N-deacetylation of chitin in alkaline solution. Carbohyd Res 303:327–332
19. Suntornsuk W, Pochanavanich P, Suntornsuk L (2002) Fungal chitosan production on food processing by-products. Process Biochem 37:727–729
20. Chang KL, SeonJeong K, Sun IK et al (2006) Preparation of chitosan microfibres using electro-wet-spinning and their electroactuation properties. Smart Mater Struct 15:607–611
21. Thome JP, Van Daele Y (1986) Adsorption of polychlorinated biphenyls (PCB) on chitosan and application to decontamination of polluted stream waters. In: Muzzarelli R, Jeuniaux C, Gooday GW (eds) Chitin in nature and technology. Plenum Press, New York, pp 551–554

Chapter 184
Study on Method for Cooking Wheat Straw Pulp at Atmosphere by Microwave Radiation Mixed-Alkali Method

Yu Deng and Zhimin Zhang

Abstract Cooking method of wheat straw pulp was investigated at ambient pressure by using microwave radiation alkali. Under the given microwave irradiation conditions, wheat straw was cooked with mixed-alkali. Single-factor and orthogonal experiments were applied to obtain the most favorable pulping conditions: 18 % of alkali, 1/6 of solid/liquid ratio, and 45 min of microwave heating time. Paper performance tests showed equal or better results from our paper product compared with those produced by conventional methods. A consistent yield (around 60.1 %) of wheat straw pulp was observed after repeated experiments.

Keywords Wheat straw · Microwave radiation · Pulp · Mixed-alkali

184.1 Introduction

In the papermaking industry, wood is the main and most common source. The large amounts of wood used to manufacture paper had raised severe supply problems, and led to many experts focused on searching for new raw materials. The output of pulp from non-wood plants has increased from 7 to 12 % of the total pulp output since the 1970s, which is two to three times higher than that of pulp from traditional wood raw materials. Our country has a large number of non-wood plant fibers that can be used for papermaking, most of which are annual plants that

Y. Deng · Z. Zhang (✉)
College of Material Science and Chemical Engineering, Tianjin University of Science and Technology, Tianjin 300457, People's Republic of China
e-mail: happyzzm@126.com

Y. Deng
Tianjin Key Laboratory of Pulp & Paper, Tianjin University of Science and Technology, Tianjin 300308, People's Republic of China

T.-C. Zhang et al. (eds.), *Proceedings of the 2012 International Conference on Applied Biotechnology (ICAB 2012)*, Lecture Notes in Electrical Engineering 251,
DOI: 10.1007/978-3-642-37925-3_184,

develop their full fiber potential in one growing season. As crop by-products, wheat straw has been mostly burned, which pollutes the environment and wastes resources. Hence, to use wheat straw for pulp papermaking is a good method for making good use of the common resources and for reducing pollution; therefore the research on wheat straw pulp has profound meaning. The microwave can make heating a quick and uniform processs, what is more, it can greatly reduce the material handling time. The pulp and paper industry needs a large number of steam heating slurries and dry paper, the heating effect of the microwave can become an energy saver in a potential good way [1, 2].

184.2 Experimental

184.2.1 Experimental Equipment, Materials, and Chemicals

Materials and chemicals: wheat straw was supplied by pulp and paper laboratories from Tianjin University of Science and Technology. Anhydrous sodium sulfite, sodium hydroxide, concentrated sulfuric acid, potassium iodide, and hyposulphite were purchased from Tianjin Chemical Reagent Factory, AR.

Instruments: NJL07-3-type microwave oven was produced by Nanjing JieQuan, Valley Beater, ZQJ-B sheet machine, shawboll-style tensile strength determinator, Elmendorf-style tear tester, GeerLai-air permeability instrument.

184.2.2 Experimental Process [3–5]

The experimental process was conducted according to the method from Chen Peirong [6]. The process on wheat straw pulping by combining microwave with mixed-alkali at atmosphere was as follows: microwave cooking at atmosphere → filtering → cleaning. Slurry was washed clean after untwining by standard fiber untwining machine, followed by the procedure of moisture equilibrium; then the yield and hardness were tested, and subsequently, beating and papermaking, testing physical properties were carried out.

184.2.3 Raw Material Pretreatment

The alkaline pulping process with microwave radiation was as follows: first remove ear, skin, and junction for air-dried wheat straw, and break into 2–3 cm pieces. Then mix all the samples and equilibrate water in an airtight vessel. Experiments and analysis were conducted after all treatments.

184.2.4 Microwave Pulping

2 g of dry wheat straw was cooked in a 200 ml conical flask. The following experiments were conducted in a certain liquid ratio and the application of different microwave powers by adding different quantity of NaOH, in order to mix wheat straw with physic liquor, the flask was shaken after every 5 min. During the experiment, the microwave power was modulated to keep a maximum cooking temperature of 100 °C, slurry was separated from black liquor after microwave radiation. The experiment was repeated twice under the same conditions.

184.2.5 Detection

184.2.5.1 Determination of Wheat Straw Raw Material Components

The analysis methods of the main components of wheat straw were carried out based on the methods from Liu Shucha [7]. The results are shown in Table 184.1.

184.2.5.2 Determination of Pulp Hardness

Pulp hardness was determined by the analysis of potassium permanganate value.

Potassium permanganate value of pulp was defined as the volume (ml) of potassium permanganate solution (0.02 M (0.1 equivalent)) consumed by 1 g of dry pulp under certain conditions, using equation:

$$\text{potassium permanganate value} = (V_1 - V_2)/G$$

Table 184.1 The component content of wheat straw

Components	Content (%)
Water	6.57
Cool water extractive	10.36
Hot water extractive	18.20
1 % NaOH extractive	46.13
Benzene-alcohol extractive	1.99
Holocellulose	71.37
Cellulose	38.76
Klason lignin	15.90

V_1 added liquid volume of 0.02 mol/l potassium permanganate, ml
V_2 consumed liquid volume of 0.1 mol/l sodium thiosulfate in titration process, ml
G the absolute dry slurry weight, g

184.2.5.3 Post Treatment and Performance Test

Yield of coarse pulp: The cooked wheat straw pulp was weighed after it was purified by spilling over, scrubbing, pumping filtration, and seasoning.

Beating: The resulting pulp was beaten by Valley beater.

Sheet: Using ZQJ-B sheet machine, and rapid sheet according to Kaiser forming method.

Measurement of breaking length: Using Shawboll-style tensile strength determinator to determine breaking length of sheet.

Measurement of tearing strength: Using Elmendorf-style tear tester to determine tearing strength of paper.

Measurement of air permeability: Using GeerLai-air permeability instrument to determine.

184.3 Results and Discussion

184.3.1 Single-Factor Experiments

Cooking of wheat straw by mixed anhydrous sodium sulfate and sodium hydroxide with microwave radiation is a complex and multiphase reaction system consisting of gas, liquid, and solid. The amount of mixed solution, solid–liquid ratio, microwave radiation power, radiation time, and alkali concentration had significant impact on the reaction rate and alkaline pulping results. The effects of microwave radiation power, radiation time, solid–liquid ratio, amount of mixed alkali as four main factors were detected.

(1) Effect of Microwave Radiation Time on Pulping

20 % of total alkali content, 8/1 of Na_2SO_3, and NaOH-use ratio, 750 W of power, 1/6 of solid–liquid ratio, 5 g of wheat straw. The results are shown in Table 184.2.

Table 184.2 Effect of microwave radiation time on pulping

Time/min	30	45	60	75	90
Hardness	24.0	23.5	23.5	23.0	22.5
Yield (%)	36.0	37.0	37.5	37.0	34.6

Table 184.3 Effect of microwave radiation power on pulping

Power/W	350	450	550	650	750
Hardness	21.0	21.5	22.0	23.0	23.5
Yield (%)	32.2	33.4	36.0	37.3	35.5

As shown in Table 184.2, microwave radiation time had little effect on the hardness, the yield of wheat straw pulp increased and then deceased with microwave radiation time increasing, the highest yield was given at 60 min, from the viewpoint of energy saving, we deduced that it was more appropriate to control time around 45 min.

(2) Effect of Microwave Radiation Power on Pulping

20 % of total alkali content, 8/1 of Na_2SO_3, and NaOH-use ratio, microwave radiation time was 45 min, 1/6 of solid-liquid ratio, 5 g of wheat straw, the results are shown in Table 184.3.

As can be seen from Table 184.3, with the power increasing, the yield and hardness of pulp gradually increased. The yield was maximum when power was 650 W, while the change was not obviously for hardness. It increased slightly at 650–750 W, so it was more appropriate when radiation power was 650 W.

(3) Effect of Ratio of Na_2SO_3 and NaOH on Pulping

20 % of total alkali content, 45 min of radiation time, 650 W of power, 1/6 of solid–liquid ratio, 5 g of wheat straw, the results are shown in Table 184.4.

Derived from Table 184.4, with the Na_2SO_3/NaOH ratio decreasing, the hardness of pulp increased and then decreased, the maximum hardness was present at 16/2, which revealed that NaOH had great effect on the separation of lignin. In contrast, the yield of wheat straw pulp decreased gradually; it decreased slightly in the range from 17/1 to 13/5. Therefore, the usage of Na_2SO_3 and NaOH was controlled at around 17/1–16/2.

(4) Effect of Total Alkali Content on Pulping

8/1 of Na_2SO_3 and NaOH-use ratio, 45 min of radiation time, 650 W of power, 1/6 of solid–liquid ratio, 5 g of wheat straw, the results are shown in Table 184.5.

Derived from Table 184.5, with total alkali content increasing, the hardness of wheat straw pulp increased gradually. When total alkali content was over 18 %,

Table 184.4 Effect of ratio of Na_2SO_3 and NaOH on pulping

Ratio	17/1	16/2	15/3	13/5	11/7	9/9
Hardness	21.0	26.0	25.0	21.0	22.0	21.5
Yield (%)	45.1	45.0	40.8	39.0	32.8	23.2

Table 184.5 Effect of total alkali content on pulping

Total alkali content (%)	16	17	18	19	20
Hardness	22.0	23.0	26.0	24.5	23.5
Yield (%)	39.0	40.0	45.0	43.0	35.5

Table 184.6 Effect of solid–liquid ratio on pulping

Ratio of solid to liquid	1/3	1/4	1/5	1/6	1/7
Hardness	26.0	25.0	24.0	23.5	20.0
Yield (%)	28.9	31.2	34.6	35.5	37.3

the hardness reduced gradually. Meanwhile, the yield of wheat straw pulp had the same trend with hardness, the maximum was given at 18 %. The results showed that 18 % of total alkali content was better.

(5) Effect of Solid–Liquid Ratio on Pulping

18 % of total alkali content, 8/1 of Na_2SO_3 and NaOH-use ratio, radiation time was 45 min, 5 g of wheat straw, the results are shown in Table 184.6.

Seen from Table 184.6, with the solid–liquid ratio increasing, the hardness of wheat straw pulp decreased gradually, while the yield tendency of wheat straw pulp was opposite under the same reaction condition; the yield increased slightly when the ratio was around 1/5–1/7, so it was better to choose a relatively smaller solid–liquid ratio. That means, to around 1/5–1/6 when feasible.

184.3.2 Orthogonal and Verification Experiments on Mixed-Alkali Pulping

184.3.2.1 Orthogonal Experiment

Orthogonal experiment was designed based on single-factor experiments, the results are shown in Table 184.7.

To optimize the technological conditions, orthogonal test was designed based on four factors and three levels, the L9(3^4) orthogonal table is chosen, factors and their levels are listed in Table 184.8.

As shown in Table 184.8, the effects of main factors on the yield were as follows: solid/liquid ratio > radiation time > total alkali content > Na_2SO_3/NaOH ratio, and the optimum conditions determined by calculation were 18 % of total alkali content, 8/1 of Na_2SO_3/NaOH ratio, 1/6 of solid–liquid ratio, microwave radiation time was 45 min.

Table 184.7 Ingredient level list

No.	A/ Microwave irradiation time (min)	B/ The ratio of solid to liquid	C/ Na_2SO_3/ NaOH	D/ Total alkali content (%)
1	25	1/4	17/1	16
2	35	1/5	16/2	18
3	45	1/6	15/3	20

Table 184.8 Orthogonal analysis list

No.	A/ Radiation time (min)	B/ The ratio of solid to liquid	C/ Na_2SO_3/ NaOH	D/ Total alkali content (%)	Yield (%)
1	1	1	1	1	19.8
2	1	2	2	2	36.4
3	1	3	3	3	34.4
4	2	1	2	3	22.0
5	2	2	3	1	30.0
6	2	3	1	2	34.4
7	3	1	3	2	31.6
8	3	2	1	3	38.2
9	3	3	2	1	42.2
K1j	90.6	73.4	92.4	92	K1j + K2j + K3j = 289
K2j	86.4	104.6	100.6	102.4	
K3j	112	111	96	94.6	
K1j/3	30.2	24.47	30.8	30.67	
K2j/3	28.8	34.87	33.53	34.13	
K3j/3	37.33	37	32	31.53	
R	8.53	12.53	2.73	3.46	

Note the radiation power was 650 W

184.3.2.2 Verification Experiments

18 % of total alkali content, 8/1 of Na_2SO_3/NaOH ratio, 1/6 of solid–liquid ratio, microwave radiation time was 45 min, microwave power was 650 W. Under the optimum process conditions, the experiments were repeated 11 times. The results showed that the yield of wheat straw pulp could be stabilized at around 59–60 % (Fig. 184.1, Table 184.9).

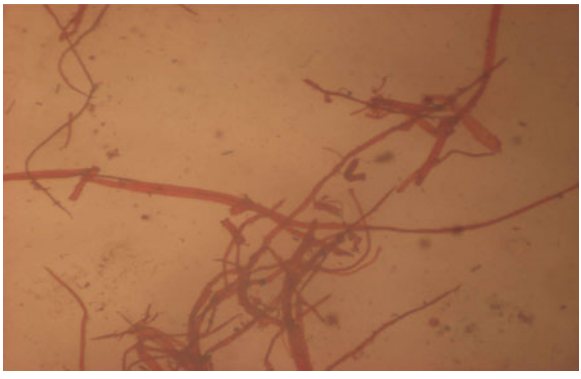

Fig. 184.1 The picture of wheat straw pulp fiber by microscope after microwave treatment

Table 184.9 Verification experiments

No.	1	2	3	4	5	6	7	8	9	10	11
Yield (%)	60.38	59.25	59.34	60.25	59.00	57.13	66.13	60.88	59.75	59.34	59.75

Table 184.10 Physical properties of microwave radiation pulping

Beating degree (°SR)	Burst index (kPa m^2/g)	Tear index (mN m^2/g)	Air permeability (μm/Pa s)	Tensile index (N m/g)
31	5.16	5.95	31.75	83.72

184.3.3 The Measurement on Physical Properties of Microwave Radiation Pulping at Atmosphere

Pulping (cooking) conditions were: 18 % of total alkali content, 8/1 of Na_2SO_3/NaOH ratio, 1/6 of solid-liquid ratio, microwave radiation time was 45 min, microwave power was 650 W. Pulp samples would be obtained through the PFI beater beating to 31°SR, paper was made by standard sheet former, and physical properties of paper disk were tested after being kept in the laboratory for 4 h with constant temperature and constant humidity.

As shown in Table 184.10, No matter tensile index, tear index, or burst index, all have a high value, which indicated microwave radiation pulping had good physical properties.

184.4 Conclusion

(1) Effects of main factors on the yield of pulping by microwave radiation are as follows: solid/liquid ratio> radiation time > total alkali content > Na_2SO_3/NaOH ratio. The optimal conditions defined by experiment are: 18 % of total alkali content, Na_2SO_3/NaOH ratio of 8/1, solid/liquid ratio of 1/6, 45 min of microwave heating time. Under the optimum conditions, the yield of wheat straw pulp can reach to 59–60 % or so.

(2) The tensile index, tear index, and burst index of the pulp which was obtained by microwave radiation in optimal conditions all had relatively higher values, embodying the better physical properties, which indicated pulping by microwave radiation has favorable maneuverability at atmosphere.

Acknowledgments Project source: National Natural Science Foundation 20976136.

References

1. Xiao ZF, Chen MD, Han GZ (2008) Research progress of mass transfer enhancement by electromagnetic field. Chem Ind Eng Pro (China) 12:1911–1913
2. Ma KJ (2009) Advances in physical fields used to enhance processes of chemical engineering. Mod Chem Ind 3:27–30
3. Zhang YJ (2010) Kraft pulping of bamboo under ultrasonic treatment. J Qd Univ Sci Technol (Nat Sci Ed) 3:262–264
4. Zhang JW, Deng Y (2010) Microwave-assisted detection method of 1% NaOH extraction. Pap Pap Mak 29:66–68
5. Li JY, Shao Q, Deng Y (2004) Application of microwave radiation technique on plant fiber bleaching. Chin Pul Pap 7:1–3
6. Chen PR (1987) Pulp and paper experiment
7. Liu SC (2003) Pulp and paper analysis and detection

Chapter 185
Biologic Chromatography for Purifying Filamentous Fungi Contaminated with Bacteria

Jianping Zhang and Feifei Sun

Abstract A method for purifying contaminated filamentous fungi was introduced and its theoretical background and application were discussed. The instrument mainly consists of a purification cup, a collection layer for the fungi, and the purification column. The steps for the assembly of the purification device include the initial preparation of the purification column, the addition of the fungal culture solution into the porous materials, and the use solid medium to create a collection layer for the purified fungi. The faster growth of the fungi compared with the bacteria, i.e., the fungi grow out of purification column into the fungal collection layer, while the bacteria stay in the purification column, which effectively purifies the contaminated fungi.

Keywords Bacteria · Biologic chromatography · Contamination · Filamentous fungi · Purity

185.1 Introduction

Microbes, such as bacteria and fungi often coexist naturally [1]. However, purified and single microbial species are often needed for scientific research and production and it is the prerequisite to all work [2, 3].

Bacteria and spore-forming filamentous fungi are easier to purify in two steps. First, the mixed microorganisms are dispersed by agitating their solution, and they

J. Zhang (✉)
School of Biology and Chemical Engineering, Jiangsu University of Science and Technology, Zhenjiang 212018, People's Republic of China
e-mail: zjpagrer@163.com

F. Sun
The Sericulture Research Institute, Chinese Academy of Agriculture Sciences, Zhenjiang 212018, People's Republic of China

T.-C. Zhang et al. (eds.), *Proceedings of the 2012 International Conference on Applied Biotechnology (ICAB 2012)*, Lecture Notes in Electrical Engineering 251,
DOI: 10.1007/978-3-642-37925-3_185,

are diluted tenfold into different concentrations. Second, the mixture is spread onto plates, cultured, and the purified bacteria or filamentous fungi are obtained from the individual colonies that form from single cells [1, 4]. The condition for getting the purified target microbes is based on their comparatively larger number in the sample and the capacity to be dispersed. Special culture condition is often used and the selective media is most frequently applied among them [5–10].

By contrast, purifying non-spore forming filamentous fungi heavily contaminated with bacteria, which fasten tightly to the mycelia, is difficult. It was often found that the filamentous fungi preserved preciously were contaminated with bacteria and the strains would be lost if not being purified effectively. Normally, it is not effective for antibiotics and selective media to be used to purify filamentous fungi.

Chromatography is normally used for isolating compounds [11]. However, this technique has not been used for purifying biomaterial such as microorganisms contaminated with other microorganisms. This research aims to apply chromatography in the purification of filamentous fungi.

185.2 Materials and Methods

185.2.1 Filamentous Fungi

Sphaeropsis sapinea contaminated with bacteria.

185.2.2 Structure of the Purification Device

The biologic purification device consists of the following eight parts as shown in Fig. 185.1.

185.2.3 Assembly of the Purification Device

Classical solid potato dextrose agar (PDA) medium was used to culture the fungi and bacteria [12]. Potatoes were peeled and cut into 0.5–1.0 cm cubes. Water was added to the potato cubes at a ratio of 1:5 (w/w) and boiled for 30 min. The resulting mixture was filtered and water was added to reach the previous water level. The potato extract solution, glucose, and agar were mixed at a ratio of 100:2:1.5 (w/w). The resulting mixture was then used as the fungal culture medium.

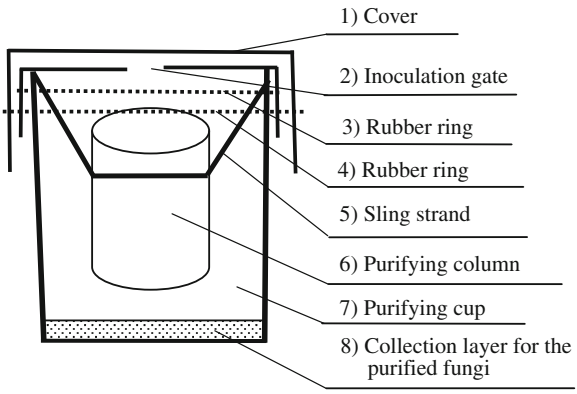

Fig. 185.1 Structure of the purification device

Fungal culture solution (PD) was prepared similar to the PDA medium, but without the agar.

Columns of desiccated tree branches with diameters smaller than the purifying cup were placed in PD for 24 h at 4 °C. Then, the branches were wrapped with plastic except the top and the bottom of the column to allow the fungi to grow from the top and out of the bottom of the column.

The collection layer for the purified fungi was placed into a purifying cup (glass beaker). Galvanized iron wire (gauge 20 to gauge 22) was used to attach the purification column. The purification column was suspended vertically in the glass with a space of about 0.5–2 cm in the purifying cup. The cup was covered with two layers: the outside cover consisted of 6–8 layers of cotton gauze or tissue-sealing film; the inner layer made of plastic film has a 1–2 cm diameter hole that acts as the inoculating gate. The covers are fastened with rubber rings. The instrument was placed vertically in a sterilizer culture was incubated

cultured with shaking

112–115 °C for 30 min. After cooling, the instrument was refrigerated for future use.

185.2.4 Purification

After the outside layer of the cover was opened, the unpurified fungi were inoculated onto the purification column via the inoculating gate. The outside layer of the cover was then replaced and the culture was incubated at 20–25 °C. When the fungi grew out of the bottom of the purifying column, the fungi were collected and saved. This procedure was performed aseptically.

185.2.5 Examination of Purifying Effect of the Filamentous Fungi

The above purified mycelia were inoculated into bouillon culture medium and cultured with shaking at 20–25 °C. If the medium remained transparent, the medium of the filamentous fungi was free from bacteria. Otherwise, the purified mycelia still carried bacteria.

185.3 Results and Discussion

185.3.1 Purifying Effect of the Filamentous Fungi

After the purified mycelia were inoculated into bouillon culture medium and cultured, the medium remained transparent, which indicated that the purified mycelia were completely free of bacteria.

185.3.2 Mechanism of Isolation and Purification of Filamentous Fungi Contaminated with Bacteria using Biologic Chromatography

The differences in the growth characteristics of fungi and bacteria and the characteristics of the materials that constitute the purification column were the basic factors that controlled the isolation and purification.

The cell growth on the top layer led to the extension of the hyphae of the filamentous fungi. The basal hyphae have a strong ability to absorb water and nutrients and they facilitate the growth of the top cells of the hyphae. Single hyphae extended forward linearly. In this way, the hyphae can span across the interstices on the medium when they grow [13].

The bacterial colonies extended to every direction. The cells in the colony abut against each other but no structure actually connected them. The nutrients required for the growth of the cells were supplied through the penetration of capillary water from the bottom cells on the surface of the medium [13]. Consequently, the bacteria grew along the smooth surface of the medium but not across large spaces.

The bacteria that contaminated the filamentous fungi were located on the surface of the hyphae and did not grow on the hyphae because nutrients and water are absent on the hyphal surfaces. However, when the bacteria grew on the plates, they constantly attached to the growing hyphae, which contaminated the hyphae with bacteria.

The purification column was made of wooden branches that contained xylem fibrocytes which consist of the combination of fiber and lignin and have good water holding potential. However, the surfaces of the fibrocytes were discontinuous and comparatively dry. Instead, the plate surface of medium was smooth and continuous, and had a water membrane on it.

Given the features of the purification column, the bacteria attached to the hyphae of the filamentous fungi stayed in their original location (including the base of the mycelia) and were unable to spread into the column. When the mycelia grew forward quickly, the top of mycelia of the filamentous fungi limited the bacterial growth. Then, the mycelia passed across the space between the purification column and into the fungi collection layer, thereby separating the mycelia of the filamentous fungi.

185.3.3 Comparison with Classical Chromatography Method

Classical chromatography such as liquid chromatography is a technique for separating and purifying mixed chemicals and sometimes single cells. The liquid chromatography consists of a liquid phase and a stationary phase. The stationary phase has different retardance to each element of the mixture of compounds (or even those that include some cells) in the mobile phase, these elements ordinarily pass one after another throughout the column. Consequently, the different compounds or cells can be separated and purified. The amount and type of compound can also be verified for quantitative and qualitative analysis using a detector in the instruments [11].

Biologic chromatography is different from classical chromatography. Using the biologic purification column to separate mixed microbiological samples, the retardance of the purification column functions similar to that in liquid chromatography. The mobile phase of the biologic chromatography is the microbiologic sample itself which grows along the biologic purification column that acts as the stationary phase. The instrument has no detector, so the samples needn't be analyzed quantitatively and qualitatively. Strict aseptic technique is required for the operation.

Several materials are available for making the biotic purification instrument. Other porous materials (such as saw dust) can be used to make the purification column but wooden branches are more convenient. Other requirements, such as selective medium that facilitates the separation of bacteria and fungi, can be chosen for the medium and the culture solution, but this is unnecessary. Beakers and other glassware can be used as purification cups. In addition, the purification column that is made of raw materials needs to be sterilized fully before use to remove preexisting microbes.

185.4 Conclusion

Based on theory of Chromatography and characteristic of filamentous fungi and bacteria in growth and their configuration of cells, the biologic chromatography for purifying filamentous fungi contaminated with bacteria is useful, effective, and easy to operate.

References

1. Ingraham JL, Ingraham CA (2004) Introduction to microbiology: a case history approach, 3rd edn. Wadsworth Publishing Company, California
2. Fang ZD (1998) Plant disease studies, 3rd edn. Chinese Agriculture Publication, Beijing
3. Labeda DP (1990) Isolation of biotechnological organisms from nature, 3rd edn. McGraw-Hill, New York
4. Ørskov J (1922) Method for the isolation of bacteria in pure culture from single cells and procedure for the direct tracing of bacterial growth on a solid medium. J Bacteriol 7(6):537–549
5. Simidu U, Hasuo K (1968) An improved medium for the isolation of bacteria from marine fish. J Gen Micro 52(3):355–360
6. King KW, Smith PH (1955) Comparisons of two media proposed for the isolation of bacteria from the rumen. J Bacteriol 70:726–729
7. Annibale AD, Rosetto F, Leonardi V et al (2006) Role of autochthonous filamentous fungi in bioremediation of a soil historically contaminated with aromatic hydrocarbons. Appl Environ Microbiol 72(1):28–36
8. Burgaud G, Le CT, Arzur D et al (2009) Diversity of culturable marine filamentous fungi from deep-sea hydrothermal vents. Environ Microbiol 11(6):1588–1600
9. Arvanitidou M, Kanellou K, Constantinides TC et al (1999) The occurrence of fungi in hospital and community potable waters. Lett Appl Microbiol 29(2):81–84
10. Eller C, Crabill MR, Bryant MP (1971) Anaerobic roll tube media for nonselective enumeration and isolation of bacteria in human feces. Appl Environ Microbiol 22(4):522–529
11. Fu RN (2005) Chromatography analysis, 2nd edn. Chemical Publication, Beijing
12. Shen P, Chen XD (2007) Microbiology experiment, 4th edn. Highly Educated Publication, Beijing
13. Zhou DQ (2002) Microbiology, 3rd edn. Highly Educated Publication, Beijing

Chapter 186
Cross-Linked Enzyme Aggregates of β-Galactosidase from Different Source by Dialdehyde Starch as Cross-Linker

Kang Wang, Yang Gao, Zhang Wang and Guangying Meng

Abstract The method of using dialdehyde starch (DAS) as cross-linking agent and bovine serum albumin (BSA) as protective agent for preparing β-galactosidase cross-linked enzyme aggregates (CLEAs) was investigated and high activity residue of 53.8 % for *K. lactis* β-galactosidase and 55.2 % for *A. oryzae* β-galactosidase was obtained. Polyethylene glycol 400 as precipitant was applied. The effect of oxidation degree of DAS and amount of bovine serum albumin (BSA) on the activity of CLEAs was discussed. The shape and surface morphology of the CLEAs were examined by SEM. Comparing with *K. lactis* β-galactosidas CLEAs, the *A. oryzae* β-galactosidase CLEAs have higher thermal stability, and better performance on the affinity toward the substrate, which related to the structure of CLEAs. *A. oryzae* β-galactosidase CLEAs was more suitable for lactose hydrolysis in industries.

Keywords β-Galactosidase · Cross-linked enzyme aggregates · Dialdehyde starch · Bovine serum albumin · Lactose hydrolysis

186.1 Introduction

Immobilization method using cross-linking reaction between enzyme molecules is an attractive strategy because it affords stable catalysts with high retention of activity. Cao et al. [1] developed such an approach and named the resulting enzymes as cross-linked enzyme aggregates (CLEAs). The resulting CLEAs proved to be active and recyclable using tens of enzymes [2]. The CLEAs stability

K. Wang (✉) · Y. Gao · Z. Wang · G. Meng
Enzyme Technology Laboratory, Chemical Engineering Research Center, School of Chemical Engineering and Technology, Tianjin University, Tianjin 300072, People's Republic of China
e-mail: wangk72@tju.edu.cn

T.-C. Zhang et al. (eds.), *Proceedings of the 2012 International Conference on Applied Biotechnology (ICAB 2012)*, Lecture Notes in Electrical Engineering 251,
DOI: 10.1007/978-3-642-37925-3_186,

versus temperatures and solvents were highly enhanced [3]. The general approach for CLEAs preparation consists of protein precipitation followed by cross-linking with glutaraldehyde (GA). β-galactosidase is a very important enzyme in the dairy industry that catalyzes the conversion of lactose into glucose and galactose. It has been reported that *Aspergillus oryzae* CLEAs β-galactosidase appeared to be more suitable for lactose hydrolysis applications [4]. However, the CLEAs of β-galactosidase cross-linked by GA showed a low activity residue (13.5 % activity yield) [4]. Mateo et al. [5] reported that the use of dextran polyaldehyde as a cross-linking agent for enzymes results in a significantly lower loss of active sites. The strategy of using a proteic feeder can also be used for preparing active CLEAs (GA as cross-linker) [6]. In order to increase activity residue of CLEAs, β-galactosidase CLEAs were prepared by dialdehyde starch (DAS) as cross-linker and bovine serum albumin (BSA) as protective agent in this paper. Dialdehyde starch (DAS) from the periodate oxidative cleavage of the C(2)–C(3) bond of the anhydroglucose units of starch polysaccharide chains found several industrial applications [7]. The immobilization of urease by DAS improved the adsorption of urea for its hydrolysis that resolved the problem for patients suffering from chronic renal failure (CRF) [8]. Furthermore, β-galactosidase from *K. lactis* and *A. oryzae* in which molecular weight, pH optima, temperature optima, and kinetic parameters that were different was investigated. The properties of CLEAs, such as thermal stability, structure, and hydrolysis ability were discussed.

186.2 Materials and Methods

186.2.1 Materials

Liquid *K. lactis* β-galactosidase (Lactozym Pure 2600L) was purchased from Novozymes Co. *A. oryzae* β-galactosidase was purchased from Sigma Co. USA (Nanjing Huibaishi Biotechnology Co., Ltd, P. R. China). O-nitrophenyl-β-D-galactopyranoside (ONPG) and coomassie brilliant blue G-250 were provided from Shanghai Baoman Biotechnology Co., Ltd. Glucose oxidase–peroxidase kit was offered from Shanghai Rongsheng Biopharmacy Co., Ltd. BSA was obtained from Tianjin Institute of Hematology. Denmark lactose was purchased from Beijing Unique Dairy Technology Business & Trading Co., Ltd, P. R. China. DAS with different oxidation degree were prepared by ourselves using the method of the periodate oxidation reaction of starch. All other chemicals used in this study were of analytical grade.

186.2.2 Preparation of β-Galactosidase CLEAs

4 mL mixture solution of β-galactosidase and BSA was added to 15 ml PEG400 for 15 min at room temperature. After that, 1 mL of 10 % (w/v) DAS solution was added and the solution (20 mL) was kept stirring for 1 h at room temperature. Then the solution was centrifuged at 9,000 rpm for 20 min and the supernatant was decanted from the aggregates. The aggregates formed were washed thoroughly with buffer and used for further studies.

186.2.3 β-Galactosidase Assay

Protein concentration was determined by the dye binding method using BSA as standard protein. Activity of free and immobilized β-galactosidase was estimated by the method using ONPG as substrate. Enzyme activity unit (U) is defined as the amount of enzyme that liberates 1 μmol of o-nitrophenol (ONP) per min under standard assay conditions. The activity of free *K. lactis* β-galactosidase and that of free *A. oryzae* β-galactosidase was 12.56 (U/mg) at 37 °C in pH 6.5 phosphate buffer and 15.71 (U/mg) at 37 °C in pH 4.5 acetate buffer in this study. Thermal stability of CLEAs was compared with that of free enzyme at different temperature and ONPG was applied as substrate. Kinetics of free enzyme as well as CLEAs were assayed by varying the ONPG concentration from 0.8 to 10 g/L. The shape and surface morphology of the CLEAs were examined using electron microscope (HITACHI make, model S-4800, Japan). Samples of CLEAs were freeze-dried prior to analysis. Lactose solution (100 mL, 0.1 M) was independently incubated with soluble and cross-linked β-galactosidase and stirred continuously in water bath for 10 h. The aliquots were taken at different times and assayed for the formation of glucose by using glucose oxidase–peroxidase kit.

186.3 Results and Discussion

Selection of precipitator is very important for preparation of CLEAs by macromolecular cross-linking agent. 1,2-dimethoxyethane (DME) was used as precipitator in works of Mateo et al. [5]. However, DME has certain toxicity. PEG 400 that is gentle and harmless was applied in our study. Moreover, it was found that the cross-link of enzyme aggregates must be carried in precipitator solution due to the low chemical binding rate of DAS, otherwise dissolution again of enzyme aggregates was obviously presented. DAS and PEG400 is good miscible. It was shown form Table 186.1 that the high activity of β-galactosidase aggregates was obtained with the concentration of PEG400 75 % (v/v). The lower concentration of PEG400 was not used due to uncompleted precipitation of protein.

Table 186.1 Activity of β-galactosidase CLEAs

Activity (%)	Free	Precipitation by 75 % PEG	CLEAs by GA	CLEA by DAS	CLEA with BSA (1:8) by DAS
K. lactis β-galactosidase	100	101	4.78	21.8	53.8
A. oryzae β-galactosidase[a]	100	–	13.5	–	–
A. oryzae β-galactosidase[b]	100	143	7.86	25.8	55.2

[a] From Ref. [4]
[b] In this work

Furthermore, the activity of CLEAs was increased by DAS as cross-linker and BSA as protective agent (Table 186.1). Mateo et al. [5] proposed that macromolecular cross-linkers are too large to penetrate into the protein active site and react with catalytically essential amino acid residues. The experimental results indicate that 10 % DAS with 80 % oxidation degree produced high activity residue of CLEAs. Lower concentration or oxidation degree of DAS may lead to uncompletely cross-link while higher concentration or oxidation degree cause the damage of the active site of enzyme by excess of aldehyde groups. When BSA added, the cross-linker will be prior to react with -NH_2 of BSA thus the active site of β-galactosidase protected. The addition of BSA can improve the activity of CLEAs and reaching maximum activity in the ratio of eight. The higher proportion of BSA could make the lower enzyme concentration and the difficult diffusion of substrates leading to the loss of activity.

Moreover, time (0.5–2 h) and temperature (4 °C-room temperature) of cross-link have little influence on the activity of CLEAs. Comparing with stirring at 4 °C for 16 h reported by Mateo et al. [5], operating for 1 h at room temperature was relatively simple.

The pH is one of the major parameters capable of shifting enzymatic activities in aqueous solution. Whether β-galactosidase was from *K. lactis* β-galactosidase or *A. oryzae* β-galactosidase, the optimum pH of CLEAs was decreased (Table 186.2), which was similar to the reported work that the optimum pH of *A. oryzae* β-galactosidase was 4.5 for free enzyme and that of was 3 for CLEAs after cross-linked by GA [4]. However, the change of optimum pH change for system by GA from reference was slightly higher than that by DAS in this work. It was indicated that macromolecular cross-linkers decreased its possible reaction with amino acid residues.

The activity of enzyme strongly depended on temperature. For CLEAs, the optimum temperature was raised and the t1/2 was delayed (Table 186.2). It was demonstrated that the immobilization procedure enhance the temperature resistance of enzyme by protecting the enzymatic configuration and as a result, the CLEAs could work better in tough environment with less loss of activity. Moreover, the ratios of Ed of free enzyme to that of CLEAs were 1.16 times for *K. lactis* β-galactosidase and 2.5 times for *A. oryzae* β-galactosidase respectively

Table 186.2 Characteristics of β-galactosidase CLEAs

Parameters	*K. lactis* β-galactosidase		*A. oryzae* β-galactosidase	
	Free	CLEAs	Free	CLEAs
pH optima	8.0	7.0	4.5	4.0
Temperature optima	30	37	55	60
$t_{1/2}$ (min)	30 (37 °C)	60 (37 °C)	12 (60 °C)	62 (60 °C)
E_d(kJ/mol)	122 (20–40 °C)	105 (20–40 °C)	86 (30–60 °C)	35 (30–60 °C)
K_m (g/L)	0.43	1.92	0.92	1.42
k_{cat} (1/min)	4.47	4.94	8.53	3.18

Note $t_{1/2}$ half-life, E_d inactivation of activation energy, K_m Michaelis constant, k_{cat} catalytic constant

(Table 186.2). It was illustrated that higher thermal stability for *A. oryzae* β-galactosidase CLEAs was obtained by these immobilization method.

Comparing with free enzyme, CLEAs was increased in Km value by 4.47-fold for *K. lactis* β-galactosidase and 1.54-fold for *A. oryzae* β-galactosidase (Table 186.2). It was indicated that the interaction of enzyme and substrate had been weakened after immobilization and *A. oryzae* β-galactosidase CLEAs had a better performance on the affinity towards the substrate than *K. lactis* β-galactosidase CLEAs. Furthermore, kcat of *K. lactis* β-galactosidase CLEAs was closed to that of free enzyme while that of *A. oryzae* β-galactosidase CLEAs was lower than that of free enzyme. These characteristics were related to the structure of CLEAs.

Figure 186.1 shows the SEM micrographs of CLEAs at a magnification of 3000×. The surface morphology of *A. oryzae* β-galactosidase CLEAs showed relatively uniform structure of the enzyme aggregates with numbers of microspheres having 1–2 microns in size, which was different from the irregular massive enzyme aggregates of *K. lactis* β-galactosidase CLEAs. The molecular weight of *K. lactis* β-galactosidase (135 kD) and *A. oryzae* β-galactosidase (90 kD) was 2 times and 1.36 times that of BSA (66 kD) respectively. During precipitation process, a certain degree of separation between *K. lactis* β-galactosidase and BSA would be appeared due to their clear difference of molecular weight, while the system of *A. oryzae* β-galactosidase and BSA would kept relatively uniform owing to their close molecular weight, which led to different shape between *K. lactis* β-galactosidase CLEAs and *A. oryzae* β-galactosidase CLEAs. Furthermore, it was considered that BSA was mainly located outside of *K. lactis* β-galactosidase CLEAs, while homogeneous mixture structure was obtained within *A. oryzae* β-galactosidase CLEAs (Fig. 186.2). Thus affinity between substrate and *K. lactis* β-galactosidase CLEAs was obviously decreased. Chemical cross-link was primarily occurred among molecules of BSA, which induced no significant change of kcat for *K. lactis* β-galactosidase system and the improvement of thermal stability of CLEAs was limited. However, it was the chemical bond between enzyme and BSA for *K. lactis A. oryzae* β-galactosidase CLEAs that the thermal stability was distinctly increased and kcat was obviously decreased.

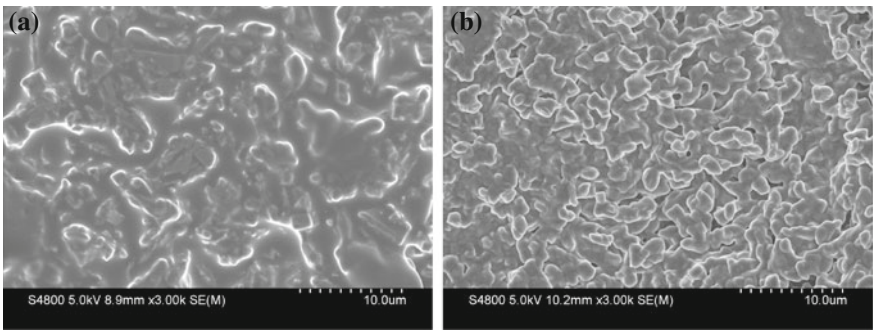

Fig. 186.1 SEM images of CLEAs. **a** *K. lactis* β-galactosidase CLEAs, **b** *A. oryzae* β-galactosidase CLEAs

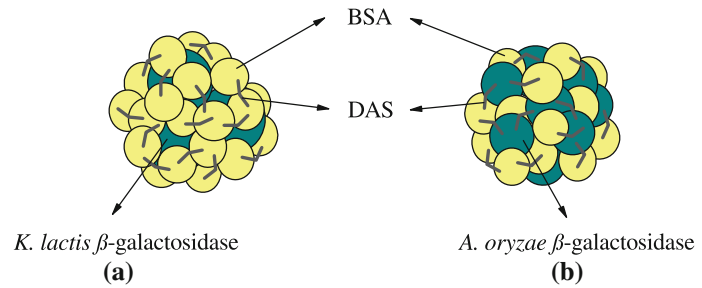

Fig. 186.2 Schematic for structure of CLEAs. **a** *K. lactis* β-galactosidase CLEAs, **b** *A. oryzae* β-galactosidase CLEAs

Figure 186.3 illustrates the hydrolysis of lactose by soluble and cross-linked β-galactosidase. For *K. lactis* β-galactosidase, glucose yield by free enzyme was higher than that by CLEAs within 10 h. However, in case of *A. oryzae* β-galactosidase, opposite results was presented, 900 mg glucose yield by CLEAs was obtained within 9 h, 450 mg glucose yield by free enzyme was appeared within 4 h and the glucose yield increased less after 4 h. It was demonstrated that *A. oryzae* β-galactosidase CLEAs was more suitable for lactose hydrolysis in industries.

It has been reported recently that a high activity residue 78 % was presented by *A. oryzae* β-galactosidase being immobilized on bioaffinity support Con A-cellulose, t1/2 at 60 °C was 35 min for free enzyme and 55 min for immobilized β-galactosidase respectively, and glucose yield by immobilized enzyme was 1.22-fold that by free enzyme within 10 h [9]. In this paper, 55 % activity residue of *A. oryzae* β-galactosidase CLEAs was obtained (Table 186.1), t1/2 at 60 °C was 12 min for free enzyme and 62 min for immobilized β-galactosidase respectively (Table 186.2), and glucose yield by immobilized enzyme was 1.87-fold that by

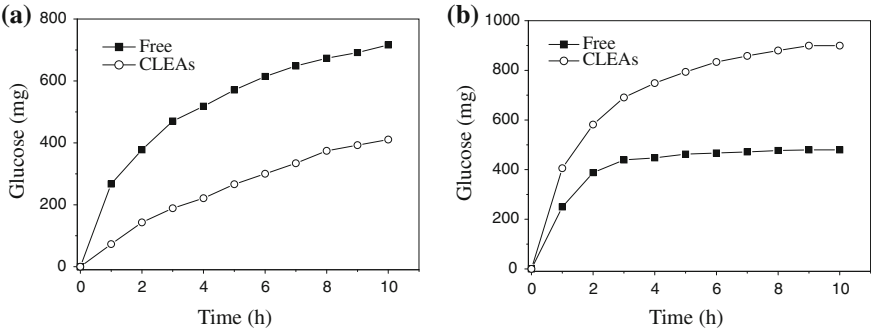

Fig. 186.3 Lactose hydrolysis. **a** *K. lactis* β-galactosidase (0.04 U/ml, pH = 6.5, 37 °C), **b** *A. oryzae* β-galactosidase (0.8 U/ml, pH = 4.5, 60 °C)

free enzyme within 10 h (Fig. 186.3b). Comparison of the literature data, though activity of CLEAs in this work was slightly lower, thermal stability and lactose hydrolysis ability was increased.

References

1. Cao L, Van Rantwijk F, Sheldon RA (2000) Cross-linked enzyme aggregates: a simple and effective method for the immobilization of Penicillin acylase. Org Lett 2:1361–1364
2. Schoevaart R, Wolbers MW, Golubovic M et al (2004) Preparation, optimization, and structures of cross-linked enzyme aggregates (CLEAs). Biotechnol Bioeng 87(6):754–762
3. Sangeetha K, Emilia AT (2008) Preparation and characterization of cross-linked enzyme aggregates (CLEA) of subtilisin for controlled release applications. Int J Biol Macromol 43:314–319
4. Gaur R, Pant H, Jain R et al (2006) Galacto-oligosaccharide synthesis by immobilized *Aspergillus oryzae* β-galactosidase. Food Chem 97:426–430
5. Mateo C, Palomo JM, van Langen LM et al (2004) A new, mild cross-linking methodology to prepare cross-linked enzyme aggregates. Biotechnol Bioeng 86:273–276
6. Shah S, Sharma A, Gupta MN (2006) Preparation of cross-linked enzyme aggregates by using bovine serum albumin as a proteic feeder. Anal Biochem 351:207–213
7. Fiedorowicz M, Para A (2006) Structural and molecular properties of dialdehyde starch. Carbohydr Polym 63:360–366
8. Nakabayashi N, Hasegawa N, Akisawa T (1985) Immobilization of urease to modified dialdehyde-starch with gelatin for removal of urea. Jpn J Polym Sci Technol 42(11):835–839 (Japanese)
9. Ansari SA, Husain Q (2010) Lactose hydrolysis by β-galactosidase immobilized on concanavalin A-cellulose in batch and continuous mode. J Mol Catal B Enzym 63:68–74

Chapter 187
Research Development on Vanadium-Dependent Haloperoxidases in Marine Algae

Tao Wang, Yong-chao Lu, Dong-mei Cao, Shu-bao Gao and Yu-shan Zhang

Abstract The halogenated marine natural products encompass a very wide range of compounds which often have important biological activities or pharmacological properties. The haloperoxidases are thought to be involved in the biosynthesis of these natural products. A new kind of haloperoxidases that contain vanadium in the active site capable of catalyzing halogenation reactions of several substrates have been subsequently isolated from a variety of organisms, particularly in marine algae. Due to their highly chemical and thermal stability, the vanadium-dependent haloperoxidases (vHPOs) attracted more attention in the last few years. The paper mainly contemplates on the types, biological properties, and molecular structures of marine algae vHPOs as well as their biochemical function and potential industrial applications.

Keywords Biologic halogenation · Halogenated products · Marine algae · Vanadium-dependent haloperoxidases

T. Wang (✉) · Y. Lu · D. Cao · S. Gao · Y. Zhang
Department of Utilizing Chemical Resource from Seawater, National Engineering Research Centre for Seawater Utilization, Institute of Seawater Desalination and Multipurpose Utilization (SOA), Tianjin 300192, People's Republic of China
e-mail: tj_wt1983@hotmail.com

T. Wang
Key Laboratory of Industrial Fermentation Microbiology, Tianjin University of Science & Technology, Ministry of Education, Tianjin 300457, People's Republic of China

T. Wang
Tianjin Key Lab of Industrial Microbiology, Tianjin University of Science and Technology, Tianjin 300457, People's Republic of China

T.-C. Zhang et al. (eds.), *Proceedings of the 2012 International Conference on Applied Biotechnology (ICAB 2012)*, Lecture Notes in Electrical Engineering 251,
DOI: 10.1007/978-3-642-37925-3_187,

187.1 Introduction

Many marine organisms, particularly the macroalgae, are frequently proved to have developed means to incorporate halogens into their metabolites that are mainly involved in antioxidants to reduce the environmental oxidative stress and chemical defenses to against opportunistic bacteria and predators [1, 2]. These halogenated compounds span a very large range from simple volatile halohydrocarbons (e.g., bromoform-, dibromomethane, methyl iodide, bromo- and chloroanisoles, etc.) to halogenated phenolic derivatives (e.g., indoles, terpenes, acetogenins, phenols, etc.) [3–6]. Since, in many cases, these halogenated marine metabolites have been found to possess biological activities of pharmacological interests, including antifungal, antibacterial, antiviral, and anti-inflammatory activities [7], the pathway of biogenesis of these compounds has intrigued marine chemists for decades.

Early on turn of the twentieth century, certain enzyme activities relative to the transformation of bromine and iodine in marine algae have been initially well documented [8, 9]. Kylin [10] postulated the involvement of an "iodide oxidase" in the thallus surface mucilage of macroalgae that was able to oxidize the iodide in seawater prior to its uptake. Wolinsky [11] and Fenical [12] invoked a possible role for haloperoxidase enzymes in the biogenesis of certain halogenated marine natural products, although this was long before haloperoxidases were discovered in marine organisms. Since then, haloperoxidases have been consequently discovered in all classes of marine organisms. According to their different active sites and reaction mechanisms, two types of marine haloperoxidases have been identified: (1) vanadium-dependent haloperoxidase (vHPO), of which vanadate is the prosthetic group [13–15], and (2) heme-dependent haloperoxidase (Heme-HPO), of which heme ion acts as the prosthetic group [16–18]. Compare with the Heme—HPO, vHPO is most prevalent and there is no change in the oxidation state of its metal center during the synthesis of halogenating agent [19]. Hence, vHPOs do not suffer from oxidative inactivation during turnover and possess relatively high tolerance for organic solvents and high temperatures [20, 21], as well as their ability to halogenate a range of organic compounds in a regio- and stereo-specific manner [7, 22], and oxidize organic sulfides in the absence of halides [23, 24]. These characteristics make them receive increasing attention as biocatalysts for producing halogen intermediate in organic synthesis. The scope of this review article includes the properties and characterizations of vHPOs from marine algae and their biological function and potential industrial applications in the biosynthesis of halogenated marine natural products.

187.2 Types and Biological Function of vHPOs

Depending on the most electronegative halogen the enzyme is capable of oxidizing, vHPOs are characterized as vanadium chloroperoxidases (vCPOs), vanadium bromoperoxidases (vBPOs), and vanadium iodoperoxidases (vIPOs).

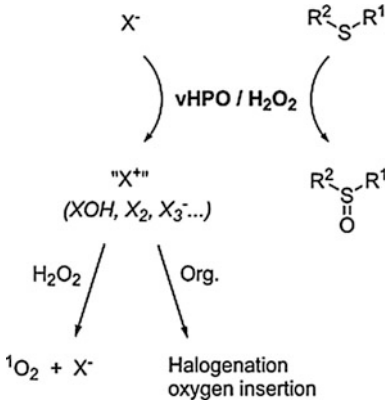

Fig. 187.1 Reactions of the vHPO/H_2O_2 system. X: Br, Cl, I. Org.: organic compound. R1, R2: alkyl, aryl [25]

In particular, chloroperoxidases can catalyze the oxidation of chloride as well as of bromide and iodide; bromoperoxidases react with bromide and iodide; whereas iodoperoxidases are specific of iodide [25]. The first vHPO to be isolated and characterized was the vBPO from the brown alga *Ascophyllum nodosum* in 1984 [26]. Subsequently, Krenn et al. [27] found it substantially contained two different kinds of vanadate proteins. To date, these enzymes have been purified and characterized in many brown alga (*Sacchoriza polyschides* [28], *Pelvetia canaliculata* [29], *Laminaria saccharin*a [30], etc.), some red (*Corallina officinalis* [31]) and green marine alga (*Cladophora glomerata* [32]), as well as in certain terrestrial lichen (*Xanthoria parietina* [33]), and more recently, in some fungi (*Curvularia inaequalis* [34], *Embellisia didymospora* [35]).

The function of vHPOs in biochemical reaction is to catalyze the oxidation of a halide (i.e., chloride, bromide, or iodide) by hydrogen peroxide, a process which results in the concomitant halogenation of organic substrates [1], as shown below.

$$H_2O_2 + X^- + R - H + H^+ \rightarrow R - X + 2H_2O \quad (1)$$

In the first step, vHPOs catalyze the oxidation of halides (X^-) by hydrogen peroxide producing a two electron oxidized halogen intermediate ("X^+" = XOH, X_2, X_3^-) [36]. In the second step, the oxidized intermediate can halogenate an appropriate organic substrate or react with another equivalent of hydrogen peroxide, forming dioxygen in the singlet-excited state ($^1O_2$) [37, 38]. In the absence of halides, vHPOs catalyze the enantioselective oxidation of sulfides into sulfoxides [39]. These sulfoxidation reactions occur at the vanadium-binding site through a direct oxygen transfer from the peroxovanadium intermediate to the sulfide [40], as shown in Fig. 187.1.

187.3 Molecular and Structural Characterization

Up to now, three X-ray crystal structures of vHPOs have been detected (Fig. 187.2), i.e., vClPO from the fungus *C. inaequalis,* which is a monomeric protein [41–43], vBrPO from the brown alga *A. nodosum* [44], which is a homodimer, and vBrPO from the red alga *C. officinalis* [31]. Interestingly, the last enzyme protein, which is associated with snyderol (2-4) biosynthesis, is a homododecameric protein arranged in a 23-point group symmetry. Thus, at the molecular level, the various monomeric states and less than 30 % identity sequences of these three proteins [19] probably indicates their differences in biological function. However, each protein shares a core structure consisting of mainly α-helices with two four-helix bundles as the main tertiary structural motif [31, 42, 43] and has an identical arrangement of amino acid residues at the vanadium active site itself. The vanadium-binding site lies at the bottom of a 15–20-Å deep funnel-shaped channel located at the core of the four-helix bundle [7, 41, 44].

Vanadium is present as a V(V) ion and is ligated to the imidazole ring of a conserved histidine residue that anchors the cofactor in a trigonal bipyramidal fashion. Three oxygen atoms of the cofactor are located in the equatorial plane, and the negative charges are compensated by an extensive hydrogen-bonding network with protonated amino acid residues in the conserved active site. Through quantum mechanics/molecular mechanics, ^{51}V solid-state NMR, and UV–visible spectroscopy studies, the resting state of the enzyme likely contains at least one hydroxyl group in the apical position [45–47]. Putatively, this position is occupied by an axial water and stabilized through a hydrogen bond with a side chain His imidazole [46].

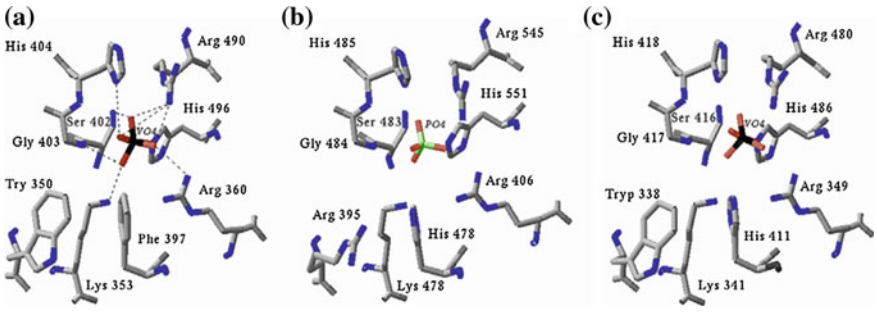

Fig. 187.2 The vanadate-binding site structure of vHPOs. **a** *C. inaequalis* vCPO, **b** *C. officinalis* vBPO, **c** *A. nodosum* vBPO. Vanadate (**a** and **c**), and the inorganic phosphate (**b**) are represented in the center of the picture and the hydrogen-bonding network, conserved in all three vHPOs, is indicated by dashed lines around the vanadate center (**a**) [25]

187.4 Perspectives of Industry Applications

In contrast to other halogenating enzymes, vHPOs activities are relatively resistant to high temperature exposures. And it has been confirmed that the enzymes are still active in oxidative conditions and in the presence of different organic solvents such as acetone, methanol or ethanol [48, 49]. These properties as well as the ability to halogenate a broad range of organic compounds of both commercial and pharmaceutical interests make vHPOs good candidates for use in industrial biotransformations [50].

Recently, a few marine algal vBPOs have been shown through in vitro chemoenzymatic conversions to catalyze the bromonium-assisted cyclization of terpenes and ethers [7, 51]. And the studies of Rehder [52] and Crans [53] have convincingly shown that various vBPOs isolated from marine red algae (e.g., *C. officinalis*, *Laurencia pacifica*, and *Plocamium cartilagineum*) catalyze the asymmetric bromination/cyclization reactions of the sesquiterpene nerolidol to the snyderol family of marine natural products. Single diastereomers of β- and γ-snyderol were produced in the enzyme reaction, whereas in the synthetic reaction, two diastereomers of each were formed. This study established the likely role of vBPOs in the biosynthesis of brominated cyclic sesquiterpenes from marine red algae and further implies that other marine algal brominated natural products may similarly be constructed. Moreover, Jiang [54] has reported an approach to produce S-/R- sulfoxides from methyl-/phenyl- sulfides catalyzed by the vHPOs isolated from marine algae. Depending on the sources of enzyme, the products are different, i.e., vHPOs from *Ascophyllum nodosum* forming R-sulfoxide, the vHPOs from *Corallina officinalis* and *C.Pilulifera* forming S-enantiomer.

187.5 Summary

Vanadium-dependent haloperoxidases is a class of new enzymes widely present in marine algae that catalyze electrophilic halogenation reactions using hydrogen peroxide to oxidize halide ion and form carbon-halogen bonds to selective organic substrates. All the vHPOs isolated to date share some common features: (1) composed of one or more subunits of relative molecular mass around 67 kDa; (2) be inactivated by dialysis against EDTA at low pH; (3) only be reactivated by restored in addition of vanadium (as vanadate) solution; and (4) seem to have similar coordination of vanadium in the active site [42–44].

Although the mechanism of their catalytic cycle has not yet been fully elucidated, the applications of vHPOs on biomimetic syntheses of chiral halogenated compounds have been developed in modern synthetic chemistry and pharmaceutical industry. Concerning its biological and environmental significance, the future researches of vHPOs will focus on the specific gene sequences that encoding vHPOs, deeply investigating their catalytic mechanism and properties and establishing more tractable systems to make them applied in wilder areas.

Acknowledgments This work was supported by a program of Key Laboratory of Industrial Fermentation Microbiology (No.2012IM003), Tianjin University of Science & Technology.

References

1. Butler A, Walker JV (1993) Marine haloperoxidases. Chem Rev 93:1937–1944
2. Kupper FC, Carpenter LJ, McFiggans GB et al (2008) Iodide accumulation provides kelp with an inorganic antioxidant impacting atmospheric chemistry. Proc Natl Acad Sci U S A 105(19):6954–6958
3. John Faulkner D (2000) Marine natural products. Nat Prod Rep 17(1):7–55
4. Manley SL, Goodwin K, North WJ (1992) Laboratory production of bromoform, methylene bromide, and methyl iodide by macroalgae and distribution in nearshore southern California waters. Limnol Oceanogr 37(8):1652–1659
5. Gschwend PM, Macfarlane JK, Newman KA (1985) Volatile halogenated organic compounds released to seawater from temperate marine Macroalgae. Science 227(4690):1033–1035
6. Gribble GW (2003) The diversity of naturally produced organohalogens. Chemosphere 52(2):289–297
7. Butler A, Carter-Franklin JN (2004) The role of vanadium bromoperoxidase in the biosynthesis of halogenated marine natural products. Nat Pro Rep 21(1):180–188
8. Atkins WRG (1914) Oxydases and their inhibitors in plant tissues. Part iii: The localisation of oxydases and catalase in some marine algae. Sci Proc Ro Dublin Soc 14:199–206
9. Reed GB (1915) Evidence for the general distribution of oxidases in plants. Bot Gaz 59(5):407–409
10. Kylin H (1930) über das vorkommen von jodiden, bromiden und jodidoxydasen bei den meeresalgen. Hoppe-Seyler's Z Physiol Chem 186(1–2):50
11. Wolinsky LE, Faulkner DJ (1976) Biomimetic approach to the synthesis of laurencia metabolites. Synthesis of 10-bromo-Alpha-chamigrene. J Org Chem 41(4):597–600
12. Fenical W (1975) Halogenation in the rhodophyta-a review. J Phycol 11(3):245–259
13. Vilter H (1983) Peroxidases from phaeophyceae iv. Fractionation and location of peroxidase isoenzymes in Ascophyllum nodosum (L.). Bot Mar 26(10):451–455
14. Wever R, Plat H, de Boer E (1985) Isolation procedure and some properties of the bromoperoxidase from the seaweed Ascophyllum nodosum. Biochim Biophys Acta Prot Struct Mol Enzym 830(2):181–186
15. Almeida M, Filipe S, Humanes M et al (2001) Vanadium haloperoxidases from brown algae of the laminariaceae family. Phytochemistry 57(5):633–642
16. Manthey JA, Hager LP (1989) Characterization of the catalytic properties of bromoperoxidase. Biochemistry 28(7):3052–3057
17. Manthey JA, Hager LP (1985) Characterization of the oxidized states of bromoperoxidase. J Biol Chem 260(17):9654–9659
18. Roach MP, Chen YP, Woodin SA et al (1997) Notomastus lobatus chloroperoxidase and amphitrite ornata dehaloperoxidase both contain histidine as their proximal heme iron ligand. Biochemistry 36(8):2197–2202
19. Winter JM, Moore BS (2009) Exploring the chemistry and biology of vanadium-dependent haloperoxidases. J Biol Chem 284(28):18577–18581
20. de Boer E, Plat H, Tromp MG et al (1987) Vanadium containing bromoperoxidase: An example of an oxidoreductase with high operational stability in aqueous and organic media. Biotechnol Bioeng 30(5):607–610
21. Coupe EE, Smyth MG, Fosberry AP et al (2007) The dodecameric vanadium-dependent haloperoxidase from the marine algae Corallina officinalis: Cloning, expression, and refolding of the recombinant enzyme. Prot Exp Pur 52(2):265–272

22. Itoh N, Hasan AK, Izumi Y, Yamada H (1988) Substrate specificity, regiospecificity and stereospecificity of halogenation reactions catalyzed by non-heme-type bromoperoxidase of Corallina pilulifera. Eur J Biochem 172(2):477–484
23. Andersson M, Willetts A, Allenmark S (1997) Asymmetric sulfoxidation catalyzed by a vanadium-containing bromoperoxidase. J Org Chem 62(24):8455–8458
24. ten Brink HB, Dekker HL, Schoemaker HE, Wever R (2000) Oxidation reactions catalyzed by vanadium chloroperoxidase from Curvularia inaequalis. J Inorg Biochem 80(1–2):91–98
25. Leblanc C, Colin C, Cosse A et al (2006) Iodine transfers in the coastal marine environment: The key role of brown algae and of their vanadium-dependent haloperoxidases. Biochimie 88(11):1773–1785
26. Vilter H (1984) Peroxidases from phaeophyceae: A vanadium(v)-dependent peroxidase from Ascophyllum nodosum. Phytochemistry 23(7):1387–1390
27. Krenn BE, Tromp MG, Wever R (1989) The brown alga Ascophyllum nodosum contains two different vanadium bromoperoxidases. J Biol Chem 264(32):19287–19292
28. Almeida M, Humanes M, Melo R et al (1998) Saccorhiza polyschides (Phaeophyceae; phyllariaceae) a new source for vanadium-dependent haloperoxidases. Phytochemistry 48(2):229–239
29. Almeida MG, Humanes M, Melo R et al (2000) Purification and characterisation of vanadium haloperoxidases from the brown alga Pelvetia canaliculata. Phytochemistry 54(1):5–11
30. de Boer E, Tromp MGM, Plat H et al (1986) Vanadium (v) as an essential element for haloperoxidase activity in marine brown algae: Purification and characterization of a vanadium (v)-containing bromoperoxidase from Laminaria saccharina. Biochim Biophys Acta Prot Struct Mol Enzym 872(1–2):104–115
31. Isupov MN, Dalby AR, Brindley AA et al (2000) Crystal structure of dodecameric vanadium-dependent bromoperoxidase from the red algae Corallina officinalis. J Mol Biol 299(4):1035–1049
32. Verdel EF, Kline PC, Wani S, Woods AE (2000) Purification and partial characterization of haloperoxidase from fresh water algae Cladophora glomerata. Comp Biochem Physiol B: Biochem Mol Biol 125(2):179–187
33. Plat H, Krenn BE, Wever R (1987) The bromoperoxidase from the lichen Xanthoria parietina is a novel vanadium enzyme. Biochem J 248(1):277–279
34. van Schijndel JWPM, Vollenbroek EGM, Wever R (1993) The chloroperoxidase from the fungus Curvularia inaequalis; a novel vanadium enzyme. Biochim Biophys Acta Prot Struct Mol Enzym 1161(2–3):249–256
35. Barnett P, Hemrika W, Dekker HL et al (1998) Isolation, characterization, and primary structure of the vanadium chloroperoxidase from the fungus Embellisia didymospora. J Biol Chem 273(36):23381–23387
36. Soedjak HS, Walker JV, Butler A (1995) Inhibition and inactivation of vanadium bromoperoxidase by the substrate hydrogen peroxide and further mechanistic studies. Biochemistry 34(39):12689–12696
37. Everett RR, Butler A (1989) Bromide-assisted hydrogen peroxide disproportionation catalyzed by vanadium bromoperoxidase: Absence of direct catalase activity and implications for the catalytic mechanism. Inorg Chem 28(3):393–395
38. Everett RR, Soedjak HS, Butler A (1990) Mechanism of dioxygen formation catalyzed by vanadium bromoperoxidase. Steady state kinetic analysis and comparison to the mechanism of bromination. J Biol Chem 265(26):15671–15679
39. Andersson M, Willetts A, Allenmark S (1997) Asymmetric sulfoxidation catalyzed by a vanadium-containing bromoperoxidase. J Org Chem 62(24):8455–8458
40. ten Brink HB, Schoemaker HE, Wever R (2001) Sulfoxidation mechanism of vanadium bromoperoxidase from Ascophyllum nodosum. Evidence for direct oxygen transfer catalysis. Eur J Biochem 268(1):132–138
41. Messerschmidt A, Wever R (1996) X-ray structure of a vanadium-containing enzyme: Chloroperoxidase from the fungus Curvularia inaequalis. Proc Natl Acad Sci 93(1):392–396

42. Macedo-Ribeiro S, Hemrika W, Renirie R et al (1999) X-ray crystal structures of active site mutants of the vanadium-containing chloroperoxidase from the fungus Curvularia inaequalis. J Biol Inorg Chem 4(2):209–219
43. Messerschmidt A, Prade L, Wever R (1997) Implications for the catalytic mechanism of the vanadium-containing enzyme chloroperoxidase from the fungus Curvularia inaequalis by x-ray structures of the native and peroxide form. Biol Chem 378(3–4):309–315
44. Weyand M, Hecht HJ, Kieß M et al (1999) X-ray structure determination of a vanadium-dependent haloperoxidase from Ascophyllum nodosum at 2.0 resolution. Biol J Mol Biol 293(3):595–611
45. Pooransingh-Margolis N, Renirie R, Hasan Z et al (2006) 51v solid-state magic angle spinning NMR spectroscopy of vanadium chloroperoxidase. J Am Chem Soc 128(15):5190–5208
46. Zhang Y, Gascón JA (2008) QM/MM investigation of structure and spectroscopic properties of a vanadium-containing peroxidase. J Inorg Biochem 102(8):1684–1690
47. Raugei S, Carloni P (2005) Structure and function of vanadium haloperoxidases. J Phys Chem B 110(8):3747–3758
48. Vilter H (1995) Vanadium-dependent haloperoxidases. Met Ions Biol Syst 31:325–362
49. Butler A, Carter JN, Simpson MT (2001) Vanadium in proteins and enzymes. In: Bertini I, Sigel A, Sigel H (eds) Handbook on metalloproteins. Marcel Dekker Inc., New York
50. Littlechild J (1999) Haloperoxidases and their role in biotransformation reactions. Curr Opin Chem Biol 3(1):28–34
51. Carter-Franklin JN, Butler A (2004) Vanadium bromoperoxidase-catalyzed biosynthesis of halogenated marine natural products. J Am Chem Soc 126(46):15060–15066
52. Rehder D (1991) The bioinorganic chemistry of vanadium. Angew Chem Int Ed 30(2):148–167
53. Crans DC, Smee JJ, Gaidamauskas E, Yang L (2004) The chemistry and biochemistry of vanadium and the biological activities exerted by vanadium compounds. Chem Rev 104(2):849–902
54. Jiang B, Huang H, Luo J, Li Z-Y (2005) Chiral sulfoxides by biooxidation of sulfides. Chin J Org Chem 25(12):1542–1547 (in Chinese)

Chapter 188
The Cells of *Gluconacetobacter xylinus* Response to Exposure

Xintong Zheng, Cheng Zhong, Miao Liu, Ainan Guo, Yanyan Li and Shiru Jia

Abstract Via direct current (DC) electric field, bacterial cellulose (BC), a biopolymer generated by *Gluconacetobacter xylinus*, was altered into its nanofibers alignment and 3-dimensional network structure in its synthesized process. In this investigation, cultures of *G. xylinus* cells exposed at DC electric field and the sham-exposed controls were respectively investigated for: the culture able count near anode and cathode, the morphological analysis of cells, BC yield, and FTIR analysis of it. Exposed samples and controls showed significant difference in cells morphology, whereas they were similar at the two poles in same condition. An exposure to DC electric field of 0, 0.25, 0.5, 0.75, and 1 V/cm produced a obviously tendency on the ratio of culture able count near anode and cathode. BC yield showed a slight increase and then sharp decrease as the electric field intensity increased. In addition, essentially unchanged in FTIR analysis of BC formed at 0 V/cm and 1 V/cm. These results combined with our previous studies can establish a conjectural theory of cells response to exposure of DC electric field which has a stimulate factor.

Keywords *Gluconacetobacter xylinus* · Bacterial cellulose · Direct current electric field · Cell morphology

188.1 Introduction

Bacterial cellulose (BC) a microbial extracellular biopolymer which is synthesized by the genera *Acetobacter*, *Rhizobium*, *Agrobacterium*, and *Sarcina* [1]. The most exhaustive invested strain is *Gluconacetobacter xylinus* (formerly known as

X. Zheng · C. Zhong · M. Liu · A. Guo · Y. Li · S. Jia (✉)
Key Laboratory of Industrial Fermentation Microbiology, Ministry of Education, Tianjin University of Science and Technology, Tianjin 300457, China
e-mail: jiashiru@tust.edu.cn

T.-C. Zhang et al. (eds.), *Proceedings of the 2012 International Conference on Applied Biotechnology (ICAB 2012)*, Lecture Notes in Electrical Engineering 251,
DOI: 10.1007/978-3-642-37925-3_188,

Acetobacter xylinum [2, 3]) which has been identified as a model microorganism for fundamental and applied research on BC [4]. One of the focal points on BC is the mechanism of its biosynthesis process and the relationship between its fiber structure and mechanical properties [5–7]. The products of BC for medical have already appeared and have been used in clinical as a commodity, such as Bio-process ®, XCell ®, and Biofill ® [8, 9]. They were applied as a graft and the scaffolds for tissue engineering such as blood vessel replacement, artificial skin, and bone tissue scaffold [10–12]. Nonetheless, one of the main constraints of BC in biomedical material field is controlling the specification of BC products. Electric field was used to control the motion of cells or particles in the electrolyte, which has been widely used for separation and aggregation [13–16]. We have previously demonstrated that the DC electric field could affect the motion of *G. xylinus* cells and bacterial cellulose synthesis [17]. It verified our hypothesis further in this work and a conjectural cell behavior model was put forward.

188.2 Materials and Methods

188.2.1 Strains

G. xylinus CGMCC No. 2955 was screened by the Key Laboratory of Industrial Microbiology of the Ministry of Education and reserved at China General Microbiological Culture Collection Center.

188.2.2 Materials

① *Liquid growth medium(v/v).* glucose 2.5 %, peptone 0.75 %, yeast extract 1 %, Na_2HPO_4 1 %, initial pH value 6.0 [18].

② *Solid growth medium.* Liquid growth medium with addition of 2 %(v/m) agar.

DC electric field culture device was used as we described previously [17]. 0, 0.25, 0.5, 0.75, and 1 V/cm were selected for the test electric field strengths.

188.2.3 Bacterial Sampling and BC Yields Measurement Methods

For seed culture, *G. xylinus* was inoculated into 100 mL of the culture medium in a 500-mL flask by shaking at 160 r/min and cultured at 30 °C for 24 h [18, 19].

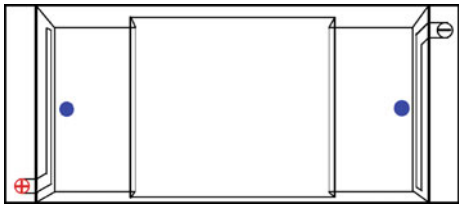

Fig. 188.1 The schematic of sampling and crossing location

Liquid growth medium contains 6 % seed poured into the electrophoresis tank, applied different DC electric field strengths, and incubated statically at 30 °C for 3 days. At the end of incubation, 1 mL medium was absorbed near anode and cathode, the position was shown in Fig. 188.1, then executed colony counts of it and prepared cells for SEM. BC was dried at 80 °C in an oven after two-step purification to constant and then weighed [20].

188.2.4 The Scanning Electron Microscope

The scanning electron microscope (SEM), Hitachi/SU-1510, was performed to observe the morphology of *G. xylinus* cells obtained from anode and cathode around. The samples prepared for the SEM experiments were immobilized by glutaraldehyde, and next dehydrated gradually by ethanol. When they were completely dry, a thin layer of gold was coated on the surface of samples and after that they were observed in SEM.

188.2.5 Fourier Transforms Infrared Spectroscopy

Infrared spectra, Vector 22, were measured samples of completely dehydrated BC by freeze dryer over the frequency range 4,000–400 cm^{-1} at the resolution of 4 cm^{-1}.

188.3 Results and Discussion

188.3.1 Observation of Cells' Distribution Under Different Electric field Strengths

In our previous works, we detected the movement of cells on semisolid swarm medium under the existence of the electric field condition [17]. It was seen that cells were migrated toward the cathode when the DC electric field applied.

Furthermore, the motion of cells would accelerate as electric field intensity increased. In this investigation, the number of colony acquired from anode and cathode after 72 h culture under different electric field strengths was counted and calculated the ratio of them. The results were shown in Table 188.1.

These results confirmed the previous conclusion further. When DC electric field was applied, the number of colonies of the cathode was always more than anode. The proportion of colony number between anode and cathode was raised as the electric field intensity increased. Combining with our previous results of mobility of cells on the semisolid swarm medium in DC electric field [17], this illustrated that the cells under the force of electric field moved toward the cathode, and the greater electric field intensity was, the more obvious tendency of cells migration would be.

188.3.2 Observation of Cell Morphology Near Anode and Cathode

The bacterial cells were obtained near anode and cathode under 0 V/cm and 1 V/cm electric field, respectively. The graph of cells micromorphology observed in SEM was shown in Fig. 188.2. It displayed that cells morphology was relatively close between anode and cathode but quite different in the two electric field intensity conditions. *G. xylinus* displayed a long rod-shaped cell about 5–6 μm long, 0.4–0.6 μm wide, and its surface was smooth in normal situation. In contrast, cells presented a stubby rod-shaped morphology at 1 V/cm electric field and a coarse surface additional. The length of cells was shortened to 2–3 μm and width was augment to 0.6–0.8 μm. It was worth mentioning that some holes appeared on the surface of cell, which exposed at 1 V/cm. This phenomenon may relate to the electroporation caused by high electric field strength.

188.3.3 The BC Yield

To verify the possible effect of DC electric field on BC yield, *G. xylinus* was exposed to 0, 0.25, 0.5, 0.75 and 1 V/cm for 72 h. The BC production presented in Fig. 188.3 corresponded to mean values and standard deviation. The data demonstrated that BC production was slightly enhanced at 0.25 V/cm compared with 0 V/cm, but dropped down rapidly over 0.5 V/cm. It was postulated that low electric field strength promoted cellular respiration and high electric field strength may undermine the synthesis site on cell membrane, even cause perforations in the membrane, leading to cell death in excessively high electric field strength.

Table 188.1 The culturable count and ratio of colony number near anode and cathode

Electric field strength (V/cm)	0	0.25	0.5	0.75	1
The culturable count near anode (cfu/mL)	$(3.81 \pm 0.25) \times 106$	$(2.58 \pm 0.44) \times 106$	$(1.76 \pm 0.26) \times 106$	$(9.55 \pm 2.76) \times 105$	$(5.95 \pm 2.05) \times 104$
The culturable count near cathode (cfu/mL)	$(3.60 \pm 0.35) \times 106$	$(5.34 \pm 0.63) \times 106$	$(3.99 \pm 0.42) \times 106$	$(3.42 \pm 0.4) \times 106$	$(4.55 \pm 0.90) \times 105$
The ratio of the colony number (Anode: Cathode)	1:0.95	1:2.07	1:2.27	1:3.58	1:7.64

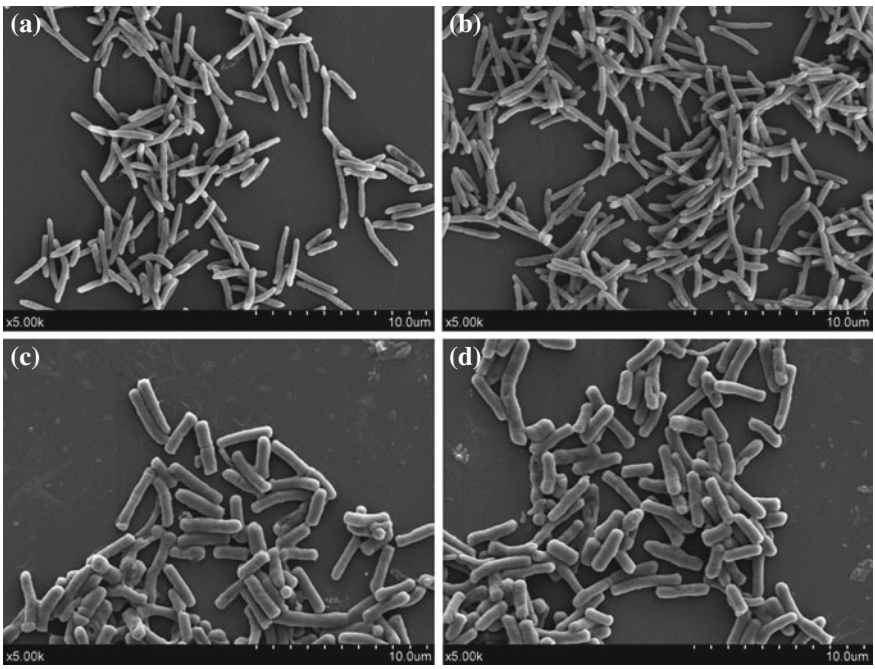

Fig. 188.2 SEM images of cells morphology acquired from anode (**a** 0 V/cm, **c** 1 V/cm) and cathode (**b** 0 V/cm, **d** 1 V/cm)

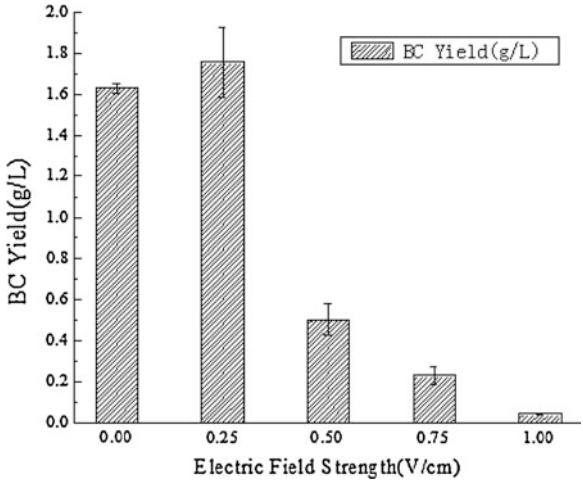

Fig. 188.3 BC yield under different electric field strengths

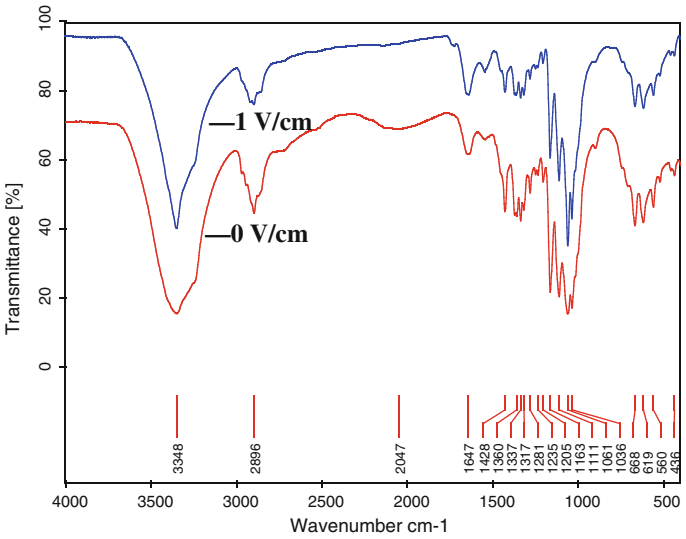

Fig. 188.4 FITR for BC membrane produced at 0 V/cm and 1 V/cm

188.3.4 Analysis of BC Microstructure

FTIR analysis of BC formed at 0 V/cm and 1 V/cm electric field was shown in Fig. 188.4. It suggested that the peak of the absorption spectra of the synthetic bacterial cellulose of different electric field strengths was almost same. Located in 1,060 cm^{-1} for the C–O–C and C–O–H bonds stretching vibration is the characteristic absorption peak of the cellulose. Absorption peak at 3,350 cm^{-1} reflects the stretching vibration of the O–H bond. The absorption peak at 2,895 cm^{-1} is generated by the stretching vibration of the O–H bond. The absorption peak at 1,428 cm^{-1} is caused by flexural vibrations of the C–H bond, its depth relates to the crystallinity of BC.

188.3.5 An Inferential Theory of G. xylinus Cells Behavior Patterns in DC Electric Field

According to the above results and previous research, we could infer how the motion of the bacterial cells under the electric field condition was changed. In normal condition, the bacterial cells had an erratic motion, and formed random cellulose 3D network, the model was shown in Fig. 188.5a. When DC electric field applied, the cells were migrated to cathode and the migration speed was proportional to the electric field strength. Furthermore, when the migration speed was over to BC generation speed, it was shown that the diameter of the fiber bundles

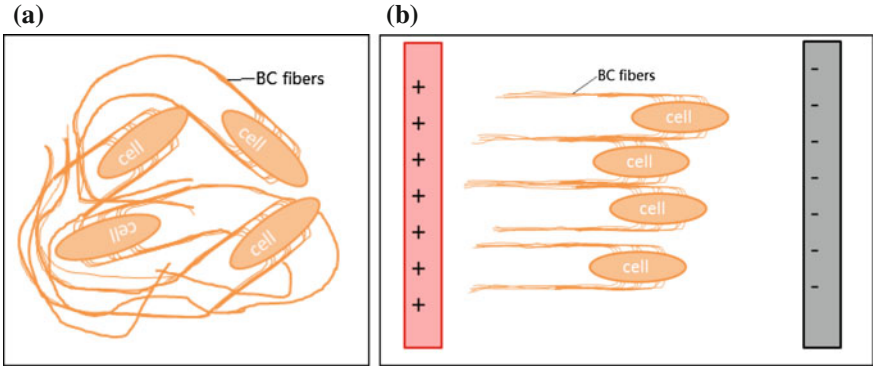

Fig. 188.5 The motion pattern of cells without electric field (**a**) and exposed to electric field (**b**)

significantly coarsened and had a certain degree of directionality compared with traditional cellulose structure [17]. BC fibers intertwined with each other into bundle due to the substantially same cell motion direction. Thus BC would have the above characteristics, as shown in Fig. 188.5b.

188.4 Conclusion

We have demonstrated that DC electric field can affect BC fibers assembly by changing the motion direction of *G. xylinus* cells in our previous work [17]. In this investigation, some further evidence was proposed and an inferential theory was founded. By studying cell behavior under DC electric field, it can provide a potential method of manipulating cells indirectly. For future research, it should be forced on the effective role of DC electric field exposure in *G. xylinus* cells and the mechanical properties of BC synthetized in different electric field condition. In particular, the possible in formation customized BC 3D structure according to application requirements through control of the electric field should be evaluated.

Acknowledgments This work was funded by the National Natural Science Foundation of China (No. 20976133 and No.21106105), the Foundation of Tianjin Educational Committee (No. 20100602), and Program for Changjiang Scholars and Innovative Research Team in University (IRT1166).

References

1. Jonas R, Farah LF (1998) Production and application of microbial cellulose. Polym Degrad Stabil 59:101–106
2. Yamada Y, Hoshino K, Ishikawa T (1997) The phylogeny of acetic acid bacteria based on the partial sequences of 16S ribosomal RNA. Biosci Biotechnol Biochem 61:1244–1251

3. Yamada Y (2000) Transfer of *Acetobacter oboediens* Sokollek et al. 1998 and Acetobacter intermedius Boesch et al. 1998 to the genus *Gluconacetobacter* as *Gluconacetobacter oboediens* comb. nov. and *Gluconacetobacter* intermedius comb. nov. Int J Syst Evol Micr 50:2225–2227
4. Cannon RE, Anderson SM (1991) Biogenesis of bacterial cellulose. Crit Rev Microbiol 17:435–477
5. Wan Y, Hong L, Jia SR et al (2006) Synthesis and characterization of hydroxyapatite–bacterial cellulose nanocomposites. Compos Sci Technol 66:1825–1832
6. Bodin A, Bäckdahl H, Fink H et al (2007) Influence of cultivation conditions on mechanical and morphological properties of bacterial cellulose tubes. Biotechnol Bioeng 97:425–434
7. Yasutake Y, Kawano S, Tajima K et al (2006) Structural characterization of the *Acetobacter xylinum* endo-β-1, 4-glucanase CMCax required for cellulose biosynthesis. Proteins 64:1069–1077
8. Fontana JD, Desouza AM, Fontana CK et al (1973) Electro tactile sensory aids for the handicapped. Presented at the 4th annual meeting biomedical engineering society. Los Angeles
9. Habibovic P, Yuan HP, Vander CM et al (2005) 3D microenvironment as essential element for osteoinduction by biomaterials. Biomaterials 26:3565–3575
10. Hoenich N (2006) Cellulose for medical applications: Past, present, and future. BioResources 1:270–280
11. Roman M, Winter WT (2004) Effect of sulfate groups from sulfuric acid hydrolysis on the thermal degradation behavior of bacterial cellulose. Biomacromolecules 5:1671–1677
12. Gatenholm P, Klemm D (2010) Bacterial nanocellulose as a renewable material for biomedical applications. MRS Bull 35:208–213
13. Gascoyne PRC, Vykoukal JV, Schwartz JA et al (2004) Dielectrophoresis-based programmable fluidic processors. Lab Chip 4:299–309
14. Pohl HA (1951) The motion and precipitation of suspensoids in divergent electric fields. Appl Phys 22:869–871
15. Shafiee H, Caldwell JL, Sano MB et al (2009) Contactless dielectrophoresis: a new technique for cell manipulation. Biomed Microdev 11:997–1006
16. Sano MB, Caldwell JL, Davalos RV (2011) Modeling and development of a low frequency contactless dielectrophoresis (cDEP) platform to sort cancer cells from dilute whole blood samples. Biosens Bioelectron 1:13–20
17. Yan L, Jia SR, Zheng XT et al (2012) The effect of growth, migration and bacterial cellulose synthesis of *Gluconacetobacter xylinus* in presence of direct current electric field condition. Adv Mater Research 22:1108–1113
18. Jia SR, Ou HY, Chen G et al (2004) Cellulose production from *Gluconobacter oxydans* TQ-B2. Biotechnol Bioproc E 9:166–170
19. Tang WH, Jia SR, Jia YY et al (2010) The influence of fermentation conditions and post-treatment methods on porosity of bacterial cellulose membrane. World J Microb Biot 26:125–131
20. Gea S, Reynolds CT, Roohpur N et al (2011) Investigation into the structural, morphological, mechanical and thermal behaviour of bacterial cellulose after a two-step purification process. Bioresour Technol 102:9105–9110

Chapter 189
Purification and Characterization of Cholinesterase from Duck Plasma

Chang Liu and Fusheng Chen

Abstract Cholinesterase from duck plasma was isolated and purified to electrophoretic homogeneity by salting out, ion-exchange chromatography on DEAE-cellulose, and gel filtration on Sephadex G-200. The enzyme was purified 278.5-fold and 17.8 % activity was recovered. Studies on the properties of the Cholinesterase showed that the optimum temperature was 37 °C and the optimum pH was 7.5–8.0. The value of Km was 2.4×10^{-5} M and the enzyme was not inhibited by excess bcetylthiocholine iodide. The presence of Ca^{2+}, Mg^{2+}, and M^{n2+} increase the enzyme activity at a concentration of 5 mM. The study showed that this cholinesterase was a valuable alternative for detecting organophosphate and carbamate pesticides of vegetables and fruits.

Keywords Cholinesterase · Duck plasma · Purification · Properties · Sensitivities

189.1 Introduction

Organophosphorus and carbamate pesticides have been widely used in the field of agriculture due to their high effectiveness for insect control. Though their use is constantly decreasing and some highly toxic compounds of them have been

C. Liu (✉)
College of Food Science and Technology, Hebei Normal University of Science and Technology, Qinhuangdao 066600, People's Republic of China
e-mail: liuchang20@sina.com

C. Liu
Key Laboratory of Food Nutrition and Safety, Ministry of Education of China, Tianjin University of Science and Technology, Tianjin 300308, People's Republic of China

F. Chen
College of Food Science and Technology, Huazhong Agriculture University, Wuhan 430070, People's Republic of China

T.-C. Zhang et al. (eds.), *Proceedings of the 2012 International Conference on Applied Biotechnology (ICAB 2012)*, Lecture Notes in Electrical Engineering 251,
DOI: 10.1007/978-3-642-37925-3_189,

forbidden in the last decades, they are still the main pesticides in many countries especially in developing countries [1, 2]. The excessive use of these pesticides often leads to residues heavily going beyond the limits. These organic toxins enter animal and human bodies directly or indirectly through the food chain or drinking water, and threat human health [3]. Affairs of poisoning owing to pesticides residues were frequently reported [4]. Traditional methods of pesticide residue include gas chromatography or HPLC, but they suffer from long analysis times, required separation/preconcentration steps and the impossibility to be used in situ [5]. So it is of great significance to develop a fast, reliable, and economically analytical method for determination of trace amounts of these pesticides.

In recent years, the enzyme inhibition method is broadly used because it is fast, simple, convenient, and without expensive equipments [6]. The principle of this method is based on the inhibiting ratio of enzyme activity according to the concentration of pesticides, thus adding the pesticide residues extracted from the fruits, vegetables, and other agricultural products into cholinesterase reaction system can detect pesticide residues rapidly [7].

Vertebrates have two types of cholinesterases (ChE): acetylcholinesterase (AChE, EC 3.1.1.7) and butyrylcholinesterase (BChE, EC 3.1.1.8), which differ in their substrate specificity [8, 9]. The cholinesterases are found in various animal tissues, such as brain, red blood cells, electric fish tissues, and animal plasma [10]. At present, the enzyme of inhibition method is mainly from head of housefly, culex, and the electric organ of electric eels [11, 12]. There is a real need to find a ChE which is more abundant in source, and easy obtainment, and it can reach the standards of pesticide inspection. Here we describe the purification and properties of a ChE from duck plasma, which may be a candidate for detection of pesticide residues.

189.2 Materials and Methods

189.2.1 Materials and Chemicals

Duck plasma, self-made (by adding fresh duck blood anticoagulant, centrifuged and collected plasma); bovine serum albumin, bcetylthiocholine iodide (BTChI), 5,5'-Dthio-bis(2-nitrobenzoic acid) (DTNB), were purchased from Sigma (St. Louis, USA); DEAE-52 ion exchange cellulose and Sephadex G-200 were purchased from Whatman Co; Coomassie brilliant blue R250 was purchase Fluka; all other chemicals used were of analytical grade.

189.2.2 Cholinesterase Activity

ChE activity assay was based on the Ellman method [13], 3 mL phosphate buffer (0.2 M, pH 8.0) and 50 μL DTNB solution (10 mg/mL) were added into a test

tube, and 50 μL of enzyme solution was added, then mixed. The mixture was incubated for 10 min at 37 °C, then 50 μL BTChI (6.5 mg/mL) was added and mixed. The yellow color produced was measured spectrophotometrically at 410 nm. Blank was also run, where phosphate buffer was used instead of enzyme.

One unit of enzyme is defined as the amount of the enzyme that catalyses the hydrolysis of 1 μM of BTChI per minute under above mentioned conditions, and all enzyme assays were preformed in triplicate [14].

189.2.3 Protein Concentration

The protein content was quantified either by measuring the absorbance at 280 nm or by Bradford Method (colorimetric protein assay at 595 nm) based on the binding of Coomassie brilliant blue dye to proteins [15].

189.2.4 Extraction and Purification of ChE

All steps were carried out at room temperature, except for salt precipitation, which was performed at 4 °C, ChE activity was measured after every purification step.

189.2.4.1 Salt Precipitation

Duck plasma was added equal volume of 20 mM phosphate buffer (pH 7.2). Solid ammonium sulphate was slowly added to duck plasma solution with shaking to obtain the 10–70 % saturation fraction. After incubation at 4 °C for 12 h, the enzymatic extract was centrifuged. The second step of precipitation was performed adding ammonium sulfate to certain saturation and incubating at 4 °C for 12 h, then centrifuged and collected supernatant. The final precipitate was dissolved in 20 mM phosphate buffer (pH 7.2) for purification. The concentration of protein and total enzyme activity was determined to confirm the most suitable saturation of ammonium sulfate dialysis.

189.2.4.2 Purification of ChE

The crude enzyme solution was loaded on DEAE-52 column (1.5 × 30 cm) equilibrated with 20 mM phosphate buffer (pH 7.8). The column was washed with the same phosphate buffer containing different concentration of NaCl (0–0.3 M) at a constant flow rate of 25 mL/h. Fractions (3 mL per tube) were collected, then protein concentration and enzyme activity were assayed. The fractions containing ChE activity were collected, and applied on Sephdex G-200 column (1.5 × 30 cm)

which was previously equilibrated with 20 mM phosphate buffer (pH 7.5) and eluted with the same buffer at flow rate of 5 mL/h. Fractions (2.5 mL per tube) was collected. Protein concentration and enzyme activity was assayed.

189.2.4.3 Gel Electrophoresis

PAGE electrophoresis of cholinesterase was carried out with discontinuous buffer system. The gel contains 8.0 % acrylamide in the resolving gel and 5 % acrylamide in the stacking gel [16].

189.2.5 Optimal Temperature and Optimal pH

The optimum temperature of ChE activity was determined by carrying out the purified ChE at selected temperatures from 20 to 50 °C in phosphate buffer (20 mM, pH 7.8). For estimation of thermal stabilities, enzyme preparations in 20 mM phosphate buffer were incubated at temperatures over the range 37–60 °C, incubation time was 60 min.

The optimal pH for the ChE was determined using BTChI as substrate. The enzyme was incubated in different pH phosphate buffer (pH 5.0–8.5). Samples were taken at regular intervals. All experiments were performed in triplicate.

189.2.6 Effect of Metal Ions

The enzyme was incubated in phosphate buffer, with addition of the following metal ion and reagents: Mg^{2+}, Ca^{2+}, Mn^{2+}, and the activity were determined thereafter using BTChI as substrate.

189.2.7 Kinetic Studies

The K_m of the purified ChE was determined by Lineweaver-Burk plots. The enzyme was incubated with BTChI of different concentrations ranging from 32.5 to 683 μM.

189.2.8 Sensitivity Test to Organophosphate and Carbamate Pesticide

The 50 μL ChE sample was added into 3 mL phosphate buffer (0.2 M, pH 8.0) including 50 μL of a certain concentration of the pesticide standard solution. The mixture was incubated for 10 min at 37 °C and then, 50 μL BTChI was added. The procedure below was the same as ChE activity assay. The nonpesticide tube was used as the blank control.

The inhibition ratio (I) of ChE activity was determined by the equation:

$$\mathrm{I}\ (\%) = (\mathrm{OD_{Blank}} - \mathrm{OD_{inhibition}}) / \mathrm{OD_{Blank}} \times 100\%$$

189.3 Results and Discussion

189.3.1 Purification of ChE

The procedures developed to purify ChE from Duck plasma are presented in Table 189.1. The crude proteins were firstly fractionated by salt precipitation. Many factors affect the salting, such as the saturation of ammonium sulfate, pH value, temperature and protein concentration and so on [3]. The concentration of protein and total enzyme activity was determined to confirm the most suitable saturation of ammonium sulfate dialysis. Firstly, ammonium sulfate was adding to the saturation of 0.25 and 0.60, then to the saturation of 0.40. Lots of other proteins were separated, but it lose some of ChE which lead to the decrease of recovery rate. After the second salting, ChE was purified 44.2 fold, and the recovery rate was 20.8 %.

After the second salting, the enzyme solution by phosphate buffer (20 mM, pH 7.8) balance DEAE-52 column, using with 0–0.3 M NaCl in phosphate buffer linear gradient elution. The results shown in Fig. 189.1, there are three protein peaks, of which the second protein peak with ChE activity was detected. Fractions associated with the peak were collected, concentrated, and subjected to Sephadex G-200 column. Sephadex G-200 gel filtration chromatography resolved the protein

Table 189.1 The purification summery of cholinesterase

Purification steps	Specific activity (U mg^{-1})	Purification fold	Yield (%)
Duck serum	21.5	1	100
The first salting out	141.8	6.6	44.2
The second salting out	939.7	44.2	20.8
DEAE-52	2830.5	132.6	18.6
SepHadex G-200	5944.1	278.5	17.8

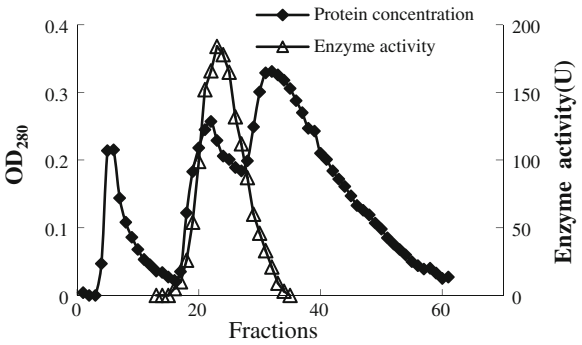

Fig. 189.1 Elution profiles of the CHE on DEAE-52

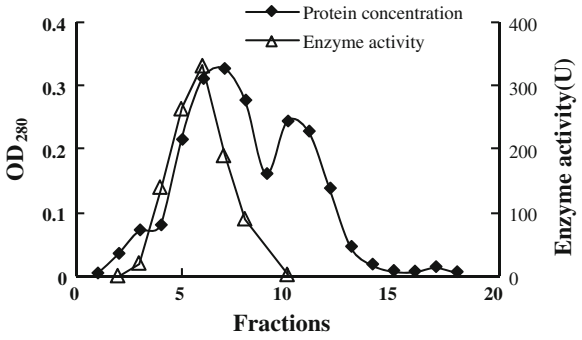

Fig. 189.2 Elution profiles of the ChE on Sephadex G-200

into two large peaks, one of which contained the ChE activity (Fig. 189.2). By these steps, the enzyme was purified 278.5 fold with a recovery of 17.8 %.

189.3.2 PAGE Gel Electrophoresis

The purified enzyme running on PAGE produced a single band when stained with coomassie brilliant blue (Fig. 189.3), whereas crude enzyme obtained by salting out has many bands that contains a lot of unwanted proteins. These results indicated that the ChE from duck plasma was purified to homogeneity by a four-step purification procedure.

189.3.3 Optimum pH and Optimum Temperature

The activity of the ChE was determined by carrying out standard assays at different pH values ranging from 5.0 to 8.5. The optimum pH of the purified ChE was around 7.5–8.0 (Fig. 189.4a).

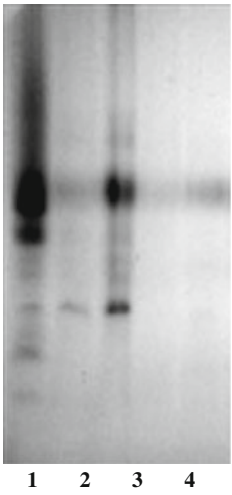

Fig. 189.3 PAGE of ChE at various purification stages Lanes. *1* Crude ChE obtained by salting out. *2* Eluate of low concentration from DEAE-52 column, *3* Eluate of high concentration from DEAE-52, *4* purified ChE by Sephadex G-200

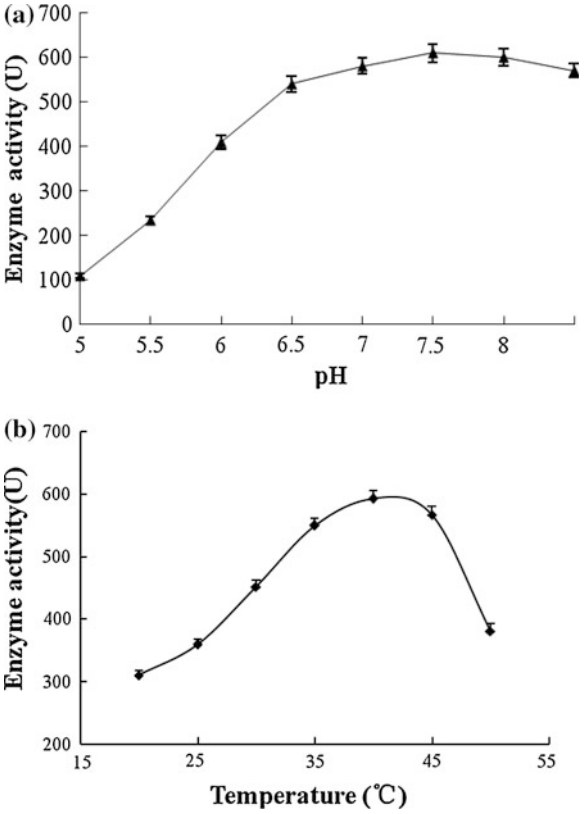

Fig. 189.4 Optimal pH (**a**) and temperature (**b**) on the activity of ChE

For estimation of the optimal temperature, the activity was determined by carrying out standard assays at temperatures over the range 20–50 °C. The enzymatic activity gradually increased in the range from 40 to 40 °C, but a decrease occurred at 45 °C. It showed maximal activity at 40 °C (Fig. 189.4b).

To estimate the thermal stability, the residual activity after an incubation of the enzyme for 60 min at different temperature was measured. The results indicated that this purified ChE was stable in a range of temperature from 37–40 °C, however it was not stable above 45 °C. 38 % relative activity was retained after 60 min of incubation at 50 °C.

189.3.4 Kinetic Parameters

According to the Lineweaver-Burk plot (Fig. 189.5), the value was calculated, which was found to be 2.4×10^{-5} M. This value is close to a number of vertebrate plasma (sheep plasma, chicken plasma) [16]. The kinetic parameters showed that ChE had a stronger affinity for BTChI. The pure enzyme activity increased in the presence of substrate concentrations from 32.5 to 683 μM, which indicated that BTChI for this enzyme has not excessive inhibition.

189.3.5 Effects of Metal Ions

Some metal ions were examined for their effects on the cholinesterase activity at a concentration of 5 mM. The presence of Ca^{2+}, Mg^{2+} and Mn^{2+} positively influenced the enzyme activity. Mg^{2+} stimulated the enzyme activity up to 119.2 %. Whereas high concentration of these metal ions inhibited the enzyme activity.

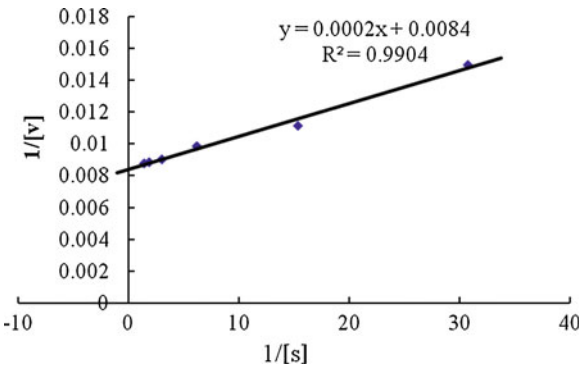

Fig. 189.5 Lineweaver-Burk plot of ChE

Table 189.2 The Linear equation of some pesticides

Pesticides	Linear equation	r^2
Dichlorphos	y = 0.6012 x + 2.2904	0.9921
Ethyl parathion	y = 0.2754 x + 0.9898	0.8779
Methyl Parathion	y = 0.5992 x + 1.6248	0.9930
Carbofuran	y = 0.6975 x + 1.4984	0.9990
Pirimicarb	y = 0.7072 x + 1.2268	0.9901
Methamidophos	y = 0.5772 x + 0.4428	0.9940
Dimethoate	y = 0.3526 x + 0.4286	0.9903
Omethoate	y = 0.5619 x + 0.1731	0.9359

189.3.6 Sensitivity Test to Organophosphate and Carbamate Pesticides

The degree of sensitivity to the pesticides was evaluated by using a linear slope obtained from a calibration graph of common logarithm of pesticide concentration versus inhibition ratio [17].

The sensitivity of ChE to 8 species of pesticides is shown in Table 189.2. It has highly sensitive to most of organophosphate and carbamate pesticides (Dichlorphos, Pirimicarb, Carbofuran and so on) with good linearity (r^2 from 0.8779 to 0.9990), but sensitivities to Methamidophos and Dimethoate were not very good. The purified ChE was shown to be high sensitive enough for detection the food samples. By calculating inhibition rate of ChE activity, the condition for pesticide residues could be estimated. The standard of detection was a dosage of inhibiting 35 % of ChE activity.

189.4 Conclusion

In summary, our study has found purified ChE is a BChE with a higher efficiency for BTChI. The nondenaturing PAGE revealed a single band. It has identical catalytic properties to those purified from different animal plasma in its pH optimum and temperature optimum for activity and stability [18, 19]. The ChE showed maximal activity at 40 °C and at pH 7.5–8.0. The enzyme is of good thermo stability and estimated a high degree of specific activity (5944.1 U/mg of protein). Further studies showed that this ChE has a high sensitivity to inhibition by some organophosphate and carbamate pesticides.

At present, the animal-origin AChE is the main enzyme used in the enzyme inhibition method for detecting organophosphate and carbamate pesticides [20]. The ChE from duck plasma obtained is more abundant, easy to obtain. This and future studies showed that this ChE was a valuable alternative for detecting organophosphate and carbamate pesticides of vegetables and fruits. The standard

of detection was a dosage of inhibiting 35 % of ChE activity. When the inhibition rate was higher than 35 %, it indicated that the sample had excessive pesticide residues. The detection time was 20 min, and several samples can be determined at the same time.

Acknowledgments This work was supported by a grant from Technology Department of Hubei Province of China (Grant NO.C2002AA207B07).

References

1. Liu T, Su H, Qu X et al (2011) Acetylcholinesterase biosensor based on 3-carboxyphenylboronic acid/reduced graphene oxid-gold nanocomposites modified electrode for amperometric detection of organophosphorus and carbamate pesticides. Sens Actuators B- Chem 160:1255–1261
2. Istamboulie G, Andreescu S, Marty JL et al (2007) Highly sensitive detection of organophosphorus insecticides using magnetic microbeads and genetically engineered acetylcholinesterase. Biosens Bioelectron 23(4):506–512
3. Li JK, Zhou YL, Wen YX et al (2009) Studies on the purification and characterization of soybean esterase, and its sensitivity to organophosphate and carbamate pesticides. Agric Sci China 8(4):455–463
4. No HY, Kim YA, Lee Y (2007) Cholinesterase-based dipstick assay for the detection of organophosphate and carbamate pesticides. Anal Chem Acta 594(1):37–43
5. Benilova IV, Arkhypova VN, Dzyadevych SV et al (2006) Soldatkin. Kinetics of human and horse sera cholinesterases inhibition with solanaceous glycoalkaloids: Study by potentiometric biosensor. Pestic Biochem Phys 86(3):203–210
6. Yücel YY, Tacal O, Ozer I (2008) Comparative effects of cationic triarylmethane phenoxazine and phenothiazine dyes on horse serum butyrylcholinesterase. Arch Biochem Biophys 478(2):201–205
7. Askar KA, Kudi AC, Moody AJ (2011) Purification of soluble acetylcholinesterase from sheep liver by affinity chromatography. Appl Biochem Biotechnol 165(1):336–346
8. Nese Cokugras A (2003) Butyrylcholinesterase: structure and physiological importance. Turk J Biochem 28(2):54–61
9. Chuiko GM (2000) Comparative study of acetylcholinesterase and butylcholinesterase in brain and serum of several freshwater fish: specific activities and in vitro inhibition by dichlorvos, an organophosphorus pesticide. Comp Bichem Phys C 27:233–234
10. Frasco MF, Fournier D, Carvalho F et al (2006) Cholinesterase from the common prawn (Palaemon serratus) eyes: Catalytic properties and sensitivity to organophosphate and carbamate compounds. Aquat Toxicol 77(4):412–421
11. Rodrigues SR, Caldeira C, Castro BB et al (2011) Cholinesterase (ChE) inhibition in pumpkinseed (Lepomis gibbosus) as environmental biomarker: ChE characterization and potential neurotoxic effects of xenobiotics. Pestic Biochem Phys 99:181–188
12. Sturm A, Assis HC, Hansen PD (1999) Cholinesterases of marine teleost fish: enzymological characterization and potential use in the monitoring of neurotoxic contamination. Mar Environ Res 47(4):389–398
13. Ellman GL, Courtney KD, Andres V et al (1961) A new and rapid colermetic determination of acetylcholinesterase activity..Biochem Pharmacol 7:88–95
14. Mohamed MA, Abdel-Gawad AS, Ghazy AE (2007) Purification and characterization of an acetylcholinesterase from the infective Juveniles of Heterorhabditis bacteriophora. Comp Bichem Phys C 146(3):314–324

15. Forget J, Livet S, Leboulenger F (2002) Partial purification and characterization of acetylchinesterase (AChE) from the estuarine copepod Eurytemora affinis (Poppe). Comp Bichem Phys C 132(1):85–92
16. Assiri AM (2003) Cholinesterase in plasma: purification and some biochemical properties. J Chem Soc Pak 25(1):63–67
17. Andreescu S, Noguer T, Magearu V et al (2002) (2002) Screen-printed electrode based on AChE for the detection of pesticides in presence of organic solvents. Talanta 57:169–176
18. Pardío VT, Ibarra N, Rodríguez MA et al (2001) Use of cholinesterase activity in monitoring organophosphate pesticide exposure of cattle produced in tropical areas. J Agric Food Chem 49:6057–6062
19. Ferrari A, Venturino A, Pechén de D'Angelo AM (2007) Muscular and brain cholinesterase sensitivities to azinphos methyl and carbaryl in the juvenile rainbow trout Oncorhynchus mykiss. Comp Biochem Physiol C 146:308–313
20. Istamboulie G, Andreescu S, Marty JL et al (2007) Highly sensitive detection of organophosphorus insecticides using magnetic microbeads and genetically engineered acetylcholinesterase. Biosens Bioelectron 23:506–512

Chapter 190
Study on the Sensitivity of Two-Line Hybrid Rice's Self-Fruitful Rates on Temperature Changes: A Numerical Study

Zhiwei Wang, Qingdai Liu and Zetian Hua

Abstract The yield of two-line hybrid rice is greatly affected by the self-fruitful rates. In the present paper, we have investigated the meteorological data related to the growth of two-line hybrid rice P88S, and found that the self-fruitful rates of different growth periods have showed some sensitivity to temperature changes. Based on a nonlinear model, we have proposed the impacts of temperature changes on self-fruitful rates have been analyzed. By numerical studies, we found that in the case of temperature fluctuating, the temperature fluctuations should account for the change of the self-fruitful rates. The results may shed light on the study of the effects of climate changes on the factors that account for the rice yields.

Keywords Hybrid rice · Sensitivity · Nonlinear model · Temperature change

190.1 Introduction

The impacts of solar radiation and temperature on rice yield remain poorly understood, despite decades of agronomic research. Current knowledge is based primarily on field trials and greenhouse experiments. These experimental studies showed that increased temperature can reduce yield [1–4]. For the two-line hybrid rice in China, the reduction of yield accounts for lower self-fruitful rate. The two-line hybrid rice was developed on the base of the three-line hybrid rice, and has been widely used because of the advantages of simplified producing procedure, free hybridization matches, and the convenience to use the hybrid advantages [5]. The low summer temperature of 1989 and the abnormal low temperature in Hunan of 1991 led to the repetition of the fertility of several photo-thermo sensitive genic

Z. Wang · Q. Liu · Z. Hua (✉)
College of Food Engineering and Biotechnology, Tianjin University of Science and Technology, Tianjin 300457, People's Republic of China
e-mail: 15904054936@139.com

T.-C. Zhang et al. (eds.), *Proceedings of the 2012 International Conference on Applied Biotechnology (ICAB 2012)*, Lecture Notes in Electrical Engineering 251,
DOI: 10.1007/978-3-642-37925-3_190,

male sterile (PTSGMS) lines, thus, the effect of the temperature on the fertility of PTSGMS lines had been paid more and more attention [6]. After a plenty of researches under natural and artificial conditions, the relations between the temperature and fertility had been clarified step by step [7].

Several studies have showed that the critical temperature of the fertility alteration has relations with the individual development stages and the lasting time [8]. Chen et al. have studied the thermosensitive sterile line with different developmental stages under the treatment of long photo (light 14 h/d) and low temperature (22–24 °C), and the results showed that some sterile lines only need 3 d to inhibit the expression of sterile genes in the meiosis stage, while other sterile lines need 7 d treatment to become fertile [9]. This study showed that the cumulative effects of the temperature. In the present article, by analyzing the fertility alteration experimental data of P88S in Hainan [10], we attempt to find the relations of some meteorological data and the corresponding self-fruitful rates.

190.2 Data and Methods

190.2.1 Data

P88S is a photo-thermo sensitive hybrid rice sterile line developed by the National Hybrid Rice Technology and Engineering Center; it is sterile in high temperature and fertile in low temperature. When the temperature is lower than 26 °C, the fertility is good, while the temperature is higher than 28 °C, it cannot easily reproduce. Moreover, when the temperature lies between 26 and 28 °C, the fertility shows instability. The fertility alteration data of P88S from Hainan was analyzed [10], and the results showed that the self-fruitful rates between Oct. 17 and Nov. 15 in 2005 are 5.0–38.5 %, which corresponded to good fertility, and the self-fruitful rates between Mar. 12 and Apr. 3 in 2006 are 0.1–14.7 %, which corresponded to bad fertility. The highest temperature during these two time spans is from about 28 to 26 °C and from 26 to 28 °C.

190.2.2 Bistable Model

In our previous work [11], we found that the dependence of the fertility or self-fruitful rates of P88S on the temperatures can be explained by bistable dynamics, one of a nonlinear dynamics. Thus we incorporated a bistable dynamical model as below:

$$\frac{dx}{dt} = \frac{1 + x^2 + \alpha\sigma_1 x^4}{1 + x^2 + \sigma_1 x^4 + \sigma_2 x^6} - Tx \tag{1}$$

Here α, $\sigma 1$, and $\sigma 2$ are control parameters that are related to the absolute fertile temperatures and the absolute sterile temperatures, T is the temperature, with the unit of centigrade, x is an order parameter that accounts for the fertility of P88S. When T is given a fixed numerical value, the solves that correspond to the change rate of the order parameter x can be solved. In this study, the critical value of x is 0.07, i.e., when $x > 0.07$, the fertility of P88S is regarded as fertile, which corresponds to a high self-fruitful rate; while when $x \leq 0.07$, the fertility is regarded as sterile, which corresponds to a low self-fruitful rate.

For P88S, the unstable fertility interval of temperatures is between about 26 and 28 °C. By computer simulations, we calculated the three parameters of the above model are: $\alpha = 3.80$, $\sigma 1 = 0.08$, and $\sigma 2 = 19{,}000$. Thus the final bistable model that accounts for the temperature-related self-fruitful rates is as below:

$$\frac{dx}{dt} = \frac{1 + x^2 + 3.80 \times 0.08x^4}{1 + x^2 + 0.08x^4 + 19000x^6} - Tx \tag{2}$$

190.2.3 Simulation Details

Using Eq. (2), we attempt to deduce the dependency of the order parameter that accounts for the fertility or the self-fruitful rate of P88S on the temperatures, both the values and the change property of the temperature. Equation (2) was simulated by computer, and we adjusted the temperatures from 25 to 29 °C, and the step is 0.001, the solved x (for $dx/dt = 0$) is the order parameter. For the temperature with variation across a period (several days), the same simulation parameters were used.

190.3 Results and Discussion

From the data of [10]. one can see that the expression of the fertility of thermosensitive sterile rice P88S is related to the cumulative effect of the temperatures. Before Oct. 17, the ear differential process of P88S were affected by high temperature for a long time, even when the temperature was declined to below 28 °C, the fertility expression was still male sterile. Until the temperature was fallen down to below 26 °C, the fertility can change to fertile. Meanwhile, before Mar. 12, the ear differential process of P88S were affected by low temperature for a long time, even when the temperature was raised up to over 26 °C, the fertility expression was still male fertile. Until the temperature was raise up to over 28 °C, the fertility can change to sterile. The results showed that the fertility of P88S between 26 and 28 °C was decided by the temperatures and the cumulative effects of the temperatures collectively.

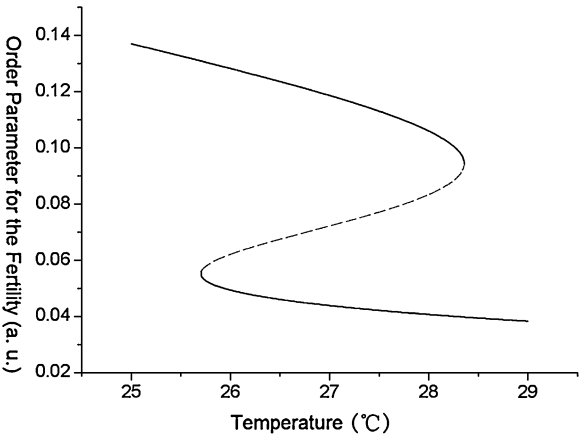

Fig. 190.1 The dependence of the order parameter of P88S sterility on the temperatures

The simulation results of Eq. (2) has only one solution when $x \leq 25.702$ and $x \geq 28.356$, while it has three solutions when $25.702 < x < 28.356$. The solutions between 25 and 29 °C are shown as below:

From Fig. 190.1 one can see that when the temperature is below 25.7 °C, P88S shows fertile, with high self-fruitful rate, while when the temperature is over 28.3 °C, P88S shows sterile, with low self-fruitful rate. Moreover, when the temperature lies between them, both of the possibilities of fertile and sterile exist. The computational results are coincide with the experiment data from [10] approximately.

Here T is a constant, while the temperature often fluctuates, and this effect must be considered. Let T = T0*[1 + A*Sin(ωt)], here A is the amplitude and ω is the frequency of the temperature fluctuation, the Gaussian fluctuation is used for simplification. From Fig. 190.1 one can see that for a given temperature between 25.7 and 28.3 °C, the state is decided by the original value. For example, if the temperature is 27 °C, the self-fruitful rate stays high if the original order parameter x is larger than 0.07, while it remains low if x is smaller than 0.07. This property would not change if the temperature fluctuation A is small, as shown by Fig. 190.2a. However, if A become larger, the self-fruitful rates may undergo a transition from high to low or from low to high, as shown by Fig. 190.2b.

The results shown in Fig. 190.2 indicate that the self-fruitful rates have showed sensitivity to temperature changes. If the temperature changes with large amplitude, the self-fruitful rates often undergo transition from 0.12 to 0.02, and the fertility is hardly to predict, which make the yield decline. There are some papers ascribe the reduction of the yield of two-line hybrid rice to abnormal low temperature. However, if the model above is reasonable, the cause is maybe the temperature fluctuation, or we can say the fluctuation is the main reason rather than the temperature value. However, since the hypothesis used in our study is simple, further experimental and theoretical studies are needed to illustrate the mechanisms of such phenomenon.

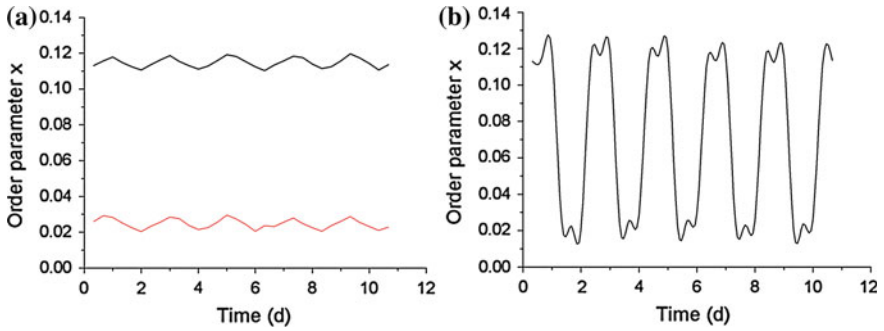

Fig. 190.2 Simulation results of Eq. (2) after considering $T = T0*[1 + A*\mathrm{Sin}(\omega t)]$. Here $T0 = 27$, $\omega = 2\pi$, and t has the unit of day. The different are **a** $A = 0.01$, and the original value of X is 0.09 (*black*) and 0.03 (*red*), respectively, **b** $A = 0.09$, and the original value of X is 0.09 or 0.03

190.4 Conclusion

In the present paper, based on the self-fruitful rates data of two-line hybrid rice P88S in Hainan and a nonlinear model we proposed, we have studied the effect of temperature fluctuations on the order parameters of the self-fruitful rates, and found that large temperature fluctuations induce the state transitions, and make the fertility unstable. The results may shed light on the study of the effects of climate changes on the factors that account for the rice yields.

Acknowledgments This work was supported by National Science Foundation of China (Grant No. 20903071, 30900339), China Postdoctoral Science Foundation (Grant No. 2011M500528, 20110490786, 2012T50231), Natural Science Foundation of Tianjin, China (Grant No. 11ZCKFNC01200), and National High-tech R&D Program of China (863 Program) (Grant No. 2011AA10A101).

References

1. Yoshida S, Parao FT (1976) Climatic influence on yield and yield components of lowland rice in the tropics. In: Proceedings of the Symposium on Climate and Rice pp 471–491
2. Yoshida S, Satake T, Mackill D (1981) High temperature stress. IRRI Res Pap 67:1–15
3. Seshu DV, Cady FB (1984) Response of rice to solar radiation and temperature estimated from international yield trails. Crop Sci 24:649–654
4. Wassmann R (2009) Climate change affecting rice production. Adv Agron 101:59–122
5. Qiu ZG (2006) Research progress and application of photo-thermo sensitive genic male sterile rice. J Anhui Agri Sci 34:5228–5230
6. Yuan LP (1992) Technical strategies of the utilization of PTGMS lines in rice. Hybrid Rice 1:1–4
7. Sun ZX (1991) Oryza sativa L.subsp.indica fertility reaction under artificial control conditions. Acta Zhejiang Argi Univ 3:101–105

8. Zhang ZG, Lu XG, Yuan LP (1992) Reflections on identification of light and temperature properties of fertility transformation of PGMR. Hybrid Rice 6:29–32
9. Chen LB, Li XZ, Zhou GQ (1993) Study of the effects of temperature on the fertility of thermo-sensitive male sterile rice. Acta Crop 19:47–54
10. Wang XN, Meng WD, Yan XW et al (2010) Fertility alteration characteristics and application of rice PTGMS line P88S in Hainan. Hybrid Rice 25(4):26–27
11. Wang ZW, Ji DW, Zhang Q, Hua ZT (2011) The construction of accumulative temperature model for fertility alteration of two-line sterile line P88S. J Anhui Agri Sci 39(29):17837–17838

Chapter 191
The Changes in Physicochemical Properties of Lacquer Wax by Physical Adsorption and UV Light

Yuan-Feng He, Cheng-Zhang Wang, Yan-he Dong, Jian-Zhong Ye, Hao Zhou and Hong-Xia Cheng

Abstract In order to make the dark green pigments fade away and broaden the appliance of lacquer wax, both physical adsorption and ultraviolet (UV) irradiation were optimized and further compared in this paper. The optimal conditions of physical discoloration could be achieved in 80 °C when 20 mL petroleum ether blends with 1 g raw wax assisted by 5 % activated carbon/kieselguhr (1:1, m/m) as an adsorbent for 30 min, twice. A good bleaching effect of lacquer wax of UV radiation can be reached in 60 °C for 60 h. The CIEL*a*b* system and Hunter whiteness formula were used to evaluate the discoloration effect. The value of peroxide, iodine, acid, and relative contents were imported to present the physical–chemical characterizations alteration. The chemical constituents variation of lacquer wax during the discoloration process was detected by GC-MS analyzer. A sharp increase of whiteness (by 54 %) occurred after these two processes and insignificant decrease in physical–chemical qualities indicated an effective and specificity method.

Keywords Chemical constituents · Lacquer wax · Physical discoloration · Rhus vernicifera · UV irradiation

191.1 Introduction

Rhus vernicifluum is a wide distribution economic tree in Asian countries, such as China, Korea, Japan, etc. The secretion of *R. vernicifluum* bark, known as lacquer sap, has been used as superior coating materials in the history of China for more than

Y.-F. He · C.-Z. Wang (✉) · Y. Dong · J.-Z. Ye · H. Zhou · H.-X. Cheng
Institute of Chemical Industry of Forest Products, CAF, Nanjing 210042, People's Republic of China
e-mail: wangczlhs@sina.com

C.-Z. Wang
Key and Open Laboratory on Forest Chemical Engineering, SFA, Nanjing 210042, People's Republic of China

T.-C. Zhang et al. (eds.), *Proceedings of the 2012 International Conference on Applied Biotechnology (ICAB 2012)*, Lecture Notes in Electrical Engineering 251,
DOI: 10.1007/978-3-642-37925-3_191,

7,000 years [1]. Lacquer sap is an absolutely natural polymer and is used as an accessory in daily life. Another important resource from lacquer trees is lacquer wax, the extraction of the seed peel of *R. vernicifluum*. The resources of lacquer trees and their seeds are abundant, with more than 500 million trees cultivated in China currently. There are about 30 species of these trees producing as much as 1.5 million tons of seeds per year, which contain large amounts of wax (about 10 %, w/w). Wax is being used for 100 years in Japan, as candles, waterproof agents, coating, especially in cosmetics, medicines, electronic photography toner, etc. Though useful and abundant, lacquer wax has not been intensely processed and utilized yet [2, 3]. The main component of lacquer wax is triglycerides, including palmitin (65 %) and stearin (30 %); however, a small amount of pigment exists that leads to an unpleasant color which restricts the utilization of lacquer wax. Activated carbon has been used to discolor the lacquer wax in China, however, the bleaching process is poor [4, 5]; what is more, activated carbon is expensive and the high viscosity of lacquer wax makes the filtration process difficult, so, how can we enhance the discoloration process? Kieselguhr is a relatively cheaper absorbent and has been used in the decoloration of oil, a blending of Kieselguhr and active carbon has been prepared to strengthen the decoloration efficiency of lacquer wax. In addition, a traditional method of producing Japan wax is sunlight irradiation [6–8]. This however depends on the weather and is time-consuming. Due to its low yield and labor-intensiveness, this old-fashioned method is uneconomical and inefficient. It is suggested that UV light irradiation may serve as an alternative and effective discoloration method without depending on weather conditions. Physical properties, major fatty acid contents, and seasonal variations of some biochemical constituents of haze wax have been investigated [9–11]; while only a few literatures reported the influence of the discoloration process on physicochemical properties of lacquer wax. The aim of this paper was to investigate the discoloration of lacquer wax via physical adsorption and UV irradiation. The changes in physical and chemical properties of lacquer wax were investigated as well.

191.2 Materials and Methods

191.2.1 Chemicals and Plant Materials

Lacquer berries were collected in November, 2010 from Ankang, Shanxi and dried at 45 °C for 10 h in the oven. The dried fruit, with less than 7.0 % water, was crushed to remove the husks and seed kernel. The remaining pulp was ground into powder and stored dry and darkness. The samples of Japan wax, produced by Araki Wax Co, Japan, were obtained from Dr. S. Noshiro (Forestry and Forest Products Research Institute, Japan). Standard methyl ethers of fatty acids were purchased from Shanghai A Pu Chemical Reagent Co, Ltd. Activated carbon, kieselguhr, and solvents were purchased from Nanjing Chemical Industries Co, Ltd.

191.2.2 Preparation of Raw Lacquer Wax

The pulp powder was extracted twice by petroleum ether (60–90 °C) with a solid–liquid ratio of 1:20 (g/mL), at 80 °C for 60 min, then the extraction was mixed, filtered, and condensed in vacuum equipment; the residue yielded raw lacquer wax with green color and 45 % weight of the pulp powder.

191.2.3 Physical Discoloration of Raw Lacquer Wax

Single factors experiments, adsorbents (activated carbon and kieselguhr), discoloration time (10, 20, 30, 40, 50, 60 min.), temperature (50, 60, 70, 80, 90 °C), and extraction times (1, 2, 3, 4) were carried out in a three-neck flask with stirrer. The orthogonal experiments were designed by $L_9(3^4)$ of three factors of ratio of raw wax to solvent (g/mL), discolor temperature, and times.

Two grams of raw wax were dissolved in petroleum ether each time. After filtrating, the filtrate was condensed under vacuum; the residue was cooled and solid lacquer wax obtained. The whiteness of the lacquer wax was then measured.

191.2.4 UV Irradiation of Raw Lacquer Wax

Two grams of raw lacquer wax was placed in a petri dish (6 cm in diameter (ID) × 1.1 cm height (H)), and irradiated under a UV lamp of 400 W. The irradiated time changes from 10 to 80 h at 50, 60, and 70 °C, respectively, the whiteness of the samples was measured after solidification.

191.2.5 Detection Method of Whiteness

The color of lacquer wax was measured using a HunterLab MiniScan@ XE Plus (Hunter Associates Laboratory Inc., USA). Color measurements (L^*, a^*, b^* values) were taken in which L^* refers to lightness, a^*, b^* relates to redness and yellowness, respectively. The wax color was indicated according to whiteness index calculated by the Hunter whiteness formula. $W = 100 - ((100 - L^*)^2 + a^{*2} + b^{*2})^{1/2}$.

191.2.6 Determination of Chemical Constituents of Lacquer Wax

The volatilization of triglycerides is low, lacquer wax should be methylated first to improve its chromatography and become easier to be separated [6–8]. 100 mg of the lacquer wax was put in a 10 mL tube and 2 mL of a 0.5 mol/L sodium solution hydroxide-methanol was added, shook, then placed in a water bath (60 °C) for 30 min. 5 ml of n-hexane was added subsequently. The constituent of lacquer wax was detected by GC–MS, equipped with an SE-30 capillary column. The injector temperature was 280 °C, gas chromatography oven was programmed to provide a constant temperature with an increased rate of 10 °C per min from 110 to 220 °C, 10 min at 110 °C and 18 min at 220 °C, Helium was used as carrier gas with a flow rate of 1 mL/min. The mass spectrometer was operated in 70 eV EI mode which scans from 29.0 to 450.0 u in the full-scan acquisition mode. The EI source had a temperature of 230 °C. Identification of the constituents of the fatty acids was based on computer matching by commercial mass spectra (NIST and WILEY Mass Spectral Search Program). The content of the constituents was calculated and expressed as a peak area percentage computed by Chemstation, an accompanying software.

191.2.7 Determination of Physical Property of Lacquer Wax

The relative density/reflect rate/acid value/saponification value/unsaponification matter content/iodine value/peroxide value of lacquer wax were measured according to GB/T5526-1985, GB/T5527-1985, GB/T5530-85, GB/T5534-1995, GB/T5535-85, GB/T5532-1985, GB/T5538-1995, respectively. Melting point of lacquer wax was analyzed by melting point apparatus.

191.2.8 Statistic Analysis

All experiments were run in triplicate, SPSS 10.0 for Windows (SPSS Inc., Chicago, IL, USA) was used to analyze the variance (ANOVA), the effect of discoloration was subject to variance and Duncan test. A value of $p < 0.05$ was considered statistically significant.

191.3 Results and Discussion

191.3.1 Physical Adsorption

Activated carbon and kieselguhr were chosen as adsorbents for the discoloration experiments, the best ratio was investigated. 100 mg of adsorbent, whose ratios of the activated carbon and kieselguhr were 0, 20, 40, 60, 80, and 100 %, respectively, combined with 40 mL petroleum ether, and 2 g lacquer wax added in the flask and heated at 80 °C for 30 min. As can be seen from Fig. 191.1a, the discoloration effect increase in the ratio of kieselguhr increased from 0 to 40 % while it decreased from 40 to 100 %; it was concluded that when kieselguhr was added with a ratio of 2:3 (kieselguhr: active carbon) it can reach an optimized decoloration effect.

Activated carbon and kieselgu with the ratio of 1:1 were chosen as adsorbent, and the doses of the adsorbent were 2.5, 5, 7.5, and 10 % (weigh to wax), respectively. Results are shown in Fig. 191.1b, as can be seen from the results, the discolored effect increased from 0 to 5 % while did not change much from 5 to 10 %, it was believed that the matter which generated color of the wax was exhausted when the content of adsorbent was above 5 %.

2 g of lacquer wax combined with 40 mL petroleum ether and, 0.1 g (5 % of weigh to lacquer wax) of adsorbent were used, which with an optimal ratio of activated carbon and kieselgu, under water bath at 80 °C, the lacquer wax was decolorated by stirring for different times, 1, 2, 3, 4, respectively, 30 min for each

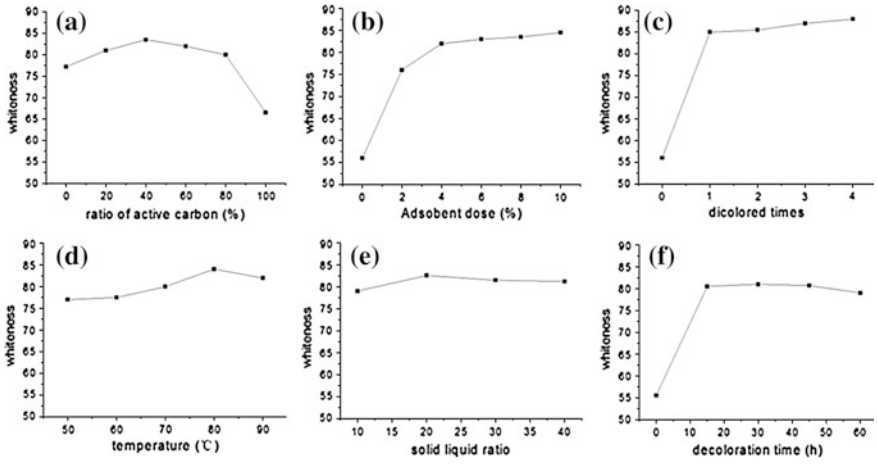

Fig. 191.1 Single factor discoloration experiments by physical adsorption. **a** selection for the ration of diatomite to activated carbon; **b** selection for the adsorbent dose; **c** selection for the discoloration times; **d** selection for temperature; **e** selection for solid-liquid ratio; **f** selection for discoloration time

procedure, the stirring speed was 120 r/min. As can be seen from Fig. 191.1c, the whiteness increased slightly after decolorated for twice.

Lacquer wax was decolorated under water bath at 50 , 60 , 70 , 80, and 90 °C for once, respectively. Results from Fig. 191.1d showed that the optimal temperature was 80 °C, and a temperature of 70 , 80, and 90 °C should be chosen to orthogonal experiment.

In the same way, the ratios of petroleum ether to lacquer wax of 1:10, 1:20, and 1:30 by discoloration time of 30, 45, and 60 min were chosen for the orthogonal experiment (Fig. 191.1e and f).

191.3.2 Orthogonal Experiments

Orthogonal experiment was devised based on the results of the single factor experiments. The conditions and experimental results of the orthogonal experiment are summarized in Table 191.1. As shown by the data in Table 191.1, the temperature was the most significant factor of the discoloration process.

K1, K2, K3 represent the whole influence of a single factor of the same leave, k1, k2, k3 value are the average values of K1, K2, K3, which correspond to the importance of the factor. Among all of the factors, the bigger the value, the more important the factor is. It was concluded that the best discoloration conditions were $A_2B_2C_3$ from Table 191.1, the optimal conditions of lacquer wax concluded from the comprehensive analysis above was choosing petroleum ether as solvent

Table 191.1 Result of orthogonal experiment

No	Temperature (°C)	Solid/liquid ratio	Time (min)	Blank rows	Whiteness
1	70 (A_1)	1:10 (B_1)	30 (C_1)	1	80.02
2	70 (A_1)	1:20 (B_2)	45 (C_2)	2	80.10
3	70 (A_1)	1:30 (B_3)	60 (C_3)	3	82.05
4	80 (A_2)	1:10 (B_1)	45 (C_2)	3	83.40
5	80 (A_2)	1:20 (B_2)	60 (C_3)	1	85.36
6	80 (A_2)	1:30 (B_3)	30 (C_1)	2	84.69
7	90 (A_3)	1:10 (B_1)	60 (C_3)	2	81.81
8	90 (A3)	1:20 (B2)	30 (C1)	3	84.84
9	90 (A3)	1:30 (B3)	45 (C2)	1	82.55
K1	242.17	245.23	249.55	247.93	T = 744.82
K2	253.45	250.30	246.05	246.60	–
K3	249.20	249.29	249.22	250.29	–
k1	80.72	81.74	83.18	82.64	–
k2	84.48	83.43	82.02	82.20	–
K3	83.07	83.10	83.07	83.43	–

K1 ~ 3 value is the sum of leave 1, 2, 3, respectively, k1 ~ 3 value is the avenge of leave 1, 2, 3, respectively; blank row corresponding to the leave number

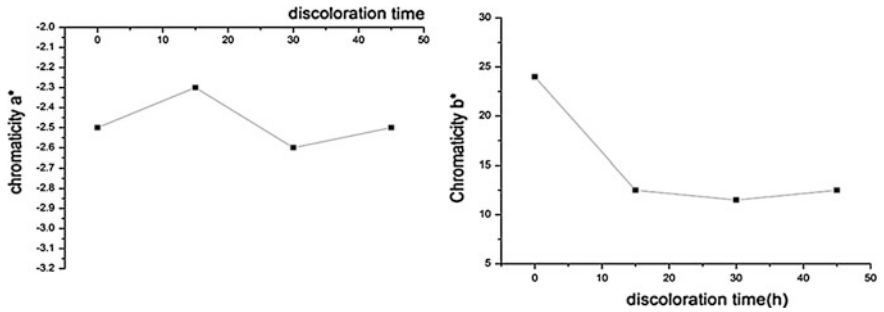

Fig. 191.2 The variation trend of chromaticity a^* and b^* with time in UV discoloration of lacquer wax

(1:20, g/mL), activated carbon-kieselguhr = 1:1 (g/g) as adsorbent which 5 % weight to wax, kept a temperature of 80 °C for 60 min, twice.

191.3.3 Changes of Chromaticity Values

a^* and b^* are the chromaticity values in the Hunter completely whiteness formula, $+a^*$ represents the redness and $-a^*$ represents the greenness, while $+b^*$ signifies yellowness and $-b^*$ represents the blueness. The changes of the chromaticity values of lacquer wax under 60 °C are shown in Fig. 191.2. As can be seen from the two figures, the color of the lacquer wax was light green and yellow, this coloration could be due to the presence of chlorophyll and carotene, respectively. The value of a^* had not changed significantly while b^* was decreased with the extension of the discoloration time, which demonstrated that the main pigment absorbed by the adsorbent is carotenoid.

191.3.4 Discoloration by UV Irradiation

Discoloration by UV irradiation was investigated as well. As can be seen from Fig. 191.3, the whiteness of the raw lacquer wax which was 55.82 could go up to 85.36 after ultraviolet discoloration. The discoloration time was the most significant factors, the longer the better as shown by Fig. 191.3. Discoloration for 60 h could achieve the best discoloration effect. The temperature had a smaller effect on the UV discoloration experiments of lacquer wax. A temperature of 60 °C could satisfy well since the melting range was from 50 to 60 °C.

The changes of the chromaticity values of the lacquer wax in 60 °C are shown in Fig. 191.4. As can be seen from the two figures, the values of a^* and b^* were decreased with the extension of the irradiation time, especially for the change of

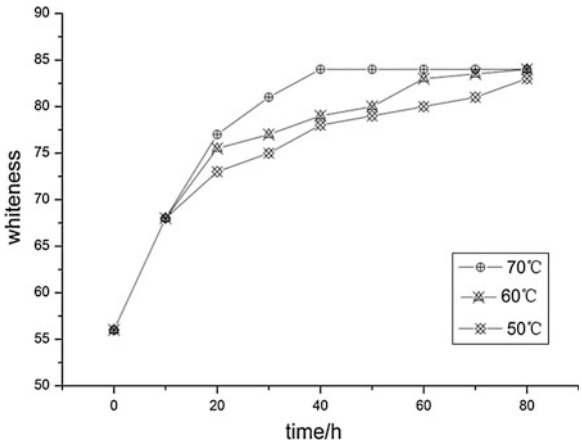

Fig. 191.3 Effect of discoloration time under different temperatures

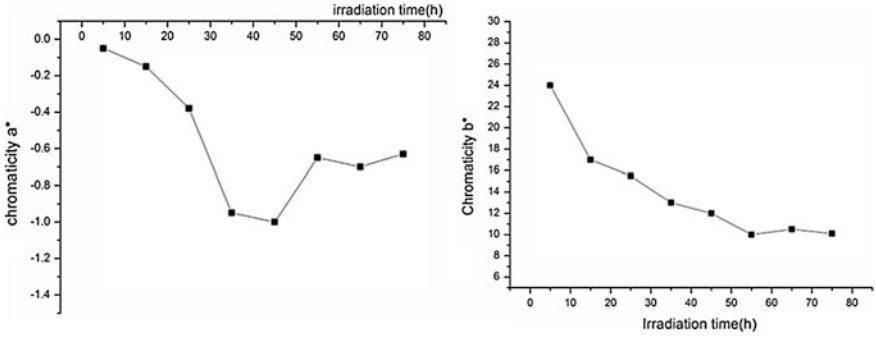

Fig. 191.4 The variation trend of chromaticity a^* and b^* with time in UV discoloration of lacquer wax

value b^*. The reason can be explained as follows, there are plenty of unsaturated group in natural pigment, which can absorb the energy of the visible light, however, double bonds were oxidized under UV irradiation and the chromospheres disappeared consequently [12–14].

Chemical constituents of the lacquer wax before and after discoloration by physical adsorption were analyzed by GC-MS. The relative content of each component were calculated according to area normalization, as can be seen from Table 191.2, the chemical constituents had not changed significantly and keep the variation of the relative contents of palmitic acid, oleic acid and stearic acid within 5 %, which attributed to the decrease of free acid adsorbed by the adsorbent, however, the relative content of three kinds of dibasic acids decreased evidently, it is indicated that dibasic acids are more easier to be absorbed by the adsorbent. Physical properties of melting point did not change obviously. However the acid

Table 191.2 Change of physicochemical properties of lacquer wax by physical adsorption

Main fatty acid	A (%)	B (%)
Myristic acid	0.896 ± 0.0107	0.853 ± 0.0104
Palmitic acid	60.121 ± 0.494	57.149 ± 0.368
Linoleic acid	0.825 ± 0.0112	0.754 ± 0.0108
Oleic acid	14.329 ± 0.213	16.102 ± 0.0198
Stearic acid	12.751 ± 0.176	13.223 ± 0.0182
Hexadecanedioic acid	0.853 ± 0.0086	0.602 ± 0.0101
Eicosanoic acid	1.655 ± 0.0232	1.534 ± 0.0196
Docosanedioic acid	0.844 ± 0.103	0682 ± 0.0084
Eicosanebioic acid	2.713 ± 0.0362	2.117 ± 0.0381
Physical properties	A	B
Melting point	52.13 ± 0.382	50.68 ± 0.292
Acid value	87.52 ± 0.837	82.98 ± 0.781
Iodine value	13.65 ± 0.196	9.95 ± 0.183
Peroxide value	6.22 ± 0.0831	3.24 ± 0.0642

A and B represent original and discoloration lacquer wax respectively ($n = 3$, $p < 0.05$)

value, iodine value, and peroxide value were slightly decreased after physical discoloration. The property of the wax was meliorated due to decreasing of peroxide value and acid value.

Chemical constituents and the relative contents of the lacquer wax which were discolored at UV light and the original lacquer wax were detected by GC-MS. The results are shown in Table 191.3. Relative contents of oleic acid and linoleic acid decreased with the irradiation time, especially for the relative content of linoleic acid as it had been completely degraded by the irradiation time of 60 h, oleic acid decreased from 14.329 to 10.213 %. The relative contents of the dibasic acids change slightly, i.e., docosanedioic acid increased from 0.844 to 1.012 %, eicosanebioic acid increased to 2.986 % with an initial content of 2.713 %, almitic acid and stearic acid did not change much. In general, substance with double bond were decomposed under UV irradiation apparently, the Iodine value varies from 13.65 to 10.36 while the Peroxide Value changed drastically from 6.22 to 206.35.

Table 191.4 showed a decrease of the iodine value from 13.65 to 10.36 with the prolonging of the UV irradiation time, which was probably due to the oxidative degradation of the unsaturated fatty acid. Earlier investigations have revealed that light irradiation was not adopted since it would induce oxidation reaction of the oil [15]. As shown in Table 191.4, an increase in irradiation time from 0 to 80 h resulted in an increase in the peroxide value from 6.22 to 206.35. It has a significant effect on the quality of the lacquer wax. Besides the organic pigments, the unsaturated fatty acids were also degraded and translated to fatty acid peroxide under UV irradiation, which resulted in the change in the quality of the wax. Therefore, an irradiation time of 60 h, which resulted in a white product with high quality, was considered as an alternative processing for the discoloration of lacquer wax.

Table 191.3 Chemical constituents of lacquer wax in different irradiation time

No	Main fatty acids	Relative contents of the fatty acids (%)				
		a	b	c	d	e
1.	Myristic acid	0.896 ± 0.0107	0.985 ± 0.0151	1.082 ± 0.0158	1.026 ± 0.0161	0.945 ± 0.0086
2.	Palmitic acid	60.121 ± 0.494	61.543 ± 0.512	60.422 ± 0.543	60.978 ± 0.576	62.184 ± 0.582
3.	Linoleic acid	0.825 ± 0.0112	0.356 ± 0.0142	0.117 ± 0.0163	0	0
4.	Oleic acid	14.329 ± 0.213	13.917 ± 0.203	12.552 ± 0.219	11.425 ± 0.216	10.213 ± 0.225
5.	Stearic acid	12.751 ± 0.176	12.988 ± 0.147	13.128 ± 0.146	13.452 ± 0.152	12.887 ± 0.166
6.	Hexadecanedioic acid	0.853 ± 0.0086	0.745 ± 0.0121	0.786 ± 0.0139	0.764 ± 0.0158	0.795 ± 0.0152
7.	Eicosanoic acid	1.655 ± 0.0232	1.682 ± 0.0255	1.901 ± 0.0177	1.847 ± 0.0198	1.883 ± 0.0301
8.	Docosanedioic acid	0.844 ± 0.103	0.943 ± 0.0201	0.977 ± 0.0298	1.045 ± 0.0104	1.012 ± 0.0196
9.	Eicosanebioic acid	2.713 ± 0.0362	2.723 ± 0.0516	2.883 ± 0.0411	2.907 ± 0.0321	2.986 ± 0.0524

a–e: Lacquer wax irradiated by UV for 0, 20, 40, 60 and 80 h, respectively ($n = 3$, $p < 0.05$)

Table 191.4 Change of physical properties of lacquer wax by UV irradiation

Physical properties	UV irradiation time/h				
	0	20	40	60	80
Melting point	52.13 ± 0.382	49.28 ± 0.586	49.88 ± 0.498	50.15 ± 0.433	50.46 ± 0.456
Acid value	87.52 ± 0.837	83.61 ± 0.954	85.41 ± 0.722	86.39 ± 0.658	84.56 ± 0.813
Iodine value	13.65 ± 0.196	12.98 ± 0.204	12.66 ± 0.211	11.49 ± 0.182	10.36 ± 0.193
Peroxide value	6.22 ± 0.0831	113.13 ± 2.35	175.22 ± 2.76	195.23 ± 3.54	206.35 ± 3.66

($n = 3$, $p < 0.05$)

191.4 Conclusion

Discoloration methods by physical adsorption, chemical, and light irradiation are common in the oil processing industry. Different colors of lacquer wax attribute to different kinds of pigments, pigments in lacquer were mainly composed of green chlorophyll, red carotene, and yellow xanthophylls. The adsorbents used in the discoloration process were a combination of activated carbon and kieselguhr, which were more cheaply and widely used in industry. Optimal discoloration conditions of lacquer wax were choosing petroleum ether as solvent (1:20, g/mL), activated carbon-kieselguhr = 1:1 (g/g) as adsorbent which 5 % weight to wax, kept a temperature of 80 °C for 30 min, twice. A high quality of lacquer wax was obtained if decolorated by a combination of kieselguhr and activated carbon. Besides, UV light irradiation was also presented as a good method to decolor the lacquer wax, which could get a similar discoloration effect (whiteness raised from 55 to 85) compared to the physical adsorption. Discoloration for 60 h could achieve a good discoloration. It is believable that UV light irradiation can serve as an alternative and effective discoloration method. In conclusion, UV irradiation is a simple and convenient method in the discoloration process of lacquer wax.

Acknowledgments The authors thank Dr XL, Lei, Jiangxi Academy of Forestry, for providing and selecting different samples. The support of this work by "International Cooperation Project (S2012GR0138)", and the "948" Cooperation Project (2009-4-58) of State Forestry Administration, China is gratefully acknowledged.

References

1. Lu R, Wan YY, Honda T (2006) Design and characterization of modified urethane lacquer coating. Progr Org Coat 57:215–222
2. Liu W, Xie BX, Yu JF (2008) Extraction Techniques of Lacquer Wax in *Rhus succedanea*. Nonw For Res 26(1):58–61
3. Dong YH, Wang CZ, Gong K (2009) Research progress on chemical constituents and comprehensive application of lacquer trees. For Ind Sci Technol 29:225–232
4. Wang YQ, Zhang FX, Zhao H (2003) Factors influencing colour of urushol wax. Chem Ind For Prod 23(2):81–83

5. Wang YQ, Sun L (2003) Research on decolorizing of urushi wax from Zhaotong. Chem Ind For Prod 37(1):17–18
6. Sionkowska A (2006) Effects of solar radiation on collagen and chitosan films. Photochem Photobiol B 82:9–15
7. Tachibana S, Sakuragi M, Sumimoto M (1989) Chemical conversion of extractives for the production of chemicals and fuels III Sunlight bleaching of urushi wax. Nipp M Gakk 35(4):356–361
8. Dal KY, Hong KN, Dong SK, Witoon P (2008) Decoloration of chitosan by UV irradiation. Carbohydr Polym 73:384–389
9. Meguro S, Kawachi S (1989) Some physical properties of haze wax correlated with major fatty acids. J Jpn Wood Res Soc 35(8):754–760
10. Meguro S, Kawachi S (1990) Major fatty acid contents of haze wax: changes during the growth and storage periods of haze seeds. J Jpn Wood Res Soc 36(2):133–138
11. Xu J, Kawachi S (1989) Seasonal variations of some biochemical constituents in Hazenoki, *Rhus succedanea*. J Jpn Wood Res Soc 35(1):30–35
12. Wang YH, Liang SZ (2000) Chemical structure and physiological functions of the carotenoids. GZ Focal Sci Tech 16(4):1–4
13. Zhao WE (2003) The antioxidant properties of carotenoids. Zhengzhou Univ Nat Sci Ed 24(1):38–46
14. Henry LK, Puspitasari-Nienaber NL, Jaren-Galan M (2000) Effects of ozone and oxygen on the degradation of carotenoids in an aqueous model system. J Agric Food Chem 48:5008–5013
15. Wang Y, Yin PH, Liang FH (2006) Bleaching of hogwash oil by oxidation/adsorption. Chn Oil For 31(7):41–43

Chapter 192
The Effect of Ethanol on Steroid Δ^1-dehydrogenase from *Arthrobacter simplex*

Jianmei Luo, Yongxin Cheng, Lina Liu, Jianfeng Wang, Yu Zheng, Yanbing Shen and Min Wang

Abstract The effects of different concentration of ethanol on enzymatic activity, thermal stability, heavy metallic ion stability, and pH stability of Δ^1-dehydrogenase from *Arthrobacter simplex* were investigated in this paper. The results showed that the introduction of no more than 6 % (v/v) of ethanol had obvious effect on pH of culture and Δ^1-dehydrogenase catalytic activity, respectively. The activation energy of deactivation (E_a) had a slight increase after the cell was treated by 2 % (v/v) of ethanol, which indicated that the addition of ethanol (2 %, v/v) could enhance the thermal stability of Δ^1-dehydrogenase. The tendency of value of half-life ($t_{1/2}$) with the content of ethanol was similar in the different concentrations of Ba^{2+}. The maximal value of $t_{1/2}$ was observed at 2 % of ethanol and then drastically decreased with the increase of ethanol. The $t_{1/2}$ value of Δ^1-dehydrogenase was obviously decreased with the increase of ethanol concentration in the buffers with the initial pH 7.0 and 10.0, respectively.

Keywords *Arthrobacter simplex* · Δ^1-dehydrogenase · Ethanol · Enzymatic activity · Enzymatic stability

192.1 Introduction

Steroid hormone production is a well-known example of the successful application of microbial biotransformation technology in large-scale industrial processes, as exemplified by the Δ^1-dehydrogenation of steroids catalyzed by *A. simplex* and the

J. Luo (✉) · Y. Cheng · L. Liu · J. Wang · Y. Zheng · Y. Shen · M. Wang
Key Laboratory of Industrial Fermentation Microbiology, Ministry of Education, Tianjin University of Science and Technology, Tianjin 300457, People's Republic of China
e-mail: luojianmei@tust.edu.cn

J. Luo · Y. Cheng · L. Liu · J. Wang · Y. Zheng · Y. Shen · M. Wang
Tianjin Key Lab of Industrial Microbiology, College of Biotechnology, Tianjin University of Science and Technology, Tianjin 300457, People's Republic of China

T.-C. Zhang et al. (eds.), *Proceedings of the 2012 International Conference on Applied Biotechnology (ICAB 2012)*, Lecture Notes in Electrical Engineering 251,
DOI: 10.1007/978-3-642-37925-3_192,

side-chain cleavage of phytosterol catalyzed by *Mycobacterium sp* [1, 2]. However, the main problem of steroid biotransformation remains its poor water solubility and low dissolution rate, which results in poor availability of substrate. As a result, a lot of efforts have been devoted to improve the solution, including the addition of the water-soluble organic co-solvent [3] or surfactant [4] or cyclodextrins (CDs) [5], the use of new organic biocatalysis technology, such as aqueous two-phase system [6], cloud point system [7], pure organic solvent system [8], and ionic liquid system [9]. All of the above methods can enhance the solubility of the substrate.

Currently, the water-soluble organic co-solvents, such as ethanol, methanol, dimethyl-formamide (DMF), and dimethyl sulfoxide are widely used in the industrial process of steroid production with the advantage of low cost and high product yield. Despite such organic solvents being toxic to biocatalysts activity and stability, organic solvent-tolerant bacteria capable of thriving in the presence of these toxic compounds have been reported for almost three decades. Solvent tolerant bacteria are being explored for their potential in industrial and environmental biotechnology [10, 11].

Most of the studies on solvent-tolerant microorganisms are focused on the effects of organic solvents on the cell growth and properties [12, 13]. Nevertheless, the key issue on the microbial transformation of steroid compounds is that their enzymes were expected to be stable and active in the presence of organic solvents.

In our previous study, *A. simplex* with the ability of Δ^1-dehydrogenation was found to grow at the concentration of ethanol (6 %) and the physiological features of microorganism had been investigated systematically [14, 15]. In order to choose a proper additive that could improve the availability of substrate with the minimum loss in enzyme activity and stability, effects of ethanol on enzymatic activity, thermal stability, heavy metal ion stability, and pH stability were further studied in this paper.

192.2 Materials and Methods

192.2.1 Materials

Cortisone acetate (CA) was supplied by Tianjin Pharmaceutical Company (99.4 % purity). Standard CA and prednisone acetate (PA) were purchased from Sigma-Aldrich Co. Ltd. Other salts and solvents were of analytic grade from Shanghai Sangon Biological Engineering Technology & Services Co. Ltd. (China).

192.2.2 Microorganism Cultivation and Preparation of Resting Cells

Arthrobacter simplex TCCC 11037 stored in our laboratory was maintained and cultivated as described previously [16]. The resting cell of *A. simplex* was prepared in two consecutive cultivation steps (18 h for seed culture and 24 h for cell cultivation, respectively). At 32 °C, the whole cells grew in 250 mL shake flasks containing 30 mL culture media on a rotary shaker (160 r/min) using 5 % (v/v) of seed culture as inoculum. The cell was centrifuged at 5000 r/min for 15 min and washed twice with KH_2PO_4-NaOH buffer (0.05 mol/L, pH 7.2). The washed cells were then resuspended in the same buffer.

192.2.3 The Effects of Ethanol on Enzymatic Activity

Equivalent washed cells (2 g dry weight per liter) were added into the prepared buffers (30 mL) containing different concentrations of ethanol (0, 2, 4 and 6 %, v/v, respectively), followed by the addition of CA to a final concentration of 1.0 g/L. They were incubated in 250 mL shake flask at 32 °C on a rotary shaker (160 r/min). Samples (500 μL) were drawn at various intervals, while continuously being shaken. The samples were extracted, filtered, and then determined by HPLC using the same method presented by Zhang [16].

192.2.4 Effect of Ethanol on pH of Reaction System

Ethanol ranging from 0 to 6 % (v/v) was added to the KH_2PO_4-NaOH buffer (0.05 mol/L, pH 7.2) and the culture media, respectively. The solutions were shaken for 10 min (32 °C, 160 r/min) and the final pH values were measured using a Metrohm 744 pH meter.

192.2.5 Enzymatic Activity Analysis of Steriod Δ^1-dehydrogenase

Enzymatic activity of Steriod Δ^1-dehydrogenase from *A. simplex* cell after different treatment was assayed by substrate conversion method. Equivalent cell was added into the buffer (30 mL), and then the substrate was added to keep the final concentrations of CA at 1.0 g/L. Bioconversion was conducted at 32 °C and 160 rpm, During the bioconversion, 500 μL samples were withdrawn periodically and analyzed by HPLC as previously described [16]. Enzymatic activity of

Δ^1-dehydrogenase was expressed by the initial conversation rate (R_a), which was estimated using linear fragments of the product accumulation time-curves. All experiments were done with two replicates at least three times.

192.2.6 Thermal Stability Analysis

Equivalent cells were resuspended into the prepared buffers containing different concentrations of ethanol (0, 2, 4 and 6 %, v/v, respectively) and incubated at various temperatures from 10 to 50 °C in a shaking water bath. At specific time intervals, 5 mL suspension was withdrawn and the remaining enzyme activity was assayed immediately by the conversion of CA as described in 'Enzymatic activity analysis of steroid Δ^1-dehydrogenase' section.

192.2.7 Heavy Metal Ion Stability Analysis

To investigate the heavy metal ion stability of Δ^1-dehydrogenase, different concentrations of Ba^{2+} (0, 0.002, 0.005, 0.01, and 0.04 mol/L, respectively) were added into the prepared buffers containing different concentrations of ethanol (0, 2, 4, and 6 %, v/v, respectively). After continuously shaking (160 r/min) for various intervals (0.5, 2, 6, and 24 h, respectively), 5 mL suspension was withdrawn at various intervals and the enzymatic activity of cell was assayed by the conversion of CA as described in the section 'Enzymatic activity analysis of steroid Δ^1-dehydrogenase'.

192.2.8 pH Stability Analysis

Buffers containing different concentrations of ethanol (0, 2, 4 and 6 %, v/v) were prepared. The initial pH of buffers were adjusted to 3.0, 5.0, 7.0, and 10.0, respectively. After incubation on a rotary shaker (160 r/min) for different intervals (0.5, 2, 6 and 24 h, respectively), 5 mL suspension was withdrawn at specific intervals for enzymatic activity analysis using the same method described in the section 'Enzymatic activity analysis of steroid Δ^1-dehydrogenase'.

192.3 Results and Discussion

192.3.1 Effect of Ethanol on pH of Reaction System

The influence of additives on the pH of the reaction medium is an important variable for the enzymatic reaction. Previous research had shown that the optimal pH for steroid Δ^1-dehydrogenase from *A. simplex* was 10.0 [17]. Different concentrations of ethanol ranging from 0 to 6 % (v/v) were added to the buffer and the medium with an initial pH of 7.2, respectively. The results were shown in Table 192.1.

The presence of ethanol had no obvious effect on the pH of the buffer and culture medium even the maximal value of increased pH was less than 0.30. The dates demonstrated that ethanol was a proper additive taking the role as the co-solvent due to the negligible effect on pH.

192.3.2 Effect of Ethanol on Δ^1-dehydrogenase Activity

The effect of ethanol on Δ^1-dehydrogenase activity was presented in Fig. 192.1.

According to Fig. 192.1, there was a slight decrease of the initial conversion rate with the increase of ethanol concentration. The maximal decrease of the initial conversion rate was less than 10 % at the concentration of ethanol (6 %, v/v), which indicated that the introduction of ethanol had no obvious effects on the *A. simplex* Δ^1-dehydrogenase catalytic activity.

192.3.3 Effect of Ethanol on Enzymatic Thermal Stability

Generally, the thermal stability of protein depends on their specific amino acid sequence. High temperatures induce an irreversible deactivation of enzymes. Meanwhile, the low temperature is good for keeping the enzyme stability.

To establish the effects of ethanol on the thermal stability of the *A. simplex* Δ^1-dehydrogenase, the cell suspensions was incubated at various temperatures in the presence of different concentrations of ethanol and the remaining activity was then

Table 192.1 Effects of ethanol on the pH of the buffer and culture medium

Initial concentration of ethanol (v/v, %)	pH of phosphate buffer	pH of medium
0	7.20	7.20
2	7.25	7.23
4	7.29	7.32
6	7.38	7.45

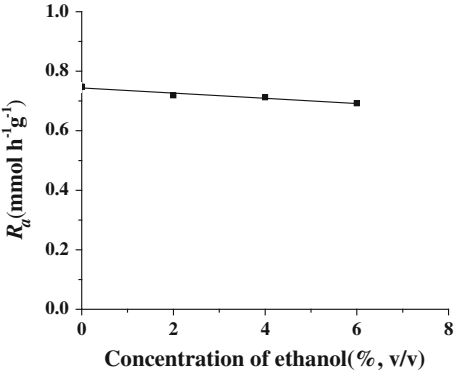

Fig. 192.1 Effect of ethanol on the initial conversion rate of Δ^1-dehydrogenase from *A. simplex*

determined. The enzymatic activity as a function of incubation time yielded linear tends and indicated first order deactivation kinetics. Therefore, the inactivation constants (k) at various temperatures were obtained from the slopes of tendency lines. Plotting ln$k$ as a function of 1/T, the Arrhenius plots in the presence of different concentrations of ethanol were showed in Fig. 192.2.

A usual assay measure of temperature-induced inactivation was the $t_{1/2}$ of the enzyme, which was defined as the time needed to decrease the initial enzyme activity by 50 %. The $t_{1/2}$ in the presence of additive was calculated from the respective inactivation constants (k) by Eq. 1.

$$t_{1/2} = 0.693/k \tag{1}$$

According to the Arrhenius' law Eq. 2

$$\ln k = \ln A - \frac{Ea}{RT} \tag{2}$$

where A is a constant, E_a is the activation energy of deactivation or thermal inactivation energy (kJ/mol), R is the universal gas constant (8.314 J/mol·K), and T is the absolute temperature (K).

According to the slope of Arrhenius plot (shown in Fig. 192.2) and Eq. 3, E_a were calculated by the multiplication of slope and R.

$$\text{slope} = \frac{Ea}{R} \tag{3}$$

The $t_{1/2}$ of the enzyme and the E_a at the different concentrations of ethanol were shown in Table 192.2. The thermal stability of Δ^1-dehydrogenase was slightly improved after the cell was treated by 2 % of ethanol and then decreased from 40.308 to 20.966 kJ/mol with the increasing concentration of ethanol.

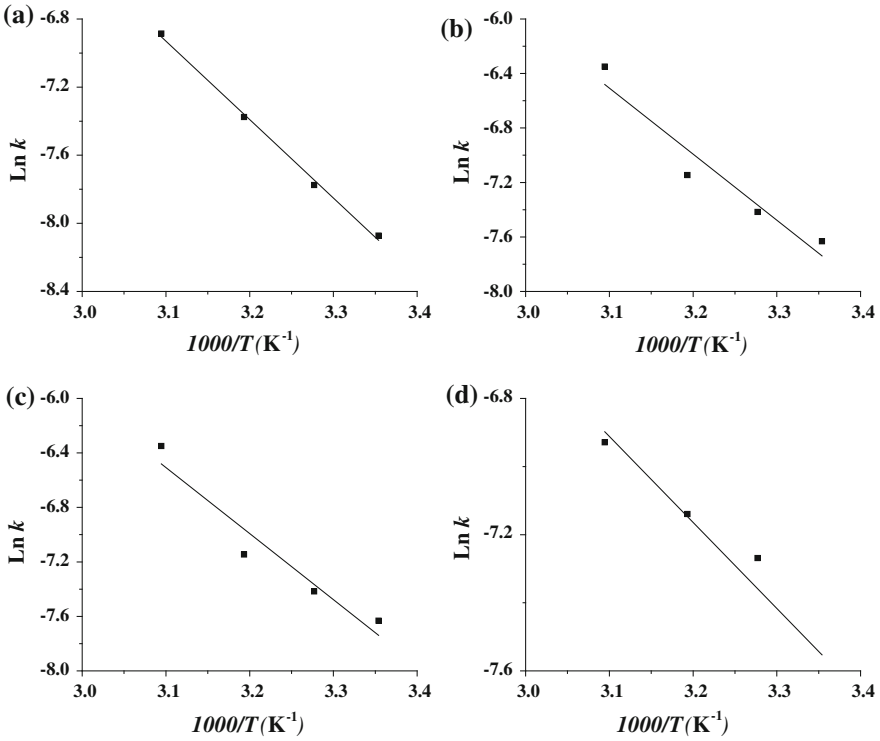

Fig. 192.2 Arrhenius plot of ln*k* versus 1/*T* in presence of ethanol: **a** 0 %, **b** 2 %, **c** 4 %, **d** 6 %

Table 192.2 The $t_{1/2}$ of the enzyme and the E_a at the different concentrations of ethanol

Initial concentration of ethanol (v/v, %)	Fitting equation	Correlation coefficient	*Ea* (kJ/mol)
0	y = −4.6046x + 7.3442	0.9972	38.283
2	y = −4.8482x + 8.5225	0.9300	40.308
4	y = −3.6339x + 3.853	0.9237	30.212
6	y = −2.5254x + 0.9173	0.9463	20.996

192.3.4 Effect of Ethanol on Heavy Metallic Ion Stability

The $t_{1/2}$ values of Δ^1-dehydrogenase after the treatment of ethanol and Ba^{2+} were shown in Fig. 192.3. The tendency of $t_{1/2}$ with the content of ethanol was similar in the different concentrations of Ba^{2+}. The maximal value of $t_{1/2}$ was observed at 2 % of ethanol and then drastically decreased with the increase of ethanol.

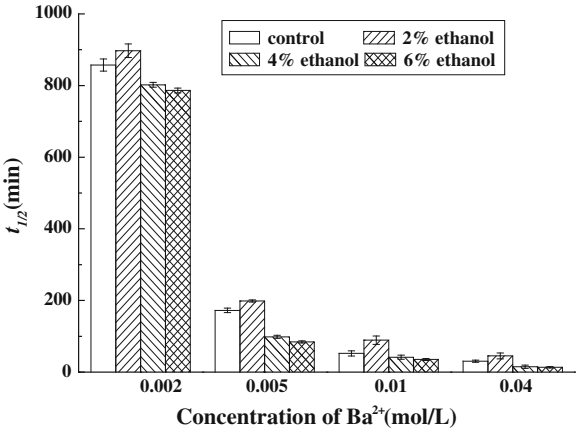

Fig. 192.3 The effect of ethanol on heavy metal stability of Δ^1-dehydrogenase

192.3.5 Effect of Ethanol on pH Stability

The $t_{1/2}$ values of Δ^1-dehydrogenase after the treatment of ethanol and the regulation of the initial pH were shown in Fig. 192.4. There was no obvious difference in $t_{1/2}$ when the concentration of ethanol was increased to 6 % (v/v) in the buffers with the initial pH 3.0 and 5.0, respectively. The $t_{1/2}$ value of Δ^1-dehydrogenase was decreased with the increase of ethanol concentration in the buffers with the initial pH 7.0 and 10.0, respectively.

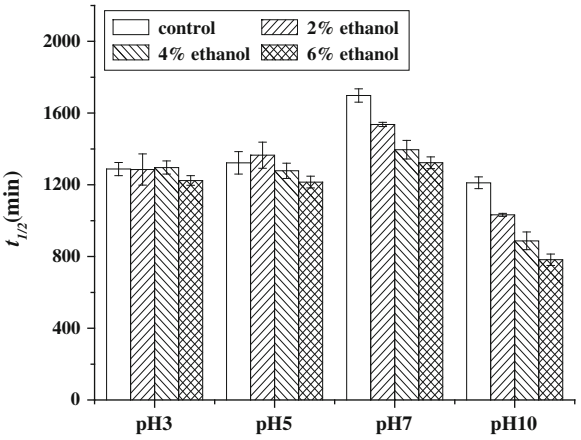

Fig. 192.4 The effect of ethanol on pH stability of Δ^1-dehydrogenase

192.4 Conclusion

The effects of different concentration of ethanol on enzymatic activity, thermal stability, heavy metallic ion stability, and pH stability of Δ^1-dehydrogenase from *A. simplex* were investigated in this paper. The results showed that the introduction of ethanol had no obvious effects on pH of culture and Δ^1-dehydrogenase catalytic activity, respectively. The E_a was slightly increased after the cell was treated by 2 % of ethanol and then decreased with the increasing concentration of ethanol, which indicated that the addition of ethanol (2 %, v/v) could enhance the thermal stability of Δ^1-dehydrogenase. The tendency of $t_{1/2}$ with the content of ethanol was almost same in the different concentrations of Ba^{2+}. The maximal value of $t_{1/2}$ was observed at 2 % of ethanol and then drastically decreased with the increase of ethanol. There was no obvious difference in $t_{1/2}$ when the concentration of ethanol was increased to 6 % (v/v) in the buffers with the initial pH 3.0 and 5.0, respectively. The $t_{1/2}$ value of Δ^1-dehydrogenase was decreased with the increase of ethanol concentration in the buffers with the initial pH 7.0 and 10.0, respectively.

Acknowledgments This work is supported by Scientific Research Foundation Project of Tianjin University of Science and Technology (No. 20100210) and Lab Opening Foundation of Tianjin University of Science and Technology (No. 1204A210).

References

1. Alexander DL, Fisher JE (1995) Advances in microbial steroid biotransformation. Steroids 60:290–294
2. Fernandes P, Cruz A, Angelova B, Pinheiro HM, Cabral JMS (2003) Microbial conversion of steroid compounds: recent developments. Enzyme Microb Technol 32:688–705
3. Simon LM, Lásló K (1998) Effects of pH value and Zn^{2+} concentration on bioactivity and structure of trypsin. J Mol Catal B Enzym 4:41–45
4. Smith M, Zahnley J (1993) Growth and cholesterol oxidation by mycobacterium species in Tween 80 medium. Appl Environ Microb 59:1425–1429
5. Bie ST, Lu FP (2008) Effect of phase composition on the bioconversion of methyltestosterone in a biphasic system. J Mol Catal B Enzym 55(1–2):1–5
6. Shen YB, Wang M, Li HN, Wang YB, Luo JM (2012) Influence of hydroxypropyl-β-cyclodextrin on phytosterol biotransformation by different strains of mycobacterium neoaurum. Ind Microb Biotechnol 39:1253–1259
7. Wang ZL, Zhao FS (2004) Microbial transformation of hydrophobic compound in cloud point system. J Mol Catal B Enzym 27(4–6):147–153
8. Griebenow K, Laureano Y (1999) Effect of prolonged exposure to organic solvents on the active site environment of subtilisin carlsberg. J Am Chem Soc 121:8157–8163
9. Rantwijk FV, Lau RM (2003) Biocatalytic transformations in ionic liquids. Trends Biotechnol 21:131–138
10. Zheng SX, Wang RZ, Xie SL (2011) Research progress in biodehydrogenation technique of steroid medicine. Chin J Biochem Pharm 32(3):251–254
11. Xue JH, Li H, Wei P (2012) Microbial metabolomics and its application in industry. Biotechnol Bull 2:20–27

12. Li SY, Ma YQ, Su YL (2012) Effect of heavy metal stress on microbial growth. Guizhou Agric Sci 40(2):90–94
13. Chen YG, Chen XM, Zhang YG (2009) The physiological mechanism of microbial heavy metals tolerance. Biotechnol Bull 10:60–65
14. Wang JF, Luo JM, Song Y (2011) The effects of ethanol on cell growth and cell characteristics of *Arthrobacter simplex* TCCC 11037. Chem Bioeng 28(3):66–69
15. Luo JM, Song Y, Wang JF, Ning J, Cheng YX (2012) Study on the effects of different kinds of organic solvents on $C_{1,2}$ dehydrogenation reaction by the analysis of *Arthrobacter simplex* cell characters. Chem Bioeng 29(5):49–53
16. Zhang LT, Wang M, Shen YB, Ma YH, Luo JM (2009) Improvement of steroid biotransformation with hydroxypropyl-β-cyclodextrin induced complexation. Appl Biochem Biotechnol 3(159):642–654
17. Choi KP, Molnár I, Yamashita M, Murooka Y (1995) Purification and characterization of the 3-ketosteroid-delta 1-dehydrogenase of *Arthrobacter simplex* produced in *Streptomyces lividans*. Mol Microbiol 117(5):1043–1049

Chapter 193
Rapid Assessment of Cell Viability of *Lactobacillus casei* after Freeze-Drying by Measurement Cell Membrane Using Flow Cytometry and Fluorescence Probes

Lin Wang, Xiaohui Liu and Jinghua Yu

Abstract Freeze-drying technique was widely used to produce commercial lactic acid bacterial starter. But cell viability and technological properties were often affected by freezing. Different methods were employed to determine bacterial cryotolerance. However, it would take several hours or days. This study aimed to develop a method of flow cytometry by using two specific fluorescent probes (cFDA and PI) to provide rapid assessment of the viability of *Lactobacillus casei* after freezing and freeze-drying. The protective effects of four different cryoprotectants were tested by this method. Results showed that cryoprotectants had positive effects on improving the viability of cell. The different protective effects compared were as follows, compound cryoprotectants > skimmed milk > lactose > monosodium glutamate. It indicated that the flow cytometry method was convenient and rapid to evaluate the viability of lactic acid bacteria.

Keywords *Lactobacillus casei* · Cryoprotectants · Freeze-drying · Viability · Flow cytometry

193.1 Introduction

Vacuum freeze-drying is widely used to produce commercial lactic acid bacterial starter, but this technique brings about undesirable side effects, such as denaturation of sensitive proteins and decreased viability of many cell types [1]. Many authors point out that it is necessary to maintain a high level of both viability and acidification activity during freezing and freeze-drying of lactic acid bacteria [2, 3]. Microbial cell survival through freeze and freeze-drying is dependent on

L. Wang · X. Liu · J. Yu (✉)
College of Food Engineering and Biotechnology, Tianjin University of Science and Technology, Tianjin 300457, People's Republic of China
e-mail: yujinghua@tust.edu.cn

T.-C. Zhang et al. (eds.), *Proceedings of the 2012 International Conference on Applied Biotechnology (ICAB 2012)*, Lecture Notes in Electrical Engineering 251,
DOI: 10.1007/978-3-642-37925-3_193,

many factors, including initial concentration of microorganisms, growth conditions, growth medium, sub-lethal treatment, centrifugation conditions, freezing rate, drying medium, retained moisture, and rehydration conditions [4]. One of the most important conditions is the composition of the medium used to suspend the organisms for freezing [5].

Starter quality is generally measured in terms of metabolism or functional activity, and the ability to reproduce and grow [6]. The viability of dairy starter cultures is traditionally quantified by the plate count technique to count the number of colony-formed on a plat. Although colony counting is the conventional method for quantitative survival studies, but there were three major drawbacks. First, it requires a long incubation time. Second, it may underestimate viable cell counts as a result of cell clumping and chain formation. Finally, it only takes the bacteria that can reproduce under the conditions provided for growth into account. As a consequence, some cells, which are known as viable but noncultivable, are not counted by this method [7].

On the basis of these considerations, more sensitive and rapid tests may be useful for providing information about the cellular viability during freezing and freeze-drying. Fluorescent techniques using specific probes have been successfully introduced for the assessment of the viability and vitality of micro-organisms. Flow cytometry is of great interest as a real-time monitoring method for viability assessment. And it makes it possible to perform a rapid count of individual cell in different status, for example, the existence of injured and 'viable but nonculturable' (VNC) cells sometimes encountered when cells are stressed [7].

Many fluorescent probes have been used to analyze different physiological parameters such as membrane integrity [8, 9], intracellular enzyme activity [10], cellular vitality [11, 12], membrane potential [13–15], and intracellular pH [16–18]. The most widely used dye for the assessment of cell viability is the esterase substrate carboxyfluorescein diacetate (cFDA), which quantifies the intracellular esterase activity. It is a non-fluorescent precursor that readily difuses across intact cell membranes and yields the positively charged green fluorescent compound, carboxyfluorescein (cF), upon hydrolysis by non-specific cellular esterases. The cF has a maximum excitation wavelength of 492 nm and an emission wavelength of 517 nm in green. Labeled cells are characterized by efficient enzymatic activity and are considered as viable cells. Another probe used for mortality studies is the nucleic acid dye, propidium iodide (PI). It is excluded by cells having intact membranes, but can enter cells with compromised membranes. It binds to DNA to form a red fluorescent DNA-complex with a maximum excitation wavelength of 535 nm and an emission wavelength of 617 nm in red. Stained cells correspond to cells having compromised or destroyed membranes and are considered as dead [12, 19]. Double stained cells correspond to cells having both enzymatic activity and compromised membranes, and are considered as stressed cells. It has been used for the viability assessment of bile salt-stressed *Bifidobacterium* [20] or acid stressed *Streptococcus macedonicus* [21]. Nevertheless, this method has never been applied to the quantification of cell survival for lactic acid bacterial starter during freezing and freeze-drying.

This investigation was to apply flow cytometry to assess and compare the viability of *Lactobacillus casei* in four different cryoprotectants in order to determine the relevance of this method for the rapid assessment of viability after freezing and freeze-drying of lactic acid starter cultures.

193.2 Materials and Methods

193.2.1 Bacterial Strain and Media

The bacterial strain *Lactobacillus casei* were grown in de Man, Rogosa and Sharpe (MRS) culture medium and were then inoculated in MRS broth. The media were sterilized at 121 °C for 15 min. After incubation at 37 °C for 12 h, cells were harvested by centrifugation at 10,000×g for 10 min at 4 °C, washed twice and resuspended to the initial cell concentration with cold sterile saline [0.85 % NaCl (w/v)]. All solutions used in the experiments were previously sterilized and manipulation was carried out aseptically.

193.2.2 Freeze Media and Sample Preparation

Four additives were tested as "protective" agents in binary aqueous solutions: monosodium glutamate [MSG; 0.42 % (w/v)], lactose5.73 % (w/v), reconstituted skimmed milk [RSM; 15.8 % (w/v)], and compound cryoprotectant (mixture of the three above). The additives and their concentration were chosen on the basis of previous studies. Distilled water was chosen as control.

193.2.3 Freeze-Drying Conditions

The mixtures were incubated at 4 °C for 1 h and frozen at −80 °C for 3 h. Frozen cells were freeze-dried using Becton Dickinson Freeze-dry System at a collector temperature of −90 °C for 24 h at 0.014 mBar.

193.2.4 Fluorescent Probes and Staining Protocols

Cells were stained with cFDA and PI (Molecular Probes, Invitrogen, USA), as previously described [7]. Before staining, cell suspensions of *L. casei* were harvested by centrifugation (10,000×g, 1 min) and then were resuspended in PBS

(pH 7.0) to reach approximately 10^6 cells/mL. Viability/mortality assays were done by dual staining of each sample to differentiate viable, dead, and stressed cells. The diluted suspension was first incubated with 10 μL of PI (1.496 mM in DMSO, Invitrogen-Molecular Probes, Chen-Yi-Xing, China) for 20 min at 37 °C. 10 μL of cFDA (21.7 μM in DMSO, Invitrogen-Molecular Probes, Chen-Yi-Xing, China) were then added and incubation took place for 10 min at 37 °C. After short centrifugation at 10,000×g for 1 min, cell pellets were re-suspended in 1 mL of PBS buffer in ice bath before analysis by flow cytometry.

193.2.5 Flow Cytometry Analyses

Flow cytometry analyses were performed as described by Aline Rault [7]. Samples were analyzed by a FACSCalibur instrument. The instrument is equipped with an argon ion laser for the excitation of the fluorescent dyes providing 15 mW at 488 nm. Filter setup was standard. All parameters were collected at logarithmic scale. cFDA fluorescent emission was detected at the FL1 channel (530 ± 15 nm), while PI at the FL2 channel (584 ± 21 nm). FACS flow solution (Becton Dickinson) was used as sheath fluid. Flowrate and cell concentration of the samples were adjusted to keep acquisition lower than 500 cells/s. At least 10,000 cells were acquired for analysis. Data were collected with the CELL Quest program (version 3.1; Becton Dickinson). Mixtures of stained and unstained cells for both cFDA and PI served as controls for adjusting detectors and compensation settings.

193.3 Results and Discussion

193.3.1 Viability and Mortality Assessment of Lactobacillus casei by Single Staining

In order to allow the differentiation of subpopulations in a sample containing heat-killed and freshly-harvested cells of *L. casei*, dead/live assays were conducted with PI/cFDA dual staining.

As illustrated in Fig. 193.1, cF- and PI-labeled populations were spatially discriminated in dot plots of FITC-A (cF fluorescence) and PE-Texas Red-A (PI fluorescence). Four kinds of subpopulations were observed with different staining characteristics. The first one was located in the lower left quadrant (Q1). It corresponded to unstained or lysed cells. The PI-labeled cells appeared on the FL2 detector in the upper left quadrant (Q2). They corresponded to dead cells. The cF-labeled cells were grouped in the lower right quadrant (Q4) and included viable cells. Finally, a double-stained population was observed in the upper right quadrant (Q3). It represented injured cells, which still displayed an esterase activity

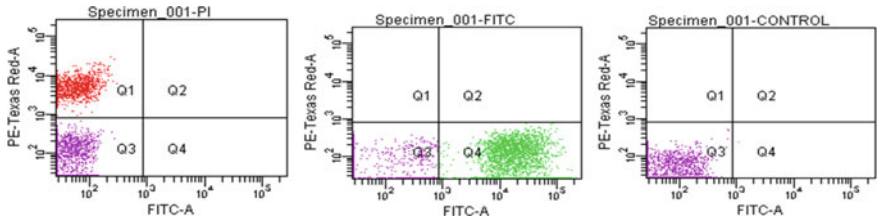

Fig. 193.1 Dot plots representing carboxyfluorescein (cFDA) and propidium iodide (PI) fluorescent signals of *L. casei.* Mixtures of freshly harvested (50 %) and heat-killed (50 %) cells were stained with PI (A) or stained with cFDA (B). Unstained cells (C)

(cF-labeled), but with a damaged membrane, thus allowing penetration of the PI probe. From these results (Fig. 193.1), a good discrimination was achieved between three different physiological states by using dual staining, viable cells, dead cells, and injured cells with damaged membranes, which were reported as stressed cells. It clearly shows that different physiological state cell can be differentiated.

193.3.2 Effect of Freezing on Viability and Mortality of Lactobacillus casei *by Double Staining*

PI and cFDA were used simultaneously for viability assessment of *Lactobacillus casei* in four different cryoprotectants after freezing and freeze-drying. Significant differences were observed in three of the four quadrants when the cells were frozen (Fig. 193.2 D-H) and freeze-dried (Fig. 193.3 I-M) in different cryoprotectants. During freezing in cryoprotectant, the relative percentage of cells in the lower right quadrant increased, whereas it diminished significantly in the upper right and left quadrants compared to freezing in distilled water. The percentage of viable cells (lower right quadrant) increased most after freezing in compound cryoprotectant compared to in distilled water, from 50.6 % to 89.4 %. No significant difference was observed when cells were frozen in compound cryoprotectant, 10 and 5.73 % RSM .

193.3.3 Effect of Freeze-Drying on Viability and Mortality of Lactobacillus casei

The viability of *L. casei* showed significant difference after freeze-dried in the selected different cryoprotectants. Compound cryoprotectant displayed a better protective effect for *L. casei* during freeze-drying than sodium glutamate and lactose, with a decrease of only 17.2 % of cF-labeled cells after freeze-drying. On the contrary, distilled water, sodium glutamate, and lactose showed the least

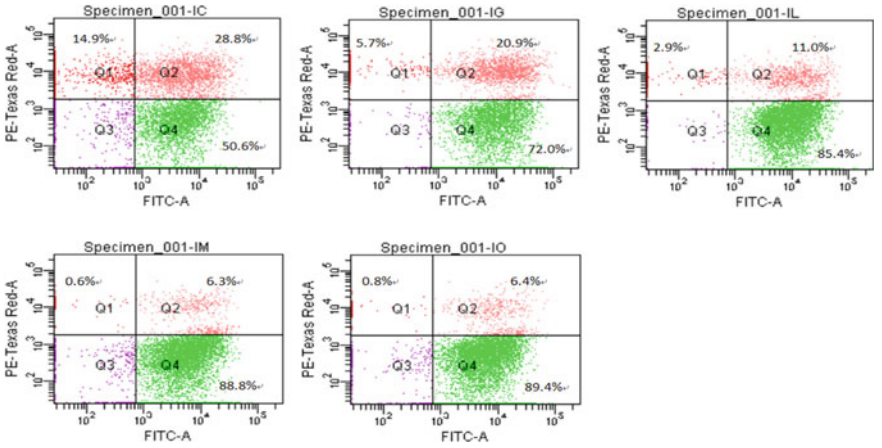

Fig. 193.2 FCM density plots of *L. casei* cells stained with 5(6)-CFDA and PI after freezing (−80 °C, 3 h). D distilled water, E 0.42 % sodium glutamate (w/v), F 5.73 % lactose (w/v), G 10 % RSM (w/v); H compound cryoprotectant (Q1: dead cells, Q2: injured cells, Q3: unstained cells, Q4: viable cells)

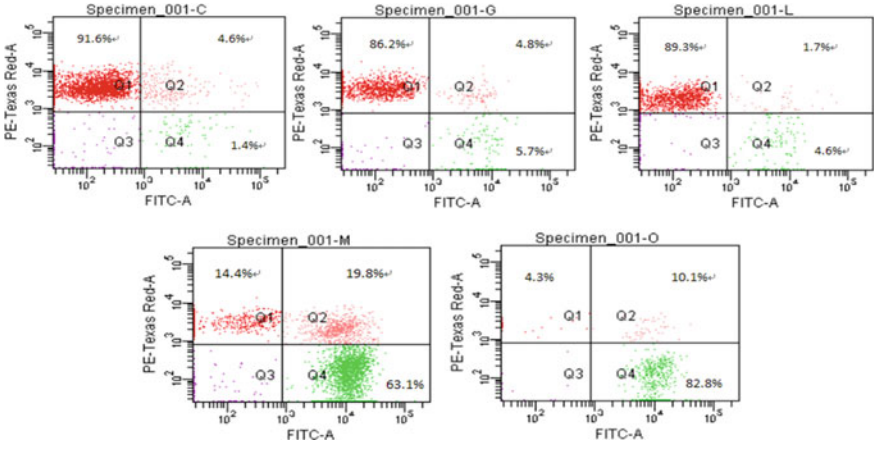

Fig. 193.3 FCM density plots of *L. casei* cells stained with 5(6)-CFDA and PI after freeze-drying. I distilled water, J 0.42 % sodium glutamate (*w/v*), K 5.73 % lactose (*w/v*), L 10 % RSM (*w/v*); M compound cryoprotectant (Q1: dead cells, Q2: injured cells, Q3: unstained cells, Q4: viable cells)

protective effect, with about 90 % of dead cells after freeze-drying (upper left quadrant). Finally, RSM displayed an intermediate protective effect, since 14.4 % of dead cells were observed after freeze-drying. By considering the stressed cells (upper right quadrant), their relative proportion was higher in RSM than in other cryoprotectants after freeze-drying.

As Figs. 193.2 and 193.3 show that viability was improved in the presence of the 5.73 % lactose, 10 % RSM, and the compound cryoprotectant during freezing. However, only the compound cryoprotectant presented a good protective effect during freeze-drying. It was also obtained that the freeze-drying process is hasher for the viability of *L. casei* than freezing.

Consequently, on the basis of these results, flow cytometry combined with fluorescent probes could be considered as an excellent tool to measure the survival cell ratio. Furthermore, it can be used to select cryoprotectant according to protective effect and to quickly evaluate cryotolerance of lactic acid bacteria. Meanwhile, the recovery capability, inactivation of intercellular enzymes, and the survival rates of *Lactobacillus casei* in the presence of four cryoprotectants were also detected (data was not shown). The result showed a similar trend with the protective effects of these cryoprotectants compared by flow cytometry method.

193.4 Conclusion

On the basis of our results, flow cytometry analysis combined with double fluorescent staining well quantified the viability of *L. casei* after freezing and freeze-drying in four different cryoprotectants. The method well-separated viable cells from stressed and dead cells. It was suitable for evaluating the loss of cell viability after freezing and during freeze-drying. Moreover, it allowed quantifying differences in the protecting effect of four cryoprotectants, when they were submitted to the same freezing and storage protocols.

More precisely, this study allowed us to classify compound cryoprotectant as a very effective protectant both during freezing and freeze-drying stages. Whereas, sodium glutamate and lactose did not show considerable effect when used singly. Consequently, it can be concluded that flow cytometry was an excellent tool for the rapid assessment of the degradation of cell viability during freezing and freeze-drying.

Acknowledgments This work was supported by the National Science & Technology Pillar Program in the Eleventh Five-year Plan Period (2009BADC1B02).

References

1. Carvalho A, Silva J (2004) Relevant factors for the preparation of freeze-dried lactic acid bacteria. Int Dairy J 14:835–847
2. Corrieu CG (1994) Viability and acidification activity of pure and mixed starters of *Streptococcus salivarius* subsp. *thermophilus* 404 and *Lactobacillus delbrueckii* subsp. *bulgaricus* 398 at the different steps of their production. Lebensm. Wiss u Technol 27:86–92
3. Conrad PB, Miller DP, Cielenski PR et al (2000) Stabilization and preservation of *Lactobacillus acidophilus in saccharide matrices*. Cryobiol 41:17–24

4. Fonseca F (2001) Operating conditions that affect the resistance of Lactic acid bacteria to freezing and frozen storage. Cryobiol 43:189–198
5. Hubalek Z (2003) Protectants used in the cryopreservation of microorganisms. Cryobiol 46:205–229
6. Joux F, Lebaron P (2000) Use of fluorescent probes to assess physiological functions of bacteria at single-cell level. Microbes Infect 2:1523–1535
7. Rault A, Beal C (2007) Multiparametric flow cytometry allows rapid assessment and comparison of lactic acid bacteria viability after freezing and during frozen storage. Cryobiol 55:35–43
8. da Silveira MG, San Romao MV, Loureiro-Dias MC et al (2002) Flow cytometric assessment of membrane integrity of ethanol-stressed *Oenococcus oeni* cells. Appl Environ Microbiol 68:6087–6093
9. Gregori G, Citterio S, Ghiani A et al (2001) Resolution of viable and membrane-compromised bacteria in freshwater and marine waters based on analytical flow cytometry and nucleic acid double staining. Appl Environ Microbiol 67:4662–4670
10. Riis SB, Pedersen HM, Sorensen NK et al (1995) Flow cytometry and acidification power test as rapid techniques for determination of the activity of starter cultures of *Lactobacillus delbrueckii subsp. bulgaricus*. Food Microbiol 12:245–250
11. Bouix M, Leveau JY (2001) Rapid assessment of yeast viability and yeast vitality during alcoholic fermentation. J Inst of Brew 107:217–225
12. Bunthof CJ, van den Braak S, Breeuwer P et al (1999) Rapid fluorescence assessment of the viability of stressed Lactococcus lactis. Appl Environ Microbiol 65:3681–3689
13. Gabier AC, Gourdon P, Reitz J et al (2005) Intracellular physiological events of *yeast Rhodotorula glutinis* during storage at 4°C. Int J Food Microbiol 105:97–109
14. Jepras RI, Carter J, Pearson SC et al (1995) Development of a robust flow cytometric assay for determining numbers of viable bacteria. Appl Environ Microbiol 61:2696–2701
15. Novo DJ, Perlmutter NG, Hunt RH et al (2000) Multiparameter flow cytometric analysis of antibiotic effects on membrane potential, membrane permeability, and bacterial counts of *Staphylococcus aureus* and *Micrococcus luteus*. Antimicrob Agents Chemother 44:827–834
16. Breeuwer P, Drocourt JL, Rombouts FM et al (1996) A novel method for continuous determination of intracellular pH in bacteria with the internally conjugated fluorescent probe 5 (and 6)-carboxy-fluorescein suc- cinimidyl ester. Appl Environ Microbiol 62:178–183
17. Rechinger KB, Siegumfeldt H (2002) Rapid assessment of cell viability of *Lactobacillus delbrueckii subsp. bulgaricus* by measurement of intracellular pH in individual cells using fluorescence ratio imaging microscopy. Int J Food Microbiol 75:53–60
18. Siegumfeldt H, Rechinger KB, Jakobsen M (1999) Use of fluorescence ratio imaging for intracellular pH determination of individual bacterial cells in mixed cultures. Microbiol 145:1703–1709
19. Breeuwer P, Abee T (2000) Assessment of viability of microorganisms employing fluorescence techniques. Int J Food Microbiol 55:193–200
20. Amor KB, Breeuwer P, Verbaarschot P et al (2002) Multiparametric flow cytometry and cell sorting for the assessment of viable, injured, and dead *Bifidobacterium* cells during bile salt stress. Appl Environ Microbiol 68:5209–5216
21. Papadimitriou K, Pratsinis H, Nebe-von-Caron G et al (2006) Rapid assessment of the physiological status of *Streptococcus macedonicus* by flow cytometry and fluorescence probes. Int J Food Microbiol 111:197–205

Chapter 194
Molecular Cloning, Characterization and Expression Analysis of a Gene Encoding Hydroxyphenylpyruvate Reductase Involved in Rosmarinic Acid Biosynthesis Pathway from *Perilla frutescens*

Xiaoling Lu, Lei Hao, Fang Wang and Chen Huang

Abstract In this study, a novel full-length cDNA of hydroxyphenylpyruvate reductase (*HPPR*) involved in rosmarinic acid (RA) biosynthesis pathway in *Perilla frutescens*is is cloned (designated as *PfHPPR*) for the first time by conserved fragment PCR and rapid amplification of cDNA ends (RACE). The cDNA of *PfHPPR* is 1723 bp long with an open reading frame (ORF) of 939 bp encoding a protein of 313 amino acid residues. Bioinformatics analysis revealed that the deduced amino acid sequence of *PfHPPR* has high homology to the other known HPPR proteins. Quantitative real-time PCR analysis of the transcription pattern indicates that the *PfHPPR* expresses constitutively in all examined tissues but most highly in leaf. Besides, the expression of *PfHPPR* can be induced by several factors such as abscisic acid (ABA), salicylic acid (SA), and ultraviolet-B radiation (UV-B).

Keywords Perilla frutescens · *PfHPPR* gene · RACE · Quantitative real-time PCR · Rosmarinic acid · Sequence analysis

X. Lu (✉) · L. Hao · F. Wang
Laboratory of Food Additives and Nutrition, College of Food Engineering and Biological Technology, Tianjin University of Science and Technology, Tianjin 300457, People's Republic of China
e-mail: lxling@tust.edu.cn

C. Huang
Tianjin Entry-Exit Inspection and Quarantine Bureau, Tianjin 300461, People's Republic of China

T.-C. Zhang et al. (eds.), *Proceedings of the 2012 International Conference on Applied Biotechnology (ICAB 2012)*, Lecture Notes in Electrical Engineering 251,
DOI: 10.1007/978-3-642-37925-3_194,

194.1 Introduction

Perilla frutescens (PfHPPR) is an annual self-fertilizing plant belonging to the family *Lamiaceae*, which have been extensively recognized worldwide as a representative oil crop and traditional Chinese medicinal herb [1, 2]. The *Perilla frutescens* accumulates a large amount of essential oil on a dry weight basis, and most of which is composed of unsaturated fatty acid such as α-Linolenic acid and various kinds of secondary metabolites with high bioactivity [3–5].

One of these metabolites is RA, an ester of caffeic acid and 3, 4-dihydroxyphenyllactic acid which is most commonly found in *Lamiaceae* and *Boraginaceae* species, and also detected in other families of dicotyledonous and monocotyledonous plants as well as in some hornworts and ferns [6]. RA has a multitude of biological activities, such as antioxidant, antibacterial, anti-inflammatory, and antimutagen [7, 8], which makes it a very valuable product for pharmaceutical and cosmetic industries. The biosynthesis of RA (Fig. 194.1) had been reported since 1970 when Ellis and Towers found that the two aromatic amino acids L-phenylalanine and L-tyrosine were the precursors for this compound [9]. L-phenylalanine is transformed to 4-coumaroyl-CoA by the three enzymes of the general phenylpropanoid pathway, phenylalanine ammonia-lyase (PAL), cinnamic acid 4-hydroxylase (C4H), and 4-coumarate: CoA-ligase (4CL) [10]. L-tyrosine is transaminated by tyrosine aminotransferase (TAT) with help of 2-oxoglutarate to 4-hydroxyphenylpyruvate [11], which is then reduced to 4-hydroxyphenyllactate by hydroxyphenylpyruvate reductase (HPPR), with NADH and NADPH serve as cofactors [12, 13]. The two intermediary precursors are esterified under release of coenzyme A by RAS, and form the first ester 4-coumaroyl-4′-hydroxyphenyllactate which is subsequently hydroxylated at position 3 and 3′ of the aromatic ring by specific membrane-bound 3 and 3′-hydroxylase activities giving rise to RA, the end product of this biosynthetic pathway [14].

At present, HPPR is completely purified and cloned from *Solenostemon scutellarioides* [15]. So far, the biosynthetic pathway for the production of rosmarinic acid in *Perilla frutescens* is not clear. In this study, a full-length *HPPR* gene is cloned from the *Perilla frutescens* and the expression pattern of this gene in different tissues including roots, stems and leaves, and leaves under various stress conditions are analyzed, respectively. Comparison of *HPPR* gene sequences from *Perilla frutescens* and other species reveals that the *HPPR* genes are structurally conserved and might possess similar functions. The cloning and characterization of the *HPPR* genes involved in RA biosynthetic pathway could greatly help to broaden our knowledge on the secondary metabolic pathway in high plants. To the best of our knowledge, this is the first time to clone and characterize the *HPPR* gene in *Perilla frutescens*.

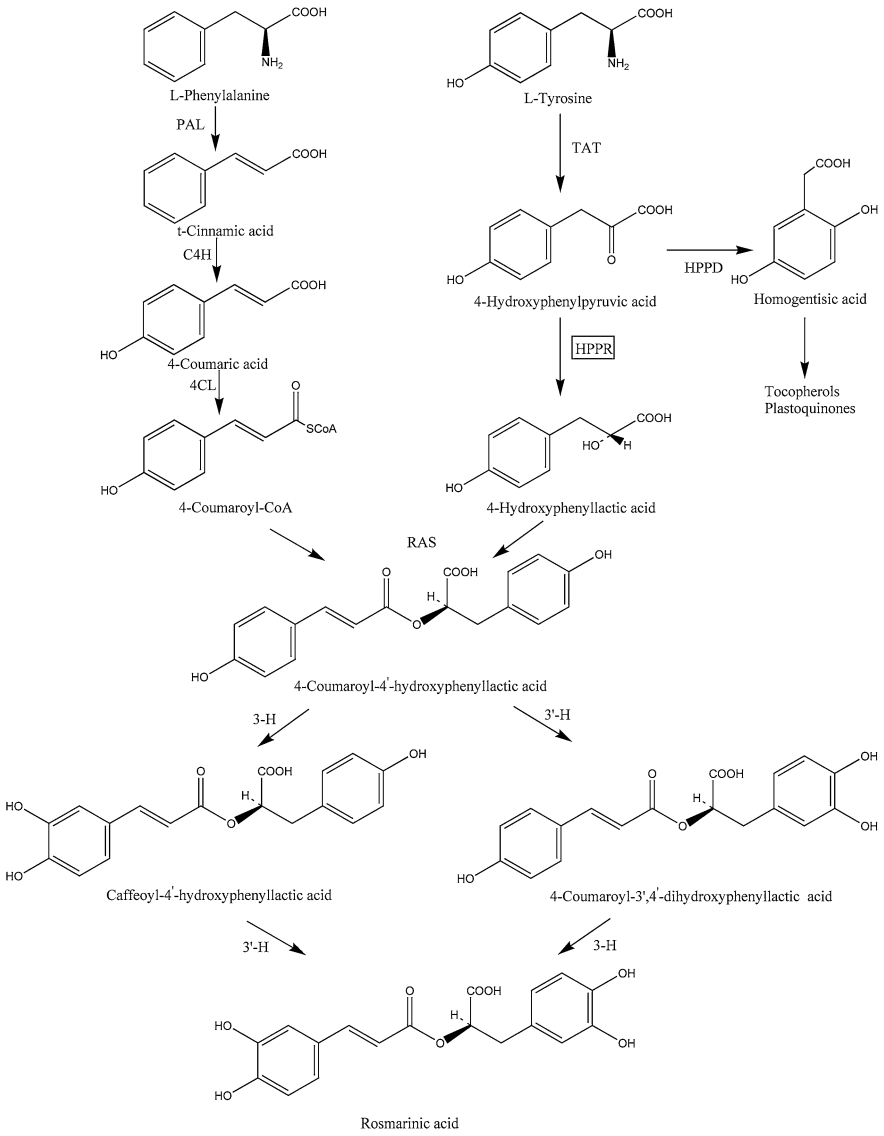

Fig. 194.1 The metabolic pathway of rosmarinic acid. Abbreviations: *TAT* tyrosine aminotransferase; *HPPR* hydroxyphenylpyruvate reductase; *PAL* phenylalanine ammonia-lyase; *4CL* 4-coumarate: CoA-ligase; *C4H* cinnamic acid 4-hydroxylase; *RAS* rosmarinic acid synthase; 3-H and 3′-H, hydroxycinnamoyl-hydroxyphenyllactate 3- and 3′-hydroxylases

194.2 Materials and Methods

194.2.1 Plant Material

Seeds of *Perilla frutescens* are pretreated with water for 1 h, washed with 75 % alcohol for 30 s, soaked in 0.1 % mercuric chloride for 7 min, and then by five rinses with bacteria free water. After this, these sterilized seeds are cultured on MS basal medium, maintained at 25 °C under 14 h light/10 h dark photoperiod cycles with light provided by cool white fluorescent lamps for 1 month until RNA isolation and various stress treatments.

194.2.2 Various Treatments

For abscisic acid (ABA) and salicylic acid (SA) treatment, the leaves are sprayed with solution of 100 μM ABA and 200 μM SA, respectively, followed by RNA isolation. The samples are collected after 0, 4, 8, 16, 24, and 48 h and the control plants are similarly treated with distilled water. For ultraviolet-B (UV-B) radiation treatment, the plants are exposed under 1,000 $\mu J/m^2$ intensity of illumination and collected after 0, 1, 2, 4, 8, and 12 h durations of treatment.

194.2.3 Isolation of RNA

The total RNA from 1-month-old *Perilla frutescens* is extracted using RNAiso Plus (TAKARA, Japan) under the manufacturer's instruction. The quality and the concentration of RNA are analyzed using 1.5 % (w/v) agarose/EtBr gel electrophoresis and spectrophotometer analysis, and the RNA samples are stored at −80 °C prior to RT-PCR and RACE analysis.

194.2.4 Molecular Cloning of Full-Length PfHPPR *cDNA*

The full-length *PfHPPR* cDNA is cloned by four successive steps.

First, highly conservative sequence is determined according to a parallel analysis of the amino acid sequence of *HPPR* gene registered in GenBank. The first-strand cDNA is synthesized from 500 ng total RNA using 50U reverse transcriptase M-MLV (TAKARA, Japan) in a 10ul reaction mixture. The mixture is heated at 70 °C for 15 min to inactivate the reverse transcriptase after incubation at 42 °C for 1 h. Then, the conserved fragment is amplified from first-strand cDNA using primer pairs PfHPPR-1 and PfHPPR-2 (Table 194.1). PCR conditions: 1 cycle with 2 min

Table 194.1 Primer sequences used for RT-PCR, RACE, and Real-time PCR

Primer types	Primer name	Primer sequence
RT-PCR primers	PfHPPR-1	5′-TAACTCAGCAGGCCGAGTCGAT-3′
	PfHPPR-2	5′-AGGTACCTCGGGCACCCTCTC-3′
RACE primers	PfHPPR3-GSP1	5′-GCATGTGCGCTGACTCCAGAAACGAC-3′
	PfHPPR3-GSP2	5′-GTGTCAGCTCTCGTGGAGGGTCG-3′
	PfHPPR5-GSP1	5′-AATCCGCCACGTCATCGGTGAGCAC-3′
	PfHPPR5-GSP2	5′-CCACGCTGAAGCACGAAACTATCTCC-3′
cDNA cloning primers	PFHPPR-HF	5′-CAATTTCTCAACTACCACTC-3′
Real-time PCR primers	RealHPPR-F	5′-TCAGCGTGGGATTGGATAA-3′
	RealHPPR-R	5′-ACTCACAAATGCGCCTCAA-3′
	RealACTIN-F	5′-GAGGTTGGATCTTGCTGGTC-3′
	RealACTIN-R	5′-GCTCGGCAGTTGTGGTAA-3′
Universal primers	SMART II A Oligonucleotide	5′-AAGCAGTGGTATCAACGCAGAGTACXXXXX-3′
	3′-CDS primer	5′-AAGCAGTGGTATCAACGCAGAGTAC$(T)_{30}$VN-3′
	5′-CDS primer	5′-$(T)_{25}$VN-3′ (N = A, C, G, or T; V = A, G, or C)
	UPM1	5′-CTAATACGACTCACTATAGGGCAAGCAGTGGTA TCAACGCAGACT-3′
	UPM2	5′-CTAATACGACTCACTATAGGGC-3′
	NUP	5′-AAGCAGTGGTATCAACGCAGAGT-3′

at 94 °C, 35 cycles with 30 s at 94 °C, 30 s at 56 °C, and 40 s at 72 °C, 1 cycle with 10 min at 72 °C. The PCR product is purified and cloned into pMD18-T vector (TAKARA, Japan) followed by sequencing.

Second, for 3′-RACE of *PfHPPR*, about 1 μg of total RNA is used to synthesize the first-strand cDNA with the 3′-RACE CDS Primer (Table 194.1) by using SMART™ RACE cDNA Amplification Kit (Clontech Laboratories Lnc, USA). Gene-specific primer PfHPPR3-GSP1 (Table 194.1, as 3′RACE first amplification primer) and gene-specific primer PfHPPR3-GSP2 (Table 194.1, as 3′RACE nest amplification primer) are designed and synthesized according to the conserved region, with 10 × Universal PrimerA Mix (UMP1 and UMP2) and Nested Universal PrimerA (NUP, Table 194.1) provided by the kit to amplify the 3′-end fragment. The PCR is conducted in accordance with the protocol provided by the manufacturer.

For 5′RACE of *PfHPPR*, about 500 ng of total RNA is used to synthesize the 5′-ready cDNA, according to the manual of the SMART™ RACE cDNA Amplification Kit with 5′-CDS primerA and SMART II A Oligonucleotide. PfHPPR5-GSP1 (as 5′RACE first amplification primer), UPM, PfHPPR5-GSP2 (as 5′RACE nest amplification primer), and NUP (Table 194.1) are used to amplify the 5′-end fragment. The PCR is conducted in accordance with the protocol provided by the manufacturer.

The 3′ and 5′-nested amplified PCR products are purified and cloned into pMD18-T vector (TAKARA, Japan) and sequenced, respectively.

By assembling the nucleotide sequences of the 3′ and 5′ RACE products, the full-length cDNA of *PfHPPR* is deduced, and then primer PFHPPR-HF (Table 194.1) and UPM are used to amplify the full-length *PfHPPR* cDNA. The PCR procedure is carried out under following conditions: 2 min at 94 °C, 35 cycles (30 s at 94 °C, 30 s at 59 °C, 2 min at 72 °C), and 10 min at 72 °C. The PCR products are fractionated on agarose gel and purified, cloned, and sequenced as depicted above.

194.2.5 Sequence Analysis of PfHPPR

Several websites and bioinformatics software are used to analyze *PfHPPR*. The amino acid sequence of *PfHPPR* is deduced and analyzed online with ProtParam tool (http://cn.expasy.org/tools/protparam.html), and the sequence comparison is conducted through database search using BLAST program (NCBI, http://www.ncbi. nlm.min.gov/). Self-optimized prediction method with alignment (SOPMA) analyses are performed online (http://www.expasy.org) [16]. Homology-based structural modeling is accomplished by Swiss-Model [17, 18], and WebLab ViewerLite 4.2 is used to display 3-D structures.

194.2.6 Expression Analysis of PfHP*PR*

Aliquots of total RNA isolated from roots, stems, and leaves of *Perilla frutescens* are treated with RNase-free DNAse to remove any contaminating genomic DNA, and its quality and integrity are checked by electrophoresis through agarose gels stained with EB. For real-time RT-PCR, first-strand cDNA is synthesized using the PrimeScript RT reagent Kit with gDNA Eraser (TAKARA) following the manufacturer's instructions. To investigate the expression pattern of *PfHPPR* in different tissues as well as the expression under elicitor treatments, real-time PCR is performed on Eppendorf Mastercycler ep Realplex4 using SYBR Premix Ex Taq™ II (Perfect Real Time) (TAKARA) according to the manufacturer's instructions.

Each real-time PCR reaction is done in 20 μL volumes containing a 10 μM concentration of each primer, 40 ng of cDNA, and 10μL of SYBR Premix Ex Tag. Thermal cycling conditions included a first denaturation step at 95 °C for 3 min, and then 40 cycles of 95 °C for 20 s, 58 °C for 20 s, and 72 °C for 20 °Cs. Fluorescence is measured at the end of each cycle. In order to confirm that only one specific PCR product is amplified, a melting curve analysis is performed by heating the PCR product from 65 to 95 °C. Negative controls missing cDNA template are included in this experiment. Expression data for *PfHPPR* are

presented as relative units after normalization to the *β-ACTIN* control, using the $2^{-\triangle\triangle CT}$ method [19, 20]. The baseline is set automatically by the software taking consistency into account. Values for mean expression and SD are calculated from the results of three independent experiments.

194.3 Results and Discussion

194.3.1 Cloning of the Full-Length PfHPPR

It is hard to directly amplify the full-length *PfHPPR* cDNA because the 5′ and 3′ untranslated sequence of *HPPR* gene is not highly homologous in species. First, a pair of primers is designed based on the conserved region founded in *Solenostemon scutellarioides* and *Salvia miltiorrhiza*, and the conserved fragment is amplified and sequenced. Second, the full-length *PfHPPR* cDNA is obtained based on the sequence of 3′ RACE cDNA fragment of 800 bp and a 5′ RACE cDNA fragment of 320 bp (Fig. 194.2), which is 1723 bp with 87 bp 5′ and 697 bp 3′ untranslated regions, and contained an ORF of 939 bp encoding 313 amino acid protein.

The nucleotide and deduced amino acid sequences of the *PfHPPR* are shown in Fig. 194.3. The putative NAD-binding is also seen in the amino acid residues of *PfHPPR*, which is identified as typical domains for the family of D-isomer-specific 2-hydroxyacid dehydrogenases [21, 22]. And the *PfHPPR* cDNA sequence is deposited in GenBank with the accession number of HM587131.

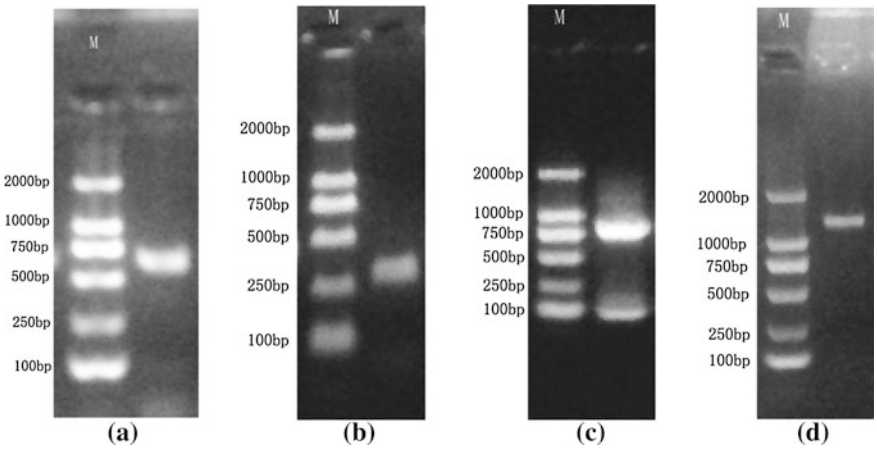

Fig. 194.2 Cloning of cDNA for *PfHPPR*. **a** PCR product of the conserved cDNA fragment; **b** PCR product of the 3′ cDNA end of *PfHPPR*; **c** PCR product of the 5′cDNA end of *PfHPPR*; **d** PCR product of the full-length cDNA of *PfHPPR*

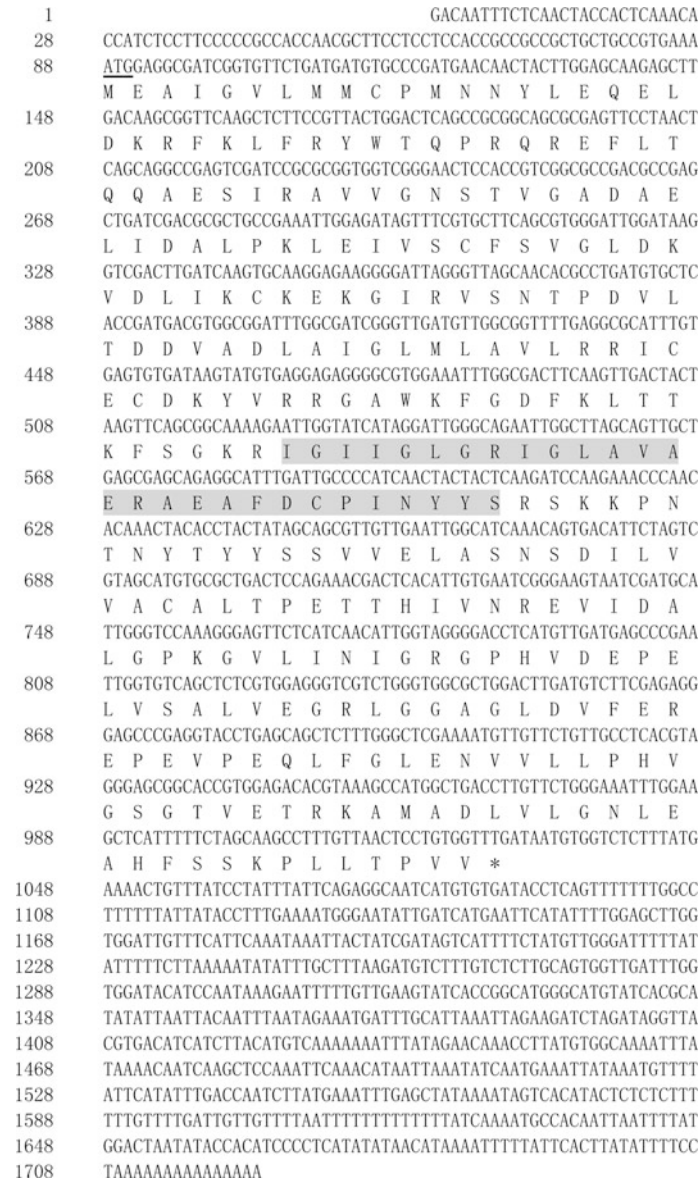

Fig. 194.3 The full-length cDNA sequence and the deduced amino acid sequence of *PfHPPR*. The start codon (ATG) is *underlined*, and the stop codon (TGA) is marked with *asterisk*. The NAD-binding domain typical of the family of D-isomer specific 2-hydroxyacid dehydrogenases is shaded

194.3.2 Bioinformatics Analysis of PfHPPR

Using the software of Compute pI/Mw Tool, the theoretical isoelectric point (pI) and molecular weight of the deduced PfHPPR protein are predicted to be 5.58 and 34 422 Da, respectively. And the sequence comparison using blast search in GenBank database reveals that the nucleotide sequence of *PfHPPR* has high homology with *HPPR* gene from other plant species such as *Solenostemon scutellarioides* (*SsHPPR*), *Salvia officinalis* (*SoHPPR*), and *Salvia miltiorrhiza* (*SmHPPR*). And the deduced amino acid sequence of PfHPPR is 93 %, 93 %, and 92 % identical to SsHPPR, SoHPPR, and SmHPPR, respectively, and is 96, 97, and 97 % similar to SsHPPR, SoHPPR, and SmHPPR, respectively, (Fig 194.4).

The secondary structure of PfHPPR is analyzed by SOPMA (Fig. 194.5) and the result reveals that the putative PfHPPR peptide mainly consisted of alpha

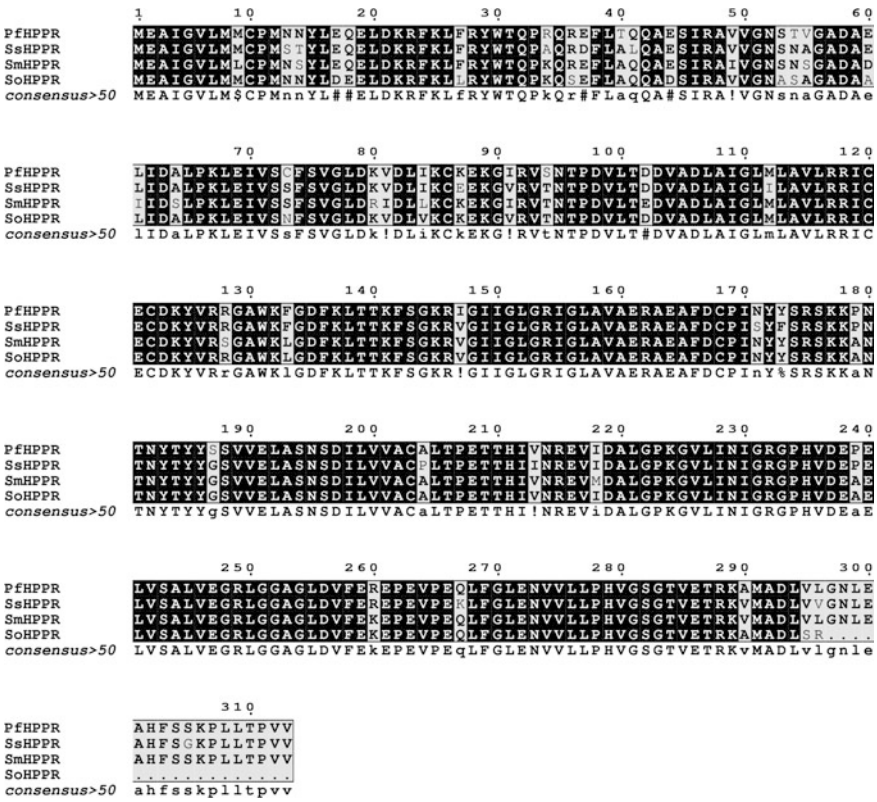

Fig. 194.4 Sequence alignment of the deduced PfHPPR protein with the following other plant HPPRs: SsHPPR (AJ507733), SoHPPR (EU924744), and SmHPPR (DQ099741). *Black boxes* indicate identical residues and gray boxes indicate the conserved residues among the aligned sequence

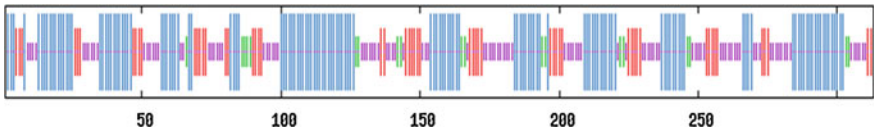

Fig. 194.5 The secondary structure of the deduced PfHPPR. In the panel the longest, middle long, short, and the shortest vertical bars represent the alpha helix, extended strand, beta turn, and random coil, respectively

helices (44.41 %) and beta turns (6.71 %), random coils (31.63 %) and extended strands (17.25 %). Penetrating through most parts of the secondary structure, alpha helices and random coils are the most abundant structural elements, while beta turns and extended strands are intermittently distributed in PfHPPR.

To better characterize the PfHPPR protein, the homology-based three-dimensional structure modeling of PfHPPR is portrayed using SWISS-MODEL and displayed by WebLab Viewerlite 4.2 (Fig 194.6). The result indicates that PfHPPR has an intricate spatial architecture which is strongly similar to *Solenostemon scutellarioides* HPPR (SsHPPR), which reveals that the PfHPPR could have the same biological activity with SsHPPR.

194.3.3 Expression Pattern of PfHPPR

In order to reveal the *PfHPPR* expression pattern in various tissues of *Perilla frutescens*, total RNA is isolated from leaf, stem, and root, respectively. The

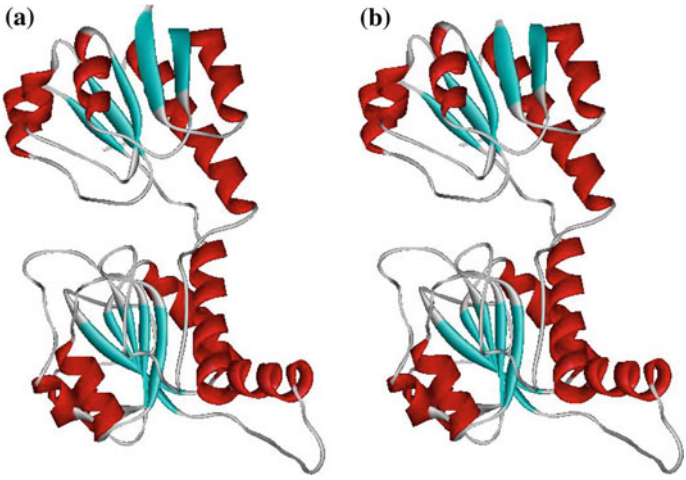

Fig. 194.6 The deduced PfHPPR (**a**) and the three-dimensional structure of SsHPPR (**b**) established by homology-based modeling. Turns and loops are indicated by *gray* lines, α-helices are indicated by *red* helices, and *β*-sheets are indicated by *blue* patches

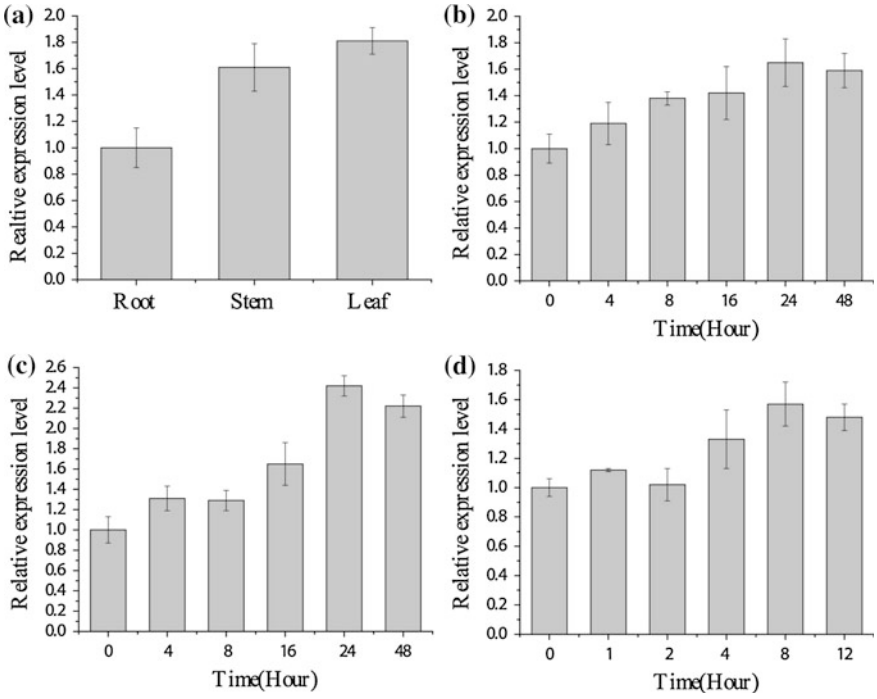

Fig. 194.7 Quantitative analysis of *PfHPPR* mRNA in different tissues (**a**) and transcription pattern of *PfHPPR* under different treatments. **b** 200 μM SA, **c** 100 μM ABA, and **d** UV-B at different time point. Error bars indicate the standard deviation for three technical replicates

transcription level of *PfHPPR* is analyzed using real-time quantitative reverse transcription PCR and the results show that *PfHPPR* can be detected in all the tested tissues with stronger expression in leaves, which suggests that it is a constitutively expressed gene (Fig 194.7a).

Because the major roles of plant secondary metabolites are to protect plants from biotic and abiotic stresses, some strategies for culture production of the metabolites based on this principle have been developed to improve the yield of such plant secondary metabolites [23–25]. In this study, *Perilla frutescens* leaves are treated with various induced factor such as SA, ABA, and UV-B, and harvested for RNA isolation at different time points to characterize the transcription pattern of *PfHPPR*.

SA, a phenolic phytohormone and key signal molecule in the systemic acquired resistance, which plays an important role in plant growth and development, and also in responses to different stresses, such as plant-pathogen interaction and ozone exposure [26, 27]. The putative *PfHPPR* expression under the SA treatment is analyzed and the results revealed that the *PfHPPR* is induced at least at transcriptional level, reaching the highest level after 24 h (Fig 194.7b).

ABA is a well-known senescence-triggering plant hormone, which acts as an important regulator of plant life and development, and especially responses to some stresses such as salt, cold and drought, or microbial defense in plants [28]. For ABA treatment, the expression levels are increased dramatically to 2.4-fold the control after 24 h and then declined (Fig 194.7c). The results in our study suggest that ABA could also stimulate the expression of *PfHPPR* gene in *Perilla frutescens*.

UV light is an abiotic stimulus, which can promote secondary metabolites accumulation to protect plants from the damaging effects of UV-B radiation [29]. And we also analyzed whether the expression of *PfHPPR* is affected under UV-B treatment, compared to control (without any stress treatment), the level of *PfHPPR* expression in leaves increases gradually along with the UV-B treatment in 24 h (Fig 194.7d).

194.4 Conclusion

In the study presented here, a new gene encoding HPPR involved in the biosynthesis of RA is cloned from *Perilla frutescens* using the RACE method. Analysis of *PfHPPR* indicates that it is 1723 bp in size, which contains a 939 bp ORF encoding a protein of 313 amino acids. Amino acid sequence analysis shows that the PfHPPR has a high sequence homology to the other HPPR proteins, which demonstrate that the *PfHPPR* belongs to the plant *HPPR* superfamily. In addition, the analysis of three-dimensional structures indicates that the PfHPPR could have the same biological activity with SsHPPR, a protein which had been purified previously, implying that they have potential functional similarities.

Expression analysis indicates that the *PfHPPR* gene expresses differently in different tissues with most highly in leaves, and *Perilla frutescens* leaves are treated with various stresses to investigate the expression profiles. In summary, considering the induction effect on the expression level, the *PfHPPR* is inferred to be an elicitor-responsive expressing gene and the result is useful to further study the expression regulation of *PfHPPR*. Our study provides information for uncovering the molecular induction mechanism in RA biosynthesis and also supplies a potential new target for enhancing the content of rosmarinic acid from *Perilla frutescens* by bioengineering means in the near future.

References

1. Honda G, Koezuka Y, Tabata M (1990) Genetic studies of color and hardness in *Perilla frutescens*. Jpn J Breed 40:469–474
2. Makino T, Ono T, Muso E (2002) Effect of *Perilla frutescens* on nitric oxide production and DNA synthesis in cultured murine vascular smooth muscle cells. Phytother Res 16:19–23

3. Shin HS, Kim SW (1994) Lipid composition of *Perilla* seed. J Am Oil Chem Soc 17:619–622
4. Kim EK, Lee SJ, Lim BO et al (2008) Antioxidative and neuroprotective effects of enzymatic extracts from leaves of *Perilla frutescens* var. japonica. Food Sci Biotechnol 17:279–286
5. Lee JH, Baek IY, Kang NS et al (2009) Optimization of extraction conditions and comparison of rosmarinic and caffeic acids from leaves of *Perilla frutescens* varieties. Food Sci Biotechnol 18:928–931
6. Petersen M, Simmonds MSJ (2003) Rosmarinic acid. Phytochemistry 62:121–125
7. Parnham MJ, Kesselring K (1985) Rosmarinic acid. Drug Future 10:756–757
8. Cuvelier ME, Richard H, Berset C (1996) Antioxidative activity and phenolic composition of pilot-plant and commercial extracts of sage and rosemary. J Am Oil Chem Soc 73:645–652
9. Ellis BE, Towers GHN (1970) Biogenesis of rosmarinic acid in Mentha. Biochem J 118:291–297
10. Karwatzki B, Petersen M, Alfermann AW (1989) Transient activity of enzymes involved in the biosynthesis of rosmarinic acid in cell suspension cultures of *Coleus blumei*. Planta Med 55:663–664
11. Ellis BE, De Eknamkul W (1987) Tyrosine aminotransferase: the entry-point enzyme of the tyrosine-derived pathway in rosmarinic acid biosynthesis. Phytochemistry 26:1941–1946
12. Hausler E, Petersen M, Alfermann AW (1991) Hydroxyphenylpyruvate reductase from cell suspension cultures of Coleus blumei Benth. Z Naturforsch C 46:371–376
13. Petersen M, Alfermann AW (1988) Two new enzymes of rosmarinic acid biosynthesis from cell cultures of *Coleus blumei*: hydroxyphenylpyruvate reductase and rosmarinic acid synthase. Z Naturforsch c 43:501–504
14. Petersen M, Hausler E, Karwatzki B, Meinhard J (1993) Proposed biosynthetic pathway for rosmarinic acid in cell cultures of *Coleus blumei*. Planta 189:10–14
15. Kim KH, Janiak V, Petersen M (2004) Purification, cloning and functional expression of hydroxyphenylpyruvate reductase involved in rosmarinic acid biosynthesis in cell cultures of *Coleus blumei*. Pl Mol Biol Rep 54:311–323
16. Geourjon C, Deleage G (1995) SOPMA: significant improvements in protein secondary structure prediction by consensus prediction from multiple alignment. Comput Appl Biosci 11:681–684
17. Guex N, Peitsch MC (1997) SWISS-MODEL and the Swiss-PdbViewer: An environment for comparative protein modeling. Electrophoresis 18:2714–2723
18. Schwede T, Kopp J, Guex N et al (2003) SWISS-MODEL: an automated protein homology-modeling sever. Nucl Acid Res 31:3381–3385
19. Kenneth J, Thomas D (2001) Analysis of relative gene expression data using real-time quantitative PCR and the $2^{-\triangle\triangle CT}$ method. Methods 25:402–408
20. Michael W (2001) A new mathematical model for relative quantification in real-time RT-PCR. Nucl Acid Res 29:2002–2007
21. Grant GA (1989) A new family of 2-hydroxyacid dehydrogenases. Biochem Biophys Res Comm 165:1371–1374
22. Kochhar S, Hunziker PE, Leong-Morgenthaler P et al (1992) Evolutionary relationship of NAD^+-Denpen- dent D-lactate dehydrogenase: comparison of primary structure of 2-hydroxy acid dehydrogenases. Biochem Biophys Res Commun 184:60–66
23. Finkelstein RR, Gampala SS (2002) Abscisic acid signaling in seeds and seedlings. Plant Cell. 14:S15–S45
24. Lin PC, Hwang SG, Endo A et al (2007) Ectopic expression of abscisic acid 2/glucose insensitive 1 in Arabidopsis promotes seed dormancy and stress tolerance. Plant Physiol 143(2):745–758
25. Ryals JA, Neuenschwander UH, Willits MG et al (1996) Systemic acquired resistance. Plant Cell 8:1809–1819
26. Zhao J, Zhu WH, Hu Q (2001) Enhanced catharanthine production in Catharanthus roseus cell cultures by combined elicitor treatment in shake flasks and bioreactors. Enzyme Microb Technol 28:673–681

27. Hayat S, Ahmad A (2007) Salicylic acid: a plant hormone. Springer, The Netherlands
28. Zhu WH, Zhao J, Hu Q, He XW (2000) Improved indole alkaloid production in *Catharanthus roseus* suspension cell cultures by various chemicals. Biotechnol Lett 22:1221–1226
29. Li JY, Oulee TM, Raba R et al (1993) Arabidopsis flavonoid mutants are hypersensitive to UV-B irradiation. Plant Cell 5:171–179

Chapter 195
Design, Synthesis, and Biological Evaluation of Nedd4 E3 Ubiquitin Ligase Small Molecule Inhibitors

Xiaoli Fu, Jie Chu, Yuyin Li, Shasha Wang, Jie Zhou, Yujie Dai and Aipo Diao

Abstract Protein ubiquitination and deubiquitination are closely associated with tumorigenesis. The incidence of most tumorigenesis associated with abnormal expression of oncogenes and tumor suppressor genes. Nedd4 is an E3 ubiquitin ligase and highly expressed in prostate cancer cells, breast cancer cells, and ovarian cancer cells [1]. Based on the three-dimensional structure of Nedd4 ubiquitin ligase and its characteristics, we used computer simulations and structural biology information to design and synthesize compounds to inhibit the activity of Nedd4 ubiquitin ligase. In this paper, we would like to report the design, synthesis, and biological activities of these compounds. Among those compounds, five new compounds have not been reported before. All the newly synthesized compounds were characterized by 1H NMR and were tested for their antitumor activities using DU145, PC3, and PNT1A cell lines. The results showed that 4-(4-chlorobenzoyl) piperazin-1-yl) (4-(phenoxymethyl) phenyl) methanone has antiproliferative activity against DU145 with an IC50 of 3.86 μM.

Keywords Nedd4 ubiquitin ligase · Antitumor · DU145 cancer cell · Inhibitor

195.1 Introduction

Ubiquitination is a way of common protein modification, which is catalyzed by a series of ubiquitination enzymes (E1, E2, E3 ubiquitin ligase) [1]. During the ubiquitination, evolutionary conserved 76 amino acid peptide chain that will be connected to the target protein substrates, to regulate the transport and degradation of the protein, as well as a variety of metabolic pathways in cells [2, 3]. The

X. Fu · J. Chu · Y. Li · S. Wang · J. Zhou · Y. Dai · A. Diao (✉)
College of Biotechnology, Tianjin University of Science and Technology, Tianjin 300457, People's Republic of China
e-mail: diaoaipo@tust.edu.cn

T.-C. Zhang et al. (eds.), *Proceedings of the 2012 International Conference on Applied Biotechnology (ICAB 2012)*, Lecture Notes in Electrical Engineering 251,
DOI: 10.1007/978-3-642-37925-3_195,

abnormal regulation of ubiquitin ligase is closely related to growth of tumors. Small molecule inhibitors of ubiquitin ligase enzyme may provide a theoretical basis for a new target for the prevention and treatment of breast cancer, ovarian cancer, inflammation, neurodegenerative diseases, and other diseases. E3 ubiquitin ligase has substrate specificity of enzymatic properties. Therefore, Nedd4 could be a new target for treatment for cancer.

Nedd4 belongs to the HECT E3 ubiquitin ligases family, which includes about 50 members. Nedd4 contains a C-terminal-specific the HECT catalytic structure and a C2 phospholipid-binding structure in the N-terminal domain. The WW domain of the Nedd4 protein comprises of a module with two highly conserved tryptophan residues, which bind to the target proteins that contain a PY motif, e.g., ppxY [4–8]. In this paper, we addressed the designing and synthesis of inhibitors to block the interaction of Nedd4 to E2.

The target compounds (5a–5e) were synthesized in five steps with piperazine as precursor through NH-Boc protecting, acylation, alkylation reaction, and so on. In order to further explore the effect of the structure for antitumor activity, we synthesized a series of compounds. To confirm the inhibition of the compound, we have tested the biological activity through MTT assay. The results indicated that 4-(4-chlorobenzoyl) piperazin-1-yl) (4-(phenoxymethyl) phenyl) methanone shows antitumor activity against DU145 cell.

195.2 Materials and Methods

All reagents and solvents used in this paper were of reagent grade. Reaction temperatures were controlled by using oil bath temperature modulator. The reaction was monitored by TLC. Merck silica gel 60 GF254 precoated plates (0.25 mm) and visualized using a combination of UV. Silica gel (particle size 200–400 mesh) was used for flash chromatography. The structure of the products was conformed by NMR. 1H NMR spectra were recorded on Bruker AM-400 NMR spectrometers in deuterated chloroform and deuterated acetone. The chemical shifts are reported in δ (ppm) against tetramethylsilane as internal standard. We analyzed the ability of 5a, 5b, 5c, 5d, and 5e for inhibiting the activity of Nedd4 in DU145 and PC3 cells. Normal prostate cell PNT1A was used as control.

195.3 Results and Discussion

195.3.1 Chemistry

Figure 195.1 demonstrates the synthesis approach to the target compound 5a–5e. There are two amino groups in the structure of piperazine, so it is difficult to

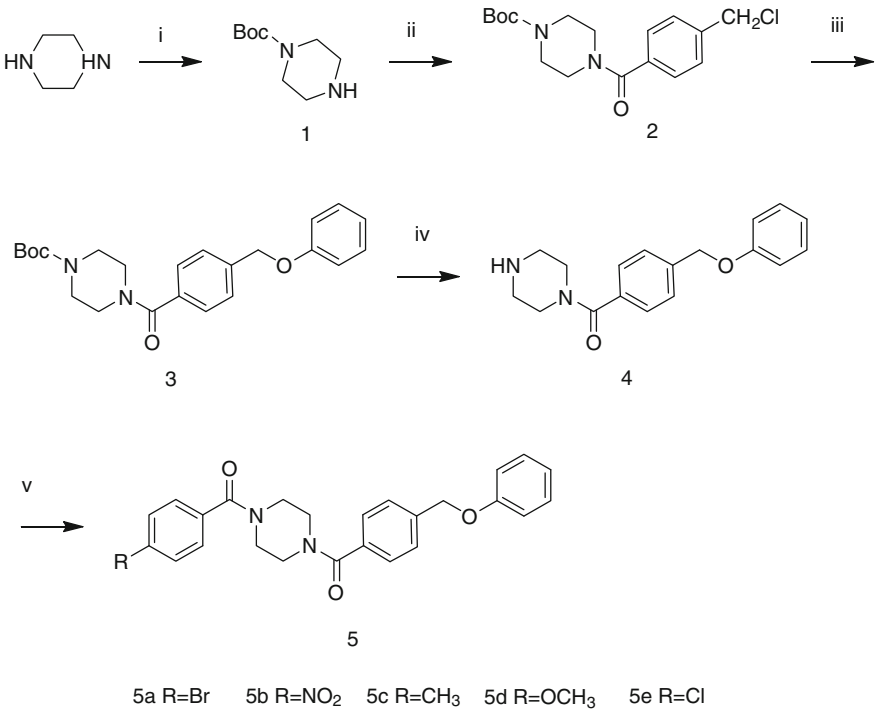

Fig. 195.1 Synthetic route of piperazine derivatives

protect either one. The general procedure for the first step was adopted from the previously reported method [9].The first step can be divided into two steps. First, Piperazine was employed to react with acetic acid to provide Piperazine titanium. The reaction must be controlled under 30 °C.It was also necessary to drop acetic acid slowly. Second, Di-tert-butyl dicarbonate was dropped slowly into the mixture on ice. Low to moderate yield of required products were obtained.

Tert-butyl 1-piperazinecarboxylate was employed to react with p-Toluoyl chloride in basic condition to provide compound 2. More attention should be paid in this step. Anhydrous condition and appropriate basic were required. Otherwise, the yields will be less than satisfactory. Compound 2 then react with Phenol to afford compound 3. TLC showed that the raw material and the product in the same position, which make it difficult to separate the product from the precursor. In that case, the precursor must be controlled to disappear completely. Compound 3 is deprotected to give Compound 4 by using TFA (Trifluoroacetic acid). Although this route provided access to the desired compound, the product exists in the form of a trifluoroacetate. The final synthesis step had to be optimized further. Yield is very low after the product was recrystallized.

Reagents and conditions: (i)CH_3CO_2Et, Toluene; (ii) K_2CO_3, CH_3COCH_3; (iii) DMF, K_2CO_3; (iv)TFA, CH_2Cl_2; (v) $(C_2H_5)_3N$, CH_2Cl_2

Table 195.1 Inhibition activity of the compound 5a, 5b, 5c, 5d, and 5e

Tested cell	Samples				
	5a	5b	5c	5d	5e
DU145(IC_{50})	>10	>10	>10	>10	3.86
PC3(IC_{50})	>10	>10	>10	>10	5.18
PNT1A(IC_{10})	>10	>10	>10	>10	>10

195.3.2 Biological Assay

The proliferation assay by MTT method was used to test which of these compounds would produce 50 % growth inhibition (IC50) in tumor cells. Nedd4 was highly expressed in prostate cancer cells, so the inhibitory activities of the above newly synthesized compounds were tested in cell lines of prostate origin: DU145, PC3, and PNT1A. The results of compounds 6a, 6b, 6c, and 6d were listed in Table 195.1. The doses employed ranged from 0.001 to 10 μM. Compounds requiring IC50 concentrations > 10 μM were considered as inactive. The result in Table 195.1 indicated that 4-(4-chlorobenzoyl) piperazin-1-yl) (4-(phenoxymethyl) phenyl) methanone have antitumor activity against DU145 and PC3 with an IC50 of 3.86 μM and 5.18 μM, but have no inhibitory effect on normal prostate cell PNT1A (IC10 > 10 μM).fetanone

195.4 Experimental

195.4.1 Experimental Section

Synthesis of Tert-butyl 1-piperazinecarboxylate [10]. A three-neck-bottom flask (500 mL) was charged with anhydrous ethanol (116.31 mL) and piperazine (20 g). The solution was stirred till the mixture became clear. Then glacial acetic acid 62.64 g (59.71 mL) was added dropwise to the mixture and the temperature should be kept under 30 °C. After all the glacial acetic acid was added to the flask the resulting solution was stirred for 15 min, and then ethanol/water (ethanol77.17 g/water111.2 g) was dropped into the mixture. The reaction mixture was stirred at room temperature for 1.5 h. When the mixture was cooled to 5 °C, Di-tert-butyl dicarbonate/anhydrous ethanol (50 g/70 g) was added dropwise, and stirred for 5 h. Insoluble product was collected by suction filtration. The solvent was removed under vacuum, till the residual solvent of the flask dropped to 70 g, stop distilling, then added 15 g water to the flask. The aqueous phase extracted with toluene (3 × 100 mL). Combined organic layers and the aqueous phase quenched with $NaHCO_3$/ice until slight precipitate appeared, then extracted with ethyl acetate (3 × 30 mL). The phases was separated and washed with water

(2 × 100 mL), finally dried over anhydrous magnesium sulfate. The ethyl acetate was removed under vacuum to afford the product with an average yield of 57.2 %.

1H NMR (CDCl3 400 MHz): δ/ppm 1.47 (s, 9H), 1.93–1.94(m, 1H), 2.81 (t, 4H), 3.38 (t, 4H)

Synthesis of Tert-butyl4-(4-(chloromethyl)benzoyl)piperazine-1-carboxylate [11]. To a solution of compound 1 (9.3 g, 0.05 mol) dissolved in acetone (50 mL) was added potassium carbonate (13.8 g, 0.1 mol) and KI (0.83 g, 5 mmol).After stirring at room temperature for 10 min, 1-(4-(chloromethyl)phenyl) ethanone (11.34 g, 0.06 mol) was added. The reaction mixture was heated under reflux for 5 h. The reaction mixture was cooled to room temperature, the resulting precipitate was removed by vacuum filtration, and the filtrate transferred to a separating funnel, where the organic phase was collected. The solvent was removed under vacuum to afford the crude which was purified by flash column chromatography (silica gel, petroleum ether/ethyl acetate 5:1), resulting in white powder 12.3 g, 72.8 %.

1H NMR (Acetone-d6 400 MHz): δ/ppm 1.47 (m, 9H), 3.41–3.82 (m, 8H), 4.78 (s, 2H), 7.43 (d, 2H), 7.57 (d, 2H)

Synthesis of Tert-butyl 4-(4-(phenoxymethyl)benzoyl)piperazine-1-carboxylate [12, 13]. To a solution of compound 2 (1.0 g, 2.95 mmol) in dry N, N-Dimethylformamide (4 mL) potassium carbonate (0.4 g, 2.95 mmol) in portions was added at room temperature. Phenol (0.28 g, 3 mmol) was added. The mixture was stirred for 6 h. The reaction mixture was poured into water (100 mL) and then extracted with dichloromethane (2 × 10 mL), washed with water (2 × 50 mL). The solvent was removed under reduced pressure to provide the crude which was purified by flash column chromatography (silica gel, petroleum ether/ethyl acetate 5:1), resulting in white powder 0.8 g, 78.4 %.

1H NMR (Acetone-d6 400 MHz): δ/ppm 1.47 (s, 9H), 341-3.82 (m, 8H), 5.18 (s, 2H), 6.97 (t, J = 7.6 Hz, 1H), 7.05 (d, 2H), 7.29 (m, 2H), 7.48 (d, 2H), 7.57 (d, 2H)

Synthesis of (4-(phenoxymethyl)phenyl)(piperazin-1-yl)methanone [14, 15]. A solution of Trifluoroacetic acid (1 mL) in dichloromethane (4 mL) was added dropwise to a mixture of compound 3 (0.5 g, 1.26 mmol) in dichloromethane (3 mL). The reaction mixture was then stirred at room temperature for 2 h. The reaction was monitored by TLC and it showed that all the products were on the base line. Water was added until the solvent was removed in vacuo. This solution was then alkalized using 1 M $NaHCO_3$ until a slight precipitate appeared (around pH 8–9), at which point the resulting precipitate was removed by vacuum filtration. The crude was purified by flash column chromatography (silica gel, petroleum ether/ethyl acetate 3:1), resulting in white powder 0.32 g, 65.7 %.

1H NMR (CDCl3 400 MHz): δ/ppm 1.93–1.94 (m, 1H), 341–3.82 (m, 8H), 5.18 (s, 2H), 6.97 (t, J = 7.6 Hz, 1H), 7.05 (d, 2H), 7.29 (m, 2H), 7.48 (d, 2H), 7.57 (d, 2H)

General method for the Synthesis of Compounds (5a–5e) [16, 17]. To a solution of compound 4 (0.2 g, 0.67 mmol) in dry dichloromethane (4 mL), $(C_2H_5)3N$ (0.14 g, 1.35 mmol) was added. After stirring for 10 min a–e (1.5 equiv) was

added, and it was stirred for an additional 4 h at room temperature. The reaction mixture was washed with 1 M $NaHCO_3$ (2 × 20 mL) then the solvent was dried with $MgSO_4$ and removed under reduced pressure to afford the crude which was purified by flash column chromatography (silica gel, petroleum ether/ethyl acetate/dichloromethane 1:1:1) to get compounds (5a–5e).

Synthesis of (4-(4-bromobenzoyl) piperazin-1-yl)(4-(phenoxymethyl)phenyl) methanone Starting from compound 4 (0.2 g, 0.67 mmol) and $(C_2H_5)3N$ (0.14 g, 1.35 mmol) and 4-bromobenzoyl chloride (0.22 g, 1.00 mmol), compound 5a was obtained in white solid, 38 % yield.

1H NMR (Acetone-d6 400 MHz): δ/ppm 3.54–3.83 (m, 8H), 5.18 (s, 2H), 6.96 (t, J = 7.6 Hz, 1H), 7.04 (d, 2H), 7.31 (t, J = 8.0, 2H), 7.44 (d, 2H), 7.50 (d, 2H), 7.57 (d, 2H), 7.65 (d, 2H)

Synthesis of (4-(4-nitrobenzoyl)piperazin-1-yl)(4-(phenoxymethyl)phenyl) methanone Starting from compound 4 (0.2 g, 0.67 mmol) and $(C_2H_5)3N$ (0.14 g, 1.35 mmol) and 4-nitrobenzoyl chloride (0.18 g, 1.00 mmol), compound 5b was obtained in white solid, 30 % yield.

1H NMR (CDCl3 400 MHz): δ/ppm 3.30–3.91 (m, 8H), 4.61 (s, 1H), 5.11 (s, 1H), 6.98 (t, 1H), 7.30 (d, 2H), 7.28–7.45 (m, 4H), 7.61 (d, 2H), 8.31 (d, 1H)

Synthesis of (4-(4-methylbenzoyl)piperazin-1-yl)(4-(phenoxymethyl)phenyl) methanone Starting from compound 4 (0.2 g, 0.67 mmol) and $(C_2H_5)3N$ (0.14 g, 1.35 mmol) and 4-methylbenzoyl chloride (0.15 g, 1.00 mmol), compound 5c was obtained in white solid, 43 % yield.

1H NMR (CDCl3 400 MHz): δ/ppm 2.38 (s, 3H), 3.34–3.78 (m, 8H), 5.20 (d, 2H), 6.96 (d, 3H), 7.26–7.33 (m,6H), 7.43 (d, 2H), 7.50 (d, 2H)

Synthesis of (4-(4-methoxybenzoyl) piperazin-1-yl)(4-(phenoxymethyl)phenyl) methanone Starting from compound 4 (0.2 g, 0.67 mmol) and $(C_2H_5)3N$ (0.14 g, 1.35 mmol) and 4-methoxybenzoyl chloride (0.17 g, 1.00 mmol), compound 5d was obtained in white solid, 44 % yield.

1H NMR (CDCl3 400 MHz): δ/ppm 3.51–3.82 (m, 8H), 3.84 (s, 3H), 5.10 (s, 1H), 5.29 (s, 1H), 6.91–6.99 (m, 4H), 7.27–7.35 (m, 3H), 7.38–7.41 (m, 4H), 4.47 (d, 1H)

Synthesis of (4-(4-chlorobenzoyl) piperazin-1-yl)(4-(phenoxymethyl)phenyl) methanone Starting from compound 4 (0.2 g, 0.67 mmol) and $(C_2H_5)3N$ (0.14 g, 1.35 mmol) and 4-chlorobenzoyl chloride (0.17 g, 1.00 mmol), compound 5e was obtained in white solid, 64 % yield.

1H NMR (CDCl3 400 MHz): δ/ppm 3.31–4.83 (m, 8H), 4.57 (s, 1H), 5.07 (s, 1H), 6.95 (d, 1H), 7.22–7.46 (m, 10H), 7.46 (d, 2H)

195.4.2 Biological Assay

The antiproliferative effects of these compounds were determined in DU145 and PC3 cells by MTT assay [18–20], with PNT1A as control. All cell lines were maintained in a humidified incubator at 37 °C and 5 % CO2/air atmosphere. The

cells were diluted to a density of 2.5 × 104 cells/mL and 200 μL was added to each well of the 96-well plates with a multichannel pipette, filled with sterile PBS in surrounding. After incubating for 24 h, 1 μL compound in DMSO was added and then cells were incubated for further 48 h (final concentrations of each compound ranged from 0.001 to 10 μM). The culture plates were incubated for 4 h after which 20 μL MTT was added to each well. Then the medium were removed from the wells and 200 μL DMSO was added into each well. After leaving for further 10 min to dissolve the formazan crystals formed, the optical density (OD) was measured at 490 and 630 nm. Cell viability was calculated from measurements of OD value according to the corresponding formula and a graph was plotted with cell viability as y-axis against drug concentration as x-axis. The inhibitory concentration by 50 % IC (50) values of compounds 5a–5e were presented in Table 195.1.

195.5 Conclusion

In conclusion, we designed and synthesized several small molecule inhibitors blocking the interaction between ubiquitin ligase E2 and Nedd4 and then tested their antitumor activities. All the target compounds were synthesized in five steps. The structures of these novel targets and all of intermediates were confirmed by 1H NMR. Biological activity test indicated that 4-(4-chlorobenzoyl) piperazin-1-yl) (4-(phenoxymethyl) phenyl) methanone has antitumor activity against DU145 and PC3 cells. The antitumor mechanism of these compounds and the relationship between compound structure and activity need to be studied next in our lab.

Acknowledgments This research is supported by the Tianjin Natural Science Foundation grant (10JCZDJC16800).

References

1. Novaro V, Radisky D (2002) 93rd annual meeting of the american association for cancer research, San Francisco, CA, USA, 6–10 April 2002. Breast Cancer Res 4:165–168
2. Xu LL, Shi Y, Petrovics G et al (2003) PMEPA1, an androgen-regulated NEDD4-binding protein, exhibits cell growth inhibitory function and decreased expression during prostate cancer progression. Cancer Res 63:4299–4304
3. Weissman A, Lowenstein L, Porat M et al (2005) The effect of hormone replacement therapy cessation on heart rate variability in postmenopausal women. Clin Auton Res 15:411–413
4. Sudol M (1996) The WW module competes with SH3 domain. Trends Biochem Sci 21:161–163
5. Macias MJ, Hyvönen M, Baraldi E et al (1996) Structure of the WW domain of a kinase-associated protein complexed with a proline-rich peptide. Nature 382:646–649

6. Chen HI, Sudol M (1995) The WW domain of Yes-associated protein binds a proline-rich ligand that differs from the consensus established for Src homology 3-binding modules. Proc Natl Acad Sci USA 92:7819–7823
7. Murillas R, Simms KS, Hatakeyama S et al (2002) Identification of developmentally expressed proteins that functionally interact with Nedd4 ubiquitin ligase. J Biol Chem 277:2897–2907
8. Wang J (2006) SUMO conjugation and cardiovasclular development. Front Biosci 14:1219–1229
9. Mulwad VV, Langi BP, Chaskar AC (2011) Synthesis of novel biologically active heterocyclic compounds from 2-oxo-2H-benzopyran-6-yl-imidazolidine. Acta Pol Pharm 68:39–47
10. Reddy KK, Ravinder T, Prasad RB et al (2011) Evaluation of the antioxidant activity of capsiate analogues in polar, nonpolar, and micellar media. J Agric Food Chem 59:564–569
11. Ruchelman AL, Man HW, Chen R et al (2011) 1,1-Diarylalkenes as anticancer agents: dual inhibitors of tubulin polymerization and phosphodiesterase 4. Bioorg Med Chem 19:56–74
12. Wesson DR (2011) Psychedelic drugs, hippie counterculture, speed and phenobarbital treatment of sedative-hypnotic dependence: a journey to the Haight Ashbury in the Sixties. J Psychoactive Drugs 43:153–164
13. Tamami B, Ghasemi S (2008) Palladium nanoparticles supported on layered hydroxide salts and their use in carbon–carbon coupling organic reactions. J Iranian Chem Soc 5:S26–S32
14. Müller C, Schöniger-Hekele M, Schernthaner R et al (2008) Percutaneous ethanol instillation therapy for hepatocellular carcinoma - a randomized controlled trial. Wien Klin Wochenschr 120:608–618
15. Biju P, Taveras A, Yu Y et al (2008) 3,4-Diamino-2,5-thiadiazole-1-oxides as potent CXCR2/CXCR1 antagonists. Bioorg Med Chem Lett 18:228–231
16. Oxford JS (2000) Zanamivir (Glaxo Wellcome). IDrugs 3:447–459
17. Kamal A, Reddy MK, Ramaiah MJ et al (2011) Synthesis of aryl-substituted naphthalene-linked pyrrolobenzodiazepine conjugates as potential anticancer agents with apoptosis-inducing ability. ChemMedChem 6:1665–1679
18. Mosmann T (1983) Rapid colorimetric assay for cellular growth and survival: application to proliferation and cytotoxicity assays. J Immunol Methods 65:55–63
19. Xu J, Wu F, Mei M (2005) MTT assay tumor chemo sensitivity. China Medicine 01:12–13
20. Miladi S, Abid N, Debarnôt C (2012) In vitro antiviral activities of extracts derived from Daucus maritimus seeds. Nat Prod Res 26:1027–1032

Chapter 196
Improvement of Electrotransformation Efficiency by Lysozyme Treatment in *Cronobacter sakazakii*

Xinjun Du, Fei Wang, Yue Ge, Lu Meng and Shuo Wang

Abstract Many *Cronobacter sakazakii* strains were poorly transformable according to our previous study. In order to improve the efficiency of electrotransformation, lysozyme treatment was introduced in preparation of the competent cells. After optimization of the parameters critical for the application of electrotransformation, including lysozyme concentration, lysozyme disposing time, electric field strength, and the time constant, efficiency of electrotransformation was raised from 7.2×10^1 to 1.16×10^3 transformants per microgram DNA. To our knowledge, this is the first time that lysozyme was used to improve the transformation efficiency in *Cronobacter*.

Keywords Lysozyme · Electrotransformation · Efficiency · *Cronobacter sakazakii*

196.1 Introduction

Cronobacter sakazakii is a gram-negative, rod-shaped, pathogenic bacterium [1] which can cause bacteraemia, meningitis, and necrotising enterocolitis in infant [2, 3]. In recent years, this bacterium has aroused more and more concern. While studies on biological characteristics, virulence, route of transmission, and epidemiology were well carried out, research works associated with genetic modification were seldom reported. In our previous studies, it was found that a large amount of *C. sakazakii* isolates were poorly transformable. Thus, establishing efficient electrotransformation system is meaningful for further research on the molecular characteristics of *C. sakazakii*.

X. Du · F. Wang · Y. Ge · L. Meng · S. Wang (✉)
Key Laboratory of Food Nutrition and Safety, Tianjin University of Science and Technology, Ministry of Education, Tianjin 300457, People's Republic of China
e-mail: s.wang@tust.edu.cn

T.-C. Zhang et al. (eds.), *Proceedings of the 2012 International Conference on Applied Biotechnology (ICAB 2012)*, Lecture Notes in Electrical Engineering 251,
DOI: 10.1007/978-3-642-37925-3_196,

Electrotransformation is well known as the most efficient way of transformation [4]. Electroporation involves the application of an instant, high-voltage pulse to a suspension of cells and DNA, resulting in reversible membrane pores and subsequent uptake of DNA [5–7]. Many research works have focused on impact-factors of electrotransformation, such as the traits of bacteria [8], sizes of plasmids [9], DNA concentration [10] voltage [11], and so on. Lysozyme was well used in transformation of gram-positive bacteria [12–14], but was seldom used to improve transformation efficiency of gram-negative bacteria. In this study, lysozyme was first introduced to improve the electrotransformation efficiency in *C. sakazakii*.

196.2 Materials and Methods

196.2.1 Materials

C. sakazakii (IQCC 10423) came from China Center of Industrial Culture Collection (Beijing, China). pET-26b plasmid was obtained from Novagen (Darmstadt, Germany). Lysozyme (LDB0308) was purchased from Sangon company (Shanghai, China).

196.2.2 Preparation of Competent Cells

The method developed by Teixeira et al. [15] was modified to prepare *C. sakazakii* competent cells. Five milliliters of Luria-Bertrani (LB) broth was inoculated with a single colony of strain IQCC 10423 and incubated overnight at 37 °C with shaking at 200 rpm. The following day, the overnight culture was diluted 100-fold in 50 ml LB broth and incubated at 37 °C with shaking at 200 rpm until exponential phase. The culture was treated with different concentrations of lysozyme and chilled on ice for 30 min. The cells were centrifuged at 1,500xg for 15 min at 4 °C. The supernatant was decanted, and the pellets were resuspended with 20 mL ice-cold sterile water and centrifuged. The washed cells were resuspended with 15 ml ice-cold sterile glycerol (10 %). After centrifugation at 1,500xg for 15 min at 4 °C, the cell pellets were suspended with 500 μl ice-cold 10 % glycerol, divided into 50 μl aliquots, and stored at −80 °C until use.

196.2.3 Electrotransformation

Modified electrotransformation procedure [16] was carried out to transform pET-26b into *C. sakazakii* competent cells. After defrosting 50 μl competent cells on

ice, 2.5 μg pET-26b plasmid was added and the mixture was incubated on ice for 30 min. The mixed DNA and cells were transferred to a chilled 2 mm gap electroporation cuvette (Bio-Rad, Hercules, California) and incubated on ice for 5 min. Electrotransformation was performed in a GenePulser Xcell electro-porator (Bio-Rad, Hercules, California). Then the cells were transferred to 1 mL of pre-heated SOC broth and cultured at 37 °C for 1 h with shaking at 200 rpm. 100 μl of cell culture was then spread onto LB plates containing 50 μg/mL kanamycin and incubated overnight at 37 °C. Triplicate experiments were conducted for each transformation condition.

196.2.4 Positive Rates Examination

Colonies on each plate were counted. Ten clones were selected randomly and further verified as positive transformants with the PCR method using pET-26b specific primers under conditions: one cycle (94 °C, 10 min); 35 cycles (94 °C, 30 s; 55 °C, 45 s; 72 °C, 45 s) followed by a last cycle (72 °C, 10 min). The positive rates of the transformants were calculated based on PCR results.

196.3 Results

196.3.1 Effect of Lysozyme Concentration on Electrotransformation Efficiency

To determine the optimum concentration of lysozyme, cell suspensions of *C. sakazakii* were treated with different amounts of lysozyme (0, 5, 10, 20, 40 μg/mL). On the same electric pulse condition (3.0 kV, 6.1 ms), different competent cells were transformed with pET-26b plasmid and the efficiencies of transformation were calculated. It was observed that at a lower lysozyme concentration there were only a few transformants. Only at lysozyme concentration of 10 μg/mL were there more number of transformants observed, and at higher lysozyme concentration also only a few transformants were obtained. As shown in Table 196.1, the highest transformation efficiency was obtained when the concentration of lysozyme was 10 μg/mL. All positive rates of different transformations are more than 90 %.

Table 196.1 Effect of lysozyme concentration on electrotransformation efficiencies

Concentration of lysozyme (μg/mL)	0	5	10	20	40
Transformants/plate	18 ± 5.9	42 ± 1.7	82 ± 26.2	78 ± 6.8	77 ± 7.4
Positive rate (%)	100	100	100	100	90
Efficiency (Positive transformants/μg DNA)	(0.72 ± 0.23) × 10^2	(1.68 ± 0.07) × 10^2	(3.28 ± 1.05) × 10^2	(3.12 ± 0.27) × 10^2	(2.78 ± 0.29) × 10^2

196.3.2 Effect of Lysozyme Disposing Time on Electrotransformation Efficiency

To determine the disposing time of lysozyme, cell suspensions of *C. sakazakii* was treated with 10 μg/mL lysozyme for different periods of time varying from 10 min to 40 min. On the same electric pulse condition (3.0 kV, 6.1 ms), different competent cells were transformed with 2.5 μg pET-26b plasmid, respectively, and the different efficiencies of transformation were obtained (Table 196.2). It was observed that at a shorter disposing time there were only a few transformants. Only at medium lysozyme disposing time of 30 min were there more number of transformants observed, and at longer disposing time also only a few transformants were obtained. The results indicate that the highest transformation efficiency could be obtained when the cells were disposed with lysozyme for 30 min.

196.3.3 Effect of Field Strength and Time Constant on Electrotransformation Efficiency

Electric pulses were also optimized in this study. Transformation efficiencies of different pulse parameters (1.8 kV, 2.5 ms; 1.5 kV, 6.1 ms; 2.0 kV, 6.1 ms;

Table 196.2 Effect of lysozyme disposing time on electrotransformation efficiency

Disposing time of lysozyme (min)	10	20	30	40
Transformants/plate	128 ± 15.1	216 ± 27.0	241 ± 20.0	124 ± 25.1
Positive rates (%)	100	90	100	90
Efficiency (Positive transformants/μg DNA)	(5.12 ± 0.60) × 10^2	(7.78 ± 1.08) × 10^2	(9.64 ± 0.72) × 10^2	(4.48 ± 1.00) × 10^2

Table 196.3 Effect of electroporation parameters on electrotransformation efficiencies

Electroporation parameters	1.8 kV, 2.5ms	1.5 kV, 6.1 ms	2.0 kV, 6.1 ms	2.5 kV, 6.1 ms	3.0 kV, 6.1 ms
Transformants/plate	176 ± 9.5	181 ± 21.6	290 ± 9.8	84 ± 24.7	119 ± 13.1
Positive rates (%)	100	100	100	100	90
Efficiency (Positive transformants/μg DNA)	(7.04 ± 0.39) × 10^2	(7.24 ± 0.86) × 10^2	(1.16 ± 0.39) 10^3	(3.36 ± 0.99) × 10^2	(4.28 ± 0.52) × 10^2

2.5 kV, 6.1 ms; 3.0 kV, 6.1 ms) were examined after the *C. sakazakii* cells being treated with 10 μg/mL lysozyme for 30 min and the results are shown in Table 196.3. Only at medium field strength of 2.5 kV were there more number of transformants observed at 6.1 ms time constant. In these five conditions, the highest (1.16 × 10^3 cfu/μg DNA) efficiency is three folds higher than the lowest one (3.36 × 10^2 cfu/μg DNA).

196.4 Discussion

Transformation is a fundamental technique for molecular biology researches. Eletrotransformation and chemical transformation are frequently used to introduce foreign materials into cells, of which the efficiency of the former is higher than the latter, and is more suitable for experiments requiring high efficiency such as establishing different antibody libraries and random mutation libraries.

Impact-factors of transformation efficiency are various, including growth condition of cells, voltage, construction of electroporation buffer solution, and concentration of plasmid [17], of which the concentration of foreign plasmid is the most effective factor [18, 19]. But when the plasmid condition is limited, the other factors can affect the transformation efficiency obviously, especially the permeability of the competent cells. Electrotransformation parameters are also effective for transformation efficiency. Therefore, in this study, lysozyme treatment and pulse parameter were optimized and more than 10-fold improvement was obtained.

Lysozymes, also known as muramidase or N-acetylmuramide glycanhydrolase, are glycoside hydrolases that damage bacterial cell walls by catalyzing hydrolysis of 1, 4-beta-linkages in peptidoglycan and chitodextrin. Though *C. sakazakii* is a kind of gram-negative bacteria with thinner peptidoglycan layer in comparison to gram-negative ones, it can also be affected by lysozyme. The positive effect on enhancing the permeability of competent cell benefits the introduction of foreign DNA.

This study provides an easy way to improve the transformation efficiency of *C. sakazakii*. It is plausible to speculate that this method is valid for other gram-negative bacteria which are poorly transformable.

Acknowledgments This work was supported in part by National Natural Science Foundation of China (Project No. 20905058), Ministry of Education Key Project of Science and Technology (Project No. 212009), and the Science and Technology Development Foundation of Tianjin Colleges and Universities (Project No. 2010ZD01).

References

1. Gurtler JB, Kornacki JL, Beuchat LR (2005) *Enterobacter sakazakii*: a coliform of increased concern to infant health. Int J Food Microbiol 104:1–34
2. Drudy D, Mullane NR, Quinn T et al (2006) *Enterobacter sakazakii*: an emerging pathogen in powdered infant formula. Clin Infect Dis 42:996–1002
3. Lai KK (2001) *Enterobacter sakazakii* infections among neonates, infants, children and adults: case reports and review of the literature. Medicine (Baltimore) 80:113–122
4. Becker DM, Guarente L (1991) Highefficiency transformation of yeast by electroporation. Methods Enzymol 194:182–187
5. Serror P, Sasaki T, Ehrlich SD et al (2002) Electroporation of *Lactobacillus delbrueckii* subsp. *bulgaricus* and *L. delbrueckii* subsp. *lactis* with various plasmids. Appl Environ Microbiol 68:46–52
6. Ackermann G, Tang YJ, Henderson JP et al (2001) Electroporation of DNA sequences from the pathogenicity locus (PaLoc) of toxinogenic Clostridium difficile into a non-toxinogenic strain. Mol Cell Probes 15:301–306
7. Wang TT, Choi YJ, Lee BH et al (2001) Transformation systems of non-Saccharomyces yeasts. Crit Rev Biotechnol 21:177–218
8. Fiedler S, Wirth R (1988) Transformation of bacteria with plasmid DNA by electroporation. Anal Biochem 170:38–44
9. Sheng Y, Mancino V, Birren B (1995) Transformation of *Escherichia coli* with large DNA molecules by electroporation. Nucleic Acids Res 23:1990–1996
10. Rittich B, Spanova A (1996) Electrotransformation of bacteria by plasmid DNAs: statistical evaluation of a model quantitatively describing the relationship between the number of electrotransformants and DNA concentration. Bioelectrochem Bioenerg 40:233–238
11. DeBruin KA, Krassowska W (1999) Modeling electroporation in a single cell. I. Effects of field strength and rest potential. Biophys J 77:1213–1224
12. Rodríguez MC, Alegre MT, Mesas JM (2007) Optimization of technical conditions for the transformation of Pediococcus acidilactici P60 by electroporation. Plasmid 58:44–50
13. Gong W, Jiang W, Yang Y (2004) Improvement of transformation and electroduction in avermectin high-producer, *Streptomyces avermitilis*. Folia Microbiologica (Praha) 49:399–405
14. Lal R, Khanna R, Dhingra N et al (1998) Development of an improved cloning vector and transformation system in Amycolatopsis mediterranei (Nocardia mediterranei). J Antibiot (Tokyo) 51:161–169
15. Teixeira KRS, Wulling M, Morgan T et al (1999) Molecular analysis of the chromosomal region encoding the nifA and nifB genes of Acetobacter diazotrophicus. FEMS Microbiol Lett 176:301–309
16. Ichimura M, Nakayama-Imaohji H, Wakimoto S et al (2010) Efficient electrotransformation of Bacteroides fragilis. Appl Environ Microbiol 76:3325–3332

17. Xue GP, Johnson JS, Dalrymple BP (1999) High osmolarity improves the electro-transformation efficiency of the gram-positive bacteria Bacillus subtilis and Bacillus licheniformis. J Microbiol Methods 34:183–191
18. Mclntyre DA, Harlander SK (1989) Genetic transformation of intact Lactococcus lactis subsp. lactis by high-voltage electroporation. Appl Environ Microbiol 55:604–610
19. Miller JF, Dower WJ, Tompkins LS (1988) High voltage electroporation of bacteria: genetic transformation of Campylobacter jejuni with plasmid DNA. Proc Natl Acad Sci USA 85:856–860

Chapter 197
Multiplex Plasmid Engineering (MPE) for Fine Tuning the Expression Level of Red Fluorescent Protein

Qun Gu, Yifan Li, Zhenquan Lin, Tao Chen, Xueming Zhao and Zhiwen Wang

Abstract Many applications of metabolic engineering need balanced expression of several genes in synthetic metabolic pathways and genetic circuits. But it is often difficult to achieve the best expression level for all the genes for a desired function due to the complexity of biological systems. Here, we present Multiplex Plasmid Engineering (MPE) for high efficient tuning the expression level of genes in plasmids. First, red fluorescent protein (*rfp*) was tested to be utilized as a reporter gene for assaying recombineering efficiency on plasmids. Then ssDNA and plasmid co-transformation technique was exploited to achieve 25 % recombineering efficiency which is compatible to genome recombination. At last, as a proof of concept experiment, MPE was applied to tune the expression level of *rfp* gene and successfully generated dispersed distribution of *rfp* expression level. Our method should potentially be used for simultaneously tuning the expression level of several genes in metabolic pathways.

Keywords Metabolic engineering · Multiplex recombineering · λ-Red recombination · Red fluorescent protein

197.1 Introduction

Recent breakthroughs in metabolic engineering have made it easier to overproduce biochemical products from renewable resources [1, 2]. Such advances include fabricating large synthetic pathways (de novo synthesized DNA sequences) and optimizing pathway expression through transcription- or translation-level engineering, which is essential to avoid buildup of toxic products. These advances

Q. Gu · Y. Li · Z. Lin · T. Chen · X. Zhao · Z. Wang (✉)
School of Chemical Engineering and Technology, Tianjin University, Tianjin 300072, People's Republic of China
e-mail: zww@tju.edu.cn

T.-C. Zhang et al. (eds.), *Proceedings of the 2012 International Conference on Applied Biotechnology (ICAB 2012)*, Lecture Notes in Electrical Engineering 251,
DOI: 10.1007/978-3-642-37925-3_197,

occur in part because of the improvements in techniques for genetically modifying large DNA molecules [3, 4]. Among these techniques, recombination-based genetic engineering (recombineering) has been the most efficient tool for engineering bacteria genomes [5].

Recombineering is highly efficient, is targeted by short (50 base) DNA homologies, is not limited by the availability of restriction sites, and can be automated to rapidly make genome-wide alterations [6, 7]. If introduced by short ssDNA recombineering, mutations could be generated on genomes at a frequency of more than 20 %, making it practical to screen the mutants after allele replacement without any selectable marker [8].

Recently, recombineering has been exploited to develop Multiplex Automated Genome Engineering (MAGE) for parallel modification of *E. coli* genome [9]. Tens of oligos were introduced into the bacteria induced for Red recombination function and several modifications could be created simultaneously. This technique was applied to optimize lycopene biosynthetic pathway and, coupled with high throughput screening, successfully generated clones with fivefold increase in lycopene production within 3 days.

In another publication, the same group of researcher found that recombineering efficiency could be greatly enhanced by a mechanism called co-selection. This enhanced technique was applied to modify 80 sites in the genome of E. coli within 40 days [10].

Most synthetic metabolic pathways and synthetic circuits were still constructed based on plasmid systems [11, 12]. Yet, MAGE has not been transferred to the engineering of plasmid systems. In this article, we introduced the engineering principle of MAGE into the modification of plasmids. We first confirmed that red fluorescent protein (*rfp)* can be used as a reporter gene for assaying allele replacement efficiency. After that, we increased recombineering efficiency for modifying multicopy number plasmid to more that 20 % by the introduction of ssDNA and plasmid co-transformation technique into plasmid recombineering. Finally, Multiplex Plasmid Engineering (MPE) was applied to fine-tune the expression level of *rfp* gene by mutagenize its ribosome biding site (RBS).

197.2 Materials and Methods

197.2.1 Bacterial Strains and Media

The recombineering strain HME68 was kindly provided by Professor Donald Court [7]. DH5α was from laboratory stock. For the plasmid selection experiment, ampicillin was added at 100 μg/ml.

197.2.2 Oligos and Plasmids

Plasmid pLX01 is a modified version of pTrc99a and was from laboratory stock. Oligos were purchased from Sangon Biotech (Table 197.1).

197.2.3 Construction of pLX02

Primer B007 was used to amplify *rfp* gene. The PCR product was digested by EcoRI and PstI, then cloned into plasmid pLX01 plasmid. Transformation of the ligation mixture into Escherichia coli DH5α generated red colonies, indicating the successfulness of the construction. The structure of the pLX02 was further checked by restriction double digestion.

197.2.4 Recombineering Methodology

The recombination assays for all experiments were performed as described by Costantino and Court [5, 6]. Briefly, HME68 were grown at 32 °C to mid-log phase (OD600 nm 0.4–0.6). The cultures were shifted to 42 °C for 15 min to induce the Red functions, then quick-chilled in an ice water slurry. The cells were washed with sterile ice cold water for 3 times in preparation for electroporation. Oligos and/or plasmid were added into electrocompetent cells. Transformations were performed at 1.80 kV, 25 mF. 1 ml of LB was added to the cuvette, and the cells were allowed to recover at 32 °C with shaking for 2 h. Cells were diluted in water or LB media and plated on LB plates with ampicillin to select for recombinants.

197.2.5 MPE Cycling

The cycling process was different from the original MAGE cycle [9]. First, Plasmids and ssDNA were co-transformed into competent HME68 cells induced

Table 197.1 Primers used in this study

Primer name	Sequence 5′ → 3′
B007F	CATAGATCTTATGGACAGCAAGCGAACCG
B007R	TCGCTGCAGTCAGAAGAACTCGTCAAGAAG
D021	ACCTTCGTACGGACGACCTTCACCTTCACCTTCGATTTCGAACTAG TGACCGTTAACGGAACCTTCCATACGAACTTTGAAACGCATGA
D033	TTGATAACGTCTTCGGAGGAAGCCATATTTTACCTCCTTAANNNNN NGCGGAGCGGCGCCCTGTGTGAAATTGTTATCCGCTCACAATT

for Red functions, in which oligo-mediated recombination occurred between plasmids and oligos. Then cells were recovered in LB media for 2 h and grown in test tubes overnight in 32 °C containing relevant antibiotics for the selection of plasmids. In the next day, plasmids were extracted from overnight cultures and then transformed with ssDNA for the next round of MPE.

197.2.6 Assay of Fluorescent Intensity

Diluted plasmid mixture after MPE were transformed into DH5α competent cells and 20 cells were randomly picked from plate for fluorescent assay. The selected cells were allow to grow overnight in LB media. The next day, the cultures were diluted for 100 times in M9 media and cells grown at 37 °C for 4 h until reached mid-log phase. The cells were kept on ice until OD600 and fluorescence intensity were measured.

197.3 Results and Discussion

197.3.1 Red Fluorescent Protein as a Reporter to Test Recombineering Efficiency

To test recombineering efficiency, *rfp* was inserted into a multicopy plasmid as a reporter gene. "RBS calculator" was used to optimize the RBS of *rfp*, aiding it to achieve the maximum expression level [13]. With an optimized RBS, *rfp* gene was cloned into pLX01 plasmid which was a modified version of pTRC99A, generating pLX02, in which the expression of *rfp* gene was controlled by a Trc promoter induced by IPTG. Oligo D021 was designed to introduce a stop codon into *rfp* on pLX02 to inactivate the gene (Fig. 197.1).

Unlike genome which is single copy, plasmid is multicopy. If some, not all, molecular of plasmid acquire mutations, the clone should contain a mixture of plasmids. Therefore, allele replacement frequency cannotbe measured directly by plating the cell after transformation, because it cannot tell how much percent of the plasmid molecular in a single cell are mutants. To test allele replacement frequency at single molecular level, the cells after recombineering were grown overnight, and the mutagenized plasmids were extracted and re-transformed. After plating the re-transformed cells, clones containing wild type pLX02 could express *rfp* gene and their formed colonies turned red after incubation. On the other hand, if ssDNA was successfully recombined with plasmid pLX02, a stop codon was introduced into the middle of *rfp* gene, blocking its expression and the colonies formed remained white. By counting the number of white and red colonies, recombineering efficiency, which equals white/(white + red) colony numbers, could be determined (Fig. 197.1).

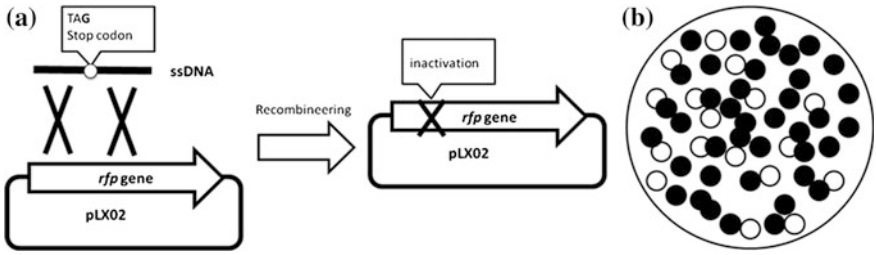

Fig. 197.1 Red fluorescent protein gene as a reporter gene to test recombineering efficiency. **a** ssDNA was transformed to target *rfp* gene on pLX02, generating a stop codon in its open reading frame, blocking its expression. **b** Cells harboring a native *rfp* gene turned red (depicted as black cycle in this figure) after 24 h of incubation. In contrast, cells harboring *rfp* gene with a stop codon generated by ssDNA recombination remained white (depicted as white cycle in this figure). Allele replacement efficiency could be determined by counting the number of red and white colonies

197.3.2 Plasmid Recombineering Efficiency Could be Largely Enhanced by Co-Transformation

With our newly developed method for the assay of allele replacement efficiency, we tested if MAGE technique could operate on plasmid preexist in recombineering cells. Oligo D021 was transformed into HME68 already harboring pLX02. Surprisingly, the allele replacement efficiency was extremely low. In contrast to the oligo-mediated recombination efficiency of more than 20 % on genome, the efficiency was about 1 % when targeting plasmids which were already resident in recombineering cells. We hypothesize that the low efficiency was due to the multicopy nature of plasmids; unlike genomes which present only one copy in cells, plasmids used in our experiment usually form approximately 50 copies. Different copies of plasmid molecular may compete with each other for ssDNA introduced and/or Red proteins with recombination functions.

If this were true, the recombineering efficiency could be increased if plasmids is co-transformed with ssDNA, because each cell should receive only one molecular of plasmid co-transformed at low concentration, which is in the similar case with genome recombineering. We tested the hypothesis by co-transform pLX02 and D021 into HME68 induced for Red function and assayed the efficiency with the method described in the previous section. Just as expected, the allele replacement efficiency was increased to about 20 % with co-transformation, which was much higher than with plasmid was resident in recombineering cells (Fig. 197.2).

We also found the efficiency could be affected by the amount of ssDNA added. Increased oligo concentration and decreased plasmid concentration led to increased allele replacement efficiency. Among tested co-transforming 20 pmol ssDNA and 0.1 ng DNA to 50 ul electrocompetent cell could reach the highest recombination efficiency (Table 197.2).

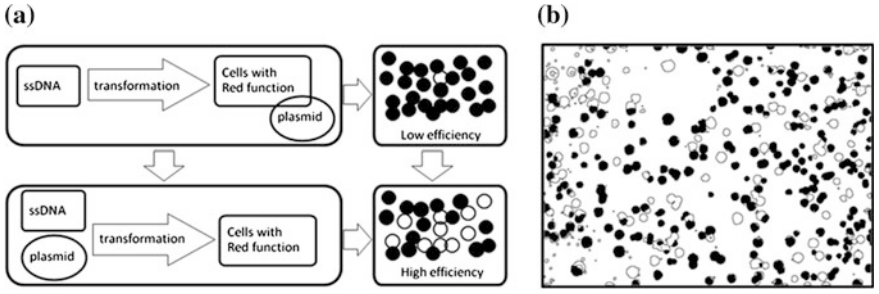

Fig. 197.2 Plasmid allele replacement efficiency was largely increased by plasmid and oligo co-transformation. **a** plasmid and oligo co-transformation led to increased recombineering efficiency than oligo transformation to cells already harboring the targeting plasmid. **b** the strategy co-transformation increased recombineering efficiency from about 1 % to about 25 %

Table 197.2 Recombineering efficiency with varying amount of oligo concentration

ssDNA added (pmol)	White colony number	Red colony number	Tatal colony number	Recombination efficiency (%)
4	120	546	666	18.02
20	109	275	384	28.39
40	18	51	69	26.09

197.3.3 Multiplex Plasmid Engineering to Tune the Expression Level of rfp *Gene*

As a test for MPE application, we used the technique to fine tuning *rfp* expression by modifying its RBS with oligo D033, which was designed to have 6 bp degenerate sequence targeting the core region of *rfp* RBS and the rest homologous with the sequence on pLX02 (Table 197.1). Different molecular of D033 oligo recombined into pLX02 create different versions of mutant *rfp* RBS, diversifying the expression level of *rfp* gene.

We ran MPE cycle with pLX02 and D033 for 15 rounds. 20 clones were randomly picked to determine the distribution of *rfp* expression in each round of 3, 6, 9, 12, 15. The results of our experiment are shown in Fig. 197.3. It could be inferred that the more rounds of MPE performed, the more dispersed distribution of *rfp* expression could be produced. After 15 rounds, the RBS intensity of the population ranged from 0 to 640 with a near linear distribution. Thus MPE can be used to tune the expression level of *rfp* gene by mutagenize its RBS, by which dispersed distribution of RFP expression level can be created.

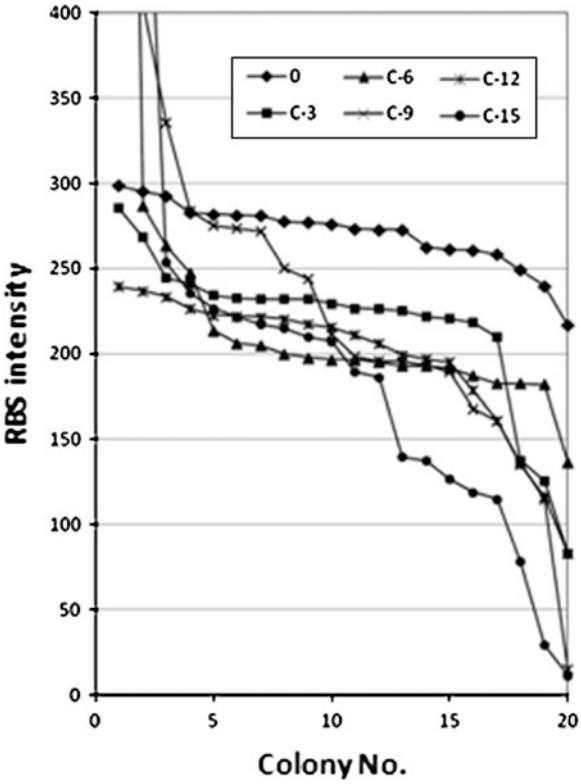

Fig. 197.3 Distribution curve of RBS intensity (fluorescent intensity) of *rfp* genes in the mutagenized population

197.4 Conclusion

In this article, we introduced multiplex engineering strategy into the modification plasmid systems. First, *rfp* gene was utilized to test allele replacement efficiency. With oligo D021 delivering a stop codon in the ORF of *rfp,* the efficiency could be simply determined by counting the number of red and white colonies. Second, the strategy of plasmid and ssDNA co-transformation was found to increase the allele replacement efficiency from 1 % to 25 % for plasmid recombineering. This large amount of enhancement allowed multiplex recombineering to be performed in plasmids without any selection markers. At last, as a proof of concept experiment, MPE was applied to tune the expression level of *rfp* gene to generate dispersed *rfp* expression level.

The method developed in our lab is multiplex and combinatorial in nature, which should be useful for fine tuning of the expression level of several genes of metabolic pathways in plasmids. This plasmid combinatorial engineering strategy could be generally applicable to optimizing metabolic pathways and genetic circuits, expanding the toolbox of metabolic engineering and synthetic biology from

conventional approaches such as rationally changing promoter strength and/or replication origin to now include tools capable of subtly controlling the expression of each gene throughout the network.

Acknowledgments This work was supported by the National 973 Project (2012CB725203, 2011CBA00804), National Natural Science Foundation of China (NSFC-21176182), Natural Science Foundation of Tianjin (12JCYBJC12900), and the Research Fund for the Doctoral Program of Higher Education (20100032120014).

References

1. Lee JW et al (2012) Systems metabolic engineering of microorganisms for natural and non-natural chemicals. Nat Chem Biol 8:536–546
2. Keasling JD (2012) Synthetic biology and the development of tools for metabolic engineering. Metab Eng 14:189–195
3. Woodruff LB, Gill RT (2011) Engineering genomes in multiplex. Curr Opin Biotechnol 22:576–583
4. Wang X, Sa N, Tian PF, Tan TW (2011) Classifying DNA assembly protocols for devising cellular architectures. Biotechnol Adv 29:156–163
5. Sharan SK, Thomason LC, Kuznetsov SG, Court DL (2009) Recombineering: a homologous recombination-based method of genetic engineering. Nat Protoc 4:206–223
6. Thomason L, Bubunenko M, Costantino N et al (2007) Recombineering: genetic engineering in bacteria using homologous recombination. Curr Protoc Mol Biol (1.16.1–1.16.24)
7. Yu DG et al (2000) An efficient recombination system for chromosome engineering in Escherichia coli. Proc Natl Acad Sci USA 97:5978–5983
8. Costantino N, Court DL (2003) Enhanced levels of lambda red-mediated recombinants in mismatch repair mutants. Proc Natl Acad Sci USA 100:15748–15753
9. Wang HH, Church GM (2011) Multiplexed genome engineering and genotyping methods applications for synthetic biology and metabolic engineering. Methods Enzymol 498:409–426
10. Carr PA et al (2012) Enhanced multiplex genome engineering through co-operative oligonucleotide co-selection. Nucleic Acids Res 40:e132
11. Martin VJJ, Pitera DJ, Withers ST, Newman JD, Keasling JD (2003) Engineering a mevalonate pathway in Escherichia coli for production of terpenoids. Nat Biotechnol 21:796–802
12. Ajikumar PK et al (2010) Isoprenoid pathway optimization for Taxol precursor overproduction in Escherichia coli. Science 330:70–74
13. Salis HM, Mirsky EA, Voigt CA (2009) Automated design of synthetic ribosome binding sites to control protein expression. Nat Biotechnol 27:946–950

Chapter 198
Study on the Influencing Conditions in the Electro-Transformation Efficiency of *Bacillus licheniformis* ATCC14580

Yihan Liu, Yanjing Xu, Shuai Fan, Jiaxin Bo, Jianling Wang and Fuping Lu

Abstract In current study, the plasmid pWB980 isolated from *Bacillus licheniformis* ATCC14580 was used to research the influencing conditions in electro-transformation efficiency of *B. licheniformis* ATCC14580 by changing the parameters of the high osmolarity electroporation method. The restriction modification system (RMS) of *B. licheniformis* was the main influence factor on the electro-transformation efficiency of *B. licheniformis*. Meanwhile, the glycine which was added in growth media resulted in a significant increase in the transformation efficiency of *B. licheniformis.* When the glycine concentration of the growth media was 7.5 mg/ml, the bacterial concentration OD_{600} 1.2–1.4 and the voltage was 21 kV/cm, a maximum value of 1.3×10^4 transformats per μg pWB980 was obtained. The results indicated that glycine was useful in improving the electro-transformation efficiency of *B. licheniformis*.

Keywords *Bacillus licheniformis* · Electro-transformation efficiency · Glycine · Restriction modification system · Transformation conditions

Y. Liu · Y. Xu · S. Fan · F. Lu (✉)
Key Laboratory of Industrial Fermentation Microbiology, Ministry of Education, Tianjin 300457, People's Republic of China
e-mail: lfp@tust.edu.cn

Y. Liu · F. Lu
National Engineering Laboratory for Industrial Enzymes, Tianjin 300457, People's Republic of China

J. Bo
Tianjin Key Laboratory of Industrial Microbiology, Tianjin 300457, People's Republic of China

Y. Liu · Y. Xu · S. Fan · J. Bo · J. Wang · F. Lu
The College of Biotechnology, Tianjin University of Science and Technology, Tianjin 300457, People's Republic of China

T.-C. Zhang et al. (eds.), *Proceedings of the 2012 International Conference on Applied Biotechnology (ICAB 2012)*, Lecture Notes in Electrical Engineering 251,
DOI: 10.1007/978-3-642-37925-3_198,

198.1 Introduction

Bacillus licheniformis is a Gram-positive and endospore-forming bacterium and it has been used for decades in the large-scale industrial production of extracellular enzymes [1, 2]. *B. licheniformis* possesses a complete protein secretory system and secrets a lot of proteins directly to culture supernatants [3]. Meanwhile, *B. licheniformis* is not a human pathogen [3] and regarded as one of microorganisms generally-regarded-as-safe[GRAS] species [4]. Furthermore, the whole genome sequence has recently been disclosed by two different groups [5, 6]. Due to these advantages above, an interesting endeavor was to develop *B. licheniformis* as an expression system for the transformation of exogenous DNA to produce heterologous proteins.

Genetic transformation provides a modern gene technology for the improvement of important industrial microorganisms by introducing exogenous genes [7]. However, the low frequency of genetic transformation regularly observed in *B. licheniformis* is a drawback [8]. For the sake of getting the high efficiency competent cells of *B. licheniformis*, several strategies have been developed, including phage transduction [9], protoplast fusion [10], and electro-transformation [8]. Electroporation is a simple and widely used technique for transformation of various bacterial species. This technique uses an electric pulse treatment of cells to make the temporary degradation of the cell wall and cytoplasmic membrane, such that DNA can efficiently enter the bacterial cells [11]. A combination of high osmolarity and high field strength may be a useful approach to improving the transformation efficiency of some gram-positive bacterial species which were able to grow in a high osmolarity medium [8]. In addition, the restriction modification system (RMS) of the host bacterium hinders the transformation of the foreign genes [12]. *B. licheniformis* defends itself from incoming foreign DNA by methylation of the foreign DNA [13]. *B. licheniformis* MW3 was obtained by targeted deletion of the hsdR loci of two type I RMS identified in *B. licheniformis* DSM13 (isogenic to ATCC14580), allowing the routine creation of transformants [13].

In this chapter, in order to improve the electro-transformation efficiency of *B. licheniformis* ATCC14580, the plasmids, respectively, isolated from *Bacillus subtilis* WB600 and *B. licheniformis* ATCC14580 was used to study the influencing conditions of the electro-transformation efficiency using the high osmolarity electroporation method [8].

198.2 Materials and Methods

198.2.1 Bacterial Strains and Plasmid DNA

B. licheniformis ATCC14580 was purchased from Chain Center of Industrial Culture Collection (CICC10101). *B. subtilis* WB600 was preserved in our laboratory. *B. licheniformis* ATCC14580 harboring pWB980 was constructed by our

laboratory. The plasmid pWB980 (3787 bp) with a high plasmid copy number (121 copies per cell) in *B. subtilis* was a generous gift from Professor Sui-Lam Wong (University of Calgary, Canada).

198.2.2 Growth Conditions and Culture Media

B. subtilis and *B. licheniformis* were cultivated for 12–16 h in Luria-Bertani (LB) medium (10 g tryptone/l, 5 g yeast extract/l, and 10 g NaCl/l) or LB medium supplemented with 1.5 % (w/v) agar (agar/LB) for growth on solid medium. Kanamycin (30 μg/ml) was added to the growth medium when necessary.

198.2.3 Transformation of B. licheniformis

To prepare electro-competent cells, an overnight culture of *B. licheniformis* was diluted to a final OD_{600} of 0.2 into 50 ml growth medium (LB containing 0.5 M sorbitol and glycine) and was grown at 37 °C to and was grown at 37 °C to different optical densities (OD_{600}: 0.6–1.8). At the same time, a range of glycine concentration (1 mg/ml-5 mg/ml) was evaluated, to examine the effect of glycine concentration in the growth medium on the growth of *B. licheniformis*. The cells were harvested by centrifugation at 4 °C and 5000x g for 5 min after cooling on ice for 10 min. Following five washes in ice-cold electroporation medium (0.5 M sorbitol, 0.5 M mannitol, and 10 % glycerol v/v), the cells were suspended in 600 μl electroporation medium. If necessary, the competent cells could be stored at −80 °C for future use until with some decrease in transformation efficiency. The electroporation was performed using the ice-cold Bio-Rad (Richmond, CA) electroporation cuvettes (1 mm gap) with 1.5 μg/ml (the terminal concentration) plasmid and 60 μl of ice-cold electrocompetent cells. After incubation for 3–5 min, the cells were exposed to a single electrical pulse using a GenePulser (BTX, ECM399) set at different electric voltages (13–25 kV/cm) resulting in time constants of 5–6 ms. The cells were then rapidly suspended in 1 ml of recovery medium (LB containing 0.5 M sorbitol and 0.38 M mannitol). After incubation at 37 °C and 180 rpm for 3 h, the cells were plated on LB plates containing 30 μg/ml kanamycin and store at 37 °C for 36–48 h for selection of transformed cells containing pWB980.

198.2.4 Plasmid Analyses

To confirm that antibiotic-resistant *B. licheniformis*, the plasmids isolated from the transformants were digested by the appropriate restriction endonucleases and verified by agarose gel electrophoresis.

198.3 Results

198.3.1 The Electro-Transformation Efficiency by DNA Source

The plasmids pWB980 isolated from *B. subtilis* WB600 and *B. licheniformis* ATCC14580, respectively, were transformed into *B. licheniformis* ATCC14580. *B. licheniformis* ATCC14580 harboring pWB980 was constructed by the previous experiment (data not shown). At the same transformation conditions ($OD_{600} = 1.0$, 1.5 μg/ml DNA), the maximum transformation efficiency of the pWB980 isolated form *B. licheniformis* ATCC14580 was 2.9×10^3 transformants per μg pWB980 at 21 kV/cm (Fig. 198.1b), which was 242-fold higher than that of the pWB980 isolated form *B. subtilis* (12 transformants per μg pWB980 at 18 kV/cm) (Fig. 198.1a). Therefore, the plasmid pWB980 isolated from *B. licheniformis* ATCC14580 was used in the further research.

198.3.2 The Effect of the Field Strength on the Electro-Transformation Efficiency

The field strength from 13 to 25 kV/cm was used to study the effect on the electro-transformation efficiency of *B. licheniformis* ATCC14580 when the cell concentration of $OD_{600} = 1.0$. The results showed that the highest transformation efficiency (2.9×10^3 transformants per μg pWB980) obtained with 21 kV/cm was 29-fold and 1.7-fold higher than those obtained at 13 kV/cm (0.1×10^3 transformants per μg pWB980) and 25 kV/cm (1.3×10^3 transformants per μg pWB980) (Fig. 198.1b).

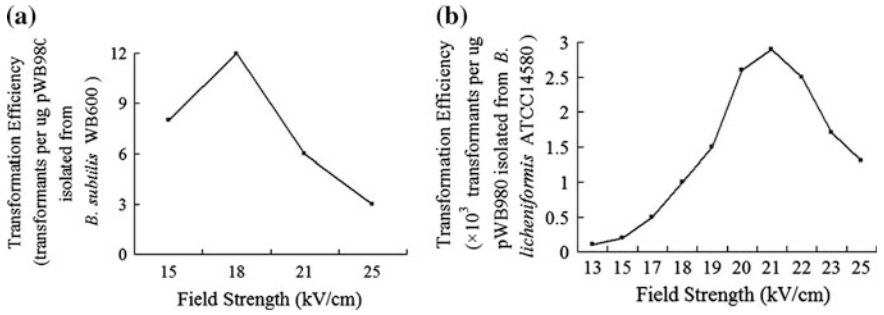

Fig. 198.1 The transformation efficiency of *B. licheniformis* ATCC14580 was influenced by the plasmids (isolated from different species). **a** the pWB980 isolated from *B. subtilis* WB600, **b** the pWB980 isolated from *B. licheniformis* ATCC14580

198.3.3 The Effect of Glycine Concentration on the Electro-Transformation Efficiency

In order to study the effect of glycine concentration on the growth of *B. licheniformis* ATCC14580, the glycine with various amounts (1, 3, 5, 7, 9, 11, 13, and 15 mg/ml) was added in the growth medium cultivating in overnight (Fig. 198.2). 1–5 mg/ml glycine in the growth medium had no significant effect on the growth of *B. licheniformis.* The inhibitory rate of glycine at concentrations of 7 mg/ml on *B. licheniformis* growth was 40 %. *B. licheniformis* ATCC14580 grew very slowly and hardly when the concentration of glycine exceeded 9 mg/ml. Therefore, 5.5, 6, 6.5, 7, 7.5, 8, 8.5, and 9 mg/ml glycine were used to study the effect on the electro-transformation efficiency. The results showed that when the growth medium contained glycine, the transformation efficiency was improved. Moreover, when 7.5 mg/ml glycine was added in the medium, the growth inhibition rate of *B. licheniformis* ATCC14580 was 50 % (Fig. 198.2a) and the transformation efficiency with 9×10^3 transformants per μg pWB980 was the highest (Fig. 198.2b) with the field strength of 21 kV/cm, the cell concentration of $OD_{600} = 1.0$, and the DNA of 1.5 μg/ml.

198.3.4 The Effect of the Cell Concentration on the Electro-Transformation Efficiency

The age of the culture is an additional factor influencing transformation. *B. licheniformis* ATCC14580 cells were cultivated to different growth phases ($OD_{600} = 0.6$–1.8) to investigate the transformation efficiency. As shown in Fig. 198.3, the results indicated that the transformation efficiency of the late exponential phase ($OD_{600} = 1.2$–1.4) cells was 1.05×10^4 transformants per μg pWB980.

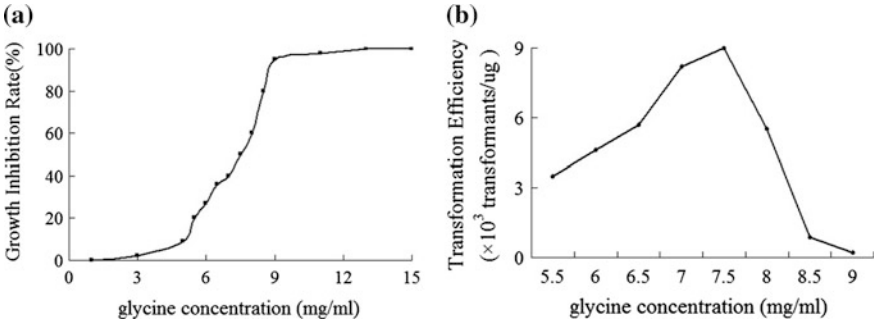

Fig. 198.2 The effect of glycine concentration. **a** The effect of glycine concentration on the growth of *B. licheniformis* ATCC14580, **b** The effect of glycine concentration on the transformation efficiency of *B. licheniformis* ATCC14580

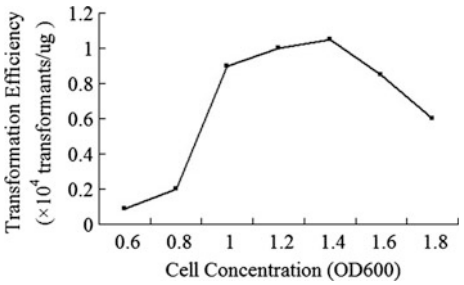

Fig. 198.3 The transformation efficiency of *B. lichiformis* is different at the various age of the strain. The other conditions: field strength (21 kV/cm), 7.5 mg/ml glycine, 1.5 μg/ml DNA

198.3.5 The Effect of the DNA Concentration on the Electro-Transformation Efficiency

DNA at the range of 0.5–5 μg/ml was used to study the effect on the electro-transformation efficiency of *B. licheniformis* ATCC14580. As shown in Fig. 198.4, the results indicated that the highest electro-transformation efficiency (1.3×10^4 transformants per μg pWB980) was obtained with 2–3 μg/ml DNA.

198.3.6 The Plasmid Analyses

The plasmids were isolated from the transformed *B. licheniformis* ATCC14580 which were cultivated in 5 ml LB (containing kanamycin 30 μg/ml) for overnight. Then the plasmids were digested by the appropriate restriction endonucleases and verified by agarose gel electrophoresis. The size of the plasmids was consentaneous with the size of pWB980 from *B. licheniformis* ATCC14580 (Fig. 198.5).

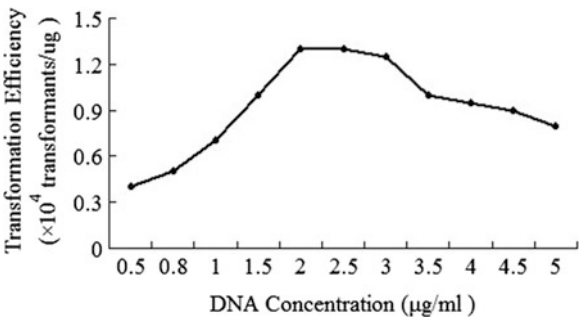

Fig. 198.4 The transformation efficiency correlates with the DNA concentration. The other conditions: field strength (21 kV/cm), 7.5 mg/ml glycine, $OD_{600} = 1.2–1.4$

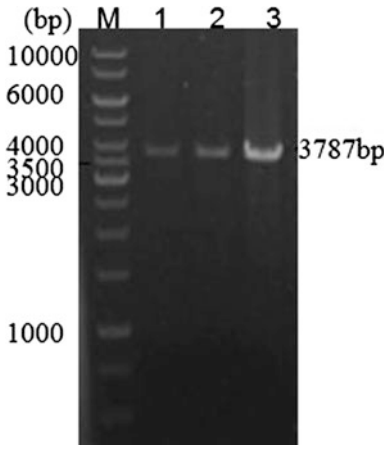

Fig. 198.5 Restriction analysis of plasmids from *B. licheniformis* ATCC14580 transformed. Lane M: 1 kb DNA ladder; *Lane 1–2* the plasmids from transformants digested by *Hin*dIII; *Lane 3* the pWB980 from *B. licheniformis* ATCC14580 digested by *Hin*dIII

198.4 Discussion

This study demonstrated that using the plasmid from *B. licheniformis*, adding glycine in the growth medium (7.5 mg/ml), increasing the field strength to high values (21 kV/cm) with the best suitable concentration of bacterium (OD_{600} = 1.2–1.4), and the optimal concentration of DNA (2–3 μg/ml) could significantly improve the electro-transformation efficiency of *B. licheniformis* ATCC14580.

As an expression system of heterologous proteins, *B. licheniformis* had the drawback that it is difficult to finally obtain a desired transformant [14]. This was mainly due to the existence of two type I restriction modification systems (RMS) in *B. licheniformis* [5, 6]. A number of bacteria depended on cutting foreign DNA with the acid of restriction endonucleases to prevent the foreign DNA into the strain, while their own genetic materials were concomitantly protected by specific methylations [13]. The knockout of the RMS gene in *B. licheniformis* DSM13 (isogenic to ATCC14580) resulted in strains being readily transformable [13]. Apparently, the transformation efficiency was influenced by the source of DNA used in this experiment. The same DNA methylation modification led to the high transformation efficiencies.

The other explanation for the difficulties in electro-transformation of gram-positive species, was that the thick and dense cell walls of gram-positive bacteria may either render the cells less vulnerable to electric fields or prevent the passage of macromolecules into cells [15]. The high values field strength for electro-transformation of gram-positive bacteria could overcome the limit to a certain degree and hence improve the transformation efficiency [8]. Meanwhile, the high osmolarity media could improve the resealing capacity of the porous cell membrane induced by electric pulse and reduce the rate of outflow of molecules from cells electrically damaged at a high field strength, which was beneficial to improvement of cell survive ability [8]. However, the efficient entry of plasmid

DNA was still obtained in electrocompetent cells with hyperosmotic solutions during electroporation [8]. In addition, the optimal concentration of glycine in growth medium of bacteria caused deficiency of the cell-wall. The mechanism was that the D-alanine residue of peptidoglycan chain was replaced by glycine, resulting in the interference for the cross linking which influenced the cell-wall biogenesis [16]. The current study demonstrated that using the pWB980 isolated from *B. licheniformis* ATCC14580 in combination with high voltages and the high osmolarity growth medium containing glycine could observably improve the transformation efficiency. Besides, the efficiency of the electro-transformation was affected by the concentration of cells and DNA, respectively.

By this study on the influencing conditions in the electro-transformation efficiency of *B. licheniformis* ATCC14580, the optimum parameters on the electro-transformation efficiency of *B. licheniformis* ATCC14580 were determined to improve its transformation efficiency. However, the transformation efficiency of *B. licheniformis* was still lower compared with that of *B. subtilis* and *E.coli*. In order for the wide application of *B. licheniformis* as an expression system, it is necessary to develop other transformation methods (such as protoplast transformation, different electro-transformation methods, and so on) to improve the transformation efficiency of *B. licheniformis.*

Acknowledgments This work was supported by the National Natural Science Fund (31101219), the National High Technology Research and Development Program ('863' Plan) (2013AA102106 and 2011AA100905-4), and the Program for Changjiang Scholars and Innovative Research Team in University (IRT1166).

References

1. Berensmeier S, Singh SA, Meens J et al (2004) Cloning of the pelA gene from *Bacillus licheniformis* 14A and biochemical characterization of recombinant, thermostable, high-alkaline pectate lyase. Appl Microbiol Biotechnol 64:560–567
2. Harwood CR (1992) *Bacillus subtilis* and its relatives: molecular biological and industrial workhorses. Trends Biotechnol 10:247–256
3. Niu DD, Shi GY, Wang ZX (2009) Research progress of high protein secretion *Bacillus licheniformis* and its industrial application. Biotechnol Bull 6:45–50
4. Hoffmann K, Wollherr A, Larsen M et al (2010) Facilitation of direct conditional knockout of essential genes in *Bacillus licheniformis* DSM13 by comparative genetic analysis and manipulation of genetic competence. Appl Environ Microbiol 76:5046–5057
5. Rey MW, Ramaiya P, Nelson BA et al (2004) Complete genome sequence of the industrial bacterium *Bacillus licheniformis* and comparisons with closely related *Bacillus* species. Genome Biol 5:R77
6. Veith B, Herzberg C, Steckel S et al (2004) The complete genome sequence of *Bacillus licheniformis* DSM13, an organism with great industrial potential. J Mol Microbiol Biotechnol 7:204–211
7. Cao GQ, Zhang XH, Zhong L et al (2011) A modified electro-transformation method for *Bacillus subtilis* and its application in the production of antimicrobial lipopeptides. Biotechnol Lett 33:1047–1051

8. Xue GP, Johnson JS, Dalrumple BP (1999) High osmolarity improves the electro-transformation efficiency of the gram-positive bacteria *Bacillus subtilis* and *Bacillus licheniformis*. J Microbiol Methods 34:183–191
9. Taylor MJ, Thorne CB (1963) Transduction of *Bacillus licheniformis* and *Bacillus subtilis* by each of phages. J Bacteriol 86:452–461
10. Waldeck J, Rammes HM, Wieland S et al (2007) Targeted deletion of genesencoding extracellular enzymes in *Bacillus licheniformis* and the impact on the secretion capability. J Biotechnol 130:124–132
11. Tsong YT (1992) Time sequence of molecular events in electroporation. In: Chang DC (ed) Guide to Electroporation and Electrofusion. Academic Press, San Diego, pp 47–60 (Chapter 4)
12. Alegre TM, Rodríguez MC, Mesas JM (2004) Transformation of *Lactobacillus plantarum* by electroporation with in vitro modified plasmid DNA. FEMS Microbiol Lett 241:73–77
13. Waschkau B, Waldeck J, Wieland S et al (2008) Generation of readily transformable *Bacillus licheniformis* mutants. Appl Microbiol Biotechnol 78:181–188
14. Niu DD, Zuo ZR, Shi GY et al (2009) High yield recombinant thermostable α-amylase production using an improved *Bacillus licheniformis* system. Microb Cell Fact 8:58–65
15. Dower WJ, Chassy BM, Trevors JT et al (1992) Protocols for the transformation of bacteria by electroporation. In: Chang DC (ed) Guide to Electroporation and Electrofusion. Academic Press, San Diego, pp 485–499
16. Wu S, Xia HZ, Cheng S (2001) A study on protoplast formation, regeneration and DNA transformation of *Streptomyces tenebrarius*. J Shenyang Pharm Univ 18:213–216

Chapter 199
Determination of Folic Acid in Serum by SPE and High Performance Liquid Chromatography with Photochemical Spectrofluorimetry

Caiju Zhou, Haijie Hu and Tong-Cun Zhang

Abstract This paper described a combined high-performance liquid chromatography (HPLC) -photochemical spectrofluorimetry/solid-phase extraction (SPE) procedure for determining the concentration of unmetabolized folic acid in human serum. After being extracted by SPE (C_{18}-H) column, the serum samples were irradiated under the UV lamp for 11 h, separated on a C_{18} HPLC column with methanol/water as the mobile phases and determined by a fluorescence detector. Fluorescence excitation and emission wavelengths were at 280 and 443 nm, respectively. The linear range was 1.9 $\sim$ 8.0 ng/mL. The recovery was from 88.9 to 123.6 % with RSD in the range of 4.1–6.4 %.

Keywords Folic acid · High-performance liquid chromatography · Photochemical spectrofluorimetry · Solid-phase extraction

199.1 Introduction

Folic acid (pteroylglutamate), a member of water-soluble vitamin B family, is used as a drug to treat anemia, mainly for megaloblastic anemia, and also for pernicious anemia as secondary treatment drug. It is also involved in the biosynthesis of amino acids and nucleic acids in the human body, and jointly promotes the formation of red blood cells with vitamin B_{12} [1]. In addition, folic acid is associated with some other diseases, including neural tube defects [2], colon cancer [3], cardiovascular disease [4], and childhood mental retardation [5]. Therefore, rapid and accurate determination of folic acid in human tissue is of great significance for

C. Zhou (✉) · H. Hu · T.-C. Zhang
Key Laboratory of Industrial Fermentation Microbiology, Ministry of Education, College of Biotechnology, Tianjin University of Science and Technology, Tianjin 300457, People's Republic of China
e-mail: zhoucaiju@yahoo.com.cn

T.-C. Zhang et al. (eds.), *Proceedings of the 2012 International Conference on Applied Biotechnology (ICAB 2012)*, Lecture Notes in Electrical Engineering 251,
DOI: 10.1007/978-3-642-37925-3_199,

the prevention, diagnosis, and treatment of diseases caused by folic acid. Due to its poor stability, complex composition, and very low content in natural samples, the analysis of folic acid is a great challenge. The accuracy and sensitivity of folic acid analysis highly depends on the merits of the extraction method as well as detection techniques. Currently, there are microbiological assay (MA), radioimmunoassay, capillary electrophoresis and HPLC [6] to determine folic acid in biological samples. There are, however, several limitations with MA, e.g., tedious laboratory work, and multiple interferences from the sample matrix [7, 8]. HPLC method has a great potential due to its rapid progress of separation and detection techniques, as well as the possibility of automatizing the purification procedure.

The objective of this work was to develop and validate a simple and sensitive HPLC method suitable for the determination of folic acid in biological samples. Folic acid has weak fluorescence, but its fluorescence intensity in hexamethylenetetramine-hydrochloric acid medium was greatly increased after UV irradiation. However, additional purification of human serum prior to HPLC analysis is necessary in case of interference from the matrix. In this paper, we set out to improve the lower quantitation limit of the methodology described by Bai Xiaohong [9]. This improved methodology involves the HPLC fractionation of unmetabolized folic acid in serum from other folate derivatives, followed by solid-phase concentration. This method is of high sensitivity, and good selectivity with satisfactory results.

199.2 Materials and Methods

An Agilent Technologies 1200 liquid chromatographic system (USA) was equipped with a vacuum degasser (G1322A), a quaternary pump (G1311A), a column thermostat (G1316A), a fluorescence detector (G1321A), and a Rheodyne sample injector with 20 mL loop. The ChemStation software controlled the whole liquid chromatographic system. Folic acid standard substance was supplied by Sigma (Sigma-Aldrich, ≥97 %, F7876). HPLC-grade acetonitrile and methanol were purchased from China National Medicines Corporation Ltd. All other reagents were of analytical grade, and doubly deionized water was used.

199.2.1 Preparation of Standard Solutions

The concentration of folic acid stock solution was 50 μg/mL. Folic acid was dissolved in an aqueous solution of 1 mol/L $NaHCO_3$. The solution was stored in a refrigerator, and was protected from light. Working standard solutions were prepared daily by mixing of the stock standard solutions in appropriate proportions and diluting with water [10].

199.2.2 Photochemical Reaction Conditions

The folic acid solution extracted from serum was dissolved with 500 μL of hexamethylenetetramine-hydrochloric acid medium (pH 5.2) and placed at 5 cm under UV light (6 w) irradiation for 1, 3, 5, 7, 10, 12, 16, and 19 h prior to the HPLC analysis.

199.2.3 Chromatographic Conditions

A Kromasil 100RP 18 endcapped (250 × 4.6 mm, 5 μm particle size, Sweden) and a guard column RP 18 (10 × 4.6 mm, 5 μm particle size, Sweden) were used for all analyses. The mobile phase of the HPLC system was delivered at a flow rate of 0.6 mL/min, consisted of H_2O/CH_3OH (40/60). The injection volume was 20 μL. The fluorimetric detector was operated at an excitation wavelength of 280 nm and at an emission wavelength of 443 nm. The SPE cartridges (C18-H, 500 mg/3 mL, BESEPR) were used for sample clean-up.

199.2.4 Experimental Methods

SPE C18-H column was treated successively with 1 mL of methanol and 1 mL of deionized water. The 400 μL human serum samples were deproteinized by the addition of 600 μL of acetonitrile. After vortex mixing for 2 min, the sample was was greatly increasedwas greatly increased 12,000 r/min for 5 min. The supernatant was subsequently applied to the solid-phase cartridge after removal of the organic solvent by N_2. The sample was retained on the sorbent for a period of time and subsequently eluted by 1 mL of aqueous sodium acetate buffer (pH 3.6). The eluent was collected in a small beaker and evaporated to dryness in a vacuum oven (60 °C). The dry residue of the vitamin fraction was reconstituted in 500 μL of hexamethylenetetramine-hydrochloric acid medium (pH 5.2), and was irradiated under UV lamp for several hours. All solutions were filtered through a 0.45 μm Teflon membrane filters prior to HPLC analyses. After 1 h, 20 μL of each solution was injected into the HPLC column.

199.2.5 Method Validation

The method was validated in agreement with the International Conference on Harmonization Guidelines (ICH, 1996) with regards to its specificity, linearity, limit of detection (LOD), accuracy, and precision. Linearity was studied by a

series of folic acid standards, covering the entire working range. Six concentration levels were used in the range 1.9 ~ 8.0 ng/mL. Regression analysis revealed calibration equation with the correlation coefficient.

The inter-day accuracy and precision were evaluated by assaying triplicate samples of blinded concentrations of folic acid representing low, middle and high concentrations. The precision was expressed as the relative standard deviation (RSD). The accuracy was determined by comparing the calculated concentration from the standard curves to the theoretical concentration.

199.3 Results and Discussion

199.3.1 Photochemical Reaction Conditions

Folic acid itself has weak fluorescence, but its fluorescence intensity in hexamethylenetetramine-hydrochloric acid medium (pH 5.2) was greatly increased after UV irradiation. With the increase of irradiation time, the fluorescence intensity of folic acid is gradually increased. When the irradiation time is in the range of 10 ~ 12 h, the peak height of folic acid reaches its maximum (Fig. 199.1).

199.3.2 Chromatographic Conditions

A reversed phase Kromasil C18 column was chosen for the separation and determination of folic acid in human serum. Preliminary studies were carried out with methanol-water at various volume ratios as mobile phase. When methanol-water (v/v 60:40) was used as mobile phase, all chromatographic peaks were well separated without overlapping peaks or tailing peaks. The flow rate was set at 0.6 mL/min. The fluorimetric detector was operated at an excitation wavelength of 280 nm, and an emission wavelength of 443 nm. Under these conditions, the

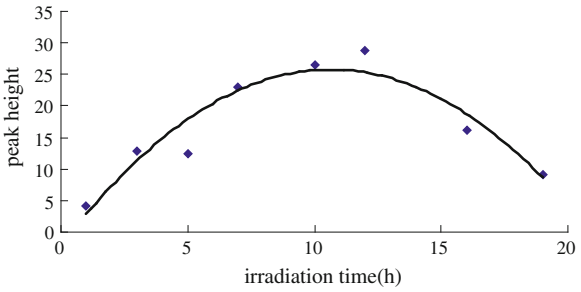

Fig. 199.1 Influence of irradiation time on fluorescence intension of folic acid

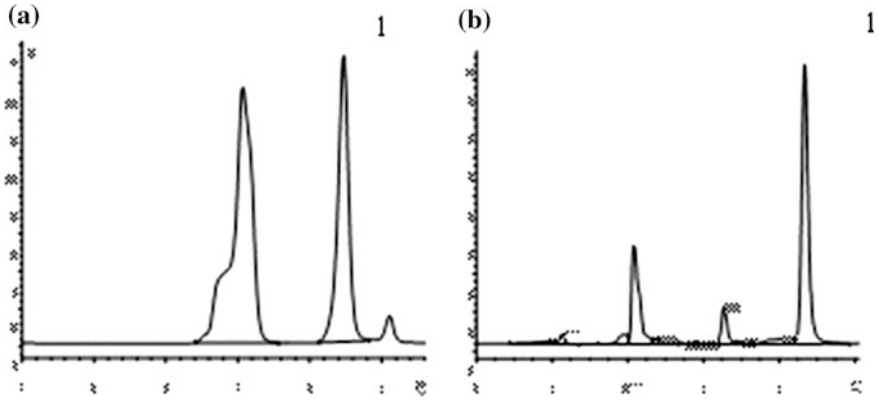

Fig. 199.2 Chromatogram of folic acid standard solution (**a**) and folic acid in human serum, with c_{18}-h extraction (**b**); 1: folic acid

representative chromatograms of folic acid in standard solution and human serum are shown in Fig. 199.2. The serum samples can be effectively adsorbed, and the eluent can separate folic acid from endogenous interfering substances.

199.3.3 Method Validation

The linearity of the method was established by calculating the calibration curves determined by the peak height folic acid at different concentrations, in the range of 1.9 ~ 8.0 ng/mL. Each sample was analyzed in triplicate. The linearity of the curves was good in the range evaluation. The equation of the calibration curve and regression coefficient

for folic acid was height = 1.3748C–1.3741, correlation coefficient (R^2) 0.9985 (see Fig. 199.3). Thus, a methodology of high sensitivity was demonstrated able to determine folic acid in human serum. Precision and accuracy data are presented in Table 199.1. As shown in Table 199.1, the recoveries were from 88.9 to 123.6 % and the relative standard deviations (RSD) were in the range of 4.1 to 6.4 % (n = 3).

199.3.4 Application of the Method

The method is suitable for analysis of biological samples, but a preconcentration step is required to reach quantitation limits. No interference from matrix or noise was noticed even after concentration. Fifteen serum samples were prepared and analyzed in order to check the applicability of the method in real clinical samples.

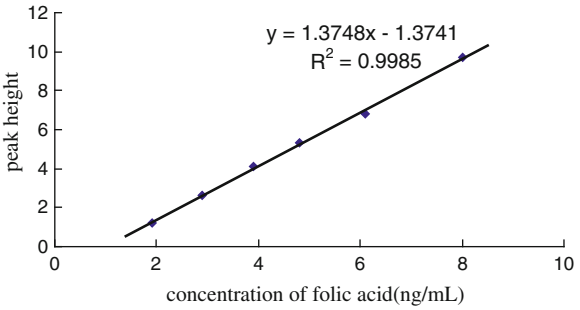

Fig. 199.3 Standard calibration curves for folic acid

Table 199.1 Precision and accuracy study for the determination of folic acid in human serum (n = 3)

	Added (ng)	Found (ng)	Recovery (%)	RSD (%)
Folic acid	0.96	0.85	88.9	4.1
	1.27	1.57	123.6	4.6
	1.35	1.54	114.3	6.4

Range of measured concentrations of folic acid in real human serum samples is 2.62 $\sim$ 3.21 ng/mL. The mean value is 2.86 $\pm$ 0.16 ng/mL with RSD 5.6 %. The values are at levels similar to those reported [10].

199.4 Conclusion

In our developed method, the folic acid in human serum was separated, identified, and quantitatively determined by SPE and high-performance liquid chromatography with photochemical spectrofluorimetry. Adequate clean-up of biological samples was achieved by the developed SPE protocol. No interference was observed in blood serum samples. Endogenous compounds from serum samples did not interfere. Real sample analysis proved the applicability of this method [11].

Acknowledgments This research was supported by the SME Technology Innovation Fund, China (Project No. 10C26211200209).

References

1. Arues BN (1999) Micronutrient deficiencies a major cause of DNA damage. Ann NY Acad Sci 89:87–106
2. Zhang SQ, Yin LJ (1994) Folic acid, vitamin B_{12} and neural tube defects. Foreign med Sci (Sect matern child health) 5:61–63

3. Song HL, Liu AH (2002) New progress on folic acid application research. Northwest Pharm J 17:38–39
4. Weir DG, Scott JM (1998) Homocysteine as a risk factor for cardiovascular and related disease nutritional implications. Nutr Res Reviews 11:311–318
5. Cheng ZP (2003) Status quo and development on neural tube defects research. Prac Prev Med 10:263–265
6. Hao L, Tang Y, Li Z (1999) Progress in folic acid determination. Chin Prac Prev Med 33:177–179
7. Holt DL, Wehling RL, Zeece MG (1988) Determination of native folates in milk and other dairy products by high-performance liquid chromatography. J Chromatogr A 449:271–279
8. Finglas PM, Wigertz K, Vahteristo L et al (1999) Standardization of HPLC techniques for the determination of naturally-occurring folates in food. Food Chem 64:245–255
9. Che X, Bai XH (2005) Determination of folic acid in plasma by solid phase extraction and high performance liquid chromatography with photochemical spectrofluorimetry. Chin Pharm J 40:1346–1349
10. Pavlos FC, Victoria FS, Robert V et al (2004) Development of a validated HPLC method for the determination of B-complex vitamins in pharmaceuticals and biological fluids after solid phase extraction. J Sep Sci 27:1181–1188
11. Smith J, Jones M Jr, Houghton L et al (1999) Future of health insurance. N Engl J Med 965:325–329

Chapter 200
Design and Synthesis of 2-Arylbenzothiazole Analogues as Novel SIRT1 Activators

Shaolong Jia, Fei Hu, Yinghao Gao, Qiuyue Wang, Yingying Wang and Erbing Hua

Abstract SIRT1 is a protein deacetylase that has emerged as a therapeutic target for the development of activators to treat diseases such as type II diabetes, cancer, cardiovascular, and neurodegenerative diseases. Resveratrol, a naturally occurring small molecule activator of SIRT1, has been reported to extend lifespan in yeast, caenorhabditis elegans, drosophila and rodents, then it also has been demonstrated to improve metabolism and glucose tolerance. Oxazolo[4,5-b]pyridines (OAP), recently showed moderate activation of SIRT1. Importantly, these compounds were more potent than resveratrol. In this work, we design and synthesize a series of compounds as novel potential SIRT1 activators through a two-step convenient synthetic procedure. Ten 2-Arylbenzothiazole analogs were characterized on the basis of 1H NMR spectral.

Keywords Synthesis · 2-Arylbenzothiazole analogs · SIRT1 activator · Type II diabetes

200.1 Introduction

The sirtuins are a family of enzymes that catalyze the NAD^+-dependent deacetylation of ε-acetyl-Lys residues of proteins [1–3]. Interest in these enzymes stems from the roles they are thought to play in human disease. Of particular interest is SIRT1, which has been implicated in a number of age-related diseases and biological functions involving cell survival, apoptosis, stress resistance, fat storage, insulin production, and glucose and lipid homeostasis [4, 5]. Moreover,

S. Jia · F. Hu · Y. Gao · Q. Wang · Y. Wang · E. Hua (✉)
Key Laboratory of Industrial Microbiology, Ministry of Education, College of Biotechnology, Tianjin University of Science and Technology, Tianjin 300457, People's Republic of China
e-mail: huarb@tust.edu.cn

T.-C. Zhang et al. (eds.), *Proceedings of the 2012 International Conference on Applied Biotechnology (ICAB 2012)*, Lecture Notes in Electrical Engineering 251,
DOI: 10.1007/978-3-642-37925-3_200,

SIRT1-activating compounds (STACs) have been developed that produce biological effects consistent with direct SIRT1 activation. At the molecular level, the mechanism by which STACs activate SIRT1 remains elusive [6–9].

Resveratrol (1), a naturally occurring small molecule activator of SIRT1, has been reported to extend lifespan in yeast [10], Caenorhabditis elegans, drosophila [11], and rodents [12]. When administered to rodents, resveratrol has been demonstrated to improve metabolism and glucose tolerance, as well as overall physical performance in various stress tests [13].

Previous studies analyzed one notable series of SIRT1 activators identified through the HTS was the oxazolo[4, 5-b]pyridines (OAP), as exemplified by compounds 2 and 3 (Fig. 200.1). These compounds showed moderate activation of SIRT1, with EC1.5 = 6 μM, 240 % max act, and 25 μM, 207 % max activation, respectively. Importantly, these compounds were more potent than resveratrol, 1, (EC1.5 = 46 μM, 200 % max act) and were amenable to analog synthesis at several different points on the scaffold [9, 14].

On that basis, numerous efforts have been devoted to discover novel activators of SIRT1. We synthesis 2-Arylbenzimidazole as newly scaffold instead of the nuclear structure of the oxazolo[4, 5-b]pyridines (OAP), then ten 2-Arylbenzothiazole analogs as the novel potential SIRT1 activators were synthesized. The aim of this work is to explore new template structures for novel potent SIRT1 activators.

200.2 Materials and Methods

200.2.1 Materials and Measurements

All reagents and solvents used were of reagent grade. Reaction temperatures were controlled by oil bath temperature modulator. Thin layer chromatography (TLC) was performed using E. Merck silica gel GF254 plates (0.25 mm). Silica gel (particle size 20–400 mesh) was used for flash chromatography. 1H spectra were recorded on Bruker AM-400 NMR spectrometers in deuterated chloroform.

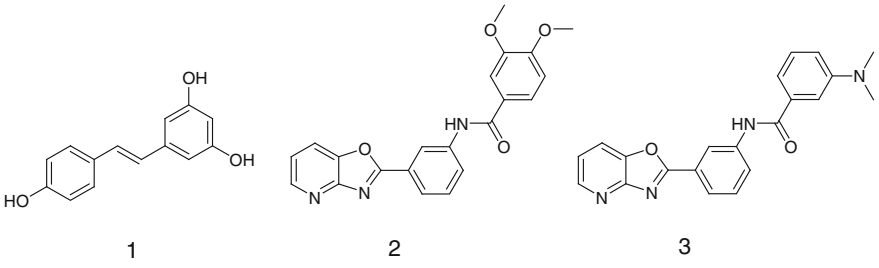

Fig. 200.1 Resveratrol (**1**), and the oxazolo[4,5-b]pyridines (**2** and **3**)

200.2.2 Experimental Methods

The route to synthesis of 2-Arylbenzothiazole intermediate and analogues was presented in Fig. 200.2.

The methods of synthesizing and purifying intermediate were as follows

2-aminobenzenethiol (4 g, 32 mmol), 3-aminoben zoic acid (4.38 g, 32 mmol), and PPA (44 g) were added into 250 mL round-bottom flask, then the reaction mixture was allowed to be heated to 180 °C by oil bath and kept reflux for 6 h. After the reaction was completely finished, the reaction mixture was poured slowly into ice water and the resulting mixture basified with solid NaOH and NaHCO3. At pH 8–10 the precipitate was filtered, washed with water and dried to obtain the crude product, which purified by flash column chromatography (silica gel, petroleum ether: ethyl acetate = 8:1).

Preperation of compounds 1–10 from intermediate1 with organic acids was as follows

In a round-bottomed flask, aromatic carboxylic acid (1.2 mmol) was dissolved in suitable amount of CH2Cl2 (25 ml), followed by adding EDCI· HCl (1.5 mmol), Et3 N (2 mmol), DMAP (0.5 mmol), and compound 1 (1 mmol). Then the reaction mixture was allowed to be heated to 50 °C and kept reflux for 6 h. After cooling the reaction mixture was poured into a 100 ml separating funnel, then water was added, and then extracted by using CH2Cl2, the organic layer was washed successively by water, saturated salt water, and then dried by sodium sulphate. These compounds were purified by flash column chromatography.

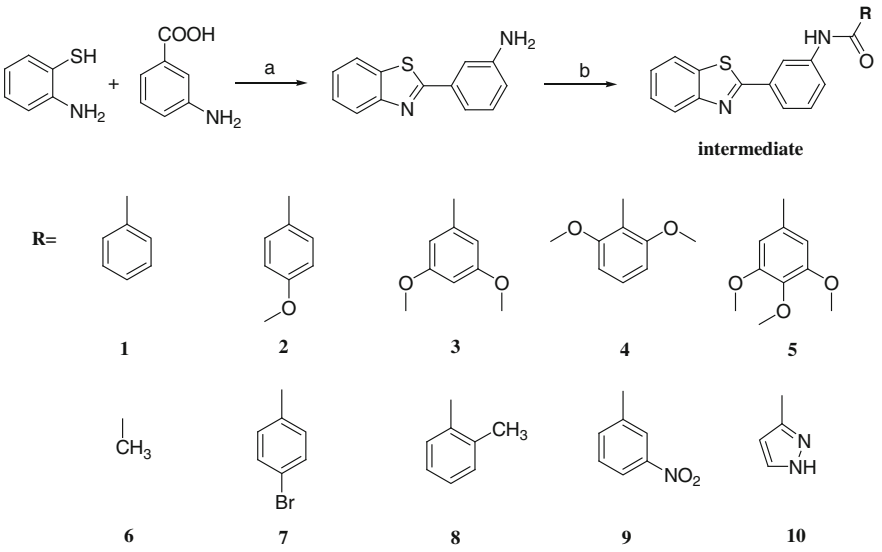

Fig. 200.2 Reagents and conditions: **a** PPA, 180 °C, 6 h; **b** CH_2Cl_2, EDCI· HCl, DMAP, Et_3N, 50 °C, 6 h

200.2.3 Syntheses

2-(2′-aniline) benzothiazole (intermediate)

A white solid, 80.5 % yield.

1H NMR (400 MHz, CDCl3)δ (ppm) 8.088 (d, $J = 8$ Hz, 1H), 7.922 (d, $J = 8$ Hz, 1H), 7.386–7.531 (m, 4H), 7.51 (t, $J = 7.6$ Hz, 2H), 7.294 (t, $J = 8$ Hz, 1H), 6.833 (dd, $J = 2$, 2.4 Hz, 1H), 3.865 (s, br, 2H).

2-Arylbenzothiazole analogs 1

A white solid, 59.7 % yield.

1H NMR (400 MHz, CDCl3)δ (ppm) 8.270 (s, 1H), 8.071 (d, $J = 8$ Hz, 1H), 7.990 (dd, $J = 1.6$, 1.6 Hz, 1H), 7.925 (d, $J = 7.2$ Hz, 2H), 7.844 (d, $J = 8$ Hz, 1H), 7.797 (d, $J = 8.4$ Hz, 2H), 7.695 (d, $J = 8.4$ Hz, 2H), 7.571 (m, 1H), 7.490–7.543 (m, 2H), 7.410 (t, $J = 8$ Hz, 1H).

2-Arylbenzothiazole analogs 2

A white solid, 52.4 % yield.

1H NMR (400 MHz, CDCl3)δ (ppm) 8.682 (s, 1H), 8.028 (d, $J = 7.2$ Hz, 2H), 7.850 (d, $J = 8$ Hz, 2H), 7.501–7.639 (m, 5H), 7.314–7,457 (m, 1H), 7.063–7.011 (m, 1H), 3.435 (s, 3H).

2-Arylbenzothiazole analogs 3

A white solid, 49.6 % yield.

1H NMR (400 MHz, CDCl3)δ (ppm) 8.280 (t, $J = 2$ Hz, 1H), 8.076 (d, $J = 8$ Hz, 1H), 7.997 (dd, $J = 2$, 1.2 Hz, 1H), 7.926 (d, $J = 8$ Hz, 2H), 7.849 (d, $J = 8$ Hz, 1H), 7.487–7.538 (m, 2H), 7.406 (t, $J = 8$ Hz, 1H), 7.016 (d, $J = 2$ Hz, 2H), 6.647 (t, $J = 2.4$ Hz, 1H), 3.871 (s, 6H).

2-Arylbenzothiazole analogs 4

A white solid, 39.5 % yield.

1H NMR (400 MHz, CDCl3)δ (ppm) 8.238 (s, br, 1H), 8.054 (d, $J = 8$ Hz, 2H), 7.910 (d, $J = 8$ Hz, 1H), 7.828 (d, $J = 8$ Hz, 1H), 7.681–7.717 (m, 1H), 7.489 (t, $J = 8$ Hz, 2H), 7.389 (t, $J = 8.4$ Hz, 1H), 7.324 (t, $J = 8.4$ Hz, 1H), 6.600 (d, $J = 8.4$ Hz, 2H), 3.841 (s, 6H).

2-Arylbenzothiazole analogs 5

A white solid, 62.5 % yield.

1H NMR (400 MHz, CDCl3)δ (ppm) 8.275 (s, br, 1H), 8.100 (d, $J = 8$ Hz, 2H), 7.954 (d, $J = 8$ Hz, 2H), 7.859 (d, $J = 8$ Hz, 1H), 7.518–7.574 (m, 2H), 7.438 (t, $J = 8$ Hz, 1H), 7.151 (s, 2H), 3.992 (s, 6H), 3.955 (s, 3H).

2-Arylbenzothiazole analogs 6

A white solid, 65.2 % yield.

1H NMR (400 MHz, CDCl3)δ (ppm) 8.138 (s, br, 1H), 8.057 (d, $J = 8$ Hz, 1H), 7.907 (d, $J = 8$ Hz, 1H), 7.814 (t, $J = 8.4$ Hz, 2H), 7.372–7.515 (m, 4H), 2.217 (s, 3H).

2-Arylbenzothiazole analogs 7

A white solid, 58.2 % yield.

1H NMR (400 MHz, CDCl3)δ (ppm) 8.273 (t, $J = 2$ Hz, 1H), 8.074 (d, $J = 8$ Hz, 1H), 7.989 (dd, $J = 1.6$, 1.6 Hz, 1H), 7.926 (d, $J = 7.2$ Hz, 2H), 7.856

(d, $J = 8$ Hz, 1H), 7.782 (d, $J = 8.4$ Hz, 2H), 7.664 (d, $J = 8.4$ Hz, 2H), 7.490–7.543 (m, 2H), 7.410 (t, $J = 8$ Hz, 1H).

2-Arylbenzothiazole analogs 8

A white solid, 41.3 % yield.

1H NMR (400 MHz, CDCl3)δ (ppm) 8.460 (s, br, 1H), 7.895 (d, $J = 7.6$ Hz, 1H), 7.811 (s, 1H), 7.635 (d, $J = 8.4$ Hz, 2H), 7.467–7.506 (m, 3H), 7.395 (t, $J = 8.4$ Hz, 1H), 7.270-7.204 (m, 4H), 2.533 (s, 3H).

2-Arylbenzothiazole analogs 9

A white solid, 45.9 % yield.

1H NMR (400 MHz, CDCl3)δ (ppm) 8.885 (t, $J = 2$ Hz, 1H), 8.713 (s, 1H), 8.478 (d, $J = 8.4$ Hz, 2H), 7.760–7.938 (m, 3H), 7.677 (d, $J = 7.6$ Hz, 1H), 7.535–7.595 (m, 2H), 7.185–7.254 (m, 2H).

2-Arylbenzothiazole analogs 10

A white solid, 37.3 % yield.

1H NMR (400 MHz, CDCl3)δ (ppm) 10.469 (s, br, 1H), 8.917 (s, br, 1H), 8.345 (s, 1H), 8.082 (d, $J = 8$ Hz, 1H), 8.032 (dd, $J = 1.2$, 1.2 Hz, 1H), 7.926 (d, $J = 8$ Hz, 1H), 7.835 (d, $J = 8$ Hz, 1H), 7.669 (d, $J = 2.4$ Hz, 1H), 7.505 (t, $J = 8$ Hz, 2H), 7.404 (t, $J = 7.6$ Hz, 1H), 7.009 (d, $J = 2.4$ Hz, 1H).

200.3 Results and Discussion

In a word, we have synthesized an intermediate and ten 2-Arylbenzothiazole analogs by using cyclization and acylation. We will carry out the cell experiment (in vitro) and mice experiment (in vivo) that test the activity of these compounds for the treatment of type II diabetes. Moreover, thiazolidinedione (TZDs) [15, 16], is also the analogs of these compounds, which has been confirmed to enhance signal transduction of insulin and its target receptor, and improve the sensitivity of insulin to its target organization to lower blood sugar effectively [17–20]. We believe this work will build basic study for looking for a new promising lead compound toward new targets.

Acknowledgments This work was supported by grants from the National Natural Science Foundation of China (grant no. 81072521) and Tianjin University of Science and Technology (grant no. 20100411).

References

1. Sauve AA, Celic I, Avalos J et al (2001) Chemistry of gene silencing: the mechanism of NAD + -dependent deacetylation reactions. Biochem 40:15456–15463
2. Sauve AA, Schramm VL (2003) Sir2 regulation by nicotinamide results from switching between base exchange and deacetylation chemistry. Biochem 42:9249–9256

3. Sauve AA, Wolberger C, Schramm VL et al (2006) The biochemistry of sirtuins. Annu Rev Biochem 75:435–465
4. Haigis MC, Sinclair DA (2010) Mammalian sirtuins: biological insights and disease relevance. Annu Rev Pathol 5:253–295
5. Baur JA (2010) Resveratrol suppresses body mass gain in a seasonal non-human primate model of obesity. Mech Ageing Dev 131:261–269
6. Dai H, Kustigian L, Carney D et al (2010) SIRT1 activation by small molecules. J Biol Chem 285:32695–32703
7. Milne JC, Lambert PD, Schenk S et al (2007) Small molecule activators of SIRT1 as therapeutics for the treatment of type 2 diabetes. Nature 450:712–716
8. Bordone L, Guarente L (2005) Calorie restriction, SIRT1 and metabolism: understanding longevity. Nature Rev. Mol. Cell Biol. 6:298–305
9. Vu CB, Bemis JE, Disch JS et al (2009) Discovery of imidazo[1,2-b]thiazole derivatives as novel SIRT1 activators. J Med Chem 52:1275–1283
10. Lamming DW, Wood JG, Sinclair DA (2004) MicroReview: Small molecules that regulate lifespan: evidence for xenohormesis. Mol Microbiol 53:1003
11. Wood JG et al (2004) Sirtuin activators mimic caloric restriction and delay ageing in metazoans. Nature 430:686–689
12. Bauer JA, Pearson KJ et al (2006) Resveratrol improves health and survival of mice on a high-calorie diet. Nature 444:337
13. Lagouge M, Argmann C, Gerhart-Hines Z et al (2006) Resveratrol improves mitochondrial function and protects against metabolic disease by activating SIRT1 and PGC-1α. J Cell 127:1109
14. Bemis JE, Vu CB, Xie R et al (2008) Abstract of Papers, 235th National Meeting of the American Chemical Society, New Orleans, LA; American Chemical Society: Washington, DC, Abstract 242
15. Willson TM, Cobb JE, Cowan DJ (1996) The Structure activity relationship between peroxisome proliferator activated receptor γagonism and the antihyperglycemic activity of thiazolidinediones. J Med Chem pp 665–668
16. Willson TM, Brown PJ, Sternbach DD (2000) The PPARs: from orphan receptors to drug discovery. J Med Chem 43(4):527–549
17. Picard F, Kurtev M, Chung N et al (2004) SIRT1 promotes fat mobilization in white adipocytes by repressing PPAR-γ. Nature 429:771–776
18. Brunet A et al (2004) Stress-dependent regulation of FOXO transcription factors by the SIRT1 deacetylase. Science 303:2011–2015
19. Luo J, Nikolaev AY, Imai S et al (2001) Negative control of p53 by Sir2α promotes cell survival under stress. Cell 107:137–148
20. Motta MC et al (2004) Mammalian SIRT1 represses forkhead transcription factors. Cell 116:551–563

Chapter 201
UV-B Irradiation Regulates Apoptosis in Yeast

Kun Chen, Nailong Liang, Jing Yang and Hua Zhao

Abstract UV-B irradiation-induced reactive oxygen species (ROS) generates apoptosis. UV-B irradiation is known as an agent to modulate apoptosis in human cells as well as plants, but the mechanisms of apoptotic regulation of *Saccharomyces cerevisiae* are not well established. The aim of our work is to evaluate the influence of continuous UV-B irradiation on defense mechanisms of antioxidants against cell death. To understand adaptive stress response during natural and artificially modulated (UV-B-induced) apoptosis, cells were adapted to sub-lethal dose of UV-B irradiation for 96 h or not. UV-B-induced apoptosis was revealed by cell death assay and DNA fragment assay. Oxidative damage induced by ROS was confirmed by SDS-PAGE. A sharply decrease of activity of antioxidant enzymes was appeared both in UV-B treated and control cells. By contrast, in continuous irradiated yeast cells, the level of SOD, CAT, and GR activity was increased by 1.1-, 1.1-, and 1.3-fold than those in control of 96 h, respectively. The contents of low-molecular weight antioxidants as trehalose and ergosterol increased but without significant changes in control. The results suggested that accumulation of antioxidants induced by UV-B would suppress apoptosis and played a main role to protect cells from death.

Keywords UV-B irradiation · *Saccharomyces cerevisiae* · Antioxidant defense mechanisms · Apoptosis · Reactive oxygen species

K. Chen · J. Yang · H. Zhao
Key Laboratory of Industrial Fermentation Microbiology, Ministry of Education, College of Bioengineering, Tianjin University of Science and Technology, Tianjin 300457, People's Republic of China

H. Zhao (✉)
Tianjin Key Laboratory of Industrial Microbiology, Tianjin 300457, People's Republic of China
e-mail: zhaohua@tust.edu.cn

N. Liang
Medical Institute, Liaocheng Vocational and Technical College, Shandong 252000, People's Republic of China

T.-C. Zhang et al. (eds.), *Proceedings of the 2012 International Conference on Applied Biotechnology (ICAB 2012)*, Lecture Notes in Electrical Engineering 251,
DOI: 10.1007/978-3-642-37925-3_201,

201.1 Introduction

Stratospheric ozone depletion leads to enhanced UV-B irradiation. UV-B irradiation is a relatively minor component of sunlight but has a substantial impact on the biosphere because of their high energy [21]. UV-B irradiation is potentially harmful to all organisms and known to cause macromolecular damage and inhibit cellular processes. Therefore, the capacity of different reproductive cells to cope with UV-B irradiation was recently investigated in the laboratory [8, 11, 15].

UV-B irradiation, however, is not solely an agent of damage. It also regulates UV-protective responses and developmental processes that act as an informational signal [14, 34]. In UV-protective responses, both enzymatic and non-enzymatic antioxidant mechanisms play a significant role against reactive oxygen species (ROS) induced oxidative damage to cells components. ROS has a central role in all cases of yeast apoptosis [20]. Superoxide dismutase (SOD), converting O^{2-} to H_2O_2, and catalase (CAT), converting H_2O_2 to water, have been reported to represent a strong enzymatic defense system to scavenge ROS in Arctic amphipods [31], and small molecule ROS scavengers (vitamins C, E, β-carotene, tralalose, ergosterol and fibrous polysaccharide, and other redox active thiols) function as free-radical chain breaking agents and singlet oxygen ($^1O^2$) quenchers [22].

Apoptosis, or programmed cell death, is a physiological cellular response to and mediated by environmental stress [29, 32]. UV-B irradiation is widely known to be used as an apoptosis agent. For instance, in plants, UV-B irradiation was reported not only to damage DNA, generate ROS, and inhibit photosynthetic reactions, but also in some cases to cause necrosis [34]. In mammalian cells, UV-B irradiation is also reported as one of the most common DNA damage and apoptosis agents [9, 18, 35].

Recently apoptosis is also discovered in unicellular organisms such as bacteria and yeast. As it is known that *Saccharomyces cerevisiae* (*S. cerevisiae*) regularly withstands fluctuations including available nutrients, temperature, and the variable presence of noxious agents such as radiation and toxic chemicals [10], we selected yeast *S. cerevisiae* as a valuable model in this study. Previous works have been investigated that UV irradiation can promote cell cycle and morphological alterations as indicative of apoptosis, and relative genes affecting UV radiation sensitivity [4, 6, 24], but the mechanisms of yeast *S. cerevisiae*, especially mechanisms by UV-B irradiation are not well established. It was found that enhanced activities of antioxidant enzymes mediated by NO can effectively protect plants from UV-B damage [27]. It was also reported that the protection of Copper, zinc-superoxide dismutase from UV-B-induced apoptosis of human keratinocytes is associated with the increased levels of antioxidant enzymes [30]. Therefore, we presume that many similarities may occur among yeast, plants, and mammalian cells. The aim of this work was mainly to address the alteration effects of continuous UV-B irradiation on cell growth and antioxidant defense mechanisms and associated activity of antioxidants in *S. cerevisiae* apoptosis.

201.2 Materials and Methods

201.2.1 Strains and UV-B Exposure

Wild-type strains *S. cerevisiae* (American Type Culture collection) were used as control strains for the comparison against UV-B stress. Prior to treat with UV-B irradiation, cells were aerobically grown in a nutrient-rich improving YEPD liquid medium (4 % (w/v), glucose; 0.5 % (w/v), yeast extract; 0.5 % (w/v), $(NH_4)_2SO_4$; 1 % (w/v), KH_2PO_4; 0.5 % (w/v), $MgSO_4 \cdot 7H_2O$; equipped with citric acid buffer at 30°C by shaking at 70 rpm for 20–30 min of recovery, and up to Mid-log phase ($OD_{600} = 1.0$). Cells were then transferred to UV-B chamber at 28–30°C on a rotary shaker (50–60 rpm) for 96 h or more. UV-B chamber was equipped with a 15 W UV-B light (Spectronics, Inc., Westbury, New York, USA) covered with new cellulose acetate film. The light ranges from 290 to 320 nm and emitted most of its energy (80 %) with an emission peak at 312 nm. UV-B irradiation was administered in a single dose of 24 J/m^2 (50 cm distance) with the aid of a UV radiometer. In the experimental stage, glucose was added to the culture and pH was adjusted regularly in order to the content of the yeast normal living.

201.2.2 Cell Death and DNA Fragmentation Assay

Cells were harvested during 0, 24, 48, 72 and 96 h irradiation under different conditions, and washed three times with deionized water and resuspended, then diluted to an optical density of 1.0 at 600 nm (OD600). 0.2 ml of each sample was then spotted on a YEPD agar media (1 % (w/v), yeast extract; 2 % (w/v), peptone; 2 % (w/v), dextrose) for 2 or 3 days at 30°C in order to monitor cell death. The viability was expressed as percent survival (100 %) and cell numbers were measured by counting of colonies for units (CFU).

In order to detect UV-B irradiation-induced apoptosis, DNA fragmentation assay was performed. Genomic DNA from S. cerevisiae was isolated according to the method described by Adams et al. [1]. Samples were precipitated with isopropanol and then electrophoresed on 2 % agarose gels. The approximate amount of DNA detected in the gel was assessed by densitometry of photographic negatives [28].

201.2.3 Protein Sample Preparation

The yeast cell walls were utilized as a proteolytic enzyme to break down and stop irradiation process. Crude cellular protein extracts were prepared according to the

method described by Ilsup et al. [13]. The protein concentration was determined by the Bradford method (Bio-Rad, Hercules, USA).

201.2.4 Activities of Enzymatic Antioxidants and Low-Molecular Weight Antioxidants Extract and Measure

The activity of SOD was assayed at 406 nm as the inhibition of quercetin oxidation by superoxide anion [7]. One unit was the amount of enzymes that one unit was determined as the amount of soluble protein of supernatant which inhibited the maximal rate of quercetin oxidation by 50 %. Catalase activity was determined with the decrease absorbance at 240 nm by the decomposition of hydrogen peroxide [19]. The activity of glutathione reductase (GR) was measured by following the consumption of NADPH in a reaction medium [7]. The content of trehalose and ergosterol was measured by the methods of Liang et al. [17] and Shang et al. [25].

201.2.5 Oxidative Damage to Proteins

Protein samples (30 mg per lane) were separated by 10 % SDS-polyacrylamide gel electrophoresis. Cellular carbonyl contents were measured at 368 nm [23]. Matrix-assisted laser desorption ionization-time of flight-mass spectrometry (MALDI-TOF-MS) was used to analyze immunochemical detection of protein carbonyls and mass spectrometry by using rabbit anti-DNP antibodies diluted 1:1000 [5].

201.3 Results

201.3.1 Cell Death and DNA Fragmentation Assay

Wild-type yeast cells were selected as a model to study whether cells survival on UV-B irradiated was decreased relative to UV-B irradiation in vitro or not. The same strains were cultivated in flasks and then were displayed under a UV-B light in phases during 24, 48, 72 and 96 h of continuous irradiation on the distance 50 cm. The survival of the UV-B irradiated cells was illustrated in Fig. 201.1, which was marked lower than the control cells ($P < 0.05$). UV-B irradiation induced apoptosis was shown in Fig. 201.2. It was clear that lane 4, 5, and 6 with a little trail which is so-called “fragmentation”. Comparison between lane 4, 5, and 6, cells treated with 24 h and 48 h has fewer fragment than ones treated with 72 h,

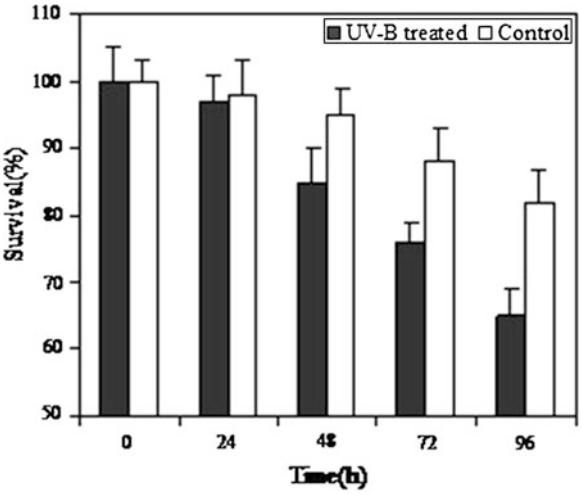

Fig. 201.1 Effect of UV-B irradiation on yeast *S. cerevisiae* cell death after 96 h of UV-B irradiation

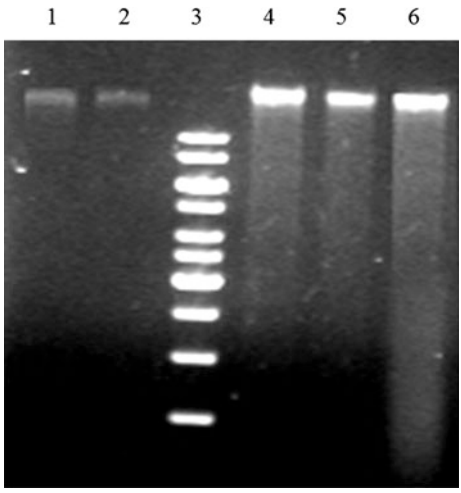

Fig. 201.2 DNA fragmentation derived from yeast *S. cerevisiae* after 96 h of UV-B irradiation

but significant different to the "no trail" lane 1, 2. Chromatin fragmentation was 15.6 % of total DNA in lane 4, 18.7 % in lane 5, and 30.1 % in lane 6.

The results are mean ± S. D.; n = 3. Hatched bar: UV-B treated; Open bar: control. $P < 0.05$ compared with control.

Lane 1, non-irradiated; Lane 2, 0 h of UV-B irradiation; Lane 3, molecular size markers; Lane 4, 24 h; Lane 5, 48 h; Lane 6,72 h. The results were mean ± S. D.; n = 3.

Table 201.1 Enzymatic and non-enzymatic defense mechanism activated by continuous UV-B irradiation compare to controls

UV-B irradiation (/h)		Enzymatic			Non-enzymatic	
		SOD	CAT	GR	Trehalose	Ergosterol
0	Stress	614.2 ± 17.0	30.7 ± 0.7	15.2 ± 0.3	110.2 ± 1.5	14.5 ± 0.5
	Control	614.2 ± 16.7	30.7 ± 0.9	15.2 ± 0.3	110.2 ± 1.7	14.5 ± 0.4
24	Stress	563.4 ± 16.7	28.6 ± 0.9	13.6 ± 0.3	112.1 ± 1.8	14.9 ± 0.3
	Control	615.4 ± 17.0	29.7 ± 0.6	14.3 ± 0.2	110.4 ± 1.6	14.8 ± 0.4
48	Stress	451.8 ± 16.0	25.4 ± 1.1	12.7 ± 0.2	114.3 ± 2.0	15.3 ± 0.5
	Control	467.3 ± 16.4	26.8 ± 1.3	12.6 ± 0.2	111.5 ± 2.1	14.9 ± 0.6
72	Stress	289.1 ± 16.4	20.2 ± 0.9	11.9 ± 0.2	114.7 ± 2.1	15.4 ± 0.5
	Control	258.6 ± 15.8	19.9 ± 0.5	10.9 ± 0.2	110.8 ± 1.9	15.0 ± 0.3
96	Stress	156.5 ± 14.9	16.1 ± 1.3	11.2 ± 0.3	112.9 ± 1.4	15.2 ± 0.4
	Control	145.1 ± 14.8	14.6 ± 0.5	9.7 ± 0.2	110.7 ± 1.5	14.7 ± 0.4

The values were expressed in U (g protein)$^{-1}$ or mg g^{-1}, the results are mean ± S. D.; n = 3

201.3.2 Activities of Enzymatic and Non-enzymatic Antioxidants

Significant reduction of activity of antioxidative enzymes was established as well as the increasing of contents of low-molecular weight antioxidants as a result of intensive exposure to UV-B irradiation in artificially modulate apoptosis was shown in Table 201.1.

In non-irradiated yeast cells, there was a transient increasing occurred during early phase, and the activity reached a maximum value at 624.9 U/mg of protein (data not shown), whereas UV-B irradiated cells decreased directly. However, the SOD activity of non-irradiated yeast cells was 11.4 % lower than the continuous UV-B irradiated cells at 96 h. Similar phenomena were happened in CAT and GR activity. The relative CAT and GR activity was finally increased by 1.1- and 1.3-fold than those in control after 96 h irradiation, respectively. On the other hand, the increasing contents of low-molecular weight antioxidants were represented as a bell-shaped curve, and the maximum content of trehalose and ergosterol (3.9 mg/g and 0.4 mg/g higher than control at the same phase) was obtained at 60 and 84 h respectively.

201.3.3 Oxidative Damage to Proteins

The degree of protein damage resulting from continuous UV-B irradiation treatment was shown in Fig. 201.3. Carbonyl contents were gradually augmented after the directly UV-B-treated conditions, whereas in control these contents were unaltered. Proteins of interest as major targets of UV-B-induced oxidative damage were also detected (Fig. 201.3b): translation elongation factor eEF-2, heat shock

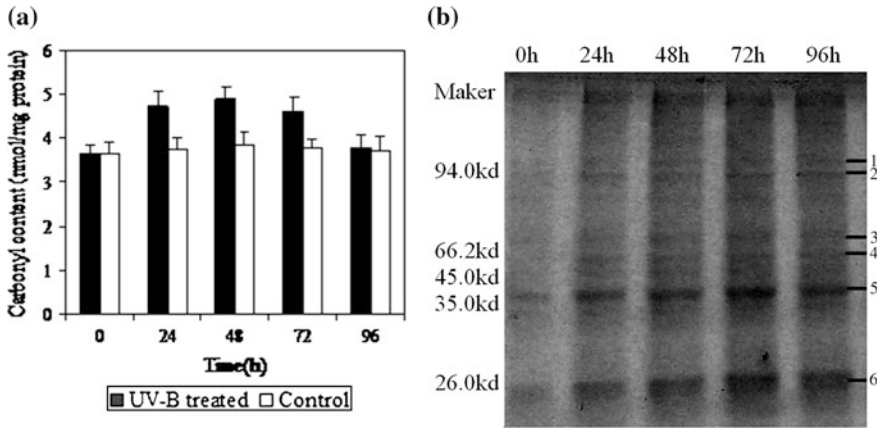

Fig. 201.3 Patterns of proteins of interest as major targets of UV-B-induced oxidative damage were detected after 96 h of UV-B irradiation **a** Carbonyl contents in treated cells. The results are mean ± S. D.; n = 3. Hatched bar: UV-B treated; Open bar: control. $P < 0.05$ compared with control. **b** Major oxidatively damaged proteins were detected by anti-2, 4-dinitrophenol-immunostaining

protein 70 (Ssa2p), pyruvate decarboxylase, enolase, glyceraldehydes-3-phosphate dehydrogenase, and 60S ribosomal protein L7.

Cellular carbonyl content and damaged proteins were detected. Exponentially growing cells (OD_{600} of 1.0) were treated with UV-B irradiation for 96 h after adaptation or not. (a) Carbonyl contents in treated cells. The results are mean ± S. D.; n = 3. Hatched bar: UV-B treated; Open bar: control. $P < 0.05$ compared with control. (b) Major oxidatively damaged proteins were detected by anti-2, 4-dinitrophenol-immunostaining. Detected bands were well-identified by matrix-assisted laser desorption ionization-time of flight-mass spectrometry (MALDI-TOF-MS) such as: (1) translation elongation factor eEF-2; (2) heat shock protein 70 (Ssa2p); (3) pyruvate decarboxylase; (4) enolase; (5) glyceraldehyde-3-phosphate dehydrogenase; (6) 60S ribosomal protein L7.

201.4 Discussion

The results obtained in this work demonstrated the relationship between continuous UV-B irradiation and cell death and apoptosis in *S. cerevisiae*. By virtue of the high homology in structure and function of yeast and mammalian, *S. cerevisiae* was used as an in vitro model to probe the response mechanism to continuous UV-B exposure. Owing to the depletion of nutrients by fast-growing cells so that slow-growing ones did not reach a detectable size, glucose and pH were adjusted regularly in order to content the yeast normal living. Earlier report has showed that the growth of fungi on the soil surface in the Antarctic terrestrial environment was

inhibited by Solar UV-B Radiation [12], our results was consistent with it (Fig. 201.1). Through manipulating apoptosis and cell death, UV-B irradiation modulated cell proliferation or differentiation was discovered. In previous study, it was well documented a typical set of morphological events including chromatin condensation, DNA and nuclear fragmentation, cell shrinkage, plasma membrane blebbing, increased numbers of cytosol vacuoles, and formation of apoptotic bodies followed by phagocytes digestion after UV-B irradiation [6]. Here, we sought to limit the study to apoptosis by using UV-B irradiation. Confirmed by DNA fragment analysis (see Fig. 201.2), it was suggested that the generation of UV-B-induced apoptosis was promoted at early stage and time-dependent. However, high survival of irradiated cells explained that UV-B irradiation was not extremely lethal to yeast cells, but has possibly an additional cellular functions for UV-B irradiation-induced apoptosis by activation of both receptor-mediated and mitochondrion-initiated cell death pathways [3].

Up to now, there was little study that has examined the oxidative damage by UV-B irradiation on *S. cerevisiae* in vitro. We augmented free ion in order to enhance higher toxic ROS generation. UV-B-induced ROS as oxidant could damage a wide range of cellular biological molecules including carbohydrates, nucleic acids, lipids, and proteins [16]. In zymograms analysis, six proteins of interest as major targets of UV-B-induced oxidative damage were shown in Fig. 201.3b. Similar manners to MD or Copper, proteins showed multiple effects on cellular physiology and server as a rapid-response mechanism to help cells confront in damage [2, 26].

Our results also provided direct evidences that UV-B irradiation are involved in antioxidant defense mechanisms. Previous researchers reported that SOD and CAT act to defend *S. cerevisiae* against hydrogen peroxide or menadione [2, 8], the SOD, CAT, and GR activity were also detected in present work. Compared to the control, the relatively increased activities under the influence of UV-B irradiation was testified protective processes in yeast cells. A strong positive correlation ($R^2 = 0.9754$, $R^2 = 0.9915$) among SOD, CAT, and GR activities has been further examined in Fig. 201.4. It was suggested that both of these activities played an important role in *S. cerevisiae* survival after continuous UV-B irradiation. These activities might represent the function of maintaining the necessary oxidant/antioxidant balance, rather than the optimal leads to development of oxidative stress. The immediate reduction of enzymatic antioxidants activity after exposure to UV-B radiation during 48 h was the evidence of already non-irreversible damages in yeast cells. And the defense against UV-B-induced ROS required to balance increments in antioxidant enzymes and cannot automatically be improved by increase in the activity of single enzymes.

In addition, an increasing contents of low-molecular weight antioxidants after UV-B irradiation in contrast to non-irradiated ones was observed, which could be considered as adaptive and protective reaction preventing from cell death. Trehalose is a non-reducing disaccharide which is account for a stress metabolite signal. For it is associated with the level of H_2O_2 (which is one of ROS), a large accumulation of trehalose in response to different kinds of stress appears to be

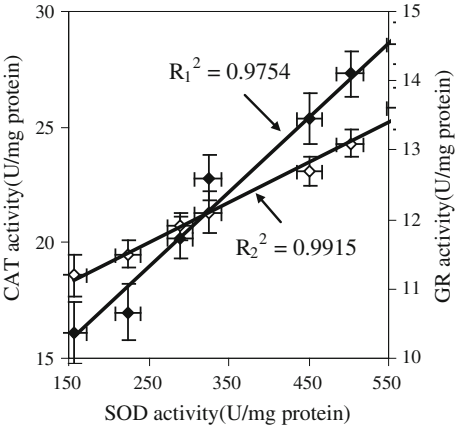

Fig. 201.4 A strong positive relationship between SOD and CAT and GR activities after 96 h of UV-B irradiation

crucial to ensure proper protection of cell integrity [33]. It is also true that spores with high trehalose content become more resistant against extreme environmental circumstances. Ergosterol is another protective substance, a main sterol in yeast cells and is responsible for structural membrane features such as integrity, fluidity, permeability, and the activity of membrane-bound enzymes [25]. UV-B irradiation also increased the contents of other low-molecular weight antioxidants. For example, it was reported that fibrous polysaccharide would remain intact under UV irradiation stress during the whole process, which could explain why cells undergoing apoptosis were, at least apparently, the same size as normal cells [6]. Thus, our results showed that both enzymatic and non-enzymatic defense mechanism could be modulating by UV-B irradiation in protective cell from apoptosis.

Our results demonstrated that increased antioxidative defense mechanism significantly suppressed UV-B-induced apoptosis. The results of DNA fragment assay indicated that the increased antioxidative defense mechanism did not protect the genome from UV-B-induced DNA damage. It is already known that overexpression of SelH decreases the ROS level and sustains cell viability in human cells [3]. Thus, we presumed that UV-B-induced genes associated with specific proteins of antioxidative defense mechanism would involve in ameliorating oxidative stress and repairing UV damage and further use of the yeast deletion collection for synthetic lethal mutants to identify among genes with roles in *S. cerevisiae* under UV-B irradiation.

Acknowledgments This work was supported by the Tanggu Technical Development Foundation Grant of Tianjin in China.

References

1. Adams A, Gottschling DE, Kaiser CA (2005) Methods in yeast genetics: a cold spring harbor laboratory course manual. Cold Spring Harbor Laboratory, New York
2. Bayliak M, Semchyshyn H, Lushchak V (2006) Effect of hydrogen peroxide on antioxidant enzyme activities in *Saccharomyces cerevisiae* is strain-specific. Biochem (Mosc) 71:1013–1020
3. Ben Jilani KE, Panee J, He Q et al (2007) Overexpression of selenoprotein H reduces Ht22 neuronal cell death after UVB irradiation by preventing superoxide formation. Int J Biol Sci 3:198–204
4. Birrell GW, Giaever G, Chu AM et al (2001) A genome-wide screen in *Saccharomyces cerevisiae* for genes affecting UV radiation sensitivity. Proc Natl Acad Sci USA 98:12608–12613
5. Cabiscol E, Piulats E, Echave P et al (2000) Oxidative stress promotes specific protein damage in *Saccharomyces cerevisiae*. J Biol Chem 275:27393–27398
6. Del Carratore R, Della Croce C, Simili M et al (2002) Cell cycle and morphological alterations as indicative of apoptosis promoted by UV irradiation in *S. cerevisiae*. Mutat Res 513:183–191
7. Fabrizio P, Liou LL, Moy VN et al (2003) SOD2 Functions downstream of Sch9 to extend longevity in yeast. Genetics 163:35–46
8. Fernandes PN, Mannarino SC, Silva CG et al (2007) Oxidative stress response in eukaryotes: effect of glutathione, superoxide dismutase and catalase on adaptation to peroxide and menadione stresses in *Saccharomyces cerevisiae*. Redox Rep 12:236–244
9. Fernández Zenoff V, Siñeriz F, Farías ME (2006) Diverse Responses to UV-B radiation and repair mechanisms of bacteria isolated from high-altitude aquatic environments. Appl Environ Microbiol 72:7857–7863
10. Gasch AP, Spellman PT, Kao CM et al (2000) Genomic expression programs in the response of yeast cells to environmental changes. Mol Biol Cell 11:4241–4257
11. Hakozaki T, Date A, Yoshii T et al (2008) Visualization and characterization of UVB-induced reactive oxygen species in a human skin equivalent model. J Arch Dermatol Res 300:s51–s56
12. Hughes KA, Lawley B, Newsham KK (2008) Solar UV-B radiation inhibits the growth of antarctic terrestrial fungi. Appl Environ Microbiol 69:1488–1491
13. Ilsup K, Haesun Y, Hitoshi I et al (2006) Genome-wide expression analyses of adaptive response against medadione-induced oxidative stress in *Saccharomyces cerevisiae* KNU5377. J Process Biochem 41:2305–2313
14. Kaiserli E, Jenkins GI (2007) UV-B promotes rapid nuclear translocation of the arabidopsis UV-B-specific signaling component UVR8 and activates its function in the nucleus. Plant Cell 19:2662–2673
15. Kim JJ, Sundin GW (2000) Regulation of the *rulAB* mutagenic DNA repair operon of pseudomonas syringae by UV-B (290–320 Nanometers) radiation and analysis of *rulAB*-mediated mutability in vitro and in planta. J Bacteriol 182:6137–6144
16. Kliebenstein DJ, Lim JE, Landry LG et al (2002) Arabidopsis *UVR8* regulates ultraviolet-B signal transduction and tolerance and contains sequence similarity to human regulator of chromatin condensation 1. Plant Physiol 130:234–243
17. Liang LK, Wang XK, Zhu KL et al (2007) Trehalose synthesis in *Saccharomycopsis fibuligera* does not respond to stress treatments. Appl Microbiol Biotechnol 74:1084–1091
18. Liu T, Biddle D, Hanks AN et al (2006) Activation of Dual Apoptotic pathways in human melanocytes and protection by survivin. J Invest Dermatol 126:2247–2256
19. Lushchak V, Semchyshyn H, Mandryk S et al (2005) Possible role of superoxide dismutases in the yeast *Saccharomyces cerevisiae* under respiratory conditions. Arch Biochem Biophys 441:35–40

20. Madeo F, Fröhlich E, Ligr M et al (1999) Oxygen stress: a regulator of apoptosis in yeast. J Cell Biol 145:757–767
21. Michael YR, Christian W, Ulrike HL (2006) Impact of ultraviolet radiation on cell structure, UV-absorbing compounds, photosynthesis, DNA damage, and germination in zoospores of Arctic *Saccorhiza dermatodea*. J Exp Botany 57:3847–3856
22. Obermüller B, Karsten U, Abele D (2005) Response of oxidative stress parameters and sunscreening compounds in arctic amphipods during experimental exposure to maximal natural UVB radiation. J Exp Mar Biol Ecol 323:100–117
23. Reznick AZ, Packer L (1994) Oxidative damage to proteins: spectrophotometric method for carbonyl assay. J Meth Enzymol 233:357–363
24. Scherens B, Goffeau A (2004) The uses of genome-wide yeast mutant collections. Genome Biol 5:229
25. Shang F, Wen S, Wang X et al (2006) High-cell-density fermentation for ergosterol production by *Saccharomyces cerevisiae*. J Biosci Bioeng 101:38–41
26. Shanmuganathan A, Avery SV, Willetts SA et al (2004) Copper-induced oxidative stress in *Saccharomyces cerevisiae* targets enzymes of the glycolytic pathway. FEBS Lett 556:253–259
27. Shi S, Wang G, Wang Y et al (2005) Protective effect of nitric oxide against oxidative stress under ultraviolet-B radiation. Nitric Oxide 13:1–9
28. Shindo Y, Hashimoto T (1998) Ultraviolet B-induced cell death in four cutaneous cell lines exhibiting different enzymatic antioxidant defences: involvement of apoptosis. J Dermatol Sci 17:140–150
29. Susan E (2007) Apoptosis: a review of programmed cell death. J Toxicol Pathol 35:495–516
30. Takahashi H, Hashimoto Y, Aoki N et al (2000) Copper, zinc-superoxide dismutase protects from ultraviolet B-induced apoptosis of *SV40*-transformed human keratinocytes: the protection is associated with the increased levels of antioxidant enzymes. J Dermatol Sci 23:12–21
31. Varengo A, Abele-Oeschger D, Burlando B (1998) Effects of low temperature on prooxidant processes and antioxidant defence systems in marine organisms. In: Pörtner HO, Playle R (ed) Cold Ocean physiology. Society for experimental biology seminar series, vol 65. Cambridge UNIV PR, Cambridge pp 212–235
32. Whitelam GC, Halliday KJ, Jenkins GI et al (2007) UV-B perception and signal transduction. In: Whitelam GC, Halliday KJ (eds) Light and plant development. Blackwell, Oxford, pp 155–182
33. Zaragoza O, González-Párraga P, Pedreño Y et al (2003) Trehalose accumulation induced during the oxidative stress response is independent of *TPS1* mRNA levels in candida albicans. Int Microbiol 6:121–125
34. Zhang B, Spandau DF, Roman A (2002) E5 protein of human papillomavirus Type 16 protects human foreskin keratinocytes from UVB-irradiation-induced apoptosis. J Virol 76:220–231
35. Zhang W, Hanks AN, Boucher K et al (2005) UVB-induced apoptosis drives clonal expansion during skin tumor development. J Carcinog 26:249–257